Advanced Structured Materials

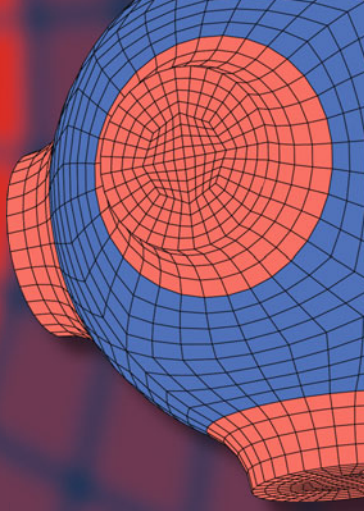

Francesco dell'Isola
Victor A. Eremeyev
Alexey Porubov *Editors*

Advances in Mechanics of Microstructured Media and Structures

Springer

Advanced Structured Materials

Volume 87

Common engineering materials reach in many applications their limits and new developments are required to fulfil increasing demands on engineering materials. The performance of materials can be increased by combining different materials to achieve better properties than a single constituent or by shaping the material or constituents in a specific structure. The interaction between material and structure may arise on different length scales, such as micro-, meso- or macroscale, and offers possible applications in quite diverse fields.

This book series addresses the fundamental relationship between materials and their structure on the overall properties (e.g. mechanical, thermal, chemical or magnetic etc.) and applications.

The topics of *Advanced Structured Materials* include but are not limited to

- classical fibre-reinforced composites (e.g. class, carbon or Aramid reinforced plastics)
- metal matrix composites (MMCs)
- micro porous composites
- micro channel materials
- multilayered materials
- cellular materials (e.g. metallic or polymer foams, sponges, hollow sphere structures)
- porous materials
- truss structures
- nanocomposite materials
- biomaterials
- nano porous metals
- concrete
- coated materials
- smart materials

Advanced Structures Material is indexed in Google Scholar and Scopus.

More information about this series at http://www.springer.com/series/8611

Francesco dell'Isola · Victor A. Eremeyev
Alexey Porubov
Editors

Advances in Mechanics of Microstructured Media and Structures

Springer

Editors
Francesco dell'Isola
Dipartimento di Ingegneria Strutturale e Geotecnica
Università di Roma "La Sapienza"
Rome
Italy

Victor A. Eremeyev
Faculty of Civil and Environmental Engineering
Gdańsk University of Technology
Gdańsk
Poland

Alexey Porubov
Department of Micromechanics of Materials
Institute of Problems in Mechanical Engineering
Saint Petersburg
Russia

ISSN 1869-8433 ISSN 1869-8441 (electronic)
Advanced Structured Materials
ISBN 978-3-319-73693-8 ISBN 978-3-319-73694-5 (eBook)
https://doi.org/10.1007/978-3-319-73694-5

Library of Congress Control Number: 2017962993

Printed on acid-free paper

This Springer imprint is published by the registered company Springer International Publishing AG part of Springer Nature
The registered company address is: Gewerbestrasse 11, 6330 Cham, Switzerland

Preface

This volume is devoted to the memory of Russian scientist Eron Aero who passed away on June 2016. His outstanding contribution to the theory of materials with internal structure starts with his first publication with his supervisor Kuvshinsky on the model of the Cosserat continuum. It appeared in early sixties and attracted great attention of scientists as an outstanding contribution in the field of generalized continua. The main finding was the obtaining of the potential and the material relationships invariant to the rigid rotation while previous models were not invariant. Throughout his life, he considered the micropolar models of solids and fluids. Nowadays, the Cosserat continuum has taken a significant place in Continuum Mechanics among other generalized models of continua such as micromorphic continua, strain-gradient media and media with internal variables. His findings in the area inspired many scientists for their fruitful scientific researches.

He also contributed to the theory of liquid crystals developing new theory for nematics based on the use of couple stresses theory. He developed strongly nonlinear continuum theory of crystalline media whose complex lattice structure consists of two sub-lattices. He suggested a principle of translational symmetry that resulted in obtaining new nonlinear equations of motion. The solutions to these equations allow us to predict deep structural rearrangements of the lattice in the field of intensive power and thermal stresses: lowering of potential barriers, switching of the inter-atomic bonds, phase transitions, fragmentation of the lattice, etc; thus, some modern experimental data may be explained. The most important Aero's publications were listed in the editorial [V. A. Eremeyev, A. V. Porubov, L. Placidi. Special Issue in Honor of Eron L Aero. *Math. Mech. Solids*. 2016. **21**(1), 3–5].

As can be seen, E. Aero was not afraid to seriously change the direction of his research and distinguished by original approaches to the solution of the problems stated by him. His vivid non-standard thinking provided a great influence on the investigations of his colleagues who discussed their tasks with him.

This volume contains contributions of scientist dealing with various aspects of mechanics of microstructured media and structures. There are papers written by the colleagues of the Institute of Problems in Mechanical Engineering of the Russian Academy of Sciences where he worked for many years, organized and headed the laboratory of Micromechanics of Materials. In particular, these works concern development of the theory of highly nonlinear dynamic processes in media having complex crystalline lattice. Also the contributions on generalized microstructured media are presented which are originally inspired by his pioneering work with Kuvshinsky. The presented here papers address the further developments in the theory of Cosserat media, liquid crystals, porous media, piezoelectrics, thermodynamics, materials with surface stresses, in applications to the metamaterials and even in the modelling of the circumsolar ring evolution.

The volume continues honouring of achievements of E. Aero started by the Special Issue of the Mathematics and Mechanics of Solids (2016, SAGE Publ.) on the occasion of his 80th anniversary.

Rome, Italy — Francesco dell'Isola
Gdańsk, Poland — Victor A. Eremeyev
Saint Petersburg, Russia — Alexey Porubov
November 2017

Contents

Some Introductory and Historical Remarks on Mechanics of Microstructured Materials

Francesco dell'Isola and Victor A. Eremeyev

Abstract Here we present few remarks on the development of the models of microstuctured media and the generalized continua.

1 Structured Media i.e. Modeling Complexity: A Change of Paradigm?

In recent literature a great attention has been paid to the so called "structured media". These are media in which the macroscopic behavior is dictated by the micro structure of the considered systems. Of course the related theory of structures, which was originated for describing the behavior of bridges and building, then applied to airplanes, spaceships and robotics uses methods and techniques which are very close. Therefore the most modern theory did exploit the results and the ideas developed in the elder one.

The standard Cauchy continuum theory is clearly not suitable to describe the physical behavior of structured continua. For a detailed discussion of this point the reader can refer for instance to [1–4].

For this reason different generalizations were proposed. The works which we consider more enlightening and systematic are those due to Germain and Eringen (see [5–7]) and we refer to [1, 4, 8–16] and references there cited for a more detailed discussion of the explored theoretical possibilities.

The ideas of Cauchy having found brave champions (see e.g. [17]) a part of the community of mechanicians did believe that the whole continuum mechanics was

F. dell'Isola
Università di Roma "La Sapienza" and International Research Center on Mathematics and Mechanics of Complex System (M&MOCS), Università dell'Aquila, L'Aquila, Italy
e-mail: francesco.dellisola@uniroma1.it

V. A. Eremeyev (✉)
Faculty of Civil and Environmental Engineering, Gdańsk University of Technology, ul. Gabriela Narutowicza 11/12, 80-233 Gdańsk, Poland
e-mail: eremeyev.victor@gmail.com

F. dell'Isola et al. (eds.), *Advances in Mechanics of Microstructured Media and Structures*, Advanced Structured Materials 87,
https://doi.org/10.1007/978-3-319-73694-5_1

covered by what is indeed a particular case. Cauchy first gradient continua, while representing a particular and very important case of continua, do not exhaust all logical and physical possibilities, when one decides to introduce a continuous model for deformable bodies (see e.g. [4, 5, 7, 18]).

This circumstance had as a consequence that mechanics needed to experience (in a small scale and in a limited subgroup rather localized in space and time) a rather sharp change of paradigm (see for the discussion of the concept of paradigm and for the particular paradigm change considered here e.g. [8, 19–25]) in order to recover the capacity of describing complexity via continuum models.

The complexity at micro level do require extra kinematic descriptors at macro level: sometimes it is enough to introduce as deformation measures higher gradients of displacements (see e.g. [6, 18]) but in general other completely independent descriptors are needed. If one limits to continua where it is enough to introduce balance of torque then one gets Cosserat continua (see the founding work [26] and e.g. the elegant contribution by [24, 27–32]).

Otherwise one needs variational principles and a family of new and completely independent kinematic descriptors as discussed e.g. in [5, 7, 18, 33, 34].

A possible way for getting well posed theory may consist in introducing homogenization techniques, by starting from a discrete or continuous micro-model being characterized by simple mechanical properties and complex geometry.

Gabrio Piola (translated in [35]) seems to have been one of the first scholars in proposing a kind of asymptotic homogenization and actually he ended by introducing peridynamics and high gradient models (see e.g. [1, 4, 8, 19]).

More recently more rigorous homogenization procedures are applied and used (see e.g. the fundamental book [36–49]) based on various functional analytical concepts, including Gamma-convergence. All these procedures however, while gaining in mathematical rigor, do not supply in general a heuristic tool: they are only to be used in order to justify mathematically a conjecture which has to be obtained via some other conceptual tools. Moreover the great majority of them assume some starting hypotheses which lead and limit to first gradient continua. However it has been proven that higher gradient models can be obtained via homogenization of highly contrasted micro structures (see e.g. [3, 50–61]). The conjecture which leads to these class of continua by means of asymptotic expansions is simple: different elasticity coefficients must be rescaled with the expansion parameter to diverge with suitably large power. This statement formulates precisely the condition of "presence of high contrast" in material parameters. This situation is exactly as for layered plates and shells with hight contrast in elastic moduli of layers. For low contrast the classic model of shear-deformable plates and shells can be applied whereas for high contrast the extended models that is layer-wised ones are necessary, see [62, 63].

It is worth to mentioned that the homogenization is a reach source for constitutive models of extended continue. For example it was used for derivation of the constitutive relations of micropolar solids in [33, 64–74].

The homogenization techniques can be applied also in in the case of microstructured coatings such as applied to produce superhydro- and oleo-phobic surfaces in order to obtain the models of surface elasticity developed by [75, 76] and by [77, 78], see e.g. [79].

It has to be remarked that in statistical mechanics some rigorous results are obtained which prove rigorously how one can get fluid continua from discrete microscopic systems (see the exhaustive reviews presented in [80–82]).

Actually while one can obtain relevant and rigorous results in homogenizing microscopically inhomogeneous systems, also including in the picture thermal phenomena for systems behaving macroscopically as fluids (see the e.g. [83–87]) and also for different class of biological systems (see e.g. [88, 89]), it is an open problem the determination, via statistical mechanics and rigorous reasonings, of micro properties leading, at macro level, to solid behavior.

Therefore one has to expect that heuristic methods, mixed micro-macro approaches and ad hoc phenomenological continuum models still play a relevant role in the efforts for describing structured media.

2 Did Piola Formulate Already A Method of Asymptotic Homogenization?

While Piola did not produce results comparable in rigor to the results cited in the previous introduction (clearly the concept of rigor in mathematical proof is changing in time and in space) he did formulate generalized continuum model, like those presented in this volume.

Homogenization procedures start by considering two different levels at which modeling is performed. We talk about respectively micro and macro descriptions and they correspond to relatively smaller or larger length scales.

As we have discussed there are two different class of homogenization results: the first class of these results is based on heuristic considerations leading to conjecture, having accepted more or less clear assumptions, that a specific set of discrete micro models, if the characteristic length-scale tends to zero, can converge to a certain macro continuous model, at least under well specified phenomenological conditions. If one is lucky (or clever enough) these heuristic analyses can lead to the identification of continuum constitutive parameters in function of the properties of the micro discrete systems.

The second class consists in producing precise mathematical results: the micro problem and the limit macro problem are compared and the difference of their solutions is estimated by introducing an upper bound, which, eventually, is proven to vanish when the homogenization parameter tends to zero. As the methods used in this second class are modern they did not belong to the generation of mathematicians of Piola: it is useful to distinguish them as results based either on the functional analysis [36, 37, 45, 49], or on Gamma-convergence (see e.g. [3, 39, 41, 42, 50, 51, 53, 54]), or on a priori estimated techniques (see e.g. [55]).

Remark that when one starts from a micro model one can reach a macro model only after having accepted suitable kinematical and simplifying assumptions. These assumptions actually characterize the macro target model and this macro model is

assumed to be able to describe the overall behavior of the micro model only in some and well specified physical instances.

Actually there are (eventually infinite) many micro motions which can correspond to a unique specifically chosen macro motion: in statistical mechanics and in any homogenization procedure one has to make a limiting choice of one specific class of micro motions for each macro motion in order to develop the macro model: this is an intrinsic characteristic of the "averaging" procedure.

Based on this correspondence one must also try to identify the evolution equations of the macro motion starting from the geometrical and mechanical properties of micro system.

We stress that it has to be recognized that Piola's contribution to mechanics must include his identification of a micro motion for a discrete lattice material particles systems in terms of a macro motion as given by the placement fields for the homogenized continuum, as functions of space and time.

This is exactly the method which he uses to formulate (see [4]) his generalized continuum macro models, which are very advanced even nowadays and which has been rediscovered more than 150 years later.

Of course one can object that Piola did not "prove" that starting from micro-motions, as solutions of micro evolution equations, and considering macro-motions, as solution of macro evolution equations, when the chosen micro-level length-scale tends to zero, the micro motions tend to produce exactly the considered macro motions, once a suitable way for measuring their distance has been introduced.

This procedure requires to preliminary find a well-posedness result for both micro and macro problems and the capacity of finding a functional space to which both macro and micro motions belong. Many different techniques have been developed: see e.g. the following references: ([3, 36, 37, 39, 41, 42, 45, 49–51, 53–55]). The reader will not be surprised to see that considered models at micro scale are sometimes infinite dimensional continuous and other times finite dimensional models: macro models, instead, are nearly always continuous.

Using his identification procedure Piola manage to formulate continuum models which are more general than those studied by Cauchy: however these last class of models attracted the attention of the majority of engineering scientists and therefore when both at micro and macro levels one considers Cauchy (i.e. first gradient) continua it is possible to find, in modern literature, many interesting results which frame homogenization in very advanced mathematic al theories: Gamma convergence and many other functional analysis concepts were developed under the push of the demands from this mechanical problem: the reader is referred for more details, for instance, to [36, 37, 39–47, 49, 90]. All mathematical results in this context are based on the rigorous proof of the convergence of micro energies to macro energies when the introduced micro scale vanishes.

It has to be remarked that Piola considers at micro-level a system of particles placed in a lattice: they may experience also long range interactions and their placement may be changed under the action of external actions. As long range interactions among particles are allowed the continuum limit which he obtains results to be a generalized continuum. Remark that Piola did not know that subsequent literature would

be bound to consider Cauchy particular class of continua: therefore he calls what in modern times are "generalized continua" simply "continua". Piola's continua, actually were bound to be rediscovered in XXI century: they are the object of the study in so called Peridynamics (see for a more detailed discussion the work [4]).

Piola seems to attribute to discrete systems a specific and relevant physical meaning, as was customary in his époque. Later science was shacked by the terrible controversy between Mach and Boltzmann. It seems to us that Piola would have shared the ideas expressed by Boltzmann. It has to be remarked that Piola had no ideas of the true dimensions of atoms and molecules and that his considerations do not include temperature. Some homogenization results (and very rigorous ones) have been obtained, for discrete systems, in statistical mechanics. With these results one can prove rigorously how fluid continua can be seen as a limit of discrete microscopic systems, see the interesting reviews in [80–82]. These results in homogenizing microscopically inhomogeneous systems, which manage to interpret thermal phenomena in systems which behave macroscopically as fluids (see e.g. the papers [83–87]) and in some biological systems (see e.g. [88, 89]), were not extended, up to now, to determine, by means of rigorous statistical mechanical methods, which are those micro properties which produce, at macro level, deformable solids.

As a consequence the old fashioned heuristic methods *à la Piola* can still be topical, as it may represent the only available conceptual tool to model some specific complex mechanical systems. An example of their application is presented in [91–93], while in [58, 59, 91] some mixed micro-macro approaches are attempted. Also numerical identifications (see e.g. [94, 95]) and ad hoc phenomenological continuum models in [2, 5, 26, 58, 59, 91–93, 96, 97] still play a relevant role in the efforts for describing structured media.

Exactly as happens in statistical mechanics the system that Piola considers at micro level is finite dimensional: in modern literature one finds less attention to the homogenization of this kind of models (see e.g. [38, 39]).

We believe that starting from lattices of interacting particles it is more natural to arrive to macro homogenized models which do not verify the basic assumptions by Cauchy: and indeed Piola did easily formulate such a kind of models. Also it has to be noticed that the modern debates and discussions questioning the use and the role of second or higher gradient continuum theories in mechanical sciences are not new.

Francesco Brioschi edited the last work by Piola translated in [35], posthumous in 1856: in the title of this work the word "controversial" appeared in a evident position. Cauchy, Navier and Poisson, changing the direction given to the French mechanics school by Lagrange and D'Alembert, did not believe any more to the powerful heuristic importance of variational methods.

More recently the French school (leaded by Paul Germain see e.g. [6, 7]) came back to the ancient ideas by Lagrange, as divulged by Piola.

Therefore we have an apparently paradoxical situation: even if the results presented by Piola are not as rigorous as required by the modern standards in the mathematical theory of homogenization, they are often, and by far, more general than those presented in the great majority of recent papers and textbooks in continuum mechanics.

We believe that the Piola's micro-macro identification procedure can be easily used as a heuristic guidance to new and very interesting rigorous results: Piola identifies macro virtual work in terms of macro kinematical descriptors by imposing its equality with micro virtual work. To do so he assumes what we want to call *Piola's Ansatz*:

(i) one assumes that a smooth macro displacement field exists which describes at this length scale the overall behavior of studied complex system,
(ii) one identifies the displacements of the particles forming the micro-lattice by means of the values of the macro displacement in the nodes of the lattice;
(iii) he identifies finite differences with derivatives and in this way he identifies the expression of macro deformation and kinetic energy and macro virtual work in terms of micro geometrical and physical properties.

In our opinion this process is due to Piola (again we are ready to discover a further occurrence of Stigler's law) and we call it: *Piola identification process*.

3 Variational Principles as a Guide for Formulating New Models: The Case of Hencky and Euler Beams

Which postulation scheme is needed when one needs to formulate new models for describing the physical behavior of systems not yet studied?

Many possible epistemological choices can be used: D'Alembert, Lagrange and Piola are among the founders of a school whose postulation is based on variational principle. The most general of such principles is the Principle of Virtual Work, of which the Hamilton Principle can be regarded as a particular case.

It is relevant to understand when this principles were introduced at first. In our opinion in many cases new mathematical models could be formulated only after having approached the problem by using the postulation scheme based on variational principles. For historical remarks on various variational principles we refer also to [98].

This opinion can be tested only by checking all possible instance of novel models, as introduced in different époques: of course in this context it is essential to determine the first formulation of a given model. Indeed once formulated a models, for instance starting from a variational principle, it is easy to reformulate it by assuming a postulation scheme based on balance principles.

From an epistemological point of view it is essential to establish if the discovery is more frequent when one starts from variational principles or if he starts from balance principles.

Therefore while the fight for priority may be futile, to establish which postulation scheme was more successful may be of relevance.

We discuss here two examples.

3.1 First Formulations of Hamilton Principle

For sure in the work by Piola published in 1825 one finds the following statement:

"Concluderemo adunque che le funzioni di t volute dalle leggi della natura e che esprimono le coordinate di tutti i punti del sistema alla fine di un tempo qualunque, hanno quelle stesse forme che rendono massima o minima la primitiva della funzione $\Omega - U - \frac{1}{2}\sum\left(dx^2 + dy^2 + dz^2\right)$ definita fra i due limiti valori del tempo".

This statement can be translated as follows:

"We will therefore conclude that the functions of the time t which are wanted by the laws of nature and which express the coordinates of all the points of the system at the end of any time whatsoever, have exactly the same forms which render maximal or minimal the primitive of the function $\Omega - U - \frac{1}{2}\sum\left(dx^2 + dy^2 + dz^2\right)$ as defined between the two limit values of the time".

Few years later such a statement has been called "the Principle of Hamilton". The reader will remark that this variational principle has been placed at the basis of the mechanics of material bodies in the two papers "On a General Method in Dynamics" which were published in the Philosophical Transactions in 1834 and 1835 (see [99]).

In [99] Hamilton writes: "But when this well known law of least, or as it might be better called, of stationary action, is applied to the determination of the actual motion of the system, it serves only to form, by the rules of the calculus of variations, the differential equations of motion of the second order, which can always be otherwise found." ....

Therefore it seems that also Hamilton needed to discuss and support his variational point of view, if he feels the need to support it by confirming its results with those obtained in another way.

"A different estimate, perhaps, will be formed of that other principle which has been introduced in the present paper, under the name of the law of varying action, in which we pass from an actual motion to another motion dynamically possible, by varying the extreme positions of the system, and (in general) the quantity H, and which serves to express, by means of a single function, not the mere differential equations of motion, but their intermediate and their final integrals."

In reading Hamilton one must deduce that he did not know Piola's previous work. There are no reasons to doubt about this fact: indeed he expresses his total admiration of the work of his predecessors and in particular those due to Lagrange. He claims:

> The theoretical development of the laws of motion of bodies is a problem of such interest and importance, that it has engaged the attention of all the most eminent mathematicians, since the invention of dynamics as a mathematical science by Galileo, and especially since the wonderful extension which was given to that science by Newton. Among the successors of those illustrious men, Lagrange has perhaps done more than any other analyst, to give extent and harmony to such deductive researches, by showing that the most varied consequences respecting the motions of systems of bodies may be derived from one radical formula; the beauty of the method so suiting the dignity of the results, as to make of his great work a kind of scientific poem.

The previous excerption by Hamilton expresses an opinion fully shared by Piola. Both Hamilton and Piola are to be considered immediate successors of Lagrange in

the leadership of the mechanical school basing the study of physical systems on a postulation which has as central point the Principle of Hamilton, or its weaker form (later used systematically by Piola) given by the Principle of Virtual Work.

We can easily accept that Hamilton and Piola are among the brightest scientists in mechanical sciences. They both regarded themselves as continuators of the work of D'Alembert, in the spirit (i.e. following his metaphysics, using Piola's expression) of Lagrange.

We cannot be sure that Piola is actually the true originator of modern generalized continuum theories: we are aware of the fact that in [100], Stigler's law of eponymy is formulated "no scientific discovery is named after its original discoverer".

3.2 Hencky Discrete Models and Euler Continuum Models for Beams

In 1825 Piola published his first scientific Memoir. Piola considers more fundamental and more physically understandable a model for planar beams based on the consideration of an "equivalent" system of bars and concentrated springs. He regards an Euler beam as the limit of a set of bars: each bar can be elongated and the relative angle between two bars can change. Both elongation and angle variations determine a variation of deformation energy, whose expression in left arbitrary. Actually Piola formulates a principle of virtual work by specifying suitable deformation energies and by determining the dual quantities of these deformations.

Piola's discrete model will be studied by Hencky nearly one century later, regarding it as an approximation of Euler beam. Piola regards as more understandable the described discrete system: he finds possible the formulation of the Euler model only regarding it as a limit of a discrete system of bars. Both Piola and Euler (see e.g. [101] for a detailed discussion of the original works of Euler and his choice of basing his investigations on variational principles) systematically formulate, as the most fundamental assumption, a principle of virtual work.

Consider that Euler was among the first authors studying the deformation of Elasticas and that Piola is one of the first authors studying Hencky type models for beams.

We can read some excerptions from the Memoir of 1825 by Piola, when he talks about elastic curves:

> In the elastic curves it occurs to have to consider internal forces as those recalled in the n 199; they can be, as we will see, of three kinds; but if one wants to conceive their action, it is possible to do so only by using the approximating polygon (193).

It is obvious then that for Piola the ontological reality resides only in discrete models, while the continua are only some mathematical tools which can be of use when looking for the solution of specific applicative problems: he relies for this on the powerful methods of mathematical analysis.

Piola continues by stating that:

> Therefore this is what we will do, by recalling that it is not important to be able to form in our mind the image of the way of action of elastic forces in the curves: for what concerns the effects, they can be found as could be found if it would not occur (occurrence which still is indispensable) the disappearance of every representation in the passage from the polygon to the curve, which is its limit (see again 193).

Here Piola states clearly the fact that he refrains from the consideration of internal forces: he considers the efforts in this direction "not important".

Finally he lists the three kinds of elasticity which can be observed in elastic curves:

At first the one related to elongations:

> The first kind of elasticity, to which one wanted to give the name of tension, is that elasticity for which, even if there were not external applied forces, one would change every side of the subtended polygon by elongation or contacting it.

then the kind related to bending

> The second kind of elasticity, or that kind of elasticity to which the recent writers have left the name without any specific adjective, is imagined to act on the angle formed by two consecutive sides of the polygon and along all the polygon itself. However, in order to find the term which this kind of elasticity has introduced in the general equation, it is convenient to determine, at first, the function F (199) which said elasticity tends to make vary.

Piola manages to determine some measures of deformation able to account for the bending, starting from the placement function of the elastic curve. In [102] the spirit of Piola is evoked to find an expression of continuous deformation energy and to formulate the equilibrium minimization problem for pantographic structures. Exactly as forecast by Piola the obtained models are generalized second gradient continua.

Then Piola proves that the limit of his Hencky type discrete beam leads exactly to the fundamental conjecture by Euler and Bernoulli: bending deformation energy depends on the curvature of the elastica.

Again quoting Piola (his Memoir 1825):

> Therefore (199) in the term $SE\delta f$ introduced by that elastic force the f will have the just determined value. As then, being R the radius of curvature, one knows that
>
> $$R = \frac{\left(Dx^2 + Dy^2 + Dz^2\right)^{\frac{3}{2}}}{\sqrt{\left\{\left(DxD^2z - DzD^2x\right)^2 + \left(DyD^2z - DzD^2y\right)^2 + \left(DxD^2y - DyD^2x\right)^2\right\}}}$$
>
> in this way it can be seen how we get
>
> $$f = \frac{Ds}{R} \qquad\qquad ''$$

To complete his analysis Piola considers beams having non planar actual configurations:

> Mister Binet (**J**) was the first author who introduced the consideration of a third kind of elasticity, and he wanted to call it torsion: this kind of elasticity had escaped the analysis of Lagrange, and nevertheless one cannot deny that it can be observed also in nature. To understand what it is [such a concept] let us consider three consecutive sides of the subtended polygon (199), and it is very well clear that the plane formed by the first two sides will not generally be the same plane which contains the last two sides: these two planes will form an angle and it is on this angle that the new elasticity is intended to act. Once called F this angle of the polygon, if we will manage to transform it into the usual form $\omega f + \omega^2 k + etc.$, we will also know the term $SE\delta f$ introduced by the torsion in the general equation (199). Again here, as in the previous paragraph and for a similar reason, I will give a new way for finding this angle.

We conclude with two remarks:

(i) Piola's mathematical investigations gave an important contribution to the modern theory of one dimensional extensional continua, moving in space and capable to store bending and twisting energy;
(ii) Piola's results established the mathematical basis of the numerical study of Euler or Hencky beams, basing the formulation of their evolution equations on the firm basis of variational principles.

4 Discrete Versus Continuous Description: An Ancient Dichotomy

Greek philosophers debated about the true ontological nature of matter. Epicurean believed in its discrete nature, as they considered atoms as the smallest indivisible constituent of matter. On the other side Heraclitus did believe that the ontological nature of matter was intrinsically continuous.

However already Archimedes was aware of the difficulty in reaching any definite conclusion about the ultimate true nature of matter (and any other physical phenomenology): in fact he was aware that any mathematical theory had a specific use limited to describe only a well determined class of phenomena.

Therefore the question concerning discrete of continuous description has to be considered simply as a matter of opportunity: in a given context which is the most suitable approach? It seems rather difficult to establish that one description between the one give by discrete models or the other one based on continuous models is the closest to reality.

Archimedes (and the modern scientists) refrain from any effort of attaining any definite truth about the ultimate nature of matter. We must be content to find the class of model which more suitably describes a given class of phenomena. It seems that also Piola accepts such a point of view. The principle of Virtual Work is at the basis of the whole set of memoirs by Piola: all the models which he considers starts from the postulation of the internal and external work functionals. He prefers to start his analysis by considering discrete models for the lattices of particles which he wants to consider and he claims to be able to understand clearly the physical meaning of such

discrete models: he believes that continuum models represent as mental construction useful to describe the behavior of discrete systems as a whole and only in some specific and well determined situations. Actually he considers continuous models as a mathematical tool to calculate solutions to equilibrium or motion problems: partial differential equations are considered in his époque (see also for instance the results by Hamilton leading to Hamilton-Jacobi partial differential equation) as a tool useful to calculate the solution of systems of ordinary differential equations having many unknown time varying function.

For those who may ask themselves how it is possible to believe that more complex PDEs may be of use in solving simpler ODEs we remark here that it can happen that PDEs can be solved with less efforts that the original ODEs: the French school in engineering sciences obtained wonderful results using this method, mainly when dealing with linearized equations. For instance De Saint Venant opened for engineering applications all the results for linear elasticity and had a great impact in engineering capacity of designing structures.

In our opinion, for Piola and many scientists of his generation, continuum mechanics represents a "computational tool". It is a "mathematical trick" which allows for computation of some solutions which are relevant in the engineering applications. As sometimes happens in science, what was born as a computational tool became a foundational concept: the choice of considering balance equations as the most fundamental concepts in mechanics (due probably to Cauchy, but who knows? Maybe Stigler's law applies also here) produced the consequence of considering the principle of virtual work as a less fundamental concept. This lead to the following oxymoron: "we prove now the theorem of the principle of virtual work". Further investigations are now needed to districate such an oxymoron and many other related ones.

The dichotomy discrete/continuous was present in the whole history of science and we cannot discuss in a small space it: such dichotomy has so many aspects which it could be a gigantic work simply to give a short review about its historical development. Piola surely consider atomistic models more fundamental, but we believe that he did not manage to arrive to a formulation close to modern statistical mechanics as he does not manage to conceive any kinetic concept leading to the concept of temperature and heat flux. Piola explicitly states that he develops mechanics with a postulation where Thermodynamics does not play any role. It is very important to remark that, in order to use computer aided simulations, leading to numerical prediction of considered phenomena, in general the literature one considers Euler-Lagrange equations (i.e. balance equations) as the most fundamental concepts to be postulated as basic principle. Then one multiplies by test functions (suitably regular) and after a painful integration by parts he is lead to get a variational principle for the continuous system which is considered. Finally one discretizes via a finite elements the obtained expression for internal and external work to compute, with a numerical integration scheme, the desired discrete approximation of the continuous field solution of the problem formulated with the continuous model.

This seems to be a vicious circle and therefore one may ask a question: is it really necessary to homogenize and then discretize again? Maybe it is much better to study the discrete system which we have at the beginning! It is possible, probably

sometimes easier, to make computations based on the discrete systems which one can postulate directly without any intermediate step. This is spirit which inspired, for instance, the papers [103–108]. Indeed they central idea of the numerical simulations presented there is simple: one does not model pantographic structures with a continuum (which is necessarily to be chosen in the class of second gradient continua). Actually such continuum is inspired by a homogenization process similar to the one due to Piola and Hencky: in order to get some meaningful numerical predictions a subsequent PE discretization is needed, which must involve suitably regular elements. On the contrary a discrete Lagrangian model is postulated since the very beginning and the numerical code needed to find the motion is adapted to use directly it.

In some sense the continual models using PDEs were widely applied since these models give some very useful tool for analytical analysis whereas discrete models require almost always numerical methods. So it was one of reasons to replace a lattice model with atoms and molecules by a continual counterpart. Nowadays, there are many developments in the theory of lattices considered as discrete systems, see e.g. [109–114].

It is remarkable how some conceptual tools initially introduced to meet the needs imposed by computing (here we consider, as examples, the partial differential equations obtained as Euler Lagrange stationarity conditions or also the Ptolemaic epicycles in the calculations needed to study, in Hellenistic époque, the mechanics of celestial bodies) may have changed their role in the process of formulating theories in different cultural paradigms.

Instead of representing a tool for getting the solution of engineering problems in a given milieux they could become the most fundamental concepts in the views of some schools.

This is what happened to PDEs: being essentially equivalent to balance equations in continuum mechanics they were regarded to supply the most fundamental conceptual tool in physics. Exactly as happened to the theory of epicycles and deferents: from being a computational tool they were transformed in middle ages as the most basic concepts in the study of celestial motion (the reader can find more details in [19, 115]).

5 Some Conclusions: History of Mechanics as a Tool in Finding Models for Fabrics, 3D Printed Prototypes and Various Complex Systems

Gabrio Piola has been an Italian scientist whose contributions have been generally neglected. However he has left a trace in mechanical and mathematical literature and his works were widely distributed in the main world libraries, although written in Italian (for instance in Vienna [116, 117] and at the University of Wisconsin, Google books could find many copies of his works). Hellinger was aware of some of

his contributions (see [9–11]) and Piola was cited also in [17]. For a more detailed discussion aimed to assess the true influence of Piola on subsequent research the reader is referred to [4] and also to [8].

Piola gives a visionary presentation of variational principles and tries to teach to his successors those methods that he believes are more suitable to invent new models. He writes in "*Intorno alle equazioni fondamentali del movimento di corpi qualsivogliono, considerati secondo la naturale loro forma e costituzione*." page 4, as translated in [118]:

> If it is well founded or not the statement that the Lagrangian methods are sufficient to the description of all mechanical phenomena, and are so powerful that they are suitable for all further possible researches, this is what shall be decided later, and before rebutting my point of view, it will be fair to leave me to expose all arguments which I have gathered to defend my point of view. I hope to clarify in the following Memoir that the only reason for which the Analytical Mechanics seemed to be insufficient in the solution of some problems, is that Lagrange, while writing the conditions for equilibrium and motion of a three dimensional body, did not detailed his model by assigning the equations relative to every material point belonging to it. If he had done this, and he could very well do it without departing from the methods imparted in his book, he would have obtained easily the same equations to which the French Geometers of our times arrived very painfully, [equations] which now are the foundation of new theories. However those results which he could not obtain, because death subtracted him to sciences before he could complete his great oeuvre, these results can be obtained by others: this is the assumption which led me to start some efforts since the years 1832 and 1835 (See the Memoir della Meccanica dei carpi naturalmente estesi inserted in the 1st Tome of Opuscoli matematici e fisici; Milano, Giusti, 1832: and the other Sulla nuova analisi per tutte le quistioni della Meccanica molecolare in the Tome XXI of these Proceedings).

Following, more or less consciously, the indication of Piola many generalized continuum or Lagrangian discrete models have been used by some successors of Lagrange:

(i) for modeling fabrics used to built reinforced composites (see e.g. [91, 93, 119–123]): the complexity at micro level of such systems very often imposes the formulation of generalized continuum models at macro level; however it must be remarked that, always using Lagrangian mechanics, such complex systems may be modeled directly by means of discrete models as done for instance in [103–108]. Hencky type models, generalizing the discrete description of Euler beams, can be very useful in formulating numerical codes suitable to predict the behavior of metamaterials and complex fabrics;

(ii) to develop more sophisticated description of deformation phenomena (see e.g. [2, 18, 26, 48, 53, 56, 57, 59, 61, 97, 124–127] and also the fundamental papers [6, 7, 24]): this effort has been, paradoxically, blocked by the undoubted success of the simpler Cauchy continuum models whose range of applicability is, however, rather limited in the considered instances;

(iii) to guide the invention of novel meta materials by using the technology of 3D printing (see e.g. [61, 91, 93, 102, 119, 123, 126, 128]): exotic behavior forecast for generalized continua can be transformed into real phenomena

occurring to objects whose internal architecture is so finely specified and whose microstructure is optimized for specific applications;

(iv) to obtain novel micro-macro identification results (see e.g. [3, 37, 50, 51, 53, 54, 58–60, 103–108, 121, 122, 129–131]): reduced order models are very useful to save computing time and to make possible the required predictions concerning the physical behavior of complex systems;

(v) to obtain interesting models of biomechanics phenomena (see e.g. [96, 132–135]): many different length scales appear in biomechanical systems and when modeling them the standard Cauchy continuum mechanics is very often not suitable to fully describe relevant phenomena.

Gabrio Piola describes in his first published work in 1825 a homogenization procedure allowing for the determination of a continuum model for a discrete systems constituted by a lattice of particles in the reference configuration. He also obtains an identification of macro parameters when micro geometrical and mechanical properties are known. Piola's homogenization procedure has been used often in the subsequent literature as it is very useful to model the behavior of complex systems.

However we are aware of Stigler's law of eponymy: therefore we do not give as granted that Piola was indeed the first scientist who did introduce the heuristic method of asymptotic homogenization which he describes in his works.

On the other hand there are some precise statements which can be assessed:

(i) many results by Piola seem to have been rediscovered also 150 years later,

(ii) Piola variational postulation of (continuum) mechanics is more encompassing than the postulation proposed by Cauchy, between 1822 and 1850),

(iii) Piola does not use tetrahedron argument, as he bases all his analysis on the principle of virtual work,

(iv) Piola prefers to start with discrete finite dimensional particle models of mechanical complex systems, and he uses the ideas and the concepts from continuum mechanics as a purely computational tool,

(v) Piola believes that all physical theories are to be based on variational principles.

In recent times many authors discussed about the need of considering large deformation measures in engineering applications. Many claimed that only linearized theories have a "utility" in engineering applications and that finite deformations "are not needed in the engineering practice". This point of view leads to miss the physical understanding of studied systems and is contradicted by the most modern technological demands. In the works by Piola all kinematical quantities are considered for large displacements and large deformations as the are the only concepts having a true physical meaning. Many scientists needed to recover this attitude in recent times. The temporary success of linearized models has actually blocked engineering sciences in the development of very interesting applications for many years.

The papers presented in this volume share the visionary point of view of Piola in many aspects and they seem to be continuing his conceptual efforts.

References

1. Auffray, N., dell'Isola, F., Eremeyev, V.A., Madeo, A., Rosi, G.: Analytical continuum mechanics à la Hamilton-Piola least action principle for second gradient continua and capillary fluids. Math. Mech. Solids **20**(4), 375–417 (2015)
2. Bertram, A., Glüge, R.: Gradient materials with internal constraints. Math. Mech. Complex Syst. **4**(1), 1–15 (2016)
3. Camar-Eddine, M., Seppecher, P.: Determination of the closure of the set of elasticity functionals. Arch. Ration. Mech. Anal. **170**(3), 211–245 (2003)
4. dell'Isola, F., Andreaus, U., Placidi, L.: At the origins and in the vanguard of peridynamics, non-local and higher-gradient continuum mechanics: an underestimated and still topical contribution of gabrio piola. Math. Mech. Solids **20**(8), 887–928 (2015)
5. Eringen, A.C., Kafadar, C.B.: Polar field theories. In: Eringen, A.C. (ed.) Continuum Physics. vol. IV, pp. 1–75. Academic Press, New York (1976)
6. Germain, P.: La méthode des puissances virtuelles en mécanique des milieux continus. première partie: théorie du second gradient. J. Mécanique **12**, 236–274 (1973)
7. Germain, P.: The method of virtual power in continuum mechanics. part 2: microstructure. SIAM J. Appl. Math. **25**(3), 556–575 (1973)
8. dell'Isola, F., Corte, A.D., Giorgio, I.: Higher-gradient continua: the legacy of Piola, Mindlin, Sedov and Toupin and some future research perspectives. Math. Mech. Solids **22**(4), 852–872 (2017)
9. Eugster, S.R., dell'Isola, F.: Exegesis of Sect. II and III. A from fundamentals of the mechanics of continua by Hellinger, E. ZAMM (2017). https://doi.org/10.1002/zamm.201600293
10. Eugster, S.R., dell'Isola, F. (2017) Exegesis of Sect. III. A from fundamentals of the mechanics of continua by E. Hellinger. ZAMM
11. Eugster, S.R., dell'Isola, F.: Exegesis of the Introduction and Sect. I from fundamentals of the mechanics of continua by Hellinger, E. ZAMM **97**(4), 477–506 (2017)
12. Maugin, G.A.: Generalized continuum mechanics: what do we mean by that? In: A MG, V MA (eds) Mechanics of Generalized Continua. One Hundred Years after the Cosserats, Springer, pp. 3–13 (2010)
13. Maugin, G.A.: A historical perspective of generalized continuum mechanics. In: Altenbach, H., Erofeev, V.I., Maugin, G.A. (eds.) Mechanics of Generalized Continua, pp. 3–19. From the Micromechanical Basics to Engineering Applications, Springer, Berlin (2011)
14. Maugin, G.A.: Generalized Continuum Mechanics: Various Paths, pp. 223–241. Springer, Dordrecht (2013)
15. Maugin, G.A.: Continuum mechanics through ages. From the Renaissance to the twentieth century, Springer, Cham (2016)
16. Maugin, G.A.: Non-Classical Continuum Mechanics: A Dictionary. Springer, Singapore (2017)
17. Truesdell, C., Noll, W.: The Non-linear Field Theories of Mechanics, 3rd edn. Springer, Berlin (2004)
18. dell'Isola, F., Seppecher, P., Madeo, A.: How contact interactions may depend on the shape of Cauchy cuts in Nth gradient continua: approach "à la D'Alembert". Zeitschrift für angewandte Mathematik und Physik **63**(6), 1119–1141 (2012)
19. dell'Isola, F., Della Corte, A., Esposito, R., Russo, L.: Some cases of unrecognized transmission of scientific knowledge: from antiquity to gabrio piolas peridynamics and generalized continuum theories. In: Generalized continua as models for classical and advanced materials, Springer, pp 77–128 (2016)
20. Kline, M.: Mathematical Thought From Ancient to Modern Times: Voll. 1,2,3, vol. 3. OUP USA (1990)
21. Kuhn, T.S.: The Structure of Scientific Revolutions, 3rd edn. University of Chicago Press (1996)
22. Sedov, L.I.: Mathematical methods for constructing new models of continuous media. Russian Math. Surv. **20**(5), 123 (1965)

23. Stillwell, J.: Exceptional objects. Am. Math. Month. **105**(9), 850–858 (1998)
24. Toupin, R.A.: Theories of elasticity with couple-stress. Arch. Ration. Mech. Anal. **17**(2), 85–112 (1964)
25. Turro, N.J.: Paradigms lost and paradigms found: Examples of science extraordinary and science pathological and how to tell the difference. Angewandte Chemie International Edition **39**(13), 2255–2259 (2000)
26. Cosserat, E., Cosserat, F.: Théorie des corps déformables. Herman et Fils, Paris (1909)
27. Mindlin, R.D.: Micro-structure in linear elasticity. Arch. Ration. Mech. Anal. **16**(1), 51–78 (1964)
28. Mindlin, R.D.: Second gradient of strain and surface-tension in linear elasticity. Int. J. Solids Struct. **1**(4), 417–438 (1965)
29. Mindlin, R.D., Eshel, N.N.: On first strain-gradient theories in linear elasticity. Int. J. Solids Struct. **4**(1), 109–124 (1968)
30. Mindlin, R.D., Tiersten, H.F.: Effects of couple-stresses in linear elasticity. Arch. Ration. Mech. Anal. **11**, 415–448 (1962)
31. Nowacki, W.: Theory of Asymmetric Elasticity. Pergamon-Press, Oxford (1986)
32. Toupin, R.A.: Elastic materials with couple-stresses. Arch. Ration. Mech. Anal. **11**(1), 385–414 (1962)
33. Eremeyev, V.A., Lebedev, L.P., Altenbach, H.: Foundations of Micropolar Mechanics. Springer, Heidelberg (2013)
34. Eringen, A.C.: Microcontinuum Field Theory. I. Foundations and Solids, Springer, New York (1999)
35. dell'Isola, F., Andreaus, U., Cazzani, A., Perego, U., Placidi, L., Ruta, G., Scerrato, D.: Di un principio controverso della meccanica analitica di lagrange e delle molteplici sue applicazioni. In: The complete works of Gabrio Piola: vol. 1 I, Springer, pp 371–590 (2014)
36. Bensoussan, A., Lions, J.L., Papanicolaou, G.: Asymptotic analysis for periodic structures, vol. 5. North-Holland, Amsterdam (1978)
37. Bakhvalov, N.S., Panasenko, G.: Homogenisation: Averaging Processes in Periodic Media: Mathematical Problems in the Mechanics of Composite Materials, Mathematical Problems in the Mechanics of Composite Materials, vol. 36. Kluwer, Dordrecht (1989)
38. Braides, A.: Gamma-convergence for Beginners, vol. 22. Clarendon Press (2002)
39. Braides, A.: A handbook of γ-convergence. North-Holland, Handbook of Differential Equations: Stationary Partial Differential Equations **3**, 101–213 (2006)
40. Braides, A., Defranceschi, A.: Homogenization of Multiple Integrals, vol. 12. Oxford University Press, Oxford (1998)
41. Braides, A., Truskinovsky, L.: Asymptotic expansions by γ-convergence. Continuum Mech. Thermodynam. **20**(1), 21–62 (2008)
42. Dal Maso, G.: An introduction to Γ-convergence, Progress in Nonlinear Differential Equations and Their Applications, vol. 8. Birkhauser, Basel (1993)
43. Hornung, U. (ed.): Homogenization and porous media, Interdisciplinary Applied Mathematics, vol. 6. Springer, New York (2012)
44. Jikov, V.V., Kozlov, S.M., Oleinik, O.A.: Homogenization of Differential Operators and Integral Functionals. Springer, Berlin (1994)
45. Kozlov, S.M.: Averaging of random operators. Matematicheskii. Sbornik **151**(2), 188–202 (1979)
46. Målqvist, A., Peterseim, D.: Localization of elliptic multiscale problems. Math. Comput. **83**(290), 2583–2603 (2014)
47. Oleinik, O.A., Shamaev, A.S., Yosifian, G.A.: Mathematical problems in elasticity and homogenization, Studies in Mathematics and its Applications, vol. 26. Elsevier, Amsterdam (1992)
48. Ostoja-Starzewski, M.: Microstructural randomness and scaling in mechanics of materials. Chapman and Hall/CRC Press, Boca Raton (2007)
49. Sanchez-Palencia, E.: Non-homogeneous Media and Vibration Theory. Lecture Notes in Physics, vol. 127. Springer, Berlin (2000)

50. Alibert, J.J., Della Corte, A.: Second-gradient continua as homogenized limit of pantographic microstructured plates: a rigorous proof. Zeitschrift für angewandte Mathematik und Physik **66**(5), 2855–2870 (2015)
51. Alibert, J.J., Seppecher, P., dell'Isola, F.: Truss modular beams with deformation energy depending on higher displacement gradients. Math. Mech. Solids **8**(1), 51–73 (2003)
52. Berlyand, L., Owhadi, H.: Flux norm approach to finite dimensional homogenization approximations with non-separated scales and high contrast. Arch. Ration. Mech. Anal. **198**(2), 677–721 (2010)
53. Camar-Eddine, M., Seppecher, P.: Non-local interactions resulting from the homogenization of a linear diffusive medium. Comptes Rendus de l'Académie des Sciences-Series I-Mathematics **332**(5), 485–490 (2001)
54. Camar-Eddine, M., Seppecher, P.: Closure of the set of diffusion functionals with respect to the mosco-convergence. Math. Models Methods Appl. Sci. **12**(08), 1153–1176 (2002)
55. Carcaterra, A., dell'Isola, F., Esposito, R., Pulvirenti, M.: Macroscopic description of microscopically strongly inhomogenous systems: A mathematical basis for the synthesis of higher gradients metamaterials. Arch. Ration. Mech. Anal. **218**(3), 1239–1262 (2015)
56. Challamel, N., Kocsis, A., Wang, C.: Higher-order gradient elasticity models applied to geometrically nonlinear discrete systems. Theor. Appl. Mech. **42**(4), 223–248 (2015)
57. Cordero, N.M., Forest, S., Busso, E.P.: Second strain gradient elasticity of nano-objects. J. Mech. Phys. Solids **97**, 92–124 (2016)
58. Javili, A., McBride, A., Mergheim, J., Steinmann, P., Schmidt, U.: Micro-to-macro transitions for continua with surface structure at the microscale. Int. J. Solids Struct. **50**(16), 2561–2572 (2013)
59. Misra, A., Poorsolhjouy, P.: Identification of higher-order elastic constants for grain assemblies based upon granular micromechanics. Math. Mech. Complex Syst. **3**(3), 285–308 (2015)
60. Pideri, C., Seppecher, P.: A second gradient material resulting from the homogenization of an heterogeneous linear elastic medium. Continuum Mech. Thermodynam. **9**(5), 241–257 (1997)
61. Trinh, D.K., Janicke, R., Auffray, N., Diebels, S., Forest, S.: Evaluation of generalized continuum substitution models for heterogeneous materials. Int. J. Multiscale Computat. Eng. **10**(6) (2012)
62. Naumenko, K., Eremeyev, V.A.: A layer-wise theory for laminated glass and photovoltaic panels. Comp. Struct. **112**, 283–291 (2014)
63. Naumenko, K., Eremeyev, V.A.: A layer-wise theory of shallow shells with thin soft core for laminated glass and photovoltaic applications. Comp. Struct. **178**, 434–446 (2017)
64. Besdo, D.: Towards a Cosserat-theory describing motion of an originally rectangular structure of blocks. Arch. Appl. Mech. **80**(1), 25–45 (2010)
65. Bigoni, D., Drugan, W.J.: Analytical derivation of Cosserat moduli via homogenization of heterogeneous elastic materials. Trans. ASME J. Appl. Mech. **74**(4), 741–753 (2007)
66. Dos Reis, F., Ganghoffer, J.: Construction of micropolar continua from the asymptotic homogenization of beam lattices. Comput. Struct. **112**, 354–363 (2012)
67. Ehlers, W., Ramm, E., Diebels, S., d'Addetta, G.D.A.: From particle ensembles to Cosserat continua: Homogenization of contact forces towards stresses and couple stresses. Int. J. Solids Struct. **40**(24), 6681–6702 (2003)
68. Goda, I., Ganghoffer, J.F.: Identification of couple-stress moduli of vertebral trabecular bone based on the 3d internal architectures. J. Mech. Behav. Biomed. Mater. **51**, 99–118 (2015)
69. Goda, I., Assidi, M., Belouettar, S., Ganghoffer, J.: A micropolar anisotropic constitutive model of cancellous bone from discrete homogenization. J. Mech. Behav. Biomed. Mater. **16**, 87–108 (2012)
70. Larsson, R., Diebels, S.: A second-order homogenization procedure for multi-scale analysis based on micropolar kinematics. Int. J. Numer. Methods Eng. **69**(12), 2485–2512 (2007)
71. Reda, H., Rahali, Y., Ganghoffer, J., Lakiss, H.: Wave propagation in 3D viscoelastic auxetic and textile materials by homogenized continuum micropolar models. Comp. Struct. **141**, 328–345 (2016)

72. Trovalusci, P., De Bellis, M.L., Ostoja-Starzewski, M., Murrali, A.: Particulate random composites homogenized as micropolar materials. Meccanica **49**(11), 2719–2727 (2014)
73. Trovalusci, P., Ostoja-Starzewski, M., De Bellis, M.L., Murrali, A.: Scale-dependent homogenization of random composites as micropolar continua. Eur. J. Mech. A/Solids **49**, 396–407 (2015)
74. Trovalusci, P., De Bellis, M.L., Masiani, R.: A multiscale description of particle composites: From lattice microstructures to micropolar continua. Comp. Part B Eng. **128**, 164–173 (2017)
75. Gurtin, M.E., Murdoch, A.I.: A continuum theory of elastic material surfaces. Arch. Ration. Mech. Anal. **57**(4), 291–323 (1975)
76. Gurtin, M.E., Murdoch, A.I.: Surface stress in solids. Int. J. Sol. Struct. **14**(6), 431–440 (1978)
77. Steigmann, D.J., Ogden, R.W.: Plane deformations of elastic solids with intrinsic boundary elasticity. Proc. Royal Soc. A **453**(1959), 853–877 (1997)
78. Steigmann, D.J., Ogden, R.W.: Elastic surface-substrate interactions. Proc. Royal Soc. A **455**(1982), 437–474 (1999)
79. Eremeyev, V.A.: On effective properties of materials at the nano-and microscales considering surface effects. Acta Mech. **227**(1), 29–42 (2016)
80. Esposito, R., Pulvirenti, M.: From particles to fluids. Handbook of mathematical fluid dynamics **3**, 1–82 (2004)
81. Pulvirenti, M.: Kinetic limits for stochastic particle systems. Lecture Notes in Mathematics pp. 96–126 (1996)
82. Saint-Raymond, L.: Hydrodynamic limits of the Boltzmann equation. 1971, Springer (2009)
83. Caprino, S., Esposito, R., Marra, R., Pulvirenti, M.: Hydrodynamic limits of the Vlasov equation. Commun. Partial Differ. Equat. **18**(5–6), 805–820 (1993)
84. Carinci, G., De Masi, A., Giardinà, C., Presutti, E.: Hydrodynamic limit in a particle system with topological interactions. Arab. J. Math. **3**(4), 381–417 (2014)
85. Carinci, G., De Masi, A., Giardinà, C., Presutti, E.: Super-hydrodynamic limit in interacting particle systems. J. Stat. Phys. **155**(5), 867–887 (2014)
86. De Masi, A., Olla, S.: Quasi-static hydrodynamic limits. J. Stat. Phys. **161**(5), 1037–1058 (2015)
87. De Masi, A., Merola, I., Presutti, E., Vignaud, Y.: Coexistence of ordered and disordered phases in Potts models in the continuum. J. Stat. Phys. **134**(2), 243–306 (2009)
88. De Masi, A., Luckhaus, S., Presutti, E.: Two scales hydrodynamic limit for a model of malignant tumor cells. Annales de l'Institut Henri Poincare (B) Probability and Statistics **43**(3):257–297 (2007)
89. De Masi, A., Galves, A., Löcherbach, E., Presutti, E.: Hydrodynamic limit for interacting neurons. J. Stat. Phys. **158**(4), 866–902 (2015)
90. Papanicolaou, G.C., Varadhan, S.S.: Boundary value problems with rapidly oscillating random coefficients. Seria Colloq Math Society Janos Bolyai **1**, 835–873 (1979)
91. Nadler, B., Papadopoulos, P., Steigmann, D.J.: Multiscale constitutive modeling and numerical simulation of fabric material. Int. J. Solids Struct. **43**(2), 206–221 (2006)
92. Steigmann, D.J.: Two-dimensional models for the combined bending and stretching of plates and shells based on three-dimensional linear elasticity. Int. J. Eng. Sci. **46**(7), 654–676 (2008)
93. Steigmann, D.J., dell'Isola, F.: Mechanical response of fabric sheets to three-dimensional bending, twisting, and stretching. Acta Mechanica Sinica **31**(3), 373–382 (2015)
94. Giorgio, I.: Numerical identification procedure between a micro-Cauchy model and a macro-second gradient model for planar pantographic structures. Zeitschrift für angewandte Mathematik und Physik **67**(4), 95 (2016)
95. Saeb S, Steinmann P, Javili A (2016) Aspects of computational homogenization at finite deformations: A unifying review from reuss' to voigt's bound. Appl. Mech. Rev. **68**(5):050,801
96. Bevill, G., Eswaran, S.K., Gupta, A., Papadopoulos, P., Keaveny, T.M.: Influence of bone volume fraction and architecture on computed large-deformation failure mechanisms in human trabecular bone. Bone **39**(6), 1218–1225 (2006)
97. Ganghoffer, J.F.: Spatial and material stress tensors in continuum mechanics of growing solid bodies. Math. Mech. Comp. Syst. **3**(4), 341–363 (2016)

98. Berdichevsky, V.: Variational Principles of Continuum Mechanics: I. Fundamentals, Springer, Heidelberg (2009)
99. Hamilton, W.R.: On a general method in dynamics; by which the study of the motions of all free systems of attracting or repelling points is reduced to the search and differentiation of one central relation, or characteristic function. Philos. Trans. Royal Soc. London **124**, 247–308 (1834)
100. Stigler, S.M.: Stigler's law of eponymy. Transactions of the New York Academy of Sciences **39** (1 Series II):147–157 (1980)
101. Benvenuto, E.: La scienza delle costruzioni e il suo sviluppo storico. Sansoni, Firenze (1981)
102. dell'Isola, F., Giorgio, I., Pawlikowski, M., Rizzi, N.: Large deformations of planar extensible beams and pantographic lattices: Heuristic homogenisation, experimental and numerical examples of equilibrium. Proc. Royal Soc. London Ser A **472**(2185): 20150, 790 (2016)
103. Turco, E., Rizzi, N.L.: Pantographic structures presenting statistically distributed defects: numerical investigations of the effects on deformation fields. Mech. Res. Commun. **77**, 65–69 (2016)
104. Turco, E., Barcz, K., Pawlikowski, M., Rizzi, N.L.: Non-standard coupled extensional and bending bias tests for planar pantographic lattices. part i: numerical simulations. Zeitschrift für angewandte Mathematik und Physik **67**(5), 122 (2016)
105. Turco, E., Barcz, K., Pawlikowski, M., Rizzi, N.L.: Non-standard coupled extensional and bending bias tests for planar pantographic lattices. part i: numerical simulations. Zeitschrift für angewandte Mathematik und Physik **67**(5), 122 (2016)
106. Turco, E., dell'Isola, F., Rizzi, N.L., Grygoruk, R., Müller, W.H., Liebold, C.: Fiber rupture in sheared planar pantographic sheets: Numerical and experimental evidence. Mech. Res. Commun. **76**, 86–90 (2016)
107. Turco, E., Golaszewski, M., Cazzani, A., Rizzi, N.L.: Large deformations induced in planar pantographic sheets by loads applied on fibers: experimental validation of a discrete lagrangian model. Mech. Res. Commun. **76**, 51–56 (2016)
108. Turco, E., Golaszewski, M., Giorgio, I., D'Annibale, F.: Pantographic lattices with non-orthogonal fibres: Experiments and their numerical simulations. Comp. Part B Eng. **118**, 1–14 (2017)
109. Born, M., Huang, K.: Dynamical Theory of Crystal Lattices. Clarendon Press, Oxford, International series of monographs on physics (1954)
110. Ostoja-Starzewski, M.: Lattice models in micromechanics. Appl. Mech. Rev. **55**(1), 35–60 (2002)
111. Porubov, A.: Modeling of strongly nonlinear effects in diatomic lattices. Arch. Appl. Mech. **84**(9–11), 1533–1538 (2014)
112. Porubov, A., Andrianov, I.: Nonlinear waves in diatomic crystals. Wave Motion **50**(7), 1153–1160 (2013)
113. Porubov, A., Antonov, I., Fradkov, A., Andrievsky, B.: Control of localized non-linear strain waves in complex crystalline lattices. Int. J. Non-Lin. Mech. **86**, 174–184 (2016)
114. Porubov, A.V., Aero, E.L., Maugin, G.A.: Two approaches to study essentially nonlinear and dispersive properties of the internal structure of materials. Phys. Rev. E **79**(4):046,608 (2009)
115. Russo, L.: The forgotten revolution: how science was born in 300 BC and why it had to be reborn. Springer Science & Business Media (2013)
116. Piola, D.G.: Sulla teorica dei cannocchiali. Memoria inserita nelle Effemeridi. Dall'Imp, Regia Stamperia, Milano (1821)
117. Piola, D.G.: Veglie di un filosofo. In: Soliani, E. (ed.) Memorie di religione, di morale e di letteratura. Tipografi Reale, Modena (1823)
118. dell'Isola, F., Maier, G., Perego, U., Andreaus, U., Esposito, R., Forest, S.: (eds) The complete works of Gabrio Piola: vol. I. Springer (2014)
119. Boutin, C., dell'Isola, F., Giorgio, I., Placidi, L.: Linear pantographic sheets: asymptotic micro-macro models identification. Math. Mech. Complex Syst. **5**(2), 127–162 (2017)
120. Gatouillat, S., Bareggi, A., Vidal-Sallé, E., Boisse, P.: Meso modelling for composite preform shaping-simulation of the loss of cohesion of the woven fibre network. Comp. Part A Appl. Sci. Manufact. **54**, 135–144 (2013)

121. Harrison, P.: Modelling the forming mechanics of engineering fabrics using a mutually constrained pantographic beam and membrane mesh. Comp. Part A Appl. Sci. Manufact. **81**, 145–157 (2016)
122. Harrison, P., Alvarez, M.F., Anderson, D.: Towards comprehensive characterisation and modelling of the forming and wrinkling mechanics of engineering fabrics. Int. J. Solids Struct. (2017)
123. Placidi, L., Barchiesi, E., Turco, E., Rizzi, N.L.: A review on 2d models for the description of pantographic fabrics. Zeitschrift für angewandte Mathematik und Physik **67**(5), 121 (2016)
124. Abali, B.E., Müller, W.H., Georgievskii, D.V.: A discrete-mechanical approach for computation of three-dimensional flows. ZAMM **93**(12), 868–881 (2013)
125. Battista, A., Cardillo, C., Del Vescovo, D., Rizzi, N.L., Turco, E.: Frequency shifts induced by large deformations in planar pantographic continua. Nanomech. Sci.Technol. Int. J. **6**(2), (2015)
126. Del Vescovo, D., Giorgio, I.: Dynamic problems for metamaterials: review of existing models and ideas for further research. Int. J. Eng. Sci. **80**, 153–172 (2014)
127. Lejeune, E., Javili, A., Linder, C.: An algorithmic approach to multi-layer wrinkling. Extreme Mech. Lett. **7**, 10–17 (2016)
128. Placidi, L., Greco, L., Bucci, S., Turco, E., Rizzi, N.L.: A second gradient formulation for a 2d fabric sheet with inextensible fibres. Zeitschrift für angewandte Mathematik und Physik **67**(5), 114 (2016)
129. Pideri C, Seppecher P (2006) Asymptotics of a non-planar rod in non-linear elasticity. Asymp. Anal. **48**(1, 2):33–54
130. Placidi, L., Andreaus, U., Della Corte, A., Lekszycki, T.: Gedanken experiments for the determination of two-dimensional linear second gradient elasticity coefficients. Zeitschrift für angewandte Mathematik und Physik **66**(6), 3699–3725 (2015)
131. Placidi, L., Andreaus, U., Giorgio, I.: Identification of two-dimensional pantographic structure via a linear d4 orthotropic second gradient elastic model. J. Eng. Math. **103**(1), 1–21 (2017)
132. Andreaus, U., Giorgio, I., Lekszycki, T.: A 2-d continuum model of a mixture of bone tissue and bio-resorbable material for simulating mass density redistribution under load slowly variable in time. ZAMM J. Appl. Mathematics and Mechanics/Zeitschrift für Angewandte Mathematik und Mechanik **94**(12), 978–1000 (2014)
133. Giorgio, I., Andreaus, U., Scerrato, D., dell'Isola, F.: A visco-poroelastic model of functional adaptation in bones reconstructed with bio-resorbable materials. Biomech. Model. Mechanobiol. **15**(5), 1325–1343 (2016)
134. Giorgio, I., Andreaus, U., Lekszycki, T., Corte, A.D.: The influence of different geometries of matrix/scaffold on the remodeling process of a bone and bioresorbable material mixture with voids. Math. Mech. Solids **22**(5), 969–987 (2017)
135. Giorgio, I., Andreaus, U., Scerrato, D., Braidotti, P.: Modeling of a non-local stimulus for bone remodeling process under cyclic load: Application to a dental implant using a bioresorbable porous material. Math. Mech. Solids **22**(9), 1790–1805 (2017)

Exact Analytical Solutions for Nonautonomic Nonlinear Klein-Fock-Gordon Equation

Eron L. Aero, A. N. Bulygin and Yu. V. Pavlov

Abstract We develop methods of construction of functionally invariant solutions $U(x, y, z, t)$ for the nonlinear nonautonomic Klein-Fock-Gordon equation. The solutions $U(x, y, z, t)$ are found in the form of an arbitrary function, which depends on one, $\tau(x, y, z, t)$, or two, $\alpha(x, y, z, t)$, $\beta(x, y, z, t)$ specially constructed functions. The functions are called ansatzes. The ansatzes (τ, α, β) are defined as solutions of the special equations (algebraic or mixed type—algebraic and partial differential equations). The equations for defining of the ansatzes contain arbitrary functions, depending on (τ, α, β). The offered methods allow to find the solution $U(x, y, z, t)$ for particular, but wide class of the nonautonomic nonlinear Klein-Fock-Gordon equations. The methods are illustrated by examples of finding exact analytical solutions of the nonautonomic Liouville equation.

1 Introduction

The nonlinear Klein-Fock-Gordon (NKFG) equation

$$U_{xx} + U_{yy} + U_{zz} - \frac{U_{tt}}{v^2} = F(U) \tag{1}$$

appears in many fields of modern natural sciences. Here $F(U)$ is arbitrary function, and the subscripts mean derivatives with respect to the corresponding variables.

Equation (1) is widely applied in fundamental and applied physics, mechanics, biology, chemistry and other fields of science, when the right hand part is a part of

Eron L. Aero—Deceased.

E. L. Aero · A. N. Bulygin (✉) · Yu. V. Pavlov
Institute for Problems in Mechanical Engineering of Russian Academy of Sciences, 61 Bol'shoy, V.O., Saint Petersburg 199178, Russia
e-mail: bulygin_an@mail.ru

Yu. V. Pavlov
e-mail: yuri.pavlov@mail.ru

F. dell'Isola et al. (eds.), *Advances in Mechanics of Microstructured Media and Structures*, Advanced Structured Materials 87,
https://doi.org/10.1007/978-3-319-73694-5_2

the exponential ($\exp nU$) hyperbolic ($\sinh nU$, $\cosh nU$), Fourier ($\sin nU$, $\cos nU$), or Taylor (U^n, $n = 1, 2, \ldots,$) series. These equations describe the different physical phenomena and model various technological processes. In case of nonhomogeneous external media or external fields the corresponding equation is the nonlinear nonautonomic Klein-Fock-Gordon equation

$$U_{xx} + U_{yy} + U_{zz} - \frac{U_{tt}}{v^2} = p(x, y, z, t)\, F(U), \tag{2}$$

where $p(x, y, z, t)$ is some function.

In literature there are practically no methods of obtaining exact analytical solutions for the nonautonomic NKFG equation. Our methods basing on construction of the functionally invariant solutions of the partial differential equations are offered below.

2 Methods of Construction of Exact Analytical Solutions for Nonautonomic NKFG Equation

The solution W of the differential equation is called functionally invariant if the complex function of $U = f(W)$ is also the solution for arbitrary function f. The function W is called ansatz. For the first time, the idea about existence of the functionally invariant solutions were suggested by Jacobi [1]. A. Forsyth has found the functionally invariant solutions of the Laplace equation, the wave equation and the Helmholtz equation [2]. The idea of C. Jacobi has been fundamentally developed by H. Bateman in relation to the theory of propagation of electromagnetic waves [3]. S.L. Sobolev and V.I. Smirnov have successfully applied method of construction of the functionally invariant solutions for the problems of diffraction and distribution of sound in homogeneous and layered media [4–6]. N.P. Erugin has made a big contribution to development of the theory [7]. Functionally invariant solutions of the autonomic NKFG and sine-Gordon equations are found by the authors in Ref. [8–12].

We will seek the solution of Eq. (2) in the form $U = f(W)$. Then Eq. (2) takes the form

$$f''\left[W_x^2 + W_y^2 + W_z^2 - \frac{W_t^2}{v^2}\right] + f'\left[W_{xx} + W_{yy} + W_{zz} - \frac{W_{tt}}{v^2}\right] = p(x, y, z, t)\, F[f(W)]. \tag{3}$$

Here and further the prime denotes derivative with respect to the argument. It is possible to make two obvious statements from Eq. (3).

Proposition 1 *If function W satisfies the equations*

$$W_x^2 + W_y^2 + W_z^2 - \frac{W_t^2}{v^2} = 0, \tag{4}$$

$$W_{xx} + W_{yy} + W_{zz} - \frac{W_{tt}}{v^2} = p(x, y, z, t), \tag{5}$$

then the solution of Eq. (2) is given by the inversion of the integral

$$\int \frac{df}{F(f)} = W(x, y, z, t). \tag{6}$$

Proposition 2 *If function W satisfies the equations*

$$W_x^2 + W_y^2 + W_z^2 - \frac{W_t^2}{v^2} = p(x, y, z, t), \tag{7}$$

$$W_{xx} + W_{yy} + W_{zz} - \frac{W_{tt}}{v^2} = 0, \tag{8}$$

then the solution of Eq. (2) is given by the inversion of the integral

$$\int \frac{df}{\sqrt{E + V(f)}} = \pm\sqrt{2}\, W(x, y, z, t). \tag{9}$$

Here $F(U) = V'(U)$, and E is a constant of integration.

So, the problem of solution of the nonautonomic Eq. (2) is reduced to finding of the function W, which satisfies Eqs. (4), (5) or (7), (8). This problem can be solved by the methods of construction of functionally invariant solutions of the partial differential equations. We will consider further that the solution of Eq. (2) is constructed if the function W satisfying to Eqs. (4), (5) or (7), (8) is found.

1st method. We will seek the solution of Eqs. (4), (5) in a form

$$W = \varphi(\tau). \tag{10}$$

Here $\varphi(\tau)$ is an arbitrary function of τ, and $\tau(x, y, z, t)$ is a root of the algebraic equation,

$$x\,\xi(\tau) + y\,\eta(\tau) + z\,\zeta(\tau) - v^2 t\tau = \frac{s^2 + q^2}{2}, \tag{11}$$

$$s^2 = x^2 + y^2 + z^2 - v^2 t^2, \tag{12}$$

$$q^2 = \xi^2(\tau) + \eta^2(\tau) + \zeta^2(\tau) - v^2\tau^2, \tag{13}$$

and $\xi(\tau), \eta(\tau), \zeta(\tau)$ are the arbitrary functions of τ.

Equation (11) defines implicit dependence τ on time and space coordinates. We calculate partial derivatives of τ of the first and second orders by the rules of differentiation of implicit functions and see that τ satisfies the equations

$$\tau_x^2 + \tau_y^2 + \tau_z^2 - \frac{\tau_t^2}{v^2} = 0, \tag{14}$$

$$\tau_{xx} + \tau_{yy} + \tau_{zz} - \frac{\tau_{tt}}{v^2} = \frac{2}{\nu}, \tag{15}$$

$$\nu = \xi_\tau(x - \xi) + \eta_\tau(y - \eta) + \zeta_\tau(z - \zeta) - v^2(t - \tau). \tag{16}$$

For Eqs. (14), (15) the expressions

$$\xi_\tau \tau_x + \eta_\tau \tau_y + \zeta_\tau \tau_z + \tau_t = 1, \tag{17}$$

$$\nu_x \tau_x + \nu_y \tau_y + \nu_z \tau_z - \frac{\nu_t \tau_t}{v^2} = 1 \tag{18}$$

are take into account.

On the base of Proposition 1 and Eqs. (14), (15) we get, that Eq. (10) is a solution of Eq. (2), if the function $f(W)$ is found from Eq. (6) and

$$p(x, y, z, t) = \frac{2}{\nu}\varphi_\tau. \tag{19}$$

It should be noted that, despite of simplicity of analytical dependence (19), the solution of the nonautonomic NKGF equation is rather general. First, $\varphi(\tau)$ is arbitrary function of τ, and, besides, ansatz τ is found from Eq. (11) which contains three arbitrary functions $\xi(\tau)$, $\eta(\tau)$, $\zeta(\tau)$.

We will seek the function W in the form

$$W = \Psi(\nu, \tau). \tag{20}$$

For this ansatz Eqs. (7), (8) are

$$W_x^2 + W_y^2 + W_z^2 - \frac{W_t^2}{v^2} = \Psi_\nu^2(2\sigma - q^2) + 2\Psi_\nu \Psi_\tau + \Psi_\tau \frac{2}{\nu}, \tag{21}$$

$$W_{xx} + W_{yy} + W_{zz} - \frac{W_{tt}}{v^2} = \frac{1}{\nu}(2\sigma - q_1^2)(\nu\Psi_\nu + \Psi)_\nu + \frac{2}{\nu}\Psi_\nu(\nu\Psi_\nu + \Psi). \tag{22}$$

Here

$$\sigma = \xi_{\tau\tau}(x - \xi) + \eta_{\tau\tau}(y - \eta) + \zeta_{\tau\tau}(z - \zeta), \tag{23}$$

$$q_1^2 = \xi_\tau^2 + \eta_\tau^2 + \zeta_\tau^2 - v^2. \tag{24}$$

At definition of Eqs. (21), (22) it is necessary to take into account (17), (18) and the equations for the function $\nu(x, y, z, t)$:

$$v_x^2 + v_y^2 + v_z^2 - \frac{v_t^2}{v^2} = 2\sigma - q_1^2, \tag{25}$$

$$v_{xx} + v_{yy} + v_{zz} - \frac{v_{tt}}{v^2} = \frac{2}{v}(2\sigma - q_1^2). \tag{26}$$

From Eq. (22) one can see, that $\Psi(v, \tau)$ will be solution of Eq. (8), i.e. the wave function, if

$$v\Psi_v + \Psi = 0, \quad \Psi(v, \tau) = \frac{\varphi(\tau)}{v}. \tag{27}$$

For this solution one has

$$W_x^2 + W_y^2 + W_z^2 - \frac{W_t^2}{v^2} = \frac{\varphi^2}{v^4}\left[2\sigma - q_1^2 - 2v\frac{\varphi_\tau}{\varphi}\right]. \tag{28}$$

On the base of Proposition 2 we come to conclusion that the ansatz W, defined by Eqs. (20), (27) is a solution of Eq. (2), if

$$p(x, y, z, t) = \frac{\varphi^2}{v^4}\left[2\sigma - q_1^2 - 2v\frac{\varphi_\tau}{\varphi}\right]. \tag{29}$$

2nd method. The ansatz τ, which is found from Eq. (11), depends on time and spatial coordinates. Set of analytical expressions for the ansatz τ can be expanded under assumption that τ in addition to space coordinates and time depends on some parameters (α, β). Naturally, the new equations are necessary in this case. Let's the equations for $\tau = \tau(x, y, z, t, \alpha, \beta)$ are

$$x\xi(\alpha, \beta, \tau) + y\eta(\alpha, \beta, \tau) + z\zeta(\alpha, \beta, \tau) - v^2 t\theta(\alpha, \beta, \tau) = \frac{s^2 + q_2^2}{2}, \tag{30}$$

$$x\xi_\alpha + y\eta_\alpha + z\zeta_\alpha - v^2 t\theta_\alpha = \frac{1}{2}\left(q_2^2\right)_\alpha, \tag{31}$$

$$x\xi_\beta + y\eta_\beta + z\zeta_\beta - v^2 t\theta_\beta = \frac{1}{2}\left(q_2^2\right)_\beta, \tag{32}$$

$$q_2^2 = \xi^2 + \eta^2 + \zeta^2 - v^2\theta^2. \tag{33}$$

Equation (30) is algebraic. It as well as Eq. (11) linearly depends on time and space coordinates, but now the coefficients ξ, η, ζ, θ are the functions not only of τ, but also of three arguments (τ, α, β). Equations (31), (32) are partial differential equations of the first order. From Eqs. (30)–(32) one can calculate the first and second order derivatives of τ with respect to time and space coordinates. These calculations allow us to prove that τ satisfies the equations

$$\tau_x^2 + \tau_y^2 + \tau_z^2 - \frac{\tau_t^2}{v^2} = 0, \tag{34}$$

$$\tau_{xx} + \tau_{yy} + \tau_{zz} - \frac{\tau_{tt}}{v^2} = p(x, y, z, t), \tag{35}$$

$$p(x, y, z, t) = \frac{1}{v}\left[3 - (\xi_x + \eta_y + \zeta_z + \theta_t)\right]. \tag{36}$$

On the basis of Eqs. (34), (35) and Proposition 1 it is possible to construct solutions of nonautonomic NKFG equation if ansatz τ is defined by Eqs. (30)–(33), and function $p(x, y, z, t)$ is given by Eq. (36).

3rd method. We will determine ansatz $\alpha(x, y, z, t)$ as a root of the algebraic equation

$$x\, l(\alpha) + y\, m(\alpha) + z\, n(\alpha) - v^2 t\, w(\alpha) + q(\alpha) = 0. \tag{37}$$

Here $l(\alpha)$, $m(\alpha)$, $n(\alpha)$, $w(\alpha)$, $q(\alpha)$ are arbitrary functions of α. Solution of Eqs. (4), (5), (7), (8) we will seek in the form

$$W = f(\alpha, \beta). \tag{38}$$

By definition

$$\beta = x\, l_\alpha + y\, m_\alpha + z\, n_\alpha - v^2 t\, w_\alpha + q_\alpha, \tag{39}$$

and $f(\alpha, \beta)$ is an arbitrary function of α, β.

From Eqs. (37), (39) it is possible to calculate the first and second order partial derivatives of $\alpha(x, y, z, t)$ and $\beta(x, y, z, t)$ with respect to space coordinates and time and to obtain that W satisfies the following equations

$$W_x^2 + W_y^2 + W_z^2 - \frac{W_t^2}{v^2} = f_\beta(l_\alpha^2 + m_\alpha^2 + n_\alpha^2 - v^2 w_\alpha^2), \tag{40}$$

$$W_{xx} + W_{yy} + W_{zz} - \frac{W_{tt}}{v^2} = \left(f_{\beta\beta} + \frac{2f_\beta}{\beta}\right)(l_\alpha^2 + m_\alpha^2 + n_\alpha^2 - v^2 w_\alpha^2). \tag{41}$$

Final form of Eqs. (40), (41) will be obtained if we impose the condition on $l(\alpha)$, $m(\alpha)$, $n(\alpha)$, $w(\alpha)$

$$l^2 + m^2 + n^2 = v^2 w^2 \tag{42}$$

and takes into account that

$$l\, l_{\alpha\alpha} + m\, m_{\alpha\alpha} + n\, n_{\alpha\alpha} - v^2 w\, w_{\alpha\alpha} = -(l_\alpha^2 + m_\alpha^2 + n_\alpha^2 - v^2 w_\alpha^2). \tag{43}$$

Let $f(\alpha, \beta)$ is a solution of equation

$$f_{\beta\beta} + \frac{2f_\beta}{\beta} = 0. \tag{44}$$

Then

$$f(\alpha, \beta) = A(\alpha) + \frac{B(\alpha)}{\beta}, \tag{45}$$

where $A(\alpha)$, $B(\alpha)$ are arbitrary functions of α. From Eqs. (40), (41) it follows that W will satisfy Eqs. (7), (8) and

$$p(x, y, z, t) = f_\beta^2(l_\alpha^2 + m_\alpha^2 + n_\alpha^2 - v^2 w_\alpha^2). \tag{46}$$

Using ansatz $\alpha(x, y, z, t)$ it is possible to find other solutions of Eqs. (40), (41). Let's construct the function

$$W = xL(\alpha) + yM(\alpha) + zN(\alpha) - v^2 tV(\alpha) + Q(\alpha), \tag{47}$$

where $L(\alpha)$, $M(\alpha)$, $N(\alpha)$, $V(\alpha)$, $Q(\alpha)$ are arbitrary functions of α, connecting with the functions $l(\alpha)$, $m(\alpha)$, $n(\alpha)$, $w(\alpha)$, $q(\alpha)$ by the simple relationships

$$L_\alpha = l, \quad M_\alpha = m, \quad N_\alpha = n, \quad V_\alpha = w, \quad Q_\alpha = q. \tag{48}$$

The function W, defined by Eq. (47), satisfies

$$W_x^2 + W_y^2 + W_z^2 - \frac{W_t^2}{v^2} = L^2 + M^2 + N^2 - v^2 V^2, \tag{49}$$

$$W_{xx} + W_{yy} + W_{zz} - \frac{W_{tt}}{v^2} = -\frac{1}{\beta}\left(l^2 + m^2 + n^2 - v^2 w^2\right). \tag{50}$$

If the functions L, M, N, V are connected by the expression,

$$L^2 + M^2 + N^2 = v^2 V^2, \tag{51}$$

then W will be solution of Eqs. (4), (5) and

$$p(x, y, z, t) = -\frac{1}{\beta}\left(l^2 + m^2 + n^2 - v^2 w^2\right). \tag{52}$$

In the case (42) the function W will satisfy Eqs. (7), (8), and

$$p(x, y, z, t) = L^2 + M^2 + N^2 - v^2 V^2. \tag{53}$$

The offered method of obtaining the function W allows to find large number of particular solutions of the nonautonomic NKFG equation by the choice of arbitrary functions $l(\alpha)$, $m(\alpha)$, $n(\alpha)$, $w(\alpha)$, $q(\alpha)$.

3 Exact Analytical Solutions for the Nonautonomic Liouville Equation

The offered methods for solution of the NKFG equation are applicable for finding of exact analytical solutions of the nonautonomic Liouville wave equation

$$U_{xx} + U_{yy} + U_{zz} - \frac{U_{tt}}{v^2} = p(x, y, z, t)\, e^U. \tag{54}$$

For illustration of the general methods we will obtain simple particular solutions.

In accordance with Eq. (6), the function

$$U = \ln \frac{1}{C - W}, \tag{55}$$

is a solution of Eq. (54), if the function $W(x, y, z, t)$ satisfies Eqs. (4), (5). If $W(x, y, z, t)$ satisfies Eqs. (7), (8), then, on the base of Eq. (9),

$$U = -2 \ln \sinh \frac{W + C}{\sqrt{2}} \tag{56}$$

is solution of (54). Here C is a constant of integration. Function $W(x, y, z, t)$ as it is stated above, can be constructed by different ways. Method **1** results in the solution $W(x, y, z, t)$ of Eq. (54) in the form of arbitrary function of the ansatz $\tau(x, y, z, t)$ and the last is a root of algebraic equation (11). To receive particular solutions, it is necessary to determine the arbitrary functions $\xi(\tau)$, $\eta(\tau)$, $\zeta(\tau)$. Let's

$$\xi = 0, \quad \eta = 0, \quad \zeta = 0, \tag{57}$$

then

$$\tau = t \pm \frac{R}{v}, \quad R = \sqrt{x^2 + y^2 + z^2}, \tag{58}$$

$$p(x, y, z, t) = \frac{2}{v} W_\tau, \quad v = \pm vR. \tag{59}$$

Thus Eq. (55) gives a solution of Liouville equation (54) in the case (57), when W is an arbitrary function of τ and $\tau(x, y, z, t)$, $p(x, y, z, t)$ are defined by Eqs. (58), (59).

Let's

$$\xi = a_1 v\tau, \ \eta = a_2 v\tau, \ \zeta = a_3 v\tau, \ a_1^2 + a_2^2 + a_3^2 = 1. \tag{60}$$

Then Eq. (55) gives a solution of Eq. (54) if

$$\tau = \frac{s^2}{2\nu}, \quad s^2 = x^2 + y^2 + z^2 - v^2 t^2, \tag{61}$$

$$p(x, y, z, t) = \frac{2}{\nu} W_\tau, \quad \nu = v(a_1 x + a_2 y + a_3 z - vt), \tag{62}$$

and W is an arbitrary function of τ, as in the case (57).

The second method for construction of exact analytical solutions of Eq. (54) is reduced in essence to finding of ansatz $\tau(x, y, z, t, \alpha, \beta)$ from Eqs. (30)–(32). These equations include four arbitrary functions $\xi(x, y, z, t, \alpha, \beta)$, $\eta(x, y, z, t, \alpha, \beta)$, $\zeta(x, y, z, t, \alpha, \beta)$ and $\theta(x, y, z, t, \alpha, \beta)$. Here we give examples of particular solutions for the cases when the functions $(\xi, \eta, \zeta, \theta)$ have rather simple analytical form. They are given by the formula (55), in which W is an arbitrary function of ansatz τ and the functions τ, $p(x, y, z, t)$ is determined by specific form of the functions $(\xi, \eta, \zeta, \theta)$.

1. $\xi = v\tau \cos\alpha \cos\beta, \quad \eta = v\tau \cos\alpha \sin\beta, \quad \zeta = v\tau \sin\alpha, \quad \theta = \tau,$

$$\tau = t \pm \frac{R}{v}, \quad p(x, y, z, t) = \pm \frac{2}{vR} W_\tau,$$

2. $\xi = v\tau \cos\alpha, \quad \eta = v\tau \sin\alpha, \quad \zeta = 0, \quad \theta = \tau,$

$$\tau = \frac{s^2}{\sqrt{x^2 + y^2} - vt}, \quad p(x, y, z, t) = \frac{4 - \frac{\tau}{\sqrt{x^2+y^2}}}{\sqrt{x^2 + y^2} - vt} W_\tau,$$

3. $\xi = \tau \cos\alpha, \quad \eta = \tau \sin\alpha, \quad \zeta = \tau \sinh\beta, \quad \theta = \frac{\tau}{v} \cosh\beta,$

$$\tau = \sqrt{x^2 + y^2} - \sqrt{v^2 t^2 - z^2}, \quad p(x, y, z, t) = \left[\frac{1}{\sqrt{x^2 + y^2}} + \frac{1}{\sqrt{v^2 t^2 - z^2}} \right] W_\tau,$$

4. $\xi = \tau \cos\alpha \sinh\beta, \quad \eta = \tau \sin\alpha \sinh\beta, \quad \zeta = \tau, \quad \theta = \frac{\tau}{v} \cosh\beta,$

$$\tau = z + \sqrt{v^2 t^2 - x^2 - y^2}, \quad p(x, y, z, t) = -\frac{2}{\sqrt{v^2 t^2 - x^2 - y^2}} W_\tau.$$

The spatial images of solution **2** are shown on Fig. 1 for the case $W(\tau) = \sin\tau$.

Thus, if the functions of $(\xi, \nu, \zeta, \theta)$ are given, then integration of Eq. (54) is actually reduced to finding the functions (τ, α, β) from the system of three equations (30)–(32). The last problem is more simple, than integration of Eq. (54).

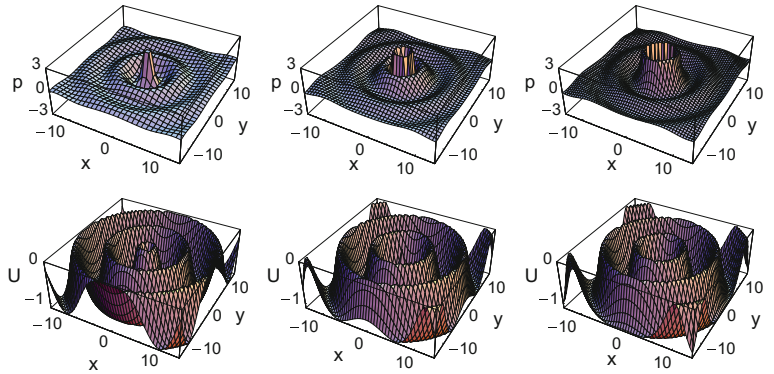

Fig. 1 The functions p and U for solution **2**, for $z = 0$, $t = 0$ (at the left), $t = 2$ (in the centre) and $t = 3$ (at the right)

In the 3-rd method of the solution of Eq. (54) it is necessary to determine the functions $l(\alpha)$, $m(\alpha)$, $n(\alpha)$, $w(\alpha)$, $q(\alpha)$ and then to find the ansatz α from Eq. (37). One can find the functions W and p with using the expression for α by two ways:

(a) by Eqs. (38), (39), (45) and (46),
(b) by Eqs. (47), (53).

The simple examples are given below.

$$(\mathbf{1}) \quad l = \alpha, \quad n = -\sqrt{2}, \quad vw = \alpha + \frac{1}{\alpha}, \quad q = 0,$$

$$\alpha = \frac{z \pm R_1}{\sqrt{2}(x - vt)}, \quad R_1 = \sqrt{z^2 - 2(x - vt)(y - vt)},$$

$$(a) \quad \beta = \pm\frac{\sqrt{2}R_1}{\alpha}, \quad p = \frac{B^2(\alpha)}{\beta^2 R_1^2}.$$

$$(b) \quad W = (x - vt)\frac{\alpha^2}{2} + (y - vt)\ln\alpha - z\sqrt{2}\alpha, \quad p = \alpha^2(2 - \ln\alpha).$$

$$(\mathbf{2}) \quad l = \frac{1}{\cosh\alpha}, \quad m = \tanh\alpha, \quad n = q = 0, \quad vw = 1,$$

$$\alpha = \ln\frac{x \pm R_2}{\sqrt{2}(vt - y)}, \quad R_2 = \sqrt{x^2 + y^2 - v^2t^2},$$

$$(a) \quad \beta = \mp\frac{R_2}{\cosh\alpha}, \quad p = \frac{B^2(\alpha)}{\beta^2 R_2^2}.$$

$$(b)\quad W = x\tan^{-1}(\sinh\alpha) + y\ln\cosh\alpha + zC - vt\alpha,\quad C = \text{const},$$

$$p = (\tan^{-1}(\sinh\alpha))^2 + \ln^2\cosh\alpha - \alpha^2 + C^2.$$

$$(\mathbf{3})\quad l = \frac{\cos 2\alpha}{2\cos\alpha},\quad m = \sin\alpha,\quad n = \frac{\sqrt{3}}{2\cos\alpha},\quad vw = \frac{1}{\cos\alpha},\quad q = 0,$$

$$\alpha = \tan^{-1}\frac{y \pm R_3}{\sigma + x},\quad R_3 = \sqrt{x^2 + y^2 - \sigma^2},\quad \sigma = 2vt - z\sqrt{3},$$

$$(a)\quad \beta = \mp\frac{R_3}{\cos\alpha},\quad p = \frac{B^2(\alpha)}{\beta^2 R_3^2}.$$

$$(b)\quad W = x\sin\alpha - y\cos\alpha - \frac{\sigma + x}{4}\ln\frac{1+\sin\alpha}{1-\sin\alpha},\quad p = 1 - \frac{\sin\alpha}{2}\ln\frac{1+\sin\alpha}{1-\sin\alpha}.$$

One can analogically construct solution of Eqs. (49), (50) and find the solution of Eq. (54) using Eq. (55).

$$(\mathbf{1})\quad L = \alpha,\quad M = \frac{1}{\alpha},\quad N = -\sqrt{2},\quad vV = \alpha + \frac{1}{\alpha},\quad Q = 0,\quad \alpha = \pm\sqrt{\frac{y - vt}{x - vt}},$$

$$W = \pm\sqrt{(x - vt)(y - vt)} - \sqrt{2}z,\quad p = \frac{\mp 1}{\sqrt{(x - vt)(y - vt)}}.$$

$$(\mathbf{2})\quad L = \frac{1}{\cosh\alpha},\quad M = \tanh\alpha,\quad N = 0,\quad vV = 1,\quad Q = 0,\quad \sinh\alpha = \frac{y}{x},$$

$$W = \sqrt{x^2 + y^2} - vt,\quad p = \frac{1}{\sqrt{x^2 + y^2}}.$$

$$(\mathbf{3})\quad L = \frac{\sqrt{2}\alpha}{1 + \alpha^2},\quad M = L,\quad N = \frac{1 - \alpha^2}{1 + \alpha^2},\quad vV = 1,\quad Q = 0,\quad \alpha = \sqrt{2}\frac{R - z}{x + y},$$

$$R = \sqrt{z^2 + \frac{(x + y)^2}{2}},\quad W = R - vt,\quad p = \frac{1}{R}.$$

The spatial images of the functions p and W are shown in Fig. 2 for the solution **3**.

In conclusion we note that solutions of Eqs. (7), (8) can be constructed using ansatzes $\sigma = x + iy$, $\tilde{\sigma} = x - iy$, $\theta = z \pm vt$. So

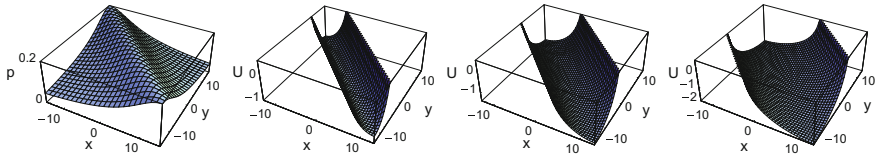

Fig. 2 The functions p (at the left) and U for the solution **3**, for $z = 0$, $t = 0.01$ (the 2nd), $t = 2$ (the 3rd) and $t = 5$ (the 4th)

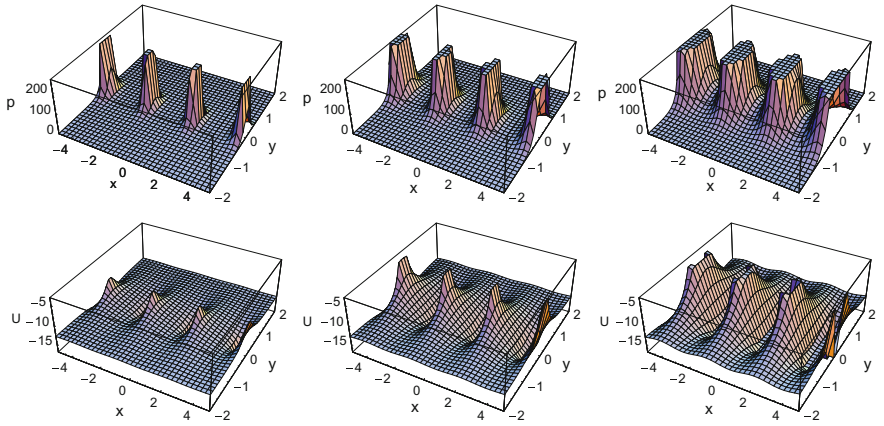

Fig. 3 The functions p and U for the solution (63), if $z = 0$, $t = 0$ (at the left), $t = 1$ (in the centre) and $t = 2$ (at the right)

$$W = \frac{f(\sigma, \theta) + f(\tilde{\sigma}, \theta)}{2} \tag{63}$$

is the real solution of Eqs. (7), (8), if $p = f_{\sigma} f_{\tilde{\sigma}}$, where $f(\sigma, \theta)$ is arbitrary function.

The spatial images of the functions p and W are shown in Fig. 3 for the solution with $f(\sigma, \theta) = e^{\theta} \tan \sigma$.

4 Conclusion

Methods of finding exact analytical solutions of the nonautonomic NKFG equation are offered. They are based on the ideas and methods of construction of functionally invariant solutions of the partial differential equations. The offered methods allow us to construct solutions of the NKFG equation in the form of arbitrary function depending on one or several ansatzes. The equations for determination of the ansatzes are given, and methods of their solution are discussed. The developed methods allow us to find exact analytical solutions of Eq. (2) for functions $p(x, y, z, t)$ of a special form. In this methods both the solution and analytical form of the function $p(x, y, z, t)$ are

found simultaneously. These solutions are particular solutions, but they have rather general form because they contain arbitrary functions.

The general methods for construction of functionally invariant solution of the NKFG equation are illustrated by examples of finding the exact analytical solutions for the nonautonomic Liouville equation.

Methods of the solution of the nonautonomic NKFG equation are given for three dimension space. However, they easily can be generalized on the spaces of arbitrary number of dimension. It is possible to hope that the developed methods will be useful to realization of nonlinear models which describe the real physical phenomena and technological processes more adequately [13].

Acknowledgements This work was supported by Russian Foundation for Basic Research, grants 16-01-00068-a and 17-01-00230-a.

References

1. Jacobi, C.G.J.: Über eine particuläre Lösung der partiellen Differentialgleichung $\frac{\partial^2 V}{\partial x^2} + \frac{\partial^2 V}{\partial y^2} + \frac{\partial^2 V}{\partial z^2} = 0$. Crelle Journal für die reine und angewandte Mathematik **36**, 113–134 (1848)
2. Forsyth, A.R.: New solutions of some of the partial differential equations of mathematical physics. Messenger Math. **27**, 99–118 (1898)
3. Bateman, H.: The Mathematical Analysis of Electrical and Optical Wave-Motion on the Basis of Maxwell's Equations. Cambridge University Press, Cambridge (1915)
4. Smirnoff, V., Soboleff, S.: Sur une méthode nouvelle dans le problème plan des vibrations élastiques. Trudy Seismologicheskogo Inst. **20**, 1–37 (1932)
5. Smirnoff, V., Soboleff, S.: Sur le problème plan des vibrations élastiques. C. R. Acad. Sci. Paris **194**, 1437–1439 (1932)
6. Sobolev, S.L.: Functionally invariant solutions of wave equation. Trudy Fiz.-Mat. Inst. V.A. Steklov **5**, 259–264 (1934)
7. Erugin, N.P.: On functionally invariant solutions. Uchenye Zap. Leningarad University **15**(96), 101–134 (1948)
8. Aero, E.L., Bulygin, A.N., Pavlov, Yu.V.: Solutions of the three-dimensional sine-Gordon equation. Theor. Math. Phys. **158**, 313–319 (2009). https://doi.org/10.1007/s11232-009-0025-3
9. Aero, E.L., Bulygin, A.N., Pavlov, Yu.V.: Solutions of generalized (3+1) sine-Gordon equation [In Russian]. Nelineinii Mir **7**, 513–517 (2009)
10. Aero, E.L., Bulygin, A.N., Pavlov, Yu.V.: New approach to the solution of the classical sine-Gordon equation and its generalizations. Differ. Equ. **47**, 1442–1452 (2011). https://doi.org/10.1134/S0012266111100077
11. Aero, E.L., Bulygin, A.N., Pavlov, Yu.V.: Functionally invariant solutions of nonlinear Klein-Fock-Gordon equation. Appl. Math. Comput. **223**, 160–166 (2013). https://doi.org/10.1016/j.amc.2013.07.088
12. Aero, E.L., Bulygin, A.N., Pavlov, Yu.V.: Solutions of the sine-Gordon equation with a variable amplitude. Theor. Math. Phys. **184**, 961–972 (2015). https://doi.org/10.1007/s11232-015-0309-8
13. Porubov, A.V., Fradkov, A.L., Andrievsky, B.R.: Feedback control for some solutions of the sine-Gordon equation. Appl. Math. Comput. **269**, 17–22 (2015)

Percolation Threshold for Elastic Problems: Self-consistent Approach and Padé Approximants

Igor V. Andrianov, Galina A. Starushenko and Vladimir A. Gabrinets

Abstract Self-consistent approximation and Padé approximants are used for calculation of percolation threshold for elasticity problem.

1 Introduction

Mathematical models of composite materials can be rather complicated as a result of the distribution and orientation of the multiple inclusions within the matrix. Properties of inclusions are usually very different of properties of matrix. If the distribution of inclusions is completely random, then with an increase in their volume fraction c_2 the chains of the contacting inclusions (clusters) are created in the material. The critical value $c_2 = c_p$, for which the cluster of an infinite length is formed, is called the percolation threshold. The properties of such composite materials cannot be described within the framework of regular or quasi-regular models, and it is necessary to use the theory of percolation. This theory was intensively developed in the recent decades [1–7]. The objectives of the theory of percolation consist in description of the correlations between the appropriate physical and geometrical characteristics of the objects under study.

Effective characteristics k_0 of a composite near the percolation threshold ($c_2 \to c_p$) are defined by the asymptotic relations like

I. V. Andrianov (✉)
Institut Für Allgemeine Mechanik, RWTH Aachen University, 64 Templergraben, Aachen 52056, Germany
e-mail: igor.andrianov@gmail.com

G. A. Starushenko
Dnipro Regional Institute of Public Administration, National Academy of Public Administration, 29 Gogol St, Dnipro 49044, Ukraine

V. A. Gabrinets
Dnipro National University of Railway Transport named after Academician V. Lazaryan, 2 Ac. Lazaryan, Dnipro 49010, Ukraine

F. dell'Isola et al. (eds.), *Advances in Mechanics of Microstructured Media and Structures*, Advanced Structured Materials 87,
https://doi.org/10.1007/978-3-319-73694-5_3

$$k_0 \sim \left|c_2 - c_p\right|^t, \tag{1}$$

where c_p is the critical volume fraction of the inclusions, t is the critical index of the corresponding physical property.

Different models of percolation media and corresponding methods of calculation of percolation threshold and the critical indices are reviewed in [1–5]. It is worth to note that until now there is a certain discrepancy between the results of different authors, especially in the 3D case.

For transport problems it is shown that Bruggeman's formula (self-consistent approximation) makes it possible to qualitatively describe the percolation threshold [2, 6, 7]. However, the accuracy of Bruggeman's formula is low. In the paper [6] a modification of Maxwell's formula is proposed based on the Padé approximant (PA), which provides a qualitative explanation of the existence of the percolation threshold.

In our paper we analyse using of self-consistent approximation and PA for calculation of percolation threshold for elasticity problem. Percolation threshold depends on the shape of inclusions. We will consider in the present paper the spherical inclusions in 3D case.

2 Self-consistent Approach

Well-known self-consistent approach [8–10] leads to the following equations for effective shear modulus μ^*, bulk modulus K^* and Poisson's coefficient ν^*:

$$\sum_{i=1}^{2} \frac{c_i}{1+\alpha^*\left(\frac{K_i}{K^*}-1\right)} = 1;\ \sum_{i=1}^{2} \frac{c_i}{1+\beta^*\left(\frac{\mu_i}{\mu^*}-1\right)} = 1;\ \nu^* = \frac{3K^* - 2\mu^*}{6K^* + 2\mu^*}, \tag{2}$$

where

$$\alpha^* = \frac{1+\nu^*}{3(1-\nu^*)},\ \beta^* = \frac{2(4-5\nu^*)}{15(1-\nu^*)};$$

K_1, μ_1 and K_2, μ_2 are the elastic constants of inclusions and matrix respectively; $c_i (i = 1, 2)$ are the volume fractions, $c_1 + c_2 = 1$.

The system of Eq. (2) admits an exact analytic solution (we do not give it due to its cumbersome nature), which allows us to obtain the expression for the effective Young's modulus E^*.

Figure 1 shows the graphs of the effective Young's modulus E^*, obtained due the solution of the system of Eq. (2), for various values of the elastic characteristics of the matrix K_2, μ_2, and inclusions K_1, μ_1.

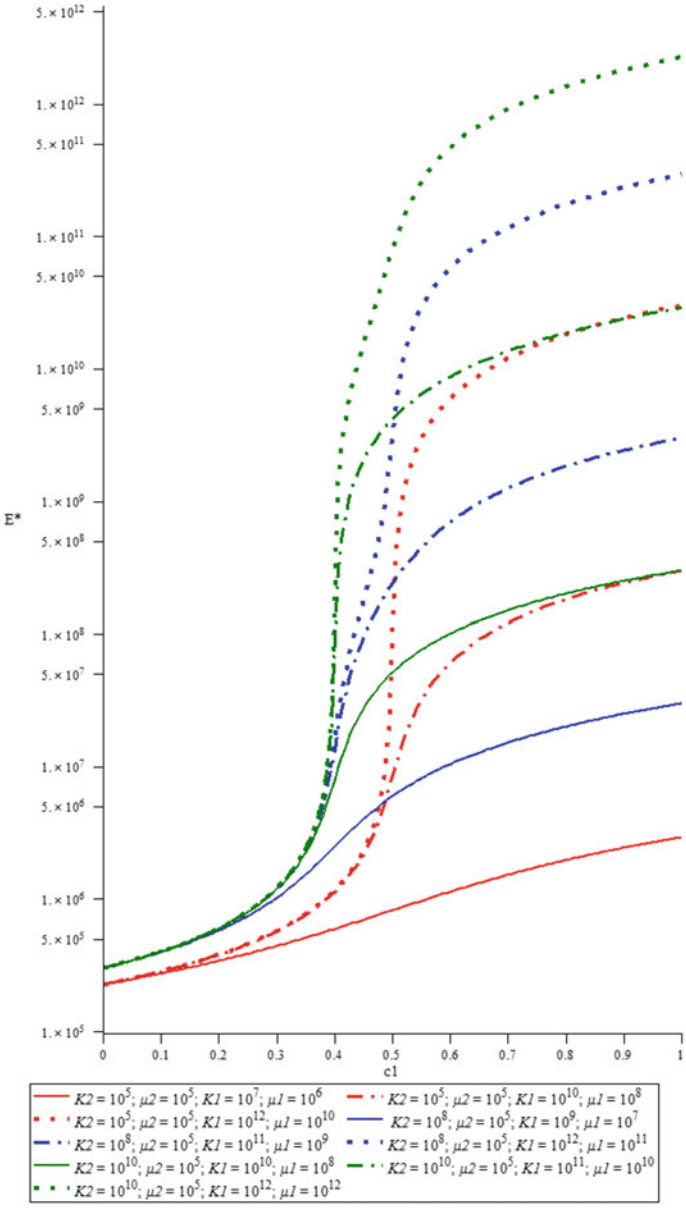

Fig. 1 Graphs of the effective Young's modulus E^* for various values of the elastic characteristics of the matrix and inclusions

Analysis of these dependences shows that in the case of rigid inclusions, whose elastic characteristics significantly exceed the values of the corresponding parameters of the matrix ($K_1 \gg K_2$, $\mu_1 \gg \mu_2$), the self-consistency solution describes a qualitatively the percolation threshold in the composite material.

In particular, for the values of the elastic constants of the matrix $K_2 = 10^{10}$, $\mu_2 = 10^5$, and inclusions $K_1 = 10^{12}$, $\mu_1 = 10^{12}$, the percolation threshold obtained by the self-consistent approach agrees with the experimental data [11], where it is shown that for the composite with the mentioned elastic characteristics the percolation threshold is located between 0.40 and 0.41.

3 Padé Approximants for Virial Expansions

Virial expansions for effective shear μ^* and bulk K^* modulus at small inclusions concentrations can be written as follows [9, 12]:

$$K^* = \left[1 + \frac{3(1-\nu_2)(K_1 - K_2)c_1}{2K_2(1-2\nu_2) + K_1(1+\nu_2)}\right] K_2; \tag{3}$$

$$\mu^* = \left[1 + \frac{15(1-\nu_2)(\mu_1 - \mu_2)c_1}{\mu_2(7-5\nu_2) + 2\mu_1(4-5\nu_2)}\right] \mu_2. \tag{4}$$

Using well-known relations

$$E = \frac{9K\mu}{3K+\mu}, \; \nu = \frac{1}{2} \cdot \frac{3K-2\mu}{3K+\mu},$$

and formulas (3), (4) one obtains effective Young's modulus E^*:

$$\begin{aligned} E^* = {} & \left[9\mu_2\left(4\mu_2^2(2-5c_1) + \mu_1(3K_2(3-5c_1) + 4\mu_1(3+5c_1)) + 5K_2\mu_1(2+3c_1)\right)\right. \\ & \times (\mu_2(4K_2(1-c_1) + 4K_1c_1) + 3K_2(-K_2c_1 + K_1(1+c_1)))]/\left[16(2-5c_1)\mu_2^4\right. \\ & + 4(3K_2(11-13c_1) + 3K_1(2+3c_1) + 4\mu_1(3+5c_1))\mu_2^3 \\ & + 3(K_2(28\mu_1(2-c_1) + 3K_1(11+15c_1)) + 4K_1\mu_1(3+17c_1))\mu_2^2 \\ & + 9K_2(K_2(4\mu_1(2-5c_1) + 9(K_1(1+c_1) - K_2c_1)) + K_1\mu_1(14+25c_1))\mu_2 \\ & \left. + 54K_2^2\mu_1(-K_2c_1 + K_1(1+c_1))\right]. \end{aligned} \tag{5}$$

The range of applicability of the virial expansion ы method is limited by the small concentrations of one of the components; therefore, the relations (3)–(5) cannot be used for large inclusions and even at a qualitative level do not describe the percolation threshold. For improving formula (5) let us use PA [13]. PA [0/1] for E^* is:

$$E^{*\,(0)}_{[0/1]}(c_1) = \frac{9K_2^2\mu_2\Delta_1^{(1)}}{K_2(3K_2+\mu_2)\Delta_1^{(1)} - (3K_2+4\mu_2)\Delta_2^{(1)}c_1}, \tag{6}$$

where

$$\Delta_1^{(1)} = (3K_1+4\mu_2)\left(6K_2\mu_1 + 9K_2\mu_2 + 12\mu_1\mu_2 + 8\mu_2^2\right);$$
$$\Delta_2^{(1)} = 45K_1K_2^2(\mu_1-\mu_2) + 3K_1K_2\mu_2(2\mu_1+3\mu_3) + 3K_2^2\mu_2(18\mu_1-23\mu_2) + 4(K_1-K_2)\mu_2^2(3\mu_1+2\mu_2).$$

Similarly, we construct a PA [1/0] for the expression obtained from (5) by replacing: $K_{1(2)} \underset{\leftarrow}{\overset{\rightarrow}{}} K_{2(1)}$, $\mu_{1(2)} \underset{\leftarrow}{\overset{\rightarrow}{}} \mu_{2(1)}$, $c_1 \to c_2$. From the physical point of view, we reversed the roles of the phases of the composite "matrix"—"inclusion". In this case, the corresponding PA is written as:

$$E^{*\,(0)}_{[1/0]}(c_2) = \frac{9K_1\mu_1}{3K_1+\mu_1} + \frac{9\mu_1(3K_1+4\mu_1)\Delta_2^{(2)}}{(3K_1+\mu_1)^2\Delta_1^{(2)}}c_2, \tag{7}$$

where $\Delta_i^{(2)} = \Delta_i^{(1)}(i=1,2)$ after change: $K_{1(2)} \underset{\leftarrow}{\overset{\rightarrow}{}} K_{2(1)}$, $\mu_{1(2)} \underset{\leftarrow}{\overset{\rightarrow}{}} \mu_{2(1)}$.

Passing in the Eq. (7) to the variable c_1 ($c_2 = 1 - c_1$), for $c_1 \to 1$ finally we have:

$$E^{*\,(1)}_{[1/0]}(c_1) = \frac{9\mu_1\left((3K_1+\mu_1)\left(K_1\Delta_1^{(2)} + \Delta_2^{(2)}\right) + \mu_1\Delta_2^{(2)} - (3K_1+4\mu_1)\Delta_2^{(2)}c_1\right)}{(3K_1+\mu_1)^2\Delta_1^{(2)}}. \tag{8}$$

In Fig. 2 at the values of the elastic constants of the matrix material and inclusions: $K_1 = 10^{12}$; $\mu_1 = 10^{12}$; $K_2 = 10^{10}$; $\mu_2 = 10^5$ graphs of the effective Young's modulus obtained using the self-consistency method (2) and using the Padé approximants (7), (8) are presented.

We can conclude that

i. the PA allows us to expand area of applicability of virial expansion substantially;
ii. a comparison with the self-consistent solution shows that the PA at zero (7) reliably describes the effective parameter right up to the percolation percolation threshold;
iii. the PA in unit (8) works well for large inclusions: the results practically coincide with the self-consistent solution.

To estimate the accuracy of the constructed PA, we use the Hill equation, which is an exact relation that does not depend on the microstructure of the composite.

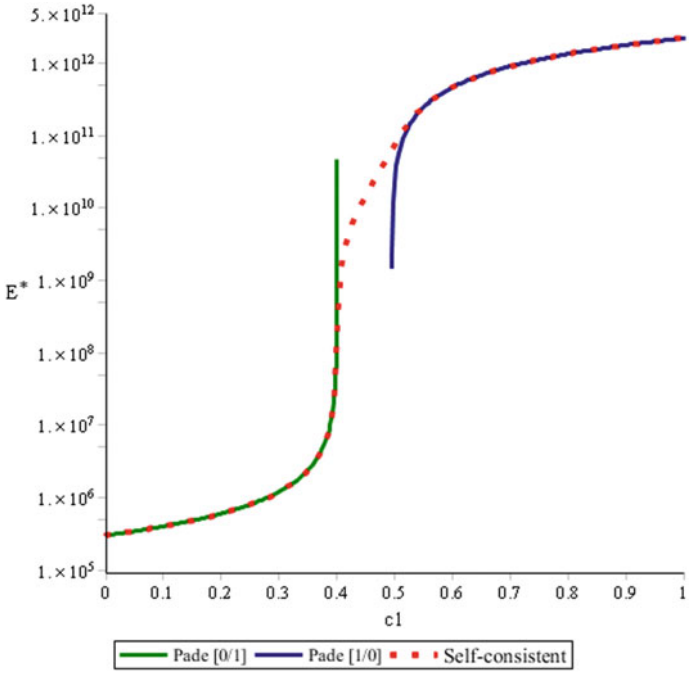

Fig. 2 Comparison of the results of calculations of the effective Young's modulus by self-consistent approach and PA of virial expansions

This equation is valid for composites consisting of isotropic components having the same shear modulus of components. For a two-dimensional two-component composite with $\mu_1 = \mu_2 = \mu$ this equation is written as:

$$\frac{1}{K^* + \mu} = \frac{c_1}{K_1 + \mu} + \frac{c_2}{K_2 + \mu}, \tag{9}$$

from which the expression of an effective bulk modulus follows directly:

$$K_H^* = \frac{(c_1 K_1 + c_2 K_2)\,\mu + K_1 K_2}{c_1 K_2 + c_2 K_1 + \mu}. \tag{10}$$

Comparison with the exact solution (10) of expression

$$K^* = \left[1 + \frac{(3K_2 + 4\mu)(K_1 - K_2)c_1}{(3K_1 + 4\mu)K_2}\right] K_2, \tag{11}$$

obtained from (3) in the particular case $\mu_1 = \mu_2 = \mu$, indicates a very limited area of applicability of the latter (Fig. 3, dashed line).

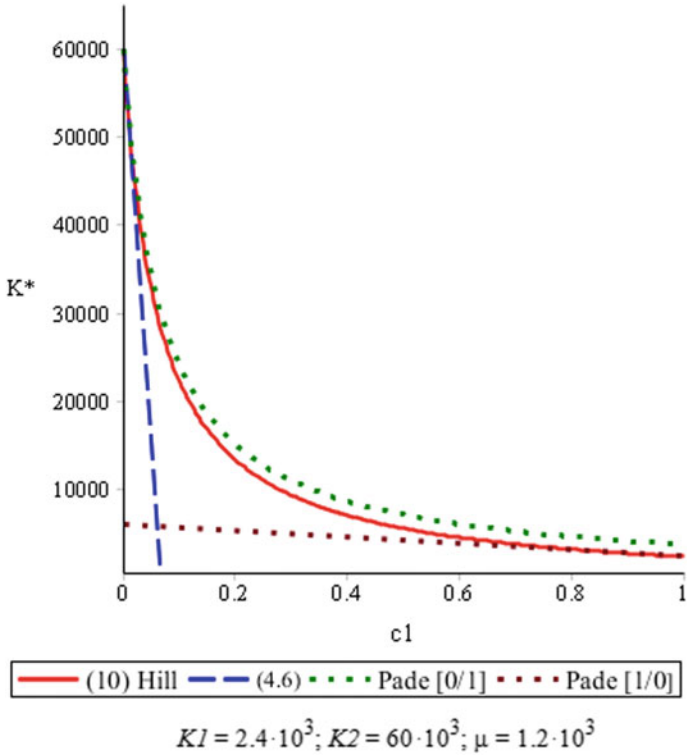

Fig. 3 Comparison of the exact solution (10) with PA (12), (13) in the special case of the same shear modulus of components

Let us transform the solution of (11) to PA [0/1] for a small concentration of inclusions $c_1 \to 0$:

$$K^{*\,(0)}_{[0/1]}(c_1) = \frac{(3K_1 + 4\mu)K_2^2}{(3K_1 + 4\mu)K_2 - (3K_2 + 4\mu)(K_1 - K_2)c_1}. \tag{12}$$

Similarly, we construct the PA [1/0] for a large concentration of inclusions $c_2 = 1 - c_1 \to 0$:

$$K^{*\,(1)}_{[1/0]}(c_1) = \frac{(3K_1 + 4\mu)K_2 - 3(K_1 - K_2)K_1 + (3K_1 + 4\mu)(K_1 - K_2)c_1}{3K_2 + 4\mu}. \tag{13}$$

The PA (12), (13) are close to the exact solution (10) for small and large inclusions, respectively (Fig. 3).

4 Conclusion

The PA (7) reliably describes the effective parameter right up to the beginning of the percolation process and "catches" the percolation threshold.

References

1. Torquato, S.: Random heterogeneous media: microstructure and improved bounds on effective properties. Appl. Mech. Rev. **44**(2), 37–76 (1991)
2. Torquato, S.: Random Heterogeneous Materials: Microstructure and Macroscopic Properties. Springer, New York (2002)
3. Sahimi, M.: Heterogeneous Materials. Springer, New York (2003)
4. Stauffer, D., Aharony, A.: Introduction to Percolation Theory, Rev. 2nd ed. Taylor & Francis, London (1994)
5. Snarskii, A.A., Bezsudnov, I.V., Sevryukov, V.A., Morozovskiy, A., Malinsky, J.: Transport Processes in Macroscopically Disordered Media (from Medium Field Theory to Percolation). Springer, New York (2016)
6. Snarskii, A.A.: Did Maxwell know about the percolation threshold? (on the fiftieth anniversary of percolation theory). Physics-Uspekhi **50**(12), 1239–1242 (2007)
7. Bergman, D.J.: The self-consistent effective medium approximation (SEMA): new tricks from an old dog. Phys. B **394**, 344–350 (2007)
8. Budiansky, B.: On the elastic moduli of some heterogeneous materials. Phys. Solids **13**, 223–227 (1965)
9. Shermergor, T.D.: The Theory of Microinhomogeneous Media. Nauka, Moscow, 1977 (in Russian)
10. Kanaun, S.K., Levin, V.M.: Self-consistent Methods for Composites, vol. 1: Static Problems. Springer, New York (2008)
11. Benguigui, L., Ron, P.: Experimental realization of superelasticity near the percolation threshold. Phys. Rev. Lett. **70**(16), 2423–2426 (1993)
12. Krivoglaz, M.A., Cherevko, A.S.: On the elastic moduli of a two-phase solid. Fiz. Met. Metalloved. **8**(2), 16–165 (1959) (in Russian)
13. Baker, G.A.: Essential of Padé Approximants. Academic Press, New York (1975)

A 1D Continuum Model for Beams with Pantographic Microstructure: Asymptotic Micro-Macro Identification and Numerical Results

Emilio Barchiesi, Francesco dell'Isola, Marco Laudato, Luca Placidi and Pierre Seppecher

Abstract In the standard asymptotic micro-macro identification theory, starting from a De Saint-Venant cylinder, it is possible to prove that, in the asymptotic limit, only flexible, inextensible, beams can be obtained at the macro-level. In the present paper we address the following problem: is it possible to find a microstructure producing in the limit, after an asymptotic micro-macro identification procedure, a continuum macro-model of a beam which can be both extensible and flexible? We prove that under certain hypotheses, exploiting the peculiar features of a pantographic microstructure, this is possible. Among the most remarkable features of the resulting model we find that the deformation energy is not of second gradient type only because it depends, like in the Euler beam model, upon the Lagrangian curvature, i.e. the projection of the second gradient of the placement function upon the normal vector to the deformed line, but also because it depends upon the projection of the second gradient of the placement on the tangent vector to the deformed line, which is the elongation gradient. Thus, a richer set of boundary conditions can be prescribed

E. Barchiesi · F. dell'Isola (✉)
Dipartimento di Ingegneria Strutturale e Geotecnica, Università degli Studi di Roma "La Sapienza", Via Eudossiana 18, 00184 Roma, Italy
e-mail: fdellisola@gmail.com

E. Barchiesi · F. dell'Isola · M. Laudato · L. Placidi · P. Seppecher
International Research Center M&MoCS, Università degli Studi dell'Aquila, Via Giovanni Gronchi 18 - Zona industriale di Pile, 67100 L'Aquila, Italy

L. Placidi
Facoltà di Ingegneria, Università Telematica Internazionale UNINETTUNO, Corso Vittorio Emanuele II 39, 00186 Roma, Italy

F. dell'Isola
Dipartimento di Ingegneria Civile, Edile, Ambientale e Architettura, Università degli Studi dell'Aquila, Via Giovanni Gronchi 18 - Zona industriale di Pile, 67100 L'Aquila, Italy

M. Laudato
Dipartimento di Ingegneria e Scienze dell'Informazione e Matematica, Università degli Studi dell'Aquila, Via Vetoio 1, 67100 L'Aquila, Coppito, Italy

P. Seppecher
Institut de Mathématiques de Toulon, Universitè de Toulon et du Var, Avenue de l'Université, BP 132, Cedex, 83957 La Garde, France

F. dell'Isola et al. (eds.), *Advances in Mechanics of Microstructured Media and Structures*, Advanced Structured Materials 87,
https://doi.org/10.1007/978-3-319-73694-5_4

for the pantographic beam model. Phase transition and elastic softening are exhibited as well. Using the resulting planar 1D continuum limit homogenized macro-model, by means of FEM analyses, we show some equilibrium shapes exhibiting highly non-standard features. Finally, we conceive that pantographic beams may be used as basic elements in double scale metamaterials to be designed in future.

Keywords Micro-macro identification · Asymptotic expansion · Pantographic beams · Continuum models

1 Introduction

Customarily, the theory of nonlinear beams is either postulated by means of a suitable least action principle in the so called "direct way" or is deduced, by means of a more or less rigorous procedure, starting from a three-dimensional elasticity theory. The first example of direct model can be found in the original paper by Euler [1]. Many epigones of Euler used this approach: a comprehensive account for this procedure can be found in e.g. Antman [2]. On the other hand, by following the procedure described by De Saint-Venant, one can try to identify the constitutive equation of an Euler type (1D) model in terms of the geometrical and mechanical properties, at micro-level, of the considered mechanical systems. This is done, in more modern textbooks, by using a more or less standard asymptotic micro-macro identification procedure, which generalizes the one used by De Saint-Venant for bodies with cylindrical shape (see for instance [3]). It can be rigorously proven, under a series of well-precised assumptions, that only flexible and inextensible beams can be obtained [4–9]. In the present paper we address the following problem: is it possible to find a microstructure producing, at the macro level and under loads of the same order of magnitude, a beam which can be both extensible and flexible? Using an asymptotic expansion and rescaling suitably the involved stiffnesses, we prove that a pantographic microstructure does induce, at the macro level, the aforementioned desired mechanical behaviour. In this paper, in an analogous fashion to that of variational asymptotic methods, and following a mathematical approach resembling that used by Piola, we have employed asymptotic expansions of kinematic descriptors directly into the postulated energy functional. Using the so obtained 1D continuum model, we show some equilibrium shapes exhibiting highly non standard features, essentially related to the complete dependence of the homogenized continuum energy density functional on the second gradient of the placement field. While in the standard finite deformation Euler beam theory the energy functional depends only on the material curvature, i.e. the normalized projection of the second gradient of the placement on the normal vector to the current configuration, the energy functional for the nearly-inextensible pantographic beam model depends also on the projection of the second gradient of the placement on the tangent vector to the current configuration. Thus, the full decomposition of the second gradient of the placement is present in the latter model. Generalized continua [10–14], and in particular higher

gradient theories, see [15] or [16] for a comprehensive review, are able to describe behaviours which cannot be accounted for in classical Cauchy theories [17–24]. In the literature, several examples can be found motivating the importance of generalized continua: electromechanical [25] and biomechanical [26–29] applications, elasticity theory [30–35], capillary fluids analysis [36], granular micromechanics [37–39], robotic systems analysis [40, 41], damage theory [42–47], and wave propagation analysis [48–52]. Furthermore, second gradient continuum models always appear when the considered micro-system is a pantographic structure [53–60]. A comprehensive review on the modeling of pantographic structures can be found in [61, 62]. Several results of numerical investigations can be found in [30, 63–71], while for an outline of recent experimental results we refer to [72, 73]. The work is organized in the following way. In Sect. 2, we discuss the geometry of the pantographic beam micromechanical model. Once the general expression for the micro-model energy is given, we restrict to the quasi-inextensibility case, where small elongation of oblique fibers is assumed. The micro-model energy is then represented as a function of the macroscopic kinematical descriptors and the further specialization to the (complete) inextensibility of the oblique fibers is considered. In Sect. 3 we perform a heuristic homogenization procedure and we discuss the feature of the 1D continuum model. In particular, we show that such a homogenization procedure gives rise to a full second gradient theory. In Sect. 4 we show results of numerical simulations in order to better highlight some non-standard features of the nearly-inextensible pantographic beam model. Finally, in Sect. 5 we postulate a generalized strain energy density which includes both the quasi-inextensible pantographic beam model and the standard Euler beam theory. Euler-Lagrange equations for this generalized strain energy density are derived together with the corresponding boundary conditions and the specializations to the two models are performed.

2 Discrete Micro-model

In this section we discuss the discrete micro-mechanical model which is employed throughout this paper. We begin giving a geometrical description and then we give a mechanical characterization, by choosing a deformation energy. It is a Hencky-type spring model with the geometrical arrangement of a pantographic strip. Once the energy of the micro-model is chosen in its general form, we assume a particular asymptotic behaviour for some relevant kinematic quantities, i.e. the elongation of oblique springs, as will be clear in the sequel. We consider the quasi-inextensibility case, i.e. the relative elongation of the oblique springs is small. As a further specialisation, the inextensibility case is considered. Finally, after having defined a micro-macro identification, we express the energy of the micro-system in terms of macroscopic kinematic descriptors to prepare the field to the homogenization procedure which will be discussed in details in the next section.

2.1 Geometry

In the spirit of [55, 59, 74], in this section we introduce a discrete-spring model (also referred to as the *micro-model*, since it resembles the features of a specific microstructure). The topology and features of the undeformed and deformed discrete-spring system are summarized in Figs. 1 and 2, respectively. In the undeformed configuration $N + 1$ material particles are arranged upon a straight line at positions P_i's, $i \in [0; N]$, with a uniform spacing ε. The basic i-th unit cell centered in P_i is formed by four springs joined together by a hinge placed at P_i. Between two oblique springs, belonging to the same cell and lying on the same diagonal, a rotational spring opposing to their relative rotation is placed. Rotational springs are colored in Fig. 1 in blue and red.

We denote with p_i the position in the deformed configuration corresponding to position P_i in the reference one. In order to completely describe the kinematics of the micro-model we have to introduce other descriptors. At this end, the length of the oblique deformed springs, indicated with $l_i^{\alpha\beta}$, is introduced, the indices α and β belonging respectively to the sets $\{1, 2\}$ and $\{D, S\}$ and referring to the first and

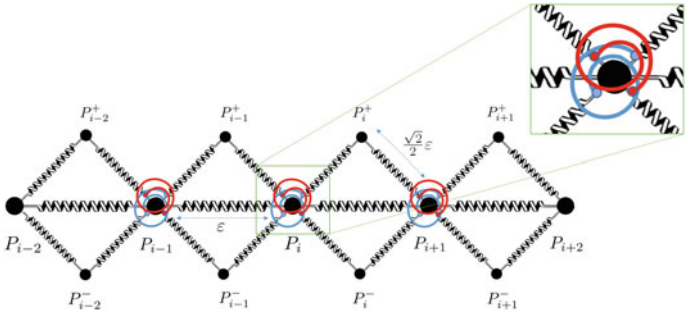

Fig. 1 Undeformed spring system resembling the micro-structure

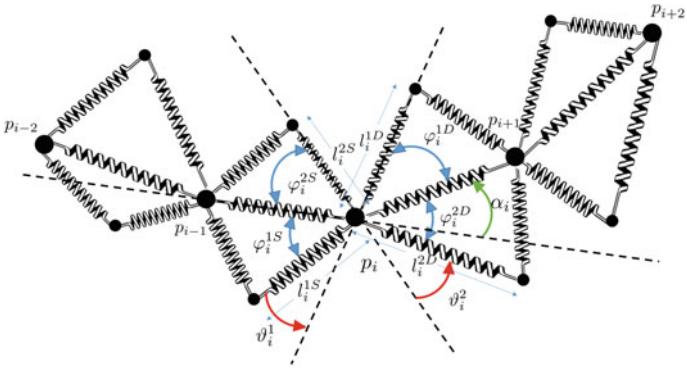

Fig. 2 Deformed spring system resembling the micro-structure

second diagonal and left and right, respectively. Referring to Fig. 2, we consider the i-th node, notwithstanding that the same quantities can be defined for each node. We define α_i as the angle between the vectors $p_i - p_{i-1}$ and $p_i - p_{i+1}$, respectively. We define as ϑ_i^α the angle measuring the deviation of two opposite oblique springs from being collinear. In order to illustrate the definition of $\varphi_i^{\alpha\beta}$, we consider the case $\alpha = 1$ and $\beta = D$. The quantity φ_i^{1D} is the angle between the vector $p_{i+1} - p_i$ and the upper oblique spring hinged at p_i. By means of elementary geometric considerations, we have that

$$\begin{aligned}
\vartheta_i^1 &= \alpha_i + \varphi_i^{1D} - \varphi_i^{1S} \\
\vartheta_i^2 &= \alpha_i + \varphi_i^{2S} - \varphi_i^{2D}, \ i \in [0; N]\,.
\end{aligned} \tag{1}$$

In the undeformed configuration, see Fig. 1, we have:

$$\begin{aligned}
l_i^{\alpha\beta} &= \frac{\sqrt{2}}{2}\varepsilon, \ \alpha = 1, 2 \quad \beta = D, \ S \quad i \in [0; N] \\
\vartheta_i^1 &= \vartheta_i^2 = 0 \\
\|p_i - p_{i-1}\| &= \varepsilon, \ i \in [0; N]\,.
\end{aligned} \tag{2}$$

Considering that $\varphi_i^{\alpha D}, \varphi_i^{\alpha S} \in [0, \pi]$, by means of the law of cosines, we get:

$$\begin{aligned}
\varphi_i^{1D} &= \cos^{-1}\left(\frac{\|p_{i+1} - p_i\|^2 + \left(l_i^{1D}\right)^2 - \left(l_{i+1}^{2S}\right)^2}{2 l_i^{1D} \|p_{i+1} - p_i\|}\right) \\
\varphi_i^{2D} &= \cos^{-1}\left(\frac{\|p_{i+1} - p_i\|^2 + \left(l_i^{2D}\right)^2 - \left(l_{i+1}^{1S}\right)^2}{2 l_i^{2D} \|p_{i+1} - p_i\|}\right) \\
\varphi_i^{1S} &= \cos^{-1}\left(\frac{\|p_i - p_{i-1}\|^2 + \left(l_i^{1S}\right)^2 - \left(l_{i-1}^{2D}\right)^2}{2 l_i^{1S} \|p_i - p_{i-1}\|}\right) \\
\varphi_i^{2S} &= \cos^{-1}\left(\frac{\|p_i - p_{i-1}\|^2 + \left(l_i^{2S}\right)^2 - \left(l_{i-1}^{1D}\right)^2}{2 l_i^{2S} \|p_i - p_{i-1}\|}\right).
\end{aligned} \tag{3}$$

2.2 Mechanical Model

The micro model energy, written as a combination of the elastic energy contributions of the springs, is defined as:

$$\mathcal{M} = \sum_i \sum_{\alpha,\beta} \frac{k^e_{\alpha\beta,i}}{2} \left(l_i^{\alpha\beta} - \frac{\sqrt{2}}{2}\varepsilon \right)^2 + \sum_i \sum_{\alpha} \frac{k^f_{\alpha,i}}{2} \left(\vartheta_i^{\alpha} \right)^2 + + \sum_i \frac{k^m_i}{2} \left(\|p_{i+1} - p_i\| - \varepsilon \right)^2 = \tag{4}$$

Reminding that $\vartheta_i^{\alpha} = \alpha_i + (-1)^{\alpha} \left(\varphi_i^{\alpha S} - \varphi_i^{\alpha D} \right)$, then (4) recasts as:

$$\mathcal{M} = \sum_i \sum_{\alpha,\beta} \frac{k^e_{\alpha\beta,i}}{2} \left(l_i^{\alpha\beta} - \frac{\sqrt{2}}{2}\varepsilon \right)^2 + \sum_i \sum_{\alpha} \frac{k^f_{\alpha,i}}{2} \left[\alpha_i + (-1)^{\alpha} \left(\varphi_i^{\alpha S} - \varphi_i^{\alpha D} \right) \right]^2 + + \sum_i \frac{k^m_i}{2} \left(\|p_{i+1} - p_i\| - \varepsilon \right)^2 . \tag{5}$$

In the next subsections we will specialize this form of the energy by means of assumptions on the properties of the micro-system. In particular, we will discuss in detail the representation of the micro-energy for the quasi-inextensibility assumption that will be made clear next and, subsequently, for the (complete) inextensibility cases.

2.3 Asymptotic Expansion and Quasi-inextensibility Assumption

We postulate that the following asymptotic expansion holds for $l_i^{\alpha\beta}$

$$l_i^{\alpha\beta} = \varepsilon \tilde{l}_{i1}^{\alpha\beta} + \varepsilon^2 \tilde{l}_{i2}^{\alpha\beta} + o\left(\varepsilon^2\right), \tag{6}$$

where the constant (with respect to ε) term is not present. We now turn to what we refer to as the quasi-inextensibility case. It consists in fixing the value of the first-order term in (6) as $\tilde{l}_{i1}^{\alpha\beta} = \frac{\sqrt{2}}{2}$. Moreover, to lighten the notation, we drop the subscript "2" of $\tilde{l}_{i2}^{\alpha\beta}$ i.e. $\tilde{l}_i^{\alpha\beta} := \tilde{l}_{i2}^{\alpha\beta}$. Hence, (6) reads as:

$$l_i^{\alpha\beta} = \frac{\sqrt{2}}{2}\varepsilon + \varepsilon^2 \tilde{l}_i^{\alpha\beta} + o\left(\varepsilon^2\right). \tag{7}$$

2.4 Piola's Ansatz

The reference shape of the macro-model is a one-dimensional straight segment $\mathcal{S}$ and we introduce on it an abscissa $s \in [0, B]$—where $B = N\varepsilon$ is the length of $\mathcal{S}$ which labels each position in $\mathcal{S}$. Proceeding as in the pioneering works of Gabrio Piola, an Italian mathematician and physicist who lived in the 1800s (see [75] for a historical review), we introduce the so-called *kinematical map*s, i.e. some fields in the macro-model that uniquely determine p_i and $\tilde{l}_i^{\alpha\beta}$:

$$\chi : [0, B] \to \mathcal{E}$$

$$\tilde{l}^{\alpha\beta} : [0, B] \to \mathbb{R}^+, \tag{8}$$

with $\mathcal{E}$ the Euclidean space on $\mathbb{V} \equiv \mathbb{R}^2$. We choose χ to be the placement function of the 1D continuum and, hence, it has to be injective. The current shape can be regarded as the image of the (sufficiently smooth) curve $\chi : [0, B] \to \mathcal{E}$ and, unlike the reference shape, it is not parameterized by its arc-length and it is not a straight line in general. In order for these fields to uniquely determine the kinematical descriptors of the micro-model (i.e. p_i and $\tilde{l}_i^{\alpha\beta}$), we use the *Piola's ansatz* and impose

$$\chi\left(s_i\right) = p_i$$

$$\tilde{l}^{\alpha\beta}\left(s_i\right) = \tilde{l}_i^{\alpha\beta}, \ \forall i \in [0; N]. \tag{9}$$

2.5 Micro-model Energy as a Function of Macro-model Descriptors

In this subsection we obtain the micro-model energy for the quasi-inextensibility case in terms of the macroscopic kinematical maps. Assuming that χ is at least twice continuously differentiable with respect to the space variable in s_i's, we have

$$\chi\left(s_{i+1}\right) = \chi\left(s_i\right) + \varepsilon\chi'\left(s_i\right) + \frac{\varepsilon^2}{2}\chi''\left(s_i\right) + o\left(\varepsilon^2\right)$$

$$\chi\left(s_{i-1}\right) = \chi\left(s_i\right) - \varepsilon\chi'\left(s_i\right) + \frac{\varepsilon^2}{2}\chi''\left(s_i\right) + o\left(\varepsilon^2\right). \tag{10}$$

Plugging (9) in (7) and (10), we get the following expressions:

$$
\begin{aligned}
l_i^{\alpha\beta} &= \frac{\sqrt{2}}{2}\varepsilon + \varepsilon^2 \tilde{l}^{\alpha\beta}\left(s_i\right) + o\left(\varepsilon^2\right) \\
p_{i+1} - p_i &= \varepsilon \chi'\left(s_i\right) + \frac{\varepsilon^2}{2}\chi''\left(s_i\right) + o\left(\varepsilon^2\right) \\
p_{i-1} - p_i &= -\varepsilon \chi'\left(s_i\right) + \frac{\varepsilon^2}{2}\chi''\left(s_i\right) + o\left(\varepsilon^2\right).
\end{aligned} \tag{11}
$$

Substituting (11) into (3) and expanding $\varphi_i^{\alpha S} - \varphi_i^{\alpha D}$ up to first-order with respect to ε, we get

$$
\begin{aligned}
&\varphi_i^{\alpha S} - \varphi_i^{\alpha D} = \\
&\frac{\frac{\sqrt{2}}{4}\left[\|\chi'\left(s_i\right)\|^2\right]' + \left[\tilde{l}^{(3-\alpha)D}\left(s_{i-1}\right) - \tilde{l}^{(3-\alpha)S}\left(s_{i+1}\right)\right]}{\|\chi'\left(s_i\right)\|\sqrt{1 - \frac{\|\chi'(s_i)\|^2}{2}}}\varepsilon + \\
&+ \frac{\left[\|\chi'\left(s_i\right)\|^2 - 1\right]\left[\tilde{l}^{\alpha S}\left(s_i\right) - \tilde{l}^{\alpha D}\left(s_i\right)\right]}{\|\chi'\left(s_i\right)\|\sqrt{1 - \frac{\|\chi'(s_i)\|^2}{2}}}\varepsilon + o\left(\varepsilon\right).
\end{aligned} \tag{12}
$$

Finally, substituting (12) in (5) yields the micro-model energy $\mathcal{M}$ as a function of the kinematical descriptors χ and $\tilde{l}^{\alpha\beta}$ of the macro-model

$$
\begin{aligned}
&\mathcal{M} = \\
&\sum_i \sum_{\alpha,\beta} \frac{k^e_{\alpha\beta,i}\varepsilon^4}{2}\left(\tilde{l}_i^{\alpha\beta}\right)^2 + \sum_i \frac{k_i^m \varepsilon^2}{2}\left(\|\chi_i'\| - 1\right)^2 + \\
&+ \sum_i \sum_\alpha \frac{k^f_{\alpha,i}\varepsilon^2}{2}\left\{\vartheta'\left(s_i\right) + (-1)^\alpha \frac{\frac{\sqrt{2}}{4}\left[\|\chi'\left(s_i\right)\|^2\right]' + \left[\tilde{l}_i^{(3-\alpha)D}\left(s_{i-1}\right) - \tilde{l}_i^{(3-\alpha)S}\left(s_{i+1}\right)\right]}{\|\chi'\left(s_i\right)\|\sqrt{1 - \frac{\|\chi'(s_i)\|^2}{2}}} + \right. \\
&\left. + (-1)^\alpha \frac{\left[\|\chi'\left(s_i\right)\|^2 - 1\right]\left[\tilde{l}_i^{\alpha S}\left(s_i\right) - \tilde{l}_i^{\alpha D}\left(s_i\right)\right]}{\|\chi'\left(s_i\right)\|\sqrt{1 - \frac{\|\chi'(s_i)\|^2}{2}}}\right\}^2,
\end{aligned} \tag{13}
$$

where $\alpha_i = \varepsilon \vartheta'\left(s_i\right)$ has been used and

$$
\vartheta' = \frac{\chi_\perp' \cdot \chi''}{\|\chi'\|^2},
$$

with $\chi'_{\perp}$ the 90° anti-clockwise rotation of χ', is the material curvature i.e. rate of change with respect to the reference abscissa of the orientation of the tangent $\chi'(s) = \rho(s)\left[\cos\vartheta(s)\,\mathbf{e}_1 + \sin\vartheta(s)\,\mathbf{e}_2\right]$ to the deformed centerline. We remark that the micro-model energy, when written in terms of macroscopic fields, contains already a contribution from the second gradient of $\chi(s)$. Finally, it is worth to be noticed that, for a fixed ε, Eq. (13) provides an upper bound for $||\chi'||$, i.e. $\|\chi'\| < \sqrt{2}$, even if no kinematic restrictions directly affect $||\chi'||$.

2.6 The Inextensibility Case

We consider now the case of inextensible oblique springs. This translates in considering $\tilde{l}_i^{\alpha\beta} = 0$ and it is referred as the *inextensibility case*. Moreover, for the sake of simplicity we consider the elastic constants of the rotational springs to satisfy $k^f_{1,i} = k^f_{2,i} := k^f_i, \forall i \in [1; N]$. We remark that $\tilde{l}_i^{\alpha\beta} = 0$ implies, through a purely geometric argument, that $\varphi^{S1}_{i+1} = \varphi^{S2}_{i+1} = \varphi^{D1}_i = \varphi^{D2}_i := \varphi_i$. Once the kinematic restrictions implied by the inextensibility assumption have been presented, we are ready to define the micro-model energy (5) as

$$\mathcal{I} =$$

$$\sum_i k^f_i \sum_\alpha \frac{\left[\alpha_i + (-1)^\alpha\left(\varphi_i - \varphi_{i-1}\right)\right]^2}{2} + \sum_i \frac{k^m_i}{2}\left(\|p_{i+1} - p_i\| - \varepsilon\right)^2. \tag{14}$$

Proceeding in analogy with the previous construction, we introduce the *kinematical map*

$$\varphi : [0, B] \to \left[0, \frac{\pi}{2}\right]$$

and, then, we perform the *Piola's ansatz* by imposing

$$\varphi\left(s_i\right) = \varphi_i, \ \forall i \in [0; N]. \tag{15}$$

Assuming both χ and φ to be at least one time continuously differentiable with respect to the space variable in s_i and taking into account the *Piola's ansatz* (15), we have

$$p_{i+1} - p_i = \varepsilon\chi'\left(s_i\right) + o(\varepsilon)$$

$$\varphi_{i-1} - \varphi_i = -\varepsilon\varphi'\left(s_i\right) + o(\varepsilon). \tag{16}$$

Substituting (16) into (14) yields the micro-model energy for the inextensibility case in terms of the kinematical quantities of the macro-model

$$\mathcal{I} =$$

$$\sum_i k_i^f \varepsilon^2 \left[\vartheta'^2\left(s_i\right) + \varphi_i'^2\left(s_i\right)\right] + \sum_i \frac{k_i^m \varepsilon^2}{2}\left(\|\chi_i'\| - 1\right)^2. \tag{17}$$

We now impose the so-called *internal connection* constraint:

$$\sqrt{2}\varepsilon \cos\varphi\left(s_i\right) = \|\chi\left(s_{i+1}\right) - \chi\left(s_i\right)\|, \tag{18}$$

which, up to ε-terms of order higher than one, reads:

$$\sqrt{2}\cos\varphi = \|\chi'\|. \tag{19}$$

This constraint ensures that, in the deformed configuration, the upper-left spring of the i-th cell is hinge-joint with the upper-right spring of the $(i-1)$-th cell, and the lower-left spring of the i-th cell is hinge-joint with lower-right spring of the $(i-1)$-th cell. Due to this constraint, the maps φ and χ are not independent and it is possible to rewrite the expression of the micro-model energy in terms of the placement field $\chi(s)$ only. Indeed, deriving (19) with respect to the space variable yields

$$-\sqrt{2}\varphi'\left(s_i\right)\sin\varphi\left(s_i\right) = \|\chi'\left(s_i\right)\|', \tag{20}$$

which, in turn, implies

$$\varphi'\left(s_i\right) = -\frac{\|\chi'\left(s_i\right)\|'}{\sqrt{2}\sin\varphi\left(s_i\right)}.$$

Reminding $\varphi \in [0, \pi]$ and taking into account (19), we get:

$$\varphi_i' = -\frac{\|\chi_i'\|'}{\sqrt{2}\sqrt{1-\cos^2\gamma_i}} = \\ = -\frac{\|\chi_i'\|'}{\sqrt{2-\|\chi_i'\|^2}}.$$

Hence, in the inextensibility case, the micro-model energy (17) can be recast, as a function of the macro-model descriptor χ only, as

$$\mathcal{I} = \sum_i k_i^f \varepsilon^2 \left[\left[\vartheta' \left(s_i \right) \right]^2 + \left(\frac{\| \chi' \left(s_i \right) \|'}{\sqrt{2 - \| \chi' \left(s_i \right) \|^2}} \right)^2 \right] + \sum_i \frac{k_i^m \varepsilon^2}{2} \left(\| \chi' \left(s_i \right) \| - 1 \right)^2 \tag{21}$$

Clearly, since the inextensibility case is just a special case of the quasi-inextensibility case, it is possible to show that this expression can be also obtained in a more direct way from (13) by setting $\tilde{l}^{\alpha S} \left(s_i \right) = 0$ and $k_{1,i}^f = k_{2,i}^f := k_i^f$.

3 Continuum-Limit Macro-model

In this section, by performing the final steps of the heuristic homogenization procedure presented throughout this paper, we derive a 1D continuum model, also referred to as the *macro-model,* associated to the aforementioned micro-structure. Besides, we analyse the quasi-inextensibility and inextensibility cases and we obtain the corresponding macro-model energies in terms of the displacement field χ.

3.1 Rescaling of Stiffnesses and Heuristic Homogenization

The preliminary step to perform the homogenization procedure consists into the definition of the quantities $\mathbb{K}_{\alpha\beta,i}^e$, $\mathbb{K}_{\alpha,i}^f$ and $\mathbb{K}_i^m$. These quantities are scale invariant, meaning that they do not depend on ε. Their role is to keep track of the asymptotic behaviour of the stiffnesses $k_{\alpha,\beta,i}^e$, $k_{\alpha,i}^f$, and k_i^m of the micro-model springs. More explicitly, we assume:

$$k_{\alpha\beta,i}^e(\varepsilon) = \frac{\mathbb{K}_{\alpha\beta,i}^e}{\varepsilon^3}; \qquad k_{\alpha,i}^f(\varepsilon) = \frac{\mathbb{K}_{\alpha,i}^f}{\varepsilon}; \qquad k_i^m(\varepsilon) = \frac{\mathbb{K}_i^m}{\varepsilon}. \tag{22}$$

We remark that in this rescaling, as ε approaches zero, the ratio between the stiffness $k_{\alpha\beta,i}^e$ of the oblique springs and the stiffness $k_{\alpha,i}^f$ will approach infinity with a rate of divergence in ε equal to two, i.e. $\frac{k_{\alpha\beta,i}^e}{k_{\alpha,i}^e} \sim \varepsilon^2$. Now, we are ready to perform the homogenization procedure. Firstly, we consider the more general quasi-inextensibility case. For simplicity, let us set

$$\mathbb{K}_{1D,i}^e = \mathbb{K}_{1S,i}^e = \mathbb{K}_{2D,i}^e = \mathbb{K}_{2S,i}^e := \mathbb{K}_i^e; \qquad \mathbb{K}_{1,i}^f = \mathbb{K}_{2,i}^f := \mathbb{K}_i^f. \tag{23}$$

Let us introduce the kinematical maps

$$\mathbb{K}^e : [0,B] \to \mathbb{R}^+; \qquad \mathbb{K}^f : [0,B] \to \mathbb{R}^+; \qquad \mathbb{K}^m : [0,B] \to \mathbb{R}^+$$

such that they satisfy the following Piola's ansatz:

$$\mathbb{K}^e\left(s_i\right) = \mathbb{K}_i^e; \qquad \mathbb{K}^f\left(s_i\right) = \mathbb{K}_i^f; \qquad \mathbb{K}^m\left(s_i\right) = \mathbb{K}_i^m. \tag{24}$$

Substituting (22) in (13), taking into account (23) and (24), and letting $\varepsilon \to 0$ yield

$$\begin{aligned}
&\mathcal{E} = \\
&\int_S \frac{\mathbb{K}^e}{2}\left(\tilde{l}^{1S}\right)^2 \mathrm{ds} + \int_S \frac{\mathbb{K}^e}{2}\left(\tilde{l}^{1D}\right)^2 \mathrm{ds} + \int_S \frac{\mathbb{K}^e}{2}\left(\tilde{l}^{2S}\right)^2 \mathrm{ds} + \int_S \frac{\mathbb{K}^e}{2}\left(\tilde{l}^{2D}\right)^2 \mathrm{ds} + \\
&+ \int_S \frac{\mathbb{K}^f}{2}\left\{\vartheta' + \frac{-\sqrt{2}\left(\|\chi'\|^2\right)' - 4\left[\left(\tilde{l}^{2D} - \tilde{l}^{2S}\right) - \left(\|\chi'\|^2 - 1\right)\left(\tilde{l}^{1D} - \tilde{l}^{1S}\right)\right]}{\|\chi'\|\sqrt{2 - \|\chi'\|^2}}\right\}^2 \mathrm{ds} + \\
&+ \int_S \frac{\mathbb{K}^f}{2}\left\{\vartheta' + \frac{\sqrt{2}\left(\|\chi'\|^2\right)' + 4\left[\left(\tilde{l}^{1D} - \tilde{l}^{1S}\right) + \left(\|\chi'\|^2 - 1\right)\left(\tilde{l}^{2S} - \tilde{l}^{2D}\right)\right]}{\|\chi'\|\sqrt{2 - \|\chi'\|^2}}\right\}^2 \mathrm{ds} + \\
&+ \int_S \frac{\mathbb{K}^m}{2}\left(\|\chi'\| - 1\right)^2 \mathrm{ds}.
\end{aligned} \tag{25}$$

which is the continuum-limit macro-model energy for a 1D pantographic beam under the hypothesis of quasi-inextensible oblique micro-springs. It is worth to remark that, when $\mathbb{K}^m = 0$, $\tilde{l}^{\alpha\beta} = 0$ and $\chi(s) = Cs\mathbf{e}_1$, with $C \in \mathbb{R}$, the beam undergoes a floppy mode i.e. (25) vanishes. Thus, under the above conditions, the configuration $\chi(s) = Cs\mathbf{e}_1$ is isoenergetic to the undeformed configuration for any C. For a fixed ε, considering $k_i^m = 0$ and $\tilde{l}_i^{\alpha\beta} = 0$ in the micro-model energy (13), we have that $\chi(s_i) = Cs_i\mathbf{e}_1$ is a floppy mode for the micro-model as well. This means that the homogenization procedure that we have carried out has preserved a key feature of the micro-model. Up to now, the expression of the continuum limit homogenized energy depends both on the kinematical maps χ and $\tilde{l}$. In the next section we show that, at equilibrium, it is possible to write the macro-energy in terms of the placement field only.

3.2 *Macro-model Energy as a Function of the Placement field*

We now equate to zero the first variations of (25) with respect to $\tilde{l}^{\alpha\beta}$'s, i.e. we look for stationary points, with respect to $\tilde{l}^{\alpha\beta}$, of (25). This is a necessary first order condition

for optimality. In the continuum limit homogenized energy no spatial derivatives of $\tilde{l}^{\alpha\beta}$ appear. Such energy depends only by linear and quadratic contributions in $\tilde{l}^{\alpha\beta}$. Hence, this process yields four algebraic linear equations in $\tilde{l}^{\alpha\beta}$. Solving these equations gives $\tilde{l}^{\alpha\beta}$ at equilibrium

$$\begin{aligned}
\tilde{l}^{1D} &= \frac{\sqrt{2}}{2}\mathbb{K}^f\left(\chi''\cdot C+\vartheta' D\right)\\
\tilde{l}^{2D} &= \frac{\sqrt{2}}{2}\mathbb{K}^f\left(\chi''\cdot C-\vartheta' D\right)\\
\tilde{l}^{1S} &= \frac{\sqrt{2}}{2}\mathbb{K}^f\left(-\chi''\cdot C-\vartheta' D\right)\\
\tilde{l}^{2S} &= \frac{\sqrt{2}}{2}\mathbb{K}^f\left(-\chi''\cdot C+\vartheta' D\right)
\end{aligned} \tag{26}$$

with

$$\begin{aligned}
C &= \frac{\chi'}{2\mathbb{K}^f\|\chi'\|^2-\frac{1}{2}\left(\mathbb{K}^e\|\chi'\|^2+8\mathbb{K}^f\right)}\\
D &= \frac{\|\chi'\|\sqrt{4\tilde{L}^2-\|\chi'\|^2}}{\mathbb{K}^e\tilde{L}^2\left(\|\chi'\|^2-2\right)-2\mathbb{K}^f\|\chi'\|^2}.
\end{aligned}$$

From (26) we can get, in some particular cases, interesting information about the properties of the pantographic beam. Firstly, let us notice that $\tilde{l}^{1D}=-\tilde{l}^{1S}$ and $\tilde{l}^{2D}=-\tilde{l}^{2S}$. Moreover, we also notice that when $\chi'=\rho\mathbf{e}_1$, with ρ independent of the abscissa s, then, as χ'' vanishes, $\tilde{l}^{\alpha\beta}=0$ i.e. the fibers undergo no elongation. Instead, when $\chi'(s)=\rho(s)\,\mathbf{e}_1$, with ρ depending on s, then $\tilde{l}^{1D}=\tilde{l}^{2D}=-\tilde{l}^{1S}=-\tilde{l}^{2S}$. This remarkable and counter-intuitive feature can be used as a possible benchmark test to validate, as ε approaches zero, a numerical scheme based on the discrete micro-model. Let us consider the case of non-zero bending curvature, i.e. $\vartheta'\neq 0$, when $\chi''\cdot C << \vartheta' D$, which implies that $\tilde{l}^{1D}=-\tilde{l}^{2D}=-\tilde{l}^{1S}=\tilde{l}^{2S}$. If $\vartheta'>0$ then $\tilde{l}^{1D},\tilde{l}^{2S}>0$ and $\tilde{l}^{2D},\tilde{l}^{1S}<0$ while, if $\vartheta'<0$ then $\tilde{l}^{1D},\tilde{l}^{2S}<0$ and $\tilde{l}^{2D},\tilde{l}^{1S}>0$. We are now ready to express the macro-model energy $\overline{\mathcal{E}}(\chi)$ as a function of the placement χ only, by substituting (26) in (25):

$$\overline{\mathcal{E}}\left(\chi\left(\cdot\right)\right) = \min_{\tilde{l}^{\alpha\beta}(\cdot)} \mathcal{E} =$$

$$\int_S \mathbb{K}^e\mathbb{K}^f \left\{ \frac{\left(\rho^2-2\right)}{\rho^2\left(\mathbb{K}^e-4\mathbb{K}^f\right)-2\mathbb{K}^e}\vartheta'^2 + \frac{\rho^2}{\left(2-\rho^2\right)\left[\rho^2\left(\mathbb{K}^e-4\mathbb{K}^f\right)+8\mathbb{K}^f\right]}\rho'^2 \right\} \mathrm{ds} +$$

$$+ \int_S \frac{\mathbb{K}^m}{2}\left(\rho-1\right)^2 \mathrm{ds} =$$

$$= \int_S \frac{\mathbb{K}^e\mathbb{K}^f\left(\|\chi'\|^2-2\right)}{\|\chi'\|^4\left[\|\chi'\|^2\left(\mathbb{K}^e-4\mathbb{K}^f\right)-2\mathbb{K}^e\right]}\left(\chi'_\perp\cdot\chi''\right)^2 \mathrm{ds} +$$

$$+ \int_S \frac{\mathbb{K}^e\mathbb{K}^f}{\left(2-\|\chi'\|^2\right)\left[\|\chi'\|^2\left(\mathbb{K}^e-4\mathbb{K}^f\right)+8\mathbb{K}^f\right]}\left(\chi'\cdot\chi''\right)^2 \mathrm{ds} +$$

$$+ \int_S \frac{\mathbb{K}^m}{2}\left(\|\chi'\|-1\right)^2 \mathrm{ds}. \tag{27}$$

We observe that, for $0 < \rho < \sqrt{2}$ and for any choice of the positive macro-stiffnesses $\mathbb{K}^e$, $\mathbb{K}^f$ and $\mathbb{K}^m$, (27) is positive definite. Moreover, not only we can classify this homogenized model as a second gradient theory, but we notice that the full second gradient χ'' of χ contributes to the strain energy. Indeed, beyond the usual term $\left(\chi'_\perp\cdot\chi''\right)$ related to the Lagrangian curvature, also the term $\left(\chi'\cdot\chi''\right)$, deriving from the presence of the oblique springs, appears. There is a remarkable feature in this model which deserves to be discussed. From (27), it is clear that in the limit $||\chi'|| \to \sqrt{2}$ the model exhibits a so-called phase transition: it locally degenerates into the model of an uniformly extensible cable, notwithstanding that $\sqrt{2}$ is an upper bound for ρ. Indeed,

$$\frac{\left(\rho^2-2\right)}{\rho^2\left(\mathbb{K}^e-4\mathbb{K}^f\right)-2\mathbb{K}^e} \to 0$$

$$\frac{\rho^2}{\left(2-\rho^2\right)\left[\rho^2\left(\mathbb{K}^e-4\mathbb{K}^f\right)+8\mathbb{K}^f\right]} \to +\infty,$$

so that no deformation energy is stored for finite bending curvature and, in order for the energy to be bounded for bounded deformations, ρ' must approach zero, meaning that the elongation must be locally uniform. Further developments of this model could consist in contemplating a phase transition to a model that, for finite bending curvature, entails a non-zero stored deformation energy.

3.2.1 Non-dimensionalization

In order to handle more easily the model in the numerical implementation and in the interpretation of the corresponding results, we turn to the use of non-dimensional

quantities. Therefore, we introduce the following non-dimensional fields:

$$s = B\bar{s}; \qquad \chi = B\overline{\chi}; \qquad \mathbb{K}^e = K\overline{\mathbb{K}}^e; \qquad \mathbb{K}^f = K\overline{\mathbb{K}}^f; \qquad \mathbb{K}^m = K^m\overline{\mathbb{K}}^m.$$

In terms of these new quantities, we can recast (27) as

$$\begin{aligned}
&\frac{K}{B}\int_0^1 \frac{\overline{\mathbb{K}}^e\overline{\mathbb{K}}^f\left(\|\overline{\chi}'\|^2-2\right)}{\|\overline{\chi}'\|^4\left[\|\overline{\chi}'\|^2\left(\overline{\mathbb{K}}^e-4\overline{\mathbb{K}}^f\right)-2\overline{\mathbb{K}}^e\right]}\left(\overline{\chi}'_\perp\cdot\overline{\chi}''\right)^2 \mathrm{d}\bar{s} + \\
&+\frac{K}{B}\int_0^1 \frac{\overline{\mathbb{K}}^e\overline{\mathbb{K}}^f\left(\overline{\chi}'\cdot\overline{\chi}''\right)^2}{\left(2-\|\overline{\chi}'\|^2\right)\left[\|\overline{\chi}'\|^2\left(\overline{\mathbb{K}}^e-4\overline{\mathbb{K}}^f\right)+8\overline{\mathbb{K}}^f\right]}\mathrm{d}\bar{s} + \\
&+K^mB\int_0^1 \frac{\overline{\mathbb{K}}^m}{2}\left(\|\overline{\chi}'\|-1\right)^2 \mathrm{d}\bar{s}
\end{aligned} \tag{28}$$

where the symbol <<$\bar{\ }$>> denotes differentiation with respect to the dimensionless abscissa $\bar{s}$.

3.3 The Inextensibility Case

Let us focus now on the inextensibility case. The homogenization procedure follows the same lines of the previous case. Indeed, keeping in mind (23) and (24), letting $\varepsilon \to 0$ in (21) yields the continuum-limit macro-model energy for the inextensibility case

$$\begin{aligned}
&\int_S \left\{\mathbb{K}^f\left[\vartheta'^2+\frac{\rho'^2}{2-\rho^2}\right]+\frac{\mathbb{K}^m}{2}(\rho-1)^2\right\}\mathrm{ds} = \\
&=\int_S\left\{\mathbb{K}^f\left[\frac{\left(\chi_\perp\cdot\chi''\right)^2}{\|\chi'\|^4}+\frac{\left(\chi\cdot\chi''\right)^2}{\|\chi'\|^2\left(2-\|\chi'\|^2\right)}\right]+\frac{\mathbb{K}^m}{2}\left(\|\chi'\|-1\right)^2\right\}\mathrm{ds}.
\end{aligned} \tag{29}$$

This result is consistent with the quasi-inextensibility case. Indeed, we could have found (29) also by letting $\mathbb{K}^e \to +\infty$ in (27). Let us remark that, also in this case, the homogenized continuum model, due to the richness of the mictrostructure, gives rise to a full second gradient theory.

3.3.1 Linearization

An interesting connection can be traced with the existing literature on the formulation of 1D continuum homogenized model for microstructured media and, in particular, for pantographic ones. Indeed, this connection is traced by considering a linearization of the pantographic beam energy in the (complete) inextensibility case. We set $\chi(s) = \begin{pmatrix} s \\ 0 \end{pmatrix} + \eta\tilde{u}$, with $\tilde{u}$ independent of η, i.e. we linearize with respect to the displacement $u = \chi(s) - \begin{pmatrix} s \\ 0 \end{pmatrix}$, and $\mathbb{K}^m = 0$. By means of simple algebra manipulations it is possible to derive the deformation energy in Eq. (5) (with $K^+ = K^-$) of [10] (see also [21]):

$$\int_S \mathbb{K}^f \|u''\|^2 \, \mathrm{ds}. \tag{30}$$

We remark that in the linearized energy (30) the transverse displacement and the axial one decouple.

4 Numerical Simulations

In the sequel, $\mathbb{K}^m = 0$ will be considered, which means that the standard quadratic additive elongation/shortening contribution to the deformation energy will be turned off. This is made in order to better highlight some non-standard features of the nearly-inextensible pantographic beam model. In this section we show numerical results for the quasi-inextensible and inextensible pantographic beam model and for the geometrically non-linear Euler model. We remind that these cases stand for $\mathbb{K}^e < +\infty$ and $\mathbb{K}^e \to +\infty$, respectively. Two benchmark tests are exploited in order to illustrate peculiar and non-standard features of the pantographic beam model. Convergence of the quasi-inextensible pantographic beam model to the completely inextensible one is shown, by means of a numerical example, as the macro-stiffness $\mathbb{K}^e$ related to elongation of the oblique springs approaches $+\infty$. This is due to the fact that, as it is clear from Eq. (25), if $\mathbb{K}^e \to +\infty$, then $\tilde{l}^{\alpha\beta} \to 0$. Of course, the same discussion and simulations can be made for the micro-model and this could be the subject of a further investigation. For the sake of self-consistence, we recall that the deformation energy of the geometrically non-linear Euler model employed in the following simulations is the following

$$\int_S \left\{ \frac{K^e}{2} \left(\|\chi'\| - 1 \right)^2 + \frac{K^b}{2} \left[\frac{\chi'' \cdot \chi''}{\|\chi'\|^2} - \left(\frac{\chi' \cdot \chi''}{\|\chi'\|^2} \right)^2 \right] \right\} \, \mathrm{ds} =$$

$$= \int_S \left\{ \frac{K^e}{2} (\rho - 1)^2 + \frac{K^b}{2} \vartheta'^2 \right\} \, \mathrm{ds}$$

and we notice that, while in the nearly-inextensible pantographic beam model both ρ and ϑ can be enforced at the boundary, for the non-linear Euler model it can be done for ϑ only, as no spatial derivative of ρ appears in the energy.

4.1 Semi-circle Test

We consider for both the nearly-inextensible pantographic beam model and the geometrically non-linear Euler beam model the reference domain to be the interval $[0, 2\pi]$. We enforce the following boundary conditions for both models

$$1.\ \chi(0) = \mathbf{0}; \quad 2.\ \chi(2\pi) = 2\mathbf{e}_{1;} \quad 3.\ \vartheta(0) = -\frac{\pi}{2}; \quad 4.\ \vartheta(2\pi) = \frac{\pi}{2}$$

and, for the nearly-inextensible pantographic beam model, we also have the following two additional constraints

$$5.\ \rho(0) = \rho_0; \quad 6.\ \rho(2\pi) = \rho_0.$$

In Fig. 3 (up) the deformed shapes for the nearly-inextensible pantographic beam model and for the geometrically non-linear Euler beam model (GNEM) are shown for different values of ρ_0 reported in the legend. In Fig. 3 (down) the elongation $\rho - 1$ for the nearly-inextensible pantographic beam model and for the geometrically non-linear Euler beam model (GNEM) is shown for different values of ρ_0 reported in the legend. It is remarkable that passing from $\rho_0 > 1$ to $\rho < 1$ there is a change of concavity in the elongation for the pantographic beam model. In Fig. 4 (up) the deformed shapes for the nearly-inextensible pantographic beam model (blue) and for the inextensible pantographic beam model (green) with $\rho_0 = 1.4$ are compared. Of course, the area spanned by the quasi-inextensible pantographic beam includes that

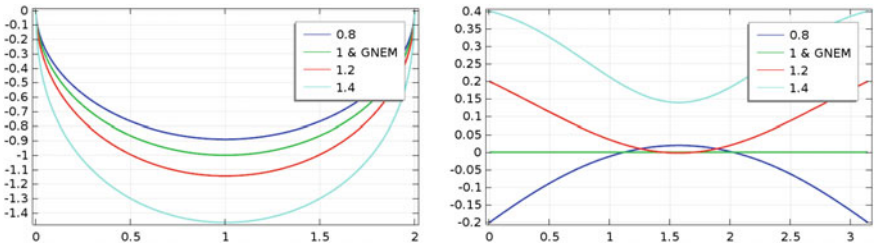

Fig. 3 Semi-circle test. Deformed shapes for the nearly-inextensible pantographic beam model and for the geometrically non-linear Euler beam model (GNEM). (left). Elongation $\rho - 1$ versus the reference abscissafor the nearly-inextensible pantographic beam model and for the geometrically non-linear Euler beam model (GNEM) (right). Numbers in the legends stands for different dimensionless values of ρ_0

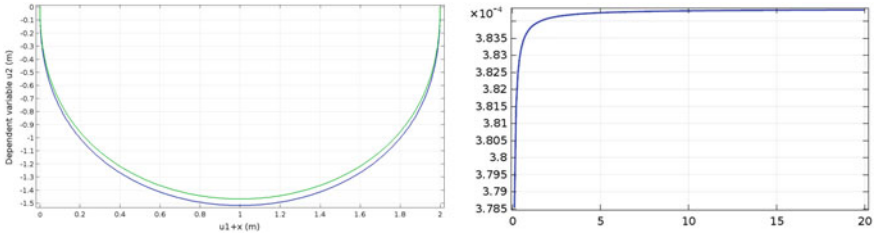

Fig. 4 Semi-circle test. Deformed shapes for the nearly-inextensible pantographic beam model (blue) and for the inextensible pantographic beam model (green) with $\rho_0 = 1.4$ (left). Energy of the nearly-inextensible pantographic beam model (ordinate) asymptotically tends to the energy of the inextensible pantographic beam model (asymptote) as $\mathbb{K}^e$ (abscissa) $\to +\infty$ (right)

of the (completely) inextensible one. In Fig. 4 (down) it is numerically shown that the energy of the nearly-inextensible pantographic beam model (ordinate) asymptotically tends to the energy of the inextensible pantographic beam model (asymptote) as $\mathbb{K}^e$ (abscissa) $\to +\infty$.

4.2 Three-Point Test

We consider for both the quasi-inextensible pantographic beam model and the geometrically non-linear Euler beam model the reference domain to be the interval $[0, 2]$. We enforce the following boundary conditions for both models:

$$1.\ \chi(0) = \mathbf{0}; \quad 2.\ \chi(1) \cdot \mathbf{e}_2 = \overline{u}; \quad 3.\ \chi(2) = \mathbf{0}; \quad 4.\ \vartheta(0) = 0; \quad 5.\ \vartheta(2) = 0.$$

In Fig. 5 the deformed shapes for the nearly-inextensible pantographic beam model (red, light blue) and for the geometrically non-linear Euler beam model (blue, green) are shown for different values of $\overline{u}$ in the legend. Figure 6 shows, for different values of the parameter $\overline{u}$, the elongation $\rho - 1$ versus the reference abscissa for the nearly-inextensible pantographic beam model. The parameter $\overline{u}$ is increasing from bottom to top. We observe that, as $\overline{u}$ increases, at some point, there is a concavity change in the elongation plot and, increasing further the parameter $\overline{u}$, curves start to intersect. This means that, for some points of the beam an increase of the prescribed displacement $\overline{u}$ implies a decrease in the elongation. Figure 7 shows the pulling force, i.e. Lagrange multiplier associated to the weak constraint $\chi(1) \cdot \mathbf{e}_2 = \overline{u}$, changed of sign, applied at the midpoint in order to vertically displace it of an amount $\overline{u}$. In the nearly-inextensible pantographic beam model (blue) negative stiffness property, also known as elastic softening, is observed, while in the geometrically non-linear Euler beam model (green) elastic softening is not observed. Figure 8 shows the plot of $\tilde{l}^{1D}$ versus reference abscissa for different values of $\overline{u}$ in the legend. Analogous plots hold for $\tilde{l}^{2D}$, $\tilde{l}^{1S}$ and $\tilde{l}^{2S}$.

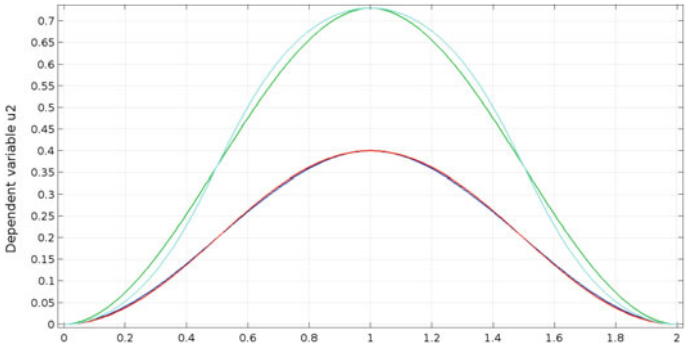

Fig. 5 Three-point test. Deformed shapes for the nearly-inextensible pantographic beam model (red, light blue) and for the geometrically non-linear Euler beam model (blue, green) for different values of $\overline{u}$ in the legend

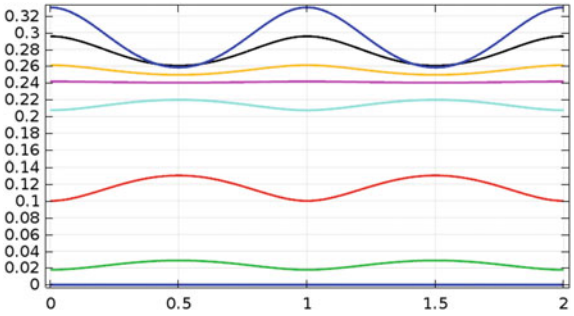

Fig. 6 Three-point test. Elongation $\rho - 1$ versus the reference abscissa for the nearly-inextensible pantographic beam model. The parameter $\overline{u}$ is increasing from bottom to top. We observe that, While increasing $\overline{u}$, there is a concavity change at some point. Increasing further the parameter $\overline{u}$, curves start to intersect

4.3 Modified Three-Point Test

We consider for both the quasi-inextensible pantographic beam model and the geometrically non-linear Euler beam model the reference domain to be the interval $[0, 2]$. We enforce the three-point test boundary conditions for both models

$$1.\ \chi(0) = \mathbf{0}; \quad 2.\ \chi(1) \cdot \mathbf{e}_2 = \overline{u}; \quad 3.\ \chi(2) = \mathbf{0}; \quad 4.\ \vartheta(0) = 0; \quad 5.\ \vartheta(2) = 0$$

with the additional condition, at the midpoint $s = 1$,

$$6.\ \rho(1) \simeq \sqrt{2}.$$

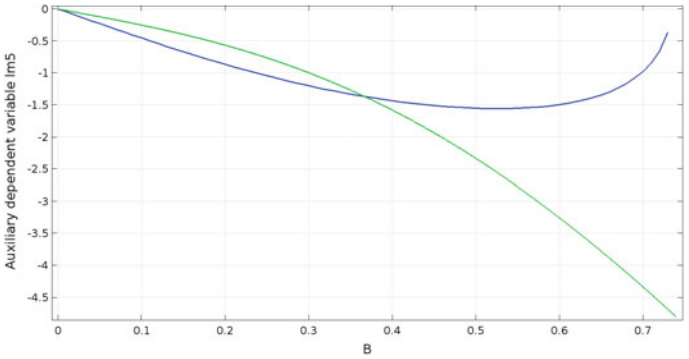

Fig. 7 Three-point test. Pulling force (i.e. Lagrange multiplier associated to the weak constraint $\chi(1) \cdot \mathbf{e}_2 = \overline{u}$), changed of sign, applied at the midpoint in order to vertically displace it of an amount $\overline{u}$ (abscissa). In the nearly-inextensible pantographic beam model (blue) elastic softening is observed, while in the geometrically non-linear beam model (green) elastic softening is not observed

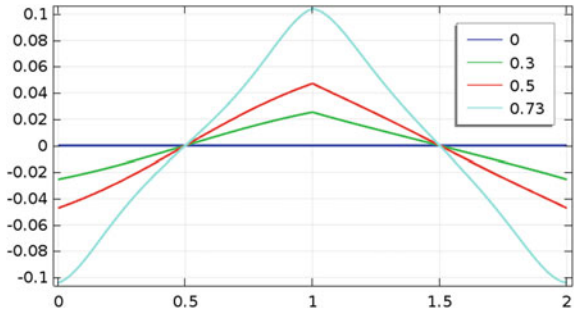

Fig. 8 Three-point test. Plot of $\tilde{l}^{1D}$ versus reference abscissa for different values of $\overline{u}$ in the legend. Analogous plots hold for $\tilde{l}^{2D}$, $\tilde{l}^{1S}$ and $\tilde{l}^{2S}$

Fig. 9 shows the deformed configuration for the nearly-inextensible pantographic beam model, while in Fig. 10 the elongation $\rho - 1$ versus the reference abscissa for the nearly-inextensible pantographic beam model is shown.

5 Euler-Lagrange Equations

Let us consider an internal (potential) unit line energy density of the form

$$W = \frac{G(\rho)}{2}\rho'^2 + \frac{F(\rho)}{2}\vartheta'^2 + H(\rho) \tag{31}$$

with ρ and ϑ such that $\chi' = \rho\left(\cos\vartheta\mathbf{e}_1 + \sin\vartheta\mathbf{e}_2\right) = \rho\mathbf{e}(\vartheta)$, and G, F, H functions from $\mathbb{R}^+ \supseteq A$ to $\mathbb{R}^+$. We recall that $\rho' = \frac{\chi''\cdot\chi'}{\|\chi'\|}$, $\vartheta' = \frac{\chi''\cdot\chi'_\perp}{\|\chi'\|^2}$. We remark that, when

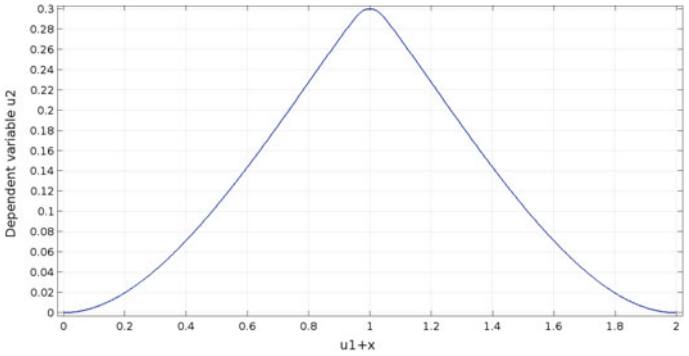

Fig. 9 Modified three-point test. Deformed configuration for the nearly-inextensible pantographic beam model

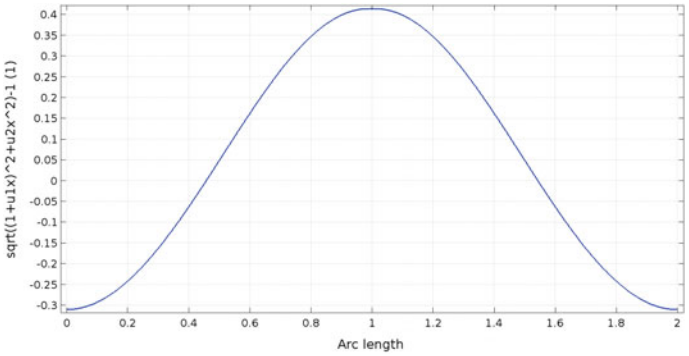

Fig. 10 Modified three-point test. Elongation $\rho - 1$ versus reference abscissa for the nearly-inextensible pantographic beam model

the specialization

$$\begin{cases} G(\rho) = 0 \\ F(\rho) = K^b \geq 0 \\ H(\rho) = \frac{K^e}{2}(\rho - 1)^2, \ K^e \geq 0 \end{cases} \tag{32}$$

of (31) is considered, we find the geometrically nonlinear Euler model while, when the specialization

$$\begin{cases} G(\rho) = \mathbb{K}^e \mathbb{K}^f \frac{\rho^2}{(2-\rho^2)\left[\rho^2\left(\mathbb{K}^e - 4\mathbb{K}^f\right) + 8\mathbb{K}^f\right]}, \ \mathbb{K}^e \geq 0, \ \mathbb{K}^f \geq 0 \\ F(\rho) = \mathbb{K}^e \mathbb{K}^f \frac{(\rho^2 - 2)}{\rho^2\left(\mathbb{K}^e - 4\mathbb{K}^f\right) - 2\mathbb{K}^e}, \ \mathbb{K}^e \geq 0, \ \mathbb{K}^f \geq 0 \\ H(\rho) = \frac{\mathbb{K}^m}{2}(\rho - 1)^2, \ \mathbb{K}^m > 0 \end{cases} \tag{33}$$

of (31) is considered, we find the nearly-inextensible pantographic beam model. We now consider the functional

$$\begin{aligned}
&\mathcal{E}(\rho(\cdot),\vartheta(\cdot),\chi(\cdot),\Lambda(\cdot)) = \\
&= \int_S \left\{ W - b^{ext}\cdot\chi - \mu^{ext}\cdot\vartheta + \Lambda\cdot\left[\chi' - \rho\mathbf{e}(\vartheta)\right] \right\} \,\mathrm{ds} + \\
&- \sum_{s=0,L} R^{ext}(s)\cdot\chi(s) - \sum_{s=0,L} M^{ext}(s)\cdot\vartheta(s),
\end{aligned} \tag{34}$$

where $\int_S b^{ext}\cdot\chi + \mu^{ext}\cdot\vartheta \,\mathrm{ds} + \sum_{s=0,L} R^{ext}(s)\cdot\chi(s) + \sum_{s=0,L} M^{ext}(s)\cdot\vartheta(s)$ is the work done by external distributed and concentrated forces and couples. The first variation of the functional $\mathcal{E}$ in (34) is

$$\begin{aligned}
&\delta\mathcal{E}(\rho(\cdot),\vartheta(\cdot),\chi(\cdot),\Lambda(\cdot),\delta\rho(\cdot),\delta\vartheta(\cdot),\delta\chi(\cdot),\delta\Lambda(\cdot)) = \\
&= \int_S \left\{ \frac{1}{2}\frac{\partial G}{\partial\rho}(\rho)\rho'^2 + \frac{1}{2}\frac{\partial F}{\partial\rho}(\rho)\vartheta'^2 + \frac{\partial H}{\partial\rho}(\rho) - \Lambda\cdot\mathbf{e}(\vartheta) - \left[G(\rho)\rho'\right]' \right\}\delta\rho \,\mathrm{ds} + \\
&+ \int_S \left\{ -\left[F(\rho)\vartheta'\right]' - \mu - \Lambda\times\chi' \right\}\delta\vartheta + \left(-b - \Lambda'\right)\cdot\delta\chi + \left[\chi' - \rho\mathbf{e}(\vartheta)\right]\cdot\delta\Lambda \,\mathrm{ds} + \\
&+ \left[G(\rho)\rho'\delta\rho\right]_0^L + \left\{\left[F(\rho)\vartheta' - M^{ext}\right]\delta\vartheta\right\}_0^L + \left[\left(\Lambda - R^{ext}\right)\cdot\delta\chi\right]_0^L = \\
&= \int_S \left\{ \frac{1}{2}\frac{\partial F}{\partial\rho}(\rho)\vartheta'^2 + \frac{\partial H}{\partial\rho}(\rho) - \frac{1}{2}\frac{\partial G}{\partial\rho}(\rho)\rho'^2 - \Lambda\cdot\mathbf{e}(\vartheta) - G(\rho)\rho'' \right\}\delta\rho \,\mathrm{ds} + \\
&+ \int_S \left\{ -\left[F(\rho)\vartheta'\right]' - \mu - \Lambda\times\chi' \right\}\delta\vartheta + \left(-b - \Lambda'\right)\cdot\delta\chi + \left[\chi' - \rho\mathbf{e}(\vartheta)\right]\cdot\delta\Lambda \,\mathrm{ds} + \\
&+ \left[G(\rho)\rho'\delta\rho\right]_0^L + \left\{\left[F(\rho)\vartheta' - M^{ext}\right]\delta\vartheta\right\}_0^L + \left[\left(\Lambda - R^{ext}\right)\cdot\delta\chi\right]_0^L.
\end{aligned}$$

By applying the Fundamental Lemma of Calculus of Variations, we find the Euler-Lagrange equations:

1. $\frac{1}{2}\frac{\partial G}{\partial\rho}(\rho)\rho'^2 + \frac{1}{2}\frac{\partial F}{\partial\rho}(\rho)\vartheta'^2 + \frac{\partial H}{\partial\rho}(\rho) - \Lambda\cdot\mathbf{e}(\vartheta) - \left[G(\rho)\rho'\right]' = 0$
2. $\left[F(\rho)\vartheta'\right]' + \mu + \Lambda\times\chi' = 0$
3. $b + \Lambda' = 0$
4. $\chi' - \rho\mathbf{e}(\vartheta) = 0$

and the corresponding boundary conditions:

$$G(\rho(0)) = 0 \vee \rho'(0) = 0 \vee \text{Dirichlet Conditions on } \rho \text{ in } s = 0$$
$$G(\rho(L)) = 0 \vee \rho'(L) = 0 \vee \text{Dirichlet Conditions on } \rho \text{ in } s = L$$

$$F(\rho(0))\vartheta'(0) - M^{ext}(0) = 0 \vee \text{Dirichlet Conditions on } \vartheta \text{ in } s = 0$$
$$F(\rho(L))\vartheta'(L) - M^{ext}(L) = 0 \vee \text{Dirichlet Conditions on } \vartheta \text{ in } s = L$$

$$\Lambda(0) - R^{ext}(0) = 0 \vee \text{Dirichlet Conditions on } \chi \text{ in } s = 0$$
$$\Lambda(L) - R^{ext}(L) = 0 \vee \text{Dirichlet Conditions on } \chi \text{ in } s = L.$$

We now analyze the two specializations (32) and (33) of (31). Let us first analyze (32). The Euler-Lagrange equations reduce to

$$\begin{aligned}
&1.\ K^e(\rho - 1) - \Lambda \cdot \mathbf{e}(\vartheta) = 0\\
&2.\ \left[K^b\vartheta'\right]' + \mu + \Lambda \times \chi' = 0\\
&3.\ b + \Lambda' = 0\\
&4.\ \chi' - \rho\mathbf{e}(\vartheta) = 0,
\end{aligned} \tag{35}$$

complemented with the following boundary conditions

$$K^b\vartheta'(0) - M^{ext}(0) = 0 \vee \text{Dirichlet Conditions on } \vartheta \text{ in } s = 0$$
$$K^b\vartheta'(L) - M^{ext}(L) = 0 \vee \text{Dirichlet Conditions on } \vartheta \text{ in } s = L$$

$$\Lambda(0) - R^{ext}(0) = 0 \vee \text{Dirichlet Conditions on } \chi \text{ in } s = 0$$
$$\Lambda(L) - R^{ext}(L) = 0 \vee \text{Dirichlet Conditions on } \chi \text{ in } s = L. \tag{36}$$

We notice that $(35)_1$ is an algebraic equation in ρ, and it gives:

$$\rho = 1 + \frac{\Lambda \cdot \mathbf{e}(\vartheta)}{K^e}. \tag{37}$$

The direct integration of Eq. $(35)_3$ gives:

$$\Lambda = \int_0^s b \, \mathrm{ds} + R^{ext}(0), \tag{38}$$

while, plugging (38) in (37) yields

$$\rho = 1 + \frac{\left[\int_0^s b \, \mathrm{ds} + R^{ext}(0)\right] \cdot \mathbf{e}(\vartheta)}{K^e}, \tag{39}$$

and plugging (39) and (38) in $(35)_2$ yields

$$\left[K^b \vartheta'\right]' + \mu + \Lambda \times \left(1 + \frac{\Lambda \cdot \mathbf{e}(\vartheta)}{K^e}\right) \mathbf{e}(\vartheta) = 0,$$

which is a 2nd order O.D.E. in the unknown ϑ. This O.D.E. is complemented with boundary conditions $(36)_{1,2}$. Finally, one recovers χ by integrating $(35)_4$ and by using the Dirichlet boundary conditions on χ. Let us turn to the study of the specialization (33) of the unit line potential energy density in Eq. (31). By explicitly computing the partial derivatives of the functions F, G, H with respect to ρ, we get the following Euler-Lagrange equations for the nearly-inextensible pantographic beam model:

1. $$\frac{\mathbb{K}^e\mathbb{K}^f\left[16\mathbb{K}^f\rho + (\mathbb{K}^e - 4\mathbb{K}^f)\rho^5\right]}{(\rho^2-2)^2\left[(\mathbb{K}^e - 4\mathbb{K}^f)\rho^2 + 8\mathbb{K}^f\right]^2}\rho'^2 - \frac{16\mathbb{K}^e\left(\mathbb{K}^f\right)^2\rho}{\left[(\mathbb{K}^e - 4\mathbb{K}^f)\rho^2 - 2\mathbb{K}^e)\right]^2}\vartheta'^2 + \mathbb{K}^m(\rho-1) - \Lambda\cdot\mathbf{e}(\vartheta) +$$
$$-\left[\mathbb{K}^e\mathbb{K}^f\frac{\rho^2\rho'}{\left(2-\rho^2\right)\left[\rho^2\left(\mathbb{K}^e - 4\mathbb{K}^f\right) + 8\mathbb{K}^f\right]}\right]' = 0$$
2. $$\left[\mathbb{K}^e\mathbb{K}^f\frac{\left(\rho^2-2\right)}{\rho^2\left(\mathbb{K}^e - 4\mathbb{K}^f\right) - 2\mathbb{K}^e}\vartheta'\right]' + \mu + \Lambda\times\chi' = 0$$
3. $b + \Lambda' = 0$
4. $\chi' - \rho\mathbf{e}(\vartheta) = 0,$

complemented with the following boundary conditions:

$$\rho'(0) = 0 \vee \text{Dirichlet Conditions on } \rho \text{ in } s = 0$$
$$\rho'(L) = 0 \vee \text{Dirichlet Conditions on } \rho \text{ in } s = L$$

$$\mathbb{K}^e\mathbb{K}^f\frac{\left(\rho^2(0)-2\right)}{\rho^2(0)\left(\mathbb{K}^e - 4\mathbb{K}^f\right) - 2\mathbb{K}^e}\vartheta'(0) - M^{ext}(0) = 0 \vee \text{Dirichlet Conditions on } \vartheta \text{ in } s = 0$$
$$\mathbb{K}^e\mathbb{K}^f\frac{\left(\rho^2(L)-2\right)}{\rho^2(L)\left(\mathbb{K}^e - 4\mathbb{K}^f\right) - 2\mathbb{K}^e}\vartheta'(L) - M^{ext}(L) = 0 \vee \text{Dirichlet Conditions on } \vartheta \text{ in } s = L$$
$$\Lambda(0) - R^{ext}(0) = 0 \vee \text{Dirichlet Conditions on } \chi \text{ in } s = 0$$
$$\Lambda(L) - R^{ext}(L) = 0 \vee \text{Dirichlet Conditions on } \chi \text{ in } s = L.$$

For the (completely) inextensible pantographic beam model, from Eq. (29) we have that:

$$
\begin{aligned}
G(\rho) &= \frac{2\mathbb{K}^f}{2-\rho^2} \\
F(\rho) &= 2\mathbb{K}^f \\
H(\rho) &= \mathbb{K}^m(\rho-1)^2.
\end{aligned}
$$

Therefore, Euler-Lagrange equations for the inextensible pantographic beam model recast as

1. $\frac{2\rho\mathbb{K}^f}{(2-\rho^2)^2}\rho'^2 + 2\mathbb{K}^m(\rho-1) - \Lambda\cdot\mathbf{e}(\vartheta) - \left[\frac{2\mathbb{K}^f}{2-\rho^2}\rho'\right] = 0'$
2. $\mu + \Lambda\times\chi' = 0$
3. $b + \Lambda' = 0$
4. $\chi' - \rho\mathbf{e}(\vartheta) = 0,$

complemented with the following boundary conditions:

$$
\begin{aligned}
&\rho'(0) = 0 \vee \text{Dirichlet Conditions on } \rho \text{ in } s = 0 \\
&\rho'(L) = 0 \vee \text{Dirichlet Conditions on } \rho \text{ in } s = L \\
&2\mathbb{K}^f\vartheta'(0) - M^{ext}(0) = 0 \vee \text{Dirichlet Conditions on } \vartheta \text{ in } s = 0 \\
&2\mathbb{K}^f\vartheta'(L) - M^{ext}(L) = 0 \vee \text{Dirichlet Conditions on } \vartheta \text{ in } s = L \\
&\Lambda(0) - R^{ext}(0) = 0 \vee \text{Dirichlet Conditions on } \chi \text{ in } s = 0 \\
&\Lambda(L) - R^{ext}(L) = 0 \vee \text{Dirichlet Conditions on } \chi \text{ in } s = L.
\end{aligned}
$$

We believe that the use of the techniques employed in [74], which have been exploited to analytically determine remarkable properties of the extensible Euler beam model in finite deformation regime, can be fruitfully applied to the examined pantographic beam model. Also the numerical exploitation of the Euler-Lagrange equations through, e.g., a shooting method, could be useful to explore the set of solutions. This might be of help in shedding light on the mathematical properties of the quasi-inextensible and inextensible pantographic beam models.

6 Conclusions

In this work, we have modeled and analyzed a pantographic microstructure giving rise, after a homogenization procedure, to a $1D$ continuum model for a beam which

exhibits many interesting non-standard features. We have provided a characterization of the kinematics of the proposed discrete Hencky-type spring model which resembles the geometrical arrangement of a pantographic strip. Once the kinematics of the micro-model has been discussed, we have given a mechanical characterization of the micro-system, by specifying the general form of the deformation energy. Subsequently, we postulated an asymptotic expansion for one of the microscopic descriptors, i.e. the elongation of the oblique springs. Besides, by choosing the value of the first-order term of this expansion, we considered the so-called quasi-inextensibility case, which corresponds to the quasi-inextensibility of the oblique springs. Successively, following the Piola's ansatz, we introduced the so-called kinematical maps, i.e. some fields in the macroscopic model that uniquely determine the microscopic kinematical descriptors. By means of these kinematical maps, namely the placement function χ and the elongation of the oblique springs $\tilde{l}^{\alpha\beta}$, we have written the micro-model energy for the quasi-inextensibility case in terms of macroscopic descriptors. The resulting micro-model energy contains already a contribution from the second gradient of $\chi(s)$ and it provides an upper bound $||\chi'|| < \sqrt{2}$, even if no kinematic restrictions directly affect $||\chi'||$. Successively, we have considered the case of (completely) inextensible oblique springs by means of two equivalent procedures. We also verified that, as it is obvious, requiring the kinematic descriptor $\tilde{l}^{\alpha\beta}$, standing for the elongation of the oblique springs, to vanish implies that the quasi-inextensible pantographic beam model specializes to the (completely) inextensible pantographic beam model. In order to give a better insight into the peculiar properties of this problem, we also derived "ab imis fundamentis" the micro-model energy of the inextensible pantographic beam model, whose kinematics is characterized by the positions p_i only, as a function of the macroscopic kinematical descriptor χ evaluated in s_i's. Following a procedure analogue to the quasi-inextensibility case, we defined the micro-model energy for the inextensibility case and, once the kinematical maps was introduced by means of the Piola's ansatz, we have written it in terms of these macroscopic descriptors. Then, we have imposed the so-called internal connection constraint, which ensures that, in the deformed configuration, the upper-left spring of the i-th cell is hinge-joint with the upper-right spring of the $(i-1)$-th cell, and the lower-left spring of the i-th cell is hinge-joint with lower-right spring of the $(i-1)$-th cell. After that, we have performed a heuristic homogenization procedure in order to derive a $1D$ continuum model, also referred to as the macro-model and characterized by its deformation energy, associated to the aforementioned microstructure in the quasi-inextensibility and inextensibility cases. The preliminary step to perform the homogenization procedure has been to define scale-invariant quantities, whose role is to keep track of the asymptotic behaviour of the stiffnesses of the micro-model springs. We first performed the homogenization procedure for the quasi-inextensibility case by computing the limit $\varepsilon \to 0$ in the expression of the micro-model energy written in terms of macroscopic kinematical descriptors. The resulting continuum-limit macro-model energy describes a $1D$ pantographic beam under the hypothesis of quasi-inextensible oblique micro-springs. The macroscopic beam, when $\mathbb{K}^m = 0$, $\tilde{l}^{\alpha\beta} = 0$, and $\chi(s) = Cs\boldsymbol{e}_1$, undergoes a floppy mode. This is

a key feature of the micro-model energy which was preserved by the homogenization procedure that we have carried out. Moreover, we observed that not only this homogenized model can be classified as a second gradient theory, but we noticed that the full second gradient χ'' of χ contributes to the strain energy. Indeed, beyond the usual term $(\chi'_{\perp} \cdot \chi'')$ related to the Lagrangian curvature, also the term $(\chi' \cdot \chi'')$, deriving from the presence of the oblique springs, appears. Finally, we remarked that, in the limit $||\chi'|| \to \sqrt{2}$, the model exhibits a so-called phase transition, i.e. it locally degenerates into the model of an uniformly extensible cable, notwithstanding that $\sqrt{2}$ is an upper bound for ρ. Subsequently, we have performed the homogenization procedure also for the (complete) inextensibility case. The homogenization procedure has followed the same lines of the quasi-inextensibility case and it yields a continuum-limit macro-model energy consistent with the quasi-inextensibility case. An interesting connection with the existing literature on $1D$ continuum homogenized models for microstructured media, and in particular for pantographic ones, has been traced by considering the linearization of the pantographic beam energy in the (complete) inextensibility case. Furthermore, it has to be remarked that, of course, what has been presented in this paper is not the only possible homogenization technique. Indeed, many other procedures, like coarse-graining, hydrodynamical limits [76–79] for many-particle systems, and computational homogenization [80–82], are being employed in literature, and they deserve to be better understood. The numerical solution of the homogenised continuum model has been addressed by means of the finite element method in three exemplary cases, trying to highlight the main differences with the classical finite deformation Euler beam model. In particular, in order to better highlight some non-standard features of the nearly-inextensible pantographic beam model, we have considered as vanishing the standard quadratic additive elongation/shortening contribution to the deformation energy. These benchmark tests were exploited in order to illustrate some peculiar features of the pantographic beam model and the convergence of the quasi-inextensible pantographic beam model to the completely inextensible one. In particular, we have performed for the nearly-inextensible pantographic beam model and for the geometrically non-linear Euler model what has been referred to as the semi-circle test, the three-point test and the modified three-point test. The weak form deriving from the stationarity of the energy functional has been projected on the basis of Hermite cubic interpolants. Further improvements of this approach could include the use of isogeometric analysis, which has found wide application for beam elements [83–91]. Indeed, spline functions employed in that approach allow to ensure higher continuity between elements and other many desirable properties. Finally, through a standard variational procedure, we have provided the explicit form of the Euler-Lagrange equations and of the corresponding boundary conditions for a general potential energy density functional which includes as particular cases the quasi-inextensible pantographic beam model and the Euler beam model. Moreover, we have given the explicit form of the Euler-Lagrange equations and of the boundary conditions for the quasi-inextensible and completely inextensible pantographic beam model. It is conceivable that pantographic beams can be used as building blocks for more complex double scale materials.

References

1. Euler, L., Carathéodory, C.: Methodus Inveniendi Lineas Curvas Maximi Minimive Proprietate Gaudentes Sive Solutio Problematis Isoperimetrici Latissimo Sensu Accepti, vol. 1. Springer Science & Business Media (1952)
2. Antman, S.S.: Nonlinear Problems of Elasticity. Mathematical Sciences, vol. 107. Springer, Berlin, New York (1995)
3. Placidi, L., Barchiesi, E., Battista, A.: An inverse method to get further analytical solutions for a class of metamaterials aimed to validate numerical integrations. In: Mathematical Modelling in Solid Mechanics, pp. 193–210. Springer (2017)
4. Murat, F., Sili, A.: Comportement asymptotique des solutions du système de l'élasticité linéarisée anisotrope hétérogène dans des cylindres minces. Comptes Rendus de l'Académie des Sciences-Series I-Mathematics **328**(2), 179–184 (1999)
5. Mora, M.G., Müller, S.: A nonlinear model for inextensible rods as a low energy γ-limit of three-dimensional nonlinear elasticity. Annales de l'IHP Analyse non linéaire **21**, 271–293 (2004)
6. Jamal, R., Sanchez-Palencia, E.: Théorie asymptotique des tiges courbes anisotropes. Comptes rendus de l'Académie des sciences. Série 1, Mathématique **322**(11), 1099–1106 (1996)
7. Pideri, C., Seppecher, P.: Asymptotics of a non-planar rod in non-linear elasticity. Asymptot. Anal. **48**(1, 2), 33–54 (2006)
8. Allaire, G.: Homogenization and two-scale convergence. SIAM J. Math. Anal. **23**(6), 1482–1518 (1992)
9. Bensoussan, A., Lions, J.-L., Papanicolaou, G.: Asymptotic Analysis for Periodic Structures, vol. 5. North-Holland Publishing Company Amsterdam (1978)
10. Alibert, J.-J., Seppecher, P., dell'Isola, F.: Truss modular beams with deformation energy depending on higher displacement gradients. Math. Mech. Solids **8**(1), 51–73 (2003)
11. Carcaterra, A., dell'Isola, F., Esposito, R., Pulvirenti, M.: Macroscopic description of microscopically strongly inhomogeneous systems: a mathematical basis for the synthesis of higher gradients metamaterials. Arch. Ration. Mech. Anal. **218**(3), 1239–1262 (2015)
12. Abali, B.E., Müller, W.H., dell'Isola, F.: Theory and computation of higher gradient elasticity theories based on action principles. Arch. Appl. Mech. 1–16 (2017)
13. Pietraszkiewicz, W., Eremeyev, V.: On natural strain measures of the non-linear micropolar continuum. Int. J. Solids Struct. **46**(3), 774–787 (2009)
14. Altenbach, H., Eremeyev, V.: On the linear theory of micropolar plates. ZAMM-Journal of Applied Mathematics and Mechanics/Zeitschrift für Angewandte Mathematik und Mechanik **89**(4), 242–256 (2009)
15. dell'Isola, F., Della Corte, A., Giorgio, I.: Higher-gradient continua: the legacy of piola, mindlin, sedov and toupin and some future research perspectives. Math. Mech. Solids (2016). https://doi.org/10.1177/1081286515616034
16. dell Isola, F., Seppecher, P., Della Corte, A.: The postulations á la d alembert and á la cauchy for higher gradient continuum theories are equivalent: a review of existing results. In: Proceedings of the Royal Society A, vol. 471, p. 20150415. The Royal Society (2015)
17. dell'Isola, F., Giorgio, I., Andreaus, U.: Elastic pantographic 2D lattices: a numerical analysis on static response and wave propagation. Proc. Est. Acad. Sci. **64**, 219–225 (2015)
18. Reiher, J.C., Giorgio, I., Bertram, A.: Finite-element analysis of polyhedra under point and line forces in second-strain gradient elasticity. J. Eng. Mech. **143**(2), 04016112 (2016)
19. Boutin, C., Giorgio, I., Placidi, L., et al.: Linear pantographic sheets: asymptotic micro-macro models identification. Math. Mech. Complex Syst. **5**(2), 127–162 (2017)
20. dell'Isola, F., Cuomo, M., Greco, L., Della Corte, A.: Bias extension test for pantographic sheets: numerical simulations based on second gradient shear energies. J. Eng. Math. 1–31 (2016)
21. Seppecher, P., Alibert, J.-J., dell'Isola, F.: Linear elastic trusses leading to continua with exotic mechanical interactions. In: Journal of Physics: Conference Series, vol. 319, p. 012018. IOP Publishing (2011)

22. Cuomo, M., dell'Isola, F., Greco, L., Rizzi, N.L.: First versus second gradient energies for planar sheets with two families of inextensible fibres: investigation on deformation boundary layers, discontinuities and geometrical instabilities. Eng. Compos. Part B (2016)
23. dell'Isola, F., Madeo, A., Seppecher, P.: Cauchy tetrahedron argument applied to higher contact interactions. Arch. Ration. Mech. Anal. **219**(3), 1305–1341 (2016)
24. Placidi, L., Greco, L., Bucci, S., Turco, E., Rizzi, N.L.: A second gradient formulation for a 2D fabric sheet with inextensible fibres. Zeitschrift für angewandte Mathematik und Physik, **67**(5)(114) (2016)
25. Enakoutsa, K., Della Corte, A., Giorgio, I.: A model for elastic flexoelectric materials including strain gradient effects. Math. Mech. Solids (2015). https://doi.org/10.1177/1081286515588638
26. Placidi, L., Andreaus, U., Giorgio, I.: Identification of two-dimensional pantographic structure via a linear d4 orthotropic second gradient elastic model. J. Eng. Math. 1–21 (2016)
27. Giorgio, I., Andreaus, U., Lekszycki, T., Della Corte, A.: The influence of different geometries of matrix/scaffold on the remodeling process of a bone and bioresorbable material mixture with voids. Math. Mech. Solids (2015). https://doi.org/10.1177/1081286515616052
28. Andreaus, U., Giorgio, I., Lekszycki, T.: A 2D continuum model of a mixture of bone tissue and bio-resorbable material for simulating mass density redistribution under load slowly variable in time. Zeitschrift für Angewandte Mathematik und Mechanik **13**, 7 (2013)
29. Andreaus, U., Giorgio, I., Madeo, A.: Modeling of the interaction between bone tissue and resorbable biomaterial as linear elastic materials with voids. Zeitschrift für angewandte Mathematik und Physik **66**(1), pp. 209–237 (2014)
30. Andreaus, U., Placidi, L., Rega, G.: Numerical simulation of the soft contact dynamics of an impacting bilinear oscillator. Commun. Nonlinear Sci. Numer. Simul. **15**(9), 2603–2616 (2010)
31. Giorgio, I., Corte, A.Della: Dynamics of 1D nonlinear pantographic continua. Nonlinear Dyn. **88**(1), 21–31 (2017)
32. Turco, E., Golaszewski, M., Giorgio, I., D'Annibale, F.: Pantographic lattices with non-orthogonal fibres: experiments and their numerical simulations. Compos. Part B: Eng. **118**, 1–14 (2017)
33. Placidi, L., Andreaus, U., Della Corte, A., Lekszycki, T.: Gedanken experiments for the determination of two-dimensional linear second gradient elasticity coefficients. Zeitschrift für angewandte Mathematik und Physik **66**(6), 3699–3725 (2015)
34. dell'Isola, F., Della Corte, A., Greco, L., Luongo, A.: Plane bias extension test for a continuum with two inextensible families of fibers: a variational treatment with lagrange multipliers and a perturbation solution. Int. J. Solids Struct. (2015)
35. Abali, B.E., Müller, W.H., Eremeyev, V.A.: Strain gradient elasticity with geometric nonlinearities and its computational evaluation. Mech. Adv. Mater. Mod. Process. **1**(1), 4 (2015)
36. Auffray, N., dell'Isola, F., Eremeyev, V., Madeo, A., Rosi, G.: Analytical continuum mechanics à la Hamilton-Piola least action principle for second gradient continua and capillary fluids. Math. Mech. Solids **20**(4), 375–417 (2015)
37. Yang, Y., Misra, A.: Micromechanics based second gradient continuum theory for shear band modeling in cohesive granular materials following damage elasticity. Int. J. Solids Struct. **49**(18), 2500–2514 (2012)
38. Misra, A., Poorsolhjouy, P.: Granular micromechanics model for damage and plasticity of cementitious materials based upon thermomechanics. Math. Mech. Solids (2015). https://doi.org/10.1177/1081286515576821
39. Misra, A.l., Singh, V.: Thermomechanics-based nonlinear rate-dependent coupled damage-plasticity granular micromechanics model. Contin. Mech. Thermodyn. **27**(4-5), 787 (2015)
40. Della Corte, A., Battista, A., dell'Isola, F.: Referential description of the evolution of a 2D swarm of robots interacting with the closer neighbors. Int. J. Non-Linear Mech. **80**, 209–220 (2016)
41. Del Vescovo, D., Giorgio, I.: Dynamic problems for metamaterials: review of existing models and ideas for further research. Int. J. Eng. Sci. **80**, 153–172 (2014)

42. Rinaldi, A., Placidi, L.: A microscale second gradient approximation of the damage parameter of quasi-brittle heterogeneous lattices. ZAMM-Journal of Applied Mathematics and Mechanics/Zeitschrift für Angewandte Mathematik und Mechanik **94**(10), 862–877 (2014)
43. Placidi, L.: A variational approach for a nonlinear 1-dimensional second gradient continuum damage model. Contin. Mech. Thermodyn. **27**(4–5), 623 (2015)
44. Madeo, A., Placidi, L., Rosi, G.: Towards the design of metamaterials with enhanced damage sensitivity: second gradient porous materials. Res. Nondestruct. Eval. **25**(2), 99–124 (2014)
45. Misra, A.: Effect of asperity damage on shear behavior of single fracture. Eng. Fract. Mech. **69**(17), 1997–2014 (2002)
46. Misra, A., Singh, V.: Micromechanical model for viscoelastic materials undergoing damage. Contin. Mech. Thermodyn. 1–16 (2013)
47. Yang, Y., Misra, A.: Higher-order stress-strain theory for damage modeling implemented in an element-free galerkin formulation. CMES-Comput. Model. Eng. Sci. **64**(1), 1–36 (2010)
48. Madeo, A., Della Corte, A., Greco, L., Neff, P.: Wave propagation in pantographic 2D lattices with internal discontinuities (2014). arXiv:1412.3926
49. Bersani, A.M., Della Corte, A., Greco, L., Neff, P.: An explicit solution for the dynamics of a taut string of finite length carrying a traveling mass: the subsonic case. Zeitschrift für angewandte Mathematik und Physik **67**(4), 108 (2016)
50. Placidi, L., dell'Isola, F., Ianiro, N., Sciarra, G.: Variational formulation of pre-stressed solid-fluid mixture theory, with an application to wave phenomena. Eur. J. Mech.-A/Solids **27**(4), 582–606 (2008)
51. Madeo, A., Barbagallo, G., d'Agostino, M., Placidi, L., Neff, P.: First evidence of non-locality in real band-gap metamaterials: determining parameters in the relaxed micromorphic model. In: Proceedings of the Royal Society A, vol. 472, p. 20160169. The Royal Society (2016)
52. Madeo, A., Neff, P., Ghiba, I., Placidi, L., Rosi, G.: Band gaps in the relaxed linear micromorphic continuum (2014). arXiv:1405.3493
53. Giorgio, I.: Numerical identification procedure between a micro-cauchy model and a macro-second gradient model for planar pantographic structures. Zeitschrift für angewandte Mathematik und Physik **67**(4)(95) (2016)
54. dell'Isola, F., Della Corte, A., Giorgio, I., Scerrato, D.: Pantographic 2D sheets: discussion of some numerical investigations and potential applications. Int. J. Non-Linear Mech. **80**, 200–208 (2016)
55. dell'Isola, F., Giorgio, I., Pawlikowski, M., Rizzi, N.: Large deformations of planar extensible beams and pantographic lattices: heuristic homogenization, experimental and numerical examples of equilibrium. In: Proceedings of the Royal Society A, vol. 472, p. 20150790. The Royal Society (2016)
56. Scerrato, D., Giorgio, I., Rizzi, N.: Three-dimensional instabilities of pantographic sheets with parabolic lattices: numerical investigations. Zeitschrift für angewandte Mathematik und Physik **67**(3), 1–19 (2016)
57. Giorgio, I., Della Corte, A., dell'Isola, F., Steigmann, D.: Buckling modes in pantographic lattices. Comptes rendus Mecanique (2016)
58. Rahali, Y., Giorgio, I., Ganghoffer, J.F., Dell'Isola, F.: Homogenization à la piola produces second gradient continuum models for linear pantographic lattices. Int. J. Eng. Sci. **97**, 148–172 (2015)
59. Alibert, J., Della, A.: Corte. Second-gradient continua as homogenized limit of pantographic microstructured plates: a rigorous proof. Zeitschrift für angewandte Mathematik und Physik **66**(5), 2855–2870 (2015)
60. Eremeyev, V.A., dell'Isola, F., Boutin, C., Steigmann, D.: Linear Pantographic Sheets: Existence and Uniqueness of Weak Solutions (2017)
61. Placidi, L., Barchiesi, E., Turco, E., Rizzi, N.L.: A review on 2D models for the description of pantographic fabrics. Zeitschrift für angewandte Mathematik und Physik, **67**(5)(121) (2016)
62. Barchiesi, E., Placidi, L.: A review on models for the 3D statics and 2D dynamics of pantographic fabrics. In: Wave Dynamics and Composite Mechanics for Microstructured Materials and Metamaterials, pp. 239–258. Springer (2017)

63. Turco, E., dell'Isola, F., Rizzi, N.L., Grygoruk, R., Müller, W.H., Liebold, C.: Fiber rupture in sheared planar pantographic sheets: numerical and experimental evidence. Mech. Res. Commun. **76**, 86–90 (2016)
64. Spagnuolo, M., Barcz, K., Pfaff, A., dell'Isola, F., Franciosi, P.: Qualitative pivot damage analysis in aluminum printed pantographic sheets: numerics and experiments. Mech. Res. Commun. (2017)
65. Battista, A., Rosa, L., dell'Erba, R., Greco, L.: Numerical investigation of a particle system compared with first and second gradient continua: Deformation and fracture phenomena. Math. Mech. Solids (2016). https://doi.org/10.1177/1081286516657889
66. Greco, L., Giorgio, I., Battista, A.: In plane shear and bending for first gradient inextensible pantographic sheets: numerical study of deformed shapes and global constraint reactions. Math. Mech. Solids (2016). https://doi.org/10.1177/1081286516651324
67. Battista, A., Cardillo, C., Del Vescovo, D., Rizzi, N.L., Turco, E.: Frequency shifts induced by large deformations in planar pantographic continua. Nanomechanics Sci. Technol. Int. J. **6**(2) (2015)
68. Turco, E., Golaszewski, M., Cazzani, A., Rizzi, N.L.: Large deformations induced in planar pantographic sheets by loads applied on fibers: experimental validation of a discrete lagrangian model. Mech. Res. Commun. **76**, 51–56 (2016)
69. Turco, E., Barcz, K., Pawlikowski, M., Rizzi, N.L.: Non-standard coupled extensional and bending bias tests for planar pantographic lattices. Part i: numerical simulations. Zeitschrift für angewandte Mathematik und Physik **67**(5), 122 (2016)
70. Turco, E., Rizzi, N.L.: Pantographic structures presenting statistically distributed defects: numerical investigations of the effects on deformation fields. Mech. Res. Commun. **77**, 65–69 (2016)
71. Turco, E., dell'Isola, F., Cazzani, A., Rizzi, N.L.: Hencky-type discrete model for pantographic structures: numerical comparison with second gradient continuum models. Zeitschrift für angewandte Mathematik und Physik **67** (2016)
72. dell'Isola, F., Lekszycki, T., Pawlikowski, M., Grygoruk, R., Greco, L.: Designing a light fabric metamaterial being highly macroscopically tough under directional extension: first experimental evidence. Zeitschrift für angewandte Mathematik und Physik **66**, 3473–3498 (2015)
73. Ganzosch, G., dell'Isola, F., Turco, E., Lekszycki, T., Müller, W.H.: Shearing tests applied to pantographic structures. Acta Polytechnica CTU Proceedings **7**, 1–6 (2016)
74. Alibert, J.-J., Della Corte, A., Giorgio, I., Battista, A.: Extensional elastica in large deformation as\gamma-limit of a discrete 1D mechanical system. Zeitschrift für angewandte Mathematik und Physik **68**(2), 42 (2017)
75. Dell'Isola, F., Andreaus, U., Placidi, L.: At the origins and in the vanguard of peridynamics, non-local and higher-gradient continuum mechanics: an underestimated and still topical contribution of gabrio piola. Math. Mech. Solids **20**(8), 887–928 (2015)
76. De Masi, A., Galves, A., Löcherbach, E., Presutti, E.: Hydrodynamic limit for interacting neurons. J. Stat. Phys. **158**(4), 866–902 (2015)
77. De Masi, A., Olla, S.: Quasi-static hydrodynamic limits. J. Stat. Phys. **161**(5), 1037–1058 (2015)
78. Carinci, G., De Masi, A., Presutti, E.: Super-hydrodynamic limit in interacting particle systems. J. Stat. Phys. **155**(5), 867–887 (2014)
79. Carinci, G., De Masi, A., Giardinà, C., Presutti, Errico: Hydrodynamic limit in a particle system with topological interactions. Arabian J. Math. **3**(4), 381–417 (2014)
80. Chatzigeorgiou, G., Javili, A., Steinmann, P.: Unified magnetomechanical homogenization framework with application to magnetorheological elastomers. Math. Mech. Solids **19**(2), 193–211 (2014)
81. Saeb, S., Steinmann, P., Javili, A.: Aspects of computational homogenization at finite deformations: a unifying review from reuss' to voigt's bound. Appl. Mech. Rev. **68**(5), 050801 (2016)
82. Javili, A., Chatzigeorgiou, G., Steinmann, P.: Computational homogenization in magnetomechanics. Int. J. Solids Struct. **50**(25), 4197–4216 (2013)

83. Cazzani, A., Malagù, M., Turco, E.: Isogeometric analysis: a powerful numerical tool for the elastic analysis of historical masonry arches. Contin. Mech. Thermodyn. **28**(1–2), 139–156 (2016)
84. Cazzani, A., Stochino, F., Turco, E.: An analytical assessment of finite element and isogeometric analysis of the whole spectrum of Timoshenko beams. ZAMM-Journal of Applied Mathematics and Mechanics/Zeitschrift für Angewandte Mathematik und Mechanik (2016)
85. Cazzani, A., Stochino, F., Turco, E.: On the whole spectrum of Timoshenko beams. Part I: a theoretical revisitation. Zeitschrift für angewandte Mathematik und Physik **67**(2), 1–30 (2016)
86. Cazzani, A., Malagù, M., Turco, E., Stochino, F.: Constitutive models for strongly curved beams in the frame of isogeometric analysis. Math. Mech. Solids **21**(2), 182–209 (2016)
87. Greco, L., Cuomo, M.: An isogeometric implicit G1 mixed finite element for Kirchhoff space rods. Comput. Methods Appl. Mech. Eng. **298**, 325–349 (2016)
88. Cuomo, M., Contrafatto, L., Greco, L.: A variational model based on isogeometric interpolation for the analysis of cracked bodies. Int. J. Eng. Sci. **80**, 173–188 (2014)
89. Greco, L., Cuomo, M.: B-spline interpolation of kirchhoff-love space rods. Comput. Methods Appl. Mech. Eng. **256**, 251–269 (2013)
90. Greco, L., Cuomo, M.: An implicit G1 multi patch B-spline interpolation for kirchhoff-love space rod. Comput. Methods Appl. Mech. Eng. **269**, 173–197 (2014)
91. Greco, L., Cuomo, M.: Consistent tangent operator for an exact kirchhoff rod model. Contin. Mech. Thermodyn. **27**(4–5), 861–877 (2015)

Numerical Simulation of Energy Localization in Dynamic Materials

Mihhail Berezovski and Arkadi Berezovski

Abstract Dynamic materials are artificially constructed in such a way that they may vary their characteristic properties in space or in time, or both, by an appropriate arrangement or control. These controlled changes in time can be provided by the application of an external (non-mechanical) field, or through a phase transition. In principle, all materials change their properties with time, but very slowly and smoothly. Changes in properties of dynamic materials should be realized in a short or quasi-nil time lapse and over a sufficiently large material region. Wave propagation is a characteristic feature for dynamic materials because it is also space and time dependent. As a simple example of the complex behavior of dynamic materials, the one-dimensional elastic wave propagation is studied numerically in periodic structures whose properties (mass density, elasticity) can be switched suddenly in space and in time. It is shown that dynamic materials have the ability to dynamically amplify, tune, and compress initial signals. The thermodynamically consistent high-resolution finite-volume numerical method is applied to the study of the wave propagation in dynamic materials. The extended analysis of the influence of inner reflections on the energy localization in the dynamic materials is presented.

1 Introduction

The wave energy redistribution in materials may result in scattering [1] or harvesting of energy [10]. Such a redistribution can be controlled via the interaction of mechanical waves with a materials microstructure [5]. For instance, unique dynamic properties of phononic crystals can be used to guide and focus elastic waves for wave-based energy harvesting and/or to design materials capable of energy absorbing [4].

M. Berezovski
Embry Riddle Aeronautical University, Daytona Beach, FL, USA
e-mail: mihhail.berezovski@erau.edu

A. Berezovski (✉)
School of Science, Tallinn University of Technology, Tallinn, Estonia
e-mail: arkadi.berezovski@cs.ioc.ee

F. dell'Isola et al. (eds.), *Advances in Mechanics of Microstructured Media and Structures*, Advanced Structured Materials 87,
https://doi.org/10.1007/978-3-319-73694-5_5

Phononic crystals are normally static in the sense that their properties are fixed in advance by their design parameters, which can limit their functionality to very specific arrangements [3]. These constraints appear to limit the usefulness and versatility of phononic crystals to predesigned narrowband operating conditions. Varying the material parameters of the scatterers in the course of time like in dynamic materials (see [6]) will modify the propagation of waves through a phononic crystal. This may enable time-dependent phononic crystals to have more robust or multiple operating regimes as compared to their static counterparts.

The localization of energy during wave propagation is the most intriguing property of dynamic materials [6, 8, 11]. Theoretical analysis of this phenomenon is possible only for zero impedance mismatch [6, 7], which is rarely happens in practice. It is worth, therefore, to study numerically a more general case with non-zero impedance mismatch.

Wave propagation in heterogeneous solids has been a subject of considerable research for many years. However, micro-structural details are rarely taken into account in large-scale structural dynamics or dynamic impact simulations. The reason is the enormous complexity of wave phenomena in highly heterogeneous media. The diversity of possible responses of materials with microstructure to dynamic loading has been recently underlined [12]. This is why the one-dimensional (in space) case is considered.

2 One-Dimensional Elasticity in Small-Strain Approximation

In general, dynamic materials are characterized by material parameters varying in space and time. In the framework of one-dimensional elasticity, this reflects in the space and time dependence of density ρ and Young's modulus E. With a standard notation (u is the elastic displacement; derivatives indicated by subscripts), the corresponding Lagrangian density has the form [11]

$$L = \frac{1}{2}\rho(x,t)(u_t)^2 - \frac{1}{2}E(x,t)(u_x)^2. \tag{1}$$

The local balance of linear momentum is then written as (no body force for the sake of simplicity)

$$\big(\rho(x,t)u_t\big)_t - \big(E(x,t)u_x\big)_x = 0. \tag{2}$$

We will consider a situation that may be easier to realize experimentally than the general case, namely, a purely inertial material inhomogeneity ($\rho = \rho(x)$) and only a time evolution of the elasticity coefficient, $E = E(t)$. In this case, we arrive at the wave equation

$$u_{tt} - c^2(x,t)u_{xx} = 0, \tag{3}$$

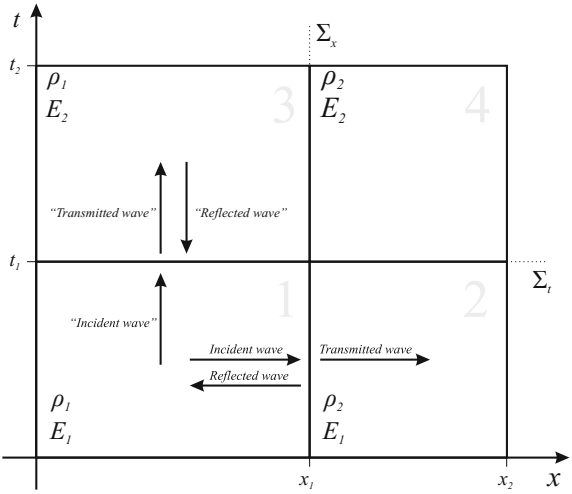

Fig. 1 Propagation diagram (adopted from [9])

which can be also represented in the form of the hyperbolic system of the first-order equations

$$v_t = c^2(x,t)\varepsilon_x, \tag{4}$$

$$\varepsilon_t = v_x, \tag{5}$$

where $v = u_t$, $\varepsilon = u_x$, and $c^2(x,t) = E(t)/\rho(x)$.

We will examine the piecewise constant variations in space and time where, in the single space dimension, discontinuities Σ_x are represented by straight lines parallel to the t-axis while discontinuities Σ_t are straight lines parallel to the x-axis (see Fig. 1). At the space-like discontinuity surface Σ_x, the continuity of the traction is represented as

$$[\![u_x]\!] = 0 \quad \text{at} \quad \Sigma_x, \tag{6}$$

and at the time-like discontinuity surface Σ_t, the continuity of momentum is reduced to [11]

$$[\![u_t]\!] = 0 \quad \text{at} \quad \Sigma_t, \tag{7}$$

where double square brackets denote the usual jump.

The system of Eqs. (4)–(5) with the use of conditions (6)–(7) at fixed discontinuity surfaces is solved numerically by means of the conservative wave-propagation algorithm [2].

3 Numerical Simulation of Dynamic Material Behavior

Our goal is to investigate the influence of impedance mismatch, up to 30%, upon the energy localization within the checkerboard structure. We also provide the analysis of the performance of the checkerboard structure for initial disturbance of different lengths (from $\lambda = 100\Delta x$ to $\lambda = 1000\Delta x$). The propagation occurs along 1D medium which can be viewed as an elastic rod. The rod is assumed homogeneous except a region of the length $l = 1000\Delta x$, where dynamic material with a checkerboard structure is maintained (Fig. 2). The homogeneous parts of the rod are used for the better observation of initial and transmitted signals as well as all reflections.

The checkerboard part consists of a finite number of equal spatial periods with total length of $l = 1000\Delta x$. We consider the case of the checkerboard structure with equal number of steps in time and space periods. The number of time periods is not limited. All the properties are normalized for better comparison of the results, i.e., the elastic velocity c_1 for the "fast" material is set equal to 1. Through all numerical experiments, we calculate the amplitude of the initial disturbance at time t_1. The amplitude of transmitted signal is measured at time t_2 in the second homogeneous part.

The performance of the checkerboard structure is studied for a range of values of its material parameters, i.e., the elastic velocities c_i and the impedances $z_i = \rho_i c_i$. We also consider the influence of the length λ of the initial disturbance.

All numerical simulations are performed by means of the conservative wave propagation algorithm [2]. This numerical scheme is stable up to the value of the Courant number equal to 1, and second-order accurate on smooth solutions. The typical computational domain is presented in Fig. 3.

Here, the checkerboard structure consists of five space periods of $P_s = 250\Delta x$ each and time periods $P_t = 250\Delta t$. The light blue color represents the "fast" material with elastic wave velocity $c_1 = 1$. The dark blue represents the "slow" material, with elastic wave velocity $c_2 = 0.7$. The impedance ratio $z = z_2/z_1$ is set to 1 in this example.

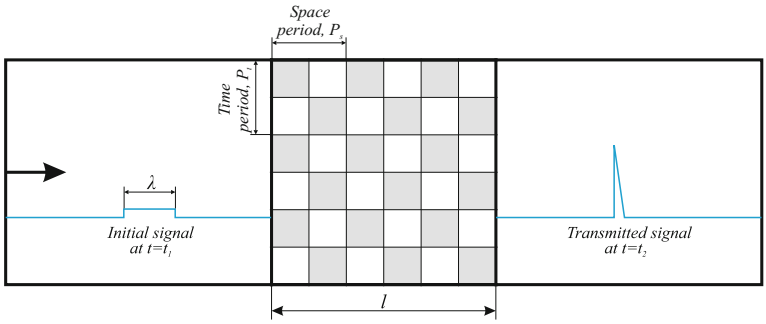

Fig. 2 Geometry of the problem

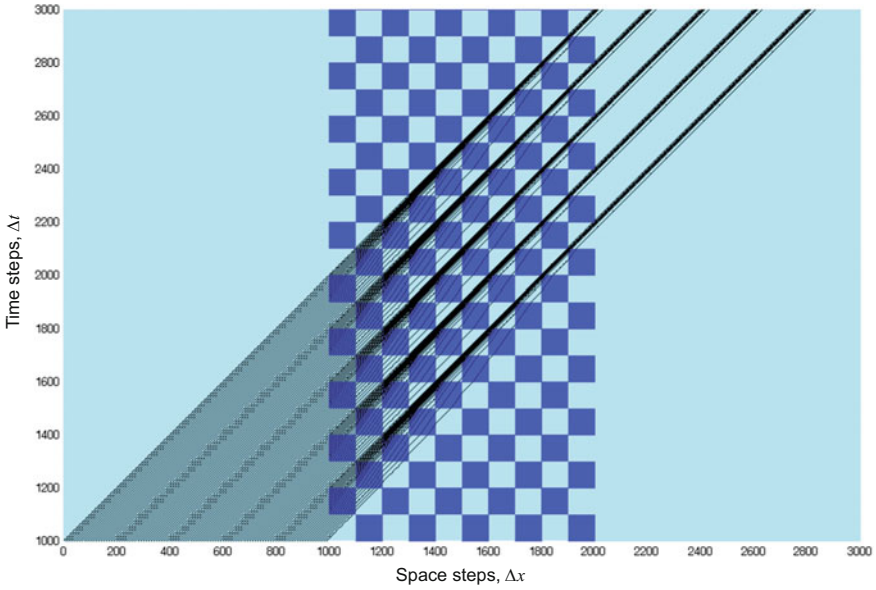

Fig. 3 Computational domain with wave routes ($P_s = 250\Delta x, P_t = 250\Delta t, c_2/c_1 = 0.7, \lambda = 1000\Delta x$)

The black dashed lines represent wave routes for the main disturbance traveling with no reflections (impedance match). We can observe the formation of five limit cycles. It should be noted that this simulation assumes the fixed length and finite numbers of space periods. The corresponding wave field is presented in Fig. 4.

The wave field evolution repeats the wave routes behavior. The transformation of the initial pulse into five peaks with higher amplitudes appears due to the limit cycles formation. In this "ideal" case with equal wave impedances, there is no reflection of waves from the material interfaces.

Our study is focused on the influence produced by a weak impedance mismatch on the energy localization. During the wave propagation through layers with different impedances we expect reflections at the material interfaces. The corresponding wave field history is presented in Fig. 5.

The main peaks of the transmitted signal almost repeat the "ideal" case with equal impedances (Fig. 4). The multiple waves reflected from spatial and temporal interfaces are clearly observed.

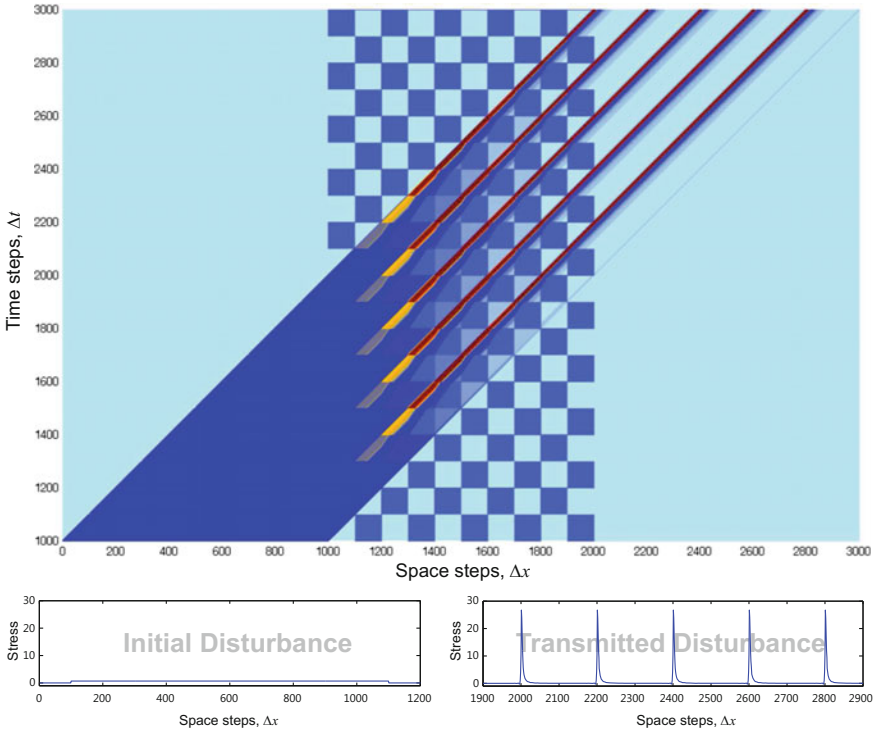

Fig. 4 Wave field time history ($P_s = 250\Delta x, P_t = 250\Delta t, c_2/c_1 = 0.7, \lambda = 1000\Delta x$)

4 Amplitude of Transmitted Pulses

4.1 Amplitude of Transmitted Pulses Versus Velocity Ratio

Now we perform simulations varying the elastic wave velocity of the "slow" material from 0.5 to 1. The length of the initial step pulse is $500\Delta x$ with amplitude equal to unity. We repeated these simulations for the impedance ratio mismatch up to 30%. The results are presented in Fig. 6.

The normalized amplitude of transmitted pulses is around 50 in the case when the elastic wave velocity in the "slow" material is two times less than in the "fast" one for this particular setting. It reaches its maximum for the velocity ratio equal approximately to 0.57. As the elastic wave velocity in "slow" material becomes closer to that in "fast" material, the amplitude of transmitted pulses becomes smaller and approaches to that in the initial disturbance.

These results show that the impedance mismatch up to 30% has very little influence on the amplitude of transmitted pulses. The normalized amplitude plots for different impedance ratios are overlapping each other.

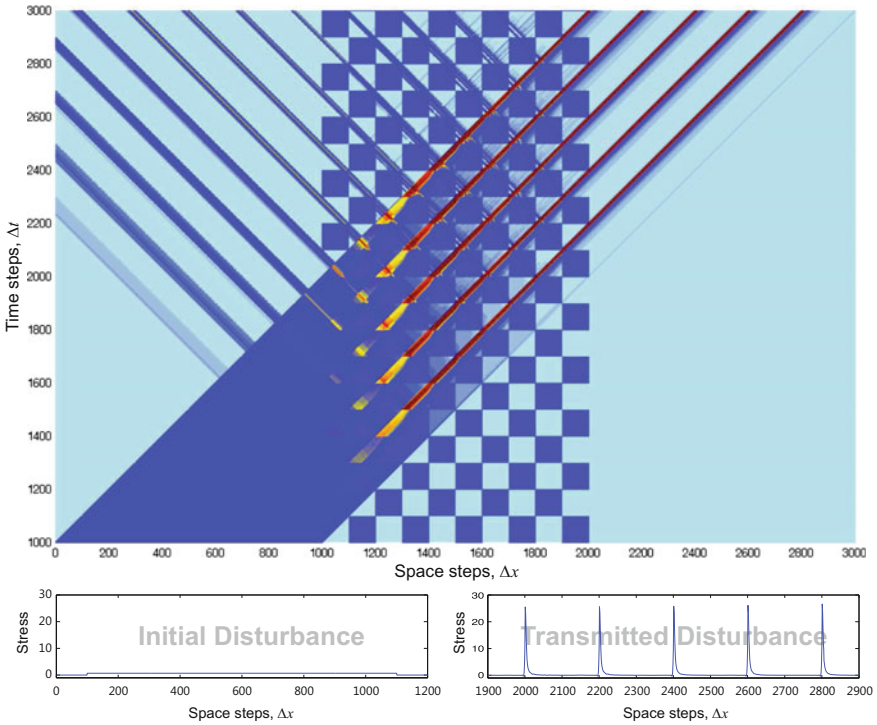

Fig. 5 Wave field time history ($P_s = 250\Delta x, P_t = 250\Delta t, c_2/c_1 = 0.7, z = 0.9, \lambda = 1000\Delta x$)

4.2 Amplitude of Transmitted Pulses Versus Wave Length

To study the behavior of a checkerboard structure for different lengths of the initial disturbance, we choose the elastic wave velocity ratio equal to 0.7. The length of initial pulse varies from $100\Delta x$ to $1000\Delta x$. The numerical simulations was repeated for impedance ratios z = 0.7, 0.8, 0.9, 1.0 and 1.1. The corresponding results are shown in Fig. 7.

It is clearly seen that the amplitude of transmitted pulses for initial signals that are shorter than the length of the space period is increased linearly with the initial wave length. Here the initial disturbance has not enough time to develop into the limit cycles due to the finite number of space periods. As the duration of initial disturbance increases, the amplitude of transmitted pulses becomes constant, because there is a sufficient time to generate well developed limit cycles with the energy localization (see Fig. 3). The average amplitude of transmitted pulses is up to 22. As before, the influence of the impedance mismatch is about 5%.

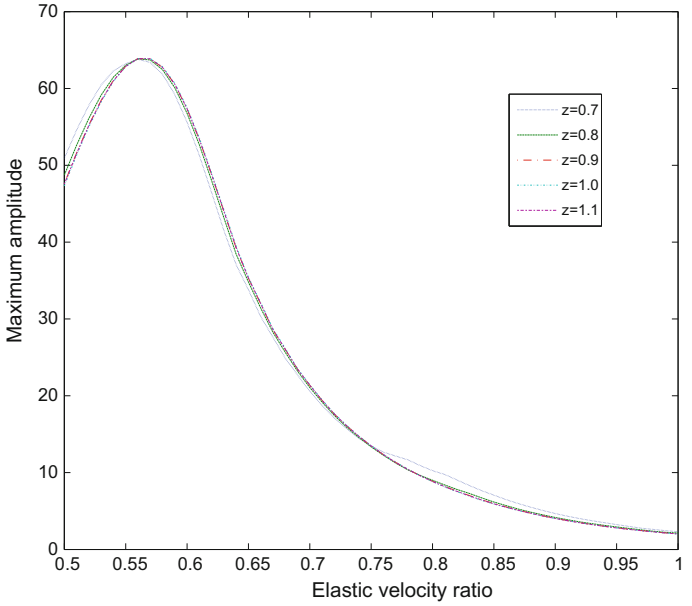

Fig. 6 Amplitude of transmitted pulse versus elastic velocity ratio for different impedance ratios z ($P_s = 250\Delta x, P_t = 250\Delta t, \lambda = 500\Delta x$)

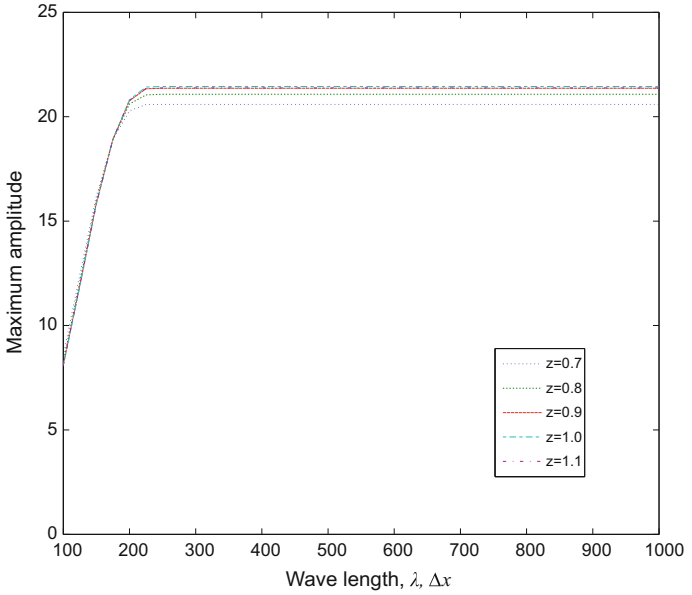

Fig. 7 Amplitude of transmitted pulse versus wave length for different impedance ratios z ($P_s = 250\Delta x, P_t = 250\Delta t, c_2/c_1 = 0.7$)

5 Conclusions

Application of the improved finite volume wave-propagation algorithm [2] allows to implement jump relations both at space-like and time-like discontinuities to simulate wave propagation in dynamic materials. It is shown that dynamic materials demonstrate a very specific transmission of signals. Indeed, the step-wise initial disturbance transforms into a train of localized pulses. The amplitude of such pulses depends on the way of switching material properties of layers, which is external in relation to the wave propagation process. This means that the amplitude of transmitted pulses can be determined only qualitatively. Nevertheless, the influence of parameters of the checkerboard structure on the amplitude of transmitted pulses can be simulated. As it is shown, the effect of a weak impedance mismatch is small, but the variation of elastic wave velocity ratio is significant. The influence of the length of the initial signal depends on the its ratio to the size of the checkerboard structure.

Acknowledgements Authors appreciate discussions with Prof. G. A. Maugin, Prof. K. A. Lurie, and Prof. S. Weekes. The first author acknowledges the support from Worcester Polytechnic Institute.

References

1. Andreassen, E., Jensen, J.S.: Analysis of phononic bandgap structures with dissipation. J. Vibr. Acoust. **135**(4), 041,015 (2013)
2. Berezovski, A., Engelbrecht, J., Maugin, G.A.: Numerical Simulation of Waves and Fronts in Inhomogeneous Solids. World Scientific Singapore (2008)
3. Deymier, P.A., et al.: Acoustic Metamaterials and Phononic Crystals. Springer (2013)
4. Hussein, M.I., Leamy, M.J., Ruzzene, M.: Dynamics of phononic materials and structures: historical origins, recent progress, and future outlook. Appl. Mech. Rev. **66**(4), 040,802 (2014)
5. Le, C., Bruns, T.E., Tortorelli, D.A.: Material microstructure optimization for linear elastodynamic energy wave management. J. Mech. Phys. Solids **60**(2), 351–378 (2012)
6. Lurie, K.A.: An Introduction to the Mathematical Theory of Dynamic Materials. Springer (2007)
7. Lurie, K.A., Weekes, S.L.: Wave propagation and energy exchange in a spatio-temporal material composite with rectangular microstructure. J. Math. Anal. Appl. **314**(1), 286–310 (2006)
8. Maugin, G.A., Rousseau, M.: Wave Momentum and Quasi-Particles in Physical Acoustics. World Scientific (2015)
9. Maugin, G.A., Rousseau, M.: Prolegomena to studies on dynamic materials and their space-time homogenization. Discret. Contin. Dyn. Syst.-Ser. S **6**(6), 1599–1608 (2013)
10. Radousky, H.B., Liang, H.: Energy harvesting: an integrated view of materials, devices and applications. Nanotechnology **23**(50), 502,001 (2012)
11. Rousseau, M., Maugin, G.A., Berezovski, M.: Elements of study on dynamic materials. Arch. Appl. Mech. **81**(7), 925–942 (2011)
12. Van Pamel, A., Sha, G., Rokhlin, S.I., Lowe, M.J.: Simulation of elastic wave propagation in heterogeneous materials. J. Acoust. Soc. Am. **141**(5), 3809–3810 (2017)

Fracture Prediction of Piezoelectric Ceramic by the 2-D Boundary Element Analysis

M. Biglar, T. Trzepieciński and F. Stachowicz

1 Introduction

Piezoelectric ceramics are widely used as sensors and multilayer actuators in many areas of industry [1], despite the absence of a fundamental understanding of their fracture behaviour [2]. Piezoelectricity is a linear effect that is related to the microscopic structure of the solid. Among piezoelectric materials, barium titanate is the most often used as a ceramic material. Barium titanate is a ferroelectric classic perovskite structure with wide-ranging material properties that depend on its composition [3, 4]. The perovskite structure ABO_3 (Fig. 1) is the arrangement where the corner-sharing oxygen octahedra are linked together in a regular cubic array with smaller cations (Ti, Zr, Sn, Nb, etc.) occupying the central octahedral B-site, and larger cations (Pb, Ba, Sr, Ca, Na, etc.) filling the interstices between octahedra in the larger A-site [5]. Several studies have been carry out in order to study the influence of compositionally modified ceramic bodies and the sintering conditions on the properties of ceramic [6]. The ceramic material which is composed of the random orientation of these piezoelectric crystallites, is inactive, i.e., the effects from the individual crystals cancel each other and no discernable piezoelectricity is present [5]. The domains are the regions of equally oriented polarization vectors. To orient the domains the pooling method can be used.

M. Biglar · T. Trzepieciński (✉) · F. Stachowicz (✉)
Faculty of Mechanical Engineering and Aeronautics, Department of Materials Forming and Processing, Rzeszow University of Technology, Al. Powst. Warszawy 8, 35-959 Rzeszów, Poland
e-mail: tomtrz@prz.edu.pl

F. Stachowicz
e-mail: stafel@prz.edu.pl

M. Biglar
e-mail: m_biglar@prz.edu.pl

F. dell'Isola et al. (eds.), *Advances in Mechanics of Microstructured Media and Structures*, Advanced Structured Materials 87,
https://doi.org/10.1007/978-3-319-73694-5_6

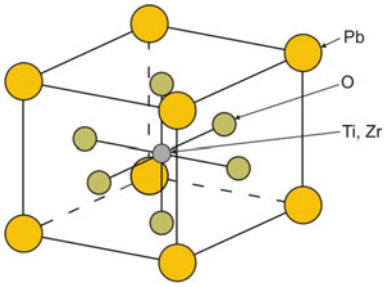

Fig. 1 Perovskite structure

This technique consist in polarizing the ceramic through the application of a static electric field.

Fracture in piezolelectrics have been investigated as an electroelastic problem by several authors. Shindo et al. [7] analysed cracks in piezoelectric layers using integral equation method. Sou et al. [8] established a fracture mechanics for ferroelectric mechanics under small-scale hysteresis conditions, which facilitates the experimental study of fracture resistance under combined mechanical and electrical loading. Wang and Singh [9] studied crack propagation in a piezoelectric lead–zirconium–titanate (PZT) material under simultaneous mechanical loading and applied electric fields using the Vickers indentation technique. They also presents a mechanism for the change in crack propagation behavior of the piezoelectric PZT material under applied electric fields. Fu and Zhang [10] conducted the compact tension tests and indentation-fracture tests to study the effects of an applied electric field on the fracture toughness K_{IC} of poled PZT ceramics. The experiments show that an applied electric field, either parallel or antiparallel to the poling direction, considerably reduces the K_{IC} value. Nonlinear three-dimensional finite element analysis was employed by Shindo et al. [11] to calculate the energy release rate for double torsion specimens based on the exacts permeabled and approximates impermeabled crack models. The results of analyses of Zhang [12] shows that for an insulating crack, the energy release rate is independent of the applied electric field either perpendicular or parallel to the crack when the electric field inside the crack is taken into account. Wilson et al. [13] proposed a new function that governs material degradation to eliminate the presence of high phase-field values in the vicinity of large electric fields. The new function is found to lead to improved brittle material behavior. The commonly used fracture criteria have been presented in [14–16].

For the numerical crack analysis in piezoelectric ceramics mostly the finite element method (FEM) was used [17]. However, the boundary element method (BEM) has proved to be a very efficient and accurate tool for analysing linear elastic crack problems. Boundary element method is one the favourite optimized numerical computational method which is used by scientist in many areas of engineering. This method is very applicable in determining the behavior of solid body which contains several numbers of cracks and holes. The common advantage of BEM compared to FEM is that the numerical discretization is restricted to the boundary only and that the dependent field quantities such as stresses and electric displacements are very

accurately approximated inside the domain by fundamental solutions [17]. The BEM is successfully applied to study the crack problems in piezoelectric structures. Xu and Rajapakse [18] developed a two-dimensional boundary element code based on the closed form Green's functions to examine stress and electric field concentration around voids. Pan [19] developed a displacement discontinuity approach to get a single domain BEM for crack problems and employed the extrapolation of the extended relative crack displacements to calculate the *K*-factors. An implementation of BEM for the analysis of piezoelectric materials with the aim to exploit their features in linear electroelastic fracture mechanics has been presented by Davì and Milazzo [20]. The problem was formulated employing generalized displacements, that is displacements and electric potential, and generalized tractions, that is tractions and electric displacement. The boundary integral equation is derived through a displacement based modified Lekhnitskii's functions [21] approach. Rajapakse and Xu [22] presented fundamental solutions for straight impermeable and conducting cracks based on set of piezoelectric Green's functions and the extended Lekhnitskii's formalism. The fracture parameters were computed based on the boundary element modelling. More recently an overview of the BEM computation of crack parameters in fracture mechanics has been provided by Aliabadi and Rooke [23].

In order to use the BEM method, one must pay attention to this fact that traction fundamental solution and displacement fundamental solution for isotropic bodies are different than anisotropic bodies. It is the most important fact that researcher have to consider it when they are using boundary element method for the investigations and studies [24].

To understand failure mechanisms of piezoelectric materials and maintain the stability of cracked piezoelectric structures operating in an environment of combined electromechanical loading, analysis of the mechanical and electrical behavior is a prerequisite [2]. In this chapter, an effective implementation of boundary element multiscale method in analyzing of fracture of barium titanate piezoelectric ceramics was introduced. Then bridges meso-scale to macro-scale by a damage parameter were performed.

2 Ferroelectricity

A ferroelectric material possesses a spontaneous polarization that can be reversed in direction by application of a realizable electric field over some temperature range [5]. The properties of ferroelectric materials are different due to the Curie temperature T_c. Below the T_c they are exhibit polarized properties and above this temperature they are not polar. Applying an electric field to multilayer actuator (Fig. 2) causes the polarization to reverse, and this gives rise to the ferroelectric hysteresis loop, relating the polarization P to the applied electric field E. A crack intensifies induction causing local hysteresis and decrease the fatigue strength of multilayer actuator. A typical field-polarization loop is presented in Fig. 3a.

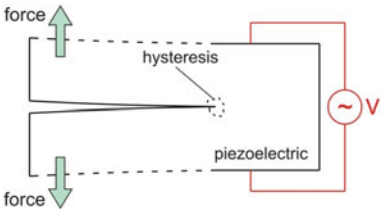

Fig. 2 Deformation of multilayer actuator layers

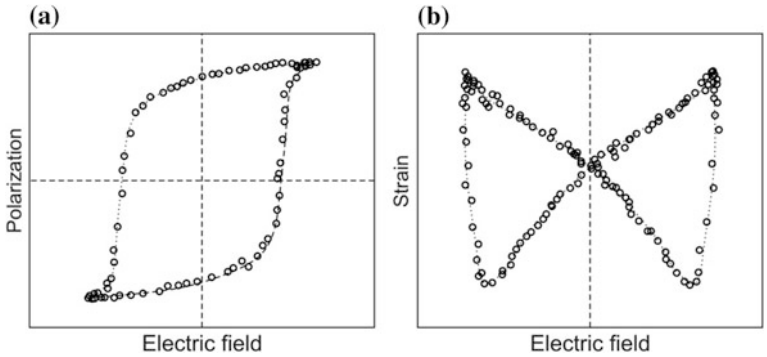

Fig. 3 Hysteresis loop of a poled piezoelectric ceramic (**a**), and butterfly loop indicating switching (**b**)

Two key parameters of the P-E loop are the coercive field E_c and the remanent polarization P_r. Once the field is switched off, the material will have a polarization equal to P_r [5]. It is commonly known, that the existence of the P-E loop is a proof that a material is ferroelectric.

Polarization switching leads to strain-electric field hysteresis referred as butterfly loop (Fig. 3b). As the electric field is applied, the converse piezoelectric effect in deformation is observed. As the field is increased, the strain comes to nonlinear with the field as domain walls start switching.

3 Constitutive Equations of Piezoelectric Ceramics

When a piezoelectric material is subjected to a mechanical stress, not only is a mechanical strain produced, but also the electric charge density is changed [8]. In contrast, when an electric field is applied to the piezoelectric material, it cause changes in the electric charge density and mechanical deformation. The behaviour between electric load and stress/strain is described by constitutive equations. Denoting **D**, **E**, **ε**, **σ** as the electric charge density vector, the electric field vector,

the strain tensor, and the stress tensor, respectively, the constitutive equations can be written as [9, 25]:

$$\mathbf{D} = \mathbf{d}\boldsymbol{\sigma} + \boldsymbol{\varepsilon}^{\sigma}\mathbf{E} \tag{1}$$

$$\mathbf{E} = -\mathbf{g}\boldsymbol{\sigma} + (\boldsymbol{\varepsilon}^{\sigma})^{-1}\mathbf{D} \tag{2}$$

$$\boldsymbol{\varepsilon} = \mathbf{C}^{\mathrm{E}}\boldsymbol{\sigma} + (\mathbf{d})^{T}\mathbf{E} \tag{3}$$

$$\boldsymbol{\sigma} = \mathbf{S}^{\mathbf{E}}\boldsymbol{\varepsilon} - \mathbf{e}\mathbf{E} \tag{4}$$

where $\mathbf{C}^{\mathbf{E}}$ is the compliance tensor measured under a constant electric field condition, $\mathbf{S}^{\mathbf{E}}$ is the elastic modulus tensor measured under a constant electric-field condition, $\boldsymbol{\varepsilon}^{\boldsymbol{\sigma}}$ is the dielectric constant tensor measured under a constant stress condition, and **d**, **e**, and **g** are the piezoelectric constant tensors.

The constant tensors are interrelated according to the relation:

$$\mathbf{d} = \boldsymbol{\varepsilon}\mathbf{g} = \mathbf{e}\mathbf{C}^{\mathbf{E}} \tag{5}$$

where T denote transposed matrix.

The physical constants for pled barium titanate are as follows: elasticity C $\sim 10^{11}$ N/m^2, permittivity ε $\sim 10^{-8}$ F/m and piezoelectricity e $\sim$ 10 C/m^2.

4 Methodology and Basic Formulations

4.1 Basic Equations for a 2-D Piezoelectric Solid

2-D piezoelectric solid in the bounded domain Ω is described by the balance equations of forces and electric charges (6), the piezoelectric constitutive Eqs. (7), (8) and the conditions on the boundary $\partial\Omega$ [17]:

$$\sigma_{\mathrm{ij},j} + b_i = 0; \quad i = 1, 2; \quad D_{j,j} - \omega_V = 0 \tag{6}$$

$$\begin{pmatrix} \sigma_{11} \\ \sigma_{22} \\ \sigma_{12} \end{pmatrix} = C \begin{pmatrix} u_{1,1} \\ u_{2,2} \\ u_{1,2} + u_{2,1} \end{pmatrix} + R^{T} \begin{pmatrix} \varnothing_{,1} \\ \varnothing_{,2} \end{pmatrix} \tag{7}$$

$$\begin{pmatrix} D_1 \\ D_2 \end{pmatrix} = R \begin{pmatrix} u_{1,1} \\ u_{2,2} \\ u_{1,2} + u_{2,1} \end{pmatrix} - K \begin{pmatrix} \varnothing_{,1} \\ \varnothing_{,2} \end{pmatrix} \tag{8}$$

where σ_{ij}, D_i, u_i, b_i $(i, j = 1, 2)$ denote the components of the stress tensor, the electric and mechanical displacements and the volume forces in a rectangular Cartesian x_1, x_2-coordinate system. ϕ is the electric potential and ω_V is the volume charge.

C, R, K are the matrices of the elastic, piezoelectric and dielectric constants c_{ij}, e_{ij}, κ_{ij} [17]:

$$C = \begin{pmatrix} c_{11} & c_{12} & 0 \\ c_{12} & c_{22} & 0 \\ 0 & 0 & c_{33} \end{pmatrix} \quad R = \begin{pmatrix} 0 & 0 & e_{13} \\ e_{21} & e_{22} & 0 \end{pmatrix} \quad K = \begin{pmatrix} \kappa_{11} & 0 \\ 0 & \kappa_{22} \end{pmatrix} \tag{9}$$

where R^{T} is transposition of matrix of R. Coefficients described by Eq. (9) characterize a transversely isotropic piezoelectric material with the x_2-axis being the poling direction.

4.2 Fundamental Solution and Stroh Formulations

The paper presents an effective implementation of boundary element multi-scale method in analyzing of piezoelectric ceramics. The presented method is applied based on constitutive equations and numerical modeling. This method can be easily used to get a better understanding of damage mechanism in the ceramic materials in order to improve the constitutive models and to support the future design of those materials. In this method the relation of boundary element method for obtaining traction in order to analysis cracked plate as well as plate with inclusion is presented. Then the basic will be used for multiscale modeling of piezoelectric ceramic.

First of all, the Stroh formulation which is applicable for obtaining fundamental solution equation of boundary element method is explained as below. In this method, the linear relation for piezoelectric materials is applied as:

$$\begin{aligned} \sigma_{ij} &= c_{ijkl} u_{k,l} + e_{lij} \varphi_{,l} \\ D_i &= e_{ikl} u_{k,l} - \kappa_{il} \varphi_{,l} \end{aligned} \tag{10}$$

In these equations, σ, D, u and φ are stress, electric displacement, displacement and u_α respectively; c, e and κ are elastic stiffnesses (elastic moduli), piezoelectric constants, dielectric constants respectively. In the next step, the equilibrium equation can be introduced as follow:

$$\sigma_{ij,j} + f_i = 0,\ D_{i,i} - q = 0 \tag{11}$$

In the case that $f_i = 0$ and absence of body charge, for two-dimensional deformation, solution of equilibrium equation which only depends on x_1 and x_2 can be considered as follow:

$$u_\alpha = a_\alpha f(x_1 + px_2) \quad \alpha = 1, 2, 3, 4 \tag{12}$$

For the $\alpha = 1 - 3$ the u_α is mechanical deformation and for $\alpha = 4$, u_α is electric field. a and p are constants which have to be determined according to properties of materials. Inserting Eq. (12) into linear piezoelectric materials relation can have following result:

$$\begin{aligned} \sigma_{ij} &= \left(c_{ijkl}a_k + e_{lij}a_4\right)(\delta_{l1} + p\delta_{l2})f' \\ D_i &= (e_{ikl}a_k - \kappa_{il}a_4)(\delta_{l1} + p\delta_{l2})f' \end{aligned} \tag{13}$$

where f' is differential of f and δ is Kronecker delta. Substitution of Eq. (13) into equilibrium equation, leads to following equation which gives solution for a_α and p:

$$\begin{aligned} &\left(c_{ijkl}a_k + e_{lij}a_4\right)\left(\delta_{j1} + p\delta_{j2}\right)(\delta_{l1} + p\delta_{l2}) = 0 \\ &(e_{ikl}a_k - \kappa_{il}a_4)(\delta_{i1} + p\delta_{i2})(\delta_{l1} + p\delta_{l2}) = 0 \end{aligned} \tag{14}$$

These equations can be written as

$$\left[\mathbf{Q} + p(\mathbf{R} + \mathbf{R}^{\mathbf{T}}) + p^2\mathbf{T}\right]\mathbf{a} = 0 \tag{15}$$

where

$$\mathbf{Q} = \begin{bmatrix} \mathbf{Q^e} & \mathbf{e_{11}} \\ \mathbf{e_{11}^T} & -\boldsymbol{\kappa}_{\mathbf{11}} \end{bmatrix}, \quad \mathbf{R} = \begin{bmatrix} \mathbf{R^e} & \mathbf{e_{21}} \\ \mathbf{e_{21}^T} & -\boldsymbol{\kappa}_{\mathbf{12}} \end{bmatrix}, \quad \mathbf{T} = \begin{bmatrix} \mathbf{T^e} & \mathbf{e_{22}} \\ \mathbf{e_{22}^T} & -\boldsymbol{\kappa}_{\mathbf{22}} \end{bmatrix} \tag{16}$$

Via this system of linear equations, the eigenvalues p and eigenvectors $a = [\,\mathrm{a}_1 \quad \mathrm{a}_2 \quad \mathrm{a}_3 \quad \mathrm{a}_4\,]$ can be approached. The matrices $\mathbf{Q^e}$, $\mathbf{R^e}$, $\mathbf{T^e}$ and $\mathrm{e_{ij}}$ are defined as follow:

$$Q_{ij}^e = c_{i1k1},\ R_{ik}^e = c_{i1k2},\ T_{ik}^e = c_{i2k2} \tag{17}$$

Nonzero solution of Eq. (15) needs to solution of calculate its determination as follow:

$$\left|\mathbf{Q} + p(\mathbf{R} + \mathbf{R}^{\mathbf{T}}) + p^2\mathbf{T}\right| = 0 \tag{18}$$

Via solving this equation eight values can be obtained for p. $p_\alpha(\alpha = 1, 2, 3, 4)$ which has positive imaginary part, leads to have eigenvector $a_\alpha(\alpha = 1, 2, 3, 4)$. Other four eigenvalues and corresponding eigenvectors can be written as follow:

$$p_{\alpha+4} = \bar{p}_\alpha, \quad a_{\alpha+4} = \bar{a}_\alpha \quad \mathrm{Im}(\overline{p}_\alpha) \rangle 0 \tag{19}$$

The result of these activities leads to have general solution for displacement and electric field in the form [26]:

$$u_i = A_{i\alpha} f_\alpha(z_\alpha) + \bar{A}_{i\alpha} \bar{f}_\alpha(z_\alpha) \quad \mathrm{i} = 1, 2, 3, 4 \tag{20}$$

which is written as

$$u_i = 2\mathrm{Re}(A_{i\alpha} f_\alpha(z_\alpha)) \quad \mathrm{i} = 1, 2, 3, 4 \tag{21}$$

Now, by differentiation of equation of displacement, the stress and electrical displacement can be obtained as follow [26]:

$$\sigma_{i1} = -\phi_{i,2}, \quad \sigma_{i2} = \phi_{i,1} \quad \mathrm{i} = 1, 2, 3, 4 \tag{22}$$

where $\phi_i = b_i f(x_1 + p x_2)$ is generalized stress and electrical displacement functional vector, the vector b is defined as

$$b = \left(\mathbf{R}^{\mathbf{T}} + p\mathbf{T}\right)\mathbf{a} = -(\mathbf{Q} + p\mathbf{R})\mathbf{a}/p \tag{23}$$

Equation (23) can be rewritten as eigenvector equation as

$$\mathbf{N} = \begin{bmatrix} \mathbf{N}_1 & \mathbf{N}_2 \\ \mathbf{N}_3 & \mathbf{N}_1^{\mathbf{T}} \end{bmatrix}, \quad \mathbf{N}\,\boldsymbol{\xi} = p\boldsymbol{\xi}, \quad \mathbf{N}^{\mathrm{T}}\boldsymbol{\eta} = p\boldsymbol{\eta} \tag{24}$$

where $\mathbf{N}_1 = -\mathbf{T}^{-\mathbf{1}}\mathbf{R}^{\mathbf{T}}$, $\mathbf{N}_2 = \mathbf{T}^{-\mathbf{1}}$, $\mathbf{N_3} = \mathbf{R}\mathbf{T}^{-\mathbf{1}}\mathbf{R}^{\mathbf{T}} - \mathbf{Q}$; $\boldsymbol{\xi} = [\mathbf{a}, \mathbf{b}]^{\mathbf{T}}$ is a right eigenvector; $\boldsymbol{\eta} = [\mathbf{b}, \mathbf{a}]^{\mathbf{T}}$ is left eigenvector of matrix $\mathbf{N}$; vector η_i and ξ_i obtained for the eigenvalue p_i and q_i can be normalized as

$$\xi_i^T \eta_j = \delta_{ij} \tag{25}$$

This rule (25) is the most important for obtaining fundamental solution via Stroh formulation for boundary element method. Without establishing this rule, the boundary element method will have accurate solution for elasticity problems. So, the general solution for electromechanical problems can be written as

$$u_i = 2\mathrm{Re}(A_{i\alpha} f_\alpha(z_\alpha)), \quad \phi_i = 2\mathrm{Re}(B_{i\alpha} f_\alpha(z_\alpha)) \quad \mathrm{i} = 1, 2, 3, 4 \tag{26}$$

where $\mathbf{A} = [\,\mathbf{a_1} \quad \mathbf{a_2} \quad \mathbf{a_3} \quad \mathbf{a_4}\,]$ and $\mathbf{B} = [\,\mathbf{b_1} \quad \mathbf{b_2} \quad \mathbf{b_3} \quad \mathbf{b_4}\,]$; $z_\alpha = x_1 + p_\alpha x_2$. Generalized solution of Stroh electroelastic problem by Stroh formulations, allows to define fundamental solution for linear force and point charge acting at point $Z_0 = (x_{01}, x_{02})$ of infinite piezoelectric medium [27]:

$$U_{ij}(X,Z_0)=\frac{1}{\pi}\mathrm{Im}\left[A_{i\alpha}A_{j\alpha}\ln Z_\alpha(X,Z_0)\right]$$
$$T_{ij}(X,Z_0)=\frac{1}{\pi}\mathrm{Im}\left[A_{i\alpha}B_{j\alpha}(n_2-n_1p_\alpha)\frac{1}{Z_\alpha(X,Z_0)}\right], \tag{27}$$

where $Z_\alpha(X,Z_0)=x_1+p_\alpha x_2-(x_{01}+p_\alpha x_{02})$.

4.3 Basic Equations of Boundary Element Method

Now it is opportunity to define boundary element method which is a numerical method based on numerical integral over boundary of model. The Eq. (28) shows the traditional boundary element equation of displacement. In this equation u and t are displacement and traction and U and T are fundamental solution for displacement and traction, respectively.

$$\frac{1}{2}u(Z_0)=\int_s U(X,Z_0)\,t(Q)\,ds(X)-\int_S T(X,Z_0)\,u(Q)\,ds(X) \tag{28}$$

The Fig. 4 shows a simple example that how the boundary integral method should be discretized over boundary of solids to obtain unknown. In this figure as it is clear, in some boundaries traction is unknown and in other ones displacement is unknown so via discrediting the Eq. (28), numerical equation can be obtained as:

$$\frac{1}{2}u^e+\sum_{e=1}^{8}\Delta T_i^e\,u^e=\sum_{e=1}^{8}\Delta U_i^e t^e \tag{29}$$

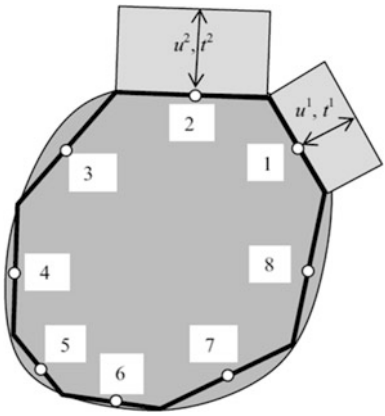

Fig. 4 Simple example of using boundary element equation in order to obtain displacement and traction

in which ΔT_i and ΔU_i can be obtained as follow:

$$\Delta T_i^e = \int_{s_e} T(X, Z_{0i}) ds_e(X) \quad \Delta U_i^e = \int_{s_e} U(X, Z_{0i}) ds_e(X) \tag{30}$$

The following linear algebraic equation can be achieved.

$$[\Delta T]\{u\} = [\Delta U]\{t\} \tag{31}$$

In the Eq. (31), $[\Delta T]$ and $[\Delta U]$ can be defined as follow:

$$\begin{bmatrix} \frac{1}{2} + \Delta T_1^1 & \Delta T_1^2 & \dots \\ \Delta T_2^1 & \frac{1}{2} + \Delta T_2^2 & \dots \\ \dots & \dots & \dots \end{bmatrix} \begin{Bmatrix} u^1 \\ u^2 \\ \vdots \end{Bmatrix} = \begin{bmatrix} \frac{1}{2} + \Delta U_1^1 & \Delta U_1^2 & \dots \\ \Delta U_2^1 & \frac{1}{2} + \Delta U_2^2 & \dots \\ \dots & \dots & \dots \end{bmatrix} \begin{Bmatrix} t^1 \\ t^2 \\ \vdots \end{Bmatrix} \tag{32}$$

Through solving these algebraic equations, the unknown parameters can be approached. One the most important application of boundary element method is solving the plate problem which contains different kinds of crack and holes. So far, some researchers investigated this kind of problem via different numerical and analytical methods. Particular attention should be paid to modelling of the singular integral near the crack tip. This issue will be discussed in future chapters of current paper. By the way, the displacement equation of boundary element method for cracked plate can be written as follow [28]:

$$\begin{aligned} \frac{1}{2} u_i(Z_0) = & \int_s U_{ij}(X, Z_0)\, t_j(X) ds(X) - \int_s T_{ij}(X, Z_0)\, u_j(X) ds(X) \\ & + \int_\Gamma U_{ij}(X, Z_0) \sum t_j(X) ds(X) - \int_\Gamma T_{ij}(X, Z_0)\, \Delta u_j(X) ds(X) \end{aligned} \tag{33}$$

In this equation, Δu is difference between displacements at crack upper and lower crack surface and $\sum t_j$ is sum of the traction at upper and lower crack surface. Generally speaking, $\sum t_j$ should be equal to zero, however, here we ignore this simplification in order to achieve correct equation for traction boundary element equation. s is boundary of main body and Γ is boundary of crack. Via differentiation of Eq. (33) and utilizing Hook's law, the following equation can be achieved which is boundary element equation for traction [28]:

$$\begin{aligned} & n_m(Z_0) \int_s D_{jlm}(X, Z_0) t_j(z) ds(X) - n_m(Z_0) \int_s W_{jlm}(X, Z_0) \frac{\partial u_j(X)}{\partial s(X)} ds(X) \\ & + n_m(Z_0) \int_\Gamma D_{jlm}(X, Z_0) \Sigma t_j(X) ds(z) - n_m(Z_0) \int_\Gamma W_{jlm}(Z, X_0) \frac{\partial \Delta u_j(Z)}{\partial s(Z)} ds(Z) \\ & = \begin{cases} \frac{1}{2} t_l(Z_0) & Z_0 \in s \\ \frac{1}{2}\left(t_l^+(Z_0) - t_l^-(Z_0)\right) & Z_0 \in \Gamma \end{cases} \end{aligned} \tag{34}$$

where $\frac{\partial \Delta u_j(Z)}{\partial s(Z)}$ is dislocation density. D and W can be written as:

$$\begin{aligned} D_{ijk}(X, Z_0) &= -\frac{1}{\pi} \mathrm{Im}\left[B_{i\alpha} A_{k\alpha} (\delta_{2j} - \delta_{1j} p_\alpha) \frac{1}{Z_\alpha(X, Z_0)} \right], \\ W_{jlm}(X, Z_0) &= c_{lmik} (\delta_{1i}\delta_{2j} - \delta_{2i}\delta_{1j}) D_{ijk}(X, Z_0) \end{aligned} \tag{35}$$

In the Eq. (34), the dislocation density can be obtained over the crack tip (Fig. 5) which is useful for obtaining stress intensity factor.

4.4 Numerical Implementation of Boundary Element Method

Similar to all of numerical methods, boundary element method needs to be discretized in order to be solved numerically. Figure 4 shows clearly that the boundary of model can be replaced by assembly of linear elements. In this subsection, some explanation about discretization of all of the boundaries of body into serious of segments will be presented. To discretized the integral over boundary to small linear element, it is essential to define variable coordinate for each element as follow,

$$x_i = N_1(\zeta) x_i^{(1)} + N_2(\zeta) x_i^{(2)}, \quad (|\zeta| \le 1) \tag{36}$$

where N_1 and N_2 as shape functions can be defined as:

$$\begin{aligned} N_1(\zeta) &= \frac{1}{2}(1 - \zeta), \\ N_2(\zeta) &= \frac{1}{2}(1 + \zeta) \end{aligned} \tag{37}$$

where $\left(x_1^{(1)}, x_1^{(2)}\right)$ and $\left(x_2^{(1)}, x_2^{(2)}\right)$ are coordinate of initial and end node of element, respectively. For general elements, traction and dislocation density can be shown as:

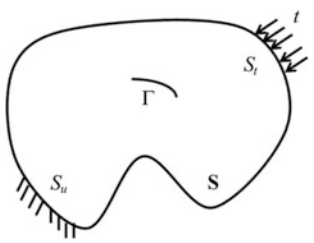

Fig. 5 Discretized boundary on the element and crack surface

$$t_i = N_1(\zeta) t_i^{(1)} + N_2(\zeta) t_i^{(2)},$$
$$\frac{\partial u_i}{\partial s} = N_1(\zeta) \frac{\partial u_i^{(1)}}{\partial s} + N_2(\zeta) \frac{\partial u_i^{(2)}}{\partial s}, \tag{38}$$

and for crack surface:

$$\sum t_i = N_1(\zeta) \sum t_i^{(1)} + N_2(\zeta) \sum t_i^{(2)},$$
$$\frac{\partial \Delta u_i}{\partial s} = N_1(\zeta) \frac{\partial \Delta u_i^{(1)}}{\partial s} + N_2(\zeta) \frac{\partial \Delta u_i^{(2)}}{\partial s}, \tag{39}$$

In the case of element on crack tip, the formulation is a little different than normal ones considering that these elements must treat singularity on the crack tip. For an element at crack tip, two different formulations can be define according to nodes, for local node 1 it can be represented by:

$$\frac{\partial \Delta u_i}{\partial s} = \frac{\partial \Delta u_i^{(1)}}{\partial s} / \sqrt{N_2(\zeta)} + N_2(\zeta) \left(\frac{\partial \Delta u_i^{(2)}}{\partial s} - \frac{\partial \Delta u_i^{(1)}}{\partial s} \right), \tag{40}$$

and for node 2, similarly it can be approximated by:

$$\frac{\partial \Delta u_i}{\partial s} = \frac{\partial \Delta u_i^{(2)}}{\partial s} / \sqrt{N_1(\zeta)} + N_1(\zeta) \left(\frac{\partial \Delta u_i^{(1)}}{\partial s} - \frac{\partial \Delta u_i^{(2)}}{\partial s} \right). \tag{41}$$

5 Multiscale Modeling

The macro-scale modeling is based on micro-continuum theories, however, paying attention to this point is necessary in order to save material integrity, no constitutive law or damage have to be considered. In the next step, by applying the boundary condition on a representative volume element (RVE) which was obtained from the calculation of macro-scale, the cohesive laws can be brought up for modeling of crack initiation and propagation in the RVE. The RVE is a small volume of microstructure that has the general characteristics of the whole microstructure such as volume fraction, morphology and randomness of the phases and over which modeling of specific characteristics is carried out [29]. All information from the micro-scale can be transferred to macro level to modify the results and model the next steps. In Fig. 6 it is shown that the calculation of micro-scale is able to provide boundary conditions for micro-scale, on the other hand, micro-scale will provide some information by which the constitutive law can be modified and possible damage can be modeled for next steps as well.

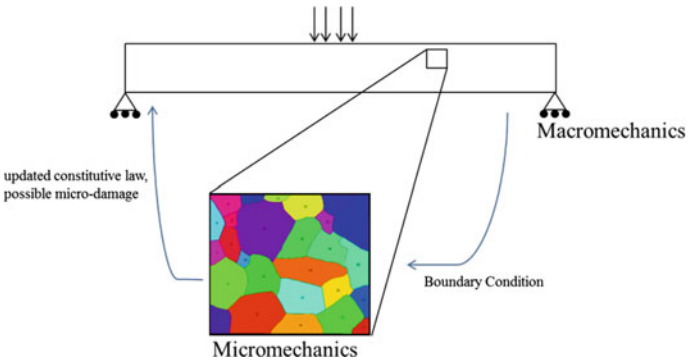

Fig. 6 Schematic view of a multiscale tension modeling

Via fundamental boundary element equation the displacement equation for each grain can be written as:

$$C_{ij}^{H}(z_k^{'})\tilde{u}_j^{H}(z_k^{'}) + \int_{S_{nc}^{H}} \tilde{T}_{ij}^{H}(z_k^{'}, z_k)\tilde{u}_j^{H}(z_k)dS_{nc}^{H} + \int_{S_c^{H}} \tilde{T}_{ij}^{H}(z_k^{'}, z_k)\tilde{u}_j^{H}(z_k)dS_c^{H}$$
$$= \int_{S_{nc}^{H}} \tilde{U}_{ij}^{H}(z_k^{'}, z_k)\tilde{t}_j^{H}(z_k)dS_{nc}^{H} + \int_{S_c^{H}} \tilde{U}_{ij}^{H}(z_k^{'}, z_k)\tilde{t}_j^{H}(z_k)dS_c^{H} \quad (42)$$

In Eq. (42), $\tilde{T}_{ij}^{H}(z_k^{'}, z_k)$ and $\tilde{U}_{ij}^{H}(z_k^{'}, z_k)$ are fundamental solutions for traction and displacement which can be obtained via Stroh formulation for each grain. S_c^{H} and S_{nc}^{H} belong to boundary of internal grain and (contact boundary) and free boundary.

6 Results and Discussion

6.1 Cracked Plate

In order to measure efficiency of presented formulation, some numerical examples were done. The Fig. 7 shows variation of stress versus the distance from crack tip. It can be concluded that the stress near crack tip has the highest amount and by moving far from crack tip, stress is decreased which show the accuracy of Eqs. (40) and (41) in treating singular integral near crack tips. The figure shows the variation of stress for three different paths with different angles. In order to show the influence of crack length on stress intensity factor, the kicked crack was simulated. The result is shown in Fig. 8. By variation of θ and increasing the length of crack, the stress intensity factor for mode one increases and after pick at $\theta = 0$ crack length decreases again to its lowest amount.

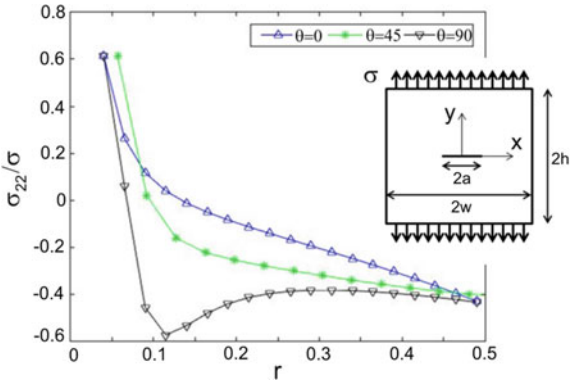

Fig. 7 Central crack in a rectangular piezoelectric plate, a/w = 0.06

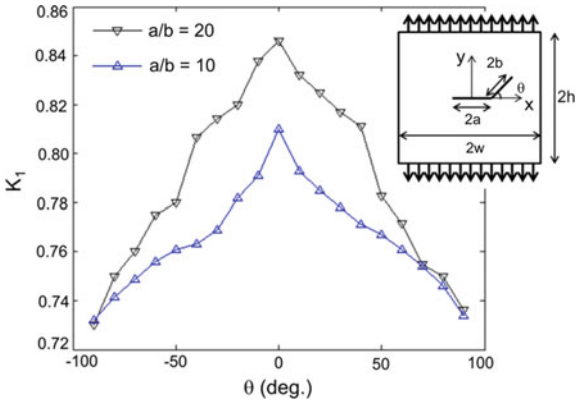

Fig. 8 Variation of the normalized mode I stress intensity factor for a/b = 10, and 20

6.2 *Piezoelectric Plate with Inclusion*

In this subsection, first some equation for plate with inclusion will be presented, the results will be discussed. In the case when there are inclusions: circular (Fig. 9a) and rectangular (Fig. 9b), boundary element integral can be written for matrix s and inclusion Γ as:

$$\begin{aligned}\frac{1}{2}u(X) &= \int_{s+\Gamma} U^0(Z_0,X)\,t(X)ds(X) - \int_{s+\Gamma} T^0(Z_0,X)\,u(X)ds(X) \quad X \in s \cup \Gamma \\ \frac{1}{2}u(X) &= \int_{\Gamma} U^1(Z_0,X)\,t(X)ds(X) - \int_{\Gamma} T^1(Z_0,X)\,u(X)ds(X) \quad X \in \Gamma\end{aligned} \tag{43}$$

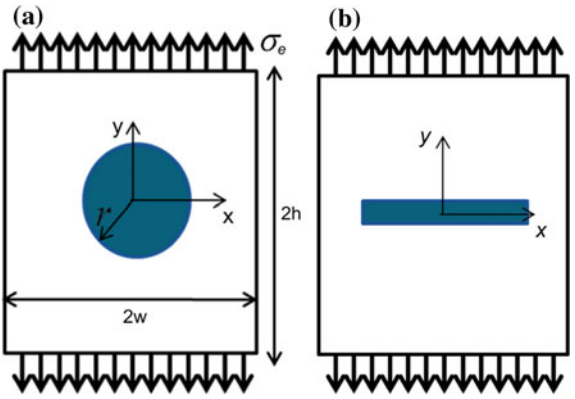

Fig. 9 The rectangular piezoelectric with circular (**a**) and rectangular (**b**) inclusion

where 0 and 1 indicate the matrix and inclusion sub domain, respectively. After discretization and using linear or quadratic elements, Eq. (43) can be expressed as:

$$\begin{bmatrix} \mathbf{A}_{11}^{0} & \mathbf{A}_{12}^{0} & \mathbf{A}_{13}^{0} \\ \mathbf{A}_{21}^{0} & \mathbf{A}_{22}^{0} & \mathbf{A}_{23}^{0} \\ \mathbf{A}_{31}^{0} & \mathbf{A}_{32}^{0} & \mathbf{A}_{33}^{0} \end{bmatrix} \begin{Bmatrix} \mathbf{U}^{0} \\ \mathbf{T}^{0} \\ \mathbf{U}^{i} \end{Bmatrix} = \begin{bmatrix} \mathbf{B}_{11}^{0} & \mathbf{B}_{12}^{0} & \mathbf{B}_{13}^{0} \\ \mathbf{B}_{21}^{0} & \mathbf{B}_{22}^{0} & \mathbf{B}_{23}^{0} \\ \mathbf{B}_{31}^{0} & \mathbf{B}_{32}^{0} & \mathbf{B}_{33}^{0} \end{bmatrix} \begin{Bmatrix} \bar{\mathbf{T}}^{0} \\ \bar{\mathbf{U}}^{0} \\ \mathbf{T}^{i0} \end{Bmatrix} \tag{44}$$

$$\mathbf{G}^{i}\mathbf{T}^{ii} = \mathbf{H}^{i}\mathbf{U}^{i}$$

where $\mathbf{U}^{0}$ and $\bar{\mathbf{T}}^{0}$ represent the unknown nodal displacement and known nodal traction, respectively, on matrix; $\mathbf{T}^{0}$ and $\bar{\mathbf{U}}^{0}$ are the unknown nodal traction and known nodal displacement on matrix; $\mathbf{U}^{i}$ is the unknown nodal displacement on interface: While $\mathbf{T}^{i0}$ and $\mathbf{T}^{ii}$ express the unknown nodal traction on the interface for the matrix and inclusion, respectively.

The results of numerical examples are presented in Figs. 10 and 11.

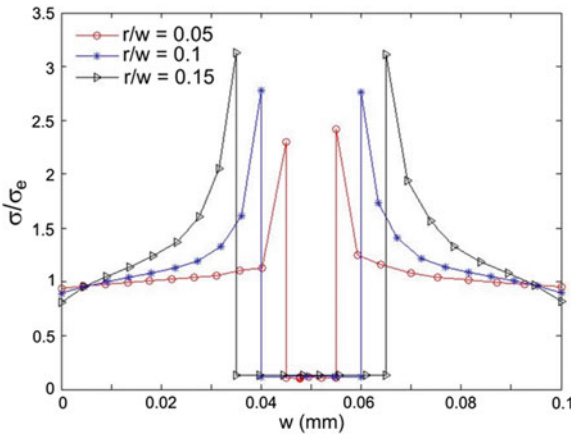

Fig. 10 Variation of stress near circular inclusion in rectangular piezoelectric plate

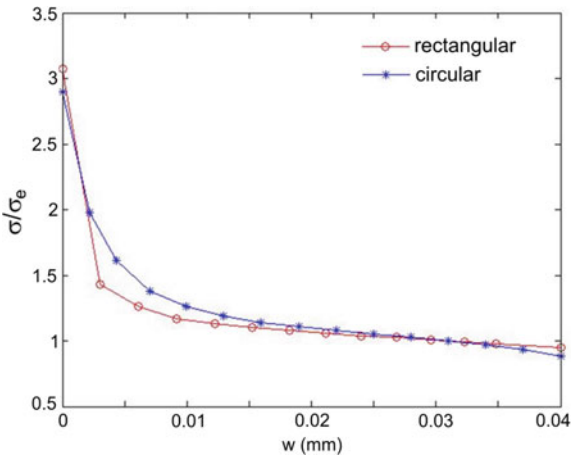

Fig. 11 Variation of stress near circular and rectangular inclusion at centre of inclusion in piezoelectric plate

It is clear from Fig. 10 that near interface of circular inclusion (which is shown in Fig. 9) and matrix, the stress has its highest amount and when it goes far from interface, the stress decrease to its lowest amounts. So, it can be concluded that inclusion can have the effect similar to hole and crack. Another point in this figure is that for bigger inclusion, the higher amount of stress can be happen. Figure 11 compares the variation of stress near interface of rectangular and circular inclusion. The length of rectangular inclusion is equal to diameter of circular one. The variation of stress near interface of both inclusions is the same which shows that stress is independent of shape of inclusion.

7 Summary

In this chapter the multiscale BEM is applied to study the crack propagation in barium titanate piezoelectric ceramic. Furthermore, the mathematical bridges meso-scale to macro-scale by the damage parameter were formulated. The developed method is applied based on the numerical modelling and constitutive equations and can be easily used to get a better understanding of damage mechanism in the ceramic materials. In this method the relation of boundary element method for obtaining traction in order to analysis cracked plate as well as plate with inclusion is presented. For obtaining fundamental solution equation of BEM the Stroh formulation is applied. It was found that the shape of interface does not have a great influence on the stress intensity. Considering the dimensions of inclusion it can be concluded that inclusion can have the effect similar to the hole and the crack; bigger inclusion leads to an increase of the stress.

Acknowledgements The research leading to these results has received funding from the People Programme (Marie Curie Actions) of the European Union's Seventh Framework Programme FP7/2007-2013/under REA grant agreement No. PITN-GA-2013-606878.

References

1. Biglar, M., Gromada, M., Stachowicz, F., Trzepieciński, T.: Optimal configuration of piezoelectric sensors and actuators for active vibration control of a plate using a genetic algorithm. Acta Mech. **226**, 3451–3462 (2015)
2. Banks-Sills, L.: Fracture criteria for piezoelectric ceramics. In: Proceedings of 13th International Conferences on Fracture, pp. 1–7, 16–21 June 2013, Beijing, China
3. Nunkumwong, J., Srisombat, L., Ananta, S.: Effect of sintering temperature on phase for-mation, microstructure and dielectric properties of nanogold modified barium titanate-ceramics. Current Appl. Phys. **14**, 1312–1317 (2014)
4. George, C.N., Thomas, J.K., Kumar, H.P., Suresh, M.K., Kumar, V.R., Wariar, P.R.S., Jose, R., Koshy, J.: Characterization, sintering and dielectric properties of nanocrystalline barium titanate synthesized through a modified combustion process. Mater. Charact. **60**, 322–326 (2009)
5. Jordan, T.L., Qunaies, Z.: Piezoelectric ceramics characterization. ICASE report no. 2001–28, Langley Research Center, Hampton, USA
6. Gromada, M., Biglar, M., Trzepieciński, T., Stachowicz, F.: Characterisation of $BaTiO_3$ piezoelectric perovskite material for multilayer actuators. Bull. Mater. Sci. (2017) Accepted for publication
7. Shindo, Y., Ozawa, E., Nowacki, J.P.: Singular stress and electric fields of cracked piezoelectric strip. Int. J. Appl. Electromagn. Mater. **1**, 77–87 (1990)
8. Suo, Z., Kuo, C.M., Barnett, D.M., Willis, J.R.: Fracture mechanics for piezoelectric ceramics. J. Mech. Phys. Solids **40**, 739–765 (1992)
9. Wang, H., Singh, R.N.: Crack propagation in piezoelectric ceramics: Effects of applied electric fields. J. Appl. Phys. **81**, 7471–7479 (1997)
10. Fu, R., Zhang, T.Y.: Effects of an electric field on the fracture toughness of poled lead zirconate titanate ceramics. J. Amer. Ceram. Soc. **83**, 1215–1218 (2000)
11. Shindo, Y., Narita, F., Mikami, M.: Double torsion testing and finite element analysis for determining the electric fracture properties of piezoelectric ceramics. J. Appl. Phys. **97**, 114109 (2005)
12. Zhang, T.Y.: Studies of fracture of piezoelectric ceramics at HKUST. Key Eng. Mater. **183–187**, 773–778 (2000)
13. Wilson, Z.A., Borden, M.J., Landis, C.M.: A phase-field model for fracture in piezelectric ceramics. Int. J. Fract. **183**, 135–153 (2013)
14. Jelitto, H., Kessler, H., Schneider, G.A., Balke, H.: Fracture behavior of poled piezoelectric PZT under mechanical and electrical loads. J. Eur. Ceram. Soc. **25**, 749–757 (2005)
15. Motola, Y., Banks-Sills, L., Fourman, V.: On fracture testing of piezoelectric ceramics. Int. J. Fract. **159**, 167–190 (2009)
16. Banks-Sills, L., Heller, L., Fourman, V.: A supplementary study on fracture tests of piezoelectric material: cracks parallel to the poling direction. Int. J. Fract. **175**, 109–125 (2012)
17. Groh, U., Kuna, M.: Efficient boundary element analysis of cracks in 2D piezoelectric structures. Int. J. Solids Struct. **42**, 2399–2416 (2005)
18. Xu, X.L., Rajapakse, R.K.N.D.: Boundary element analysis of piezoelectric solids with defects. Compos. Eng. B **29**, 655–669 (1998)
19. Pan, E.: A BEM analysis of fracture mechanics in 2D anisotropic piezoelectric solids. Eng. Anal. Bound. Elem. **23**, 67–76 (1999)

20. Davì, G., Milazzo, A.: Multidomain boundary integral formulation for piezoelectric materials fracture mechanics. Int. J. Solids Struct. **38**, 7065–7078 (2001)
21. Lekhnitskii, S.G.: Theory of Elasticity of an Anisotropic Body. Holden-Day, San Francisco, USA (1963)
22. Rajapakse, R.K.N.D., Xu, X.L.: Boundary element modelling of cracks in piezoelectric solids. Eng. Anal. Bound. Elem. **25**, 771–781 (2001)
23. Aliabadi, M.H., Rooke, D.P.: Numerical Fracture Mechanics. Kluwer Academic Publisher, Dordrecht/Boston/London (1991)
24. Snyder, M.D., Cruse, T.A.: Boundary-integral equation analysis of cracked anisotropic plates. Int. J. Fract. **11**, 315–328 (1975)
25. Katz, H.W.: Solid State Magnetic and Dielectric Devices. Wiley, New York (1959)
26. Fang, D., Liu, J.: Fracture Mechanics of Piezoelectric and Ferroelectric Solids. Springer Verlag, Berlin (2013)
27. Pasternak, I.: Doubly periodic arrays of cracks and thin inhomogeneities in an infinite magnetoelectroelastic medium. Eng. Anal. Bound. Elem. **36**, 799–811 (2012)
28. Liew, K.M., Sun, Y., Kitipornchai, S.: Boundary element-free method for fracture analysis of 2-D anisotropic piezoelectric solids. Int. J. Num. Meth. Eng. **69**, 729–749 (2007)
29. Snyder, M.D., Cruse, T.A.: Boundary-integral equation analysis of cracked anisotropic plates. Int. J. Fract. Mech. **11**, 315–328 (1975)

Rotational Waves in Microstructured Materials

Vladimir I. Erofeev and Igor S. Pavlov

Abstract A brief review of theoretical representations and experimental data on rotational motions of elements of a continuous medium is given. Description of wave rotational motions is impossible in the framework of the classical theory of elasticity, but it is allowed within the scope of generalized continua models (the Cosserat microspolar model, moment and gradient models, etc.). The numerical modeling of the parameters of the Cosserat medium is carried out by the structural modeling method, and the ranges of existence of rotational waves are determined for some crystals with cubic symmetry. A new approach to the solution of the problem of rotational motions is offered for the "geological block" continuum, namely, A.V. Vikulin's model, in which the stresses are described by a symmetric tensor. Geological and geophysical data are presented that confirm both rotational approaches to describing the blocks and plates composing a geomedium, and the existence of rotational waves.

1 Introduction

One of the main ways of describing the deformation of solids is the classical theory of elasticity considering a medium as a continuum of material points possessing, in general, three translational degrees of freedom. However, yet in the middle of the 19th century, works began to appear with deviations from the canons of the classical continuum (see, for example [1–5]). In 1909, the brothers Eugne and Franois

V. I. Erofeev (✉) · I. S. Pavlov
Mechanical Engineering Research Institute of Russian Academy
of Sciences IPM RAN, 85 Belinskogo str., 603024 Nizhny Novgorod, Russia
e-mail: erof.vi@yandex.ru

I. S. Pavlov
e-mail: ispavlov@mail.ru

V. I. Erofeev · I. S. Pavlov
Nizhny Novgorod Lobachevsky State University, 23 Gagarin av.,
603950 Nizhny Novgorod, Russia

F. dell'Isola et al. (eds.), *Advances in Mechanics of Microstructured Media and Structures*, Advanced Structured Materials 87,
https://doi.org/10.1007/978-3-319-73694-5_7

Cosserat laid the theoretical foundations of one of the first (and at this moment, perhaps, the best known) continuum models of an elastic medium that cannot be described within the scope of the classical theory of elasticity [6]. The Cosserat medium named in their honor consists of solid non-deformable body-particles having three translational and three rotational degrees of freedom.

In the three-dimensional case, the linear dynamic equations of the Cosserat continuum can be written in the vector form:

$$\rho\frac{\partial^2\mathbf{u}}{\partial t^2} - (\lambda + 2\mu)\text{grad}\,\text{div}\,\mathbf{u} + (\mu + \alpha)\text{rot}\,\text{rot}\,\mathbf{u} - 2\alpha\text{rot}\,\boldsymbol{\Phi} = 0, \tag{1}$$

$$J_i\frac{\partial^2\boldsymbol{\Phi}}{\partial t^2} - (\beta + 2\gamma)\text{grad}\,\text{div}\,\boldsymbol{\Phi} + (\gamma + \varepsilon)\,\text{rot}\,\boldsymbol{\Phi} - 2\alpha\text{rot}\,u + 4\alpha\boldsymbol{\Phi} = 0, \tag{2}$$

where $\mathbf{u}$ is the displacement vector, $\boldsymbol{\Phi}$ is the vector of rotation angles of an element of a medium in the reference frame related to its mass center, J_i are the corresponding inertia moments of elements of a medium, ρ is the density of a medium, λ and μ are Lame constants corresponding to the classical theory of elasticity, α, β, γ, and ε are the parameters of the Cosserat medium.

In this system, Eq. (1) characterizes propagation of translational waves (dilatation and shear waves) in a medium, but, in distinct from the classical case, shear waves are linearly related to rotational waves, the propagation of which is described by Eq. (2). The propagation of rotational wave perturbations in the Cosserat medium occurs by means of a moment (noncentral) interaction of its elements with each other.

The Cosserat theory is a mathematical description of such a phenomenon as rotational waves. Is it possible to observe them experimentally?

In the middle of 1930s and early 1940s, experimental physicists paid attention to the importance of taking into account the rotational degrees of freedom of the elements (particles) of the medium. Thus, the experiments of B. Bauer and M. Mag are very interesting [7]. They compared the scattering spectra for heavy and light water. From the comparison of spectra of these two substances, which molecules have approximately the same mass, but different moments of inertia, the authors made a conclusion about existence of both translational and rotational oscillations of molecules. J. Bernal and J. Tamm [8] explained the differences between some physical properties of light and heavy water under the assumption about the existence of rotational oscillations.

In 1940 E.F. Gross [7] observed the effect of variation of the wavelength of scattered light in a liquid associated with orientation fluctuations of anisotropic molecules. He remarked that the axes of molecules can rotate by a significant angle, if the oscillation period is much larger than the relaxation time. Later, E.F. Gross and A.V. Korshunov established experimentally [9] that in crystals of some organic substances (for instance, benzene and naphthalene) the scattering spectrum of small frequencies is associated with rotational vibrations of molecules. The scattering spectrum is the most intensive in substances, which molecules have a large optical anisotropy (carbon disulfide, naphthalene, benzene). The crystal lattices of such

substances consist of large molecules. In them, the intermolecular forces are usually much larger than the van der Waals forces acting between the molecules; therefore, the molecules can be regarded as solid bodies oscillating with respect to each other. There are translational oscillations of molecules, rotational oscillations, as well as mixed translational-rotational oscillations. Experimental studies of oscillations in such crystals, carried out by Raman scattering, have shown that in the vicinity of the Rayleigh lines there are characteristic scattering lines due to the rotational nature of molecular oscillations [10, 11]. In experiments on spectrograms of light scattering in organic substances, estimates have been obtained for the threshold frequency of benzene and naphthalene [10].

From the beginning of the 1960s generalized models of the Cosserat continuum are intensively developed [12]: the theory of oriented media, asymmetric, multipolar, micromorphic, gradient theories of elasticity. So, on the basis of assumption of the rotational interaction of particles of elongated shape in an anisotropic elastic medium, E.L. Aero and E.V. Kuvshinsky [13, 14] generalized the phenomenological theory of elasticity in order to explain some anomalies in the dynamic behavior of plastics, to which the classical theory of elasticity did not provide a satisfactory treatment. Later, the idea of an "oriented" continuum, each point of which is assigned a direction (the field of a director), was developed in the theory of liquid crystals [15, 16], where the director waves in liquid crystals are, in fact, analogues of rotational waves in solids, however, like spin waves in ferromagnets [17]. Chapter 4 of the monograph [17] by A.I. Akhiezer, et al. deals with the analysis of coupled spin and acoustic waves in ferromagnets. Elastic waves are considered in the framework of the classical theory without taking into account microrotations, but it is shown that, due to the relatedness of the elastic deformations with the magnetic field of spins, the stress tensor is no longer symmetric, i.e., in an elastic ferromagnet there appear couple stresses at the excitation of the spin waves. In the monograph by V.E. Lyamov [18] it was shown that the account of microrotations in crystals leads to the appearance of the spatial dispersion and new wave modes.

In the last 30 years, the processes of propagation and interaction of elastic (acoustic) waves in microstructured solids have been extensively studied theoretically and experimentally (see, e.g., [19–33]). And the first experiments on acoustics of microstructured solids were performed yet in 1970 by G.N. Savin et al. [34, 35]. The authors established the correlation between the grain size in different metals and aluminum alloys and the dispersion of the acoustic wave. Dispersion of the ultrasound waves was observed by V.I. Erofeev and V.M. Rodyushkin in an artificial composite—ferrite pellets in epoxy resin [36]. The appearance of a wave dispersion "forbidden" by the classical theory of elasticity can be explained, in particular, by the influence of rotational modes. Moreover, A.I. Potapov and V.M. Rodyushkin [37] experimentally observed the transfer of momentum in a microstructured material with the velocity that is distinct from the longitudinal wave velocity. A clear separation of the impact pulse into two components was observed in this case. This fact indicates that pulse is carried by two types of oscillations differing from each other in velocity.

Nevertheless, still nobody could observe experimentally the propagation of rotational waves in "laboratory conditions". So, the question arises: "Why?".

The method of ***structural modeling*** [26, 38] is used in this work for answer this question. This method is an alternative to the continuum approach to constructing models of microstructured media, within the scope of which the Cosserat brothers obtained Eqs. (1) and (2). These equations contain material constants, which relation with a material structure is not clear. Such constants have to be determined experimentally. This especially regards to the generalized models of the Cosserat continuum [30, 39]. However, the structural modeling does not have this drawback.

2 Basic Stages of the Structural Modeling

Elaboration of a structural model starts with the selection of a certain minimum volume (a structural cell that is analog of the periodicity cell in the crystalline material) in the bulk of a material represented by a regular or a quasiregular lattice consisting of particles of finite sizes. Such a cell is capable of reflecting the main features of the macroscopic behavior of this material [40, 41]. As a rule, a structural cell represents a particle, which behavior is characterized by interaction with its environment and is described by kinematic variables. For instance, domains, granules, fullerenes, nanotubes, or clusters of nanoparticles can play the role of such bodies. Sometimes, particles are represented as material points—i.e. centers of forces possessing properties of mass, charge, and so on [42, 43]. It is assumed that the interaction forces decrease rapidly with growing of distance and they can be neglected if the distance between the points exceeds the "molecular action radius".

At the second stage, the simulation of force interactions is carried out. Since small deviations of the particles from the equilibrium states are considered, the force and moment interactions of the particles can be described by a power-law potential. In the harmonic approximation, the interaction potential is a quadratic form of the variables of a state of the system. The potential energy per lattice cell is equal to the potential energy of the particle interacting with its neighbors.

In phenomenological theories, material constants must be measured in experiments. Their connection with the geometric structure and force interactions in the crystal lattice is unclear. Only some restrictions on their values can be obtained from the general energy considerations and symmetry conditions. However, the structural approach enables one to find an explicit relationship between the elements of the force matrices and the lattice parameters.

In mechanics of deformable solids, the structural modeling involves, instead of a field description of the interaction of particles, entering an equivalent force scheme in the form of a system of rods or springs transmitting forces and moments between the structural elements [44–46]. In this paper, a spring model is used. When a scheme of force interactions is introduced, round particles are replaced, for convenience, by inscribed polygons, the shape of which repeats the shape of a cell. The springs

modeling transfer of force interactions between the particles are assumed to be fixed at the vertices of polygons and have different coefficients of elasticity.

Due to expressions for the kinetic and potential energy that were obtained at the previous stages, it is possible to make up differential-difference equations describing the lattice dynamics. Such equations represent Lagrange equations of the second kind

$$\frac{d}{dt}\left(\frac{\partial L}{\partial \dot{q}_{i,j}^{(l)}}\right) - \frac{\partial L}{\partial q_{i,j}^{(l)}} = 0,$$

where $L = T_{i,j} - U_{i,j}$ is the Lagrange function, which is equal to the difference between the kinetic and potential energy of a cell, $q_{i,j}^{(l)}$ are the generalized coordinates, $\dot{q}_{i,j}^{(l)}$ are the generalized velocities.

A transition from discrete models to continual ones is performed by extrapolating the functions specified at discrete points by continuous fields of displacements and micro-rotations. For long-wavelength perturbations, when $\Lambda \gg a$ (where λl is a characteristic spatial scale of deformation), discrete labels i and j can be changed by means of a continuous spatial variables $x = ia$ and $y = ja$. In this case, the functions specified at discrete points are interpolated by the continuous functions and their partial derivatives in accordance with the standard Taylor formula. Depending on the number of interpolation terms, one can consider various approximations of a discrete model of a microstructured medium and elaborate a hierarchy of quasi-continuum models.

At the final stage, identification of a model is performed. The goal of identification is the construction of the best (optimal) model on the basis of experimental observations. Identification is divided by *structural* and *parametric*. *The structural identification* is a choice of the optimal form of equations for a mathematical model. *The parametric identification* is a determination by the experimental data of the values of the parameters of the mathematical model ensuring the agreement of the model values with the experimental data, provided that the model and the object are subjected to similar influences. Such identification also includes a numerical simulation of experiment and a choice of the model parameters from the condition of the best coincidence of calculation and experimental results.

The structural modeling began from the works of M. Born on the theory of crystal lattices and, until recently, it developed, mainly, in the framework of the solid state physics [47, 48]. In Russia, the founder of structural modeling was the pupil of A.G. Stoletov professor of Moscow University N.P. Kasterin (1869–1947) [49, 50]. Using this method, he investigated dispersion of sound waves. Particular attention is paid in the structural modeling method to the study of the propagation and interaction of elementary excitations—quasiparticles (phonons, magnons, excitons, etc.) and various defects inherent in real bodies [51]. Both quantum and classical approaches to the analysis of dynamic processes are organically combined within the scope of this direction [52]. As distinct from a continuum, structural models in explicit form contain the geometric parameters of the structure—the size and shape of the

particles, on which, ultimately, the effective moduli of elasticity of various orders depend [26]. By changing these parameters, we can control the physical and mechanical properties of a medium that cannot be done in principle within the scope of the continual description. The clear coupling between a structure and macroparameters of a medium discloses major opportunities for the purposeful design of materials with specified properties. Shortcomings of the structural modeling are absence of universality of modeling procedure and complexity of the accounting of nonlinear and nonlocal effects of interparticle interactions.

Structural models enable one not only to reveal the qualitative influence of local structure on the effective moduli of elasticity, but also to perform numerical estimations of their quantities; these being generally unavailable from continual models of the Cosserat type. In this paper, it will be shown how the velocity and the threshold frequency of rotational waves, as well as the parameters of the Cosserat medium can be numerically estimated due to the structural modeling method.

3 The Discrete Model of a Square Lattice

When the two-dimensional Cosserat continuum consisting of centrally symmetric particles is considered [45, 53–55], Eqs. (1) and (2) are substantially simplified. In this case, the Lagrange function has the form:

$$L = \frac{\rho}{2}\left(u_t^2 + w_t^2 + R^2\varphi_t^2\right) - \frac{1}{2}[B(u_x^2 + w_y^2) + (\mu + \frac{\kappa}{2})(w_x^2 + u_y^2) + \\ +\gamma(\varphi_x^2 + \varphi_y^2) + (\lambda + \mu - \frac{\kappa}{2})(u_x w_y + u_y w_x) + 2\kappa(w_x - u_y)\varphi + 2\kappa\varphi^2]. \tag{3}$$

Here ρ is the density of the medium, B is a macroelasticity constant of the second order, λ and μ are Lame constants, and γ and κ are phenomenological constants to be found from experiments. In the case of the isotropic Cosserat continuum, parameter B is not independent, it is related to Lame constants:

$$B = \lambda + 2\mu.$$

Further, let us start constructing an alternative model of a medium, which will enable one to establish an analytic relationship between the macroelasticity constants and the microstructure parameters.

We consider a square lattice (Fig. 1) consisting of homogeneous round particles (granules or grains) with mass M and diameter d. At the initial states, the mass centers of the particles are located at the lattice sites and the nearest distance between them equals a along both x- and y- axes. The lattice sites N are enumerated using couple of indices: the index i determines the site location along the horizontal x-axis, and j defines the site position along the vertical y-axis. Each particle has three degrees of freedom: the mass centre displacements $u_{ij}(t)$ and $w_{ij}(t)$, respectively, along the

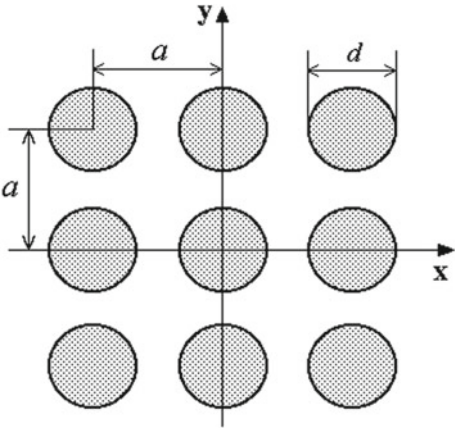

Fig. 1 A square lattice of round particles

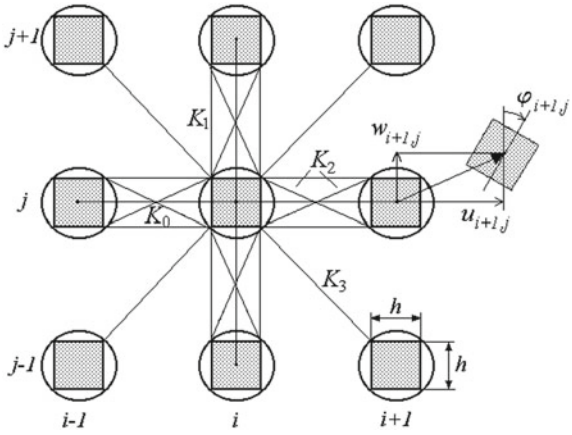

Fig. 2 Scheme of the force interactions between the particles and kinematics

x- and y-axes and the rotation $\varphi_{ij}\,(t)$ with respect to the axis passing through the mass centre of the particle (Fig. 2).

The kinetic energy of a cell is considered to be equal to the kinetic energy of a particle:

$$T_{i,j} = \frac{M}{2}\left(\dot{u}_{i,j}^2 + \dot{w}_{i,j}^2\right) + \frac{J}{2}\dot{\varphi}_{i,j}^2, \tag{4}$$

where $J = Md^2/8 = MR^2$ is the moment of inertia of the particle about the axis passing through its mass centre, $R = d/\sqrt{8}$ is the inertia radius of the particle. The upper dots denote derivatives with respect to time.

Only small deviations of the particles from the equilibrium position will be considered. The displacements of the grains are assumed to be small in comparison with the sizes of the unit cell of the lattice under consideration. The potential energy per cell is provided by the interaction of the particle N with the eight nearest neighbors

along the lattice, the first four of which are situated at a distance a from N (these are the particles of the first coordination sphere), and the other four are located on the diagonals of the square lattice (the particles of the second coordination sphere) and is described by the formula:

$$U_N = \frac{1}{2}\left(\sum_{n=1}^{4}\frac{K_0}{2}D_{0n}^2 + \sum_{n=1}^{8}\frac{K_1}{2}D_{1n}^2 + \sum_{n=1}^{8}\frac{K_2}{2}D_{2n}^2 + \sum_{n=1}^{4}\frac{K_3}{2}D_{3n}^2\right), \tag{5}$$

where D_{ln} ($l = 0, 1, 2, 3$) are elongations of the springs of four types, which are numbered in an arbitrary order and connect the particle with its neighbors. The central springs with rigidity K_0 and the non-central ones with rigidity K_1 simulate the interaction of granules during tension-compression of the material. The springs K_1 are also responsible for transmitting moments arising when the particles rotate. The springs with rigidity K_2 characterize the force interactions of particles under shear deformations in the material. Finally, the springs K_3 describe the interactions of the central particle with the grains of the second coordination sphere. For the convenience of further calculations, we assume that the points of connection of the central springs lie in the centers of the round particles, and the springs of the other three types—at the vertices of a square with the side $h = d/\sqrt{2}$ that is entered in a round particle (Fig. 2). In addition, expression (5) involves the extra factor 1/2, because the potential energy of each of the springs is uniformly divided between the two neighboring particles connected by the spring.

Entering the designations $\Delta u_i = u_{i,j} - u_{i-1,j}$ and $\Delta u_j = u_{i,j} - u_{i,j-1}$, one can calculate the expressions for the elongations of the springs D_{ln} in the approximation of smallness of the quantities $\Delta u_i \sim \Delta w_i \sim \Delta u_j \sim \Delta w_j \sim a\varepsilon$, $\Delta\varphi_i \sim \Delta\varphi_j \sim \varepsilon^{3/2}$, $\Phi_i \sim \sqrt{\varepsilon}$, where $\Phi_i = \left(\varphi_{i-1,j} + \varphi_{i,j}\right)/2 \ll \pi/2$ and ε is the measure of the cell deformation. Substitution of these expressions into (5) leads to the Lagrange function $L = T_{i,j} - U_{i,j}$ for the (i, j)-particle with accuracy up to quadratic terms. Then, using the Lagrange equations of the second kind, it is possible to obtain differential-difference equations describing the lattice dynamics. Such equations are useful for numerical simulation of the system response to external dynamic forcing in the wide frequency range, up to threshold values. However, for a comparison of the proposed mathematical model of a microstructured medium with the known theories of solids it is convenient to pass over from the discrete to the continuous description.

4 Continual (Long-Wavelength) Approximation

In order to compare the structural model of a medium with the known models of a solid, it is expedient to pass from a discrete description to a continuous one. In the case of long-wavelength perturbations, when $a/\Lambda \ll 1$ (Λ is the characteristic spatial scale of deformation), it is possible to change discrete variables i and j by continuous spatial variables $x = ia$ and $y = ja$. In this case, the functions $u_{ij}(t)$,

$w_{ij}(t)$, and $\varphi_{ij}(t)$ given at discrete points are interpolated by the continuous functions $u(x, y, t)$, $w(x, y, t)$, and $\varphi(x, y, t)$. Depending on the degree of approximation, we can consider different continual models. In the first approximation, we arrive at the following Lagrange function of the microstructured medium:

$$L = \frac{M}{2}\left(u_t^2 + w_t^2 + R^2\varphi_t^2\right) - \frac{M}{2}[c_1^2(u_x^2 + w_y^2) + c_2^2(w_x^2 + u_y^2) + \\ + R^2c_3^2(\varphi_x^2 + \varphi_y^2) + s^2(u_x w_y + u_y w_x) + 2\beta^2(w_x - u_y)\varphi + 2\beta^2\varphi^2]. \tag{6}$$

It is obvious that the Lagrange functions (6) and (26) coincide up to the coefficients. Using the Lagrange function (6), a set of differential equations of the first approximation describing the dynamic processes in a two-dimensional crystalline medium with a cubic symmetry, is derived in agreement with Hamilton's variational principle:

$$u_{tt} = c_1^2 u_{xx} + c_2^2 u_{yy} + s^2 w_{xy} - \beta^2\varphi_y,$$

$$w_{tt} = c_2^2 w_{xx} + c_1^2 w_{yy} + s^2 u_{xy} + \beta^2\varphi_x, \tag{7}$$

$$R^2\varphi_{tt} = R^2c_3^2(\varphi_{xx} + \varphi_{yy}) + \beta^2(u_y - w_x) - 2\beta^2\varphi.$$

Here, the following notations have been introduced: c_i ($i = 1$ to 3) are the velocities of propagation of longitudinal, transverse, and rotational waves, respectively, s is the coefficient of coupling between the longitudinal and transverse deformations, β is the dispersion parameter. It should be noted that the rotational wave has a dispersion of wave-guide (Klein-Gordon) type and therefore $_3$ represents the asymptotic value of the phase and group velocities of the waves in the high-frequency range.

Dependences of the coefficients of Eq. (7) on the force constants K_0, K_1, K_2, K_3, the lattice period a and the particle size $h = d/\sqrt{2}$ (d is diameter of the particle) have the following form [27]:

$$c_1^2 = \frac{a^2}{M}\left(K_0 + 2K_1 + \frac{2(a-h)^2}{(a-h)^2 + h^2}K_2 + K_3\right),$$

$$c_2^2 = \frac{a^2}{M}\left(\frac{2h^2}{(a-h)^2 + h^2}K_2 + K_3\right), \tag{8}$$

$$c_3^2 = \frac{a^2h^2}{2MR^2}\left(K_1 + \frac{a^2}{(a-h)^2 + h^2}K_2\right),$$

$$s^2 = \frac{2a^2}{M}K_3, \beta^2 = \frac{2a^2}{M}\left(\frac{h^2}{(a-h)^2 + h^2}K_2\right).$$

It follows from Eq. (8) that some parameters are not independent in the proposed model:

$$2c_2^2 - s^2 = 2\beta^2. \tag{9}$$

From comparison of the Lagarange functions (6) and (26) one can establish the following relationships between their coefficients:

$$c_1^2 = \frac{B}{\rho}, \quad c_2^2 = \frac{2\mu + \kappa}{2\rho}, \quad s^2 = \frac{2\lambda + 2\mu - \kappa}{2\rho}, \quad c_3^2 = \frac{\gamma}{\rho R^2}, \quad \beta^2 = \frac{\kappa}{\rho}. \tag{10}$$

Analysis of dependencies (8) emphasizes the importance of taking into account the springs of all four types in the considered model: $s = 0$ at $K_3 = 0$; $\beta = 0$ for $K_2 = 0$; if $K_1 = 0$, then parameters β and c_3 are interrelated: $\beta^2 = \frac{h^2}{a^2} c_3^2$ that is equivalent to the relationship $\kappa = \frac{4}{a^2}\gamma$ in the Cosserat model (it is obvious that such rigid relationships between the parameters essentially narrow the scope of the model) and, at last, account of the springs K_0 the springs ensures the superiority of the velocity of the longitudinal wave over the velocities of transverse and rotational waves.

Analysis of the dispersion properties of Eq. (7) shows [27] that the rotational wave has a critical frequency $\omega_0 = 4\beta/d$, below which it does not propagate.

It is obviously that from Eq. (10) it is possible to establish also inverse relations that could be used to calculate values of the parameters of the Cosserat medium for known values of $_1$, $_2$, s, c_3, and ω_0. However, it is very difficult to measure experimentally the last two parameters from the five given ones. To solve the problem of numerical estimation of the parameters of the Cosserat medium, the velocity and the critical frequency of the rotation wave (c_3 and ω_0), we compare Eq. (7) with the two-dimensional equations of the classical theory of elasticity for media with a cubic symmetry:

$$\rho u_{tt} = C_{11} u_{xx} + C_{44} u_{yy} + \left(C_{12} + C_{44}\right) w_{xy}, \tag{11}$$

$$\rho w_{tt} = C_{44} w_{xx} + C_{11} w_{yy} + \left(C_{12} + C_{44}\right) u_{xy}.$$

But since the correspondence between Eqs. (11) and (7) is observed only in the field of frequencies less than ω_0 [27], we shall first consider the low-frequency approximation of Eq. (7).

5 The Low-Frequency (Two-Mode) Approximation

In the low-frequency approximation ($\omega < \omega_0$) microrotations of particles of a medium are not independent, they are determined by a displacement field. The interrelationship between the microrotations φj and displacements u and w can be found from the third Eq. (7) by the method of stepwise approximations. In the first approximation

$$\varphi(x,t) \approx \frac{1}{2}\left(u_y - w_x\right). \tag{12}$$

This is the classical relationship of the theory of elasticity, which relates the rotations of particles in the medium to the vorticity of the displacement field. In the framework of the Cosserat theory, it corresponds to the case of a continuum with constrained particle rotation, when the rotational degree of freedom is "frozen". In this case, in the medium, as in the classical theory, there are only two translational degrees of freedom, and the Lagrange function L takes on the form:

$$L = \frac{M}{2}\left(u_t^2 + w_t^2 + \frac{R^2}{4}(u_{yt} - w_{xt})^2\right) -$$

$$-\frac{M}{2}[c_1^2(u_x^2 + w_y^2) + c_2^2(w_x^2 + u_y^2) + \frac{R^2}{4}c_3^2((u_{xy} - w_{xx})^2 + (u_{yy} - w_{xy})^2) + \tag{13}$$

$$+ s^2(u_x w_y + u_y w_x) - \frac{\beta^2}{2}(w_x - u_y)^2].$$

Additional terms appear in (13) that contain second derivatives of the displacement field, which are absent in the classical theory of elasticity. Information on the microstructure of the medium is saved in these terms. The terms u_{yt} and w_{xt} take into account the contribution of the rotational motions to the kinetic energy, and the terms with spatial derivatives u_{xy}, w_{xx} and etc. describe the contribution to the potential energy of the stresses provided by bending of the lattice. From (13) it is possible to obtain the equations of the gradient theory of elasticity [56] containing terms with the higher-order derivatives (in this case, the fourth order):

$$u_{tt} - c_1^2 u_{xx} - (c_2^2 - \frac{\beta^2}{2})u_{yy} - (s^2 + \frac{\beta^2}{2})w_{xy} =$$

$$= \frac{R^2}{4}\frac{\partial}{\partial y}\left[\frac{\partial^2}{\partial t^2}\left(u_y - w_x\right) - c_3^2 \Delta\left(u_y - w_x\right)\right],$$

$$w_{tt} - (c_2^2 - \frac{\beta^2}{2})w_{xx} - c_1^2 w_{yy} - (s^2 + \frac{\beta^2}{2})u_{xy} =$$

$$= -\frac{R^2}{4}\frac{\partial}{\partial x}\left[\frac{\partial^2}{\partial t^2}\left(u_y - w_x\right) - c_3^2 \Delta\left(u_y - w_x\right)\right]. \tag{14}$$

Here the symbol Δ means the two-dimensional Laplacian: $\Delta = \partial^2/\partial x^2 + \partial^2/\partial y^2$.

Equations such as (17) are usually called *equations of the second-order gradient theory of elasticity*, as the terms with spatial fourth-order derivatives take into account the coupled stresses arising at the translational displacements of the particles. From Eq. (17) it follows that in the considered low-frequency approximation, the transverse wave velocity is diminished by quantity $\beta/2$, and parameter s^2 increases by the same quantity.

It should be emphasized that, in spite of the absence of microrotations in Eq. (14), the microstructure of the medium affected the coefficients of these equations—in the low-frequency approximation, the coefficients changed at u_{yy}, w_{xy}, w_{xx}, and u_{xy} in comparison with the initial Eq. (7).

6 The Parametric Identification Problem

After neglecting the higher-order derivatives in Eq. (14) we will compare such equations with Eq. (11). As a result, the following relations yield:

$$c_1^2 = \frac{C_{11}}{\rho}, \quad c_2^2 = \frac{2C_{44} - C_{12}}{\rho}, \quad s^2 = \frac{2C_{12}}{\rho}, \quad \beta^2 = \frac{2(C_{44} - C_{12})}{\rho}. \tag{15}$$

It should be noted that relation (9) follows from (15), as well as from (8). Taking into account equation $C_{11} - C_{12} = 2\rho v^2$ [57], where v is the transverse wave velocity in the crystallographic direction <110>, one can obtain relation

$$s^2 = 2c_1^2 - 4v^2. \tag{16}$$

Consequently, relations (15) can be rewritten in the form:

$$C_{11} = \rho c_1^2, \quad C_{12} = \rho(c_1^2 - 2v^2), \quad C_{44} = \rho(c_1^2 + c_2^2 - 2v^2)/2. \tag{17}$$

Formulas (17) can be useful for determination of the effective elasticity moduli of a microstructured medium by means of acoustic measurements. Due to equalities (15)–(17), any system of basis quantities can be easy used: (A_1, A_2, s), (A_1, A_2, v), or (C_{11}, C_{12}, C_{44}). Thus, using Eqs. (17), (16) and (8), the second-order elasticity constants can be expressed in terms of the microstructure parameters as follows:

$$C_{11} = \frac{K_0 + 2K_1 + K_3}{a} + \frac{2(a\sqrt{2} - d)^2}{d^2 + (a\sqrt{2} - d)^2}\frac{K_2}{a},$$

$$C_{12} = \frac{K_3}{a}, \quad C_{44} = \frac{d^2}{d^2 + (a\sqrt{2} - d)^2}\frac{K_2}{a} + \frac{K_3}{a}. \tag{18}$$

Equalities (18) contain, on the one hand, 4 parameters of interparticle (force and moment) interactions (K_0, K_1, K_2, K_3), and on the other hand, only 3 elastic moduli of the second order (C_{11}, C_{12}, C_{44}). Therefore, in order to find the dependences inverse to Eq. (18), it is necessary to introduce an additional relationship between

the parameters of interparticle interactions: $\mathrm{K} = K_0/K_1$. Account of this relationship leads to the following dependences inverse to (18):

$$\frac{K_1}{a} = \frac{1}{2+\mathrm{K}}\left[C_{11} - C_{12} - 2\left(C_{44} - C_{12}\right)\left(\frac{\sqrt{2}}{p} - 1\right)^2\right],$$

$$\frac{K_2}{a} = \left(C_{44} - C_{12}\right)\left(1 + \left(\frac{\sqrt{2}}{p} - 1\right)^2\right), \quad \frac{K_3}{a} = C_{12}, \tag{19}$$

where $p = d/a$ is the relative size of the particles.

If to substitute relations (17) into Eq. (19), it is possible to express the parameters of interparticle interactions also in terms of the elastic wave velocities and the size of the particles:

$$\frac{K_3}{a} = \rho(c_1^2 - 2v^2), \frac{K_2}{a} = \frac{\rho}{2}\left(c_2^2 - c_1^2 + 2v^2\right)\left(1 + \left(\frac{\sqrt{2}}{p} - 1\right)^2\right),$$

$$\frac{K_1}{a} = \frac{\rho}{\mathrm{K}+2}\left[2v^2 + \left(\frac{\sqrt{2}}{p} - 1\right)^2 (c_1^2 - c_2^2 - 4v^2)\right]. \tag{20}$$

Due to relations (19) or (20), using the experimentally measured values of the elasticity constants (or the elastic wave velocities) and the relative particle size, it is possible to calculate the parameters of the force and moment interactions between the particles. And these parameters, in its turn, will allow us to obtain numerical estimates of all the macroconstants of the medium, the values of which are very difficult to measure experimentally. In particular, this concerns the velocity and critical frequency of the rotational wave, the Cosserat medium parameters, the nonlinearity coefficients [58], etc.

7 Numerical Estimates of Macroparameters

Due to the dependences (8) of the rotational wave velocity c_3 on the microstructure parameters and Eqs. (19) and (20), it is possible to express c_3 in terms of the experimentally determined values:

$$c_3 = \sqrt{\frac{2}{\rho(\mathrm{K}+2)}\left[C_{11}+C_{12}-2C_{44}+\frac{\mathrm{K}+4p\sqrt{2}-2}{p^2}\left(C_{44}-C_{12}\right)\right]} \tag{21}$$

or

$$c_3 = \sqrt{\frac{2}{\mathrm{K}+2}\left(A_1^2-A_2^2+\frac{(A_2^2-c_1^2+2v^2)(2p\sqrt{2}+\mathrm{K})}{p^2}\right)}. \tag{22}$$

Thus, if the elasticity constants are given, then the velocities of the elastic waves are found from the equalities that are inverse to Eq. (21):

$$A_1 = \sqrt{\frac{C_{11}}{\rho}}, \quad A_2 = \sqrt{\frac{2C_{44}-C_{12}}{\rho}}, \quad v = \sqrt{(C_{11}-C_{12})/2\rho}. \tag{23}$$

The normalized critical frequency has the form:

$$\omega_0 d = 4\sqrt{2\left|C_{44}-C_{12}\right|/\rho}. \tag{24}$$

The practical problem of identifying the Cosserat continuum is of current interest for some real heterogeneous materials suitable for the application of this model [59, 60]. However, reliable results concerning determination model parameters that would be confirmed by different researchers at least in the simplest case of an elastic isotropic Cosserat continuum are quite rare [61]. The mentioned above procedure for estimating macroparameters of a medium that is based on the method of structural modeling can help in solving this problem. Thus, the inverse relation to (10), taking into account Eq. (15), has the following form:

$$B = \rho c_1^2 = C_{11}, \quad \lambda = \rho(c_2^2-\beta^2) = C_{12}, \quad \mu = \rho(c_2^2-\frac{\beta^2}{2}) = C_{44},$$

$$\kappa = \rho\beta^2 = 2(C_{44}-C_{12}), \quad \gamma = \rho R^2 c_3^2. \tag{25}$$

It follows from (25) that not all constants of the Cosserat medium can be expressed in terms of the second-order elasticity constants—for γ it is possible only in the case of additional assumptions about the values of $\mathrm{K} = K_0/K_1$ and $p = d/a$. It should be noted that similar relationships were obtained in [45], but there the dependence of the material constants on the particle size remained unclear.

Theoretical estimates of the velocity and the normalized threshold frequency of the rotational wave, as well as the values of the elasticity coefficients in the Cosserat theory are given in Table 1 for some crystals with cubic symmetry: lithium fluoride (LiF), sodium fluoride (NaF), sodium bromide (NaBr), and fullerite (C_{60}). Moreover, this Table also contains the values of the elasticity constants C_{11}, C_{12}, and C_{44}, as well as the density ρ taken from known experimental (see [62] for

Table 1 Structural parameters for crystals with cubic symmetry

	Structural parameters		Crystals			
			LiF	NaF	NaBr	C_{60}
Experimental data	Density (kg/m^3)	ρ	2600	2800	3200	1720
	Elasticity constants (GPa)	C_{11}	113.00	97.00	32.55	14.9
		C_{12}	48.00	25.60	13.14	6.9
		C_{44}	63.00	28.00	19.26	8.1
Calculated characteristics	Wave velocities (m/s)	c_1	6593	5890	3190	2943
		c_2	5477	3295	2045	2325
		v	3536	3571	1741	1525
		c_3	5659	2896	1092	2036
	Normalised threshold frequency of rotational waves $\omega_0 d$ (m/s)	$\omega_0 d$	13587	5237	1095	4781
	Elasticity coefficients in the Cosserat theory (GPa)	λ	48.00	25.60	13.14	6.9
		μ	63.00	28.00	13.26	8.1
		γ/R^2	83.28	23.49	3.81	7.1
		κ	30.00	4.8	0.24	2.4
	Normalised parameters of force interactions between the particles (GPa)	K_0/a	46.01	58.19	16.11	6.01
		K_1/a	4.601	5.819	1.611	0.601
		K_2/a	19.897	3.183	0.159	1.592
		K_3/a	48.00	25.60	13.14	6.90

alkaline-galloid crystals at room temperature) and theoretical data (see [63], where the modified Lennard-Jones intermolecular potential was used for estimates of the elastic moduli of a simple cubic lattice of fullerite C_{60} at low temperatures). The rotational wave velocity has been calculated using Eq. (21), the elastic wave velocities along the crystallographic directions $< 100 >$ and $< 110 >$ have been calculated from formula (23) and, at last, the parameters of force interactions—due to formulas (19). All calculations were performed for $p = 0.9$ and $\mathrm{K} = 10$ (the central interactions dominate).

It is clear from this table that the rotational wave velocity is minimal for majority of the considered materials, and the threshold frequencies lie in the hypersonic range. So if it is to be supposed that the size of a crystal grain $d = 10\ \mathrm{nm} = 10^{-8}\ \mathrm{m}$, then for hypothetical crystalline material with elasticity constants and density, as for NaBr, $\omega_0 \approx 2.721 \times 10^{11}\ \mathrm{s}^{-1}$, and for material with parameters of LiF $\omega_0 \approx 1.359 \times 10^{12}\ \mathrm{s}^{-1}$. These values are of the same order as the theoretical estimates of the threshold frequency of rotational waves in crystals with a hexagonal lattice [27]

and experimentally determined values of the corresponding quantity in organic crystals [9–11] (for example, $\omega_0 \approx 6 \times 10^{11}\ \mathrm{s}^{-1}$ for naphthalene crystal). Therefore, in the sonic and ultrasonic ranges the microrotation waves can be neglected. However, their presence can be of principal importance for high-frequency processes. At the same time, according to formula (24), with a significant growing of the particle size of the medium, the threshold frequency of rotational waves substantially decreases, i.e. the range of propagation of rotational waves is substantially expanded.

The mentioned above data testify that for a more complete and comprehensive understanding of the rotational mechanics of the particles of a medium, first of all, it is necessary to use such models, which elementary volumes are sufficiently large and, hence, their particles have enough large moments of inertia. Such media include our planet Earth, which elements are geophysical blocks, tectonic plates and geological structures.

8 About the Role of Rotational Factor in Geodynamics

Many geologists (A.P. Karpinsky, D.I. Mushketov, I.S. Shatsky, B.L. Lichkov, P.S. Voronov, A.L. Yanshin, V.E. Khain et al.) wrote about the importance of rotational movements and their relationship with the stressed state of the Earth [64, p. 11]. Geodynamic models, based on ideas about the importance of rotational movements, began to be developed in the late 1950s (see the works of N.V. Stovas [65], K.F. Tyapkin and M.M. Dovbnich [66], etc.). In these works, the Earth was represented as a single monolithic body, the calculation of stresses in which was carried out taking into account the rotation of the Earth.

Recent data of geological and geophysical research argue that the Earth's crust consists of non-point particles-blocks that are able to rotate. Thus, according to [67, 68], the state of the Earth's crust is determined by the "inner motion potential" [69] and "self-energy" [70]. Within the scope of the mechanical concept, motion with such properties can occur only under the influence of own angular momentums of the blocks [69], in fact, their spins. The Earth's rotation around its axis with angular velocity Ω and the rotational movements of crust blocks provided by "own moments" $J\Omega$, where J is the moment of inertia of the spherical block, play an important role in geodynamics.

So, geophysical observations made during a long time interval enabled one, for example, to formulate a conclusion that Easter Island ($300 \times 400\ \mathrm{km}^2$) in the Pacific Ocean for 5 million years (it is time of its existence) has turned almost by 90° [71] that corresponds to the angular velocity 0.5π rad/5×10^6 years $\approx 3 \times 10^{-7}$ rad/year.

Moreover, Siberian platform performs a rather complex motion as a rigid plate. In the period 2.5–1 billion years ago it was located, mainly, in the equatorial and low northern latitudes, performing quasi-oscillation rotations relative to the meridian with amplitude up to 45°, whereas in the period 1.6–1 billion years ago it turned counterclockwise at the angle of about 90° [72].

GPS observations using 323 points in the Central Asian range (65–85 N, 35–55 E, Tien Shan) showed that the whole area, as expected, moves to the north with the velocities up to 10 mm/year. At the same time, blocks with sizes of 50–200 km are distinguished, which rotate in different directions with the velocities up to 5 mm/year [73].

Recently, rotational waves are increasingly being studied in problems of geodynamics—one of the branches of the Earth sciences, which "elementary" structures reach the sizes of a planetary scale. Thus, V.N. Nikolayevskiy and his co-authors studied nonlinear interactions of longitudinal waves and rotational waves in the framework of the Cosserat model applying to seismoacoustic and geodynamic problems [74]. In the framework of a gradient-consistent model of a medium with complex structure, they attempted to explain an ultrasound generation during the propagation of seismic waves. Considering the lithosphere of the Earth in the framework of the Cosserat continuum, V.N. Nikolaevsky and his co-authors simulated a lot of geodynamic wave motions observed on the surface of the Earth, including global tectonic waves having, apparently, a rotational nature.

As an alternative to the Cosserat theory, A.V. Vikulin with his co-authors developed a "rotational" approach to solving geodynamic problems (see, for example, [75, 76]). This approach is based on the following assumptions: an elementary part of the rotating solid body—the Earth's crust block—is, first of all, a rigid non-deformable volume; secondly, its motion occurs under the action of its own moment; thirdly, such a motion leads to change of the stress state of the crust surrounding the block. In this model, in contrast to the Cosserat theory, the stress tensor is symmetric and the rotational motions of a block generating its own elastic field and interacting with the intrinsic elastic fields of other equal-sized blocks of a chain are described by the sine-Gordon equation in the dimensionless form [76]:

$$\frac{\partial^2 \varphi}{\partial t^2} - \frac{\partial^2 \varphi}{\partial x^2} - \sin \varphi = 0. \tag{26}$$

Within the framework of this rotational model it is possible to describe the whole range of geodynamic velocities of rotational waves that are typical both for geophysical and geological processes—from slow rotational waves ($\leq 10^{-2}$ sm/s) characterizing redistribution of tectonic stresses up to fast seismic waves (1–10 km/s) [76–78].

The so-called "earth" waves are of special interest. They represent visually observed humps on the surface of the Earth, which propagate along its surface even from earthquake focuses. For example, "during the earthquake … on the concrete road and sidewalks the waves propagated of 1.2–1.8 m in height and 3 m in length, but no cracks appeared on the concrete"! Or an other example: in summer of 2011, a quite large part of the coast of the Taman Peninsula, 435 m in length and 50 m in width, probably for a month, rose with a maximum amplitude up to 3.4 m. At the same time, neither seismic, nor volcanic (mud) activity was not observed in the region of uplift [79]. Detailed reviews of works on such movements of a geomedium and their extensive bibliography can be found in Refs. [80–82]. According to these reviews, geophysical and geological data [83] on such "slow" movements of a geomedium

enabled geologists in the 1930s to introduce into consideration rheidity or superplastic deformations of the Earth [84].

It should be noted that in analyzing the mechanism of arising of pendular, in fact, rotational waves in laboratory conditions, mining engineers noted the effect of the "disappearance" of friction between interacting blocks [85]. Rheidity properties, apparently, can be an explanation of the "vortex" motions of a geomedium that were described above. It is clear why geophysicists and seismologists have not seriously considered "earth" waves: their existence is impossible within the scope of the classical theory of elasticity. Probably, such movements are, in fact, like tsunami waves in the ocean, gravitational waves in the Earth's crust. The physics of such waves and their polarization can be studied in the framework of rotational representations (see, for example [86–88]).

9 Conclusions

The classical theory of elasticity considers a medium as a continuum of material points possessing only translational degrees of freedom. However, in fact, a medium consists, as a rule, of relatively large bodies that can perform not only translational displacements, but also rotate with respect to each other. In the conditions of a "laboratory" medium, the account of rotational motions of its particles is necessary when high-frequency wave processes are considered. However, with growing the medium scale and the particle size, the frequency range of the wave process, in the study of which it is necessary to take into account rotations of the particles of the medium, decreases. The necessity for such an accounting is especially clearly manifested during consideration of wave processes in geomedia. At present, rotational movements of blocks of the Earth's crust are no longer a hypothesis, but an experimentally established fact that is confirmed by lots of data obtained by various methods and by different groups of researchers in many regions of the Earth. And in geodynamics there is majority of experimental confirmations of the existence of rotational waves that were mathematically described back in 1909 by the Cosserat brothers.

Acknowledgements The research was carried out under the financial support of the Russian Foundation for Basic Research (projects NN 18-08-00715-a, 16-08-00971-a, and 16-08-00776-).

References

1. Mac Cullagh, J.: An essay towards a dynamical theory of crystalline reflection and refraction. Trans. R. Irish. Acad. Sci. **21**, 17–50 (1839)
2. Clebsch, A.: Theorie der Elastizitt tester Korper, 424 pp. Leipzig (1862)
3. Kirchhoff, G.: Vorlesungen Uber Mathematische Physik, 466 pp. Mechanik, Leipzig (1874)
4. Duhem, P.: Hidrodynamique, Elasticit. Acoustique. Paris (1891)

5. Voigt, W.: Theoretische Studien uber die Elastizitatsverhaltnisse der Krystalle. Abn. Ges. Wiss. Gottingen **34** (1887)
6. Cosserat, E., Cosserat, F.: Theorie des Corps Deformables, 226 pp. Librairie Scientifique A. Hermann et Fils, Paris (1909) (Reprint, 2009)
7. Gross, E.F.: Light scattering and relaxation phenomena in liquids. Doklady Akademii Nauk SSSR **28**(9), 788–793 (1940) (in Russian)
8. Bernal, J.D., Tamm, G.R.: Nature **135**, 229 (1935)
9. Gross, E.F., Korshunov, A.V.: Rotational oscillations of molecules in a crystal lattice of organic substances and scattering spectra. JETP **16**(1), 53–59 (1946). In the book [10], pp. 100–105 (in Russian)
10. Gross, E.F.: Izbrannye Trudy (Selected Papers). Nauka, Leningrad (1976) (in Russian)
11. Gross E.F., Korshunov A.V., Sel'kin V.A.: Raman spectra of small frequencies of crystals of para-, meta- and orthoiodiobenzenes. JETP **20**, 293–296 (1950) (in Russian)
12. Kroner, E. (ed.) Mechanics of generalized continua. In: Proceedings of the IUTAM-Symposium on the Generalized Cosserat Continuum and The Continuum Theory of Dislocations with Applications, Freudenstadt and Stuttgart, 1967. Springer, Heidelberg (1968)
13. Aero, E.L., Kuvshinskii, E.V.: Basic equations of the theory of elasticity of media with rotational interaction of particles. Fiz. Tverd. Tela (Phys. Solid State) **2**(7), 1399–1409 (1960) (in Russian)
14. Kuvshinskii, E.V., Aero, E.L.: Continuum theory of asymmetric elasticity. Account of internal rotation. Fiz. Tverd. Tela (Phys. Solid State) **5**(9), 2591–2598 (1963) (in Russian)
15. Lee, J.D., Eringen, A.C.: Wave propagation in nematic liquid crystals. J. Chem. Phys. **54**(12), 5027–5034 (1971)
16. Lee, J.D., Eringen, A.C.: Continuum theory of smectic liquid crystal. J. Chem. Phys. **58**(10), 4203–4211 (1973)
17. Akhiezer, A.I., Bar'yakhtar, V.G., Peletminskii, S.V.: Spin Waves. Nauka, Moscow (1967). North_Holland, Amsterdam (1968)
18. Lyamov, V.E.: Polarization Effects and Anisotropy of the Interaction of Acoustic Waves in Crystals. Mosk. Gos. Univ., Moscow (1983) (in Russian)
19. Pouget, J., Askar, A., Maugin, G.A.: Lattice model for elastic ferroelectric crystals: microscopic approach. Phys. Rev. B **33**, 6304–6325 (1986)
20. Pouget, J., Maugin, G.A.: Nonlinear dynamics of oriented elastic solid. J. Elast. Part 1,2 **22**, 135–155, 157–183 (1989)
21. Erofeev, V.I.: Synchronous interactions of longitudinal and rotation waves in a nonlinearity elastic Cosserat medium. Acoust. Phys. **40**(2), 247–252 (1994)
22. Erofeyev, V.I.: Wave Processes in Solids with Microstructure, 256 pp. World Scientific Publishing, New Jersey, London, Singapore, Hong Kong, Bangalore, Taipei (2003)
23. Potapov, A.I., Pavlov, I.S., Maugin, G.A.: Nonlinear wave interactions in 1D crystals with complex lattice. Wave Motion **29**, 297–312 (1999)
24. Vasiliev, A.A, Dmitriev, S.V., Miroshnichenko, A.E.: Multi-field continuum theory for medium with microscopic rotations. Int. J. Solids Struct. **42**, 6245–6260 (2005)
25. Vasiliev, A.A., Miroshnichenko, A.E., Ruzzene, M.: Multifield model for Cosserat media. J. Mech. Materi Struct. **3**(7), 1365–1382 (2008)
26. Pavlov, I.S., Potapov, A.I.: Structural models in mechanics of nanocrystalline media. Dokl. Phys. **53**(7), 408–412 (2008)
27. Potapov, A.I., Pavlov, I.S., Lisina, S.A.: Acoustic identification of nanocrystalline media. J. Sound Vib. **322**(3), 564–580 (2009)
28. Potapov, A.I., Pavlov, I.S., Lisina, S.A.: Identification of nanocrystalline media by acoustic spectroscopy methods. Acoust. Phy. **56**(4), 588–596 (2010)
29. Pavlov, I.S.: Acoustic identification of the anisotropic nanocrystalline medium with non-dense packing of particles. Acoust. Phys. **56**(6), 924–934 (2010)
30. Maugin, G.A., Metrikine, A.V. (eds.) Mechanics of Generalized Continua. One Hundred Years After the Cosserats, 337 pp. Springer (2010)

31. Erofeev, V.I., Pavlov, I.S., Leontiev, N.V.: A mathematical model for investigation of nonlinear wave processes in a 2D granular medium consisting of spherical particles. Compo. Mech. Comput. Appl. Int. J. **4**(3), 239–255 (2013)
32. Erofeev, V.I., Kazhaev, V.V., Pavlov, I.S. Nonlinear localized strain waves in a 2D medium with microstructure. In: Altenbach, H., et al. (eds.) Generalized Continua as Models for Materials, 91 Advanced Structured Materials 22, pp. 91–110. © Springer, Heidelberg (2013). https://doi.org/10.1007/978-3-642-36394-8_6
33. Pavlov, I.S., Vasiliev, A.A., Porubov, A.V.: Dispersion properties of the phononic crystal consisting of ellipse-shaped particles. J. Sound Vib. **384**, 163–176 (2016)
34. Savin, G.N., Lukashev, A.A., Lysko, E.M., Veremeenko, S.V., Agas'ev, G.G.: Propagation of elastic waves in the Cosserat continuum with constrained particle rotation. Prikl. Mekh. (Appl. Mech.) **6**(6), 37–40 (1970) (in Russian)
35. Savin, G.N., Lukashev, A.A., Lysko, E.M.: Propagation of elastic waves in a solid with microstructure. Prikl. Mekh. (Appl. Mech.) **6**(7), 48–52 (1970) (in Russian)
36. Erofeyev, V.I., Rodyushkin, V.M.: Observation of the dispersion of elastic waves in a granular composite and a mathematical model for its description. Sov. Phys. Acoust. **38**(6), 611–612 (1992)
37. Potapov, A.I., Rodyushkin, V.M.: Experimental investigation of strain waves in materials with microstructure. Acoust. Phys. **47**(1), 347–352 (2001)
38. Li, C., Chou, T.-W.: A structural mechanics approach for the analysis of carbon nanotubes. Int. J. Solids Struct. **40**, 2487–2499 (2003)
39. Altenbach, H., Maugin, G.A., Erofeev, V.I. (eds.): Mechanics of Generalized Continua, 350 pp. Springer, Heidelberg (2011)
40. Broberg, K.B.: The cell model of materials. Comput. Mech. **19**, 447–452 (1997)
41. Ghoniem, N.M., et al.: Multiscale modelling of nanomechanics and micromechanics: an overview. Phil. Mag. **83**(31–34), 3475–3528 (2003)
42. Pouget, J.: Lattice dynamics and stability of modulated-strain structures for elastic phase transitions in alloys. Phys. Rev. B **48**(2), 864–875 (1993)
43. Cleland, A.N.: Foundations of Nanomechanics: From Solid-state Theory to Device Applications. Springer, Berlin (2003)
44. Ostoja-Starzewski, M., Sheng, P.Y., Alzebdeh, K.: Spring network models in elasticity and fracture of composites and polycrystals. Comput. Mater. Sci. **7**, 82–93 (1996)
45. Suiker, A.S.J., Metrikine, A.V., de Borst, R.: Comparison of wave propagation characteristics of the Cosserat continuum model and corresponding discrete lattice models. Int. J. Solids Struct. **38**, 1563–1583 (2001)
46. Suiker, A.S.J., Metrikine, A.V., de Borst, R.: Dynamic behaviour of a layer of discrete particles. Part 1: Analysis of body waves and eigenmodes. J. Sound Vib. **240**(1), 1–18 (2001)
47. Born, M., Huang, K.: Dynamical Theory of Crystal Lattices. Clarendon Press, Oxford (1954)
48. Brillouin, L., Parodi, M.: Wave Propagation in Periodic Structures. McGrawHill, New York (1946)
49. Kasterin, N.P.: On dispersion of sound waves in a heterogeneous medium. Zhurnal russkogo fiziko-khimicheskogo obshestva. J. Russ. Phys. Chem. Soc. **30**(3A), 61–78 (1898) (in Russian)
50. Kasterin, N.P.: On propagation of waves in heterogeneous media. Part 1. Sound waves. University Press, Moscow (1903) (in Russian)
51. Kaganov, M.I.: Electrons, Phonons, Magnons, 268 pp. English Translation. Mir Publishers, Moscow (1981)
52. Kosevich, A.M.: The Crystal Lattice. Wiley-VCH, Berlin (1999)
53. Kunin, I.A.: Elastic Media with Microstructure, vol. 2. Springer, Berlin (1983)
54. Nowacki, W.: Theory of Micropolar Elasticity. J. Springer, Wien (1970)
55. Eringen, A.C.: Microcontinuum Field Theories. 1: Foundation and Solids. Springer, New York (1999)
56. Vanin, G.A.: Gradient theory of elasticity. Izv. AN. MTT [Mechanics of Solids], No. 1, pp. 46–53 (1999)

57. Fedorov, V.I.: Theory of Elastic Waves in Crystals. Nauka, Moscow (1965). Plenum Press, New York (1968)
58. Pavlov, I.S.: On estimation of the nonlinearity coefficients of a granular medium by the structural modeling method. Vestnik Nizhegorodskogo Universiteta (Nizhny Novgorod State University Proceedings) (6), pp. 143–152 (2012) (in Russian)
59. Kulesh, M.A., Matveenko, V.P., Shardakov, I.N.: Propagation of surface elastic waves in the Cosserat medium. Acoust. Phys. **52**(2), 186–193 (2006). https://doi.org/10.1134/s1063771006020114
60. Kulesh, M.A., Grekova, E.F., Shardakov, I.N.: The problem of surface wave propagation in a reduced Cosserat medium. Acoust. Phys. **55**(2), 218–226 (2009). https://doi.org/10.1134/S1063771009020110
61. Adamov, A.A.: On calculation effects in solving the boundary problems for the isotropic homogeneous Cosserat continuum. In: Proceedings of VI Russian Conference "Mechanicsb of Microheterogeneous Materials and Fracture". Yekaterinburg (Russia) (2010). http://book.uraic.ru/project/conf/txt/008/2010/mmp2.htm
62. Frantsevich, I.N., Voronov, F.F., Bakuta, S.A.: Elastic constants and elasticity moduli of metals and nonmetals. In: Frantsevich, I.N. (ed.) Reference Book. Naukova Dumka, Kiev (1982) (in Russian)
63. Yildirim, T., Harris, A.B.: Lattice dynamics of solids C_{60}. Phys. Rev. B **46**, 7878–7896 (1992)
64. Milanovskii, E.E.: Rotational Processes in Geology and Physics. KomKniga, Moscow (2007) (in Russian)
65. Stovas, M.V.: The Selected Works, 155 pp. Nedra, Moscow (1975) (in Russian)
66. Tyapkin, K.F., Dovbnich, M.M.: New Rotation Hypothesis of Structure Development and Its Geological Mathematically Ground, 342 pp. Donetsk: Knowledge (2009) (in Russian)
67. Kurlenya, M.V., Oparin, V.N.: Problems of nonlinear geomechanics. Part I. J. Min. Sci. **35**(3), 216 (1999)
68. Sadovsky, M.A., Bolkhovitinov, L.G., Pisarenko, V.F.: Deformation of Geophysical Medium and Seismic Process. Science Press, Moscow (1987)
69. Peive, A.V.: Tectonics and Magmatism. Izv. AN SSSR, Series: Geology (3), 36 pp (1961)
70. Ponomarev, V.S., Energy Saturation of Geological Environment. Trudy Geol. Inst. RAN (582), 379 (2008)
71. Mezhdunarodnyi geologo-geofizicheskii atlas Tikhogo okeana (International Geological-Geophysical Atlas of the Pacific Ocean). Saint-Petersburg, Moscow. Mezhpravit. okeanograf. komm. (2003)
72. Veselovsky, R.V., Pavlov, V.E., Petrov, P.Yu.: New paleomagnetic data on anabarsky heave and uchuro-maisky region and their role in paleogeography and geological correlation of the riphean of the siberian platform. Fiz. Zemli (7), 3 (2009) (in Russian)
73. Kuzikov, S.I., Mukhamediev, Sh.A.: Structure of the present-day velocity field of the crust in the area of the Central-Asian GPS network. Izv. Phys. Solid Earth **46**(7), 584–601 (2010). https://doi.org/10.1134/S1069351310070037
74. Nikolaevskiy, V.N.: Geomechanics and Fluidodynamics. Kluwer Academic Publishers, Dordrecht (1996)
75. Vikulin, A.V., Ivanchin, A.G.: Modern concept of block hierarchy in the structure of geomedium and its implications in geosciences. J. Min. Sci. **49**(3), 395–408 (2013). https://doi.org/10.1134/S1062739149030076
76. Vikulin, A.V., Makhmudov, K.F., Ivanchin, A.G., Gerus, A.I., Dolgaya, A.A.: On wave and rheidity properties of the Earth's crust. Phys. Solid State **58**(3), 561 (2016)
77. Vikulin, A.V., Ivanchin, A.G.: Model of a seismic process. Vychislit. Tekhnol. **2**(2), 20–25 (1997)
78. Mikhailov, D.N., Nikolaevskiy, V.N.: Tectonic waves of the rotational type generating seismic signals. Izv. Phys. Solid Earth **36**, 895 (2000)
79. Popkov, V.I., Popkov, I.V., Fomenko, V.A., Glazyrin, E.A.: A catastrophic tectonic event in summer 2011 in the Taman peninsula. Dokl. Earth Sci. **448**(2), 172–174 (2013)

80. Poletaev, A.I.: On the Understanding Role and Importance of Rotation Factor in the Earth Formation and Evolution: Facts, Discussion, and Conclusions, 200 pp. LIBROKOM Publisher, Moscow (2011) (in Russian)
81. Vikulin, A.V.: World of Vortex Motions. Kamchatka State Technical University, Petropavlovsk-Kamchatskii (2008) (in Russian)
82. Vikulin, A.V.: Physics of the Earth and Geodynamics. Kamchatka State University, Petropavlovsk-Kamchatskii (2009) (in Russian)
83. Nikolayev, A.N.: Aspects of geophysics of XXI century. In: Nikolaev, A.V. (ed.) Problems of Geophysics in the 21st Century, pp. 7–16. Nauka, Moscow (2003)
84. Carey, S.W.: The rheid concept in geotectonics. Bull. Geol. Soc. Austral. **1**, 67–117 (1954)
85. Oparin, V.N., Yushkin, V.F., Simonov, B.F., Nazarov, L.A., Vostrikov, V.I., Pogarskii, Yu.V: Geomechanical and Technical Bases of Enhancement of Oil Recovery in Vibration Wave Technology. Nauka, Novosibirsk (2010) (in Russian)
86. Bulletin Seismological Society of America **99**(2B), 945–1486 (2009)
87. Teisseyre, R., Nakeo, M., Majewski, E. (eds.) Earthquake Source Asymmetry, Structural Media and Rotation Effects, 582 pp. Springer, Heidelberg (2006)
88. Teisseyre, R., Nagahama, H., Majewski, E. (eds.) Physics of Asymmetric Continua: Extreme and Fracture Processes: Earthquake Rotation and Solution Waves, 293 pp. Springer, Heidelberg (2008)

Localized Magnetoelastic Waves in a One and Two Dimensional Medium

Vladimir I. Erofeev and Alexey O. Malkhanov

Abstract The impact of external magnetic field on the generation of localized waves in non-linear conductive rod and plate has been studied. We have obtained evolutionary equations which describe the propagation of one- and two-dimensional nonlinear magnetoelastic. It has been shown that parameters of waves depend on both intension and spatial orientation of the magnetic field.

1 Introduction

Nowadays the problems of interaction of deformational, electromagnetic and thermal fields in conductive bodies are being actively studied [1–9]. The topicality of such a research is tightly connected with the development of methods of non-destructive control of materials and ways of the electrodynamical generation and reception of acoustic waves [10].

The significance of such problems is defined by the progress in the technology of thermomechanical processing of the bulky parts of constructions [11]. Warming-through material acts as one of the manufacturing operations, it reduces the stiffness of the material during sintering of powders and composites before processing. Placing the sample in a strong magnetic field creates additional opportunities for even distribution of heat, leading to a leveling of the temperature field and an increase in the heating rate during the induction processing. Near-surface currents interact with the magnetic field, which leads to the generation of acoustic waves in the environment, which, in turn, cause the induction currents in the medium and the associated quasi-stationary electromagnetic fields. Viscous and Joule dissipation which are linked to acousto-electromagnetic waves leads to the formation of additional distributed sources of heat.

V. I. Erofeev (✉) · A. O. Malkhanov
Mechanical Engineering Research Institute of RAS, Nizhny Novgorod, Russia
e-mail: erof.vi@yandex.ru

F. dell'Isola et al. (eds.), *Advances in Mechanics of Microstructured Media and Structures*, Advanced Structured Materials 87,
https://doi.org/10.1007/978-3-319-73694-5_8

The most problems of magnetoacoustics are considered in the linear approximation and the one-dimensional setting. Accounting for non-linearity is generally limited to non-linear interaction of elastic and electromagnetic field [4] and the nonlinearity associated with the thermal stresses [12]. Important for acoustics of solids physical nonlinearity, accounted, for example, in [13, 14], has not yet received in magnetoacoustics due consideration.

In this paper, we study the propagation of magnetoelastic waves in a two dimensional plate and three-dimensional nonlinear elastic medium.

2 Equations of Magnetoelasticity

In magnetoelasticity, the influence of the magnetic field on the deformation field is described employing the Lorentz forces [15]:

$$\mathbf{F}_m = \rho_e \mathbf{E} + \mathbf{j} \times \mathbf{B}, \tag{2.1}$$

which are introduced into equations of motion of an elastic body

$$\rho \frac{\partial^2 \mathbf{u}}{\partial t^2} = \left(K + \frac{1}{3}G\right) \text{grad div}\, \mathbf{u} + G\Delta \mathbf{u} + \mathbf{F}_{nonlinear} + \mathbf{F}_m. \tag{2.2}$$

Here $\mathbf{E}$ is the intensity of the magnetic field; $\mathbf{j}$ is the vector of the electric current density, $\mathbf{B}$ is the magnetic induction vector; ρ_e is the volumetric density of the electric charges; $\mathbf{u}$ is the displacement vector; K is the compression modulus, G is the shear modulus; ρ is the density of the material; t is the time. The force $\mathbf{F}_{nonlinear}$ includes elements which result from the consideration of elastic nonlinearity. If only the quadratic nonlinearity is taken into account, then the components of the vector can be represented through the gradients of displacements as follows [14]:

$$\begin{aligned} F_i = &\left(G + \frac{A}{4}\right)\left(u_{l,kk}u_{l,i} + u_{i,l}u_{l,kk} + 2u_{l,k}u_{i,lk}\right) \\ &+ \left(K + \frac{1}{3}G + \frac{A}{4} + B\right)\left(u_{l,k}u_{l,ik} + u_{i,l}u_{k,lk}\right) \\ &+ \left(K - \frac{2}{3}G + B\right)u_{l,l}u_{i,kk} + (B + 2C)u_{l,l}u_{k,ki} \\ &+ \left(K + \frac{1}{3}G + \frac{A}{4} + B\right)\left(u_{l,k}u_{l,ki} + u_{i,l}u_{k,lk}\right), \end{aligned} \tag{2.3}$$

here *A, B, C*—are the Landau constants, index after comma means differentiation with respect to the corresponding coordinate, repeating indices mean summation.

The form of nonlinear items when cubical nonlinearity is considered can be found in work [14].

From the Maxwell equations, one can obtain equations for the electric and magnetic inductions **D** and **B**, respectively:

$$\frac{\partial \mathbf{D}}{\partial t} = \operatorname{rot} \mathbf{H} - \mathbf{j}, \tag{2.4}$$

$$\frac{\partial \mathbf{B}}{\partial t} = \operatorname{rot}\left[\frac{\partial \mathbf{u}}{\partial t} \times \mathbf{B}\right] + \frac{1}{\mu_e \sigma} \Delta \mathbf{B}, \tag{2.5}$$

which should be added by the electromagnetic equations of state [15]:

$$\mathbf{j} = \sigma \mathbf{E}, \tag{2.6}$$

$$\mathbf{D} = \varepsilon_e \mathbf{E}, \tag{2.7}$$

$$\mathbf{B} = \mu_e \mathbf{H} \tag{2.8}$$

These equations should be solved together with Eqs. (2.1), (2.2). Here **H** is intensity of the magnetic field, σ is the conductivity, ε_e is the permittivity and и μ_e is the magnetic conductivity.

In magnetoelasticity, both the biasing current $(\partial \mathbf{D}/\partial t = 0)$ and the density of free electric charges $(\rho_e = 0)$ are neglected. Due to this, equations of magnetoelasticity can be written as follows:

$$\rho \frac{\partial^2 \mathbf{u}}{\partial t^2} = \left(K + \frac{1}{3} G\right) \operatorname{grad} \operatorname{div} \mathbf{u} + G \Delta \mathbf{u} + \mathbf{F}_{\mathbf{He}\,\boldsymbol{\pi}} + \mu_e (\operatorname{rot} \mathbf{H} \times \mathbf{H}), \tag{2.9}$$

$$\frac{\partial \mathbf{H}}{\partial t} = \operatorname{rot}\left[\frac{\partial \mathbf{u}}{\partial \tau} \times \mathbf{H}\right] + \frac{1}{\mu_e \sigma} \Delta \mathbf{H}. \tag{2.10}$$

We will study the case when the external constant magnetic field with the intensity H_0, has arbitrary spatial orientation which can be defined though angles $0 \le \theta \le \pi$, $0 \le \varphi < 2\pi$.

The total magnetic field consists of its permanent value and the perturbations that result from the interaction with the strain:

$$\mathbf{H} = H_0 \mathbf{n} + \mathbf{h}, \tag{2.11}$$

where **n** is the normal vector, **h** is a small disturbance of the magnetic field. In this case a small perturbation and the total magnetic field vectors are as follows:

$$\mathbf{H} = \left(H_0 \sin\theta \cos\varphi + h_x,\ H_0 \sin\theta \sin\varphi + h_y,\ H_0 \cos\theta + h_z\right) \tag{2.12}$$

3 Rod

Let us consider the propagation of longitudinal waves in a rod which has been places into external magnetic field (Fig. 1)

In this case relations for displacements vector, small disturbances of magnetic field and total magnetic field vectors will take the form:

$$\mathbf{u} = (u_x,\ 0,\ 0),\ \mathbf{h} = \left(h_x,\ h_y,\ h_z\right),\ \mathbf{H} = \left(H_0 \cos\varphi + h_z,\ h_y,\ H_0 \sin\varphi + h_z\right).$$

System of magnetoelasticity equation in this case will as follows:

$$\begin{aligned}
&\frac{\partial^2 u_x}{\partial t^2} - c_0^2\left(1 + \frac{6\alpha_1}{E}\frac{\partial u_x}{\partial x}\right)\frac{\partial^2 u_x}{\partial x^2} - \nu^2 R^2 \frac{\partial^2}{\partial x^2}\left(\frac{\partial^2 u_x}{\partial t^2} - c_\tau^2 \frac{\partial^2 u_x}{\partial x^2}\right)\\
&+ \tfrac{1}{4\pi\rho}\left[H_z \tfrac{\partial H_z}{\partial x} - H_y \tfrac{\partial H_y}{\partial x}\right] = 0,\\
&\frac{\partial H_x}{\partial t} - \frac{c^2}{4\pi\sigma}\frac{\partial^2 H_x}{\partial x^2} = 0,\\
&\frac{\partial H_y}{\partial t} + H_y \frac{\partial^2 u_x}{\partial x \partial t} + \frac{\partial H_y}{\partial x}\frac{\partial u_x}{\partial t} - \frac{c^2}{4\pi\sigma}\frac{\partial^2 H_y}{\partial x^2} = 0,\\
&\frac{\partial H_z}{\partial t} + H_z \frac{\partial^2 u_x}{\partial x \partial t} + \frac{\partial H_z}{\partial x}\frac{\partial u_x}{\partial t} - \frac{c^2}{4\pi\sigma}\frac{\partial^2 H_z}{\partial x^2} = 0.
\end{aligned} \tag{3.1}$$

We take into account that we can neglect the components (h_x), $\left(h_y\right)$, (H_x), $\left(H_y\right)$ due to the structure of the equations of smallness of items which are included these components.

For the further research, we need to obtain the evolutionary equation. To achieve that, we make the change of the variables and introduce a small parameter. Let us rewrite system (3.1) in the form

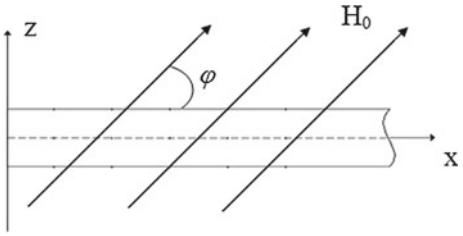

Fig. 1 Rod in a spatial oriented magnetic field

$$\begin{aligned}
&\frac{\partial G}{\partial \tau} - c_0^2\left(1 + \frac{6\alpha_1}{E}Q\right)\frac{\partial Q}{\partial x_1} - \nu^2 R^2 \frac{\partial^2}{\partial x_1^2}\left(\frac{\partial G}{\partial \tau} - c_\tau^2 \frac{\partial Q}{\partial x_1}\right) \\
&+ \frac{1}{4\pi\rho}(H_0 \sin\varphi + h_z)\frac{\partial h_z}{\partial x_1} = 0, \\
&\frac{\partial Q}{\partial \tau} - \frac{\partial G}{\partial x_1} = 0, \\
&\frac{\partial h_z}{\partial \tau} + (H_0 \sin\varphi + h_z)\frac{\partial G}{\partial x_1} + G\frac{\partial h_z}{\partial x_1} - \frac{c^2}{4\pi\sigma}\frac{\partial^2 h_z}{\partial x_1^2} = 0.
\end{aligned} \tag{3.2}$$

Here $Q = \frac{\partial u}{\partial x}$ is the deformation, $G = \frac{\partial u}{\partial \tau}$, ν is the Poisson coefficient, $R = \sqrt{J_0/F}$ is the polar radius of gyration, $J_0 = \int_F (x_2^2 + x_3^2)dF$ is the polar moment of inertia, F is the area of cross-section of the rod, $E = \frac{\mu(3\lambda + 2\mu)}{\lambda + \mu}$ is the modulus of elasticity, $\alpha_1 = \frac{E}{2} + \frac{3\lambda}{2} + A + B(1 - 2\nu) + \frac{C}{3}(1 - 6\nu)$ is the elastic nonlinearity coefficient.

We introduce non-dimensional variables

$$\begin{aligned}
&U = Q,\ V = \frac{G}{c_0},\ W = \frac{h_z}{H_0}, \\
&\tilde{x}_1 = \frac{1}{\nu R}x_1,\ \tilde{\tau} = \frac{c_0}{\nu R}\tau
\end{aligned} \tag{3.3}$$

$$x = \tilde{x}_1 - V_p\tilde{\tau},\ t = \varepsilon\tilde{\tau} \tag{3.4}$$

where V_p is a characteristic wave velocity, not known in advance, ε is a small parameter.

Substituting (3.3) and (3.4) into (3.2) and omitting items one of the second order and higher, we obtain the following systems of equations:

$$\begin{aligned}
&-V_p\frac{\partial V}{\partial x} - \frac{\partial U}{\partial x} + \frac{c_A^2 \sin^2\varphi}{c_0^2}\frac{\partial W}{\partial x} = 0, \\
&-V_p\frac{\partial U}{\partial x} - \frac{\partial V}{\partial x} = 0, \\
&-V_p\frac{\partial W}{\partial x} + \frac{\partial V}{\partial x} = 0.
\end{aligned} \tag{3.5}$$

$$\begin{aligned}
&\frac{\partial V}{\partial t} - \frac{6\alpha_1}{E}U\frac{\partial U}{\partial x} + V_p\frac{\partial^3 V}{\partial x^3} + \frac{c_\tau^2}{c_0^2}\frac{\partial^3 U}{\partial x^3} + \frac{c_A^2 \sin^2\varphi}{c_0^2}W\frac{\partial W}{\partial x} = 0, \\
&\frac{\partial W}{\partial t} + W\frac{\partial V}{\partial x} + V\frac{\partial W}{\partial x} - \frac{c^2}{4\pi\sigma c_0 \nu R}\frac{\partial^2 W}{\partial x^2} = 0.
\end{aligned} \tag{3.6}$$

which represent zero and first dimensionless approximations of the system (3.2), respectively. Using the 2nd and 3rd equations in (3.5), we obtain the connection between the functions:

$$U = -W,\ V = -V_p U, \tag{3.7}$$

and from the 1st equation we determine the velocity:

$$V_p = \sqrt{1 + \frac{c_A^2 \sin^2 \varphi}{c_0^2}}. \tag{3.8}$$

Substituting (3.7) and (3.8) into (3.6) and summing the obtained equations, we transform it to the equation of the form

$$\frac{\partial U}{\partial t} - \alpha U \frac{\partial U}{\partial x} + \beta \frac{\partial^3 U}{\partial x^3} - \delta \frac{\partial^2 U}{\partial x^2} = 0. \tag{3.9}$$

Here $\alpha = \frac{\frac{c_A^2 \sin^2 \varphi}{c_0^2} - \frac{6\alpha_1}{E} + 2V_p}{1+V_p}$, $\beta = \frac{V_p^2 - \frac{c_t^2}{c_0^2}}{1+V_p}$, $\delta = \frac{c^2}{4\pi \cdot \sigma c_0 \nu R(1+V_p)}$.

Equation (3.9) represents Korteweg-de Vries-Burgers equation [16]. This equation has a localized solution in the form of a soliton that can be represented as a blast wave:

$$\begin{aligned} &U = A \cdot \exp(\xi)\ \sec \mathrm{h}^2 \left(\frac{\xi}{2}\right),\ \xi = \xi_0 (x - 2at), \\ &\xi_0 = \sqrt{-\frac{a}{3\beta}},\ a = -\frac{3\delta^2}{25\beta}, \\ &A = -\frac{a}{\alpha},\ V_k = 2a, \Delta = \frac{2}{\xi_0}. \end{aligned} \tag{3.10}$$

Let us study the influence of magnetic field orientation on the parameters of the wave. The variations of parameters according to the angles are shown when $c_A/c_l = 0.2$.

In the Figs. 2, 3 and 4 the dependencies of velocity, width and amplitude on external magnetic field orientation are depicted.

From the figures it is clear that amplitude and velocity have their maximum value when magnetic field is parallel to the direction of propagation of the localized wave and have their minimum value when the magnetic field is transverse the direction of wave propagation. Similar conclusions can be made regarding the width of the localized wave: it takes its maximum value when the field is transverse to the direction of wave propagation and has its minimum when the field and direction of the wave propagation are is codirectional.

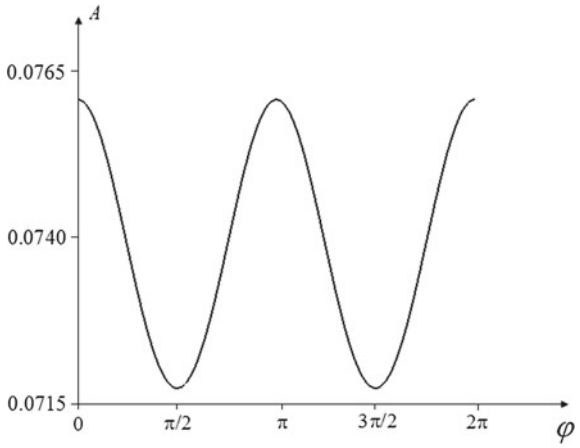

Fig. 2 Amplitude dependence on magnetic field orientation

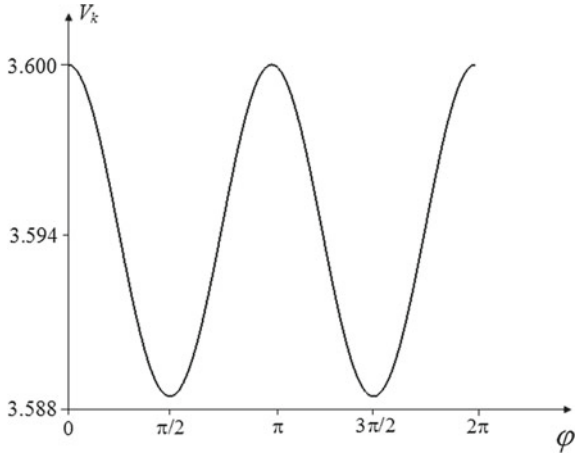

Fig. 3 Velocity dependence on magnetic field orientation

Let us estimate the relative influence of orientation and intensity of the magnetic field (for transverse field orientation) on the mentioned above parameters. These estimations are given in the (Table 1).

Here $\Delta Ak1$, $\Delta Vk1$, $\Delta\Delta k1$—the magnitudes of variations of amplitude, velocity and width of the localized wave on the intensity of transverse oriented magnetic field, $\Delta Ak2$, $\Delta Vk2$, $\Delta\Delta k2$—the magnitudes of variations of amplitude, velocity and width of the same solution when spatial orientation of the field changes in the interval $[0, 2\pi]$ and the magnetic field has constant intensity. From the Table 1 it is clear that maximal influence of the magnetic field can be achieved for transversal magnetic field orientation. The ratios of the mentioned above values can be up to 6%.

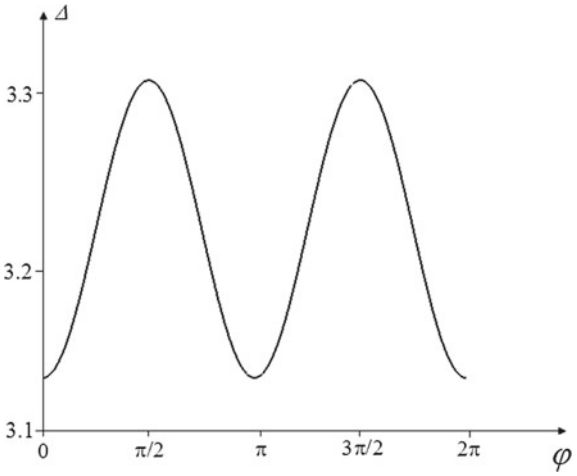

Fig. 4 Width dependence on magnetic field orientation

Table 1 Relative influence of magnetic field orientation and intensity on amplitude, velocity and width of the wave

		$\Delta Ak2/\Delta Ak1 * 100\%$	$\Delta Vk2/\Delta Vk1 * 100\%$	$\Delta\Delta k2/\Delta\Delta k1 * 100\%$
$\Delta Ak1$	0.5	1.00%		
$\Delta Ak2$	0.005			
$\Delta Vk1$	0.2		6.00%	
$\Delta Vk2$	0.012			
$\Delta\Delta k1$	4			3.75%
$\Delta\Delta k2$	0.15			

4 Plate

Let us consider the propagation of longitudinal waves in nonlinear elastic homogeneous plate in an external magnetic field (Fig. 5).

It is well known that [17], the idea of bringing three-dimensional equations of elasticity theory to two-dimensional equations of equilibrium or dynamics of the plates is to express the quantities describing the stress-strain state at any point of the body, through the new values, which vary along the medial surface of the plate. The transition from an infinite number of degrees of freedom in the normal direction $\vec{x}_\perp = (x_2, x_3)$ to a finite number of degrees of freedom (finite number of modes) is performed by approximating the displacement with polynomials. It is usually in the powers of the transverse coordinates, and as a small parameter serves the relative thickness of the plate $2k_z h$, where h—half-thickness of a plate, k_z—a normal component of wave vector.

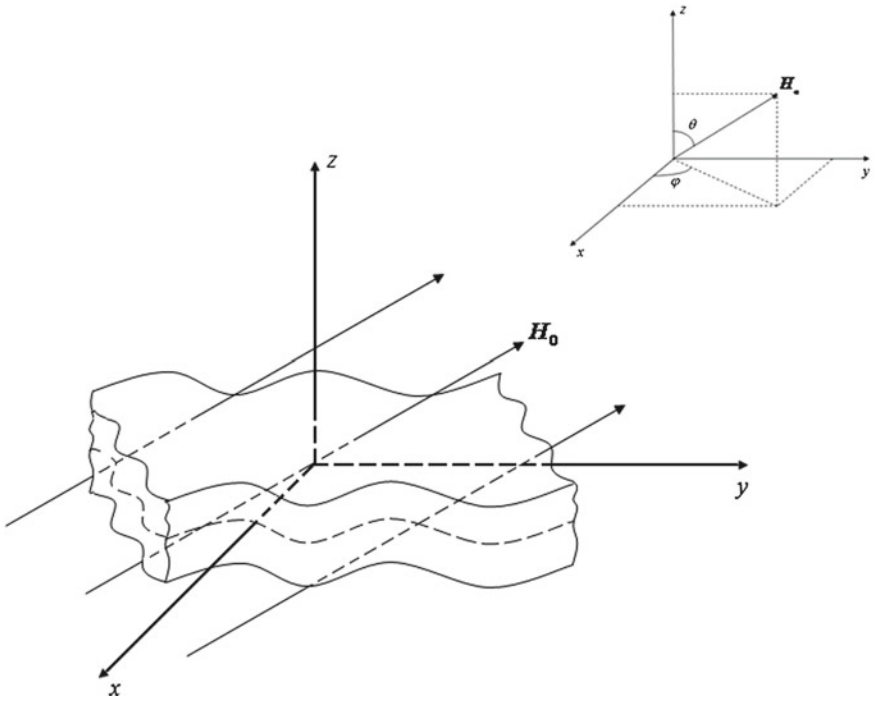

Fig. 5 Plate in a spatial oriented magnetic field

To frequencies $\omega h < c_l$, (c_l—propagation velocity of longitudinal elastic waves in an infinite medium, $c_l = \sqrt{\frac{K+4/3G}{\rho}}$) the following approximation of the displacement [17]:

$$u_1 = u(x, y, t),\ u_2 = v(x, y, t),\ u_3 = -\frac{3K-2G}{3K+4G} \cdot z \cdot div\vec{V} \tag{5.1}$$

where u, v—denote the displacement of the middle of the plate; $x = x_1$; $y = x_2$; $z = x_3$; $\vec{V} = \begin{pmatrix} u \\ v \end{pmatrix}$. Magnetoelasticity equations for a plate undergoing a longitudinal vibration can be written as follows:

$$
\begin{aligned}
&\frac{\partial^2 u}{\partial t^2} - c_p^2 \frac{\partial^2 u}{\partial x^2} - \left(c_l^2 - c_\tau^2\right) \frac{\partial^2 v}{\partial x \partial y} - c_\tau^2 \frac{\partial^2 u}{\partial y^2} - \\
&\quad - \frac{h^2}{3} \frac{(3K-2G)^2}{(3K+4G)^2} \left(\frac{\partial^4 u}{\partial x^2 \partial t^2} + \frac{\partial^4 v}{\partial x \partial y \partial t^2} \right) + \\
&\quad + \frac{c_\tau^2 h^2}{3} \frac{(3K-2G)^2}{(3K+4G)^2} \left(\frac{\partial^4 u}{\partial x^4} + \frac{\partial^4 u}{\partial x^2 \partial y^2} + \frac{\partial^4 v}{\partial x^3 \partial y} + \frac{\partial^4 v}{\partial x \partial y^3} \right) + \\
&\quad + \frac{1}{4\pi\rho} H_0 \frac{\partial h_z}{\partial x} = \\
&= \alpha_1 \frac{\partial u}{\partial x} \frac{\partial^2 u}{\partial x^2} + \alpha_2 \left[2 \frac{\partial}{\partial y} \left(\frac{\partial u}{\partial y} + \frac{\partial v}{\partial x} \right) \left(\frac{\partial u}{\partial x} + \frac{\partial v}{\partial y} \right) + \frac{\partial}{\partial x} \left(\frac{\partial u}{\partial y} + \frac{\partial v}{\partial x} \right)^2 \right] + \\
&\quad + \alpha_3 \frac{\partial v}{\partial y} \frac{\partial^2 v}{\partial x \partial y} + \alpha_4 \frac{\partial v}{\partial x} \frac{\partial^2 v}{\partial x^2} - \\
&\quad - \frac{1}{4\pi\rho} \left[(H_0 \cos\theta + h_z) \frac{\partial h_z}{\partial x} + \left(H_0 \sin\theta \, \sin\varphi + h_y\right) \left(\frac{\partial h_y}{\partial x} - \frac{\partial h_x}{\partial y} \right) \right]; \\
&\frac{\partial^2 v}{\partial t^2} - c_p^2 \frac{\partial^2 v}{\partial y^2} - \left(c_l^2 - c_\tau^2\right) \frac{\partial^2 u}{\partial y \partial x} - c_\tau^2 \frac{\partial^2 v}{\partial x^2} - \\
&\quad - \frac{h^2}{3} \frac{(3K-2G)^2}{(3K+4G)^2} \left(\frac{\partial^4 v}{\partial y^2 \partial t^2} + \frac{\partial^4 u}{\partial y \partial x \partial t^2} \right) + \\
&\quad + \frac{c_\tau^2 h^2}{3} \frac{(3K-2G)^2}{(3K+4G)^2} \left(\frac{\partial^4 v}{\partial y^4} + \frac{\partial^4 v}{\partial y^2 \partial x^2} + \frac{\partial^4 u}{\partial y^3 \partial x} + \frac{\partial^4 u}{\partial y \partial x^3} \right) + \\
&\quad + \frac{1}{4\pi\rho} H_0 \frac{\partial h_z}{\partial y} = \\
&= \alpha_1 \frac{\partial v}{\partial y} \frac{\partial^2 v}{\partial y^2} + + \alpha_2 \left[2 \frac{\partial}{\partial x} \left(\frac{\partial v}{\partial x} + \frac{\partial u}{\partial y} \right) \left(\frac{\partial v}{\partial y} + \frac{\partial u}{\partial x} \right) + \frac{\partial}{\partial y} \left(\frac{\partial v}{\partial x} + \frac{\partial u}{\partial y} \right)^2 \right] + \\
&\quad + \alpha_3 \frac{\partial u}{\partial x} \frac{\partial^2 u}{\partial y \partial x} + \alpha_4 \frac{\partial u}{\partial y} \frac{\partial^2 u}{\partial y^2} - \\
&\quad - \frac{1}{4\pi\rho} \left[(H_0 \cos\theta + h_z) \frac{\partial h_z}{\partial y} - (H_0 \sin\theta \, \cos\varphi + h_x) \left(\frac{\partial h_y}{\partial x} - \frac{\partial h_x}{\partial y} \right) \right]; \\
&\frac{\partial h_x}{\partial t} = \frac{\partial}{\partial y} \left(\left(H_0 \sin\theta \, \sin\varphi + h_y\right) \frac{\partial u}{\partial t} - (H_0 \sin\theta \, \cos\varphi + h_x) \frac{\partial v}{\partial t} \right) + \\
&\quad + \frac{1}{\mu_e \sigma} \left(\frac{\partial^2 h_x}{\partial x^2} + \frac{\partial^2 h_x}{\partial y^2} \right); \\
&\frac{\partial h_y}{\partial t} = - \frac{\partial}{\partial x} \left(\left(H_0 \sin\theta \, \sin\varphi + h_y\right) \frac{\partial u}{\partial t} - (H_0 \sin\theta \, \cos\varphi + h_x) \frac{\partial v}{\partial t} \right) + \\
&\quad + \frac{1}{\mu_e \sigma} \left(\frac{\partial^2 h_y}{\partial x^2} + \frac{\partial^2 h_y}{\partial y^2} \right); \\
&\frac{\partial h_z}{\partial t} = - \frac{\partial}{\partial x} \left[(H_0 \cos\theta + h_z) \frac{\partial u}{\partial t} \right] - \frac{\partial}{\partial y} \left[(H_0 \cos\theta + h_z) \frac{\partial v}{\partial t} \right] + \frac{1}{\mu_e \sigma} \left(\frac{\partial^2 h_z}{\partial x^2} + \frac{\partial^2 h_z}{\partial y^2} \right);
\end{aligned}
\tag{5.2}
$$

Here $c_p = c_l\sqrt{1-\frac{\left(c_l^2-2c_\tau^2\right)^2}{c_l^4}}$ is the velocity with which would extend the longitudinal wave in the plate in the absence of geometric dispersion and interaction with the magnetic field; c_τ—propagation velocity of elastic shear waves in an infinite medium; $c_\tau = \sqrt{\frac{G}{\rho}}$.

Consider the propagation of the beam longitudinal waves along the x axis, restricting the area in which the parameters of nonlinearity, dispersion and diffraction of the same order $(\sim\varepsilon)$. Suppose that a beam of waves is a limited, slightly divergent and close to a plane wave.

Let us introduce the "ray" coordinates:

$$\begin{aligned} &x' = \frac{x}{\Lambda},\ y' = \frac{y}{\Lambda},\ t' = \frac{c_l t}{\Lambda}, \\ &\xi = x' - \tilde{c}t';\ \eta = \varepsilon x';\ \chi = \sqrt{\varepsilon}y' \end{aligned} \tag{5.3}$$

and new functions

$$\begin{aligned} &u = u;\ v = \sqrt{\varepsilon}v; \\ &h_z = h_z;\ h_x = \sqrt{\varepsilon}h_x;\ h_y = \sqrt{\varepsilon}h_y. \end{aligned} \tag{5.4}$$

Here, Λ is the wave's length, $\tilde{c}$—character dimensionless velocity of the wave, previously unknown.

The choice of variables in the form (5.3) and replacement (5.4) reflect the fact that, by virtue of nonlinearity, dispersion and diffraction divergence, the displacements and the components of the magnetic field varies both along the beam propagation direction $(\sim\varepsilon)$, and across $(\sim\sqrt{\varepsilon})$.

Substituting (5.3), (5.4) into (5.2) and holding down the only terms with order of ε not higher than the first, we get the evolutionary equation for axial (longitudinal) strain $U = \partial u/\partial\xi$:

$$\frac{\partial}{\partial\xi}\left(\frac{\partial U}{\partial\eta} + \alpha U\frac{\partial U}{\partial\xi} + \beta\frac{\partial^3 U}{\partial\xi^3} - \delta\frac{\partial^2 U}{\partial\xi^2}\right) + \gamma\frac{\partial^2 U}{\partial\chi^2} = 0, \tag{5.5}$$

where

$$\alpha = \frac{3 - \frac{c_A^2\left(1-\left(\frac{H_x}{H}\right)^2\right)}{c_l^2} - 6\frac{(3K-2G)^2}{(3K+4G)^2}\left(1-\left(\frac{c_\tau}{c_l}\right)^2\right) + \left(\frac{c_p}{c_l}\right)^2 g}{2\left(2\left(\frac{c_p}{c_l}\right)^2 + \left(\frac{c_A}{c_l}\right)^2\right)} - 1,$$

$$\beta = \frac{h^2}{6}\frac{(3K-2G)^2}{(3K+4G)^2}\frac{\left(\frac{c_p}{c_l}\right)^2 + \frac{c_A^2\left(1-\left(\frac{H_x}{H}\right)^2\right)}{c_l^2} - \left(\frac{c_\tau}{c_l}\right)^2}{2\left(\frac{c_p}{c_l}\right)^2 + \left(\frac{c_A}{c_l}\right)^2},$$

$$\delta = \frac{1}{2\mu_e \sigma \Lambda c_l \sqrt{\left(\frac{c_p}{c_l}\right)^2 + \frac{c_A^2\left(1-\left(\frac{H_x}{H}\right)^2\right)}{c_l^2}}},$$

$$\gamma = \frac{1 + \frac{c_A^2\left(1-\left(\frac{H_x}{H}\right)^2\right)}{c_l^2} - \left(\frac{c_\tau}{c_l}\right)^2\left(2-\left(\frac{c_p}{c_l}\right)^2\right)}{2\left(2\left(\frac{c_p}{c_l}\right)^2 + \frac{c_A^2\left(1-\left(\frac{H_x}{H}\right)^2\right)}{c_l^2}\right)\left(\left(\frac{c_p}{c_l}\right)^2 + \frac{c_A^2\left(1-\left(\frac{H_x}{H}\right)^2\right)}{c_l^2} - \left(\frac{c_\tau}{c_l}\right)^2\right)},$$

$$g = \frac{2A+6B+2C}{\rho c_l^2}, \tilde{c} = \sqrt{c_p^2 + c_A^2\left(1-\left(\frac{H_x}{H}\right)^2\right)},$$

Here $c_A = \sqrt{H_0^2/4\pi\rho}$ is the Alfven wave velocity [18]. Equation (5.5) generalizes the well-known model equations of Khokhlov-Zabolotskaya-Kuznetsov [16] and Kadomtsev–Petviashvili [16], which follow from (5.3), when $\beta = 0$ and $\delta = 0$ respectively.

To obtain an analytical solution "by simplest equations method" [19] we take as a simple Riccati equation.

$$Y_z = -Y^2 + aY + b, \tag{5.6}$$

which has a solution in the following form:

$$Y(z) = \frac{1}{2}a + \frac{\sqrt{4b+a^2}}{2}\tanh\left[\frac{1}{2}\sqrt{4b+a^2}(z+C_2)\right], \tag{5.7}$$

where a and b define the later of the over determined system of equations.

Equation (5.7) is of the order of singularity, which is equal to two, so the solution of the equation will be sought in the form of:

$$U(z) = A_0 + A_1 Y + A_2 Y^2 + B_1\left(\frac{Y_z}{Y}\right) + B_2\left(\frac{Y_z}{Y}\right)^2, \tag{5.8}$$

here $z = k_0\xi + k_1\chi + k_2\eta$, A_i, B_i—arbitrary constants. In the form of (5.6) we obtain:

$$\begin{aligned} U(z) = {} & (A_2+B_2)Y^2 + (A_1 - B_1 - 2aB_2)Y + A_0 + aB_1 \\ & + B_2(a^2-2b) + \frac{bB_1 + 2abB_2}{Y} + \frac{B_2 b^2}{Y^2} \end{aligned} \tag{5.9}$$

Substituting (5.9) into (5.5) and equating terms with the same degree of Y_z, we obtain a system of equations, because of the cumbersome nature of which we show here only the first two equations:

$$\left(\frac{1}{2}\alpha B_2^2 + 6\beta B_2\right)^4 = 0,\ \left(14\beta B_2\alpha + \alpha B_1 B_2 + 2\beta B_1 + 2a\alpha B_2^2 + 2\delta B_2\right)b^3 = 0\ldots \tag{5.10}$$

Solution of the system is as follows:

$$A_2 = -\frac{12\beta}{\alpha},\ a = -\frac{1}{5}\frac{\delta}{\beta},\ A_0 = A_1 = B_1 = B_2 = b = 0 \tag{5.11}$$

Then the exact solution of Eq. (5.5) takes the form of a shock wave:

$$U(\xi, \chi, \eta) = -\frac{3}{25}\frac{\delta^2}{\alpha\beta}\left(-1 + \tanh\left(\frac{k_0\xi + k_1\chi + k_2\eta}{2}\right)\right)^2, \tag{5.12}$$

where is $k_0 = \frac{1}{5}\frac{\delta}{\beta}$, $k_2 = -\frac{6}{125}\frac{\delta^3}{\beta^2} + \frac{5\beta\gamma k_1^2}{\delta}$, k_1—is an arbitrary constant. The requirement of positive definiteness of the velocity of the wave ($k_2 > 0$) imposes a restriction on the k_1 coefficient: $k_1^2 > \frac{6}{625}\frac{\delta^4}{\gamma\beta^3}$. Defining the arbitrary constants as follows:

$$k_1 = \frac{\sqrt{7}}{25}\frac{\delta^2}{\sqrt{\gamma\beta^3}},\ k_2 = \frac{1}{125}\frac{\delta^3}{\beta^2} \tag{5.13}$$

we obtain expressions for the amplitude and width of the beam along the axes:

$$A = -\frac{3}{25}\frac{\delta^2}{\alpha\beta},\ \Delta_\xi = \frac{10\beta}{\delta},\ \Delta_\eta = \frac{250\beta^2}{\delta^3},\ \Delta_\chi = \frac{50}{\sqrt{7}}\frac{\sqrt{\gamma\beta^3}}{\delta^2} \tag{5.14}$$

Let's study the change in the width of the beam along each coordinate axis, depending on the orientation of the external magnetic field. The variations of parameters according to the angles are shown when $c_A/c_l = 0.5 \times 10^{-3}$. The expression for the width of the beam along the axis defined by (5.14) in which the coefficients of the Eq. (5.12) depend on angles $0 \le \theta \le \pi$, $0 \le \varphi < 2\pi$.

The following are the results of the analysis of the width of the wave beam along the coordinate axes. In contrast to the amplitude, the width of the beam along the coordinate axes of a minimum value, where the amplitude is maximum and, conversely, is maximal at the angles corresponding to the minimum values of the amplitude.

Figure 6 represents the surface $A(\varphi, \theta)$, which represents the dependence of the wave's beam magnitude on angles θ and φ:

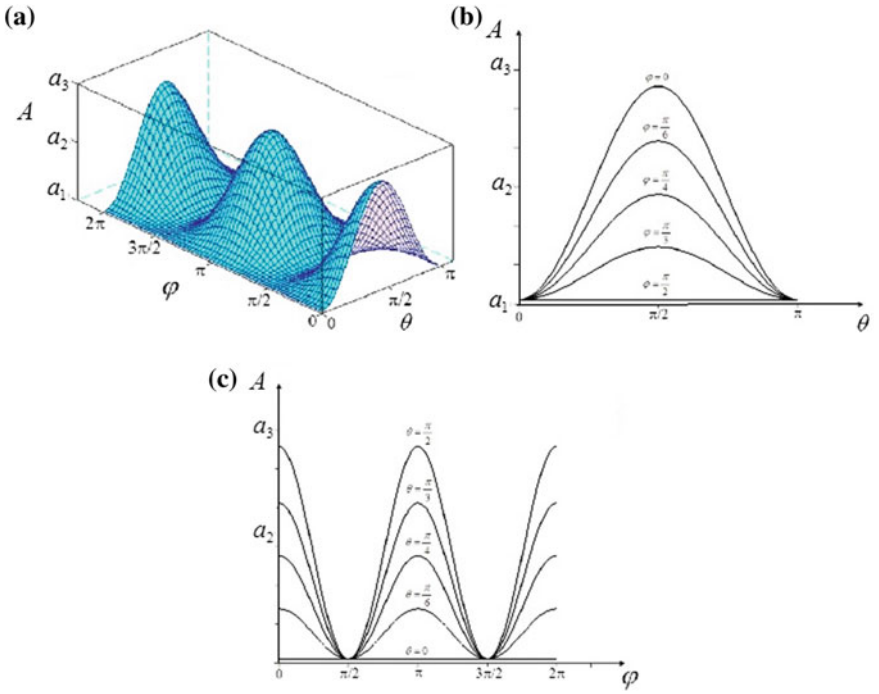

Fig. 6 **a** Surface $A(\varphi, \theta)$, **b** intersections of the surface $A(\varphi, \theta)$ by planes $\varphi = \text{const}$, **c** intersections of the plane $A(\varphi, \theta)$ by planes $\theta = \text{const}$

Table 2 The values of a_1, a_2 and a_3 for Fig. 6

	a_1	a_2	a_3
$A(\varphi, \theta)$	2.898242	2.898244	2.898246

The values of a_1, a_2, a_3 for the surface are presented in the Table 2.

We can see from Fig. 6b, which represents cross-sections of the surface $\Delta_\varsigma(\varphi, \theta)$ by planes $\varphi = \text{const}$, that with the rising of angle φ on the interval $\left[0, \frac{\pi}{2}\right]$ the width of the wave's beam along ζ axis decreases.

By similar reasoning for cross-sections of the surface $\Delta_\varsigma(\varphi, \theta)$ by planes $\theta = \text{const}$, which are shown in Fig. 6c, we can make a conclusion that with the growth of angle θ on the interval $\left[0, \frac{\pi}{2}\right]$ the width of the wave's beam along χ axis goes up.

Surfaces $\Delta_\xi(\varphi, \theta)$, $\Delta_\eta(\varphi, \theta)$ и $\Delta_\chi(\varphi, \theta)$, which represent the dependence of the wave's beam width along ξ, η and χ axis, on angles θ and φ formally identical and are shown in Fig. 7a:

The values of a_1, a_2, a_3 for each surface are presented in the Table 3.

As it follows from (Fig. 7b), which shows the intersections of surfaces $\Delta_\xi(\varphi, \theta)$, $\Delta_\eta(\varphi, \theta)$ and $\Delta_\chi(\varphi, \theta)$ by planes $\varphi = \text{const}$, with the growth of angle φ on the interval $\left[0, \frac{\pi}{2}\right]$ the width of the wave's beam along ξ, η and χ axis increases.

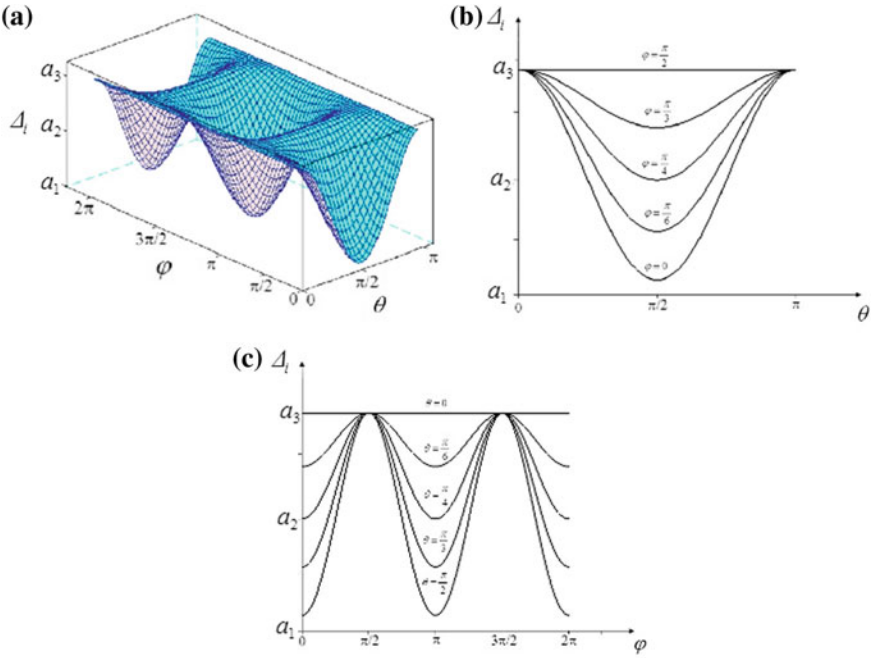

Fig. 7 **a** Surface $\Delta_i = (i = \xi, \eta, \chi)$, **b** intersections of the surface $\Delta_i = (i = \xi, \eta, \chi)$ by planes $\varphi = \text{const}$, **c** intersections of the surface $\Delta_i = (i = \xi, \eta, \chi)$ by planes $\theta = \text{const}$

Table 3 The values of a_1, a_2 and a_3 for Fig. 7

	a_1	a_2	a_3
$\Delta_\xi(\phi, \theta)$	5.67698×10^{-5}	5.67704×10^{-5}	5.67708×10^{-5}
$\Delta_\eta(\phi, \theta)$	3.049614×10^{-7}	3.0496120×10^{-7}	3.049626×10^{-7}
$\Delta_\chi(\phi, \theta)$	3.392165×10^{-6}	3.392169×10^{-6}	3.392173×10^{-6}

From the analysis of the cross-section of surfaces $\Delta_\xi(\varphi, \theta)$, $\Delta_\eta(\varphi, \theta)$ and $\Delta_\chi(\varphi, \theta)$ by planes $\theta = \text{const}$, which are represented in (Fig. 7c), we make a conclusion that with the increase of angle θ on the interval $\left[0, \frac{\pi}{2}\right]$ the width of the wave's beam along axis ξ, η and χ goes down.

The relative comparison of the influence of the magnetic field orientation and strength at its transverse orientation on the direction of wave propagation is shown in the Table 4.

Here $\Delta U_0 1$, $\Delta\Delta_\xi 1$, $\Delta\Delta_\eta 1$, $\Delta\Delta_\chi 1$—the variation of the magnitude and widths of the solution (5.12) along coordinate axis on the intensity of transverse oriented magnetic field, $\Delta U_0 2$, $\Delta\Delta_\xi 2$, $\Delta\Delta_\eta 2$, $\Delta\Delta_\chi 2$—the variation of the magnitude and

Table 4 Relative influence of the magnetic field orientation and strength at its transverse orientation on the direction of the wave propagation

		$\Delta U_0 2/\Delta U_0 1 *100\%$	$\Delta\Delta_\xi 2/\Delta\Delta_\xi 1 * 100\%$	$\Delta\Delta_\eta 2/\Delta\Delta_\eta 1 * 100\%$	$\Delta\Delta_\chi 2/\Delta\Delta_\chi 1 * 100\%$
$\Delta U_0 1$	1.5	26.67%			
$\Delta U_0 2$	0.4				
$\Delta\Delta_\xi 1$	0.03		13.33%		
$\Delta\Delta_\xi 2$	0.004				
$\Delta\Delta_\eta 1$	0.008			7.50%	
$\Delta\Delta_\eta 2$	0.0006				
$\Delta\Delta_\chi 1$	0.0025				8.00%
$\Delta\Delta_\chi 2$	0.0002				

widths of the solution (5.12) along coordinate axis when spatial orientation of the field changes in the interval $[0, 2\pi]$ and the magnetic field has constant intensity. The ratios of the mentioned above values can be up to 27%.

5 Conclusions

Thus we have studied the influence of orientation of external magnetic field on parameters of localized waves which propagate in one- and two-dimensional medium (rod and plate). The analytical dependencies have been obtained.

Acknowledgements The research was carried out under the financial support of the Russian Scientific Foundation (project no. 14-19-01637).

References

1. Ambartsumyan, S.A., Bagdasaryan, G.E., Belubekyan, M.V.: Magnetoelasticity of Thin Plates and Shells. Nauka, Moscow (1977) (in Russian)
2. Bagdasaryan, G.E., Danoyan, Z.N.: Electro-Magneto-Elastic Waves. Publishing House of Yerevan State University, Yerevan (2006) (in Russian)
3. Selezov, I.T., Selezova, L.V.: Waves in Magnetoelastic Media. Naukova Dumka, Kiev (1975) (in Russian)
4. Podstrigach, Ya.S., Burak, Ya.I., Kondrat, V.F.: Magnetotermoelastisity of Electrically Conductive Bodies. Naukova Dumka, Kiev (1982) (in Russian)
5. Sibgatullin, N.R.: Vibrations and Waves in Strong Gravitational and Electromagnetic Fields. Nauka, Moscow (1984) (in Russian)
6. Nowacki, W.: Electromagnetic Effects in Solids. Mir, Moscow (1986) (in Russian)
7. Maugin, G.A.: Continuum Mechanics of Electromagnetic Solids. North-Holland, Amsterdam (1988)

8. Kaliski, S., Rymarz, C.z., Sobczyk, K.: Vibration and Waves. Elsevier, Amsterdam (1992)
9. Bardzokas, D.I., Kudryavtsev, B.A., Senik, N.A.: Wave Propagation in Electromagnetoelastic Media. Editorial URSS, Moscow (2005)
10. Klyuev, V.V. (ed.): Non-Destructive Testing: A Handbook in 8 Volumes, Vol. 6: Magnetic Methods of Control. Optical Control. Radio Wave Control. Mashinostroenie, Moscow (2006) (in Russian)
11. Uglov, A.A. (ed.): Physico-Chemical Processes of Processing Materials with Consentrated Energy Flows. Nauka, Moscow (1989) (in Russian)
12. Ghaleb, A.F., Ayad, M.M.: Nonlinear waves in thermo-magnetoelasticity I. Basic equations II. Wave generation in a perfect electric conductor. Int. J. Appl. Electromagn. Mech. **9**(4), 339–357, 359–379 (1998)
13. Kulikovskii, A.G., Sveshnikova, E.I.: Nonlinear Waves in Elastic Media. CRC Press, New York (1995)
14. Erofeyev, V.I.: Wave Processes in Solids with Microstructure. World Scientific, Singapore (2003)
15. Landau, L.D., Lifshitz, E.M.: Electrodynamics of Continuous Media. Pergamon Press, Oxford (1984)
16. Porubov, A.V.: Amplification of Nonlinear Strain Waves in Solids. World Scientific, Singapore (2003)
17. Erofeev, V., Potapov, A., Soldatov, I.: Nonlinear Waves in Elastic Systems. Lambert Academic Publishing, Saarbrucken (2015)
18. Bagdoev, A.G., Erofeyev, V.I., Shekoyan, A.V.: Wave Dynamics of Generalized Continua. Springer, Heidelberg (2016)
19. Kydryashov, N.A.: Simplest equation method to look for exact solutions of nonlinear differential equations. Chaos Solitons Fractals **24,** 1217–1231 (2005)

Waves in Elastic Reduced Cosserat Medium with Anisotropy in the Term Coupling Rotational and Translational Strains or in the Dynamic Term

Elena F. Grekova

Abstract We consider wave propagation in a special kind of elastic micropolar continuum: reduced Cosserat medium possessing an anisotropic term coupling rotational and translational strains or anisotropy in the tensor of inertia of point bodies. This medium consists of point bodies which are infinitesimal rigid bodies that can perform independent translations and turns. Reduced Cosserat medium is a Cosserat medium that does not react on the gradient of turn of point bodies. We consider linear theory. In the isotropic case the P-wave is the same as in the classical medium, and shear-rotational waves are dispersive and one branch has a cut-off frequency. Anisotropy in elastic properties allows to introduce a coupling term between these waves. We consider some classes of anisotropy and special directions of wave propagation, and also waves in the vicinity of the characteristic frequency of the medium. We find that the shear-rotational wave splits, and that in some cases the P-wave also becomes dispersional and has a band gap, in another case there exist shear-rotational and mixed wave, both having these properties. Then we consider a reduced Cosserat medium with isotropic elastic properties but with non-spherical tensor of inertia (equal in its initial position for all point bodies). The pressure wave in such a medium is the same as in the classical medium (non-dispersive). The shear-rotational wave changes essentially. For axial symmetry its dispersion graph has two boundary frequencies and two cut-off frequencies.

1 Introduction

Many works are devoted to the mechanics of media whose point bodies have rotational degrees of freedom. For the first time such a 3D medium was considered by Cosserat [1]. Later on its theory was developed by Kafadar and Eringen [2]. Zhilin and Altenbach developed a method to obtain constitutive equations of 2D elastic

E. F. Grekova (✉)
Institute of Problems of Mechanical Engineering, Russian Academy of Sciences,
Bolshoy pr. V.O., 61, 199178 St. Petersburg, Russia
e-mail: elgreco@pdmi.ras.ru

F. dell'Isola et al. (eds.), *Advances in Mechanics of Microstructured Media and Structures*, Advanced Structured Materials 87,
https://doi.org/10.1007/978-3-319-73694-5_9

polar medium [3] that can be applied also for the 3D case. Among various books on elastic Cosserat continua one can mention books [4–6]. Many other eminent scientists, such as C. Truesdell, V.A. Palmov, Green, Naghdi, E.L. Aero made important contributions into the theory of micropolar continua. Waves in 1D nonlinear Cosserat continuum are investigated in [7]. Depending on the different type of Cosserat continua and restrictions on the strain energy we have to use different strain measures and obtain specific type of constitutive equations [8–10].

Elastic reduced Cosserat medium is a medium whose particles possess independent translational and rotational degrees of freedom, but it does not react to the gradient of turn of point bodies (Fig. 1). Schwartz et al. [11] have suggested to consider such a medium in its isotropic linear variant to describe granular materials. This is a special case of Cosserat medium with a specific restriction.

Waves in the reduced Cosserat continuum were investigated in [12, 13]. In the isotropic case the P-wave is the same as in the classical medium, but the shear-rotational wave has a band gap, limited by the boundary and cut-off frequencies. Thus reduced Cosserat medium is a single negative acoustic metamaterial. Near these frequencies one observes a strong dispersion (Fig. 2).

In the anisotropic case for a particular coupling between rotational and volumetric translational strains [14] we see that for most directions of wave propagations we have mixed waves instead of P-wave, always dispersive and almost always having a band gap, and when the pure P-wave exists, it also has the same character. However, only particular type of coupling was considered, and anisotropy in the tensor of inertia was not taken into account. A part of this work devoted to the anisotropic coupling in the elastic energy was started with collaboration with Dr. Gérard C. Herman (1954–2006) and some preliminary results were obtained.

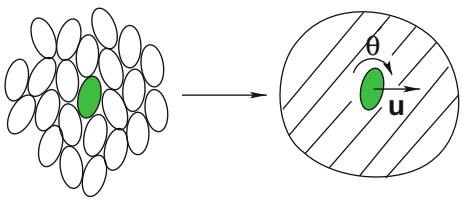

Fig. 1 Reduced Cosserat continuum with anisotropy in elastic and inertial characteristics

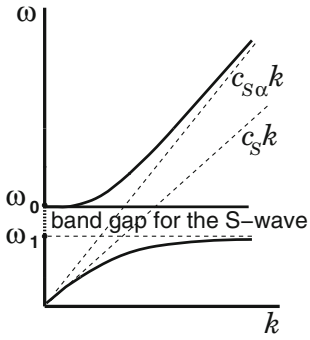

Fig. 2 Dispersion curves for the shear-rotational waves in the isotropic reduced Cosserat continuum. Velocities at low and high frequencies $c_s = \sqrt{\mu/\rho}$, $c_{s\alpha} = \sqrt{(\mu+\alpha)/\rho}$, respectively

The author regrets she cannot discuss this work with Prof. Eron L. Aero. She will keep warm recollections on the period when she had an honour to be his colleague.

2 General Equations for Reduced Cosserat Medium

Reduced Cosserat medium is an enhanced continuum. Each its point body is characterized by the mass density ρ, density of the tensor of inertia $\mathbf{I}$, position vector $\mathbf{R}$, turn tensor $\mathbf{P}$, linear velocity $\mathbf{v} = \dot{\mathbf{R}}$ and angular velocity $\boldsymbol{\omega}$ that satisfies Poisson equation $\dot{\mathbf{P}} = \boldsymbol{\omega} \times \mathbf{P}$. In the reference configuration $\mathbf{R} = \mathbf{r}$, and $\mathbf{P} = \mathbf{E}$, being $\mathbf{E}$ the identity tensor.

In such a medium the density of the kinetic energy is

$$\rho K = \frac{1}{2}\rho \mathbf{v}^2 + \frac{1}{2}\boldsymbol{\omega} \cdot \mathbf{I} \cdot \boldsymbol{\omega}. \tag{1}$$

Reduced Cosserat medium by definition does not produce work on the gradient of angular velocity. This results in absence of couple stresses, however, Cauchy force stress tensor $\boldsymbol{\tau}$ has an antisymmetric part. Laws of balance of force and moment for the reduced Cosserat continuum in absence of external loads are

$$\nabla \cdot \boldsymbol{\tau} = \rho \ddot{\mathbf{u}}, \tag{2}$$

$$\boldsymbol{\tau}_{\times} = (\mathbf{I} \cdot \boldsymbol{\omega})^{\cdot}. \tag{3}$$

Here $\boldsymbol{\tau}_{\times} = \tau^{mn}\mathbf{e}_m \times \mathbf{e}_n$ is the vectorial invariant of stress tensor $\boldsymbol{\tau}$. Inertia tensor $\mathbf{I}$ in the actual configuration equals

$$\mathbf{I} = \mathbf{P} \cdot \mathbf{I}_0 \cdot \mathbf{P}^{\top}, \tag{4}$$

where $\mathbf{I}_0$ is its value in the reference configuration.

If we consider the linear case, we may introduce infinitesimal translational ($\mathbf{u}$) and angular ($\boldsymbol{\theta}$) displacements: $\mathbf{u} = \mathbf{R} - \mathbf{r}$, $\mathbf{P} = \mathbf{E} + \boldsymbol{\theta} \times \mathbf{E}$. Note that in the linear approximation $\dot{\mathbf{P}} = \dot{\boldsymbol{\theta}} \times \mathbf{E} = \dot{\boldsymbol{\theta}} \times \mathbf{P} + o^2(1)$, therefore $\boldsymbol{\omega} = \dot{\boldsymbol{\theta}}$ up to the orders of the higher order. At the same time

$$\mathbf{I} = \mathbf{P} \cdot \mathbf{I}_0 \cdot \mathbf{P}^{\top} = (\mathbf{E} + \boldsymbol{\theta} \times \mathbf{E}) \cdot \mathbf{I}_0 \cdot (\mathbf{E} - \boldsymbol{\theta} \times \mathbf{E}) = \mathbf{I}_0 + o(1), \tag{5}$$

$$(\mathbf{I} \cdot \boldsymbol{\omega})^{\cdot} = (\mathbf{I}_0 \cdot \dot{\boldsymbol{\theta}})^{\cdot} + o^2(1) = \mathbf{I}_0 \cdot \ddot{\boldsymbol{\theta}} + o^2(1). \tag{6}$$

Therefore in the linear case the dynamic term of the balance of moment looks in the same way as if the tensor of inertia would be static. Also, instead of density one may use the density in the reference configuration.

The density of the strain energy in the linear elastic theory can be written as

$$\rho U = \frac{1}{2}\mathbf{g}^{\top} \cdot \cdot \mathbf{X} \cdot \cdot \mathbf{g}, \tag{7}$$

where $\mathbf{g} = \nabla \mathbf{u} + \boldsymbol{\theta} \times \mathbf{E}$ is the strain tensor, and $\mathbf{X}$ is a (anisotropic) tensor of elastic constants, $X^{mnkl} = X^{lknm}$ [12]. Unlike to the case of the full Cosserat medium, ρU does not depend on $\nabla \boldsymbol{\theta}$.

The constitutive equations of the reduced Cosserat continuum are

$$\boldsymbol{\tau} = \frac{\partial \rho U}{\partial \mathbf{g}} = \mathbf{X} \cdot \cdot (\nabla \mathbf{u} + \boldsymbol{\theta} \times \mathbf{E}). \tag{8}$$

Tensor of elastic constants $\mathbf{X}$ has components that respond to the translational strain $\nabla \mathbf{u}^S$ causing the symmetric part of stress tensor, components that respond to the rotational strain $\boldsymbol{\theta} - \nabla \times \mathbf{u}/2$ causing antisymmetric part of stresses, and the coupling term (causing some symmetric stress due to the rotational strain and antisymmetric stress due to translational strain). This kind of specific coupling could be useful for modelling solid-like grains and rocks, since in these materials hydrostatic pressure may result in shear and rotation on the local level.

Indeed, representing the strain tensor $\mathbf{g}$ as a sum of translational and rotational strain $\mathbf{g} = \nabla \mathbf{u}^S + (\nabla \mathbf{u} + \boldsymbol{\theta} \times \mathbf{E})^A$, $\mathbf{g}^{\top} = \nabla \mathbf{u}^S - (\nabla \mathbf{u} + \boldsymbol{\theta} \times \mathbf{E})^A$, we may write down (7) as

$$\begin{aligned} 2\rho U = {} & \nabla \mathbf{u}^S \cdot \cdot \mathbf{C} \cdot \cdot \nabla \mathbf{u}^S - (\nabla \mathbf{u}^A + \boldsymbol{\theta} \times \mathbf{E}) \cdot \cdot \boldsymbol{\alpha} \cdot \cdot (\nabla \mathbf{u}^A + \boldsymbol{\theta} \times \mathbf{E}) \\ & + \nabla \mathbf{u}^S \cdot \cdot (\mathbf{S}^l \mathbf{n}_l \times \mathbf{E}) \cdot \cdot (\nabla \mathbf{u}^A + \boldsymbol{\theta} \times \mathbf{E}) + (\nabla \mathbf{u}^A + \boldsymbol{\theta} \times \mathbf{E}) \cdot \cdot (\mathbf{n}_l \times \mathbf{E}\mathbf{S}^l) \cdot \cdot \nabla \mathbf{u}^S, \end{aligned} \tag{9}$$

$$\mathbf{X} = \mathbf{C} + \boldsymbol{\alpha} + \mathbf{S}^l \mathbf{n}_l \times \mathbf{E} - \mathbf{n}_l \times \mathbf{E}\mathbf{S}^l. \tag{10}$$

Here $\mathbf{C}$ is the tensor of elastic constants analogous to what we use in the classical theory, $\boldsymbol{\alpha}$ is a tensor of elastic constants that make the medium resist to rotational strain causing $\boldsymbol{\tau}_{\times}$, and the last line represents the coupling term of general kind, with $\mathbf{n}_l$ vectors and $\mathbf{S}^l$ symmetric tensors of elastic constants. Such an isotropic coupling does not exist for symmetry reasons. Note that the sign of $\mathbf{n}_l$ is chosen here in a different way than in [14].

In what follows we will consider isotropic $\mathbf{C} = \lambda \mathbf{E}\mathbf{E} + 2\mu(\mathbf{e}_m \mathbf{e}_n)^S (\mathbf{e}^m \mathbf{e}^n)^S$, λ and μ being Lamé constants, isotropic $\boldsymbol{\alpha} = -\alpha(\mathbf{e}_m \mathbf{e}_n)^A (\mathbf{e}^m \mathbf{e}^n)^A$ (the corresponding part of the rotational strain energy will be equal to $\frac{1}{2}\alpha(\boldsymbol{\theta} - \nabla \times \mathbf{u}/2)^2$).

Stress tensor in this case is equal to

$$\begin{aligned} \boldsymbol{\tau} = {} & \lambda \nabla \cdot \mathbf{u} + 2\mu(\nabla \mathbf{u})^S + \alpha(\nabla \mathbf{u} + \boldsymbol{\theta} \times \mathbf{E})^A \\ & + (\mathbf{S}^l \mathbf{n}_l \times \mathbf{E} - \mathbf{n}_l \times \mathbf{E}\mathbf{S}^l) \cdot \cdot (\nabla \mathbf{u} + \boldsymbol{\theta} \times \mathbf{E}) \\ = {} & \lambda \nabla \cdot \mathbf{u} + 2\mu(\nabla \mathbf{u})^S + \alpha(\nabla \mathbf{u} + \boldsymbol{\theta} \times \mathbf{E})^A \\ & - \mathbf{S}^l \mathbf{n}_l \cdot (2\boldsymbol{\theta} - \nabla \times \mathbf{u}) - \mathbf{E} \times \mathbf{n}_l \mathbf{S}^l \cdot \cdot \nabla \mathbf{u}^S. \end{aligned} \tag{11}$$

Note that $[\mathbf{n}_l \times \mathbf{E}]_\times = -2\mathbf{n}_l$. Therefore dynamic Eq. (3) can be written in displacements as

$$\begin{aligned}(\lambda+2\mu)\nabla\nabla\cdot\mathbf{u}-(\mu+\alpha)\nabla\times(\nabla\times\mathbf{u})+2\alpha\nabla\times\boldsymbol{\theta}\\ -\nabla\cdot\mathbf{S}^l\mathbf{n}_l\cdot(2\boldsymbol{\theta}-\nabla\times\mathbf{u})-\nabla\times\mathbf{n}_l\mathbf{S}^l\cdot\cdot\nabla\mathbf{u}^S=\rho\ddot{\mathbf{u}},\\ -4\alpha\boldsymbol{\theta}+2\alpha\nabla\times\mathbf{u}+2\mathbf{n}_l\mathbf{S}^l\cdot\cdot\nabla\mathbf{u}^S=\mathbf{I}_0\cdot\ddot{\boldsymbol{\theta}}.\end{aligned}\tag{12}$$

Let us look for the plane wave solution: $\mathbf{u}=\mathbf{u}_0e^{i(\mathbf{k}\cdot\mathbf{r}+\omega t)}, \boldsymbol{\theta}=\boldsymbol{\theta}_0e^{i(\mathbf{k}\cdot\mathbf{r}+\omega t)}$. Denote $k=|\mathbf{k}|, \hat{\mathbf{k}}=\mathbf{k}/k$. Then we obtain, using the symmetry of $\mathbf{S}^l$,

$$\begin{aligned}-(\lambda+2\mu)\mathbf{k}\mathbf{k}\cdot\mathbf{u}_0-(\mu+\alpha)k^2(\mathbf{E}-\hat{\mathbf{k}}\hat{\mathbf{k}})\cdot\mathbf{u}_0-\mathbf{k}\cdot\mathbf{S}^l\mathbf{n}_l\cdot\mathbf{k}\mathbf{u}_0+\mathbf{k}\times\mathbf{n}_l\mathbf{S}^l\cdot\cdot\mathbf{k}\mathbf{u}_0\\ +2i(\alpha\mathbf{k}\times\boldsymbol{\theta}_0-\mathbf{k}\cdot\mathbf{S}^l\mathbf{n}_l\cdot\boldsymbol{\theta}_0)=-\rho\omega^2\mathbf{u}_0,\\ 2i(\alpha\mathbf{k}\times\mathbf{u}_0+\mathbf{n}_l\mathbf{S}^l\cdot\cdot\mathbf{k}\mathbf{u}_0)=4\alpha\boldsymbol{\theta}_0-\omega^2\mathbf{I}_0\cdot\boldsymbol{\theta}_0.\end{aligned}\tag{13}$$

We will consider separately two cases: (1) spherical inertia tensor and non-zero anisotropic coupling, (2) isotropic elasticity with axisymmetric inertia tensor. In all cases we will consider homogeneous material with the same initial axis of symmetry of the tensor of inertia. The scheme we will apply is the following: to express $\boldsymbol{\theta}_0$ via $\mathbf{u}_0$ via the second equation of (13), substitute it into the first equation of (13) obtaining the reduced spectral problem for $\mathbf{u}$, and find its solution.

3 Reduced Cosserat Medium with an Anisotropic Coupling Between Translational and Rotational Strains and Spherical Tensor of Inertia

Let the density of the tensor of inertia be $I\mathbf{E}$, i.e. consider a spherical tensor of inertia. Denote $\omega_0^2=4\alpha/I$. In this case the second equation of (13) takes the form

$$(\omega_0^2-\omega^2)\boldsymbol{\theta}_0=i\left(\frac{\omega_0^2}{2}\mathbf{k}\times\mathbf{u}_0+\frac{2\mathbf{n}_l\mathbf{S}^l\cdot\mathbf{k}}{I}\cdot\mathbf{u}_0\right).\tag{14}$$

We have to consider separately the case $\omega=\omega_0$. One can see that Eq. (13) allow solution $\boldsymbol{\theta}=\boldsymbol{\theta}_0e^{i(\mathbf{k}\cdot\mathbf{r}+\omega t)}$, $\mathbf{u}\equiv\mathbf{0}$ if $\boldsymbol{\theta}_0$ satisfies requirement

$$\alpha\nabla\times\boldsymbol{\theta}_0-\nabla\cdot\mathbf{S}^l\mathbf{n}_l\cdot\boldsymbol{\theta}_0=0\tag{15}$$

(in particular, if $\boldsymbol{\theta}_0$ does not change in space).

Otherwise we may express $\boldsymbol{\theta}_0$ as

$$\boldsymbol{\theta}_0 = i\frac{\omega_0^2}{2(\omega_0^2-\omega^2)^{-1}}(\mathbf{k}\times\mathbf{u}_0 + \frac{\mathbf{n}_l\mathbf{S}^l\cdot\mathbf{k}}{\alpha}\cdot\mathbf{u}_0). \tag{16}$$

Calculate

$$2i\,\mathbf{k}\times\boldsymbol{\theta}_0 = -\frac{\omega_0^2}{(\omega_0^2-\omega^2)^{-1}}((\mathbf{kk}-k^2\mathbf{E})\cdot\mathbf{u}_0) + \mathbf{k}\times\frac{\mathbf{n}_l\mathbf{S}^l\cdot\mathbf{k}}{\alpha}\cdot\mathbf{u}_0), \tag{17}$$

$$2i\,\mathbf{k}\cdot\mathbf{S}^l\mathbf{n}_l\cdot\boldsymbol{\theta}_0 = -\frac{\omega_0^2}{(\omega_0^2-\omega^2)^{-1}}\mathbf{k}\cdot\mathbf{S}^l\mathbf{n}_l\cdot(\mathbf{k}\times\mathbf{u}_0 + \frac{\mathbf{n}_m\mathbf{S}^m\cdot\mathbf{k}}{\alpha}\cdot\mathbf{u}_0). \tag{18}$$

Substituting these expressions into the second equation of (13), we obtain reduced spectral problem

$$\rho\omega^2\mathbf{u} - (\lambda+2\mu)k^2\hat{\mathbf{k}}\hat{\mathbf{k}}\cdot\mathbf{u} - (\mu+\alpha\frac{\omega^2}{\omega^2-\omega_0^2})k^2(\mathbf{E}-\hat{\mathbf{k}}\hat{\mathbf{k}})\cdot\mathbf{u}$$
$$-(\frac{\omega^2k^2}{\omega^2-\omega_0^2}(\hat{\mathbf{k}}\cdot\mathbf{S}^l\mathbf{n}_l\times\hat{\mathbf{k}} - \hat{\mathbf{k}}\times\mathbf{n}_l\hat{\mathbf{k}}\cdot\mathbf{S}^l) + \frac{\omega_0^2k^2}{\alpha(\omega^2-\omega_0^2)}\hat{\mathbf{k}}\cdot\mathbf{S}^l\mathbf{n}_l\cdot\mathbf{n}_m\mathbf{S}^m\cdot\hat{\mathbf{k}})\cdot\mathbf{u} = 0 \tag{19}$$

It is easy to see that large anisotropy may destabilize the medium. Indeed, if eigen values (χ_i) of $\hat{\mathbf{k}}\cdot\mathbf{S}^l\mathbf{n}_l\cdot\mathbf{n}_m\mathbf{S}^m\cdot\hat{\mathbf{k}}$ are much larger than $\alpha(\lambda+\mu+\alpha)$, the spectral problem up to higher order terms looks in the following way

$$(\rho\omega^2\mathbf{E} + \frac{\omega_0^2k^2}{\alpha(\omega^2-\omega_0^2)}\hat{\mathbf{k}}\cdot\mathbf{S}^l\mathbf{n}_l\cdot\mathbf{n}_m\mathbf{S}^m\cdot\hat{\mathbf{k}})\cdot\mathbf{u} = 0 \tag{20}$$

which has solutions

$$k^2 = -\frac{\alpha\rho}{\chi_i}\omega^2(\omega^2-\omega_0^2) \tag{21}$$

The graph of dispersion relation is shown in Fig. 3. We see that the medium is unstable.

If we consider infinitesimal anisotropy, it will change essentially the dispersion curves near points of intersection of partial dispersion curves (for an isotropic medium) for the longitudinal and shear-rotational waves and near ω_0. However, the number of branches increases since the shear-rotational branch splits. Asymptotical analysis shows that we obtain in the vicinity of these points three dispersion branches instead of two ones. Preliminary investigation demonstrates that in some cases these dispersion curves may have decreasing parts near the point of intersection of longitudinal and shear-rotational partial dispersion curves. However, this question

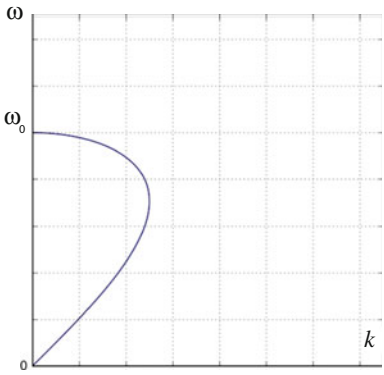

Fig. 3 Large anisotropy may lead to the instabilities

needs further investigation. We shall consider various particular cases (with finite or infinitesimal anisotropy) when we can resolve the problem, in particular, in vicinity of ω_0.

3.1 Tensors $\mathbf{S}^l$ with the Same Eigen Vector

Consider the case when there is a common eigen vector (denote it $\mathbf{e}_1$) for all $\mathbf{S}_l$. Then, if $\hat{\mathbf{k}} = \mathbf{e}_1$, there is a corresponding shear wave with the same dispersion relation as for the isotropic medium (Fig. 2).

$$\frac{\omega^2}{(\mu+\alpha)/\rho}\,\frac{\omega^2-\omega_0^2}{\omega^2-\omega_1^2} = k^2, \qquad \omega_1^2 = \frac{\mu}{\mu+\alpha}\omega_0^2. \tag{22}$$

Indeed, let $\hat{\mathbf{k}} = \mathbf{e}_1$. In this case $\hat{\mathbf{k}} \cdot \mathbf{S}^l = S_1^{(l)}\mathbf{e}_1$. Then $\hat{\mathbf{k}} \cdot \mathbf{S}^l\mathbf{n}_l = \mathbf{e}_1 S_l^{(1)}\mathbf{n}_l \stackrel{\text{def}}{=} \mathbf{e}_1\mathbf{N}$. In this case the reduced spectral problem takes the form

$$\rho\omega^2\mathbf{u} - (\lambda+2\mu)k^2\mathbf{e}_1\mathbf{e}_1\cdot\mathbf{u} - (\mu+\alpha\frac{\omega^2}{\omega^2-\omega_0^2})k^2(\mathbf{E}-\mathbf{e}_1\mathbf{e}_1)\cdot\mathbf{u}$$
$$-(\frac{\omega^2k^2}{\omega^2-\omega_0^2}(\mathbf{e}_1\mathbf{N}\times\mathbf{e}_1 - \mathbf{e}_1\times\mathbf{N}\mathbf{e}_1) + \frac{N^2\omega_0^2k^2}{\alpha(\omega^2-\omega_0^2)}\mathbf{e}_1\mathbf{e}_1)\cdot\mathbf{u} = 0 \tag{23}$$

If $\mathbf{u}_0$ is collinear to $\mathbf{e}_1 \times (\mathbf{N}\times\mathbf{e}_1) = \mathbf{N}\cdot(\mathbf{E}-\mathbf{e}_1\mathbf{e}_1)$, we obtain

$$\rho\omega^2 = \mu + \alpha\frac{\omega^2}{\omega^2-\omega_0^2}, \tag{24}$$

which is the same as (22). In case if $\mathbf{N}$ is collinear to $\mathbf{e}_1$, it is easy to see that there exist also a P-wave with an analogous dispersion relation

$$k^2 = \frac{\omega^2}{(\lambda + 2\mu - N^2/\alpha)/\rho} \frac{\omega^2 - \omega_0^2}{\omega^2 - \omega_{1p}^2}, \qquad \omega_{1p}^2 = \frac{\lambda + 2\mu - N^2/\alpha}{\lambda + 2\mu} \omega_0^2. \tag{25}$$

If $N^2 > \alpha(\lambda + 2\mu)$, this branch exists only at $\omega \geqslant \omega_0$.

In general, spectral problem (23) is identical to the case of volumetric-rotational axisymmetric coupling considered in [14]. Only in our case the direction of propagation $\mathbf{e}_1$ is fixed and, depending on $\mathbf{e}_1 \cdot \mathbf{N}$ which is given by the anisotropy of the medium, we have to find out which waves exist and which not. In particular, if $\mathbf{e}_1$ is not collinear neither orthogonal to $\mathbf{N}$, there exist a mixed longitudinal-shear-rotational wave, having a band gap, highly dispersive near this band gap. The number of branches depends on the parameters (if the anisotropy is not too large, there are two branches having a boundary frequency). For the case when $\mathbf{e}_1$ is orthogonal to $\mathbf{N}$, for some domains of parameters the band gap does not exist, but always the wave has a highly dispersive domain. Typical dispersion curves (for $\mathbf{e}_1 \cdot \mathbf{N} \neq 0$) are presented in Fig. 4.

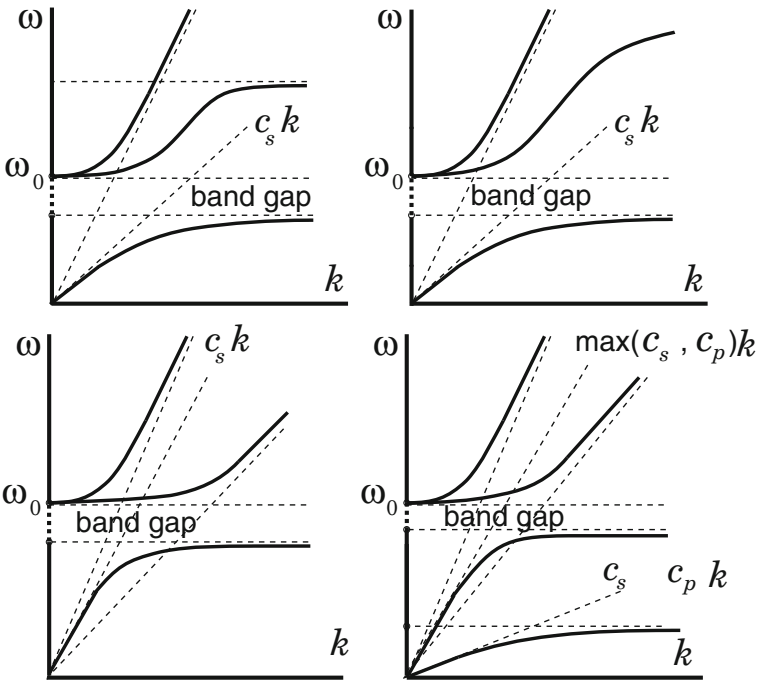

Fig. 4 Dispersion curves for $\mathbf{S}^l$ having the same eigen vector. Wave propagation along this vector. Various domains of parameters from large to small anisotropy

3.2 *In the Vicinity of ω_0*

Note that anisotropy plays a very important role at ω close to ω_0: anisotropic terms in (19) become much larger than the term corresponding to the partial dispersion relation for the longitudinal wave. We will see that dispersion curves, generally speaking, split in the vicinity of ω_0.

3.2.1 Finite Anisotropy

If it is a finite anisotropy, the term with it becomes predominant (as well as a part of term corresponding to the shear-rotational wave in the isotropic medium). At $\omega \to \omega_0$ we have $k^2\omega^2/(\omega^2 - \omega_0^2) >> k^2$, and therefore the reduced spectral problem (19) up to the terms of higher order looks as

$$(\rho\omega^2\mathbf{E} - \frac{\omega^2 k^2}{\omega^2 - \omega_0^2}(\alpha(\mathbf{E} - \hat{\mathbf{k}}\hat{\mathbf{k}}) + 2(\hat{\mathbf{k}} \cdot \mathbf{S}^l\mathbf{n}_l \times \hat{\mathbf{k}})^S - \frac{\omega_0^2}{\alpha\omega^2}\hat{\mathbf{k}} \cdot \mathbf{S}^l\mathbf{n}_l \cdot \mathbf{n}_m\mathbf{S}^m \cdot \hat{\mathbf{k}}) \cdot \mathbf{u} = 0 \quad (26)$$

This can be simplified as

$$(\rho\omega_0\mathbf{E} - \frac{k^2}{2(\omega - \omega_0)}(\alpha(\mathbf{E} - \hat{\mathbf{k}}\hat{\mathbf{k}}) + 2(\hat{\mathbf{k}} \cdot \mathbf{S}^l\mathbf{n}_l \times \hat{\mathbf{k}})^S - \frac{\hat{\mathbf{k}} \cdot \mathbf{S}^l\mathbf{n}_l \cdot \mathbf{n}_m\mathbf{S}^m \cdot \hat{\mathbf{k}}}{\alpha}) \cdot \mathbf{u} = 0 \quad (27)$$

Though we cannot find eigen vectors and eigen values for the general kind of anisotropy, we see that from (27) it follows that $k^2 \propto \omega - \omega_0$ at $\omega \to \omega_0$ and that, generally speaking (for general kind of anisotropy), there are three branches of the dispersion curve corresponding to three different eigen vectors of the spectral problem, determined by the anisotropy. We see also that ω_0 is limiting a band gap for each of these branches.

3.2.2 Infinitesimal Anisotropy

If anisotropy is infinitesimal ($\mathbf{S}^l\mathbf{n}_l/\alpha = O(\varepsilon)$), then in the vicinity of ω_0 we obtain two branches which are both close to the shear-rotational branch of the isotropic medium:

$$k^2 = (\omega - \omega_0)\frac{2\rho\omega_0}{\alpha + O(\varepsilon)} \quad (28)$$

and, if tensor $2(\hat{\mathbf{k}} \cdot \mathbf{S}^l \mathbf{n}_l \times \hat{\mathbf{k}})^S - \hat{\mathbf{k}} \cdot \mathbf{S}^l \mathbf{n}_l \cdot \mathbf{n}_m \mathbf{S}^m \cdot \hat{\mathbf{k}}/\alpha$ does not lie in the plane orthogonal to $\hat{\mathbf{k}}$, also the third branch that is almost horizontal:

$$k^2 = (\omega - \omega_0)\frac{2\rho\omega_0}{O(\varepsilon)}. \tag{29}$$

Since the anisotropy is infinitesimal but fixed for each material, it is also a parabola but with a small coefficient at k^2.

4 Reduced Cosserat Medium with Isotropic Elastic Energy and Axisymmetric Tensor of Inertia

4.1 General Case of Inertia Tensor: P-Wave and Special Shear-Rotational Waves

Consider reduced Cosserat medium with non-spherical tensor of inertia, but the same one in each point of space in the reference configuration. If the elastic tensors of the reduced Cosserat medium are isotropic, spectral problem (13) can be written as

$$\begin{gathered} -(\lambda + 2\mu)\mathbf{k}\mathbf{k} \cdot \mathbf{u}_0 - (\mu + \alpha)k^2(\mathbf{E} - \hat{\mathbf{k}}\hat{\mathbf{k}}) \cdot \mathbf{u}_0 + 2i\alpha\mathbf{k} \times \boldsymbol{\theta}_0 = -\rho\omega^2\mathbf{u}_0, \\ 2i\alpha\mathbf{k} \times \mathbf{u}_0 = 4\alpha\boldsymbol{\theta}_0 - \omega^2\mathbf{I}_0 \cdot \boldsymbol{\theta}_0. \end{gathered} \tag{30}$$

We see that if $\mathbf{I}_0 = I^k \mathbf{i}_k \mathbf{i}_k$, we have solutions of (12) $\mathbf{u} = \mathbf{0}, \boldsymbol{\theta} = \theta_0^k \mathbf{i}_k e^{i\omega_{0k}t}$, where $\omega_{0k}^2 = 4\alpha/I_k$, provided $\nabla \times \theta_0^k \mathbf{i}_k = \mathbf{0}$. In case if $\omega \neq \omega_{0k}$, we may express $\boldsymbol{\theta}_0$ via the second equation of (30) and substitute it in the first one:

$$\boldsymbol{\theta} = \frac{i}{2}\boldsymbol{\Omega} \cdot (\mathbf{k} \times \mathbf{u}_0) = \frac{i}{2}(\boldsymbol{\Omega} \times \mathbf{k}) \cdot \mathbf{u}_0, \tag{31}$$

$$\boldsymbol{\Omega} = (1 - \frac{\omega^2}{\omega_{0k}^2})^{-1}\mathbf{i}_k\mathbf{i}_k = -\frac{\omega_{0k}^2}{\omega^2 - \omega_{0k}^2}\mathbf{i}_k\mathbf{i}_k. \tag{32}$$

Thus we obtain

$$2i\alpha\mathbf{k} \times \boldsymbol{\theta}_0 = (\mathbf{k} \times \frac{\omega_{0k}^2}{\omega^2 - \omega_{0k}^2}\mathbf{i}_k\mathbf{i}_k \times \mathbf{k}) \cdot \mathbf{u}_0. \tag{33}$$

Spectral problem (30) can be reduced to

$$(\rho\omega^2\mathbf{E} - (\lambda + 2\mu)\mathbf{k}\mathbf{k} - (\mu + \alpha)k^2(\mathbf{E} - \hat{\mathbf{k}}\hat{\mathbf{k}}) + \alpha k^2\hat{\mathbf{k}} \times \frac{\omega_{0k}^2\mathbf{i}_k\mathbf{i}_k}{\omega^2 - \omega_{0k}^2} \times \hat{\mathbf{k}}) \cdot \mathbf{u}_0 = 0. \tag{34}$$

We see that the anisotropy in the density of tensor of inertia (provided its homogeneous distribution in the reference configuration) does not affect the P-wave. Indeed, (34) allows solution $\mathbf{u}_0 = u_0\hat{\mathbf{k}}$, $\omega = \sqrt{(\lambda + 2\mu)/\rho}k$.

We also see that if $\hat{\mathbf{k}}$ coincides with one of principal axes of the tensor of inertia, say, $\hat{\mathbf{k}} = \mathbf{i}_1$, then solutions for shear-rotational waves $\mathbf{u}_0 = u_0\mathbf{i}_2$ and $\mathbf{u}_0 = u_0\mathbf{i}_3$ exist, each of them having dispersion relation analogous to (22), the same as for isotropic medium, where instead of ω_0 we have to substitute ω_{02} or ω_{03}, respectively.

4.2 Axisymmetric Tensor of Inertia

Let $\mathbf{I}_0 = I(\mathbf{E} - \mathbf{nn}) + I_1\mathbf{nn}$. Corresponding characteristic frequencies will be denoted as ω_0 and ω_n. Then the reduced spectral problem (34) can be written as

$$(\rho\omega^2\mathbf{E} - (\lambda + 2\mu)\mathbf{kk} - (\mu + \alpha)k^2(\mathbf{E} - \hat{\mathbf{k}}\hat{\mathbf{k}}) + \alpha k^2\hat{\mathbf{k}} \times \frac{\omega_0^2(\mathbf{E} - \mathbf{nn})}{\omega^2 - \omega_0^2} \times \hat{\mathbf{k}} + \alpha k^2\hat{\mathbf{k}} \times \frac{\omega_n^2\mathbf{nn}}{\omega^2 - \omega_n^2} \times \hat{\mathbf{k}}) \cdot \mathbf{u}_0 = 0. \tag{35}$$

Simplifying, we obtain

$$(\rho\omega^2\mathbf{E} - (\lambda + 2\mu)\mathbf{kk} - (\mu + \frac{\alpha\omega^2}{\omega^2 - \omega_0^2})k^2(\mathbf{E} - \hat{\mathbf{k}}\hat{\mathbf{k}}) + \alpha k^2(\frac{\omega_n^2}{\omega^2 - \omega_n^2} - \frac{\omega_0^2}{\omega^2 - \omega_0^2})\hat{\mathbf{k}} \times \mathbf{nn} \times \hat{\mathbf{k}}) \cdot \mathbf{u}_0 = 0. \tag{36}$$

It is easy to see that, analogously to the case of the axisymmetric coupling between volumetric and rotational strain considered in [14] and to the case of $\mathbf{S}^l$ having the same eigen vector, along which the wave propagates (Sect. 3), there exist a shear wave with the dispersion relation (22), the same as in the isotropic medium (Fig. 2). Indeed, if $\mathbf{u}_0 = u_0\hat{\mathbf{k}} \times (\hat{\mathbf{k}} \times \mathbf{n})$, we have the dispersion relation (22).

Another shear-rotational wave has the eigen vector which is collinear to $\hat{\mathbf{k}} \times \mathbf{n}$. Indeed, if $\mathbf{u}_0 = u_0\hat{\mathbf{k}} \times \mathbf{n}$, we obtain from (36)

$$\rho\omega^2 - (\mu + \frac{\alpha\omega^2}{\omega^2 - \omega_0^2})k^2 - \alpha k^2(\frac{\omega_n^2}{\omega^2 - \omega_n^2} - \frac{\omega_0^2}{\omega^2 - \omega_0^2})|\hat{\mathbf{k}} \times \mathbf{n}|^2 = 0. \tag{37}$$

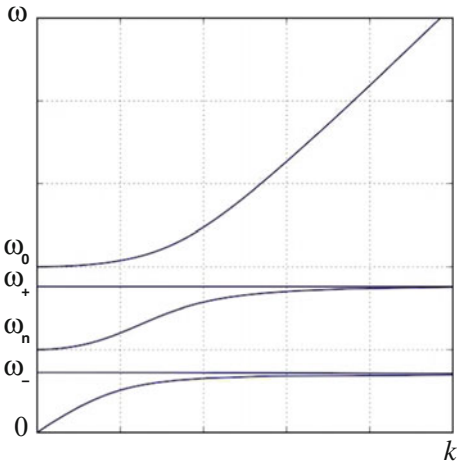

Fig. 5 Shear-rotational wave in the reduced Cosserat medium with isotropic elastic properties and axisymmetric tensor of inertia

This results in

$$k^2 = \frac{\omega^2}{c_{s\alpha}^2}\left(1 + \left(\frac{\omega_0^2(\hat{\mathbf{k}}\cdot\mathbf{n})^2}{\omega^2-\omega_0^2} + \frac{\omega_n^2(\hat{\mathbf{k}}\times\mathbf{n})^2}{\omega^2-\omega_n^2}\right)\frac{\alpha}{\mu+\alpha}\right)^{-1} \tag{38}$$

This dispersion relation also can be written as

$$k^2 = \frac{\omega^2}{c_{s\alpha}^2}\frac{(\omega^2-\omega_0^2)(\omega^2-\omega_n^2)}{(\omega^2-\omega_+^2)(\omega^2-\omega_-^2)} \tag{39}$$

Here characteristic frequencies ω_1, ω_{1n} satisfy relations

$$\omega_\pm^2 = \frac{1}{2}\Big(\omega_0^2(1-\xi_s) + \omega_n^2(1-\xi_c) \pm \sqrt{(\omega_0^2(1-\xi_s) + \omega_n^2(1-\xi_c))^2 - \omega_0^2\omega_n^2(1-\xi)}\Big), \tag{40}$$

where $0 < \xi = \alpha/(\mu+\alpha) < 1, \xi_s = \xi|\hat{\mathbf{k}}\times\mathbf{n}|, \xi_c = \xi|\hat{\mathbf{k}}\cdot\mathbf{n}|, \xi_s + \xi_c = \xi$. Simple algebra shows that both roots are positive, and that

$$\max(\omega_0^2(1-\xi_s), \omega_n^2(1-\xi_c)) < \omega_+^2 < \omega_0^2(1-\xi_s) + \omega_n^2(1-\xi_c), \tag{41}$$

$$0 < \omega_-^2 < \min(\omega_0^2(1-\xi_s), \omega_n^2(1-\xi_c)) \tag{42}$$

Typical dispersion graphs are shown in Fig. 5.

5 Conclusion

We have considered waves in two kinds of elastic linear reduced Cosserat continua (Cosserat media that do not react on the gradient of turn): with anisotropic coupling between translational and rotational strains and for non-spherical tensor of inertia. In previous studies it was shown that for the isotropic case the longitudinal wave is non-dispersive while the shear-rotational wave has a band gap and is highly dispersive in its vicinity. For the first case some classes of anisotropic coupling and particular plane waves were considered, as well as plane waves with frequencies close to the characteristic frequency. We have found out that in most cases the anisotropy makes the shear-rotational wave split and induces existence of mixed dispersive waves. In those cases when the pure pressure wave exists, it becomes dispersive and has a band gap. For the case of non-spherical tensor of inertia, when point bodies in the initial configuration have the same orientation and inertia moments, it was shown that the pressure wave is not influenced, it is not dispersive. Shear-rotational waves are dispersive and have a band gap or band gaps. Their dispersion relations were found for particular directions of the wave propagation for the general case of tensor of inertia and for any direction of wave propagation for axisymmetric tensor of inertia. In the last case this dispersion relation is more sophisticated than for an isotropic medium, and, generally speaking, has two band gaps. Thus it is also a single negative acoustic metamaterial for certain types of waves.

Acknowledgements This work was supported by the Russian Foundation for Basic Research (grant 17-01-00230), by Spanish Government Agency Ministerio de Economía y Competitividad (project No. FIS2014-54539-P) and by Andalusian Government (Junta de Andalucía), support for research group FQM-253.

References

1. Cosserat, E.F.: Théorie des corps déformables. Paris, Hermann (1909) (in French)
2. Kafadar, C.B., Eringen, A.C.: Micropolar media—I: the classical theory. Int. J. Eng. Sci. **9**(3), 271–305 (1971)
3. Zhilin, P.A., Altenbach, H.: The theory of elastic simple shells. Adv. Mech. **11**(4), 107–147 (1988) (in Russian)
4. Eremeyev, V.A., Lebedev, L.P., Altenbach, H.: Foundations of Micropolar Mechanics. Springer Science and Business Media (2013)
5. Eringen, A.C., Maugin, G.A.: Electrodynamics of Continua I: Foundations and Solid Media. Springer Science and Business Media (2012)
6. Erofeyev, V.I.: Wave Processes in Solids with Microstructure, vol. 8. World Scientific (2003)
7. Porubov, A.V., Aero, E.L., Maugin, G.A.: Two approaches to study essentially nonlinear and dispersive properties of the internal structure of materials. Phys. Rev. E **79**, 046608 (2009)
8. Eremeyev, V.A., Pietraszkiewicz, W.: Material symmetry group of the non-linear polar-elastic continuum. Int. J. Solids Struct. **49**(14), 1993–2005 (2012)
9. Eremeyev, V.A., Pietraszkiewicz, W.: Material symmetry group and constitutive equations of micropolar anisotropic elastic solids. Math. Mech. Solids **21**(2), 210–221 (2016)
10. Pietraszkiewicz, W., Eremeyev, V.A.: On natural strain measures of the non-linear micropolar continuum. Int. J. Solids Struct. **46**(3), 774–787 (2009)

11. Schwartz, L.M., Johnson, D.L., Feng, S.: Vibrational modes in granular materials. Phys. Rev. Lett. **52**(10), 831 (1984)
12. Grekova, E.F., Kulesh, M.A., Herman, G.C.: Waves in linear elastic media with microrotations, Part 2: Isotropic reduced Cosserat model. Bull. Seismol. Soc. Am. **99**(2B), 1423–1428 (2009)
13. Kulesh, M.A., Grekova, E.F., Shardakov, I.N.: The problem of surface wave propagation in a reduced Cosserat medium. Acoust. Phys. **55**(2), 218–226 (2009)
14. Grekova, E.F.: Plane waves in the linear elastic reduced Cosserat medium with a finite axially symmetric coupling between volumetric and rotational strains. Math. Mech. Solids **21**(1), 73–93 (2016)

Modeling Stress-Affected Chemical Reactions in Solids–A Rational Mechanics Approach

Polina Grigoreva, Elena N. Vilchevskaya and Wolfgang H. Müller

Abstract In materials science the inluence of mechanical stresses on chemical reactions in solids is typically introduced empirically as part of diffusion or reaction coefficients by means of an Arrhenius ansatz. However, more recently an alternative approach based on rational mechanics was proposed, where the stresses affect the chemical process at the reaction front by a driving force given by the normal component of the chemical affinity tensor, which is composed of the chemical potential (or Eshelby) tensors characteristic of the reaction. In this paper the repercussions from both types of models will be investigated and compared to each other. As a specific example the process of silicon oxidation will be considered. However, the proposed alternative method could also be applied to other binary reactions in solids accompanied by eigenstrain formation. Moreover, an attempt is made to introduce the effect of all stress components on bulk diffusion in a logical fashion leading to a tensorial expression of the diffusion coefficient. Several model calculations are performed, mostly in explicit closed form, so that the effect of the various involved parameters can easily be studied.

P. Grigoreva (✉) · E. N. Vilchevskaya
Peter the Great Saint-Petersburg Polytechnic University, Politekhnicheskaya 29,
195251 St. Petersburg, Russia
e-mail: polina.grigoreva239@gmail.com

E. N. Vilchevskaya
e-mail: vilchevska@gmail.com

E. N. Vilchevskaya
Institute for Problems in Mechanical Engineering of the Russian Academy of Sciences,
Bol'shoy pr. 61, V.O., 199178 St. Petersburg, Russia

W. H. Müller
Institute of Mechanics, Chair of Continuum Mechanics and Constitutive Theory,
Technische Universität Berlin, Einsteinufer 5, 10587 Berlin, Germany
e-mail: whmueller1000@gmail.com

F. dell'Isola et al. (eds.), *Advances in Mechanics of Microstructured Media and Structures*, Advanced Structured Materials 87,
https://doi.org/10.1007/978-3-319-73694-5_10

1 Introduction

The interdependencies between chemical reactions and deformation processes in deformable solids remain of interest for both fundamental science as well as engineering applications. In this paper we are going to study the influence of mechanical stresses on the kinetics of a chemical reaction between solid and gaseous constituents, namely:

$$n_- B_- + n_* B_* \to n_+ B_+, \tag{1}$$

where B_- and B_+ refer to the deformable solid constituents, and B_* to the diffusive gas constituent; n_-, n_+ and n_* are stoichiometric coefficients. We assume that the reaction is localized at the reaction front, Γ, which separates the regions occupied by the initial and transformed materials. The reaction is sustained by diffusion of the gas constituent B_* from the outside to the interface of the chemical reaction. The formation of silicon dioxide, $Si + O_2 \to SiO_2$, is an example for such kind of a reaction.

Thus, the reaction involves two processes—bulk diffusion of the gas through the transformed material and the chemical reaction itself. Both processes may depend on the mechanical stresses. The influence of external and internal stresses on the reaction front kinetics was examined by many researchers and a number of models have been developed. For example, Kao in [19, 20] started modeling the stresses in cylindrical structures and postulated a coupling between the reaction rate and the radial stress component. One year later Sutarya and Oldham [29] became even more specific. Following the tradition of materials science, they relate the impact of the normal stress, σ_{nn}, and of pressure, p, empirically to two constitutive quantities, first, the surface reaction rate parameter, k_*, and second, the diffusion coefficient, D in terms of an exponential Boltzmann ansatz, namely:

$$k_* = k_0(T) \exp\left(\frac{\sigma_{nn} V_k}{kT}\right), \qquad D = D_0(T) \exp\left(-\frac{pV_d}{kT}\right), \tag{2}$$

where k_0 and D_0 are temperature dependent reaction and diffusion coefficients for the stress-free case, k is Boltzmann's constant, T absolute temperature, V_k and V_d are two fitting parameters, which have the dimension of a volume. Note that the dependencies of the parameters on stresses were introduced heuristically. The choice of the parameters of the models was based on adjusting theoretical results and experimental data on the oxidation kinetics.

Stresses may also affect the diffusion process through additional stress dependent terms in the diffusion equation (see, e.g., [1, 4, 22, 23, 30]). Note that these additional terms are usually connected with a volumetric or stiffness change of the solid material or due to change of the gas concentration [3, 4].

Another approach in order to take the influence of the stress-strain state at a chemical reaction front on the velocity of the front propagation into account was presented recently in [9–13] in terms of rational continuum theory. It is based on an

expression for the chemical affinity tensor, which, on the one hand side, allows to take the stress-effect into account within the classical paradigm of physical chemistry. On the other hand side it demonstrates that in solids the reaction rate at an oriented surface element depends on the orientation of the element with respect to the stresses.

In the present paper we want to compare the impact of a stress-dependent affinity and a stress-dependent diffusion on the kinetics of the chemical reaction front. Within the first approach, stresses affect the propagation of the chemical reaction front as they appear in the expression for the chemical affinity and in a corresponding kinetic equation, which relates the chemical affinity with the reaction rate. The second approach reduces the problem of stress-assisted chemical reaction front propagation to a diffusion problem with a proper choice of a diffusion model and stress dependent parameters of the model. Since the expression for the chemical affinity tensor was derived within the so-called solid skeleton approach, where the transformed material is considered to act as a skeleton for the diffusing gas constituent and additional deformations of the skeleton, which could be produced by the gas constituent, are neglected, we will not consider additional terms in the diffusion equation and concentrate only on a dependence of the diffusion coefficient on stresses. Usually, in models of stress-dependent diffusion a scalar characteristic of the stress tensor is used. This characteristic can be defined in different ways, e.g., as a pressure, as a normal stress, as an intensity of shear stresses, and the choice between them is made intuitively. In this work, we also make an attempt to relate the diffusion coefficient with the stress or the strain tensor in a physically reasonable way, namely, with the deformations of the solid skeleton, which leads to a tensorial diffusion model.

Based on the chemical affinity model accompanied with different diffusion models we shall evaluate the kinetics of the chemical reaction front propagation for various boundary-value problems. The obtained results will be compared in order to investigate how stress-assisted diffusion affects the chemical reaction front propagation, which of the diffusion coefficients exerts a stronger influence on the chemical reaction front kinetics, and to obtain the range of values of the external loads, at which the dependence of the diffusion coefficient on the stresses in comparison with the stress-affected chemical affinity can be neglected and considered as constant.

2 Problem Statement

2.1 Chemical Affinity and Chemical Reaction Kinetics

The notion of chemical affinity, A, was introduced by de Donde and Gibbs [5, 14] (see also [26]) as a factor conjugate to the reaction rate, ω, in an expression of dissipation due to the chemical reaction. It was shown that the chemical affinity is equal to the combination of the chemical potential of reaction constituents:

$$A = -\sum n_k M_k \mu_k, \tag{3}$$

where μ_k is the chemical potential per unit mass and M_k is the molar mass of the kth constituent. The stoichiometric coefficient n_k contributes to the sum with a plus sign if the k-th constituent is produced in the reaction and with a minus sign if the kth constituent is consumed.

The chemical affinity acts as a generalized force (a.k.a. thermodynamic force, driving force) behind the chemical reaction. Then a kinetic equation was formulated, which determines the reaction rate as a function of the chemical affinity. The reaction rate dependence on the affinity forms an additional constitutive equation. For example, in [15] the following kinetic equation was introduced:

$$\omega = k_* c \left\{ 1 - \exp\left(-\frac{A}{RT} \right) \right\}. \tag{4}$$

In here c is the molar concentration of the gas constituent, and R denotes the ideal gas constant.

In the case of chemical reactions in gases and fluids, stresses are determined by a scalar value, the pressure. Thus the chemical potentials and the chemical affinity are scalars. In the case of solid phases the chemical potential becomes a tensor. This was motivated by the fact that phase equilibrium at the interface in a deformable solid has to depend on the interface orientation with respect to the stress. As a result, the chemical affinity must also be a tensor. The tensorial nature of the chemical potential and the chemical affinity have also been discussed in [27, 28].

The expression of the chemical affinity tensor was obtained as a result of the analysis of the mass, linear momentum and energy balance equations and the entropy inequality written down for a chemical reaction between gaseous and solid constituents of arbitrary rheology [9] (see also [10] and the Appendix in [12]). Specifically, it was shown that the reaction rate at the oriented area element with a normal $\boldsymbol{n}$ is conjugate to the normal component of the chemical affinity tensor $A_{nn} = \boldsymbol{n} \cdot \boldsymbol{A} \cdot \boldsymbol{n}$ of the tensor $\boldsymbol{A}$ in the expression for the dissipation due to the chemical reaction front propagation.

For the case of linear elastic solid constituents the normal component of the chemical affinity was specified in [12, 31]. A quasi-static case was considered and it was supposed that there is no sliding at the reaction front. Also, for the sake of simplicity, a thermal effect of the reaction and the input of pressure into stresses were ignored. Then the normal component of the chemical affinity tensor can be written as:

$$A_{nn} = \frac{n_- M_-}{\rho_-} \left[\gamma(T) + \frac{1}{2}\boldsymbol{\sigma}_- : \boldsymbol{\varepsilon}_- - \frac{1}{2}\boldsymbol{\sigma}_+ : (\boldsymbol{\varepsilon}_+ - \boldsymbol{\varepsilon}_{\mathrm{ch}}) + \frac{1}{2}\boldsymbol{\sigma}_+ : (\boldsymbol{\varepsilon}_+ - \boldsymbol{\varepsilon}_-) \right] + n_* RT \ln \frac{c(\Gamma)}{c_*}, \tag{5}$$

where M_- is the molar mass and ρ_- is the density of a solid component B_-; $\boldsymbol{\sigma}_- = \boldsymbol{C}_- : \boldsymbol{\varepsilon}_-$ and $\boldsymbol{\sigma}_+ = \boldsymbol{C}_+ : (\boldsymbol{\varepsilon}_+ - \boldsymbol{\varepsilon}_{\mathrm{ch}})$ are Cauchy stress tensors, $\boldsymbol{C}_\pm$ are tensors of the elastic moduli of the solid constituents, $\boldsymbol{\varepsilon}_\pm$ are deformation tensors, $c(\Gamma)$ is the concentration

of the gas at the reaction front. Moreover, c_* is a reference concentration, which has to be chosen suitably. One possible way is to identify it with the gas solubility in the transformed material B_+. $\boldsymbol{\varepsilon}_{\text{ch}}$ is the strain due to chemical transformation. We assume that it is of isotropic volumetric nature, i.e., $\boldsymbol{\varepsilon}_{\text{ch}} = \varepsilon_{\text{ch}}\mathbf{I}$, where $\mathbf{I}$ is the unit tensor. The parameter $\gamma(T)$ is determined by the chemical energies of the constituents. If the temperature T is given, $\gamma(T)$ is a parameter of the model.

If we replace the scalar chemical affinity by the normal component of the chemical affinity tensor in (4), the reaction rate is given by:

$$\omega = k_* c \left\{ 1 - \exp\left(-\frac{A_{nn}}{RT} \right) \right\}. \tag{6}$$

Hence, from the mass balance at the reaction front we have $\rho\_V = n\_M\_\omega$, where V is the normal component of the reaction front velocity. We obtain:

$$V = \frac{n\_M\_}{\rho\_} k_* c \left\{ 1 - \exp\left(-\frac{A_{nn}}{RT} \right) \right\}. \tag{7}$$

The reaction front propagates only if $A_{nn} > 0$. The case of $A_{nn} = 0$ corresponds to chemical equilibrium and to a stationary chemical reaction front. Thus the equilibrium concentration of component B_*, c_{eq}, on the reaction front can be found from the equation $A_{nn} = 0$:

$$\frac{n\_M\_}{\rho\_} \left(\gamma(T) + \frac{1}{2}\boldsymbol{\sigma}\_ : \boldsymbol{\varepsilon}\_ - \frac{1}{2}\boldsymbol{\sigma}_+ : (\boldsymbol{\varepsilon}_+ - \boldsymbol{\varepsilon}_{\text{ch}}) + \boldsymbol{\sigma}_+ : (\boldsymbol{\varepsilon}_+ - \boldsymbol{\varepsilon}\_) \right) + n_* RT \ln \frac{c_{\text{eq}}}{c_*} = 0. \tag{8}$$

If the equilibrium concentration, c_{eq}, is found, and the current concentration $c(\Gamma)$ is determined by solving the diffusion problem, then the normal component of the chemical affinity tensor can be calculated from:

$$A_{nn} = n_* \left(\ln \frac{c(\Gamma)}{c_*} - \ln \frac{c_{\text{eq}}}{c_*} \right) = \ln \left(\frac{c(\Gamma)}{c_{\text{eq}}} \right)^{n_*}. \tag{9}$$

In this case the normal component of the reaction front velocity is:

$$V = \frac{n\_M\_}{\rho\_} k_* c(\Gamma) \left(1 - \left(\frac{c_{\text{eq}}}{c(\Gamma)} \right)^{n_*} \right). \tag{10}$$

Consequently, the problem reduces to the following tasks: Find the stress-strain state at the reaction front, find the equilibrium concentration c_{eq} from Eq. (8), find the concentration at the front of the reaction $c(\Gamma)$ from the solution of the diffusion problem, substitute c_{eq} and $c(\Gamma)$ to the formula for the velocity of the chemical reaction front (10), and, finally, integrate Eq. (10) in order to find the dependence of the chemical reaction front position on time.

2.2 Diffusion Problem

The concentration of the gas at the reaction front and within the transformed material will develop according to a diffusion equation. Following Fick's law the simplest one is:

$$\frac{\partial c}{\partial t} = \nabla \cdot (D \nabla c), \tag{11}$$

where D is the diffusion coefficient. We assume that the diffusion process is steady-state because it goes much faster than the front propagation process. Then this equation takes the form:

$$\nabla \cdot (D \nabla c) = 0. \tag{12}$$

The boundary conditions read:

$$D\frac{\partial c}{\partial n} + \alpha(c_* - c) = 0 \quad \text{at } \Omega, \quad D\frac{\partial c}{\partial n} + n_* k_* c \left(1 - \left(\frac{c_{\text{eq}}}{c}\right)^{n_*}\right) = 0 \quad \text{at } \Gamma. \tag{13}$$

The first condition follows from mass flux continuity on the outer surface of the body Ω. Here n is an outward normal to B_+, α is the surface mass transfer coefficient in B_+. If $\alpha \gg D$, then the first condition degenerates to $c = c_*$ and corresponds to prescribing the concentration at the outer boundary. The second condition follows from the mass balance at the reaction front Γ. It means that all of the diffusion flux is consumed by the chemical reaction.

Three different diffusion models will be considered. In the first one a constant diffusion coefficient is used. The second one is based on the widely used dependence of the diffusion coefficient on the pressure [21, 25, 34]:

$$D = D_0 \exp\left(-\frac{pV_d}{kT}\right), \qquad p = -\frac{1}{3}\left(\sigma_{11}^+ + \sigma_{22}^+ + \sigma_{33}^+\right). \tag{14}$$

It was mentioned before that this expression for the diffusion coefficient is of phenomenological nature and based on intuitive assessment of experimental data [29].

The arguments leading to the third model are slightly more complex: In order to obtain a dependence of the diffusion coefficient on the stress-state state of the solid material based on a rational continuum theory, we consider a two component system consisting of solid and gaseous constituents. For simplicity we consider a stationary one-dimensional diffusion, $\rho_{\text{g}} = \rho_{\text{g}}(x_1)$, $\mathrm{d}u_{\text{g}}/\mathrm{d}t = V_{\text{g}}(x_1)$, $\mathrm{d}u_{\text{s}}/\mathrm{d}t = V_{\text{s}}(x_1)$, where u_{s} and u_{g} are displacements of the solid and gas constituents respectively, and assume that the solid is an isotropic linear elastic material. Then the equations of momentum balance for the gas and solid components and the mass balance for the gas component read:

$$\begin{cases} \frac{E_+(1-\nu_+)}{(1+\nu_+)(1-2\nu_+)}\frac{\mathrm{d}^2 u_\mathrm{s}}{\mathrm{d}x_1^2} + f_\mathrm{sg} = 0, \\ \frac{\mathrm{d}p_\mathrm{g}}{\mathrm{d}x_1} - f_\mathrm{sg} = 0, \\ \frac{\mathrm{d}\left(\rho_g V_g\right)}{\mathrm{d}x_1} = 0. \end{cases} \tag{15}$$

In here E_+ and ν_+ are Young's modulus and Poisson's ratio of the material B_+, $f_\mathrm{sg} = \rho_\mathrm{g} a \left(V_\mathrm{s} - V_\mathrm{g}\right)$ is a viscous interaction force between the gas and the solid components, where $V_\mathrm{s} - V_\mathrm{g}$ is the relative velocity between the solid and the gas, and a is a parameter of viscous friction, which can depend on the strain (stress) field of the solid. We assume that the gas is ideal, thus $p_\mathrm{g} = \frac{RT}{M_g}\rho_\mathrm{g}$. The solution of the system of equations is $u_s = c_1 \exp(-c_2 x_1) + c_3 x_1 + \frac{RT}{M_g a} c_2 t + c_4$, where c_1, c_2, c_3, c_4 are constants of integration. Then the diffusion flux defined by $j = \rho_\mathrm{g}\left(V_\mathrm{s} - V_\mathrm{g}\right)$ is equal to $j = \frac{\lambda_+ + 2\mu_+}{a} c_1 c_2^2 \exp(-c_2 x_1)$, $\lambda_+ = \frac{E_+\nu_+}{(1+\nu_+)(1-2\nu_+)}$ and $\mu_+ = \frac{E_+}{2(1+\nu_+)}$ being Lamé's constants. By comparing these two expressions and by taking into account that the gas concentration is $c = \rho_g / M_g$, one realizes that the diffusion flux is proportional to the gradient of the gas concentration, $j = \frac{RT}{a}\frac{\mathrm{d}c}{\mathrm{d}x_1}$, which leads to Fick's law with the diffusion coefficient being $\frac{RT}{a}$. Thus deformations in a solid can affect the diffusion process only through the parameter a. Similar results were obtained in [17, 18].

The silicon dioxide forming during silicon oxidation in the so-called LOCOS process (= LOCal Oxidation of Silicon, cf., [33]) is amorphous, and in this case of bulk diffusion the flux moves through the space between the irregular quasi-tetrahedral network (see [2]). The parameter a defines how easily the gas molecules can diffuse. Consequently, it depends on the space between the tetrahedra. In order to consider mechanical loads, we assume that the parameter a is inversely related to deformations changing the inter-tetrahedral space in the plane perpendicular to the diffusion flux. In other words, it is assumed that the deformation along the direction of the diffusion flux, ε_{11}, does not affect the diffusion. Then the diffusion coefficient in the x_1 direction is:

$$D = D_0\big(1 + \beta(\varepsilon_{22} + \varepsilon_{33})\big), \tag{16}$$

where β is a constant parameter.

Hence in the 3D case we arrive at a model of tensorial diffusion where the diffusion coefficient depends on the direction of the flux:

$$\mathbf{D} = D_0 \begin{bmatrix} 1 + \beta_1\left(\varepsilon_{22} + \varepsilon_{33}\right) & 0 & 0 \\ 0 & 1 + \beta_2\left(\varepsilon_{11} + \varepsilon_{33}\right) & 0 \\ 0 & 0 & 1 + \beta_3\left(\varepsilon_{22} + \varepsilon_{11}\right) \end{bmatrix}. \tag{17}$$

In order to compare the kinetics of the chemical reaction front with diffusion coefficients given by (14) and (16), we need an estimate for the unknown parameter

β. If we expand (14), rewrite it in terms of strains by using Hooke's law, and compare the result with (16), we will see that these two approaches agree if the parameter β is of the order of $\beta_* = \frac{V_d E_+}{(1-2\nu_+)Tk}$.

Note that, in general, these two approaches give different results. For example in the case of the uniaxial stretching in the direction of the diffusion flux, the phenomenological approach (14) leads to increasing of the diffusivity while the tensorial diffusion (16) retards the diffusion since the inter-tetrahedral space in the plane perpendicular to the diffusion flux decreases due to the Poisson effect.

3 Analytical Solutions of Some Boundary-Value Problems

3.1 A Two-Dimensional Planar Reaction Front

We consider a 3D rectangular block of dimensions $x_1 \in \left[-l_1, l_1\right]$, $x_2 \in \left[-l_2, l_2\right]$, $x_3 \in [0, H]$ (cf., Fig. 1) consisting of two solid blocks "+" and "−", which are separated by a planar reaction front at position $x_3 = h$. Because of the symmetry we assume that the concentration does not depend on the x_1- and x_2-coordinates, so that $c = c(x_3)$, $c(\Gamma) = c(h)$. The solution we seek must fulfill several restraints on the various boundaries and along the chemical reaction front. First, the bottom and the top of the system are free of tractions. Second, the traction vector must be continuous at the chemical reaction front. Third, coherency conditions apply at the chemical reaction front.

Two cases of boundary conditions on the faces perpendicular to the reaction front are considered, either displacements $\boldsymbol{u}_1 = u_1\boldsymbol{e}_1, \boldsymbol{u}_2 = u_2\boldsymbol{e}_2$ or tractions integrally equivalent to $\boldsymbol{F}_1 = F_1\boldsymbol{e}_1, \boldsymbol{F}_2 = F_2\boldsymbol{e}_2$ are prescribed. Both displacement and traction boundary-value problem statements fit within the assumption that

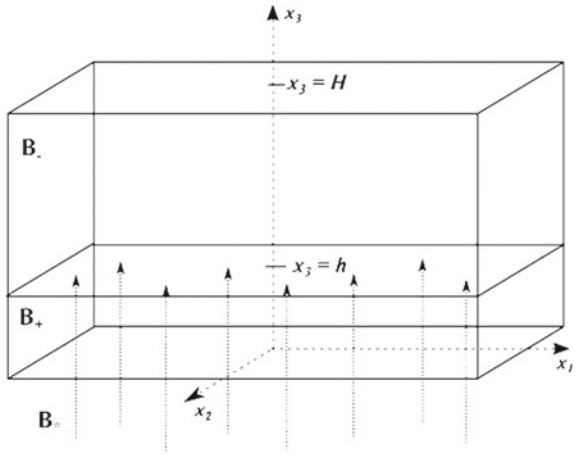

Fig. 1 Planar reaction front

$$\sigma_{33}^{\pm} = 0. \tag{18}$$

3.1.1 Prescribed Displacements

If the displacement components u_1, u_2 are given, the strain is uniformly distributed over the height of the block:

$$\varepsilon_{11,22}^{-} = \varepsilon_{11,22}^{+} = \varepsilon_{1,2}^{0} = \frac{u_{1,2}}{l_{1,2}}. \tag{19}$$

Moreover, the shear strains vanish, so that $\varepsilon_{ij}^{\pm} = 0$, if $i \neq j$. Because $\sigma_{33}^{\pm} = 0$, ε_{33}^{-}, ε_{33}^{+} can be calculated from Hooke's law, and then the normal component of the chemical affinity is:

$$A_{nn} = \frac{n_- M_-}{\rho_-}\left[\gamma(T) + \left(\frac{E_-}{1-\nu_-^2} - \frac{E_+}{1-\nu_+^2}\right)\left(\left(\varepsilon_1^0\right)^2 + \left(\varepsilon_2^0\right)^2\right) + \right. \tag{20}$$

$$\left. 2\left(\frac{\nu_- E_-}{1-\nu_-^2} - \frac{\nu_+ E_+}{1-\nu_+^2}\right)\varepsilon_1^0\varepsilon_2^0 + \frac{2E_+}{(1-\nu_+)}\varepsilon_{\mathrm{ch}}(\varepsilon_1^0 + \varepsilon_2^0) - \frac{2E_+}{(1-\nu_+)}\varepsilon_{\mathrm{ch}}^2\right] + n_* RT \ln\frac{c(\Gamma)}{c_*}.$$

The reaction propagates only if $A_{nn} > 0$. Hence, without the external load ($\varepsilon_1^0 = 0$, $\varepsilon_2^0 = 0$), the reaction front propagates only if energy parameter is large enough:

$$\gamma > \gamma_* = \frac{2E_+}{1-\nu_+}\varepsilon_{\mathrm{ch}}^2. \tag{21}$$

If $\gamma = \gamma_*$, then the reaction is blocked if

$$\left(\frac{E_-}{1-\nu_-^2} - \frac{E_+}{1-\nu_+^2}\right)\left(\left(\varepsilon_1^0\right)^2 + \left(\varepsilon_2^0\right)^2\right) + \left(\frac{\nu_- E_-}{1-\nu_-^2} - \frac{\nu_+ E_+}{1-\nu_+^2}\right)\varepsilon_1^0\varepsilon_2^0 + \tag{22}$$

$$\frac{E_+}{(1-\nu_+)}\varepsilon_{\mathrm{ch}}(\varepsilon_1^0 + \varepsilon_2^0) < 0.$$

Equation (14) can be rewritten as:

$$D = D_0 \exp\left(\frac{V_d}{kT}\frac{E_+}{3(1-\nu_+)}\left(\varepsilon_1^0 + \varepsilon_2^0 - 2\varepsilon_{\mathrm{ch}}\right)\right). \tag{23}$$

Since D depends only on the parameters of the materials and prescribed strains, and does not depend on the x_3-coordinate, the stationary diffusion equation (12) takes the form:

$$\Delta c = 0 \quad \Rightarrow \quad \frac{\partial^2 c}{\partial x_3^2} = 0, \tag{24}$$

and we conclude that the concentration profile must be linear, $c = c_1 x_3 + c_2$. From the boundary conditions (13) we can obtain explicit relations for the two constants of integration c_1 and c_2. Then, by Eq. (10), the reaction front velocity is:

$$V = \frac{M\_k_* D\alpha(c_* - c_{\text{eq}})}{\rho_- \left(D\alpha + k_* \alpha h - D k_*\right)}. \tag{25}$$

If we use the diffusion coefficient shown in Eq. (16), which also does not depend on the x_3-coordinate, we obtain the same solution.
From here on, having in mind the reaction of silicon oxidation, we shall put n_* and n_- equal to one. By introducing non-dimensional parameters,

$$\xi = \frac{h}{H},\ t_* = \frac{M\_k_* c_*}{H\rho_-} t,\ \kappa_1 = \frac{k_* H}{D_0},\ \kappa_2 = \frac{k_*}{\alpha}, \tag{26}$$

we can rewrite Eq. (25) as

$$\frac{\mathrm{d}\xi}{\mathrm{d}t_*} = \frac{1 - c_{\text{eq}}/c_*}{1 + \kappa_1 \xi + \kappa_2} \tag{27}$$

for a constant diffusivity coefficient and as

$$\frac{\mathrm{d}\xi}{\mathrm{d}t_*} = \frac{1 - c_{\text{eq}}/c_*}{1 + \frac{\kappa_1 \xi}{\bar{A}} + \kappa_2} \tag{28}$$

for a stress-dependent diffusion coefficient, where $\bar{A} = \exp\left(\frac{V_d}{kT}\frac{E_+}{3(1-\nu_+)}\right.$ $\left.\left(\varepsilon_1^0 + \varepsilon_2^0 - 2\varepsilon_{\text{ch}}\right)\right)$, if we define the coefficient by Eq. (14), and $\bar{A} = 1 + \beta\left(\varepsilon_1^0 + \varepsilon_2^0\right)$, if we use the coefficient of Eq. (16). As a result, the expression for dependence of growth of new material on time is:

$$\xi = -\frac{\kappa_2 + 1}{\kappa_1} + \sqrt{\left(\frac{\kappa_2 + 1}{\kappa_1}\right)^2 + \frac{2\left(1 - \frac{c_{\text{eq}}}{c}\right)t}{\kappa_1}} \tag{29}$$

for a constant diffusion coefficient, and

$$\xi = -\frac{\bar{A}(\kappa_2 + 1)}{\kappa_1} + \sqrt{\left(\frac{\bar{A}(\kappa_2 + 1)}{\kappa_1}\right)^2 + \frac{2\bar{A}\left(1 - \frac{c_{\text{eq}}}{c}\right)t}{\kappa_1}}. \tag{30}$$

for a stress-dependent diffusion coefficient.

3.1.2 Prescribed Tractions

We start by choosing the following semi-inverse ansatz for the strains,

$$\varepsilon^{\pm}_{11,22} = A^{\pm}_{1,2} x_3 + B^{\pm}_{1,2}, \tag{31}$$

where $A^{\pm}_{1,2}$ and $B^{\pm}_{1,2}$ are constants. Due to the continuity conditions for the displacement one can find that $A^{+}_{1,2} = A^{-}_{1,2} = A_{1,2}$ and $B^{+}_{1,2} = B^{-}_{1,2} = B_{1,2}$. Then the displacements are:

$$u^{+}_{1,2} = u^{-}_{1,2} = A_{1,2} x_3 + B_{1,2}, \qquad u^{\pm}_3 = -\frac{1}{2} A_1 x_1^2 - \frac{1}{2} A_2 x_2^2 + f^{\pm}(x_3), \tag{32}$$

and hence $\varepsilon^{\pm}_{ij} = 0$ for $i \neq j$.

By using Hooke's law we find for the missing strain components:

$$\varepsilon^{\pm}_{33} = -\frac{\nu_{\pm}}{1-\nu_{\pm}} \big((A_1 + A_2) x_3 + B_1 + B_2 \big) + \frac{1+\nu_{\pm}}{1-\nu_{+}} \varepsilon^{\pm}_{\mathrm{ch}}, \quad \varepsilon^{+}_{\mathrm{ch}} = \varepsilon_{\mathrm{ch}}, \quad \varepsilon^{-}_{\mathrm{ch}} = 0, \tag{33}$$

and for the normal stresses:

$$\begin{aligned} \sigma^{\pm}_{11} &= \frac{E_{\pm}}{1-\nu^2_{\pm}} \big((A_1 + \nu_{\pm} A_2) x_3 + B_1 + \nu_{\pm} B_2 \big) - \frac{E_{\pm}}{1-\nu_{+}} \varepsilon^{\pm}_{\mathrm{ch}}, \\ \sigma^{\pm}_{22} &= \frac{E_{\pm}}{1-\nu^2_{\pm}} \big((\nu_{\pm} A_1 + A_2) x_3 + \nu_{\pm} B_1 + B_2 \big) - \frac{E_{\pm}}{1-\nu_{+}} \varepsilon^{\pm}_{\mathrm{ch}}. \end{aligned} \tag{34}$$

The four remaining constants can be obtained from the equations for equilibrium of forces and moments:

$$\begin{aligned} \int_0^H \sigma^0_{1,2} \, \mathrm{d}x_3 &= \int_0^h \sigma^{+}_{11,22}\Big|_{x_{1,2}=l_{1,2}} \mathrm{d}x_3 + \int_h^H \sigma^{-}_{11,22}\Big|_{x_{1,2}=l_{1,2}} \mathrm{d}x_3, \quad \sigma^0_{1,2} = \frac{F_{1,2}}{H}, \\ \int_0^H x_3 \sigma^0_{1,2} \, \mathrm{d}x_3 &= \int_0^h x_3 \sigma^{+}_{11,22}\Big|_{x_{1,2}=l_{1,2}} \mathrm{d}x_3 + \int_h^H x_3 \sigma^{-}_{11,22}\Big|_{x_{1,2}=l_{1,2}} \mathrm{d}x_3. \end{aligned} \tag{35}$$

In contrast to the prescribed displacements, the stress-strain state on the chemical reaction front depends on the front position. However, in the case of a constant diffusion coefficient the gas concentration at the chemical reaction front is found from (24), the expression for the front velocity is analogous to (25), and the equilibrium concentration can be found from Eq. (20) by replacing $\varepsilon^0_{1,2}$ by $A_{1,2}(h, F_{1,2}) x_3 + B_{1,2}(h, F_{1,2})$.

The non-constant diffusion coefficient in this case also depends on the reaction front position and has the form:

$$D = D_0 \exp\left(\frac{E_+ V_d}{3kT(1-\nu_+)}\left(\left(A_1 + A_2\right)x_3 + B_1 + B_2 - 2\varepsilon_{\text{ch}}\right)\right). \tag{36}$$

Then the diffusion problem (12) reads:

$$\frac{\partial}{\partial x_3}\left(D_0 \exp(\widetilde{A}x_3 + \widetilde{B})\frac{\partial c}{\partial x_3}\right) = 0 \quad \Rightarrow \quad \frac{\mathrm{d}^2 c}{\mathrm{d}{x_3}^2} + \widetilde{A}\frac{\mathrm{d}c}{\mathrm{d}x_3} = 0, \tag{37}$$

where $\widetilde{A} = A_1 + A_2$, $\widetilde{B} = B_1 + B_2 - 2\varepsilon_{\text{ch}}$.

The solution of this equation results in an exponential profile for the concentration, $c = c_1 \exp(-\widetilde{A}x_3) + c_2$, where c_1 and c_2 can be found from the boundary condition (13). Finally, the normal component of the reaction front velocity has the following form:

$$V = \frac{M_-}{\rho_-}\frac{D_0 \exp(\widetilde{B})\widetilde{A}\alpha c_* k_* \left(1 - \frac{c_{\text{eq}}}{c_*}\right)}{D_0 \exp(\widetilde{B})\widetilde{A}\left(\alpha + k_*\right) + \alpha k_*\left(1 - \exp(-\widetilde{A}h)\right)}, \tag{38}$$

and, by using the notations (26), we can rewrite it as:

$$\frac{\mathrm{d}\xi}{\mathrm{d}t_*} = \frac{1 - \frac{c_{\text{eq}}}{c_*}}{1 + \frac{\kappa_1}{\exp(\widetilde{B})\widetilde{A}}\left(1 - \exp(-\widetilde{A}\xi)\right) + \kappa_2}. \tag{39}$$

The solution to (39) is too lengthy to be presented here, because of the dependence of $\widetilde{A}$ and $\widetilde{B}$ on the reaction front position.

3.2 *Spherical Reaction Front*

We consider a spherical body $r \in \left[0, r_{\text{o}}\right]$ (cf., Fig. 2) subjected to an external pressure $p = -\sigma_0$ or to a fixed radial displacement u_0 at the outer surface. Let the reaction front propagate from the outer surface. Due to the symmetry of the problem we suppose that the reaction front is represented by a spherical surface at position $r = r_{\text{i}}$. It is also assumed that the concentration does not depend on the ϑ- and φ-coordinates, and is a function of r only, $c = c(r)$, $c(\Gamma) = c(r_{\text{i}})$.

The displacements can be found from Lamé's solution for spheres:

$$u_r = Ar + \frac{B}{r^2}. \tag{40}$$

The constants $A_\pm$ and $B_\pm$ are determined from the displacement and traction continuity conditions at the reaction front and non-singularity of the solution at the body

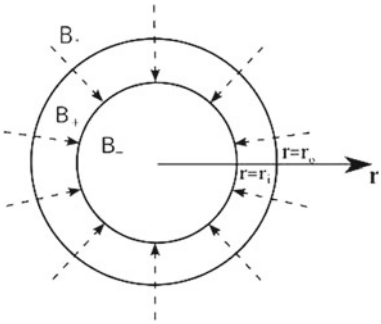

Fig. 2 Spherical reaction front

center. Hence, the radial component of the displacement is:

$$u_- = A_- r, \quad u_+ = A_+ r + \frac{(A_- - A_+) r_\mathrm{i}^3}{r^2}, \tag{41}$$

where:

$$A_+ = A_- \frac{(1-2\nu_+)\left(E_-(1+\nu_+) + 2E_+(1-2\nu_-)\right)}{3E_+(1-2\nu_-)(1-\nu_+)} + \frac{E_+}{1-2\nu_+}\varepsilon_\mathrm{ch}. \tag{42}$$

The parameter A_- can be found from the boundary condition. If the displacement $u_0(r_\mathrm{o})$ is given as the boundary condition then:

$$A_- = \frac{\left(\lambda_+ + 2\mu_+\right)\frac{3u_0}{r_\mathrm{o}} - 3k_+\left(1-\xi^3\right)\varepsilon_\mathrm{ch}}{3k_- + 4\mu_+ + 3\left(k_+ - k_-\right)\xi^3}, \tag{43}$$

and if the traction is prescribed:

$$A_- = \frac{\left(\lambda_+ + 2\mu_+\right)\sigma_0 + 4k_+\mu_+\left(1-\xi^3\right)\varepsilon_\mathrm{ch}}{k_+\left(3k_- + 4\mu_+\right) - 4\mu_+\left(k_+ - k_-\right)\xi^3}, \tag{44}$$

where $k_\pm = \frac{E_\pm}{3(1-2\nu_\pm)}$ is the bulk modulus.

From here on we put $\xi = \frac{r_\mathrm{i}}{r_\mathrm{o}}$ and, as a result, the relation for the equilibrium concentration has the form:

$$\frac{M_-}{\rho_-}\left[\gamma(T) + \frac{1}{2(\lambda_+ + 2\mu_+)}(12(k_- - k_+)\mu_+ A_-^2 + 3k_+(3k_- + 8\mu_+)A_{-_\mathrm{ch}} - 12\mu_+ k_+ \varepsilon_\mathrm{ch}^2)\right] + RT\ln\frac{c(\xi)}{c_*} = 0. \tag{45}$$

The diffusion equation in spherical coordinates reads:

$$D\frac{\mathrm{d}^2c}{\mathrm{d}\zeta^2}+\left(\frac{\mathrm{d}D}{\mathrm{d}\zeta}+\frac{2}{\zeta}D\right)\frac{\mathrm{d}c}{\mathrm{d}\zeta}=0,\qquad \zeta=\frac{r}{r_\mathrm{o}}. \tag{46}$$

Note that in this problem

$$\mathrm{Tr}\,\boldsymbol{\sigma}^+=\sigma_r^+ +\sigma_\varphi^+ +\sigma_\vartheta^+ =\frac{E_+}{1-2\nu_+}\left(A_+-\varepsilon_\mathrm{ch}\right), \tag{47}$$

and, since A_+ does not depend on r, and, consequently, on ζ, the diffusion coefficient (14) does also not depend on ζ. Thus, for a constant diffusion coefficient and for the phenomenological diffusion coefficient (14), it follows from (46) that the differential equation for the concentration has the form:

$$\frac{\mathrm{d}^2c}{\mathrm{d}\zeta^2}+\frac{2}{\zeta}\frac{\mathrm{d}c}{\mathrm{d}\zeta}=0. \tag{48}$$

The solution of this equation is

$$c=\frac{c_1}{\zeta}+c_2.$$

The two constants of integration, c_1 and c_2, can be determined from the boundary conditions shown in Eq. (13).

By using non-dimensional parameters:

$$\xi=\frac{h}{r_\mathrm{o}},\ t_*=\frac{M_-k_*c_*}{r_\mathrm{o}\rho_-}t,\ \kappa_1=\frac{k_*r_\mathrm{o}}{D_0},\ \kappa_2=\frac{k_*}{\alpha}, \tag{49}$$

we obtain the differential equation of the chemical reaction front propagation:

$$\frac{\mathrm{d}\xi}{\mathrm{d}t_*}=\frac{1-c_\mathrm{eq}/c_*}{1+\kappa_1\xi-\kappa_1\xi^2+\kappa_2\xi^2} \tag{50}$$

for a constant diffusion coefficient and

$$\frac{\mathrm{d}\xi}{\mathrm{d}t_*}=\frac{1-c_\mathrm{eq}/c_*}{1+\kappa_1/\bar{B}\,\xi-\kappa_1/\bar{B}\,\xi^2+\kappa_2\xi^2} \tag{51}$$

for the diffusion coefficient (14), where $\bar{B}=\exp\left(\frac{V_d}{kT}\frac{E_+}{1-2\nu_+}\left(A_+-\varepsilon_\mathrm{ch}\right)\right)$.

Substitution of $\tilde{\xi}=1-\xi$ yields an equation for the growth of a relative thickness of the transformed layer.

Now we turn to the tensorial diffusion coefficient (16) which in this case is equal to $D = D_0\big(1 + \beta(\varepsilon^+_{\varphi\varphi} + \varepsilon^+_{\theta\theta})\big)$. By taking into account that

$$\varepsilon^+_{\varphi\varphi} = \varepsilon^+_{\theta\theta} = A_+ + (A_- - A_+)\frac{\xi^3}{r^3}$$

the differential equation for the concentration becomes:

$$\left(1 + 2\beta\left(A_+ + \frac{B\xi^3}{\zeta^3}\right)\right)\frac{\mathrm{d}^2c}{\mathrm{d}\zeta^2} + \frac{2\big(\zeta^3(1 + 2A_+\beta) - B\beta\xi^3\big)}{\zeta^4}\frac{\mathrm{d}c}{\mathrm{d}\zeta} = 0. \tag{52}$$

By putting $p = 1 + 2\beta A_+$, $q = 2B\beta$ and by taking the boundary conditions into account, we obtain the velocity of the chemical reaction front propagation:

$$V = \frac{6p^{2/3}q^{1/3}\alpha D_0(c_* - c_{\mathrm{eq}})}{k_* r_{\mathrm{o}}\alpha\xi\left(2\sqrt{3}(f_1 + f_2) + f_3\right) + 6p^{2/3}q^{1/3}(\alpha + k_*\xi^2)D_0}, \tag{53}$$

where $f_1 = \tan^{-1}\frac{2\sqrt[3]{\frac{p}{q}}-1}{\sqrt{3}}$, $f_2 = \tan^{-1}\frac{1-\frac{2}{\xi}\sqrt[3]{\frac{p}{q}}}{\sqrt{3}}$, $f_3 = \ln\frac{(p+q)}{(p+q\xi^3)}\left(\frac{p^{1/3}+q^{1/3}\xi}{p^{1/3}+q^{1/3}}\right)^3$. Silicon dioxide is a rather brittle material. The corresponding volume change is very high and the transformation stresses would become enormous with increasing layer thickness. Hence, for physical reasons, it does not make sense to consider predicted thicknesses of a transformed silicon layer more than above half of the whole material thickness. This means that $0.5 < \xi < 1$. By using a power series expansion near $\xi = 1$ and by introducing non-dimensional parameters (49) we obtain:

$$\frac{\mathrm{d}\xi}{\mathrm{d}t_*} = \frac{(1 + 2A_-\beta)(1 - c_{\mathrm{eq}}/c_*)}{(1 + 2A_-\beta)(1 + \kappa_2\xi^2) + \kappa_1\xi - \kappa_1\xi^2}. \tag{54}$$

After substituting $\tilde{\xi} = 1 - \xi$ we have obtained a differential equation for the relative thickness of the transformed layer.

4 Numerical Calculations

4.1 Material Parameters

Further calculations were made for dry silicon oxidation as an example of the reaction (1). The material parameters of the reaction are given in Table 1. The choice of the values ρ_-/M_-, $E_\pm$ and $\nu_\pm$ corresponds approximately to polysilicon and to silicon dioxide (see, e.g., [8, 16]). The values for k_*, α were taken from [6]. The value

Table 1 Material parameters

Parameters	Constituent B_-	Constituent B_+
Young's modulus E, GPa	163	60
Poisson's ratio ν	0.23	0.17
Transformation strain ε_{ch}	–	0.03
ρ/M, mol/m^3	8.29e4	Out of use
Temperature, K	1173	
Diffusivity coefficient D_0, m^2/s	6.61E-14	
Reaction rate constant k_*, m/s	0.36E-6	
Gas phase transport coefficient		
α, m/s	Out of use	0.028

for D_0 differs considerably in publications: In [7] and in [24] it is about 3 orders higher than in [6]. Note that silicon oxidation is accompanied by a large increase in molar volume ($\varepsilon_{\text{ch}} \approx 0.3$), which would lead to enormous internal stresses. However, since silica is not a purely elastic solid, a part of the intrinsic strain will relax due to viscosity. Since the aim of the present paper is to compare a stress effect on the chemical reaction kinetics through stress-dependent diffusion and chemical affinity for the simplest case of linear elastic solid constituents we take $\varepsilon_{\text{ch}} = 0.03$. This corresponds to a small strain approach and ignores the viscous behavior. Thus the parameters in Table 1 may be considered as parameters of some artificial material. The value of the energy parameter, γ_*, which is used for calculations, can be calculated from Eq. (21) by using the introduced values for the elastic parameters and ε_{ch}.

4.2 Results for the Planar Chemical Reaction Front

Let us first consider the case of prescribed displacements or strains. We start with a demonstration of the main features of the chemical reaction kinetics in dependence on the various parameters of the model. After that the growth of the new material layer for different diffusion models will be investigated.

In Fig. 3 the relation between equilibrium concentration, $\frac{c_{\text{eq}}}{c_*}$, and externally applied strains, ε_1^0 and ε_2^0, is investigated for a constant diffusion coefficient. It is seen that for given values of ε_2^0 stretching in the second direction leads to overall lower values of equilibrium concentration (blue dashed line), whereas compression has the opposite effect (red dotted curve). Increasing or decreasing the energy parameter γ shifts the curves up or down, respectively. Small energy parameters may lead to $\frac{c_{\text{eq}}}{c_*} > 1$. This means that the reaction may come to a standstill.

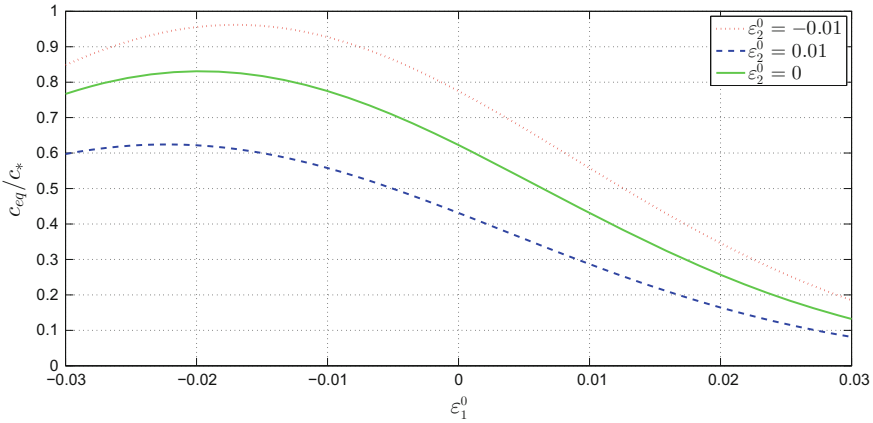

Fig. 3 Dependence of $\frac{c_{eq}}{c_*}$ on ε_1^0 at different ε_2^0, $\gamma = 3.6\gamma_*$

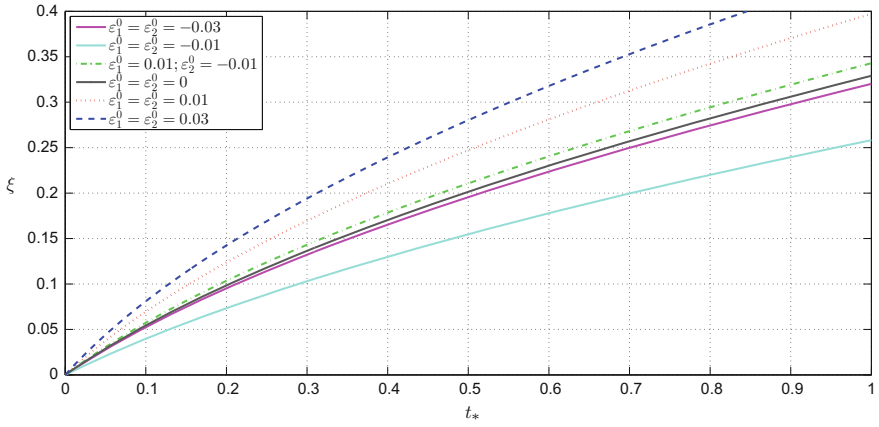

Fig. 4 Dependence of relative thickness ξ on normalized time t_* for the block, $\gamma = 3.6\gamma_*$, displacements are prescribed

The dependence of the relative thickness of the new material layer on time is presented in Fig. 4. One can see that biaxial stretching accelerates the reaction and that biaxial compression leads to retardation. The combination of deformations of different signs does not have a significant effect on the reaction kinetics.

In order to compare the chemical reaction front propagation as predicted by different diffusion models we evaluate the difference between fronts kinetics for constant and stress-dependent diffusivity, denoted by $\text{Difference}, \% = (\xi(D) - \xi(D_0)) \cdot 100\%$. We start with the phenomenological diffusion coefficient (14). Dependencies of the relative difference on normalized time for different values of the external load are presented in Fig. 5. It is seen that if stress dependent diffusivity is taken

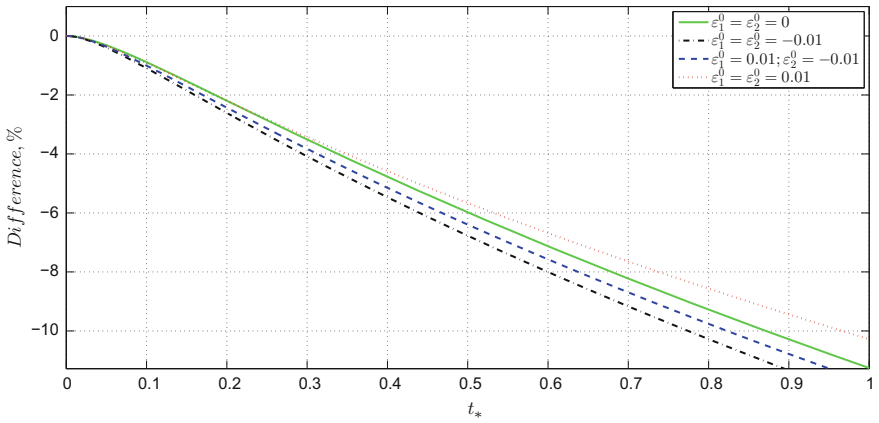

Fig. 5 Dependence of relative difference on normalized time t_* for the block, $\gamma = 3.6\gamma_*$, displacements are prescribed

into consideration the growth of new material layer is retarded (negative values for Difference). The difference is the greater the more the block is compressed.

Note that at $t_* = 0.5$ we have typically ξ-values of already 0.25, which go up to 0.4 for $t_* = 1$. Difference values between 5–20% are predicted. Indeed, this is not very small. However, recall that our linear elastic model becomes totally unrealistic at such high values for ξ, because the real eigenstrain is much higher than the assumed one and viscous relaxation must then be taken into account. Moreover, the material may also simply break, if the stresses are too high, which adds another limitation to our models.

Moreover, since different sources quote totally different values for the diffusion we plot the curves for a significantly greater value of the diffusion coefficient, D_0. From Fig. 6 it is seen that by increasing D_0 the difference between the two approaches will decrease.

In Fig. 7 we consider the phenomenological and the tensorial diffusion coefficients, (14) and (16), respectively. In the case of prescribed stretching strains the propagation of the chemical reaction front for tensorial diffusion goes faster, if compared to a constant diffusion coefficient. In the case of compressive strains the propagation is always retarded, but in both cases the difference between approaches is relatively small and may be neglected.

The difference between the approaches becomes more evident from Fig. 8. For the cases of stretching as well as for compressive strains the relative difference between the kinetics of transformed material layer growth with constant diffusion coefficient and tensor diffusion coefficient (16) does not exceed 6%.

In summary we may conclude that if the displacements or strains are given as a boundary condition the effect of the stress-affected diffusion on the planar front kinetics is relatively small and may be neglected.

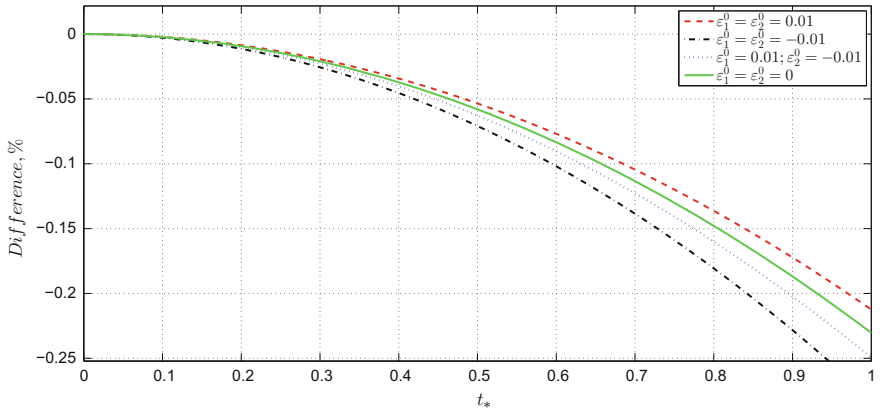

Fig. 6 Dependence of relative difference on normalized time t_* for the block, $\gamma = 3.6\gamma_*$, $\widetilde{D}_0 = 1000D_0$, displacements are prescribed

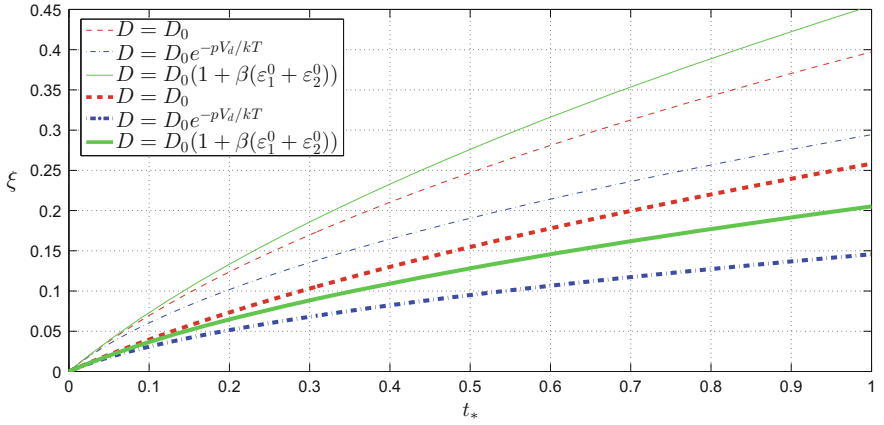

Fig. 7 Dependence of relative thickness ξ on normalized time t_* for the block, $\beta = \beta_*$, $\gamma = 3.6\gamma_*$, thin lines correspond to $\varepsilon_1^0 = \varepsilon_2^0 = 0.01$, bold lines correspond to $\varepsilon_1^0 = \varepsilon_2^0 = -0.01$

Now we consider the case of prescribed stress. In contrast to the prescription of displacements the equilibrium concentration and, as a result, the chemical reaction front velocity depend on the height of the oxidation layer, i.e., the progress of the oxidation. Figure 9 shows the growth of the new material layer for a constant diffusion coefficient and for various values of externally applied normalized stresses:

$$\bar{\sigma}_{1,2} = \frac{E_+}{1 - \nu_+^2}\sigma_{1,2}^0$$

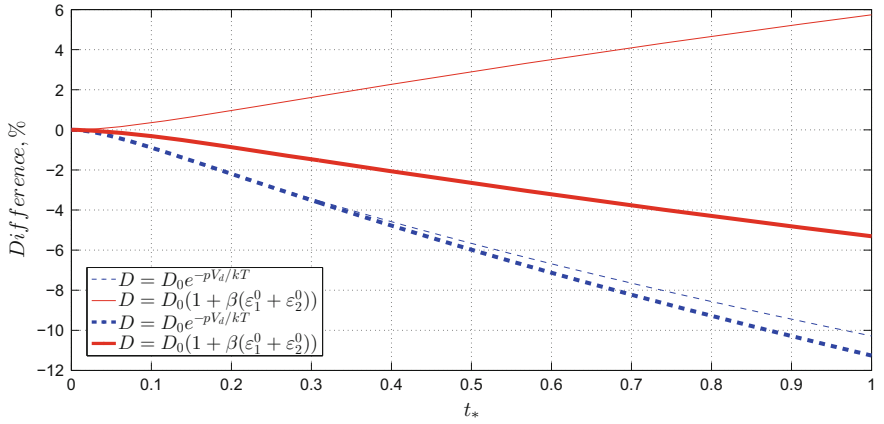

Fig. 8 Dependence of relative difference on normalized time t_* for the block, thin lines correspond to $\varepsilon_1^0 = \varepsilon_2^0 = 0.01$, bold lines correspond to $\varepsilon_1^0 = \varepsilon_2^0 = -0.01$

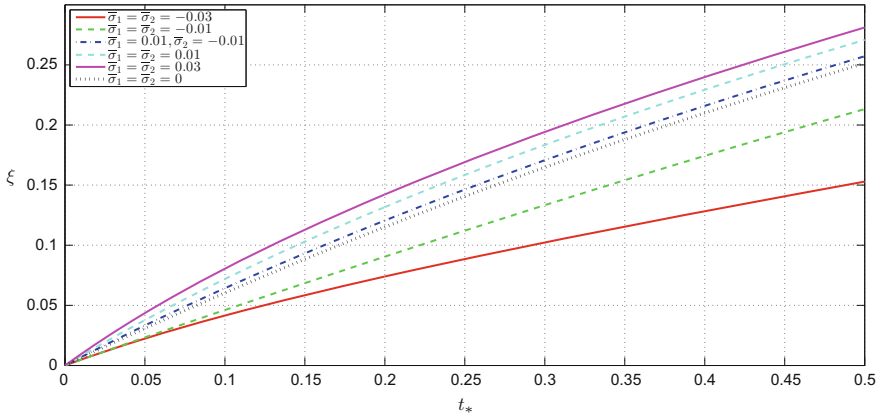

Fig. 9 Dependence of relative thickness ξ on normalized time t_*, $\gamma = 3.6\gamma_*$, stresses are prescribed

Analogously to the case of prescribed strains compression slows down the propagation of the reaction front and tension leads to its acceleration.

A comparison of the chemical reaction front propagation for a constant diffusion coefficient and the phenomenological diffusion coefficient (14) is presented in Fig. 10. Once more we must conclude that when taking the dependence of the diffusion coefficient on stresses into account the reaction will be retarded. External compression increases the difference between the approaches but the quantity Difference is still not large. Additional calculations as in Fig. 6 show that it becomes even smaller if the diffusion coefficient D_0 is increased.

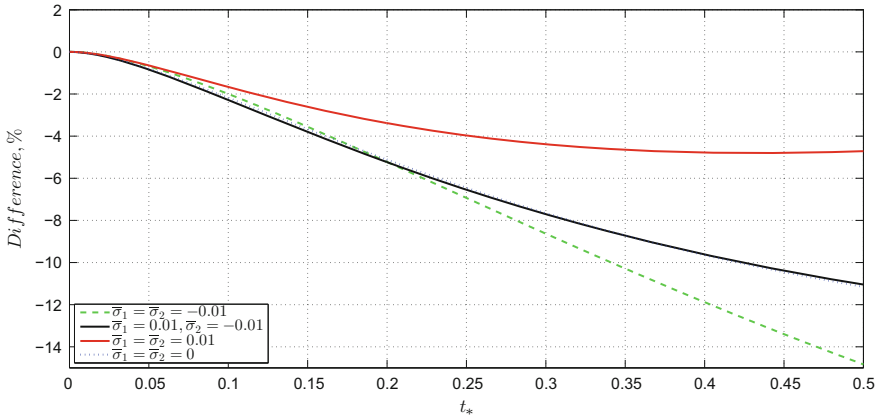

Fig. 10 Dependence of relative difference on normalized time t_* for the block, $\gamma = 3.6\gamma_*$, stresses are prescribed

If the tensorial diffusion coefficient is considered results similar to the case of fixed displacements are obtained. The characteristics of curves remains analogous to those of Fig. 8 but the absolute value of the quantity Difference decreases.

4.3 Results for a Spherical Chemical Reaction Front

The dependencies of the equilibrium concentration on the chemical reaction front position and a detailed investigation of front kinetics in spherically symmetric problems at constant D_0 were presented in [13, 32]. In the present paper we consider only the influence of stress-dependent diffusion on the velocity of the chemical reaction front. In other words we compare the solutions of Eqs. (50), (51) and (54).

Let us first consider the phenomenological diffusion coefficient (14). The results of the comparison of the different approaches for different values of fixed displacement at the body surface are shown in Fig. 11. The situation is analogous to the planar reaction front propagation: When taking the dependence of the diffusion coefficient on stresses into account the growth of the transformed layer is in general retarded. The reason of this retardation are the transformation strains. For fixed boundary conditions accumulated transformation strains create compressive internal stresses, which in turn slow down the diffusion process.

Finally, Fig. 12 shows the analogue to Fig. 11 but for stress loading. As before one can see that the stress-assisted diffusion retards the chemical reaction front propagation. However, the difference between the approaches is slightly smaller in the case of prescribed stresses than in the case of fixed displacements, since in the former case the boundaries of the body are not fixed and can expand more freely due to chemical transformations, with a smaller amount of compressive internal stresses.

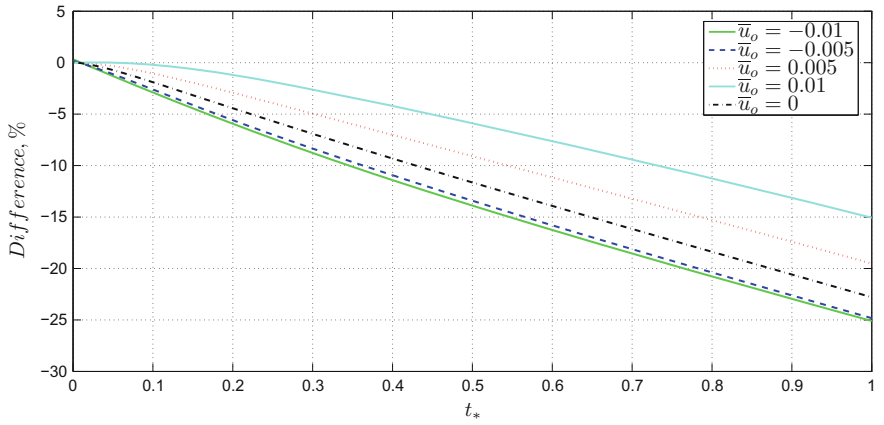

Fig. 11 Dependence of relative difference on normalized time t_* for the sphere, $\gamma = 3.6\gamma_*$, strains are prescribed ($\bar{u}_0 = u_0/r_0$)

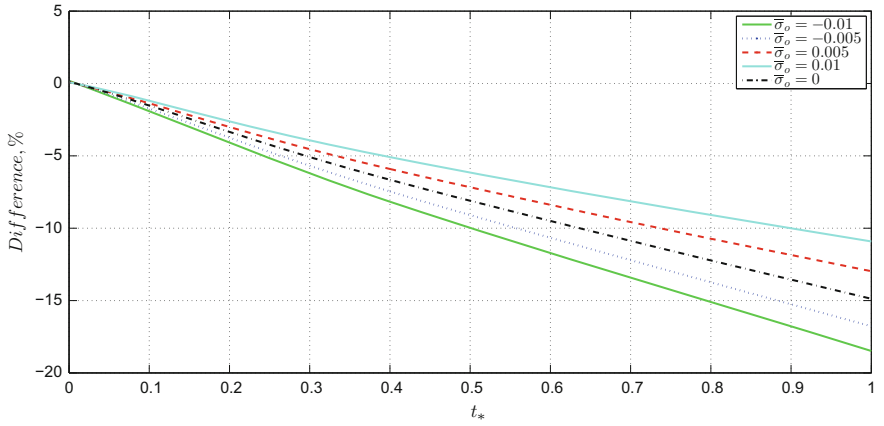

Fig. 12 Dependence of relative difference on normalized time t_* for the sphere, $\gamma = 3.6\gamma_*$, stresses are prescribed

Nevertheless, in comparison with Fig. 10 the influence of the stress-assisted diffusion is more significant even for tensile stresses. Therefore, if one chooses the dependence of diffusivity on stresses in the form of (14), then for this boundary-value problem the dependence of the diffusion coefficient on the stresses should eventually be considered even when obtaining estimated results.

Reaction front kinetics for all three diffusion coefficients and stretching and compressive external displacements are presented in Figs. 13 and 14, respectively. In both cases the difference between the kinetics of transformed material layer growth with a constant diffusion coefficient and the tensor diffusion coefficient (16) is less than

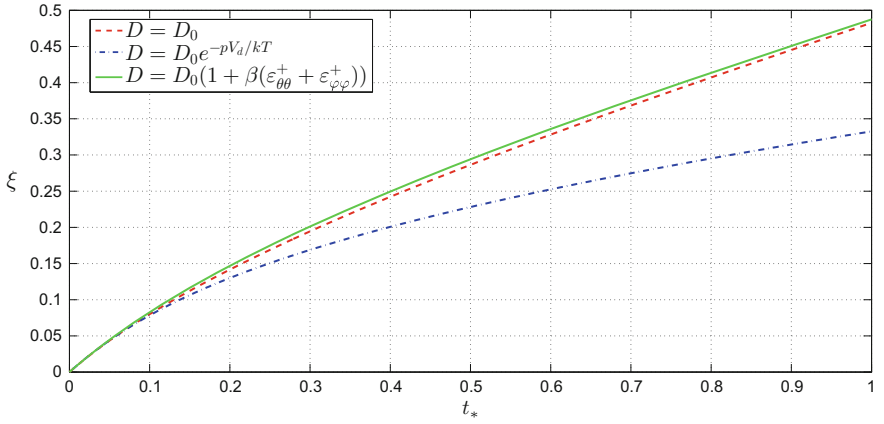

Fig. 13 Dependence of relative thickness ξ on normalized time t_* for the sphere, $\beta = \beta_*, \gamma = 3.6\gamma_*$, $\overline{u}_o = 0.01$

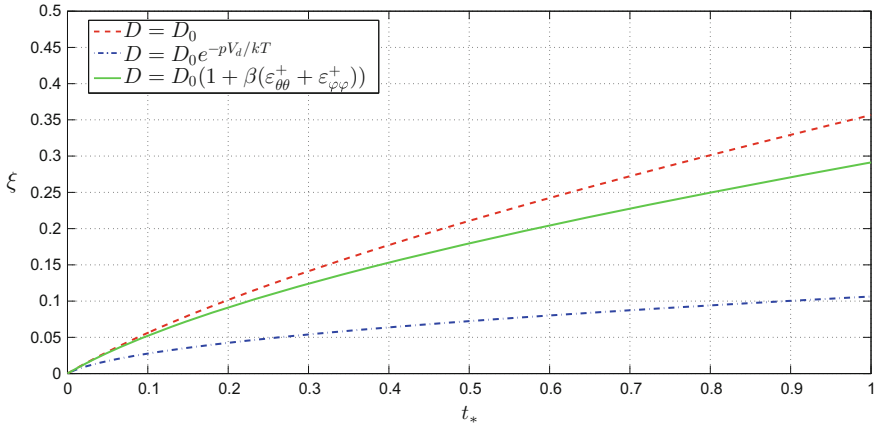

Fig. 14 Dependence of relative thickness ξ on normalized time t_* for the sphere, $\beta = \beta_*, \gamma = 3.6\gamma_*$, $\overline{u}_o = -0.01$

the same difference for a constant diffusion coefficient and the empirical diffusion coefficient (14), especially for stretching (positive displacement). A reason for this is that the internal stresses appearing due to the transformation strain are rather significant especially under compression and have a noticeable effect on the diffusivity, while strains in the $\vartheta - \varphi$-plane are small at the fixed radial displacement of the outer surface and only slightly affect on the diffusion coefficient.

The difference between the approaches becomes more evident from Figs. 15 and 16. In the case of stretching as well as of compressive strains the relative difference between the kinetics of transformed material layer growth with constant diffusion

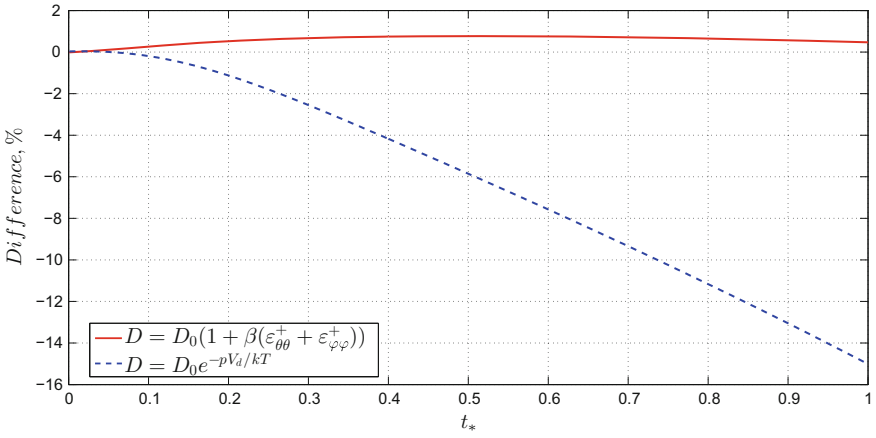

Fig. 15 Dependence of relative difference on normalized time t_* for the sphere, $\overline{u}_o = 0.01$

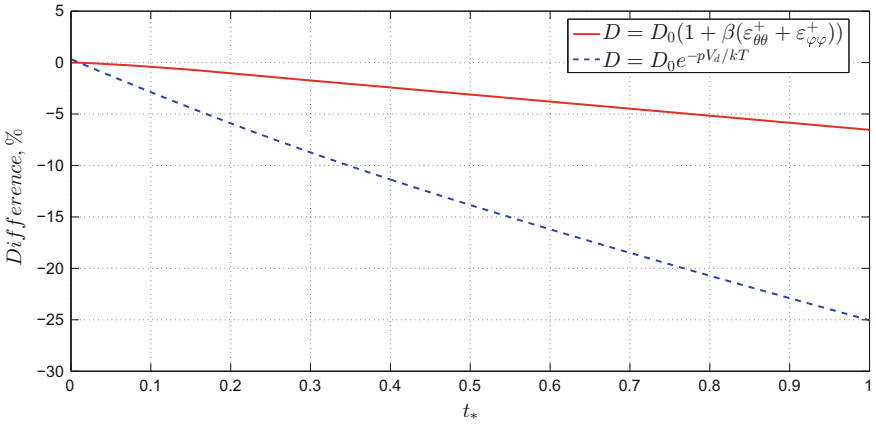

Fig. 16 Dependence of relative difference on normalized time t_* for the sphere, $\overline{u}_o = -0.01$

coefficient and tensor diffusion coefficient (16) does not exceed 7%. Therefore, if the rationally introduced tensor diffusion coefficient (16) is taken into account for calculations that do not require high accuracy and only estimate the model, one can neglect the difference and disregard the dependence of the diffusion coefficient on the mechanical stresses.

The same characteristic for the difference and kinetics behavior holds in case of prescribed stresses, but in this case the relative difference does not exceed 5% (not shown here). Hence for this diffusion coefficient one can neglect the difference and disregard the dependence of the diffusion coefficient on the mechanical stresses with rather high accuracy.

5 Summary and Conclusions

In this work we investigated the impact of the stress-driven diffusion on the velocity of the chemical reaction front propagation. We used the model of a chemical affinity tensor and also considered the dependence of the diffusion coefficient on mechanical loads. In addition to considering a phenomenologically motivated stress dependence of the diffusion coefficient in Eq. (14) the diffusion process was also investigated based on a rationally formulated model of tensor diffusion, Eq. (16). The kinetics of the chemical reaction front propagation as a function of the applied external loads was investigated for two boundary-value problems, a rectangular block in a plane-stressed state and a body with spherical symmetry. A comparison of the results for three types of diffusion law was made, one with a constant diffusion coefficient, the phenomenologically motivated (14) one, and the tensorial, rational based approach (16) as proposed in this paper.

Based upon the obtained results we may conclude that in the case of the planar chemical reaction front the dependencies of the diffusion coefficient on the mechanical stresses hardly affect the chemical reaction front propagation. This makes it possible to neglect the influence of the stresses on the diffusion process and to simplify further calculations, since the use of a constant diffusion coefficient reduces the number of necessary model parameters and, accordingly, the number of experiments and calculations necessary to find these parameters.

In the case of the spherical reaction front, the influence of taking into account the stress-assisted diffusion strongly depends on the considered diffusion model. The widely used dependence of the diffusion coefficient on the pressure has a significant impact on the kinetics of the chemical reaction front, especially in the case of prescribed displacements. This happens because an additional deformation of the chemical transformation occurs as a result of the chemical reaction. Since for specified (i.e., fixed) displacements at the boundary, the spherical body cannot expand at all, the transformation strains cause large compressive stresses inside the transformed material, which in turn, significantly decrease the diffusion coefficient and retard the chemical reaction front propagation.

The proposed tensor diffusion coefficient hardly affects the chemical reaction front propagation. This happens because in this coefficient a stress component that acts in the direction of the diffusion flux mildly affects the propagation velocity of the diffusion flux since it does not deform the solid body skeleton sufficiently to make a significant change of the distance between the cells of the material and, accordingly, to change the permeability of the material. Thus, in this case, the difference between the kinetics is sufficiently small to be neglected.

Acknowledgements This work was supported by a grant from the Russian Foundation for Basic Research (17-51-12055).

References

1. Aloke, P.: Thermodynamics, Diffusion and the Kirkendall Effect in Solids. Springer, Heidelberg (2014)
2. Björkman, T., Kurasch, S., Lehtinen, O., Kotakoski, J., Yazyev, O.V., Srivastava, A., Skakalova, V., Smet, J.H., Kaiser, U., Krasheninnikov, A.V.: Defects in bilayer silica and graphene: common trends in diverse hexagonal two-dimensional systems. Sci. Rep. 3482 (2013)
3. Cui, Z., Gao, F., Qu, J.: A finite deformation stress-dependent chemical potential and its applications to lithium-ion batteries. Mech. Phys. Solids **60**, 1280–1295 (2012)
4. Cui, Z., Gao, F., Qu, J.: Interface-reaction controlled diffusion in binary solids with applications to lithiation of silicon in lithium-ion batteries. Mech. Phys. Solids **61**(2), 293–310 (2013)
5. De Donde, T.: Thermodynamic Theory of Affinity: A Book of Principles. Oxford University Press (1936)
6. Deal, B., Grove, A.: General relationship for the thermal oxisation of silicon. Appl. Phys. **36**(12), 57–75 (1965)
7. Delph, T.: Intrinsic strain in SiO_2 thin films. Appl. Phys. **83**, 785–792 (1998)
8. El-Kareh, B.: Fundamentals of Semiconductor Processing Technologies. Kluwer Academic (1995)
9. Freidin, A.: Chemical affinity tensor and stress-assist chemical reactions front propagation in solids. In: ASME 2013 International Mechanical Engineering Congress and Exposition, 13–21 Nov 2013, San Diego, California, USA (2014)
10. Freidin, A.B.: On a chemical affinity tensor for chemical reactions in deformable solids. Mech. Solids **50**(3), 260–285 (2015)
11. Freidin, A.B., Korolev, I.K., Aleshchenko, S.P., Vilchevskaya, E.N.: Chemical affinity tensor and chemical reaction front propagation: theory and FE-simulations. Int. J. Fract. 1–15 (2016)
12. Freidin, A.B., Korolev, I.K., Vilchevskaya, E.N.: Stress-assist chemical reactions front propagation in deformable solids. Int. J. Eng. Sci. **83**, 57–75 (2014)
13. Freidin, A.B., Morozov, N., Vilchevskaya, E.N., Petrenko, S.: Chemical reactions in spherically symmetric problems of mechanochemistry. Acta Mech. **227**(1), 43–56 (2016)
14. Gibbs, J.: The Collected Works of J.W. Gibbs, Vol. 1: Thermodynamics. Yale University Press (1948)
15. Glansdorff, P., Prigogine, I.: Thermodynamic Theory of Structure, Stability and Fluctuation. Wiley Interscience, London (1971)
16. Hopcroft, M.A., Nix, W.D., Kenny, T.W.: What is the Young's modulus of silicon? Microelectromec. Syst. **19**(2), 229 (2010)
17. Indeitsev, D., Mochalova, Y.: Mechanics of multi-component media with exchange of mass and non-classical supplies. Dyn. Mech. Syst. Var. Mass **557**, 165–194 (2014)
18. Indeitsev, D.A., Semenov, B.N., Sterlin, M.D.: The phenomenon of localization of diffusion process in a dynamically deformed solid. Dokl. Phys. **57**(4), 321–335 (2012)
19. Kao, D., McVitie, J., Nix, W., Saraswat, K.: Two dimensional silicon oxidation experiment and theory. IEDM Tech. Dig. **275**, 388–391 (1985)
20. Kao, D., McVitie, J., Nix, W., Saraswat, K.: Two dimensional thermal oxidation of silicon-I. Experiments. IEEE Trans. Electron Devices **ED-34**, 1008–1017 (1987)
21. Kao, D., McVitie, J., Nix, W., Saraswat, K.: Two-dimensional thermal oxidation of silicon. II. Modeling stress effects in wet oxides. IEEE Trans. Electron Device **35**(1), 25–37 (1988)
22. Knyazeva, A.: Model of medium with diffusion and internal surfaces and some applied problems. Mater. Phys. Mech. **7**, 29–36 (2004)
23. Knyazeva, A.G.: Cross effects in solid media with diffusion. J. Appl. Mech. Tech. Phys. **44**(3), 373–384 (2003)
24. Lin, M.: Stress effects and oxidant diffusion in the planar oxidation. Ph.D. thesis, Lehigh University (1999)
25. Loeffel, K., Lallit, A.: A chemo-thermo-mechanically coupled theory for elasticviscoplastic deformation, diffusion, and volumetric swelling due to a chemical reaction. Int. J. Plast. **27**(9), 1409–1431 (2011)

26. Prigogine, I., Defay, R.: Chemical Thermodynamics. Longmans, Green, London (1988)
27. Rusanov, A.: Surface thermodynamics revisited. Surf. Sci. Rep. **58**, 111–239 (2005)
28. Rusanov, A.I.: Thermodynamic Foundations of Mechanochemistry. Nauka, Saint-Petersburg (2006)
29. Sutardja, P., Oldham, W.: Modeling of stress effects in silicon oxidation. IEEE Trans. Electron Device **36**(11), 2415–2421 (1989)
30. Toribio, J.: Role of drawing-induced residual stresses and strains in the hydrogen embrittlement susceptibility of prestressing steels. Corros. Sci. **10**, 3346–3355 (2011)
31. Vilchevskaya, E., Freidin, A.: On kinetics of chemical reaction fronts in elastic solids. Surf. Eff. Solid Mech. 105–117 (2013)
32. Vilchevskaya, E., Freidin, A., Morozov, N.: Chemical reaction front kinetics in spherically-symmetric problems of mechanochemistry. Dokl. Phys. **60**(4), 175–179 (2015)
33. Wikipedia: LOCOS. https://en.wikipedia.org/wiki/LOCOS (2016)
34. Yen, J.: H., J.G.: Stress effect on the kinetics of silicon thermal oxidation. Appl. Phys. **89**(5), 3027–3032 (2001)

Structural Transformations of Material Under Dynamic Loading

D. A. Indeitsev, B. N. Semenov, D. Yu. Skubov and D. S. Vavilov

Abstract The present paper is devoted to a two-component model of material with nonlinear interaction force, which describes the dynamics of crystalline lattice transformation under shock-wave loading. The governing equations are written for the center of mass displacement and relevant displacement of the components, which is considered to be an internal degree of freedom, responsible for structural transformations. Basing on the analogy between the continuum equations and the corresponding discrete model, we carry out the investigation of the quenching of a non-stationary wave due to the dissipation of energy into structural conversions and estimate the duration of this process. The obtained analytical results are confirmed by the numeric calculations performed by finite difference method.

1 Introduction

At present one of the main tools for studying properties of materials under dynamic deformation is the shock-wave loading of the samples performed by metal impactors, accelerated by explosion or gas gun to velocities varying from hundreds of m/s to several km/s. The scheme of generation and registration of shock waves is presented in Fig. 1.

In these experiments the particle velocity on the back side of the sample is measured by the interferometer. A round plate with a thickness of 2–15 mm is

D. A. Indeitsev · B. N. Semenov · D. Yu. Skubov · D. S. Vavilov (✉)
Institute for Problems in Mechanical Engineering, V.O., Bolshoj pr., 61, 199178 St. Petersburg, Russia
e-mail: londr@yandex.ru

D. A. Indeitsev · B. N. Semenov
St. Petersburg University, Universitetskaya Emb., 13B, 199034 St. Petersburg, Russia

D. A. Indeitsev · B. N. Semenov · D. Yu. Skubov
St. Petersburg Polytechnic University, Polytechnicheskaya, 29, 195251 St. Petersburg, Russia

D. S. Vavilov
Mozhaisky Military Space Academy, Jdanovskaya 13, 197198 St. Petersburg, Russia

F. dell'Isola et al. (eds.), *Advances in Mechanics of Microstructured Media and Structures*, Advanced Structured Materials 87,
https://doi.org/10.1007/978-3-319-73694-5_11

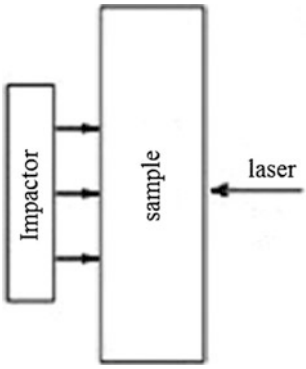

Fig. 1 Scheme of generation and registration of shock waves

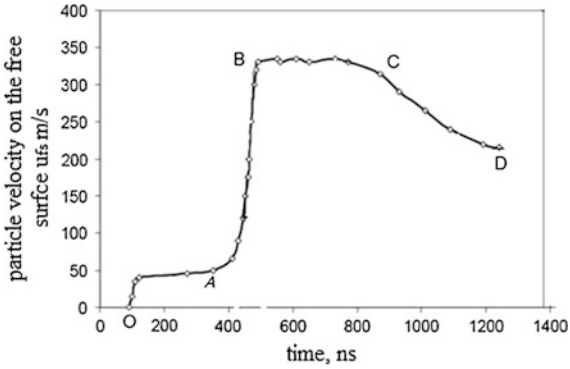

Fig. 2 Typical time profile

usually used for this purpose. Its diameter is chosen in such way that the deformation can be considered as uniaxial. A typical time profile of the particle velocity of a metal sample is depicted in Fig. 2 [1].

It consists of four main sections: the OA curve is an elastic precursor, after which the plastic front AB begins to develop, then the dependence goes to the plateau BC, where the velocity remains almost constant, and finally, the unloading front (section CD) follows. The velocity profile contains the key information about the dynamic properties of the material. It allows to calculate such important characteristics as the spall strength [2] and the dynamic yield strength, and to investigate the question of their dependence on temperature [3, 4]. It is also often used to construct the constitutive equations, to create phenomenological models of deformation and fracture [5, 6] or, conversely, to compare an experimental data with predictions of a mathematical model [7].

One of the interesting and promising directions in the mechanics of solids is the studying of the phase transition of material at high deformation rates, when a complex rearrangement of the crystal structure occurs in extremely short times not exceeding several microseconds [8, 9]. With the help of micro structural analysis, it was established that in a certain range of impactor velocities, propagation of the

shock wave leads to nucleation of reticulate structures of 0.1–0.3 μm in diameter that do not disappear after removal of the stress [10]. It was shown that grains with this structure have a higher hardness than the "pure" material, resulting in increasing of the spall strength. At the macro level, the process of structure formation is revealed through energy losses, which can be observed experimentally. The point is that in case of their absence when the wave impedances of the impactor and the target are equal, the particle velocity is two times less than the velocity of the impactor. On the other hand, it is well known that the doubling of the particle velocity takes place on the free surface. Thus, in the ideal case $U_{imp} = U_{fs}$. This ratio is satisfied up to a certain critical value of the impact velocity, however, with its further increase, it is violated and a so-called velocity defect is formed $U_{def} = U_{imp} - U_{fs}$ (Fig. 3). Its appearance is caused by the existence of the energy threshold of the structural instability of the crystal lattice [1].

It turns out that in a certain range of impacts, a significant part of the energy is spent on the transformation of the internal structure. This process is usually accompanied by rapid oscillations on the plastic front (Fig. 4), which appear immediately after the propagation of an elastic precursor.

Their duration doesn't exceed 0.15–0.3 μs. They indicate that the transformation of the structure is a complex dynamic process involving several scale levels [11]. Note that this result was obtained for a wide class of metallic materials. It indicates the necessity of creating models which take into account the transition of material to a new state.

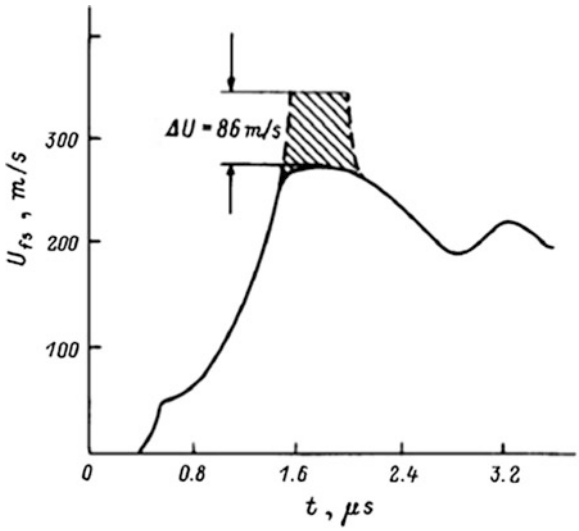

Fig. 3 Velocity defect on the time profile

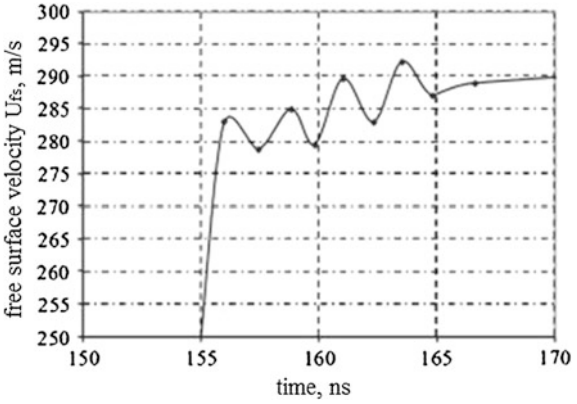

Fig. 4 Oscillations on the plastic front

2 Two-Component Model

Consider a two-component medium [12] consisting of two almost similar lattices, connected by nonlinear interaction force. Suppose that its analytical expression contains two terms

$$R = R_1(u_1 - u_2) + R_2(\dot{u}_1 - \dot{u}_2) \tag{2.1}$$

The first one is determined by nonlinear elastic force and the second one describes the dissipation. Here $u_k (k = 1, 2)$ denotes the displacement of each component. Defining the unknown functions R_1 and R_2, we should consider the possibility of internal transformations. It means, that nonlinear force is obliged to have several equilibrium positions. Besides that, it should take into account the periodicity of crystalline structure. Then one of the simplest variants for function is

$$R = K \sin \lambda z + \nu \dot{z}, \tag{2.2}$$

where K defines its maximum value and ν characterizes dissipation. The parameter $\lambda = \frac{2\pi}{d}$ is inversely proportional to the period of the lattice d. The role of internal degree of freedom is performed by the relative displacement of the components $z = u_1 - u_2$, while the center of mass displacement $U = \frac{\rho_{10} u_1 + \rho_{20} u_2}{\rho_{10} + \rho_{20}}$ [13] is considered to be a measurable macro-parameter. If Hooke's law $\sigma_k = E_k \frac{\partial u_k}{\partial x}$ $(k = 1, 2)$ is valid, then after introducing dimensionless variables $\tilde{x} = \frac{x\omega}{c_1}$, $\tilde{t} = \omega t$, $\tilde{U} = U\lambda$, $\tilde{z} = z\lambda$, $\tilde{\sigma} = \frac{c_1 \lambda \sigma}{\omega^* (E_1 + E_2)}$, $\tilde{\nu} = \frac{\nu \omega^*}{K\lambda}$, where $\omega^* = c_1 \sqrt{\frac{(1 - \chi\delta) K\lambda}{(1 - \chi) E_1}}$ and $\sigma = \sigma_1 + \sigma_2$, one can write governing equations in 1D case as

$$\begin{aligned}&\frac{\partial^2\widetilde{U}}{\partial\tilde{x}^2}-\frac{1}{c_u^2}\frac{\partial^2\widetilde{U}}{\partial\tilde{t}^2}=\alpha\frac{\partial^2\tilde{z}}{\partial\tilde{x}^2}\\&\frac{\partial^2\tilde{z}}{\partial\tilde{x}^2}-\frac{1}{c_z^2}\frac{\partial^2\tilde{z}}{\partial\tilde{t}^2}=\sin\tilde{z}+\tilde{\nu}\dot{\tilde{z}}+\delta\frac{\partial^2\widetilde{U}}{\partial\tilde{t}^2}\end{aligned}. \tag{2.3}$$

Here the following notation is used: $c_u^2=\frac{(1-\chi\delta)}{1-\delta}$, $c_z^2=\frac{1}{1-\chi\delta}$, $\alpha=\frac{(1-\chi)\chi\delta}{1-\chi\delta}$. The sound velocity of the first component is signified as $c_1=\sqrt{\frac{E_1}{\rho_1}}$, the coefficient $\chi=\frac{\rho_1}{\rho_1+\rho_2}$ denotes its mass fraction and the small parameter $\delta=1-\frac{c_1^2}{c_2^2}$ characterizes the difference in physical properties of the lattices. Further, for example, we assume that $\chi=1/2$ and $\delta=0.1$. Equation (2.3) with zero initial conditions are considered in the semi-finite region $0\le\tilde{x}<\infty$. The stress on the boundary $\tilde{x}=0$ is given in the form of the short rectangular pulse $\tilde{\sigma}_{imp}(\tilde{t})=\tilde{\sigma}_0(H(\tilde{t})-H(\tilde{t}-\tilde{t}_0))$ of $\tilde{t}_0$ duration. Here $H(\tilde{t})$ is the unit step function. If we suppose that the stress on the boundary is distributed proportionally to the density of the components, then the boundary conditions for Eq. (2.3) have the form

$$\begin{aligned}&\left.\frac{\partial\widetilde{U}}{\partial\tilde{x}}\right|_{\tilde{x}=0}=\tilde{\sigma}_{imp}(\tilde{t})\left(1+\frac{\chi(1-\chi)\delta^2}{1-\delta}\right)\\&\left.\frac{\partial\tilde{z}}{\partial\tilde{x}}\right|_{\tilde{x}=0}=\frac{\tilde{\sigma}_{imp}(\tilde{t})\delta}{1-\delta}\end{aligned}. \tag{2.4}$$

The standard type of boundary conditions is applied at infinity: $\tilde{U}\big|_{\xi\to\infty}=0$, $\tilde{z}\big|_{\xi\to\infty}=0$. Neglecting the terms of order δ, it is possible to present the initial boundary value problem as

$$\begin{aligned}&\frac{\partial^2\widetilde{U}}{\partial\tilde{x}^2}-\frac{\partial^2\widetilde{U}}{\partial\tilde{t}^2}=\frac{\delta}{4}\frac{\partial^2\tilde{z}}{\partial\tilde{x}^2}\\&\frac{\partial^2\tilde{z}}{\partial\tilde{x}^2}-\frac{\partial^2\tilde{z}}{\partial\tilde{t}^2}=\sin\tilde{z}+\nu\dot{\tilde{z}}+\delta\frac{\partial^2\widetilde{U}}{\partial\tilde{t}^2}\\&\left.\frac{\partial\widetilde{U}}{\partial\tilde{x}}\right|_{\tilde{x}=0}=\tilde{\sigma}_{imp}(\tilde{t})\\&\left.\frac{\partial\tilde{z}}{\partial\tilde{x}}\right|_{\tilde{x}=0}=\tilde{\sigma}_{imp}(\tilde{t})\delta\end{aligned}. \tag{2.5}$$

The graph of dispersions curves for system (2.5), described by the equation

$$\omega^4-\omega^2\left(2k^2+1\right)+k^4+k^2=0, \tag{2.6}$$

where k is the wave number and ω signifies the frequency, is depicted in Fig. 5.

It consists of two branches. The lower one corresponds to the center of mass displacement, and the upper one—to the relative motion. Its dynamics is described with the second equation of system (2.3). It is represented by the nonlinear Klein-Gordon equation complemented by additional term, which expresses the influence of inertia forces. This equation plays an important role in the theory of nonlinear waves, since it is very often used in different types of applications [14, 15], such as physics of dislocations, simulation of seismic phenomena, the description of Josephson junctions and etc. The exact solution for Eq. (2.5) can be easily obtained

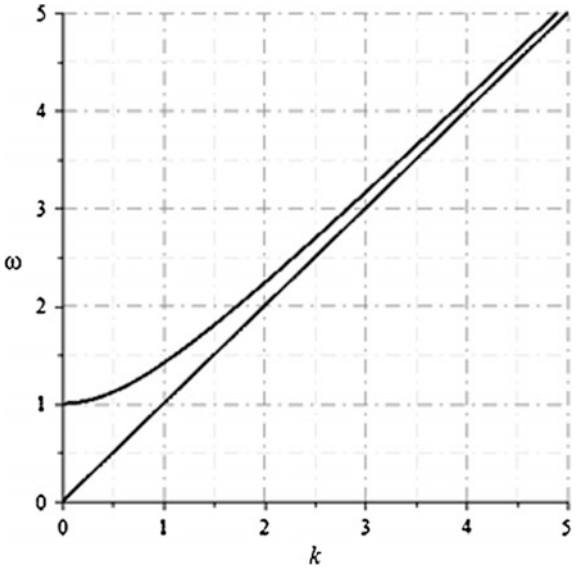

Fig. 5 Dispersion curves

for stationary waves of soliton type, but here we deal with the Cauchy problem and, therefore, it seems reasonable to think about applying numeric methods. However, a considerable difficulty exists in defining the values of parameters for numeric solution and providing the estimation of time required for the system to reach the desired state. In this regard, there is an urgent necessity for the approximate analytical expressions, allowing at least qualitatively to predict dynamics of the model and to separate the physical phenomena from the effects brought by applying numerical integration.

3 Discrete Model

For describing structural transformations we suggest to apply the method of variable interval [16]. This method is similar to Galerkin procedure, but in contrast to the traditional approach the length of the interval, where the expansion is carried out, is unknown function of time. For hyperbolic equations this function coincides with the region covered by wave perturbation. The method of variable interval turns out to be productive for construction of approximate solutions of non stationary problems. Finally, a continuous problem is reduced to the ordinary equations describing dynamics of a single element from the rheological model of material. For one-component medium this element is represented by a spring pendulum, whereas in the present case it is the nonlinear system of the coupled oscillators (Fig. 6) with close natural frequencies.

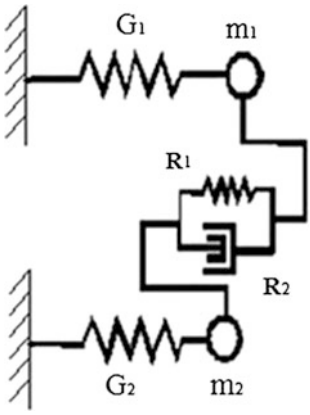

Fig. 6 Coupled oscillators

If their masses are equal, their behavior is described with the following system of equations:

$$\begin{aligned} &\ddot{x}+x=\tfrac{\delta z}{4} \\ &\ddot{z}+n\dot{z}+z+\kappa\,\sin z=\delta x \end{aligned}. \tag{3.1}$$

The center of mass displacement $x=\frac{1}{2}(x_1+x_2)$ and the relative displacement $z=x_1-x_2$ are introduced analogously to Eq. (2.3). Differentiating in (5) is performed by the dimensionless time $\tau=\omega_1 t$, where $\omega_1=\sqrt{\frac{G_1}{m_1}}$ is one of the partial frequencies. Small parameter $\delta=\frac{\omega_2^2-\omega_1^2}{\omega_1^2}$ is equal to their relative difference. The coefficient κ describes the nonlinear interaction between the masses. Subsequently, it is assumed that it is equal to the minimum value $(\kappa=1)$, providing non-convexity for potential energy of z. Initial velocity V_0 is given in order to disturb the system from equilibrium position. If V_0 is small, there is no interaction between two degrees freedom. But when it exceeds the critical value, the dynamics of the system changes dramatically. The oscillations of x, obtained by numerical integration at $n=0.022$ are depicted in Fig. 2 by dashed line.

The specific feature of the process for sufficiently large value of V_0 is the time point separating two different regimes. Note that the amplitude of oscillations at the second one is reduced in comparison with initial value. In order to obtain an analytical expression demonstrating this effect, let us suppose that the process of switching happens immediately at the point τ_*. Then the nonlinear term in Eq. (3.1) can be written as $\kappa_0 \sin z\delta_0(\tau-\tau_*)$, where $\delta_0(\tau)$ signifies delta function. The parameters τ_* and κ_0 are found by means of Laplace transform. Under the accepted assumptions the solution of system (3.1) in the image space has the form

$$x^L(p) = \frac{(p^2+1)V_0 - \delta/4\,\kappa_0 \sin z(\tau_*) e^{-p\tau_*}}{(p^2+1)^2 - \delta^2/4}$$
$$z^L(p) = \frac{V_0\delta - (p^2+1)\kappa_0 \sin z(\tau_*) e^{-p\tau_*}}{(p^2+1)^2 - \delta^2/4} \tag{3.2}$$

To switch the regime of oscillations we should leave only one of the natural frequencies. Such situation is possible if one of the poles of the function $x^L(p)$ coincides with the root of the numerator. This requirement leads to the following expressions for unknown parameters:

$$\tau_* = \frac{\pi k}{1 - \varepsilon/4} \tag{3.3}$$

$$\kappa_0 \sin z(\tau_*) = (-1)^{k+1} 2V_0, \tag{3.4}$$

where k is integer. Its value can be determined from energy balance, if we equate the work of the friction forces on the time interval $[0, \tau_*]$ to the energy jump at τ_* in the problem with delta function. With the selected values of parameters $k = 27$. The analytical solution obtained by taking the inverse Laplace transform is presented in Fig. 7. by solid line. It correlates well with the result of numeric integration.

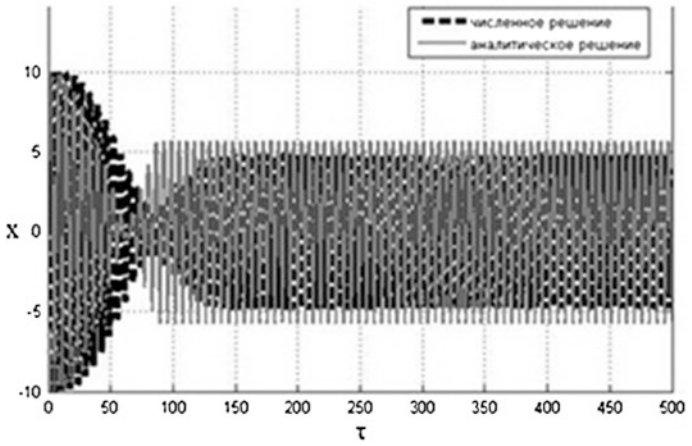

Fig. 7 Center of mass oscillations

4 Continuous Model

After the process of energy transition was demonstrated in the oscillator, it is quite reasonable to expect the same effect in continuous model. However, talking about continuum immediately raises a number of additional issues. The first and foremost is the determination of the distance, at which the structural transformation takes place. The evaluation of this parameter is a problem of great importance both for experiment and numeric simulation. Let us apply the method of variable interval for Eq. (2.5), seeking their solution as $\widetilde{U} = \sum_{n=1}^{N} Q_n(\tilde{t}) \cos\frac{\pi(2n+1)\tilde{x}}{2l} H(l-\tilde{x})$, $\tilde{z} = \sum_{n=1}^{N} q_n(\tilde{t}) \cos\frac{\pi(2n+1)\tilde{x}}{2l} H(l-\tilde{x})$. After multiplying them by the form and integrating between 0 and $l=\tilde{t}$ we obtain the system of equations for the functions $Q(t)$ and $q(t)$

$$\begin{aligned} &\ddot{Q} + \Omega^2 Q = \tfrac{\Omega^2 \delta q}{4} - \tfrac{2\sigma_{imp}(\tilde{t})}{lm^2} \\ &\ddot{q} + \nu\dot{q} + \Omega^2 q + 2J_1(q) = -\delta\ddot{Q} - \tfrac{2\sigma_{imp}\delta}{l} \end{aligned}, \tag{4.1}$$

where $\Omega = \frac{\pi(2n+1)}{2l}$ is the frequency of the corresponding form. Here $J_1(q)$ denotes Bessel function of the first kind. After excluding $\ddot{Q}$ from the second equation and introducing dimensionless time $\tau = \Omega t$ the system (4.1) can be written as

$$\begin{aligned} &\ddot{Q} + Q = \tfrac{\delta q}{4} - \tfrac{2\sigma_{imp}(\tau/\Omega)}{\Omega^2 lm^2} \\ &\ddot{q} + \tfrac{\nu}{\Omega}\dot{q} + q + \tfrac{2}{\Omega^2} J_1(q) = \delta Q \end{aligned}. \tag{4.2}$$

These equations resemble the equations of the discrete model. Therefore, all the transformations that were carried out with Eq. (3.1) are applicable to system (4.2). Using instead of external loading delta function $\delta_0(t)$ in the right part of the first equation, we obtain:

$$\begin{aligned} &\ddot{Q} + Q = \tfrac{\delta q}{4} - \tfrac{2\sigma_{imp}(\tau/\Omega)}{\Omega^2 lm^2} \\ &\ddot{q} + \tfrac{\nu}{\Omega}\dot{q} + q + \tfrac{2}{\Omega^2} J_1(q) = \delta Q \end{aligned}. \tag{4.3}$$

The parameter τ_* in the discrete model has been found by using condition (3.3) of leaving only one natural frequency in the system of coupled oscillators. This condition for Eq. (4.3) is preserved, where as the analogue of expression (3.4) has the form

$$-\frac{2\sigma_0}{l} = \frac{(-1)^k J_1(q(\tau_*))}{\Omega}, \; k = 1, 2, \; \ldots \tag{4.4}$$

Here the role of parameter that determine the magnitude of momentum, required for switching the system form one regime to another, is carried out by the distance

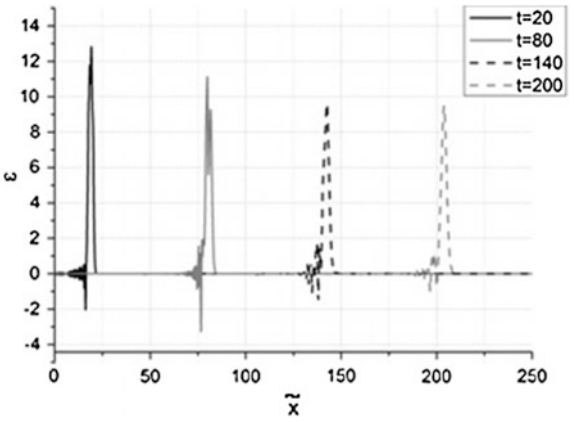

Fig. 8 Strain distribution

at which the structural transformation starts. It follows from relation (4.4) that this distance can be estimated by

$$l_* = \tau_* \sqrt{-\frac{(-1)^k}{\sin\frac{\delta\tau_*}{4}\cos\tau_*}} \tag{4.5}$$

Substituting $\delta = 0.1$, $k = 27$ one can find, that $l_* \approx 127$. The obtained result is confirmed by numeric calculation performed by finite difference method. The strain distribution, demonstrating the reduction of initial pulse is depicted in Fig. 8. The transition of the relevant displacement to the new equilibrium, which is treated in the model as a structural transformation, is demonstrated in Fig. 9.

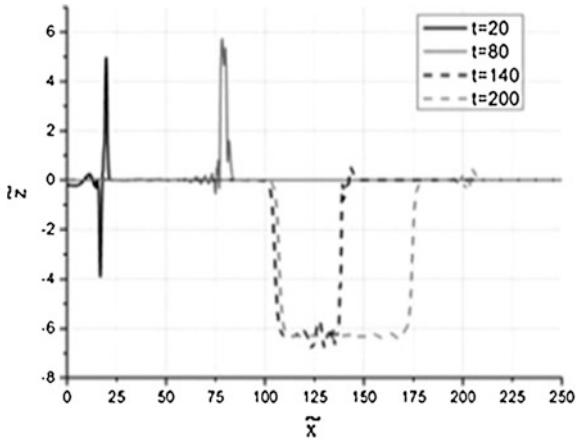

Fig. 9 Distribution of the relevant displacement

5 Conclusion

The present paper is devoted to investigation of structural transformations in solids under mechanical impact. The consideration is based on two-component model with nonlinear interaction force, which takes into account a periodic structure of the lattice. On macro-level this process is revealed through energy transfer to internal degree of freedom, which is represented by the relative displacement of the components. The investigation of the problem is performed by reducing the equations of continuous medium to dynamics of the single element from its rheological model. Such approach allows to estimate the duration of structural transformations and to demonstrate the quenching of non-stationary wave due to latent degrees of freedom. Also it is shown that the relative displacement takes another equilibrium position, corresponding to a new state of material.

References

1. Mescheryakov, Y.I., et al.: Dissipative structures in copper under impact deformation. Phys. Mesomech. **10**(5–6), 275–280 (2007)
2. Grady, D.E.: The spall strength of condensed matter. J. Mech. Phys. Solids **36**(3), 353–384 (1988)
3. Petrov, Y.V., Sitnikova, Y.V.: Temperature dependence of spall strength and the effect of anomalous temperatures in shock-wave loading. Tech. Phys. **50**(8), 1034–1037 (2005)
4. Kanel, G.I., Razorenov, S.V.: Anomalies in the temperature dependences of the bulk and shear strength of aluminum single crystals in the submicrosecond range. Phys. Solid State **43** (5), 871–877 (2001)
5. McQueen, R.G., et al.: The equation of state of solids from shock wave studies. High Velocity Impact phenom. 293 (1970)
6. Morozov, N.F., Petrov, Y.V.: Incubation time based testing of materials. Eur. J. Mech. A/ Solids **25**(4), 670–676 (2006)
7. Indeitsev, D.A., et al.: Multi-scale model of steady-wave shock in medium with relaxation. Acta Mech. **226**(3), 917–930 (2015)
8. Duvall, G.E., Graham, R.A.: Phase transitions under shock-wave loading. Rev. Mod. Phys. **49** (3), 523 (1977)
9. Hixson, R.S., et al.: Acoustic velocities and phase transitions in molybdenum under strong shock compression. Phys. Rev. Lett. **62**(6), 637 (1989)
10. Meshcheryakov, Y.I., et al.: Dynamic structures in shock-loaded copper. Phys. Rev B **78**(6) (2008)
11. Barakhtin, B.K., Meshcheryakov, Y.I., Savenkov, G.G.: Dynamic and fractal properties of SP-28 steel under high-rate loading. Zh. Tekh. Fiz. **68**(10), 43–49 (1998)
12. Indeitsev, D.A., Naumov, V.N., Semenov, B.N.: Dynamic effects in materials of complex structure. Mech. Solids **42**(5), 672–691 (2007)
13. Aero, E.L., Bulygin, A.N.: Strongly nonlinear theory of nanostructure formation owing to elastic and nonelastic strains in crystalline solids. Mech. Solids **42**(5), 807–822 (2007)
14. Braun, O.M., Kivshar, Y.: The Frenkel-Kontorova model: concepts, methods, and applications. Springer Science & Business Media (2013)
15. Dehghan, M., Shokri, A.: Numerical solution of the nonlinear Klein-Gordon equation using radial basis functions. J. Comput. Appl. Math. **230**(2), 400–410 (2009)
16. Slepian, L.I.: Non-stationary elastic waves (1972)

One-Dimensional Heat Conduction and Entropy Production

A. M. Krivtsov, A. A. Sokolov, W. H. Müller and A. B. Freidin

Abstract This review paper analyzes the entropy concept and the second law of thermodynamics in the context of one-dimensional media. For simplicity, only thermal processes are taken into account and mechanical motions are neglected. The relation between entropy and temperature and the constraints on the direction of the heat flux are discussed. A comparison with the approach of P. A. Zhilin and the approach based on statistical mechanics is presented. The obtained conclusions are applied to three models: classical, hyperbolic and ballistic heat conduction. It is shown that the concept according to which heat flows from hot to cold is consistent only with the classical model. The peculiarities of the entropy definition and the second law of thermodynamics formulation for non-classical systems are discussed.

A. M. Krivtsov · A. A. Sokolov (✉) · A. B. Freidin
Peter the Great Saint Petersburg Polytechnic University,
Politekhnicheskaya str. 29, St. Petersburg, Russia
e-mail: sokolovalexey1@gmail.com

A. M. Krivtsov
e-mail: akrivtsov@bk.ru

A. B. Freidin
e-mail: alexander.freidin@gmail.com

A. M. Krivtsov · A. B. Freidin
Institute for Problems in Mechanical Engineering, Russian Academy of Sciences,
V.O., Bolshoj pr., 61, St. Petersburg, Russia

A. A. Sokolov · W. H. Müller
Technische Universität Berlin, Einsteinufer 5, 10587 Berlin, Germany
e-mail: wolfgang.h.mueller@tu-berlin.de

A. B. Freidin
St. Petersburg University, Universitetsky Pr. 28, Peterhof, St. Petersburg, Russia

F. dell'Isola et al. (eds.), *Advances in Mechanics of Microstructured Media and Structures*, Advanced Structured Materials 87,
https://doi.org/10.1007/978-3-319-73694-5_12

1 Introduction

The concept of entropy is one of the most ambiguous in connection with the description of thermal processes. The reason for this is that there is no unique approach for analysis of non-equilibrium thermal processes. Therefore in this work we analyze thermal processes by using one of the simplest models: a homogeneous one-dimensional medium without mechanical motions. In this case, the equation of the energy balance can be written in the form

$$\rho \dot{U} = -h', \tag{1}$$

where ρ is the density, U is the (specific) internal (in the present case purely thermal) energy, h is the heat flux, the dot and the prime denote the time and spatial derivatives, respectively. In our case the thermal energy depends only on temperature T, thus

$$\dot{U} = c_V \dot{T}, \tag{2}$$

where c_V is the specific heat capacity at constant volume. If the temperature deviations are small, then the heat capacity can be treated as a constant. The relation between the heat flux and the temperature is usually described by Fourier's law [1, 2]:

$$h = -\kappa T' \quad \Rightarrow \quad \dot{T} = \beta T'' \tag{3}$$

As a result, we obtain the classical heat conduction equation, where κ is the thermal conductivity coefficient and $\beta = \kappa/(\rho c_V)$ is the thermal diffusivity coefficient. The equation is obtained by substituting Fourier's law together with relation (2) into the energy balance equation (1). The heat equation (3) describes the diffusive propagation of heat. It is widely used, but it has a number of drawbacks, such as an absence of a thermal front and an infinite speed of a signal propagation. This problem can be avoided by modification of Fourier's law, which leads to the equation of hyperbolic heat conduction (Maxwell, Cattaneo, Veronotte, Lykov) [3, 4]

$$\dot{h} + \frac{1}{\tau} h = -\frac{\kappa}{\tau} T' \quad \Rightarrow \quad \ddot{T} + \frac{1}{\tau} \dot{T} = \frac{\beta}{\tau} T''. \tag{4}$$

However, in this equation, another problem arises. It is difficult to provide an accurate physical interpretation and calculation of the relaxation time τ. Another alternative to Fourier's law leads to the equation of ballistic heat propagation [5]:

$$\dot{h} + \frac{1}{t} h = -\rho c_V c^2 T' \quad \Rightarrow \quad \ddot{T} + \frac{1}{t} \dot{T} = c^2 T'', \tag{5}$$

where the constant c is the speed of sound in the media. Equation (5) contains the variable physical time t instead of the constant relaxation time τ. The ballistic heat equation (5) describes the evolution of an instantaneous thermal perturbation at $t = 0$

in the most simple model of a one-dimensional harmonic crystal. Such a perturbation can be realized by an ultrafast laser heating [6].

Fourier's law (3) represents the intuitive idea that the heat must flow from hot to cold. Equations (4) and (5) allow for the reverse situation—when the heat flows from cold to hot. The reason for this is that these equations have inertial terms (due to the term $\ddot{T}$). In inertial processes, the direction of the media's reaction does not necessarily coincide with the direction of the external perturbation. However, in this case a serious question arises: does this behavior of the system contradict the second law of thermodynamics? This question is analyzed in the current work.

2 The Simplest Thermodynamics of a One-Dimensional Medium

2.1 Energy Balance Equations

Let us consider the simplest theory for a one-dimensional continuous medium. We only consider the process of heat propagation, neglecting mechanical motions. In this case, the energy balance equation for a certain material volume can be written in the form:

$$\dot{\mathscr{U}} = \mathscr{Q}, \tag{6}$$

where $\mathscr{U}$ is the internal energy of the considered volume, $\mathscr{Q}$ is the rate of heat supply to the system, the dot denotes the time derivative. These quantities can be written in the form:

$$\mathscr{U} = \int_V \rho U \, \mathrm{d}V, \qquad \mathscr{Q} = -\int_\Gamma \nu h \, \mathrm{d}\Gamma + \int_V \rho r \, \mathrm{d}V, \tag{7}$$

where ρ is the density (related to the number of particles per unit volume or length), U is the specific energy (per particle), h is the heat flux, r is the volumetric heat supply, V is the one-dimensional volume (length) of the media, Γ is the boundary, $\nu = \pm 1$ is the one-dimensional normal (the direction indication coefficient).

Since there are no mechanical motions, the volume V does not change and the density ρ is constant. For the one-dimensional crystal it is fulfilled that $\rho = 1/a$, where a is the initial distance between neighboring particles. Following [7] notations V, Γ and ν are used that are analogues of the corresponding quantities for a three-dimensional continuous medium. For a one-dimensional medium the volume V is some interval of the spatial coordinate $x \in [x_1, x_2]$, the boundary Γ are the points x_1 and x_2. The coefficient ν has the values $\nu = -1$ for $x = x_1$ and $\nu = +1$ for $x = x_2$ and is an analogue of the normal vector of the three-dimensional case. Thus, the integrals used in (7) can be written in the form

$$\int_V f \,\mathrm{d}V = \mathrm{d}\int_{x_1}^{x_2} f(x)\,\mathrm{d}x\,, \qquad \int_\Gamma \nu f \,\mathrm{d}\Gamma = f(x)\Big|_{x_1}^{x_2} = \int_{x_1}^{x_2} f'(x)\,\mathrm{d}x. \tag{8}$$

Here the volume integration is replaced by the boundary integration. This replacement is an analogue of the Gauss-Ostrogradsky formula but for the one-dimensional case. Substitution of the quantities (7) to the balance equation (6) with the use of (8) after contracting the domain of integration into a point ($x_1 \to x_2$) yields the differential form for the energy balance equation:

$$\rho\dot{U} = -h' + \rho r, \tag{9}$$

where the prime denotes the derivative with respect to the spatial coordinate x.

2.2 Entropy and the Second Law of Thermodynamics

Entropy is introduced as an additive function of volume:

$$\mathscr{S} = \int_V \rho S \,\mathrm{d}V, \tag{10}$$

where S is the specific entropy (per particle). The rate of entropy change has two components:

$$\dot{\mathscr{S}} = \dot{\mathscr{S}}^i + \dot{\mathscr{S}}^e, \tag{11}$$

where the index i denotes the entropy production due to internal processes in the system, and the index e is related to the change of entropy due to the heat transfer across the boundary. The second term in (11) is defined by the relation

$$\dot{\mathscr{S}}^e = -\int_\Gamma \nu \frac{h}{T} \,\mathrm{d}\Gamma + \int_V \rho \frac{r}{T} \,\mathrm{d}V, \tag{12}$$

where T is the temperature. Formula (12) is based on the principle that an elementary increment of the entropy caused by an external heat supply is equal to an elementary heat transfer to the system divided by the temperature at the considered point: $\delta S^e = \delta Q/T$. For the entropy production due to internal processes in the system there is no analogous definition. The following inequality for the entropy production is postulated instead:

$$\dot{\mathscr{S}}^i \geq 0, \tag{13}$$

which is one of the forms of *the second law of thermodynamics*.

Inequality (13) can also be formulated as [8]:

$$\dot{\mathscr{S}} \geq \dot{\mathscr{S}}^e. \tag{14}$$

According to [8], this relation is the *Clausius-Duhem inequality*. Its formulation reads [8]: The rate of change of the entropy of a material body is not less than the rate of entropy supplied to this body from the outside.[1] Obviously, this formulation is equivalent to formulation (13): the internal production of entropy is non-negative. The formulation (13) is shorter and contains only one concept, so it may be preferable from a methodical point of view.

Substitution of the relations (10)–(12) into the inequalities (13) and (14) with the use of (8) yields

$$\dot{\mathscr{S}}^i = \int_V \left(\rho \dot{S} + \left(\frac{h}{T} \right)' - \rho \frac{r}{T} \right) \mathrm{d}V \geq 0. \tag{15}$$

Since the volume is arbitrary, we obtain the local form of the Clausius-Duhem inequality:

$$\rho \dot{S} + \left(\frac{h}{T} \right)' - \rho \frac{r}{T} \geq 0 \qquad \Longleftrightarrow \qquad \rho T \dot{S} + h' - \rho r - \frac{hT'}{T} \geq 0. \tag{16}$$

2.3 Dissipative Inequality

By using the energy balance equation (9), we transform the inequality (16) to

$$\rho(T\dot{S} - \dot{U}) - \frac{hT'}{T} \geq 0. \tag{17}$$

This inequality can be written in the form of the *universal dissipative inequality* [8]:

$$\boldsymbol{\Phi} - \frac{hT'}{T} \geq 0, \tag{18}$$

where

$$\boldsymbol{\Phi} \overset{\text{def}}{=} \rho(T\dot{S} - \dot{U}) = -\rho(S\dot{T} + \dot{\Psi}) \tag{19}$$

is called dissipative function. The second form of expression (19) contains the (Helmholtz) free energy Ψ:

$$\Psi \overset{\text{def}}{=} U - TS. \tag{20}$$

[1] Literally it is said in [8]: "the rate of change of internal entropy…". However, the word "internal" is used only as an antithesis to entropy coming from outside. Therefore, this notation of "internal entropy" is equivalent to the notation of "entropy" used in the current work. Moreover, one cannot divide the entropy into internal and external. Entropy supply is different—it can be associated with a transfer from outside or with an internal processes. After entropy has entered the system, it "mixes," and it is impossible to divide it into internal and external.

The free energy is widely used in continuum mechanics [8], but in this paper we use the internal energy U, since it enables a clearer physical interpretation in context with the considered problem. Let us consider the universal dissipative inequality (18). It contains the dissipative function Φ and the term hT'/T. When mechanical motions are also taken into account, the dissipative function contains one more term, describing the dissipation of the mechanical energy. The second term characterizes the relation between the direction of the heat flux and the temperature gradient. As it will be shown later, in our case the inequality (18) splits in two relations:

$$\Phi = 0\,, \qquad hT' \le 0. \tag{21}$$

The first of them demonstrates the absence of dissipation in the system. The second one is the the so-called *Fourier's inequality* [8]. According to *Fourier's inequality* [8] the direction of the heat flux is opposite to the temperature gradient.

2.4 Constitutive Equation

Let the internal energy be a function of the entropy. Then we have:

$$U = U(S) \quad \Rightarrow \quad \dot{U} = \frac{\mathrm{d}U}{\mathrm{d}S}\,\dot{S}. \tag{22}$$

Substituting of this expression to inequality (17) yields

$$\rho\left(T - \frac{\mathrm{d}U}{\mathrm{d}S}\right)\dot{S} - \frac{hT'}{T} \ge 0. \tag{23}$$

Assuming that T and U do not depend on $\dot{S}$, and that $\dot{S}$ can take arbitrary values,[2] we obtain from (23):

$$T = \frac{\mathrm{d}U}{\mathrm{d}S}\,, \qquad hT' \le 0. \tag{24}$$

The first expression gives the relation between the internal energy, entropy and temperature, the second inequality (Fourier's inequality) means that heat flows in the direction opposite to the temperature gradient (from hot to cold).

Let us suppose that the temperature deviations are small so that the heat capacity can assumed to be a constant. Postulating further that the internal energy is a function of temperature, we obtain:

$$\mathrm{d}U = c_V \mathrm{d}T, \tag{25}$$

[2] Due to external heat supply (12) any value for quantity $\dot{S}$ can be realized.

where c_V is a constant: the heat capacity of the medium at a constant volume.[3] Furthermore we will show later in (43) that in the case of a harmonic crystal $c_V \equiv k_B$. Substituting (25) into (24), we obtain that:

$$T = c_V \frac{\mathrm{d}T}{\mathrm{d}S} \quad \Rightarrow \quad \dot{S} = c_V \frac{\dot{T}}{T} \quad \Rightarrow \quad S = S_0 + c_V \ln\left(\frac{T}{T_0}\right), \tag{26}$$

where S_0 and T_0 are the initial values of the corresponding quantities in the given spatial point.

Using that $T - T_0 \ll T_0$ and the third equation from (26), we obtain the approximate formula

$$S \approx S_0 + c_V \frac{T - T_0}{T_0}. \tag{27}$$

Note that (26) formally contradicts the third law of thermodynamics [8], which claims that as the absolute temperature tends to zero the entropy should also tend to zero. In our case it is not fulfilled. The reason for this contradiction is that only small deviations of the temperature are considered, so that the heat capacity is treated as a constant. In the general case the heat capacity will tend to zero as the temperature decreases, which allows to fulfill the third law of thermodynamics. However, the specific heat capacity of a harmonic crystal is constant at all temperatures, so this question requires additional analysis.

Let us now consider the second consequence of the second law of thermodynamics, Fourier's inequality: $hT' \le 0$. If Fourier's law (3) is fulfilled we have

$$h = -\kappa T' \quad \Rightarrow \quad hT' = -\frac{1}{\kappa} h^2 \le 0. \tag{28}$$

Thus, to fulfill the second law of thermodynamics the thermal conductivity should be nonnegative. However, for the hyperbolic and for the ballistic heat conduction, Eqs. (4) and (5), respectively, we obtain

$$\dot{h} + \frac{1}{\tau} h = -\frac{\kappa}{\tau} T' \quad \Rightarrow \quad hT' = -\frac{1}{\kappa}\left(h^2 + \frac{\tau}{2}\left(h^2\right)^{\cdot}\right); \tag{29}$$

$$\dot{h} + \frac{1}{t} h = -\rho\, c_V c^2\, T' \quad \Rightarrow \quad hT' = -\frac{1}{\rho\, c_V c^2}\left(h^2 + \frac{t}{2}\left(h^2\right)^{\cdot}\right). \tag{30}$$

In both cases, Fourier's inequality will be satisfied if the absolute value of the heat flux increases. If, however, the absolute value of the heat flux decreases rapidly enough, then the inequality can be violated, and, consequently, heat can flow in the opposite direction: from cold to hot. Thus, the formulation of the second law of thermodynamics in the form presented above is not valid for the hyperbolic and the ballistic heat conduction.

[3] Since there are no mechanical motions, the volume remains unchanged.

2.5 Modification of the Constitutive Equation

The relations (29) and (30) show that Fourier's inequality can be violated for the hyperbolic and ballistic heat conduction. Does this mean a violation of the second law of thermodynamics? Non-equilibrium thermodynamics has possible solutions for this contradiction. Following [9, 10] it can be accepted that the entropy is a function of the internal energy and the heat flux:

$$S = S(U, h^2) \quad \Rightarrow \quad \dot{S} = \frac{\partial S}{\partial U}\,\dot{U} + 2\frac{\partial S}{\partial h^2}\dot{h}h. \tag{31}$$

Here h^2 is used since the entropy does not depend on the heat flux direction (according to the principal of material objectivity). Substituting this relation to the inequality (17) we obtain the following form of the Clausius-Duhem inequality:

$$\rho\left(T\frac{\partial S}{\partial U} - 1\right)\dot{U} + h\left(2\rho T\frac{\partial S}{\partial h^2}\dot{h} - \frac{T'}{T}\right) \geq 0. \tag{32}$$

Applying the approach used in derivation of (24) and assuming that S and T are independent of $\dot{U}$, one obtains

$$\frac{\partial S}{\partial U} = \frac{1}{T}, \qquad h\left(2\rho T^2\frac{\partial S}{\partial h^2}\dot{h} - T'\right) \geq 0. \tag{33}$$

In accordance with (33), the following constitutive equation for the heat flux can be formulated based on a linear thermodynamic approach:

$$h = \kappa\left(2\rho T^2\frac{\partial S}{\partial h^2}\dot{h} - T'\right). \tag{34}$$

Following [9, 10] let us assume that

$$\frac{\partial S}{\partial h^2} = -\frac{\tau}{2\kappa\rho T^2}, \tag{35}$$

where τ is the relaxation time. Then (34) yields the differential relation between the heat flux and the temperature:

$$\dot{h} + \frac{1}{\tau}\,h = -\frac{\kappa}{\tau}\,T', \tag{36}$$

which corresponds to the equation of hyperbolic heat conduction. Substitution of (35) and the first equality from (33) to (31) gives the following equation for the entropy:

$$\dot{S}(U, h) = \frac{1}{T}\,\dot{U} - \frac{\tau}{\kappa\rho T^2}\,\dot{h}h. \tag{37}$$

Thus, the second law of thermodynamics (13) and its consequence—the Clausius-Duhem inequality in the form (16)—were used. Then two assumptions were made: (1) the entropy is a function of the internal energy and the heat flux, (2) relation (35), the form of which was chosen to satisfy the hyperbolic heat equation. This allows to obtain the equation of hyperbolic heat conduction (36) in consistence with the second law of thermodynamics (13).

3 The Approach of P. A. Zhilin

Let us represent the approach of Pavel A. Zhilin [11] to the definition of the entropy in the context of the considered problem. The proposed interpretation of P. A. Zhilin's approach is a personal interpretation of one of the authors of this work (A. M. Krivtsov) and it may differ from other interpretations. Let us consider the energy balance equation (9)

$$\rho \dot{U} = -h' + \rho r. \tag{38}$$

The peculiarity of P. A. Zhilin's approach is that in the general case the arguments of the internal energy are not specified a priori. Instead they should be determined from the energy balance equation. However, this primarily concerns the tensor parameters of state corresponding to the mechanical motion: it is difficult to choose an appropriate form of these parameters without the energy balance equation analysis. In the considered case the mechanical motion is absent, and there is the only one scalar state parameter. Therefore it should be assumed that the internal energy is a function of specific entropy S, then

$$U = U(S) \quad \Rightarrow \quad \dot{U} = T\dot{S}, \qquad T \overset{\text{def}}{=} \frac{\mathrm{d}U}{\mathrm{d}S}. \tag{39}$$

The entropy characterizes the dependence of the internal energy on the ignored degrees of freedom. Temperature is introduced as a coefficient at the entropy time-derivative in the representation of the internal energy time-derivative. Temperature characterizes the energy of the motion via the ignored degrees of freedom. The entropy is the parameter conjugate to the temperature. The temperature is considered as a measurable parameter and the entropy is not. Measurability necessitates the existence of a device (e.g., a thermometer), allowing to measure the considered physical quantity directly.

Thus relation (39)

$$T = \frac{\mathrm{d}U}{\mathrm{d}S} \tag{40}$$

is a consequence of two statements (a) internal energy depends on entropy, (b) temperature is the coefficient at the entropy time-derivative. This is the important difference between P. A. Zhilin's approach and the approaches considered in the previous

sections, where the relation (40) is a consequence of the second law of thermodynamics.

In the approach of P. A. Zhilin the second law of thermodynamics is not considered as a general law of nature. It is replaced by a number of particular laws. The following inequalities are used:

$$\boldsymbol{\Phi} \geq 0\,, \qquad hT' \leq 0. \tag{41}$$

The first inequality (the dissipative function is not negative)[4] means that dissipation always leads to a loss of energy. The second inequality is Fourier's inequality, which represents the experimental fact that the heat always flows from hot to cold—*the zeroth law of thermodynamics*.[5] In the approach presented above, two inequalities are combined in one (18)

$$\boldsymbol{\Phi} - \frac{hT'}{T} \geq 0, \tag{42}$$

—*the universal dissipative inequality* [8], which represents the second law of thermodynamics in the form of Clausius-Duhem.

It is obvious that inequality (42) is a consequence of the inequalities (41), but the reverse is not true. In Ref. [11] the inequality (42) is said to be too weak for practical applications. If we demand that the inequality (41) is the basic assumption, then we need to prove that there are cases when (42) is fulfilled and (41) is not. If this cannot be shown, then the fundamental nature of the universal dissipative inequality (41) may be in doubt.

In the considered problem the mechanical motion is absent and consequently $\boldsymbol{\Phi} \equiv 0$ and the both approaches lead to Fourier's inequality. This inequality, as it was shown above, is not fulfilled for the systems where the heat propagation is inertial. Resolving this contradiction will be different for each approach. From the point of view of P. A. Zhilin's approach, nothing crucial happens if Fourier's inequality is not fulfilled. From this point of view that it is a particular law, its non-fullfillment does not affect any further derivations. Fourier's inequality can be replaced by some other inequality, and maybe even discarded. From the point of view of the approaches based on the second law of thermodynamics, the situation is more complicated. The violation of Fourier's inequality requires modification of the derivation of the universal dissipative inequality. This modification can be obtained either by changing the formulation of the second law, or by introducing additional state variables.

[4] This inequality is sometimes called the Planck inequality or the Clausius-Planck inequality, however, in monograph [11] these terms are not used.

[5] In monograph [11] the term "Fourier's inequality" is not mentioned, instead the term "zeroth law of thermodynamics" is used.

4 Harmonic Crystal

Simple lattice models provide an attractive playground to investigate thermomechanical processes at the microscale [2, 5, 12, 13]. Let us consider the application of the equations obtained above for the model of a one-dimensional harmonic crystal. By considering this model it is possible to derive equations which describe the distribution of heat (5) from the dynamic equations of the lattice [5]. The derivation of these equations does not require the concept of entropy and the second law of thermodynamics. However, this model can be used for testing thermodynamical concepts in the case of nonequilibrium processes.

4.1 Kinetic Temperature

The heat motions in a harmonic crystal are the chaotic oscillations of atoms near their equilibrium positions. The internal energy is the mechanical energy of these oscillations, which can be divided into kinetic and potential parts. The following equations holds:

$$U = K + \Pi\,, \qquad \Pi = K = \frac{d}{2}\,k_B T\,, \qquad d = 1 \quad \Rightarrow \quad U = k_B T. \tag{43}$$

The potential and kinetic energies, Π and K, are equal because: (1) the crystal is harmonic [14], and (2) the process of heat propagation is much slower than the process of energy equalization [15]. Therefore the potential and kinetic energies satisfy the conditions of the virial theorem [16], according to which in a sufficiently long time for a harmonic system these energies should became equal. The relation (43) between the kinetic energy and the temperature is valid because we consider *the kinetic temperature* of the crystal. Comparing relations (43) and (25) we see that the heat capacity for the harmonic crystal is equal to Boltzmann's constant: $c_V = k_B$. Let us note that expression (25) was obtained under the assumption that the temperature has small deviations comparing to it's absolute value. For the harmonic crystal these conditions are not obligatory: there is an explicit relation between the internal energy and the temperature. Therefore, for the harmonic crystal expression (43) has a wider range of applicability than expression (25) for an arbitrary medium.

Substitution of relation (43) between the internal energy and the temperature into Eq. (9) and inequality (17) gives

$$\rho k_B \dot{T} = -h' + \rho r\,, \qquad \rho T\dot{S} - \rho k_B \dot{T} - \frac{hT'}{T} \geq 0. \tag{44}$$

By using the constitutive equations for h and r the first expression yields a closed equation for the heat propagation. In particular, expression (5) for the heat flux in

the harmonic crystal in the absence of volumetric heat input ($r = 0$) [5] results in the equation of the ballistic heat conduction (5):

$$\ddot{T} + \frac{1}{t}\dot{T} = c^2 T''. \tag{45}$$

The inequality in (44) allows to derive an entropy formula in a way similar to (26). It is sufficient to assume that the entropy is a function of the temperature $S = S(T)$. Then the inequality from (44) takes the form

$$\rho\left(T\frac{\mathrm{d}S}{\mathrm{d}T} - k_B\right)\dot{T} - \frac{hT'}{T} \geq 0. \tag{46}$$

Since $\dot{T}$ is arbitrary we obtain

$$T\frac{\mathrm{d}S}{\mathrm{d}T} = k_B\,, \qquad hT' \leq 0. \tag{47}$$

Exactly the same result is obtained if we assume that the temperature is a function of the entropy: $T = T(S)$. The first expression in (47) gives the relation between entropy and the temperature which was considered above. In the case of the harmonic crystal it takes the form

$$S = S_0 + k_B \ln\left(\frac{T}{T_0}\right), \tag{48}$$

where S_0 and T_0 are the initial values of temperature and entropy at a given point in space. Thus, we obtain an explicit relation between temperature and the entropy for each point of the media. The second relation from (47) is Fourier's inequality. In the next section it will be shown that this inequality can be violated for the harmonic crystal. If we limit our consideration to small deviations of temperature T from its initial value T_0 then an approximate formula similar to (27) can be obtained:

$$S \approx S_0 + k_B\frac{T - T_0}{T_0}. \tag{49}$$

In the case considered above, both the logarithmic and the linear equations, (26) and (27), respectively, are approximate. For the harmonic crystal, however, the logarithmic dependence (48) is exact, while the linear relation (49) is valid only for small temperature deviations.

4.2 Direction of the Heat Flux

From the thermodynamic analysis presented above it follows that for a harmonic crystal Fourier's inequality should be fulfilled:

$$hT' \le 0. \tag{50}$$

This means that the direction of the heat flux should be opposite to the temperature gradient. In other words, the heat should flow from hot to cold. However, for a harmonic crystal this condition can either be satisfied or not, depending on the considered initial problem. In [5] it was shown that in the case of instantaneous thermal perturbation the heat propagation in the harmonic crystal is described by equation

$$\dot{h} + \frac{1}{t}\, h = -k_B \rho c^2\, T'. \tag{51}$$

Then we have

$$hT' = -\frac{1}{k_B \rho c^2}\left(h^2 + \frac{t}{2}\left(h^2\right)^{\cdot}\right). \tag{52}$$

From this formula, as well as from formula (30), it follows that for a sufficiently fast decrease of the heat flux Fourier's inequality may be violated. This happens due to the inertial nature of the heat propagation in harmonic crystals, for example, if we solve the ballistic heat equation for a localized temperature distribution (e.g., a rectangular one) [17].

4.3 Entropy for the Harmonic Crystal

For a harmonic crystal the propagation of heat is ballistic—the heat flux can be represented as a superposition of harmonic waves. In addition, the equation of the ballistic heat conduction (45) can be interpreted as reversible in the following sense: it is invariant with respect to replacement of t by $-t$. Let us show, however, that the entropy in the harmonic crystal is not constant. The first of the inequalities shown in Eq. (16) takes the following form in the case of constant entropy ($\dot{S} = 0$) and zero volumetric heat supply ($r = 0$)

$$\left(\frac{h}{T}\right)' \ge 0. \tag{53}$$

This means that the ratio h/T is not decreasing with x. But this is in contradiction with the problem symmetry: both positive and negative directions of x axis are equivalent from the symmetry point of view.

Let us show the violation of the inequality (53) in a particular case, a sinusoidal initial temperature field, $T_0(x) = A \sin \kappa x + B$, where A and B are positive constants with the dimension of temperature, κ is the wave number. In this case the inequality (53) can be satisfied only if h/T is constant. However, according to [5] the solution for the sinusoidal initial temperature distribution has the form:

$$T(t,x) = AJ_0(\kappa ct)\sin \kappa x + B\,, \qquad h(t,x) = -Ak_B \rho c J_1(\kappa ct)\cos \kappa x. \tag{54}$$

Substitution of these formulae to (53) yields

$$\frac{h}{T} = -\frac{Ak_B\rho c J_1(\kappa ct)\cos\kappa x}{AJ_0(\kappa ct)\sin\kappa x + B} \neq \text{const}. \tag{55}$$

Here c is the speed of sound in the harmonic crystal, J_n is the Bessel function. Thus, these contradictions prove that the entropy of the harmonic crystal generally is not constant.

5 Statistical Mechanics

Further above the relation (48) between the entropy and the temperature for a harmonic crystal and Fourier's inequality $hT' \leq 0$ were obtained. In general, Fourier's inequality is not satisfied for the harmonic crystal. This questions the applicability of the formula (45) for the entropy. However, this formula can also be obtained from statistical mechanics [18]:

$$S = k_B \ln\left(\frac{2\pi eU}{h_P\,\omega_e}\right), \tag{56}$$

where S is the specific entropy, U is the specific heat energy, e is Euler's number, h_P is Planck's constant, and ω_e is the elementary frequency.[6] This formula was obtained on the basis of the Boltzmann principle, which relates entropy to the logarithm of the number of possible microstates of the macroscopic system. Equation (56) is derived analytically for a one-dimensional thermodynamically equilibrated harmonic crystal with fixed boundary conditions. By assuming in accordance with (43) that $U = k_B T$ we obtain from (56)

$$S = k_B \ln T + C\,, \qquad C \overset{\text{def}}{=} \ln\left(\frac{2\pi ek_B}{h_P\,\omega_e}\right). \tag{57}$$

This formula is obtained from statistical mechanics. From a thermodynamical approach the similar formula (48) can be obtained:

$$S = k_B \ln T + C\,, \qquad C \overset{\text{def}}{=} S_0 - k_B \ln T_0. \tag{58}$$

Formulae (57) and (58) are equal if the initial entropy and temperature are related by (57). Then the initial entropy can be defined as

$$S_0 = k_B \ln\left(\frac{2\pi ek_B T_0}{h_P\,\omega_e}\right). \tag{59}$$

[6] $\omega_e = \sqrt{C/m}$: the frequency of a particle with the mass m on a spring with the stiffness C, which is $C = \Pi''(a)$, where Π is the potential of the atomic interaction, a is the lattice step.

Thus, statistical mechanics confirms the relation between the entropy and the temperature, Eq. (26), which was obtained above by the thermodynamical approach.

6 Conclusions and Closing Remarks

In the paper, three approaches to the definition of the entropy are considered:

1. The classical thermodynamics approach based on the Clausius-Duhem inequality [8].
2. The approach by P. A. Zhilin [11].
3. The approach of classical statistical mechanics [18].

For the considered system, all three approaches lead to the same differential relation connecting the temperature T, the specific internal energy U, and the specific entropy S:

$$T = \frac{\mathrm{d}U}{\mathrm{d}S}. \tag{60}$$

If the heat capacity c_V is constant, the relation (60) between entropy and temperature is:

$$S = c_V \ln T + C, \tag{61}$$

where C is a constant determined by the initial values S and T at a given point in space. Furthermore, the first approach leads to Fourier's inequality:

$$hT' \leq 0, \tag{62}$$

which means that the heat flux h has the direction in which the temperature decreases. This inequality holds for the classical model of heat conduction (3), but it is in contradiction with models that describe inertial heat transport, such as the hyperbolic (4) or the ballistic (5) heat conduction. In these models the heat can flow in the direction of the temperature increase (form cold to hot). This could be an argument against these models. On principle this could question Eq. (4), which is empirical. But Eq. (5) is analytically derived from the dynamics of the crystal lattice and it is a strict mathematical consequence of the equations of the lattice dynamics.

There are two possible solutions to avoid this contradiction, namely, a change of the formulation of the second law of thermodynamics or consideration of additional state variables. Another explanation, according to P. A. Zhilin, is that the second law of thermodynamics is not a general law. Instead of it, he formulates a set of particular laws, such as Fourier's inequality (61). If this inequality is not fullfilled for specific systems, it is not crucial and shows the peculiarity of such systems. However, for the classical approach, the violation of (61) is critical, since it questions the second law of thermodynamics, which is fundamental for this approach.

Let us introduce possible ways of eliminating this contradiction. It can be made by introduction of additional state variables.

- In Sect. 2.5 it was shown that if the entropy is a function of the fluxes, second law of thermodynamics in the formulation (13) is satisfied. This approach, by choosing the expression for $\partial S/\partial h^2$ (relation (35)), allows to obtain different models of heat conduction. In book [9] the mentioned above variant is analysed, which leads to the hyperbolic heat conduction equation.
- It was shown in [5] that a full description of the thermal processes in a harmonic crystal requires the consideration of an infinite number of generalized (nonlocal) temperatures, in addition to the kinetic temperature. So it makes sense to assume that the entropy of a harmonic crystal also depends on generalized temperatures.
- When we consider slow motions (which are associated with heat propagation), fast processes are neglected. This leads to equalization of kinetic and potential energies. This is also an irreversible process, which leads to the entropy increase.

One of these approaches can be possible solution in order to fulfill the second law of thermodynamics in the considered models of heat conduction.

In conclusion, we want to discuss the concept of irreversibility. The equations of the classical and the hyperbolic heat conduction, Eqs. (4) and (5), respectively, are not invariant with respect to reversing time (the substitution of t by $-t$). This makes them different from, for example, the wave equation. It is usually accepted that this is directly connected with irreversibility of these equations. However, the equation of the ballistic heat conduction

$$\ddot{T} + \frac{1}{t}\,\dot{T} = c^2 T'' \tag{63}$$

is invariant with respect to time reversion: its form remains unchanged when t is substituted by $-t$. On the other hand, it describes irreversible processes: for example, damping of the sinusoidal initial temperature perturbation. Moreover, it was shown in Sect. 4.3 that the entropy for this process is not constant. Therefore, it turns out that the process reversibility is not directly related to the equation invariance with respect to time reversion.

Acknowledgements The authors of this work would like to thank E. A. Ivanova and E. N. Vilchevskaya for the useful discussions.

References

1. Cannon, J.R.: The One-Dimensional Heat Equation. Cambridge University Press (1984)
2. Lepri, S., Livi, R., Politi, A.: Thermal conduction in classical low-dimensional lattices. Phys. Rep. **377**, 1–80 (2003)
3. Cattaneo, C.: Sur une forme de l'équation de la chaleur éliminant le paradoxe d'une propagation instantane. Comptes Rendus **247**, 431–433 (1958)

4. Vernotte, P.: Les paradoxes de la theorie continue de l'équation de la chaleur. Comptes Rendus **246**, 3154–3155 (1958)
5. Krivtsov, A.M.: Heat transfer in infinite harmonic one-dimensional crystals. Dokl. Phys. **60**(9), 407–411 (2015)
6. Indeitsev, D., Osipova, E.: Two-temperature model of optical excitation of acoustic waves in conductors. Dokl. Phys. **62**(6), 538–541 (2017)
7. Krivtsov, A.M.: Deformation and fracture of solids with microstructure. Moscow, Fizmatlit. 304 p. (2007) (in Russian)
8. Palmov, V.: Vibrations of Elasto-Plastic Bodies. Springer, Berlin, Heidelberg (1998)
9. Jou, D., Lebon, G., Casas-Vazquez, J.: Extended Irreversible Thermodynamics. Springer, Netherlands (2010)
10. Müller, I., Ruggeri, T.: Extended Thermodynamics. Springer, New York (1993)
11. Zhilin, P.A.: Rational mechanics of continuous media, 584 pp. Publishing of Polytechnic University (2012)
12. Babenkov, M.B., Krivtsov, A.M., Tsvetkov, D.V.: Energy oscillations in a one-dimensional harmonic crystal on an elastic substrate. Phys. Mesomech. **19**(3), 282–290 (2016)
13. Berinskii, I.: Elastic networks to model auxetic properties of cellular materials. Int. J. Mech. Sci. **115**, 481 (2016)
14. Krivtsov, A.M.: Energy oscillations in a one-dimensional crystal. Dokl. Phys. **59**(9), 427–430 (2014)
15. Kuzkin, V.A., Krivtsov, A.M.: Fast and slow thermal processes in harmonic scalar lattices. J. Phys.: Condens. Matter **29**(50), 505401 (2017)
16. Hoover, W.G., Hoover, C.G.: Simulation and Control of Chaotic Nonequilibrium Systems. Advanced Series in Nonlinear Dynamics, vol. 27, 324 p. World Scientific (2015)
17. Sokolov, A.A., Krivtsov, A.M., Müller, W.H.: Localized heat perturbation in harmonic 1D crystals: solutions for an equation of anomalous heat conduction. Phys. Mesomech. **20**(3), 305–310 (2017)
18. Krivtsov, A.M.: A microcanonical distribution for a one-dimensional chain. The document from 12/12/2013–08/01/2014. 32 pp. (unpublished)

Model of Media with Conserved Dislocation. Special Cases: Cosserat Model, Aero-Kuvshinskii Media Model, Porous Media Model

S. A. Lurie, P. A. Belov and L. N. Rabinskiy

Abstract A sequential presentation of the theory of media by conserved dislocations as a variant of the theory of media with a microstructure (according to Mindlin's definition) is given as well as a rather complete description of the particular variants of the theory, relevant from an applied point of view: Cosserat and Aero–Kuvshinskii media, porous media, media with "twinning". The correctness of the formulation of models is determined by the use of a "kinematic" variational principle based on a formal description of the kinematics of media, the formulation of kinematic constraints for media of different complexity, and the construction of the corresponding potential energy of deformation using the Lagrange multiplier procedure. A system of defining relations is established and an agreed formulation of the boundary value problem is formulated. In this paper, much attention is paid to the analysis of the physical side of models of the media studied. The interpretation of all physical characteristics responsible for nonclassical effects is proposed, and a description of the spectrum of adhesive mechanical parameters is given. The generalized Aero-Kuvshinskii hypothesis about the proportionality of free and constrained distortions is proposed.

Keywords Continuous media with microstructure · Classification of dislocations
Kinematic interpretation of dislocations · Conserved dislocations
Variational kinematic principle · Generalized Mindlin and Cosserat media models
Aero-Kuvshinskii media model

S. A. Lurie (✉)
Institute of Applied Mechanics of Russian Academy of Science,
Moscow, Russia
e-mail: salurie@mail.ru

S. A. Lurie
Lomonosov State University, Moscow, Russia

S. A. Lurie
Dorodnicyn Computing Centre of FRC CSC RAS, Moscow, Russia

P. A. Belov · L. N. Rabinskiy
Moscow Aviation Institute, Moscow, Russia

F. dell'Isola et al. (eds.), *Advances in Mechanics of Microstructured Media and Structures*, Advanced Structured Materials 87,
https://doi.org/10.1007/978-3-319-73694-5_13

1 Introduction

Significant achievements in the creation of new materials with micro- and nanostructures and related technologies are due to success in the experimental and theoretical study of atomic structures, properties and behavior of defects such as dislocations and disclinations. It is known that in many cases defects are formed already at the stage of manufacturing many new materials. Such materials include: nano- and non-crystalline materials, amorphous crystalline compounds, nanocomposites, quasicrystalline, nanocrystalline, and some others [1–5]. The development of continuum models of defects beyond the classical elasticity appears to be very important for the description not only limited to the short-range interactions typical for the interaction of defects, but also for the modeling of size-dependent effects in elasticity and plasticity.

The kinematics of defects is a basis in development of phenomenological continuum models in the theory of defects. Firstly, the kinematics of defects (inconsistencies) is the most important element in application of the variational methods for the description of the higher order energetically consistent continuum gradient models, see [6–10]. Indeed, the kinematics of defects allows to establish a set of arguments for the correct formulation of the variation of energy functional. Secondly, the kinematic analysis allows to establish the relation between the different types of defects and to analyze the reasons and conditions for their generation and disappearance [11–16]. Moreover, kinematic analysis makes it possible to establish links between defective continuous models and pseudocontinuum models [17], gradient models [7, 15, 16, 18–21] and also models of adhesion interactions [22]. In the work [21] a special case of the theory of media with conserved dislocations was elaborated on the base of kinematic analysis and variational approach. We must note that adhesion models and its applications intensive elaborated in the recent works [23, 24].

Nevertheless, the possibilities of the theory of media with conserved dislocations are much broader in our view, and are not exhausted by the results obtained.

The study of the formulated theory is conducted in three main directions:

1. Formulation and solution of test problems for the cases realized in the experiment for the purpose of identifying nonclassical parameters of the medium, appearing in the defining equations of the theory.
2. Formulation and solution of problems forecasting/predicting unknown nonclassical effects for the formulation and conduct of relevant experiments.
3. The study of particular models arising from the general theory, and their identification with known models that exist autonomously.

This work is in the mainstream of research in the third direction and is devoted to the study of models of porous media, the models of Mindlin [9, 10], Cosserat [25] and Aero-Kuvshinskii [17]. We study correct particular models of media with a microstructure (by the definition of Mindlin), a system of defining relations is established, and a consistent statement of the boundary value problem is formulated.

It is shown that the considered media models not only simulate scale effects analogous to cohesive interactions, but also form the basis for describing a wide range of adhesion interactions. Considerable attention is paid to the analysis of the physical side of the model. A general version of media with persistent dislocations develops in the first part of the article. Then we give a complete mathematical description of particular models that have important applied value. Sequences of theories of media with conserved dislocations are consecutively presented: for the classical Cosserat medium, the Aero-Kuvshinskii medium, the porous medium and the medium with "twinning".

2 Theory of Medium with Conserved Dislocations

For the construction of media models, a variant of the "kinematic" variational principle is used, when, according to the given kinematic relationships, the form of the energy functional for the investigated medium is found and the force interactions corresponding to the introduced kinematic bonds are established. The model of the media is completely determined by the variety of the introduced kinematic constraints. Therefore, a special place in the exposition of the theory of media with a microstructure is given to the analysis of kinematic relations.

2.1 Kinematic Model

Let us write the known relations for the displacement vector R_i, obtained by formal integration of asymmetric Cauchy relations:

$$R_i = R_i^0 + \int_{M_0}^{M_x} (\gamma_{ij} + \frac{1}{3}\theta\delta_{ij} - \omega_k e_{ijk})dx_j \tag{1}$$

Where γ_{ij} is the tensor deviator of deformation, θ is the volumetric deformation, ω_k is the vector of elastic rotations (pseudovector), with δ_{ij} denoting the Kronecker, e_{ijk} is the permutation symbol.

The description of the kinematic models of nonclassical media by analyzing the homogeneous Papkovich equations, which are the conditions for the existence of a curvilinear integral in the determination of the displacement vector (1):

$$(\gamma_{in} + \theta\delta_{in}/3 - \omega_k e_{ink})_{,m} e_{nmj} = 0 \tag{2}$$

The homogeneous Papkovich Eq. (2) can be interpreted as a criterion for the existence of a vector potential (1) R_i. Consequently, when (2) is satisfied, the displacement vector R_i is a vector potential for the distortion tensor D^1_{ij}:

$$D^1_{ij} = \gamma_{ij} + \theta\delta_{ij}/3 - \omega_k e_{ijk} = R_{i,j} \tag{3}$$

In this case, the differential form $dR_i = D^1_{ij}dx_j$ is a total differential.

Let us now consider the inhomogeneous Papkovich equations:

$$\left(\gamma_{in} + \theta\delta_{in}/3 - \omega_k e_{ink}\right)_{,m} e_{nmj} = \Xi_{ij} \tag{4}$$

The quantity Ξ_{ij} is a pseudo-tensor-source of dislocations [13] of the second rank, its sign changes when the right triple of unit vectors is replaced by the left. This pseudotensor obeys the differential conservation law, which follows easily from (4):

$$\Xi_{ij,j} = 0 \tag{5}$$

As in the case of homogeneous Papkovich Eq. (2), we can formally introduce the vector of defective displacements D^2_i as the difference of the displacements of two infinitely close points by means of the relation $dD^2_i = D^2_{ij}dx_j$. However, here the linear differential form dD^2_i is no longer a total differential and the Eq. (1) for defective displacements is not integrable. We will say that a defect displacement field is defined by the vector D_i, in which, along with the continuous part R_i, there is also a discontinuous part D^2_i (displacement discontinuity vector or dislocation vector). The solution D_{ij} of the inhomogeneous Papkovich Eq. (4) can be represented as the sum of the solution of the homogeneous Papkovich equation $D^1_{ij} = R_{i,j}$ and the particular solution D^2_{ij} of the inhomogeneous Papkovich equations: $D_{ij} = R_{i,j} + D^2_{ij}$. We represent the asymmetric tensor D^1_{ij} in the form of an expansion into a tensor deviator γ^1_{ij}, the spherical tensor $\theta^1\delta_{ij}$, and the antisymmetric tensor $\omega^1_k e_{ijk}$. In turn, we write the antisymmetric tensor through the pseudovector of the rotations $\omega^1_k : D^1_{ij} = \gamma^1_{ij} + \theta^1\delta_{ij}/3 - \omega^1_k e_{ijk}$, where

$$\gamma^1_{ij} = R_{i,j}/2 + R_{j,i}/2 - R_{k,k}\delta_{ij}/3, \quad \theta^1 = R_{k,k}, \quad \omega^1_k = -R_{i,j}e_{ijk}/2.$$

For a particular solution of the inhomogeneous Papkovich Eq. (4) there is no continuous vector potential, i.e., it cannot be represented in the form (3). For it one can write only the following symmetric representation:

$$D^2_{ij} = \gamma^2_{ij} + \theta^2\delta_{ij}/3 - \omega^2_k e_{ijk}$$

It is obvious that along with D_{ij}^2 as independent "generalized displacements" one can consider the quantities $\gamma_{ij}^2, \omega_k^2$ and θ^2.

The general solution of the inhomogeneous Papkovich Eq. (4) can be written in a symmetric form:

$$D_{ij} = D_{ij}^1 + D_{ij}^2 = \gamma_{ij} + \theta\delta_{ij}/3 - \omega_k e_{ijk}$$

where:

$$\begin{aligned}\gamma_{ij} &= \gamma_{ij}^1 + \gamma_{ij}^2 = (R_{i,j}/2 + R_{j,i}/2 - R_{k,k}\delta_{ij}/3) + \gamma_{ij}^2\\ \omega_k &= \omega_k^1 + \omega_k^2 = -R_{i,j}e_{ijk}/2 + \omega_k^2\\ \theta &= \theta^1 + \theta^2 = R_{k,k} + \theta^2\end{aligned}$$

Using the terminology of the kinematics of the Cosserat mediums, we will call $\omega_k^1 = -R_{i,j}e_{ijk}/2$ as constrained rotation, a ω_k^2 is the free rotation or spin. Similarly, we will call γ_{ij}^1 and θ^1 as constrained or joint deformations, and γ_{ij}^2, and θ^2 as free or incompatible deformations. Accordingly, we introduce the definitions of tensors of free/incompatible D_{ij}^2 and constrained/joint D_{ij}^1 distortion.

The kinematic model of media with conserved dislocations is described by generalized Papkovich relations (4) and Cauchy relations for constrained distortion (3).

The kinematics of such media has the following structure:

1. The defective displacement field D_i is a superposition of two fields—a continuous field (displacements) and a discontinuity field D_i^2 (dislocations): $D_i = D_i^1 + D_i^2 = R_i + D_i^2$;
2. The discontinuity field of displacements D_i^2 (dislocations) is integrally expressed in terms of the fields of free strains and spins according to formulas analogous to Cesaro's formulas: $D_i^2 = \int\limits_{M_0}^{M_x} (\gamma_{ij}^2 + \theta^2\delta_{ij}/3 - \omega_k^2 e_{ijk})dy_j$

   However, unlike Cesaro's formulas, here the integrand does not satisfy the integrability conditions,

$$(\gamma_{in}^2 + \theta^2\delta_{in}/3 - \omega_k^2 e_{ink})_{,m} e_{nmj} = \Xi_{ij} \neq 0 \tag{6}$$

   i.e., the curvilinear integral depends on the trajectory of integration, and hence the vector field D_i^2 is not continuous.
3. The Cauchy relations generalized to defective media with conserved dislocations take place: $D_{ij} = D_{ij}^1 + D_{ij}^2 = R_{i,j} + D_{ij}^2$.
4. There are three types of dislocations $(D_i^2)_\gamma$, $(D_i^2)_\theta$ and $(D_i^2)_\omega$:

$$
\begin{aligned}
D_i^2 &= \int_{M_0}^{M_x} (\gamma_{ij}^2 + \theta^2 \delta_{ij}/3 - \omega_k^2 e_{ijk}) dy_j \\
&= \int_{M_0}^{M_x} \gamma_{ij}^2 dy_j + (1/3) \int_{M_0}^{M_x} \theta^2 dy_i - \int_{M_0}^{M_x} \omega_k^2 e_{ijk} dy_j \\
&= (D_i^2)_\gamma + (D_i^2)_\theta + (D_i^2)_\omega
\end{aligned}
\tag{7}
$$

Let's call $(D_i^2)_\gamma = \int_{M_0}^{M_x} \gamma_{ij}^2 dy_j$ as γ-dislocations, $(D_i^2)_\theta = (1/3) \int_{M_0}^{M_x} \theta^2 dy_i$ as θ-dislocations and $(D_i^2)_\omega = -\int_{M_0}^{M_x} \omega_k^2 e_{ijk} dy_j$ as ω-dislocations. The pseudotensor of the "incompatibility" of displacements Ξ_{ij} is the de Vit's pseudotensor of the dislocation density [13]:

$$
\Xi_{ij} = D_{in,m}^2 e_{nmj} = (\gamma_{in}^2 + \theta^2 \delta_{in}/3 - \omega_k^2 e_{ink})_{,m} e_{nmj}
$$

5. To each type of dislocations associated with γ_{ij}^2, ω_k^2 and θ^2, respectively, one can associate one's own pseudotensor-source type of the corresponding dislocations:

$$
\begin{aligned}
\Xi_{ij} &= (\gamma_{in}^2 + \theta^2 \delta_{in}/3 - \omega_k^2 e_{ink})_{,m} e_{nmj} \\
&= \gamma_{in,m}^2 e_{nmj} + \theta_{,m}^2 e_{imj}/3 - \omega_{k,m}^2 e_{nki} e_{nmj} \\
&= (\Xi_{ij})_\gamma + (\Xi_{ij})_\theta + (\Xi_{ij})_\omega
\end{aligned}
\tag{8}
$$

The quantities $(\Xi_{ij})_\gamma$, $(\Xi_{ij})_\theta$ and $(\Xi_{ij})_\omega$ in the expansion (8) are sources of three types of dislocations, respectively: γ-dislocations, θ-dislocations and ω-dislocations, the determination of which was given above by formulas (7).

6. There is a differential law for the conservation of dislocations, which follows from the definition of the dislocation tensor: $\Xi_{ij,j} = 0$. Sources $(\Xi_{ij})_\gamma$, $(\Xi_{ij})_\theta$ and $(\Xi_{ij})_\omega$ of introduced types of dislocations also satisfy the conservation law individually.
7. The integral analog of the law of conservation of dislocations obviously has the following form:

$$
\iiint \Xi_{ij,j} dV = \oiint \Xi_{ij} n_j dF = 0.
$$

We note that as a measure of damage (dislocations), we can choose the tensor flux Ξ_{ij} through the plane in which the chosen plane contour lies. Indeed, let the closed surface consist of an arbitrary surface spanned by a two-dimensional shape and a plane containing this flat contour. Then from the integral law of conservation follows: $\iint_F \Xi_{ij} n_j dF = -n_j \iint_0 \Xi_{ij} dF$, where F is an arbitrary surface spanned by a flat contour. In other words, the flow of a tensor Ξ_{ij} through any surface spanned by a two-dimensional shape is the same.

It follows from the above analysis (see also [21]) that the concept of a defect in a continuous medium is complex and can be determined by means of a complex of tensor objects. For dislocations such a complex of objects is: a pseudotensor-source of dislocations Ξ_{ij}; tensor of free distortion of the second rank D^2_{ij}; vector (first-rank tensor) of discontinuous displacements D^2_i, which has the physical meaning of the dislocation vector. One can also include here the corresponding Burgers vector, which can be obtained from (7) by combining the initial M_0 and final M_x points of the planar integration trajectory (n_n is a constant normal vector to the plane of the trajectory of integration):

$$b_i = \oint D^2_{ij} dx_j = \oint D^2_{ij} s_j ds = \oint D^2_{ij} v_m n_n e_{jmn} ds$$
$$= n_n \iint D^2_{ij,\,m} e_{jmn} dF = n_n \iint \Xi_{in} dF$$

where s_j is the unit vector tangent to the two-dimensional shape n_i is the vector of the unit normal to the plane of the trajectory, and the vectors s_j, v_m, n_n form a triple of unit vectors associated with the current point of the shape.

The kinematic analysis of the model allows us to establish a complete set of generalized kinematic variables necessary for the formulation of the functional and the corresponding variational equation of the model. In the case under consideration, for a medium with a field of conserved dislocations, the generalized kinematic variables are continuous quantities R_i, D^2_{ij} and their gradients $R_{i,j} = D^1_{ij}, D^2_{ij,\,k} = D^2_{ijk}$. A new natural classification of dislocations is proposed. We propose a classification, given by formula (7), which reflects the energy independence of the identified varieties of dislocations. In what follows, it will be shown that the potential energies of the types of dislocations are proportional $\gamma^2_{ij}\gamma^2_{ij}, \theta^2\theta^2, \omega^2_k\omega^2_k$ and do not have cross terms. Therefore, the potential energies of the introduced types of dislocations are additive, they can exist separately and independently of other types of dislocations. Therefore, the potential energies of the introduced types of dislocations are additive, they can exist separately and independently of other types of dislocations.

2.2 Variational Formulation of Model

In [19–21], a "kinematic" variational principle for constructing media models was formulated. In accordance with this, kinematic constraints are determined in the media, the possible work of internal forces is postulated as a possible work of reactive stresses on kinematic constraints inherent in the media. Possible work of internal forces is represented in the form of a linear form of variations of its arguments. This form can be integrated for conservative media. As a result, the potential energy is determined. For linear media, the potential energy is a quadratic form of its arguments.

For the "simplest" theory of media with conserved dislocations, such kinematic constraints are the inhomogeneous Papkovich equations for free distortion and the homogeneous Papkovich equations for constrained distortion. The homogeneous Papkovich equations for constrained distortion can be integrated in a general form. Their solution is asymmetric Cauchy relations. Thus, in accordance with the "kinematic" variational principle, the possible work of internal forces should be presented in the form:

$$\overline{\delta U} = \iiint [\sigma_{ij}\delta(D^1_{ij} - R_{i,j}) + m_{ij}\delta(\Xi_{ij} - D^2_{in,m}e_{nmj})]dV \tag{9}$$

where $\overline{\delta U}$—possible work of internal forces, in the general case—a linear form of variation of its arguments; σ_{ij} and m_{ij}—the tensors of the Lagrange multipliers, which have the physical meaning of reactive force factors ensuring the performance of the corresponding kinematic constraints.

Let us represent $\overline{\delta U}$ in (9) as a linear form of variations of its arguments. Using integration by parts in terms containing derivatives, we can obtain:

$$\begin{aligned}\overline{\delta U} = &\iiint [\sigma_{ij}\delta D^1_{ij} + \sigma_{ij,j}\delta R_i + m_{ij}\delta\Xi_{ij} + m_{ij,m}e_{nmj}\delta D^2_{in}]dV \\ &+ \oiint [-\sigma_{ij}n_j\delta R_i - m_{ij}n_m e_{nmj}\delta D^2_{in}]dF\end{aligned} \tag{10}$$

Then there is such a potential U (potential energy) that the possible work $\overline{\delta U}$ in (10) is a variation of this potential:

$$\overline{\delta U} = \delta U, U = \iiint U_V dV + \oiint U_F dF, U_V = U_V(R_i, D^1_{ij}, D^2_{ij}, \Xi_{ij}), U_F = U_F(R_i, D^2_{ij}).$$

In the future, we exclude the displacement vector from the lists of arguments for the densities of the potential energy. Then the considered generalized model of a medium with scale effects will not contradict in the particular case of the classical

theory and the known experimental data. This issue will be further discussed. As a result, we obtain:

$$U = \iiint U_V dV + \oiint U_F dF, \quad U_V = U_V(D_{ij}^1, D_{ij}^2, \Xi_{ij}) \\ U_F = U_F(D_{ij}^2) \tag{11}$$

Taking into account the list of arguments in (11) and the integrability of the possible variational of internal forces $\overline{\delta U}$ in the volume, we obviously obtain:

$$\sigma_{ij}^1 = \partial U_V / \partial D_{ij}^1, \quad \sigma_{ij}^2 = \partial U_V / \partial D_{ij}^2, \quad m_{ij} = \partial U_V / \partial \Xi_{ij} \tag{12a}$$

Accordingly, on the surface the integrability of the possible variational of internal forces $\overline{\delta U}$ gives the following analogs of the Green's formulas for adhesive stresses:

$$a_{ij}^2 = \partial U_F / \partial D_{ij}^2 \tag{12b}$$

Formulas (12a, 12b) should be treated as generalized Green's formulas for volume and surface stresses. These relations enable us to write the Lagrangian and find the corresponding Euler equations:

$$\delta L = \iiint [(\sigma_{ij,j}^1 + P_i^V)\delta R_i - (m_{in,m} e_{nmj} + \sigma_{ij}^2)\delta D_{ij}^2] dV \\ + \oiint [(P_i^F - \sigma_{ij}^1 n_j)\delta R_i + (m_{in} n_m e_{nmj} - a_{ij}^2)\delta D_{ij}^2] dF = 0 \tag{13}$$

2.3 Constitutive Equations

Let us again consider the density of potential energy in the volume and on the surface. We confine ourselves to the consideration of physically linear media. Then U_V is defined as the quadratic form of its arguments:

$$2U_V = 2U_V(D_{ij}^1; D_{ij}^2; \Xi_{ij}) \\ = C_{ijnm}^{11} D_{ij}^1 D_{nm}^1 - 2C_{ijnm}^{12} D_{ij}^1 D_{nm}^2 + C_{ijnm}^{22} D_{ij}^2 D_{nm}^2 + C_{ijnm}^{33} \Xi_{ij} \Xi_{nm} \tag{14}$$

When obtaining (14), the following well-founded simplifications were introduced:

1. The coefficient of the term $R_i R_i$ is assumed to be zero in (14). Otherwise, the operator of the equilibrium equations would have the form of Helmholtz equations, which excludes the existence of homogeneous stress-strain states.

2. The coefficients for all other bilinear components including the displacement vector are also zero. Otherwise, in the absence of a term that is quadratic relative to displacements, the bulk density of the potential energy would not be positive definite. The structure of the tensors of the elastic moduli $C^{pq}_{ijnm}, (p,q=1,2)$ in (14) is determined by their expansion in terms of isotropic tensors of the fourth rank, constructed as the product of a pair of Kronecker tensors with all possible permutations of the indices:

$$\begin{gathered} C^{pq}_{ijnm} = C^{pq}_1 \delta_{ij}\delta_{nm} + C^{pq}_2 \delta_{in}\delta_{jm} + C^{pq}_3 \delta_{im}\delta_{jn} \\ C^{pq}_1 = \lambda^{pq} \quad C^{pq}_2 = \mu^{pq} + \chi^{pq} \quad C^{pq}_3 = \mu^{pq} - \chi^{pq} \end{gathered} \tag{15}$$

where λ^{11}, μ^{11} are the Lame constants, χ^{11} is a third, nonclassical, Lame coefficient, other coefficients $\lambda^{pq}, \mu^{pq}, \chi^{pq}$ are their nonclassical counterparts.

Finally, taking into account (15) we can write the following expression for the volumetric density of the potential energy U_V:

$$\begin{aligned} 2U_V = {} & \mu^{11}\gamma^1_{nm}\gamma^1_{nm} - 2\mu^{12}\gamma^1_{nm}\gamma^2_{nm} + \mu^{22}\gamma^2_{nm}\gamma^2_{nm} \\ & + [(2\mu^{11} + 3\lambda^{11})\theta^1\theta^1 - 2(2\mu^{12} + 3\lambda^{12})\theta^1\theta^2 + (2\mu^{11} + 3\lambda^{11})\theta^2\theta^2]/3 \\ & + 4[\chi^{11}\omega^1_{nm}\omega^1_{nm} - 2\chi^{12}\omega^1_{nm}\omega^2_{nm} + \chi^{22}\omega^2_{nm}\omega^2_{nm}] \\ & + C^{33}_{ijnm}(D^2_{ia,b}e_{abj})(D^2_{nc,d}e_{cdm}) \end{aligned}$$

Note that part of the density of potential energy $C^{33}_{ijnm}\Xi_{ij}\Xi_{nm}$ (see Eq. (14)) associated with the pseudo-tensor-source of dislocations Ξ_{ij} determines the rapidly changing, local part of the potential energy dislocations:

$$C^{33}_{ijnm}\Xi_{ij}\Xi_{nm} = (C^{33}_{ijnm}e_{abj}e_{cdm})D^2_{ia,b}D^2_{nc,d} = C^{33}_{iabncd}D^2_{ia,b}D^2_{nc,d}$$

The remaining part of the density of potential energy is slowly changing and is defined as the sum of the potential energies of three types of dislocations: γ-dislocations, θ-dislocations and ω-dislocations. Consequently, the slowly varying part of the deformation energy does not contain cross terms from these types of dislocations and is an additive form with respect to the components of free distortion.

We note that integral estimates can be used to estimate the damage to media. Therefore, in these problems, for approximate estimates, it is probably possible to neglect the local, rapidly varying part of the energy. In this case also, additivity exists in the expansion of the potential energy density with respect to the components of free distortion. This circumstance is used as a additional justification for the new classification of the types of dislocations proposed by formulas (7).

Using Green Eq. (12a, 12b) the generalized equations of the Hooke law (12a, 12b) can be written in the form:

$$\sigma_{ij}^1 = C_{ijnm}^{11} R_{n,m} - C_{ijnm}^{12} D_{nm}^2, \quad \sigma_{ij}^2 = -C_{ijnm}^{21} R_{n,m} + C_{ijnm}^{22} D_{nm}^2,$$
$$m_{ij} = C_{ijnm}^{33} \Xi_{nm} \tag{16}$$

It follows from (16) that in addition to the tensor of "classical" stresses σ_{ij}^1, additional force factors—"dislocation" stresses σ_{ij}^2 occur in such media.

Let's assume that $C_{ijnm}^{12} = 0$. In this case, the general boundary value problem decomposes into a boundary value problem with respect to displacements R_i and a boundary value problem with respect to free distortion D_{ij}^2. The first boundary value problem with respect to displacements under the additional assumption $\chi^{11} = 0$ (the theory of elasticity with a symmetric stress tensor) coincides with the classical theory of elasticity and the stresses σ_{ij}^1 acquires the meaning of classical stresses. Consequently, in the considered case, the boundary-value problem for the components of the free distortion tensor is homogeneous which corresponds to the case of the absence of dislocations. As a result, if $C_{ijnm}^{12} = 0$ then the model is reduced to the case of the defectless continuous medium. The above arguments allow us to formulate the following natural interpretation for the elastic moduli $\mu^{11}, 2\mu^{11} + \lambda^{11}, \chi^{11}$ that are not damaged by the dislocations. We must take $\chi^{11} = 0$ for the symmetric classical theory of elasticity.

For the case when $C_{ijnm}^{12} \neq 0$, the mutual disturbance of a classical displacement field and purely dislocational states occur. The cross-linked terms in the generalized Hooke's law Eq. (16) for σ_{ij}^1 and σ_{ij}^2 reflect these disturbances. Similar consideration provides the algorithm for solving the general boundary-value problem using the method of successive approximations.

We note that for a smooth surface there always exists a naturally distinguished direction—the normal to the surface. The Hooke law equations for internal stresses on the surface must have a transversally isotropic character and, as a result, the kinematic factors associated with the normal to the surface and with the tangent plane will be unequal to these Hooke law equations. Let us investigate in more detail the surface density of the potential energy. To do this, first consider the expression for the surface part of the possible work. The first term in it completely corresponds to the classical representation. It appears as a result of integrating by parts the expression $\iiint \sigma_{ij}^1 \delta R_{i,j} dV$ in the equality (10). The second term in the expression for the surface part of a possible work is nonclassical, due to its appearance of a "kinematic" variational principle of model construction and is related to the surface energy of adhesion U_F.

Consider this term in more detail:

$$\begin{aligned} &\oiint m_{ij} n_m \vartheta_{nmj} \delta D_{in}^2 dF \\ &= \oiint m_{ij} n_m \vartheta_{nmj} \delta D_{ik}^2 (\delta_{kn} - n_k n_n) dF + \oiint m_{ij} n_m \vartheta_{nmj} \delta D_{ik}^2 n_k n_n dF \end{aligned} \tag{17}$$

We note that $n_n n_m e_{nmj} = 0$ is as a convolution of a symmetric tensor $n_p n_q$ with an antisymmetric pseudotensor e_{pqj}. Consequently, the work of the moment stresses (17) on the surface of the body does not occur on all nine components of the free distortion tensor D^2_{in}, but only on six of them $D^2_{ik}(\delta_{kn} - n_k n_n)$:

$$\oiint m_{ij} n_m \eth_{nmj} \delta D^2_{in} dF = \oiint m_{ij} n_m e_{nmj} \delta D^2_{ik} (\delta_{kn} - n_k n_n) dF \tag{18}$$

On the basis of (18), the surface density of the potential energy has the form:

$$U_F = a_{ijnm} D^2_{np} (\delta_{pm} - n_p n_m) D^2_{iq} (\delta_{qj} - n_q n_j)/2 \tag{19}$$

Generalized equations of Hooke's law on a surface are given by the relations (12a, 12b). We note that the surface density of the potential energy does not depend on the displacement vector. Otherwise, this leads to systematic corrections to the static boundary conditions of the classical solution and contradicts the available experimental data.

It is important to note that the lemma (18) allows us to refine the list of arguments for the surface density of the potential energy in (19). This refined list of arguments is now determined by the six "flat" components of the free distortion tensor $D^2_{im}(\delta_{pm} - n_p n_m)$: $U_F = U_F(D^2_{ik}(\delta_{kj} - n_k n_j))$. One can, however, retain the original form of the Hooke's law equations on the surface of the body and the expression for the density of the surface potential energy:

$$\begin{aligned} 2U_F &= a_{ijnm} D^2_{np} (\delta_{pm} - n_p n_m) D^2_{iq} (\delta_{qj} - n_q n_j) \\ &= a_{ijnm} (\delta_{pm} - n_p n_m)(\delta_{qj} - n_q n_j) D^2_{np} D^2_{iq} = a^*_{ijnm} D^2_{nm} D^2_{ij} \end{aligned}$$

In this case, it should be borne in mind that then the tensor of adhesion moduli a^*_{ijnm} must satisfy the conditions:

$$\begin{aligned} a^*_{ijnm} &= a_{ijnm}(\delta_{pm} - n_p n_m)(\delta_{qj} - n_q n_j), \\ a^*_{ijnm} n_m &= a_{ijnm}(\delta_{pm} n_m - n_p n_m n_m)(\delta_{qj} - n_q n_j) \equiv 0 \\ a^*_{ijnm} n_j &= a_{ijnm}(\delta_{pm} - n_p n_m)(\delta_{qj} n_j - n_q n_j n_j) \equiv 0 \end{aligned} \tag{20}$$

The structure of the tensor of the adhesion moduli a^*_{ijnm} (hereinafter we shall not put an asterisk) is determined by its expansion in terms of fourth-rank tensors, constructed as all possible products of pairs of "flat" Kronecker tensors of the form $(\delta_{ij} - n_i n_j)$ and tensors formed by the product of vectors of the unit normal of the form $n_i n_j$, with all possible permutations of the indices. We also take into account condition (20).

One can see that in this case the general structure of the tensor of the adhesion moduli has the form of

$$\begin{aligned} a_{ijnm} = [&\lambda^F(\delta_{ij} - n_i n_j)(\delta_{nm} - n_n n_m) + \delta^F n_i n_n(\delta_{jm} - n_j n_m) \\ &+ (\mu^F + \chi^F)(\delta_{in} - n_i n_n)(\delta_{jm} - n_j n_m) \\ &+ (\mu^F - \chi^F)(\delta_{im} - n_i n_m)(\delta_{jn} - n_j n_n)], \end{aligned} \tag{21}$$

where μ^F, λ^F, χ^F and δ^F—adhesion moduli.

Let us consider the surface density of the potential energy and give a physical interpretation of the adhesive components, taking into account the relations (19) and (21). The free distortion is written in the form of tensor decomposition into a "flat" deviator:

$$\begin{aligned} {}^2\gamma_{ij} = &(1/2)D^2_{nm}(\delta_{in} - n_i n_n)(\delta_{jm} - n_j n_m) \\ &+ (1/2)D^2_{nm}(\delta_{jn} - n_j n_n)(\delta_{im} - n_i n_m) \\ &- (1/2)D^2_{nm}(\delta_{ij} - n_i n_j)(\delta_{nm} - n_n n_m), \end{aligned}$$

"flat" spherical tensor: ${}^2\theta = D^2_{nm}(\delta_{nm} - n_n n_m)$

"flat" antisymmetric tensor:

$$\begin{aligned} {}^2\omega_{ij} = &(1/2)D^2_{nm}(\delta_{in} - n_i n_n)(\delta_{jm} - n_j n_m) \\ &- (1/2)D^2_{nm}(\delta_{jn} - n_j n_n)(\delta_{im} - n_i n_m) \end{aligned}$$

and the "flat" vector of the angles of rotation of the surface during its bending:

$${}^2\alpha_i = D^2_{nm} n_n(\delta_{mi} - n_m n_i)$$

The upper left index "2" emphasizes the fact that the corresponding components of the free distortion tensor are calculated on the surface of the body. As a result, we get:

$$D^2_{ik}(\delta_{jk} - n_j n_k) = {}^2\gamma_{ij} + {}^2\theta(\delta_{ij} - n_i n_j)/2 + {}^2\omega_{ij} + {}^2\alpha_j n_i \tag{22}$$

Taking into account (21), we can verify that the tensor of free distortion on the surface, represented in the form of expansion (22), converts the potential energy of adhesion to the "canonical" form:

$$\begin{aligned} 2U_F = &(\mu^F + \lambda^F)({}^2\theta^2\theta) + 2\mu^F({}^2\gamma_{ij}{}^2\gamma_{ij}) \\ &+ 2\chi^F({}^2\omega_{ij}{}^2\omega_{ij}) + \delta^F({}^2\alpha_k{}^2\alpha_k) \end{aligned} \tag{23}$$

The canonicity of the potential energy (23) gives grounds to assert the existence of four energetically independent types of adhesion interactions (the absence of cross terms). Each interaction is characterized by its adhesion modulus.

Thus, a complete and correct model of media with conserved dislocations is given. This model is defined by the Lagrangian that can be written using equations for the potential energy in the volume (11), (14) and on the surface (23):

$$L = A - (1/2)\iiint \{C^{11}_{ijnm} R_{n,m} R_{i,j} - 2C^{12}_{ijnm} R_{n,m} D^2_{ij} + C^{22}_{ijnm} D^2_{nm} D^2_{ij} + C^{33}_{ijnm} \Xi_{nm} \Xi_{ij}\} dV - (1/2) \oiint a_{ijnm} D^2_{nm} D^2_{ij} dF \tag{24}$$

On the basis of the carried out kinematic analysis, a different classification of dislocations is proposed, which makes it possible to distinguish three types of dislocations: γ-dislocations, θ-dislocations, ω-dislocations. This classification gives a new both physical and kinematic interpretation of dislocations, since it reflects the relationship of dislocations with the formation of "twinning" γ, with a change in volume θ (porosity) and with twisting ω (spins). The proposed classification, in fact, makes it possible to predict particular cases of media with conserved dislocations, when only one or two types of dislocations dominate in the medium. In such particular models, it is possible to reduce the number of degrees of freedom, which greatly facilitates the study of certain properties of media with conserved dislocations. Let us recall that twelve degrees of freedom are assigned to each point of a medium with conserved dislocations: three displacement components R_i, three rotation components ω^2_k and six deformation components $D^2_{ij} = \varepsilon^2_{ij} = \gamma^2_{ij} + \theta^2 \delta_{ij}/3$.

Special case 1. Dominant are dislocations generated only by free turns ω^2_k. This is a "classical" version of the model of Cosserat mediums with six degrees of freedom R_i and ω^2_k. In such medium $\gamma^2_{ij} = 0$ and $\theta^2 = 0$. The free distortion tensor is given by $D^2_{ij} = -\omega^2_k e_{ijk}$.

Special case 2. Dominant are dislocations, generated only by a free change in volume θ^2. This is a model of a porous medium with four degrees of freedom R_i, θ^2. In such medium $\omega^2_k = 0$ and $\gamma^2_{ij} = 0$. The free distortion tensor is given by $D^2_{ij} = \theta^2 \delta_{ij}/3$.

Special case 3. The dominant are dislocations, generated only by a free change in shape ("twinning") γ^2_{ij}. This is a model of a medium with "twinning" with eight degrees of freedom R_i, γ^2_{ij}. In such medium $\omega^2_k = 0$ and $\theta^2 = 0$. It is obvious that in this case $D^2_{ij} = \gamma^2_{ij}$.

We turn to the study of these particular models. It is proposed to consistently note the following points: to indicate the corresponding kinematic relations; to write down the system of defining equations of models; to represent the Lagrangian and give a complete variational formulation of the models; to obtain a system of resolving equations, write them relative to the displacement vector and the components of the free distortion tensor; to write the expansion of the total solution to the "classical" state and the "cohesive" state, which is proposed to be considered as corrections to the classical solution, determined by taking into account the scale effects within the framework of these models.

3 Cosserat Medium (Special Case of Medium with Conserved Dislocations)

Let us consider a particular case of medium with conserved dislocations, when the free distortion tensor $D_{ij}^2 = \gamma_{ij}^2 + \theta^2\delta_{ij}/3 - \omega_k^2 e_{ijk}$ is determined only by free rotations, and the free deformations are equal to zero $\gamma_{ij}^2 = 0, \theta^2 = 0$. In this case we have a medium with six independent degrees of freedom-three components of the displacement vector R_i and three components of the free rotation pseudovector ω_k^2. Each point of such a continuum behaves like an absolutely rigid body: it can move and rotate, unlike points of the Cauchy medium that can only move. Let us construct such a special case of the theory of media with conserved dislocations and compare the corresponding boundary value problems. The free distortion tensor is defined here by the relation:

$$D_{ij}^2 = (-\omega_k^2 e_{ijk}) \tag{25}$$

The pseudotensor of dislocations Ξ_{ij} is written as follows:

$$\Xi_{ij} = -\omega_{k,m}^2 e_{ink} e_{nmj} = -\omega_{k,m}^2(\delta_{km}\delta_{ij} - \delta_{kj}\delta_{im}) = (\omega_{j,i}^2 - \omega_{k,k}^2\delta_{ij})$$

The Lagrangian of the Cosserat theory is written as a special case of the Lagrangian (24):

$$\begin{aligned} L = A - (1/2)\iiint & [C_{ijnm}^{11} R_{n,m} R_{i,j} - 2(C_{ijnm}^{12} e_{ijk}) R_{n,m}\omega_k^2 \\ & + (C_{ijnm}^{22} e_{ijp} e_{nmq})\omega_p^2\omega_q^2 \\ & + (C_{ijnm}^{33} - C_{qqnm}^{33}\delta_{ij} - C_{ijpp}^{33}\delta_{nm} + C_{ppqq}^{33}\delta_{ij}\delta_{nm})\omega_{i,j}^2\omega_{n,m}^2]dV \\ & - (1/2)\iiint (a_{ijnm} e_{ijp} e_{nmq})\omega_p^2\omega_q^2 dV \end{aligned} \tag{26}$$

We note that the following convolutions of the elastic moduli take place

$$\begin{aligned} & C_{ijnm}^{pq}\vartheta_{ijk} = 2\chi^{pq} e_{nmk} \\ & C_{ijnm}^{pq}\vartheta_{ijk}\vartheta_{nml} = 4\chi^{pq}\delta_{kl} \\ & C_{ijnm}^{33} - C_{ppnm}^{33}\delta_{ij} - C_{ijqq}^{33}\delta_{nm} + C_{ppqq}^{33}\delta_{ij}\delta_{nm} \\ & = (2\mu^{33} + 4\lambda^{33})\delta_{ij}\delta_{nm} + (\mu^{33} + \chi^{33})\delta_{in}\delta_{jm} + (\mu^{33} - \chi^{33})\delta_{im}\delta_{jn} \\ & a_{ijnm}\vartheta_{ijk}\vartheta_{nml} = \delta^F(\delta_{kl} - n_k n_l) + 4\chi^F n_k n_l \end{aligned} \tag{27}$$

Then, taking into account formulas (15), (25)–(27), the Lagrangian of the Cosserat medium (26) acquires the following final form:

$$
\begin{aligned}
L = A - (1/2)\iiint \{ & [(1/3)(2\mu^{11} + 3\lambda^{11})\theta^1\theta^1 + \mu^{11}\gamma^1_{nm}\gamma^1_{nm}] \\
& + 4\chi^{11}\omega^1_k\omega^1_k + 8\chi^{12}\omega^1_k\omega^2_k + 4\chi^{22}\omega^2_k\omega^2_k \\
& + [(2\mu^{33} + 4\lambda^{33})\delta_{ij}\delta_{nm}/3 + (\mu^{33} + \chi^{33})\delta_{in}\delta_{jm} \\
& + (\mu^{33} - \chi^{33})\delta_{im}\delta_{jn}]\omega^2_{i,j}\omega^2_{n,m}\} dV \\
& - (1/2)\oiint [\delta^F(\delta_{kl} - n_k n_l) + 4\chi^F n_k n_l]\omega^2_k\omega^2_l dF
\end{aligned}
\tag{28}
$$

The Lagrangian (28) allows us to write down the Hooke law equations for Cosserat media:

$$
\begin{aligned}
\sigma_{ij} &= \frac{\partial U_V}{\partial R_{i,j}} = [(2\mu^{11} + 3\lambda^{11})/3]\theta^1\delta_{ij} + 2\mu^{11}\gamma^1_{ij} \\
&\qquad - 2(\chi^{11}\omega^1_k + \chi^{12}\omega^2_k)e_{ijk} \\
p_k &= \frac{\partial U_V}{\partial \omega^2_k} = 4(\chi^{21}\omega^1_k + \chi^{22}\omega^2_k) \\
m_{ij} &= \frac{\partial U_V}{\partial \omega^2_{i,j}} = [2(\mu^{33} + 2\lambda^{33})\delta_{ij}\delta_{nm}/3 + (\mu^{33} + \chi^{33})\delta_{in}\delta_{jm} \\
&\qquad + (\mu^{33} - \chi^{33})\delta_{im}\delta_{jn}]\omega^2_{n,m} \\
a_k &= \frac{\partial U_F}{\partial \omega^2_k} = [\delta^F(\delta_{kl} - n_k n_l) + 4\chi^F n_k n_l]\omega^2_l
\end{aligned}
\tag{29}
$$

As a result, the variational equation of the theory of Cosserat's media becomes:

$$
\begin{aligned}
\delta L = & \iiint [(\sigma_{ij,j} + P^V_i)\delta R_i + (m_{ij,j} - p_i)\delta\omega^2_i] dV \\
& + \oiint [(P^F_i - \sigma_{ij}n_j)\delta R_i - (m_{ij}n_j + a_i)\delta\omega^2_i] dF = 0
\end{aligned}
\tag{30}
$$

Using (29) the equilibrium equations in (30) are easily rewritten in kinematic variables:

$$
(\mu^{11} + \chi^{11})(\Delta R_i - R_{j,ji}) + (2\mu^{11} + \lambda^{11})R_{j,ji} + 2\chi^{12}\omega^2_{n,m}e_{nmi} + P^V_i = 0, \tag{31}
$$

$$
(\mu^{33} + \chi^{33})[(\Delta\omega^2_i - \omega^2_{j,ji}) + 4]\omega^2_{j,ji} - 4\chi^{22}\omega^2_i + 2\chi^{12}R_{n,m}e_{nmi} = 0. \tag{32}
$$

3.1 Direct Integration of System of Equilibrium Equations

Let us take the rotor from the equations of equilibrium of forces:

$$2\chi^{12}(\Delta\omega_i^2 - \omega_{j,ji}^2) = (\mu^{11} + \chi^{11})\Delta R_{n,m} e_{nmi} + P_{n,m}^V e_{nmi} \tag{33}$$

Using last equation let's exclude $(\Delta\omega_i^2 - \omega_{j,ji}^2)$ from the equations of equilibrium of moments (32) with the help of (33) Then we obtain a general solution of the equations of the theory of Cosserat mediums for spins:

$$\begin{aligned}\omega_i^2 = {} & 4l_\omega^2\omega_{j,ji}^2 + (1/2)[\chi^{12}R_{n,m}e_{nmi} + l_\omega^2(\mu^{11} + \chi^{11})\Delta R_{n,m}e_{nmi}]/\chi^{22} \\ & + (l_\omega^2/2\chi^{12})P_{n,m}^V e_{nmi}\end{aligned} \tag{34}$$

Here $l_\omega^2 = (\mu^{33} + \chi^{33})/4\chi^{22}$.

Taking the divergence of the equations of equilibrium of the moments (32), we immediately obtain an equation for the divergence of the spins:

$$(\mu^{33} + \lambda^{33})\Delta\omega_{k,k}^2 - \chi^{22}\omega_{k,k}^2 = 0 \tag{35}$$

Let us calculate the rotor spin from (33):

$$\begin{aligned}2\chi^{12}\omega_{p,q}^2 e_{pqi} = {} & -(\chi^{12}\chi^{12}/\chi^{22})(\Delta R_i - R_{j,ji}) \\ & -(\mu^{11} + \chi^{11})l_\omega^2\Delta(\Delta R_i - R_{j,ji}) - l_\omega^2(\Delta P_i^V - P_{j,ji}^V)\end{aligned} \tag{36}$$

We can exclude the rotor spin from the equilibrium Eq. (31) using last equation. Then we obtain:

$$\begin{aligned}&(2\mu^{11} + \lambda^{11})R_{j,ji} + (\mu^{11} + \chi^{11} - \chi^{12}\chi^{12}/\chi^{22})(\Delta R_i - R_{j,ji}) + P_i^V \\ &-(\mu^{11} + \chi^{11})l_\omega^2\Delta(\Delta R_i - R_{j,ji}) - l_\omega^2(\Delta P_i^V - P_{j,ji}^V) = 0\end{aligned} \tag{37}$$

Equation (34) indeed gives a general solution for the spins, which is constructed from the general solutions of the Eqs. (35) and (37) by means of the equality (36).

It follows that the system of equations of the theory of Cosserat mediums reduces to the homogeneous Helmholtz Eq. (35) with respect to the spin divergence and the system of fourth-order equations of a special form (36) with respect to the displacement vector. The algebraic equation for the spins (34) can then be interpreted as the expansion of the spins by the sum of the operators from the

fundamental solutions of Eqs. (35) and (37). A special form of the equations of equilibrium of forces in displacements (37) is determined by the fact that the potential part of the displacement vector in the Cosserat media remains classical:

$$(2\mu^{11}+\lambda^{11})\Delta R_{k,k}+P^{V}_{k,k}=0 \tag{38}$$

Let us pay attention to the fact that the Young's modulus $E_0=(2\mu^{11}+\lambda^{11})$ in (38) is not damaged by dislocations and is a supermodulus. The Cosserat medium is a special case of media with conserved dislocations in which only one type of dislocation dominates—the ω-dislocations.

At the same time, the vortex part satisfies the equations not of the second but of the fourth order

$$\begin{aligned}&(\mu^{11}+\chi^{11}-\chi^{12}\chi^{12}/\chi^{22})\Delta(R_{i,j}-R_{j,i})-(\mu^{11}+\chi^{11})l^2_{\omega}\Delta\Delta(R_{i,j}-R_{j,i})\\&\quad+(P^{V}_{i,j}-P^{V}_{j,i})-l^2_{\omega}\Delta(P^{V}_{i,j}-P^{V}_{j,i})=0\end{aligned}$$

Here the situation is different. Even assuming the moment modulus $l^2_{\omega}=(\mu^{33}+\chi^{33})/4\chi^{22}$ is to be zero, we will get the effect of damage—instead of the modulus χ^{11} we will get a damaged ω-dislocation modulus $(\chi^{11}-\chi^{12}\chi^{12}/\chi^{22})$.

3.2 Physical Interpretation of Fundamental Solutions

By fundamental solutions we mean a system of linearly independent functions that satisfy a system of homogeneous resolving equations. This system of functions is sufficient for solving the corresponding mixed boundary-value problem. Let us introduce the "classical" equilibrium operator:

$$L_{ij}(\ldots)=E_0\partial^2(\ldots)_{,ij}+G_{\omega}[\Delta(\ldots)\delta_{ij}-\partial^2(\ldots)_{,ij}] \tag{39}$$

Here the quotes are set to emphasize the fact that there is a global effect in the theory of media with persistent dislocations—the damage of modulus G_0 and replacement with a modulus G_{ω}. By a direct verification we prove the commutativity Lemma:

$$[\Delta(\ldots)\delta_{ij}-\partial^2(\ldots)_{,ij}]L_{kj}R_j=G_{\omega}\Delta(\Delta R_i-R_{j,ij})=L_{ik}[\Delta(\ldots)\delta_{ij}-\partial^2(\ldots)_{,ij}]R_j$$

Then, following the Lemma the equilibrium Eq. (37) can be represented as the product of operators:

$$\begin{aligned}&\{(\ldots)\delta_{ik} - l_\omega^2 G_0/G_\omega[\Delta(\ldots)\delta_{ij} - \partial^2(\ldots)_{,ij}]\}(L_{kj}R_j + P_k^V)\\&\quad + l_\omega^2(G_0 - G_\omega)/G_\omega(\Delta P_i^V - P_{k,ij}^V) = 0\end{aligned} \tag{40}$$

Let's define the vector of cohesive displacements u_k:

$$u_k = -(l_\omega^2/G_\omega)(L_{kj}R_j + P_k^V) \tag{41}$$

Then the equations of equilibrium (40) lead to the equations that determine the equilibrium of the corresponding cohesive forces:

$$\begin{aligned}&G_0(\Delta u_i - u_{k,ik}) - (G_\omega/l_\omega^2)u_i\\&\quad + l_\omega^2[(G_0 - G_\omega)/G_\omega](\Delta P_i^V - P_{k,ik}^V) = 0\end{aligned} \tag{42}$$

It follows from (42) that in the Cosserat medium the cohesive displacement vector is a purely vortex vector:

$$u_{i,i} = 0 \tag{43}$$

Using (43) in the investigation of (41), we do not arrive at a contradiction, when we obtain (38).

Let us rewrite the definition of cohesive displacements (41) in the following form:

$$L_{kj}R_j + [P_k^V + (G_\omega/l_\omega^2)u_k] = 0 \tag{44}$$

It follows from (44) that if one can formulate its own boundary-value problem for cohesive displacements, the general solution of the theory of Cosserat mediums for displacements reduces to solving the system of equations of the "classical" theory of elasticity with an effective volume force having a vortex component.

Let us define a "classical" displacements:

$$U_i = (R_j + G_0/G_\omega u_j - R_j^*) \tag{45}$$

where vector R_i^* is the particular solution of the equation:

$$\begin{aligned}&E_0 R_{j,ij}^* + G_\omega(\Delta R_i^* - R_{j,ij}^*)\\&\quad + l_\omega^2[(G_0 + G_\omega)/G_\omega](\Delta P_i^V - P_{k,ik}^V) = 0\end{aligned} \tag{46}$$

Then, taking into account Eqs. (41), (42), (45) we establish that the Eq. (46) can be rewritten in the terms of the "classical" displacements. Other word the "classical" displacements satisfy the "classical" equations of equilibrium (see Eq. (39)):

$$L_{ik}U_k + P_i^V = 0 \tag{47}$$

Thus, we have got a general solution of the system of equilibrium equations in the theory of Cosserat mediums (see Eqs. (45)–(47)):

$$R_i = U_i - G_0/G_\omega u_i + R_i^* \tag{48}$$

The general solution (34) of the system of equilibrium equations for the moments in the theory of Cosserat mediums can be rewritten in terms of classical U_i and cohesive u_i displacements (48):

$$\begin{aligned}\omega_i^2 = {} & (4l_\omega^2)\omega_{k,ik}^2 + (\chi^{12}/2\chi^{22})U_{n,m}e_{nmi} \\ & - (G_0/2\chi^{12})(G_0/G_\omega)u_{n,m}e_{nmi} \\ & + (\chi^{12}/2\chi^{22})R_{n,m}^* e_{nmi} - (l_\omega^2/G_\omega)(\chi^{12}/2\chi^{22})P_{n,m}^V e_{nmi}\end{aligned}$$

Thus, the construction of a general solution of the theory of Cosserat mediums is reduced to the definition of six fundamental solutions: classical displacements U_i having three independent components, cohesive displacements u_i having two independent components, and a pseudoscalar $\omega_{k,k}^2$. Correspondingly, the bound boundary value problem (29), (30) gives six boundary conditions at each nonsingular point of the surface of the body.

3.3 Aero-Kuvshinskii Model

The fundamental solution of the theory of Cosserat's media, is defined as the general solution of the homogeneous Helmholtz Eq. (34). If we formally search for the slowly varying part of the solution of this equation, neglecting the Laplacian of the function in comparison with the function itself, we will obtain:

$$\omega_{k,k}^2 = 4l_\omega^2 \Delta\omega_{k,k}^2 \approx 0 \tag{49}$$

This means that when constructing a slowly varying part of the solution, we can neglect the fundamental solution that determines the purely dislocation kinematic state. The general solution for the spins will then (49) be completely determined by the displacement field, as follows from (34):

$$\begin{aligned}\omega_i^2 = {} & (\chi^{12}/\chi^{22})\omega_i^1 \\ & + l_\omega^2[(\mu^{11} + \chi^{11})/\chi^{12}]\Delta\omega_i^1 - (l_\omega^2/2\chi^{12})P_{n,m}^V e_{nmi}\end{aligned} \tag{50}$$

Here $\omega_i^1 = -(1/2)R_{n,m}e_{nmi}$.

The approximate solution (50) in the theory of Cosserat mediums can be interpreted as a hypothesis about the existence of a kinematic connection between spins and displacement vortices. This hypothesis allows us to formulate a correct variational formulation of the corresponding boundary-value problem. The Aero-Kuvshinskii model, in turn, is a more "rigid" special case of the Cosserat model than the formula (50) proposed above.

A special case (50) is the hypothesis of proportionality of spins to constrained rotations. It is this hypothesis that leads to the Aero-Kuvshinskii model:

$$\omega_k^2 = -(\chi^{12}/\chi^{22})R_{p,q}e_{pqk} = 2(\chi^{12}/\chi^{22})\omega_k^1 \tag{51}$$

With such a "hard" hypothesis, spins can be algebraically excluded from the Cosserat Lagrangian. Thus, in the Aero-Kuvshinskii model, only displacements can be chosen as the main unknowns, and Lagrangian can be formulated with respect to them. At the same time, we should pay attention to this fact, that the dislocation density in the Aero-Kuvshinskii model is different from zero. The nonzero spins ω_k^2 are related by the hypothesis (51) with displacements. They determine the corresponding nonzero pseudotensor-source of dislocations in the theory of Aero-Kuvshinskii:

$$\Xi_{ij} = (\omega_{j,i}^2 - \omega_{k,k}^2\delta_{ij}) = (\chi^{12}/\chi^{22})R_{p,iq}e_{pqj} \neq 0$$

As a result, we obtain the variational equation of the Aero-Kuvshinskii model from the variational equation of the Cosserat model (28)–(30), taking into account the additionally introduced kinematic constraint (51):

$$\begin{aligned}
\delta L &= \iiint [(\sigma_{ij,j} + P_i^V)\delta R_i + (m_{ij,j} - p_i)\delta\omega_i^2]dV \\
&\quad + \oiint [(P_i^F - \sigma_{ij}n_j)\delta R_i - (m_{ij}n_j + a_i)\delta\omega_i^2]dF \\
&= \iiint [(\sigma_{ij,j} + P_i^V)\delta R_i - \mu_k^V e_{ijk}\delta R_{i,j}]dV \\
&\quad + \oiint [(P_i^F - \sigma_{ij}n_j)\delta R_i + \mu_k^F e_{ijk}\delta R_{i,j}]dF \\
&= \iiint (\sigma_{ij,j} + \mu_{k,j}^V e_{ijk} + P_i^V)\delta R_i dV \\
&\quad + \oiint \{[P_i^F - (\sigma_{ij} + \mu_k^V e_{ijk})n_j - \mu_{k,p}^F(\delta_{pj} - n_p n_j)e_{ijk}]\delta R_i \\
&\quad + \mu_k^F n_j\, e_{ijk}\delta(R_{i,p}n_p)\}dF + \sum \oint \mu_k^F v_j e_{ijk}\delta R_i ds = 0
\end{aligned}$$

For brevity we introduced the notation:

$$\mu_k^V = (1/2)(\chi^{12}/\chi^{22})(m_{kl,l} - p_k)$$
$$\mu_k^F = (1/2)(\chi^{12}/\chi^{22})(m_{kl}n_l + a_k)$$

Thus, as a consequence of simplifying hypotheses, both the Cosserat medium model and the Aero-Kuvshinskii medium model are obtained from the model of a medium with conserved dislocations. We note that a characteristic feature of the Aero-Kuvshinskii medium model is that at each nonsingular point of the surface the variational equation gives not six (as in the Cosserat model) but five boundary conditions:

$$\begin{aligned}&(\mu_k^F n_j e_{ijk})\delta(R_{i,q}n_q) = (\mu_k^F n_j e_{ijk})\delta(R_{p,q}\delta_{pi}n_q)\\ &= (\mu_k^F n_j e_{ijk})\delta(R_{p,q}(\delta_{pi} - n_p n_i + n_p n_i)n_q)\\ &= (\mu_k^F n_j e_{ijk})\delta(R_{p,q}(\delta_{pi} - n_p n_i)n_q) + (\mu_k^F n_j e_{ijk})\delta(R_{p,q}n_p)n_q\end{aligned}$$

It is easy to verify this by paying attention to the convolution identically equal to zero $n_i n_j e_{ijk} \equiv 0$. Finally, the variational equation of the Aero-Kuvshinskii media acquires the following final form:

$$\begin{aligned}\delta L = &\iiint (\sigma_{ij,j} + \mu_{k,j}^V e_{ijk} + P_i^V)\delta R_i dV\\ &+ \oiint \{[P_i^F - (\sigma_{ij} + \mu_k^V e_{ijk})n_j - \mu_{k,p}^F(\delta_{pj} - n_p n_j)\, e_{ijk}]\delta R_i\\ &+ \mu_k^F n_j\, e_{ijk}\delta(R_{p,q}n_q)(\delta_{pi} - n_p n_i)\}dF\\ &+ \sum \oint \mu_k^F v_j\, e_{ijk}\delta R_i ds = 0\end{aligned} \tag{52}$$

We have specially considered here the model of Aero-Kuvshinskii (52) as an applied model in the framework of the theory of Cosserat mediums for the following reasons:

1. The Aero-Kuvshinskii model is formulated only in displacements, that are conveniently and visually.
2. The basic properties of the medium are described by equations in displacements, however, the boundary value problem is simpler.

The hypothesis of Aero-Kuvshinskii on the proportionality of spins and vortices allows us to transfer this hypothesis to the general case of media with conserved dislocations and to formulate the generalized Aero-Kuvshinskii hypothesis in the following form:

$$d_{ij}^{\Xi} = aR_{k,k}\delta_{ij} + bR_{i,j} + cR_{i,j} \tag{53}$$

The Aero-Kuvshinskii conjecture in the form (53) will make it possible to formulate the applied theory of the medium with conserved dislocations in displacements with six boundary conditions at each nonsingular point of the surface of the body.

4 Theory of Porous Media

We consider the following special case of a general theory in which only θ-dislocations dominate. Let's formulate simplifying hypotheses. Deviator of free distortion tensor is zero and spins are equal to zero:

$$\gamma_{ij}^{2} = 0, \omega_{k}^{2} = 0 \tag{54}$$

Free distortion tensor takes the form:

$$d_{ij}^{2} = (1/3)\theta^{2}\delta_{ij} \tag{55}$$

Consequently, the pseudotensor-source of dislocations is written as follows:

$$\Xi_{ij} = d_{in,m}^{2} e_{nmj} = (-1/3)\theta_{,k}^{2} e_{ijk} \tag{56}$$

According to with (54)–(56) the Lagrangian takes the form:

$$\begin{aligned} L = A - (1/2)\iiint \{ & C_{ijnm}^{11} R_{n,m} R_{i,j} - 2C_{ijnm}^{12} R_{n,m}(1/3)\theta^{2}\delta_{ij} \\ & + C_{ijnm}^{22}((1/3)\theta^{2}\delta_{nm})((1/3)\theta^{2}\delta_{ij}) + C_{ijnm}^{33}((1/3)\theta_{,p}^{2} e_{nmp})((1/3)\theta_{,q}^{2} e_{ijq})\} dV \\ & - (1/2)\oiint A_{ijnm}((1/3)\theta^{2}\delta_{nm})((1/3)\theta^{2}\delta_{ij}) dF \end{aligned}$$

Let us calculate the convolutions of the modulus tensors that appeared in Lagrangian after simplifying hypotheses, assuming that $\chi^{11} = 0$:

$$\begin{aligned} & (A_{ijnm}\delta_{ij}\delta_{nm}) = 4(\mu^{F} + \lambda^{F}), \quad (C_{ijnm}^{12}\delta_{ij}) = (2\mu^{12} + 3\lambda^{12})\delta_{nm}, \\ & (C_{ijnm}^{22}\delta_{ij}\delta_{nm}) = 3(2\mu^{22} + 3\lambda^{22}), \quad (C_{ijnm}^{33} e_{ijp} e_{nmq}) = 4\chi^{33}\delta_{pq} \end{aligned}$$

Then, substituting the convolutions into Lagrangian we obtain the final formulation of the functional for porous media:

$$L = A - (1/2)\iiint \{2\mu^{11}\gamma^1_{ij}\gamma^1_{ij} + (1/3)(2\mu^{11} + 3\lambda^{11})\theta^1\theta^1 - (2/3)(2\mu^{12} + 3\lambda^{12})\theta^1\theta^2 + (1/3)(2\mu^{22} + 3\lambda^{22})\theta^2\theta^2 + (4/9)\chi^{33}\theta^2_{,k}\theta^2_{,k}\}dV - (1/2)\oiint \{(4/9)(\mu^F + \lambda^F)\theta^2\theta^2\}dF \tag{57}$$

In accordance with (57), the Hooke's law equations for the theory of porous media take the form of:

$$\sigma_{ij} = \frac{\partial U_V}{\partial(R_{i,j})} = 2\mu^{11}\gamma^1_{ij} + (1/3)K^{11}\theta^1\delta_{ij} - (1/3)K^{12}\theta^2\delta_{ij}$$
$$p_{kk} = \frac{\partial U_V}{\partial\theta^\Xi} = -(1/3)K^{12}\theta^1 + (1/3)K^{22}\theta^2, \quad m_k = \frac{\partial U_V}{\partial(\theta^2_{,k})} = (4/9)\chi^{33}\theta^2_{,k} \tag{58}$$

where $K^{pq} = (2\mu^{pq} + 3\lambda^{pq})$.

We note that here (58), as in Cosserat's theory, dislocation stresses and moments are also determined. The moment vector in this case coincides in direction with the gradient of porosity and is an important characteristic in studying the evolution of cracks in a porous medium.

Let us write down the basic variational equality of the theory of porous media:

$$\delta L = \iiint \{[\mu^{11}\Delta R_i + (\mu^{11} + \lambda^{11})R_{j,ij} - (1/3)K^{12}\theta^2_{,i} + P^V_i]\delta R_i + (1/3)[(4/3)\chi^{33}\Delta\theta^2 - K^{22}\theta^2 + K^{12}\theta^1]\delta\theta^2\}dV + \oiint \{P^F_i - [\mu^{11}R_{i,k}n_k + \mu^{11}R_{j,i}n_j + \lambda^{11}R_{k,k}n_i - K^{12}\theta^2 n_i]\}\delta R_i dF - (4/9)\oiint \{\chi^{33}\theta^2_{,k}n_k + (\mu^F + \lambda^F)\theta^2\}\delta\theta^2 dF = 0 \tag{59}$$

The variational Eq. (59), and constitutive Eq. (58) give a complete description of the boundary-value problem of the theory of porous media: there are four resolving equations with respect to four unknown functions R_i, θ^Ξ, and four boundary conditions at each nonsingular point of the surface.

4.1 Identification of Moduli

In the absence of pores (i.e., $(2\mu^{12} + 3\lambda^{12}) = 0$), the displacement vector is a solution to the classical theory of elasticity, and the moduli μ^{11} and λ^{11} are the Lame classical parameters of the ideal, unaffected θ-dislocations, of the medium,

$\mu^{11} = G, \quad 2\mu^{11} + \lambda^{11} = E$. For $(2\mu^{12} + 3\lambda^{12}) \neq 0$, the boundary-value problem does not decay, and θ-dislocations (pores) are not zero. We will seek an approximate solution in the form:

$$R_i = (1/3)\theta^1 x_i, \quad \theta^1 = Const\_1, \quad \theta^2 = Const\_2 \tag{60}$$

at $P_i^V = 0$ and $P_i^F = \Delta P n_i$, where ΔP—the increment of the constant value of the external load normal to the surface of the body.

Using (60) and solving by Ritz method, we get:

$$\begin{aligned} &\{-[((2\mu^{22} + 3\lambda^{22})/3)V + (4/9)(\mu^F + \lambda^F)F]\theta^2 \\ &\quad + (1/3)(2\mu^{12} + 3\lambda^{12})\theta^1 V\}\delta\theta^2 \\ &\quad + \{\Delta P - (2\mu^{11} + 3\lambda^{11})\theta^1 + (2\mu^{12} + 3\lambda^{12})\theta^2]\}V\delta\theta^1 = 0 \end{aligned} \tag{61}$$

Here it is taken into account that

$$V = (1/3)\iiint (\partial x_i/\partial x_j)\delta_{ij}dV = (1/3)\oiint x_i n_j \delta_{ij} dF = (1/3)\oiint x_i n_i dF$$
$$\oiint x_i n_i dF = 3V$$

The solution of (61) is the following relations:

$$\theta^1 = (\Delta P/3K^{11})(1 + S_F)/S, \quad \theta^2 = (\Delta P/K^{11})(K^{12}/K^{22})/S \tag{62}$$

where

$$S = [1 + (4/3)(\mu^F + \lambda^F)/(2\mu^{22} + 3\lambda^{22})(F/V) - (K^{12}/K^{11})(K^{12}/K^{22})]$$
$$S_F = (4/3)(\mu^F + \lambda^F)/(2\mu^{22} + 3\lambda^{22})(F/V)$$

Let's define the total volume change:

$$\Delta V = \iiint (D_{ij}^1 + D_{ij}^2)\delta_{ij}dV = \iiint R_{i,j}dV + \iiint \theta^{\Xi}dV \tag{63}$$

Here $R_{i,j}$ it can be interpreted as a local change in volume $\left(\iiint R_{i,i}dV = \oiint R_i n_i dF\right)$ of undamaged material, but θ^2 as a local change in volume due to reversible "opening" of pores.

Taking into account the solution of (62), Eq. (63) takes the form:

$$(\Delta P/K^{11})[1 + S_F + (K^{11}/K^{22})]/S = \Delta V/V \tag{64}$$

Taking into account (64), the solution of (62) can be rewritten in the form of:

$$\theta^1 = (1+S_F)/[1+S_F+K^{12}/K^{22}](\Delta V/V) = (1-f_\theta)(\Delta V/V)$$
$$\theta^2 = (K^{12}/K^{22})/[1+S_F+K^{12}/K^{22}](\Delta V/V) = f_\theta(\Delta V/V) \tag{65}$$

The solution in the form of (65) provides a basis for treating the medium, damaged by persistent θ-dislocations, as a finely dispersed composite in which the ideal medium with a relative volume fraction $(1-f_\theta)$ plays the role of the matrix, and the role of the inclusions is θ-dislocations with a relative volume fraction f_θ. Thus, it possible to treat a combination of nonclassical moduli f_θ as the relative volume fraction of θ-dislocations:

$$f_\theta = (K^{12}/K^{22})/[1+S_F+K^{12}/K^{22}] \tag{66}$$

Accordingly, (64) makes it possible to treat a combination of nonclassical moduli K_θ as an effective bulk modulus of such a composite:

$$K_\theta = K^{11}S/[1+S_F+K^{12}/K^{22}] \tag{67}$$

It is seen from (67) that the volume compression modulus K_θ, which is damaged by the conserved θ-dislocations, is always smaller than the ideal bulk compression modulus $K^{11} = (2\mu^{11}+3\lambda^{11})$. Thus, relations (66) and (67) are established between the formal parameters of the medium and the experimentally measurable parameters G, E, f_θ and K_θ. It should be noted that in accordance with the proposed interpretations, the term $(1/2)\iiint (1/3)(2\mu^{11}+3\lambda^{11})\theta^1\theta^1 dV$ in the Lagrangian of porous media acquires the meaning of the potential energy of changing the volume of an intact part of the medium material, the term $(1/2)\iiint (1/3)(2\mu^{22}+3\lambda^{22})\theta^2\theta^2 dV$—of the potential energy of the formation of a new volume in the damaged medium due to the reversible "opening" of the pores, and the term $(1/2)\iiint (1/3)(2\mu^{12}+3\lambda^{12})\theta^1\theta^2 dV$—of the potential pore interaction energy with an intact part of the medium material. Accordingly, the nonclassical modulus $(2\mu^{22}+3\lambda^{22})$ acquires the meaning of the energy of formation of a unit volume due to the reversible "opening" of the pores, and the nonclassical modulus $(2\mu^{12}+3\lambda^{12})$ acquires the meaning of the energy of formation of a unit volume due to a single change in the volume of the intact part of the medium material.

Similar arguments and interpretations can be made for the surface of the body. Let's give the definition of the total change in the surface of the body:

$$\Delta F = (D^1_{ij}+D^2_{ij})(\delta_{ij}-n_i n_j)dF = \oiint_{i,j}(\delta_{ij}-n_i n_j)dFR + \oiint (2/3)\theta^2 dF \tag{68}$$

The first term (68) gives the definition of the local area change due to stretching $\Delta F_{elastic}/F$:

$$\Delta F_{elastic}/F = R_{i,j}(\delta_{ij} - n_i n_j) \tag{69}$$

The second term (68) gives the definition of the area change due to the formation of a new surface associated with the reversible opening of pores on the surface $\Delta F_{pores}/F$:

$$\Delta F_{pores}/F = (2/3)\theta^2 \tag{70}$$

From (62) to (68) it follows that:

$$\begin{gathered} \oiint R_{i,j}(\delta_{ij} - n_i n_j)dF = (2/3)(\Delta P/K_\theta) f_\theta F, \\ \oiint (2/3)\theta^2 dF = (2/3)(\Delta P/K_\theta)(1 - f_\theta)F \\ \Delta F/F = (2/3)(\Delta P/K_\theta) = (2/3)(\Delta V/V) \end{gathered} \tag{71}$$

It follows from (65) to (71) that both the distribution of the volume change and the distribution of the surface change with respect to the stretching and reversible formation of the new geometry in porous media are realized in the same proportion. The coefficient of proportionality $k = f_\theta/(1 - f_\theta)$ is determined by the relative volume fraction of θ-dislocations. Let us consider the "classical" static boundary conditions:

$$P_i^F n_i = (2\mu^{11} + \lambda^{11})(R_{i,k} n_k) n_i + \lambda^{11} R_{i,j}(\delta_{ij} - n_i n_j) - (1/3)(2\mu^{12} + 3\lambda^{12})\theta^2 \tag{72}$$

Let's define the hydrostatic pressure:

$$p = (2\mu^{11} + 3\lambda^{11})R_{k,k} - (2\mu^{12} + 3\lambda^{12})\theta^2 \tag{73}$$

It turned out that:

$$(R_{i,k} n_k) n_i = p/K^{11} - R_{i,j}(\delta_{ij} - n_i n_j) + (K^{12}/K^{11})\theta^2 \tag{74}$$

The boundary condition (72) with allowance for (73) and (74) gives:

$$P_i^F n_i = [(2\mu^{11} + \lambda^{11})/K^{11}]p - 2\mu^{11} R_{i,j}(\delta_{ij} - n_i n_j) + (4/3)\mu^{11}(K^{12}/K^{11})\theta^2$$

Let us write down the last equation for the pressure and take into account the definitions (69) and (70):

$$\begin{aligned} p = {} & [K^{11}/(2\mu^{11} + \lambda^{11})]\Delta P + 2\mu^{11}[K^{11}/(2\mu^{11} + \lambda^{11})](\Delta F_{elastic}/F) \\ & - 2\mu^{11}[K^{12}/(2\mu^{11} + \lambda^{11})](\Delta F_{pores}/F) \end{aligned} \tag{75}$$

Thus, in addition to the classical surface tension, activated complex theory also describes the process of reversible formation of a new surface due to the opening of pores on the surface. The change in the total area due to the formation of a new surface is determined through the expression (70). Hence, it can be concluded that the density of the surface potential energy in the activated complex theory is determined completely by the energy of the formation of a new surface:

$$U_F = (1/2)(\mu^F + \lambda^F)(\Delta F_{pores}/F)(\Delta F_{pores}/F) \tag{76}$$

In this case, the modulus $K^F = (\mu^F + \lambda^F)$ in the theory of porous media should be treated unambiguously as the doubled energy of formation of a unit surface. Indeed, when $\Delta F_{pores}/F = 1,$ it follows from (76) that:

$$(\mu^F + \lambda^F) = 2U_F|_{(\Delta F_{pores}/F)=1} = K^F \tag{77}$$

Thus, (66), (67) and (77) have been established between the formal parameters of the medium and the experimentally measurable parameters G, E, f_θ, K_θ and K^F. The physical meaning of the remaining sixth formal parameter χ^{33} can hardly be clarified with the help of a polynomial solution, since any polynomial solution determines a slowly varying part of the solution. The formal parameter χ^{33}, on the contrary, determines the rapidly changing part of the solution. To clarify its physical meaning, it is necessary to formulate and solve the boundary value problem for some rapidly changing local state.

4.2 General Solution in Theory of Porous Media

We represent the system of four equilibrium equations for the theory of porous media in the form of a subsystem of three equilibrium equations in displacements and one equation with respect to porosity θ^2. To do this, let's define the Laplacian from the porosity θ^2 of the "classical" equilibrium equations and exclude it from the scalar equilibrium equation (in the same way as was done in the construction of the general solution of the equations of the theory of Cosserat mediums):

$$\begin{aligned}\theta^2 = {} & (K^{12}/K^{22})R_{k,k} + (2\mu^{11} + \lambda^{11})[(4\chi^{33}/K^{22})/K^{12})]\Delta R_{k,k} \\ & + [(4\chi^{33}/K^{22})/K^{12})]P^V_{k,k}\end{aligned} \tag{78}$$

$$\begin{aligned}&\mu^{11}(\Delta R_i - R_{j,ji}) + [2\mu^{11} + \lambda^{11} - (1/3)K^{12}(K^{12}/K^{22})]R_{j,ji} \\ &- (1/3)[(4\chi^{33}(2\mu^{11} + \lambda^{11})/K^{22})]\Delta R_{j,ji} + P^V_i - (1/3)[(4\chi^{33}/K^{22})]P^V_{j,ji} = 0\end{aligned} \tag{79}$$

Thus, the theory of porous media can be formulated in displacements. Equation (78) allow to find value of porosity, if displacement vector is known.

Let us investigate the structure of the general solution of the formulated system. First we assign a "classical" equilibrium operator $L_{ij}(\ldots)$ and represent the operator of system (79) as the product of two operators. One of these operators is the "classical" equilibrium operator. This operator defines the fundamental solution corresponding to the "classical" displacement vector. The second operator must determine the "cohesive" displacements ("cohesive" field). Accordingly, a linear combination of fundamental solutions will give a general solution to the theory of porous media. Let's implement this procedure. A "classical" equilibrium operator $L_{ij}(\ldots)$ has view:

$$\begin{aligned} L_{ij}(\ldots) = {} & \mu^{11}[\Delta(\ldots)\delta_{ij} - (\ldots)_{,ij}] \\ & + [2\mu^{11} + \lambda^{11} - (1/3)K^{12}(K^{12}/K^{22})](\ldots)_{,ij} \end{aligned} \tag{80}$$

It follows immediately from (80), that

$$\Delta(R_{j,j}) = (1/[2\mu^{11} + \lambda^{11} - (1/3)K^{12}(K^{12}/K^{22})])(L_{ij}R_j)_{,i}$$

Eliminating $\Delta(R_{j,j})$ from (79), we will obtain:

$$\begin{aligned} & (L_{ij}R_j + P_i^V) - \frac{[(4\chi^{33}(2\mu^{11} + \lambda^{11})/K^{22})]}{3[2\mu^{11} + \lambda^{11} - (1/3)K^{12}(K^{12}/K^{22})]}(L_{kj}R_j + P_k^V)_{,ik} \\ & + \frac{4\chi^{33}(K^{12}/K^{22})^2}{9[2\mu^{11} + \lambda^{11} - (1/3)K^{12}(K^{12}/K^{22})]}P_{k,ik}^V = 0 \end{aligned}$$

Let's introduce the definition of the length of a cohesive field l_θ for porous media:

$$l_\theta^2 = \frac{[(4\chi^{33}(2\mu^{11} + \lambda^{11})/K^{22})]}{3[2\mu^{11} + \lambda^{11} - (1/3)K^{12}(K^{12}/K^{22})]} \tag{81}$$

Thus, all relations (66), (67), (77) and (81) are established between the formal parameters of the porous medium $\mu^{11}, \lambda^{11}, K^{12}, K^{22}, (\mu^F + \lambda^F), \chi^{33}$ and the experimentally measurable parameters $G, E, f_\theta, K_\theta, K^F$ and l_θ.

It is important to note that taking into account (81), we can rewrite Eq. (79), in the form of a product of operators:

$$\begin{aligned} & [(\ldots)\delta_{ik} - l_\theta^2(\ldots)_{,ik}](L_{kj}R_j + P_k^V) \\ & + l_\theta^2(1/3)(K^{12}/K^{22})[K^{12}/(2\mu^{11} + \lambda^{11})]P_{k,ik}^V = 0 \end{aligned}$$

The found operator of the "cohesive" field makes it possible to determine "cohesive" displacements:

$$u_k = -(l_\theta^2/[2\mu^{11} + \lambda^{11} - (1/3)K^{12}(K^{12}/K^{22})])(L_{kj}R_j + P_k^V) \tag{82}$$

and the equations of equilibrium of "cohesive" forces:

$$u_{k,ik} - (1/l_\theta^2)u_i + \frac{(K^{12}/K^{22})[K^{12}/(2\mu^{11} + \lambda^{11})]}{3[2\mu^{11} + \lambda^{11} - (1/3)K^{12}(K^{12}/K^{22})]} P_{k,ik}^V = 0 \tag{83}$$

Taking the rotor (83), we can verify that in porous media cohesive displacements are potential:

$$u_{i,j} - u_{j,i} = 0 \tag{84}$$

Therefore, introducing potential u, we reduce the vector Eq. (83) to the scalar one:

$$\begin{aligned} &u_i = u_{,i} \\ &\Delta u - (1/l_\theta^2)u + \frac{(K^{12}/K^{22})[K^{12}/(2\mu^{11} + \lambda^{11})]}{3[2\mu^{11} + \lambda^{11} - (1/3)K^{12}(K^{12}/K^{22})]} P_{k,k}^V = 0 \end{aligned} \tag{85}$$

The equation of the cohesive field (85) allow to determine the scale parameter l_θ (multiscale effects) in (81), (83). Equation (79) can be represented in the form:

$$L_{ij}(R_j + u_j - R_j^*) + P_i^V = 0 \tag{86}$$

where R_j^* is a particular solution of system:

$$\begin{aligned} &\mu^{11}(\Delta R_i^* - R_{j,ij}^*) + [2\mu^{11} + \lambda^{11} - (1/3)K^{12}(K^{12}/K^{22})]R_{j,ij}^* \\ &\quad + (1/3)(K^{12}/K^{22})[K^{12}/(2\mu^{11} + \lambda^{11})]P_{k,ij}^V = 0 \end{aligned}$$

Equation (86) has the form of a "classical" equilibrium operator over a certain vector. It is natural to define this vector as a vector of classical displacements U_i:

$$U_i = R_i + u_i - R_i^* \tag{87}$$

Using (87), we obtain:

$$L_{ij}U_j + P_i^V = 0 \tag{88}$$

Rewriting (87) with respect to the total displacement vector, we obtain the general solution of the equations of the theory of porous media:

$$R_i = U_i - u_{,i} + R_i^* \tag{89}$$

where U_i—the fundamental solution corresponding to the "classical" equilibrium Eq. (89), u is the fundamental solution corresponding to the cohesive field (85). Thus, instead of the four unknown functions R_i and θ^2, the problem is formulated with respect to classical displacements U_i and the potential of cohesive displacements u.

5 Model of Media with "Twinning"

Let us consider the third special case of the general theory, when γ-dislocations dominate. In this case $\theta^2 = 0$ and $\omega_k^2 = 0$, and the tensor of free distortion has view $D_{ij}^2 = \gamma_{ij}^2$. Accordingly, the pseudotensor-source of dislocations is transformed:

$$\Xi_{ij} = \gamma_{in,m}^2 \vartheta_{nmj} \tag{90}$$

The Lagrangian for media with twinning is obtained as a special case of the general theory with allowance for kinematic model $D_{ij}^2 = \gamma_{ij}^2$ and (90):

$$\begin{aligned} L = A - (1/2) \iiint \{ C_{ijnm}^{11} R_{n,m} R_{i,j} - 4\mu^{12} R_{i,j} \gamma_{ij}^2 + 2\mu^{22} \gamma_{ij}^2 \gamma_{ij}^2 + C_{ijnm}^{33} \Xi_{nm} \Xi_{ij} \} dV \\ - (1/2) \oiint a_{ijnm} \gamma_{nm}^2 \gamma_{ij}^2 dF \end{aligned} \tag{91}$$

Equations of the Hooke law in media with twinning follow from (91) and have the form:

$$\begin{aligned} \sigma_{ij} &= \frac{\partial U_V}{\partial R_{i,j}} = C_{ijnm}^{11} R_{n,m} - 2\mu^{12} \gamma_{ij}^2, p_{ij} = \frac{\partial U_V}{\partial \gamma_{ij}^2} = 2(-\mu^{21} \gamma_{ij}^1 + \mu^{22} \gamma_{ij}^2) \\ m_{ij} &= \frac{\partial U_V}{\partial \Xi_{ij}} = C_{ijnm}^{33} \Xi_{nm} = \mu^{33} (\gamma_{ip,q} e_{pqj} + \gamma_{jp,q} e_{pqi}) + \chi^{33} (\gamma_{ip,q} e_{pqj} - \gamma_{jp,q} e_{pqi}) \\ a_{ij} &= \frac{\partial U_F}{\partial \gamma_{ij}^2} = a_{ijnm}^{11} \gamma_{nm}^2 = [\mu^F (\delta_{in} - n_i n_n)(\delta_{jm} - n_j n_m) \\ &\quad + \mu^F (\delta_{im} - n_i n_m)(\delta_{jn} - n_j n_n) \\ &\quad + \lambda^F n_i n_j n_n n_m + \delta^F n_i n_n (\delta_{jm} - n_j n_m)] \gamma_{nm}^2 \end{aligned} \tag{92}$$

Taking into account (91), (92), we will obtain the variational equation of the theory of media with twinning:

$$\delta L = \iiint \{(\sigma_{ij,j} + P_i^V)\delta R_i - (m_{in,m}\vartheta_{nmj} + p_{ij})\delta\gamma_{ij}^2\} dV + \oiint \{(P_i^F - \sigma_{ij}n_j)\delta R_i + (m_{in}n_m\vartheta_{nmj} - a_{ij})\delta\gamma_{ij}^2\} dF = 0 \tag{93}$$

As can be seen from the Euler Eqs. (93), (92) each point of the investigated medium has eight degrees of freedom: three components of the displacement vector R_i and five independent components of the deviator tensor γ_{ij}^2. The boundary conditions on the surface of the body are also determined by eight degrees of freedom. Equilibrium equations as a whole contain six formal parameters of the medium.

5.1 Fundamental Solutions

To isolate the subsystem of equations by the displacement vector, we take the divergence of the tensor equation of equilibrium of the moments and exclude $\gamma_{ij,j}^2$ from it, determined from the vector equilibrium equation:

$$\begin{aligned} &2\mu^{12}\gamma_{ij,j}^2 = \mu^{11}(\Delta R_i - R_{j,ji}) + (2\mu^{11} + \lambda^{11})R_{j,ji} + P_i^V \\ &G_D(\Delta R_i - R_{j,ji}) + E_D R_{j,ji} + P_i^V \\ &\quad - (\chi^{33}/3\mu^{22})[(2\mu^{11} + \lambda^{11})\Delta R_{j,ji} + P_{j,ji}^V] \\ &\quad - [(\mu^{33} + \chi^{33})/4\mu^{22}][\mu^{11}\Delta(\Delta R_i - R_{j,ji}) + (\Delta P_i^V - P_{j,ji}^V)] = 0 \end{aligned} \tag{94}$$

Thus, equilibrium equations for displacements are formulated.

Let's show that the displacement vector R_i can be represented in terms of two fundamental vectors. The first vector U_i is a vector of "classical" displacements that satisfies the "classical" equilibrium equations. The second vector u_i is the cohesive displacement vector. The definition of "classical" U_i and cohesive u_i displacements follows the same pattern as in the theory of Cosserat mediums and in the theory of porous media described above:

$$U_j = R_j - (\chi^{33}/3\mu^{22})(E/E_D)R_{k,kj} - [(\mu^{33} + \chi^{33})/4\mu^{22}](G/G_D)(\Delta R_j - R_{k,kj})$$
$$u_j = -L_{jk}R_k/C, \quad L_{jk}(\ldots) = E_D(\ldots)_{,jk} + G_D[\Delta(\ldots)\delta_{jk} - (\ldots)_{,jk}]$$

where: C—is some normalization dimension multiplier [Pa/m^2], and

$$E_D = [4(\mu^{11}\mu^{22} - \mu^{12}\mu^{12})/3\mu^{22}] + (2\mu^{11} + 3\lambda^{11})/3$$
$$G_D = (\mu^{11}\mu^{22} - \mu^{12}\mu^{12})/\mu^{22}$$

Note that we use the definition of "classical" in order to emphasize the difference between this operator and the classical Lame operator. In this operator there are not ideal moduli $\mu^{11} = G, \quad 2\mu^{11} + \lambda^{11} = E,$ but defective moduli $\mu^{11} > G_D, \quad 2\mu^{11} + \lambda^{11} > E_D$. After substitution of R_i in the Eq. (94), they acquire the form of "classical" equilibrium equations with a modified load, depending on the second derivatives of the volume forces:

$$L_{ij}U_j + P_i^V - (\chi^{33}/3\mu^{22})P_{j,ji}^V - [(\mu^{33} + \chi^{33})/4\mu^{22}](\Delta P_i^V - P_{j,ji}^V) = 0 \tag{95}$$

The volume load in the "classical" Eq. (95) is modified due to the influence of dislocations, which are reflected by the multipliers for the derivatives in (95).

After u_j substitution in the resolving equations, they acquire the form of equilibrium equations for the "cohesive" interactions of the "basic" model:

$$\begin{aligned} &C\{(\chi^{33}/3\mu^{22})(E/E_D)u_{j,ji} + [(\mu^{33} + \chi^{33})/4\mu^{22}](G/G_D)(\Delta u_i - u_{j,ji}) - u_i\} \\ &+ P_i^V - (\chi^{33}/3\mu^{22})P_{j,ji}^V - [(\mu^{33} + \chi^{33})/4\mu^{22}](\Delta P_i^V - P_{j,ji}^V) = 0 \end{aligned} \tag{96}$$

Let's assume that the cohesive moduli μ^{33} and χ^{33} are proportional, so that the second-order operator in the above Eq. (96) coincides with the classical operator Lame. Then we can establish that $R_i = U_i - u_i$. Thus, we can find six fundamental solutions U_i and u_i. With known displacements, the system of tensor equations of moments with the aid of first Eq. (94) can be transformed to inhomogeneous equations with respect to twinning, with right-hand sides that depend on displacements. Then, solution of these tensor equations can be constructed as the sum of the general solution of a homogeneous equations and the particular solutions.

6 Conclusion

In this paper, based on the variational kinematic approach [16–21], a complete and correct model of media with conserved dislocations is given. On the basis of the kinematic analysis, a new classification of dislocations is proposed, which makes it possible to distinguish three types of dislocations: γ-dislocations, θ-dislocations, and ω-dislocations. This classification gives a new kinematic interpretation of dislocations, since it reflects the relationship of dislocations with the shape change —γ, with a change in volume θ (porosity) and with twisting ω (spins). Partial theories are considered in which one of the three types of dislocations dominates.

As an example of applied theory, the theory of Aero-Kuvshinskii media is considered, the characteristic feature of which is the formulation of the boundary-value problem only with respect to the displacement vector. Dislocations are determined after the solution by differentiation. Generalizations of Aero-Kuvshinskii hypotheses about the proportionality of free and constrained

distortion are formulated, which makes it possible to construct an applied version of the theory with a reduced number of boundary conditions (six boundary conditions in common case instead of nine).

Acknowledgements This work was supported particular by the Russian Foundation for Basic Research project No. 15-01-03649 and 16-01-00623, 17-01-00837.

References

1. Dislocations in Solids, 1st edn. In: Hirth, J. (eds.) A tribute to F.R.N. Nabarro, vol. 14, p. 650 (2008)
2. Maugin, G.A.: Material forces: concepts and applications. Appl. Mech. Rev. **48**, 213–245 (1995)
3. Likhachev, V.A., Volkov, A.E., Shudegov, V.E.: Continuum theory of defects. Leningrad State Univ. Publ. 228, Leningrad (in Russian) (1986)
4. Nabarro, F.R.N.: Theory of Crystal Dislocations. Oxford University Press, Oxford (1967)
5. Gutkin, M.Y.: Elastic behavior of defects in nanomatarials. I model for infinite and semi-infinite media. Rev. Adv. Mater. Sci. **13**, 125–161 (2006)
6. Fleck, N.A., Hutchinson, J.W.: A phenomenological theory for strain gradient effects in plasticity. J. Mech. Phys. Solids **41**, 1825–1857 (1993)
7. Fleck, N.A., Hutchinson, J.W.: A reformulation of strain gradient plasticity. J. Mech. Phys. Solids **49**, 2245–2271 (2001)
8. Fleck, N.A., Hutchinson, J.W.: Strain gradient plasticity. Adv. Appl. Mech. **33**, 295–361 (1997)
9. Mindlin, R.D.: Micro-structure in linear elasticity. Arch. Ration. Mech. Anal. **1**, 51–78 (1964)
10. Mindlin, R.D., Tiersten, H.F.: Effects of the couple-stress in linear elasticity. Arch. Ration. Mech. Anal. **11**, 415–448 (1962)
11. Kroner, E.: Dislocations and continuum mechanics. Appl. Mech. Rev. **15**, 599–606 (1962)
12. Kroner, E.: Gauge field theories of defects in solids. Stuttgart Max-Plank Inst. (1982)
13. De Wit, R.: Theory of dislocations: continuous and discrete disclinations in isotropic elasticity. J. Res. Nat. Bur. Stand. **77A**(3), 359–368 (1973)
14. De Wit, R.: The continual theory of the stationary dislocations. Solid State Phys. **10**, 249 (1960)
15. Aifantis, E.C.: Strain gradient interpretation of size effects. Int. J. Fract. **95**, 299–314 (1999)
16. Gao, H., Huang, Y., Nix, W.D., Hutchinson, J.W.: Mechanism-based strain gradient plasticity —I. Theory. J. Mech. Phys. Solids **47**, 1239–1263 (1999)
17. Aero, E.L., Kuvshinskii, E.V.: Fundamental equations of elasticity theory for the media with a rotational interaction of particles. Fiz. Tverd. Tela **2**, 1399–1409 (1960)
18. Lurie, S.A., Belov, P.A., Tuchkova, N.P.: Gradient theory of media with conserved dislocations: application to microstructured materials. In: Maugin, G.A., Metrikine, A.V. (eds.) One hundred years after the Cosserats, advances in mechanics and mathematics, vol. 21, pp. 223–234. Springer, Heidelberg (2010)
19. Belov, P.A., Lurie, S.A.: Mathematical theory of directness media. Gradient Theories, Formulations, Hierarchy. Analysis. Applications, p. 337. Palmarium Academic Publishing (2014)
20. Lurie, S.A., Belov, P.A., Volkov-Bogorodsky, D.B., Tuchkova, N.P.: Interphase layer theory and application in the mechanics of composite materials. J. Mat. Sci. **41**(20), 6693–6707 (2006)
21. Belov, P.A., Lurie, S.A.: A continuum model of microheterogeneous media. J. Appl. Math. Mech. **73**(5), 599–608 (2009)

22. Lurie, S., Belov, P., Altenbach, H.: Classification of gradient adhesion theories across length scale. Generalized Continua as Models for Classical and Advanced Materials Series, vol. 42, pp. 261–277 (2016)
23. Altenbach, H., Eremeyev, V.A.: On the shell theory on the nanoscale with surface stresses. Int. J. Eng. Sci. **49**(12), 1294–1301 (2011)
24. Eremeyev, V.A.: On effective properties of materials at the nano-and microscales considering surface effects. Acta Mech. **227**(1), 29–42 (2016)
25. Cosserat, E., Cosserat, F.: Theore des corps deformables. Hermann, Paris (1909)

Numerical Simulation of Circumsolar Ring Evolution

A. S. Murachev, D. V. Tsvetkov, E. M. Galimov and A. M. Krivtsov

Abstract The results of the computer simulation for the circumsolar gas-dust cloud evolution are presented. The particle dynamics method is used. We show that gas-dust clusters can be formed in ring-shaped structures of protoplanetary disks. It is demonstrated that the clusters are formed as a result of the counteracting of the self-gravitational force of the ring and the gravity of the Sun. This process has a probabilistic nature. The range of the system parameters providing the clusters formation is obtained. Different scenarios of the ring evolution are observed and analyzed. The considered gas-dust clusters can be precursors for the further formation of the planet-satellite systems.

1 Introduction

Gas and dust play an important role in a planet formation [5, 18]. According to existing astrophysical theories, the process of star formation leads to the appearance of an accretion gas-dust disks around young stars [1]. Under certain conditions, planetary

A. S. Murachev (✉) · D. V. Tsvetkov · A. M. Krivtsov
Peter the Great Saint Petersburg Polytechnic University,
Politekhnicheskaya Street 29, St. Petersburg, Russia
e-mail: andrey.murachev@gmail.com

D. V. Tsvetkov
e-mail: dvtsvetkov@ya.ru

A. M. Krivtsov
e-mail: akrivtsov@bk.ru

E. M. Galimov
Vernadsky Institute of Geochemistry and Analytical Chemistry of Russian
Academy of Sciences, Kosygina Street 19, St. Petersburg, Russia
e-mail: galimov@geokhi.ru

A. M. Krivtsov
Institute for Problems in Mechanical Engineering, Russian Academy of Sciences,
V.O., Bolshoj pr., 61, St. Petersburg, Russia
e-mail: akrivtsov@bk.ru

F. dell'Isola et al. (eds.), *Advances in Mechanics of Microstructured Media and Structures*, Advanced Structured Materials 87,
https://doi.org/10.1007/978-3-319-73694-5_14

systems can be formed from such accretion disks [16]. Recently, the high resolution submillimeter ALMA telescope made it possible to obtain magnificent images of protoplanetary systems from other stars [2, 4]. The observations show bright dust rings in the disk, separated by dark gaps. The origin of these structures is not entirely clear and is still a matter of debate, but it is likely that such structures can be associated with the planets formation. In particular, ring-shaped structures can concentrate and also prevent solid particles accretion onto star [19, 21].

Thus, the probable scenario of the circumstellar disk evolution is formation of gas-dust rings, which is confirmed by the mentioned above observations and the computer simulations [6, 15, 20]. These rings can be treated as protoplanetary rings since the planet formation process is likely to take place in these high density areas. The asteroid ring in the Solar system also can be considered as a result of a protoplanetary ring evolution were the planet formation process for some reasons was not completed (probably due to the Jupiter influence).

In the present paper we present a computer model of the protoplanetary ring clustering. The paper is based on the hypothesis of academician E.M. Galimov of planets formation [9–11]. We assume that the solid phase early occurrence and growth is not the only way of the protoplanetary nebula evolution. The appearance of gravitational instabilities in protoplanetary disks along with particle growth leads to the formation of separate gas-dust clouds. These clouds collide with each other, grow in size, and after they reach an appropriate size and some additional conditions are fulfilled then planet-satellite systems can be formed as a result of their rotational collapse [11].

We use the particle dynamics method [13] to explore the protoplanetary disk evolution. The particles are represented as a point masses that interact with each other and with the central star. The method allows to find the numerical solution of the N-body problem as a function of time. One of the important peculiarities of this work in comparison with other works studying the cluster formation using the particles dynamics method [7, 8, 12, 15, 17] is the nature of the interparticle force. The considered force contains three main terms: the gravitational attraction, the soft gas-aided repulsion, and the dissipative term. We optimize the calculations with the modified Barnes-Hut algorithm [14] which in contrast to the classical algorithm [3] efficiently works for both short-range and long-range forces.

Each cluster can be considered as a separated gas-dust cloud in the protoplanetary disk. The previous computer simulations [11, 14] showed that under certain conditions, a planet with its satellite (e.g. the Earth-Moon system) can be formed as a result of a rotational collapse of such gas-dust cloud. In particulary, our results can be used as initial condition for the study of the Earth-Moon formation hypothesis [10, 11].

2 The Model

The protoplanetary ring is modeled as a set of particles interacting via prescribed forces. Initial particle co-ordinates have a uniform random distribution in an oblate spheroid with semi-axes $R_{\max}$ and R_s, where $R_s/R_{\max} \ll 1$ without central cylindrical

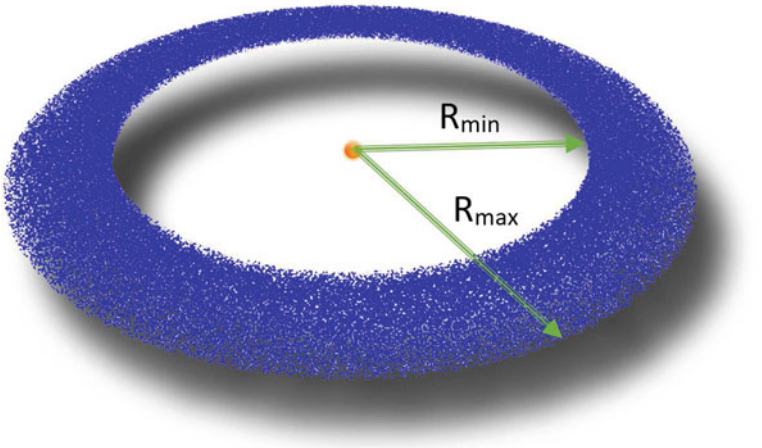

Fig. 1 The initial configuration of a protoplanetary disk

part with radius $R_{\min}$ (see Fig. 1). Further for simplicity directions in the ring plane will be called horizontal directions, the direction orthogonal to the ring plane—the vertical direction. The initial velocity of each particle is a sum of regular and random terms:

$$\boldsymbol{v} \stackrel{\text{def}}{=} \dot{\mathbf{r}} = \boldsymbol{v}_{\mathbf{reg}} + \boldsymbol{v}_{\mathbf{rand}}. \tag{1}$$

The regular component is defined as $\boldsymbol{v}_{\text{reg}} = \boldsymbol{\omega}_0 \times \boldsymbol{r}$, where $\boldsymbol{r}$ is the particle radius-vector and $\boldsymbol{\omega}_0$ is a vertical vector of the initial angular velocity of the particle. The absolute value of this vector is

$$\omega_0 = |\boldsymbol{\omega}_0| = \sqrt{\frac{\gamma M_{\text{sun}}}{r^3}}, \qquad r = |\boldsymbol{r}|, \tag{2}$$

where m is the particle mass, M_{sun} is the mass of the central star (further, for simplicity, the Sun), and γ is the gravitational constant. The random velocity components $\boldsymbol{v}_{\text{rand}}$ are randomly distributed in a spheroid with semi-axis $0.7v_{\text{reg}}$ and $0.055v_{\text{reg}}$ (horizontal and vertical, respectively), where $v_{\text{reg}} = |\boldsymbol{v}_{\text{reg}}|$.

The motion of the particles is described by the equations of Newtonian dynamics:

$$\begin{gathered} m\ddot{\boldsymbol{r}}_k = \sum_{n=1}^{N} \frac{1}{r_{kn}} f(r_{kn}, \dot{r}_{kn}) \boldsymbol{r}_{kn} + \boldsymbol{F}_k, \\ \boldsymbol{r}_{kn} = \boldsymbol{r}_k - \boldsymbol{r}_n, \qquad r_{kn} = |\boldsymbol{r}_{kn}|; \qquad k = 1, 2, \ldots, N, \end{gathered} \tag{3}$$

where N is the number of particles, $\boldsymbol{r}_k$ is the radius-vector of the k^{th} particle, $f(r, \dot{r})$ is the interparticle interaction force and

$$\boldsymbol{F}_k = \gamma \frac{M_{\text{sun}} m}{r_k^3} \boldsymbol{r}_k \tag{4}$$

is the gravitational force between the Sun and k^{th} particle, and M_{sun} is the Sun mass. The main part of the interparticle force f is the gravitational attraction that is a long-range force. In addition, we assumed that each particle in the heated state emits gaseous substances. The evaporating gas forms gas shells around the particles. This leads to the mutual repulsion of the particles. Energy loss in the interaction of the gas shells is taken into account by introducing an additional dissipative force. Thus, the interaction force consists of three components: the gravitational attraction, the gas repulsions, and the dissipation [11]:

$$f(r, \dot{r}) = \frac{A_1}{r^2} + \frac{A_2}{r^p} + \frac{A_3}{r^q} \dot{r}. \tag{5}$$

The first term in Eq. (5) corresponds to the gravitational force, where $A_1 = \gamma m^2$. The second term is the short-range repulsive force, where $A_2 = -A_1 a^{p-2}$, a is the particle diameter (the equilibrium distance between two particles), and $p = 7$. The third term in Eq. (5) describes non-conservative interaction between particles, where $A_3 = \beta A_2$, $\beta = \sqrt{11a^3/(25\gamma m)}$, and $q = p + 1$. The value of β is chosen to have a moderate dissipation in the system, the value of q is chosen to keep proportional the second and the third terms in Eq. (5) when the interparticle distance is changed. Then Eq. (5) can be rewritten in the form [11]

$$f(r, \dot{r}) = \gamma \frac{m^2}{a^2} \left[\left(\frac{a}{r} \right)^p \left(1 - \beta \frac{\dot{r}}{r} \right) - \left(\frac{a}{r} \right)^2 \right]. \tag{6}$$

The evolution of the protoplanetary ring depends on many parameters. The main goal of the study is to define the values of parameters that govern clustering in the protoplanetary system. The following main dimensionless parameters can be outlined: the dimensionless disk internal radius R_{min}/a, the shape ratio $W_r = R_{\text{max}}/R_{\text{min}}$, the mass ratio $M_s = M_{\text{sun}}/M$, and the dimensionless particle concentration n/n_0, where n is the average number of particle per unit volume, $n_0 = \frac{\pi}{3\sqrt{2}}$ is the particle close packing concentration. The oblateness $R_s/R_{\text{max}} = 0.04$ for all the systems under study. Three values of the mass ratio $M_s = 5,\ 10,\ 20$ will be considered. The number of particles is set indirectly as a function of the dimensionless particle concentration and the dimensionless disk volume (volume divided by a^3). The average number of particles in our calculations is about 700 000.

We carried out about one and a half thousand calculations of the protoplanetary rings evolution. Each calculation takes time from 3 to 10 revolutions of a particle having an initial angular velocity ω_0.

3 The Numerical Method

The particle dynamics method allows to calculate trajectories of all the particles in the system. Therefore, it is able to describe the whole system evolution. However, taking into account interactions between all particles leads to the complexity $O(N^2)$ at each step of integration. For the modeling of the planetary system formation hundreds of thousands or even millions of particles are needed. Computer resources that are needed to model such systems in the case of the complexity $O(N^2)$ are unacceptable. The traditionally way out of this situation is the use of approximate calculations of interaction forces. The Barnes-Hut algorithm [3] is one of such methods. This is a hierarchical method that is based on combining close particles into groups and calculating the total potential approximation of the group. However, the classical Barnes-Hut method is suitable only for certain stages of the system evolution. In such stages, the particles should be distributed fairly evenly in space. When clusters are formed, where the concentrations of particles in order exceed the concentration in the surrounding space, the rate of calculation drops drastically.

In this paper we use the modified Barnes-Hut method [14] to solve this problem. The modified Barnes-Hut method accelerates the calculations for the case of a essentially inhomogeneous spatial particles distribution. The modified algorithm allows to increase substantially the calculation speed without loss of accuracy. The modified method was applied to calculate the evolution of the gas-dust cloud for studying Moon and Earth system formation [11].

4 The Simulation Results

4.1 The Protoplanetary Rings Evolution

Let us consider the evolution of one of the systems where the clustering occurs. Figure 2 shows radial distribution of the average particles concentration in sequential moments of time. The average particle concentration at a given radial distance is

$$n = \frac{N_r}{S_r a}, \tag{7}$$

where N_r is the number of particles at the distance $r+\Delta r$ from the system center, Δr is numerical step of the radius and $S_r = \pi(r+\Delta r)^2 - \pi r^2$ is the area of the median plane of the protoplanetary ring. Figure 2 shows 15 graphs corresponding to 15 consecutive moments of time. It is clearly seen that the peaks of concentration appear in the late stages of the protoplanetary ring evolution, where each peak corresponds to a cluster.

The computations show that if the clusters were not formed during several first orbital periods then they are never formed. This conclusion is confirmed by the nature

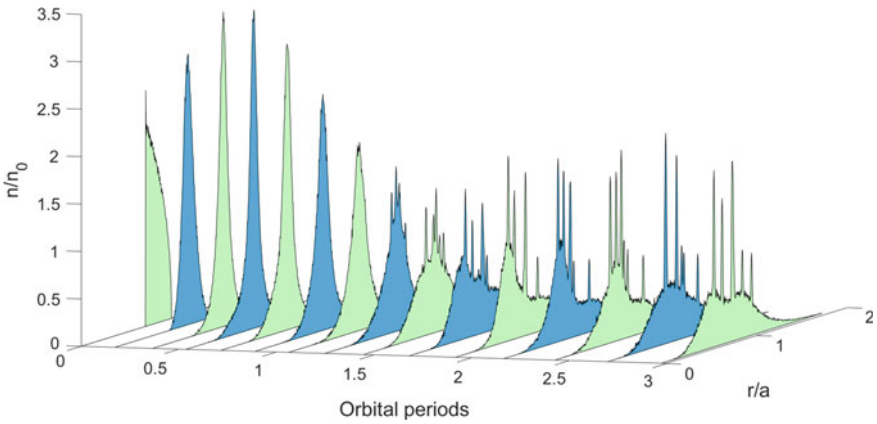

Fig. 2 Time evolution of the radial density in the ring. $R_{\min}/a = 200, W_r = 1.4, M_s = 10, n/n_0 = 0.1$

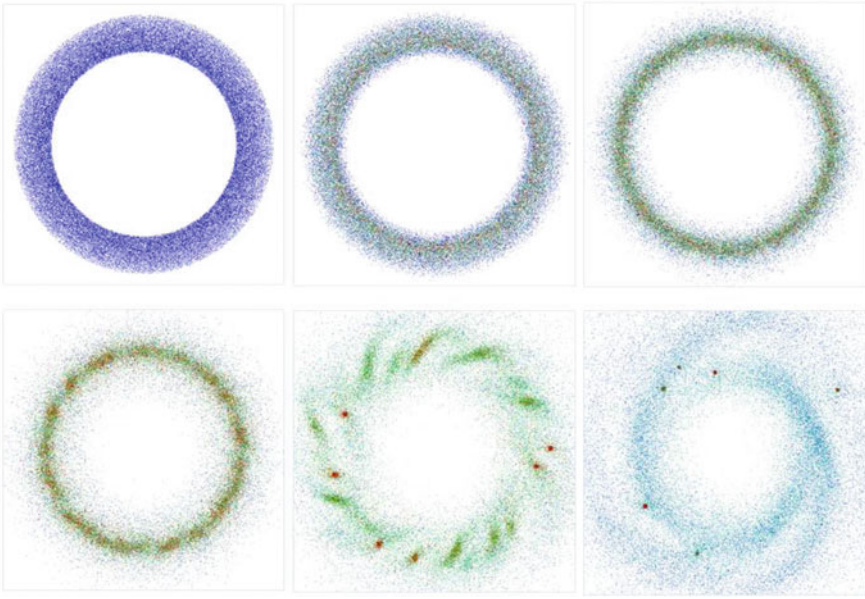

Fig. 3 The typical evolution of a protoplanetary ring. $R_{\min}/a = 200, W_r = 1.4, M_s = 10, n/n_0 = 0.1$

of the cluster formation in the ring. There are three stages in the evolution of the protoplanetary ring, which we can distinguish (see Fig. 3):

Stage 1. The stage of initial particles uniform distribution in the protoplanetary ring.
Stage 2. The stage of counteracting. Two processes occur simultaneously. The whole subsequent evolution of the system is determined by a process which is

more dominant. The first process is attraction of the particles to the protoplanetary ring mean radius $r_m = r + \Delta r/2$. The regions with increased concentration formed by gravitational instabilities accumulate particles from the surrounding space. The second process is the particle attraction to the Sun (the center of the system). Particles that fall on the Sun pull other particles behind them. There is an effect that looks like an avalanche.

Stage 3. The equilibrium stage. The clusters formation stops or the system comes to a homogeneous state at this stage. Generally, many gravitational instabilities are appear, but most of the gravitational instabilities are destroyed during the orbital motion. If the regions with increased concentration are massive, they collapses into a cluster. Clusters interact with each other. Most clusters collide. After such collisions some clusters are disrupted and some clusters are combined. Such collisions continue until the orbits of the clusters become stable.

The result of the third stage depends on the mass of the ring, the radius and the width of the protoplanetary ring. These values determine how many particles will fall on the sun and how many particles will remain in the orbit. If the gravitational instabilities have sufficient mass then they form the clusters, but if they do not have sufficient mass, they break down and their particles scatter in space. Thus in the most cases the clustering can be determined in a relatively short time and long simulations observing many revolutions around the Sun are not needed.

4.2 The Clustering Conditions

More than thousand simulations of the evolution of the protoplanetary rings with different parameters were preformed. The results of all calculations were divided in two classes according to the type of clustering: systems in which clustering is predominantly observed (for analysis of a set of similar systems) and systems in which clustering is predominantly not observed. The simulation results shows that a continuous and smooth boundary between two classes of clustering is observed in the parametric space of $(n/n_0, R_{\max}/R_{\min})$—see Figs. 4 and 5. The figures show that the greater is the concentration of particles in the protoplanetary ring and the greater is the relative width of the ring, the easier clusters formation is initiated. The systems that are close to the boundary can not be assigned to any of the classes with certainty. Such systems have similar probability of both clustering and no clustering. The system position relative to the classes boundary allows to predict the clustering in the system without calculations.

The dependence of the boundary position on the relative mass $M_s = M_{\text{sun}}/M$ was also investigated. The boundary lines were found for $M_s = 5, 10, 20$. The smaller the value of M_s is, the higher is the boundary line (see Fig. 6). These results can be interpreted as follows: the smaller is the influence of the central star, the more likely is the clustering. Gradually, clusters accumulate more and more particles in

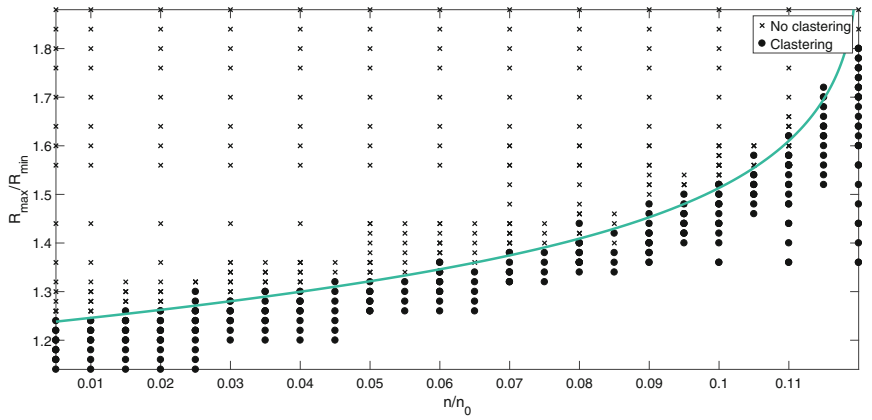

Fig. 4 The clustering diagram. $R_{\min}/a = 200, M_s = 10$

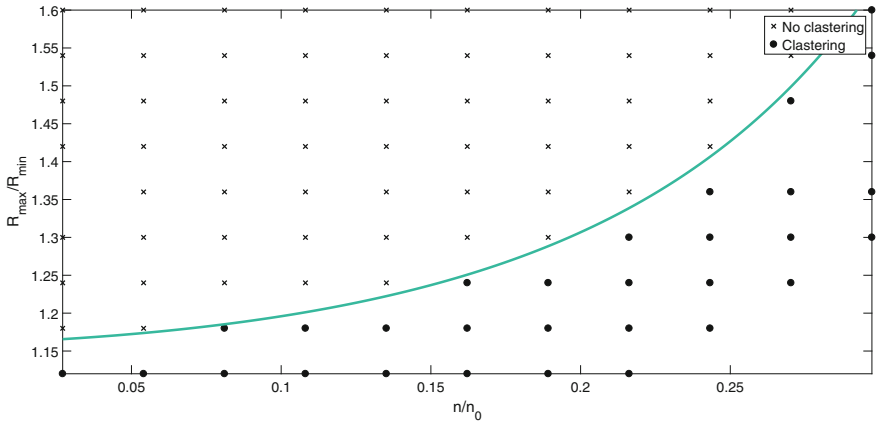

Fig. 5 The clustering diagram. $R_{\min}/a = 200, M_s = 20$

themselves, some clusters merge and some are destroyed. In our experiments, clusters accumulate up to 60% of all system particles (see Fig. 7). Over time, the clusters reach permanent orbits, but the system in which clustering occurred becomes stable usually only when one or two clusters are left in it.

5 Conclusions

The paper studies evolution of the circumsolar (or a circumstellar) rings. The evolution of the rings is simulated by the particle dynamics method. The long-range gravitational forces, the short-range dissipative forces, and the repulsive forces between

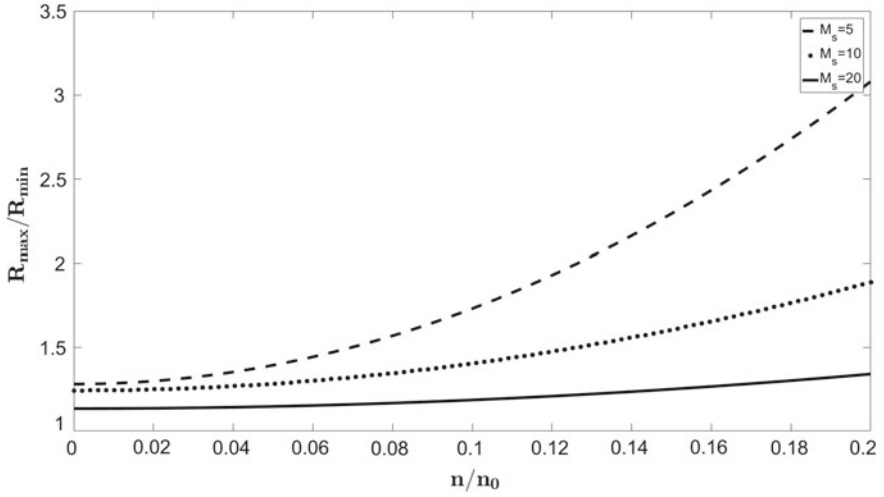

Fig. 6 The classes boundaries for several values of M_s. $R_{\min}/a = 200$

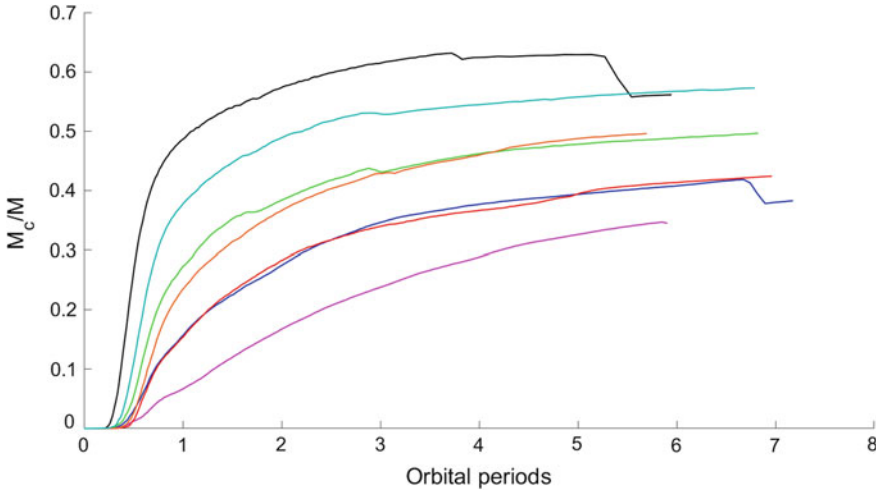

Fig. 7 Change in time the mass ratio of all clusters to the system mass. $R_{\min}/a = 200, M_s = 10$. M_c is the total clusters mass and M is the disk mass. The thresholds on some lines correspond to the clusters destruction by mutual collisions or by falling to the Sun

particles are taken into account. Also, the gravitational force from the central star is applied.

It is demonstrated that there are two main forces affecting the cluster formation in the ring: the self-gravitation of the protoplanetary ring and the gravity of the central star. The first force promotes clustering, the second force hinders it. The balance of these forces determines the formation of clusters. Also, the process of cluster formation is affected by the unique initial distribution of the particles co-ordinates and velocities. Therefore, generally speaking, the possibility of clustering can be estimated only in a statistical sense.

We have found that there is a continuously smooth boundary, which separates systems with and without clustering. The influence of the ring shape, density, and its relative (according to the central star) mass on the boundary position was investigated. The computer modeling shows that in the circumsolar ring the clusters are formed in the regions with an increased concentration of particles. If the concentration of particles is above a certain threshold, then the clusters appear. Then the clusters grow by accumulating particles from the surrounding space. Clusters also interact with each other. Usually after several revolutions only one or two clusters survived, and these clusters have stable orbits.

The further evolution of the clusters has not been studied in the present paper. However previous works [10, 11, 14] have shown that the rotational collapse of a localized gas-dust cloud can lead to the formation of the planet-satellite systems. Such a scenario is possible if the force of the particles interaction can no longer equilibrate the cluster. In particular, the results of the present paper can serve as initial conditions for study of the Earth-Moon formation from a gas-dust cloud, localized on its orbit around the Sun [11].

This research was supported by the Fundamental Research Program of the Presidium of the Russian Academy of Sciences No. 22 “The Evolution of the Organic World and the Planetary Processes”.

References

1. Andre, P., Montmerle, T.: From T Tauri stars protostars: circumstellar material and young stellar objects in the Ophiuchi cloud. Astrophys. J. **420** (1994)
2. Andrews, S.M., Wilner, D.J., Zhu, Z., Birnstiel, T., Carpenter, J.M., Pérez, L. M., Bai, X.-N., Öberg, K. I., Hughes, M., Isella, A.: Ringed substructure and a gap at 1 au in the nearest protoplanetary disk. Astrophys. J. Lett. **820**, L40 (2016)
3. Barnes, J., Hut, P. A.: A heirarchical O(N log N) force calculation algorithm. Nature **324** (1986)
4. Brogan, C.L., et al.: (ALMA Partnership), The 2014 ALMA long baseline campaign: first results from high angular resolution observations toward the HL Tau region. Astrophys. J. Lett. **808**, L3 (2015)
5. Desch, S.: Astromineralogy: dust in another solar system. Nature **431** (2004)
6. Dolgoleva, G.V., Legkostupov, M.S., Pliner, L.A.: Numerical simulation of gravitational instability of the Sun protoplanetary disk in the one-dimensional approximation. Part I. A homogeneous isotropic medium. Keldysh Inst. prepr. **049** (2016) (In Russian)
7. Eneev, T.M.: Ring compression of the matter in a drop model of a protoplanetary disc. Astron. Vestn. **27**, 5 (1993)

8. Eneev, T.M., Kozlov, N.N.: The problems of simulation of planetary systems accumulation processes. Adv. Space Res. **1**, 8 (1981)
9. Galimov, E.M., Krivtsov, A.M.: Origin of the Earth-Moon system. J. Earth Syst. Sci. **114** (2005)
10. Galimov, E.M.: Formation of the Moon and the Earth from a common supraplanetary gas-dust cloud. Geochem. Int. **49** (2011)
11. Galimov, E.M, Krivtsov, A.M.: Origin of the Moon. New Concept. Geochemistry and Dynamics, pp. 168. De Gruyter (2012)
12. Hellary, P., Nelson, R.P.: Global models of planetary system formation in radiatively-inefficient protoplanetary discs. Mon. Not. R. Astron. Soc. Lett. **419** (2012)
13. Hockney, R.W., Eastwood, J.W.: Computer Simulation Using Particles. Institute of Physics, Adam Hilger, Bristol (1988)
14. Le-Zakharov, A.A., Krivtsov, A.M.: Development of algorithms for computing the collisional dynamics of gravitating particles to simulate the formation of the Earth-Moon system through the gravitational collapse of a dust cloud. In: Galimov, E.M. (ed.) Problems of Biosphere Origin and Evolution. Nova Science Publishers, NY (2012)
15. Marov, M. Ja., Dorofeeva, V.A., Rusol, A.V., Kolesnichenko, A.V., Korolev, A.E., Samylkin, A. A., Makalkin, A.B., Ziglina, I.N.: Simulation the formation and early evolution of preplanetary bodies. In: Galimov, E., Krasand, M. (ed.) Problems of Origin and Evolution of the Biosphere, pp. 640. Moscow (2013) (in Russian)
16. Montmerle, T., Augereau, J.C., Chaussidon, M., Gounelle, M., Marty, B., Morbidelli A.: Solar system formation and early evolution: the first 100 million years. Earth Moon Planets **98** (2006)
17. Ogihara, M., Kobayashi, H.: Inutsuka, S.-i.: *N*-body simulations of terrestrial planet formation under the influence of a hot jupiter. Astrophys. J. **787**(2) (2014)
18. Okamoto, Y. K., Kataza, H., Honda, M., Yamashita, T., Onaka, T., Watanabe, J., Miyata, T., Sako, S., Fujiyoshi, T., Sakon, I.: An early extrasolar planetary system revealed by planetesimal belts in bold β Pictoris. Nature **431** (2004)
19. Pinilla, P., Benisty, M., Birnstiel, T.: Ring shaped dust accumulation in transition disks. Astron. Astrophys. **545**, A81 (2012)
20. Snytnikov, V.N., Dudnikova, G.I., Gleaves, J.T., Nikitin, S.A., Parmon, V.N., Stoyanovsky, V.O., Vshivkov, V.A., Yablonsky, G.S., Zakharenko, V.S.: Space chemical reactor of protoplanetary disk. Adv. Space Res. **30**, 6 (2002)
21. Zhu, Z., Nelson, R. P., Dong, R., Espaillat, C., Hartmann, L.: Dust filtration by planet-induced gap edges: implications for transitional disks. Astrophys. J. **755** (2012)

Two-Dimensional Modeling of Diatomic Lattice

A. V. Porubov

Abstract The two-dimensional nonlinear continuum expressions for the kinetic and potential energies are obtained for nonlinear diatomic lattice. The linear part of the energy is reconstructed using a continuum limit of the two-dimensional discrete model of the lattice. The discrete model considers neighboring spring-like interactions between masses in the lattice for derivation of equations of motion. A connection between the parameters of the lattice and the constants of the continuum model is established. The nonlinear part is added into the continuum model directly in a phenomenological manner. The expressions obtained are useful for finding a solution of a boundary value nonlinear problem.

1 Introduction

One of the last scientific problems considered by Eron Aero, was highly nonlinear continuum theory of diatomic lattices [1–4]. In particular, a one-dimensional (1D) model has been developed to account for strongly nonlinear strain waves in diatomic crystalline materials [1–3],

$$\rho U_{tt} - E\, U_{xx} \;=\; S(\cos(V) - 1)_x, \tag{1}$$

$$\mu V_{tt} - \kappa V_{xx} \;=\; (SU_x - p)\sin(V), \tag{2}$$

where

$$U \;=\; \frac{m_1 U_1 + m_2 U_2}{m_1 + m_2},\; V \;=\; \frac{U_1 - U_2}{h},$$

A. V. Porubov (✉)
Institute for Problems in Mechanical Engineering, Bolshoy 61, V.O.,
St. Petersburg 199178, Russia
e-mail: alexey.porubov@gmail.com

A. V. Porubov
Peter the Great St. Petersburg Polytechnic University (SPbPU), Polytechicheskaya st., 29,
St. Petersburg 195251, Russia

F. dell'Isola et al. (eds.), *Advances in Mechanics of Microstructured Media and Structures*, Advanced Structured Materials 87,
https://doi.org/10.1007/978-3-319-73694-5_15

U_i are the displacements of the masses m_i in the diatomic lattice, E, S, p, ρ, μ, κ are the parameters of the model. The Eqs. (1), (2) were obtained in [1, 2] starting from the continuum viewpoint without reference to the discrete equations for diatomic lattice, and some assumptions were done when constructing the expression for the energy of deformation. Also, a two-dimensional (2D) extension of the model (1), (2) was suggested in [4].

A completely continuum modeling was used in all above mentioned works. It is of interest to see how the models relate to a continuum limit of the discrete diatomic model. The 1D case was examined in [5] for nonlinearity described by the sine function and in [6] for weakly nonlinear case when nonlinear terms are of the power series nature.

The interest to diatomic lattices arose many years ago that is reflected in many books and reviews, see, e.g., [7–12]. The theory of diatomic lattices generalizes well developed nonlinear theory of monoatomic lattices that considers not only solid lattices but also the granular media and photonic lattices, see, e.g., [7–12]. Usually, the diatomic lattice is a primary object of the study while a continuum limit is employed to better understand the behavior of the lattice [7, 8, 13–17]. Both linear [7, 13] and weakly nonlinear [8, 12, 14, 15, 17–19] models are considered when weak nonlinearity is approximated by the power series in displacements.

The function V in Eqs. (1), (2) accounts for an influence of microstructure of a material. Large variation of V allows us to describe cardinal rearrangements of the lattice structure, dynamic behavior of a defect of the lattice, twinning etc. Similar description of a microstructure may be found in the chain with an additional rotational degree of freedom [20, 21]. Additional degrees of freedom are also incorporated into the discrete model via coupled stresses, see, e.g., [22]. The interest in the dynamic behaviour of micro-structured materials has grown tremendously with the recent manufacture and synthesis of new manifold strongly discrete and layered systems, artificial lattices of nanodots and other micro-elements while the classical theories of elasticity and magnetism cannot explain some of the experimental data concerning the properties of such materials with complicated microstructure. This is particularly true for materials of new types such as nano-crystalline alloys, ceramic composites, some biological materials (tissues), multi-layered magnetic films and elastic plates, artificial lattices, elastic and optical wave guides with a net of passive and active elements or corrugated internal structure, granular materials, and compounds exhibiting damage under experimental conditions of high speeds of deformation (or high frequencies of vibrations) [20, 23, 24].

In this paper, a procedure of obtaining expressions for kinetic and potential energy for diatomic lattice is developed in the 2D consideration. The procedure is based on the use of the continuum limit of the original discrete model. For this purpose, discrete equations of motion are obtained in Sect. 2 using the model where interactions between elements of the lattice (masses) are modelled by elastic springs that allows us to obtain the expressions for the elastic forces. Then the continuum limit of the equations is obtained in Sect. 3.1. The continuum variables having physical sense of macrostrain and relative micro-displacement are introduced and equations are rewritten in new variables in Sect. 3.2. Then the energies are reconstructed to

satisfy equations of motion. The energies are written in new variables in Sect. 3.3. Finally a nonlinear part of energy is introduced in a phenomenological manner in Sect. 3.4.

2 Discrete Equations

Let us consider a square lattice discrete structure with the particles having alternate masses m_1, m_2, see Fig. 1. The interactions between masses in this diatomic lattice are modeled by springs. The linearly elastic rigidities of horizontal and vertical springs is assumed to be equal to C_1 while the linearly elastic rigidity of the diagonal springs is C_2. The relative distance in the unstrained state is assumed to be equal to h. The horizontal and vertical displacements of particle m, n are denoted by $x_{m,n}$, $y_{m,n}$ for the masses m_1 and by $X_{m,n}$, $Y_{m,n}$ for the masses m_2.

Consider first particle with mass m_1 interacting with its neighbors as shown in Fig. 1 (Left). The kinetic energy is

$$T_1 = \frac{1}{2} m_1 \left(\dot{x}_{m,n}^2 + \dot{y}_{m,n}^2 \right),$$

while the potential energy is

$$\Pi_1 = \frac{1}{2} C_1 \sum_{i=1}^{4} \triangle l_i^2 + \frac{1}{2} C_2 \sum_{i=5}^{8} \triangle l_i^2,$$

where elongations of the springs, $\triangle l_i$ are

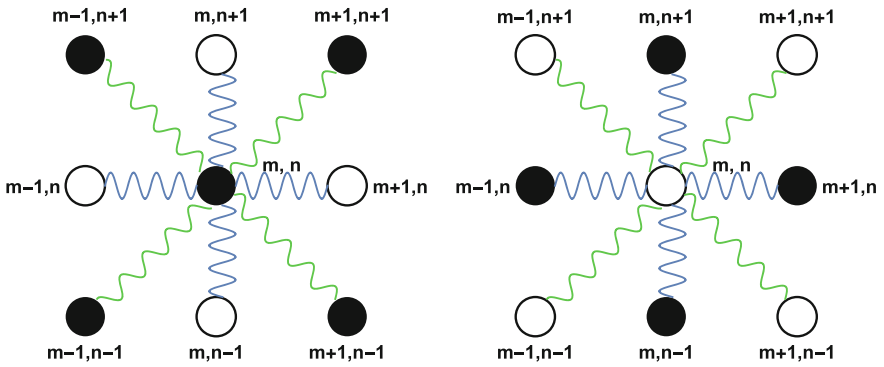

Fig. 1 Two-dimensional diatomic lattice. Left: interaction of the mass m_1 (black circle) with its neighbors. Right: interaction of the mass m_2 (transparent circle) with its neighbors

$$\triangle l_1 = X_{m+1,n} - x_{m,n}, \ \triangle l_2 = Y_{m,n+1} - y_{m,n},$$

$$\triangle l_3 = x_{m,n} - X_{m-1,n}, \ \triangle l_4 = y_{m,n} - Y_{m,n-1}$$

$$\triangle l_5 = \frac{1}{\sqrt{2}}\left(x_{m+1,n+1} - x_{m,n} + y_{m+1,n+1} - y_{m,n}\right),$$

$$\triangle l_6 = \frac{1}{\sqrt{2}}\left(x_{m,n} - x_{m-1,n+1} + y_{m-1,n+1} - y_{m,n}\right),$$

$$\triangle l_7 = \frac{1}{\sqrt{2}}\left(x_{m,n} - x_{m-1,n-1} + y_{m,n} - y_{m-1,n-1}\right),$$

$$\triangle l_8 = \frac{1}{\sqrt{2}}\left(x_{m+1,n-1} - x_{m,n} + y_{m,n} - y_{m+1,n-1}\right).$$

Then the Lagrangian, $L_1 = T_1 - \Pi_1$, may be composed, and the Hamilton-Ostrogradsky variational principle is applied to obtain the discrete governing equations of motion for masses m_1,

$$m_1\ddot{x}_m - C_1(X_{m+1,n} - 2x_{m,n} + X_{m-1,n}) - \frac{C_2}{2}\Big(x_{m+1,n+1} - 2x_{m,n} + x_{m-1,n+1} +$$

$$y_{m+1,n+1} - y_{m-1,n+1} + x_{m+1,n-1} - 2x_{m,n} + x_{m-1,n-1} + y_{m-1,n-1} - y_{m+1,n-1}\Big) = 0, \tag{3}$$

$$m_1\ddot{y}_m - C_1(Y_{m,n+1} - 2y_{m,n} + Y_{m,n-1}) - \frac{C_2}{2}\Big(y_{m+1,n+1} - 2y_{m,n} + y_{m-1,n+1} +$$

$$x_{m+1,n+1} - x_{m-1,n+1} + y_{m+1,n-1} - 2y_{m,n} + y_{m-1,n-1} + x_{m-1,n-1} - x_{m+1,n-1}\Big) = 0. \tag{4}$$

Similarly, equations of motion for masses m_2 may be obtained, see Fig. 1 (Right). Here

$$T_2 = \frac{1}{2}m_1\left(\dot{X}^2_{m,n} + \dot{Y}^2_{m,n}\right),$$

while the potential energy is

$$\Pi_2 = \frac{1}{2}C_1\sum_{i=1}^{4}\triangle L_i^2 + \frac{1}{2}C_2\sum_{i=5}^{8}\triangle L_i^2,$$

where elongations of the springs, $\triangle L_i$ are

$$\triangle l_1 = x_{m+1,n} - X_{m,n}, \ \triangle l_2 = y_{m,n+1} - Y_{m,n},$$

$$\triangle l_3 = X_{m,n} - x_{m-1,n},\ \triangle l_4 = Y_{m,n} - y_{m,n-1}$$

$$\triangle l_5 = \frac{1}{\sqrt{2}}\left(X_{m+1,n+1} - X_{m,n} + Y_{m+1,n+1} - Y_{m,n}\right),$$

$$\triangle l_6 = \frac{1}{\sqrt{2}}\left(X_{m,n} - X_{m-1,n+1} + Y_{m-1,n+1} - Y_{m,n}\right),$$

$$\triangle l_7 = \frac{1}{\sqrt{2}}\left(X_{m,n} - X_{m-1,n-1} + Y_{m,n} - Y_{m-1,n-1}\right),$$

$$\triangle l_8 = \frac{1}{\sqrt{2}}\left(X_{m+1,n-1} - X_{m,n} + Y_{m,n} - Y_{m+1,n-1}\right).$$

Then the equations of motion for masses m_2 are

$$m_2\ddot{X}_m - C_1(x_{m+1,n} - 2X_{m,n} + x_{m-1,n}) - \frac{C_2}{2}\Big(X_{m+1,n+1} - 2X_{m,n} + X_{m-1,n+1} +$$

$$Y_{m+1,n+1} - Y_{m-1,n+1} + X_{m+1,n-1} - 2X_{m,n} + X_{m-1,n-1} + Y_{m-1,n-1} - Y_{m+1,n-1}\Big) = 0, \tag{5}$$

$$m_2\ddot{Y}_m - C_1(y_{m,n+1} - 2Y_{m,n} + y_{m,n-1}) - \frac{C_2}{2}\Big(Y_{m+1,n+1} - 2Y_{m,n} + Y_{m-1,n+1} +$$

$$X_{m+1,n+1} - X_{m-1,n+1} + Y_{m+1,n-1} - 2Y_{m,n} + Y_{m-1,n-1} + X_{m-1,n-1} - X_{m+1,n-1}\Big) = 0. \tag{6}$$

3 Continuum Modeling

3.1 Continuum Limit of Discrete Equation

When $h << 1$, one assumes that the continuum displacements of the masses m_1, $x_{m,n}$, $y_{m,n}$, are $u_1(x, y, t)$, $v_1(x, y, t)$ while for displacements of the masses m_2, $X_{m,n}$, $Y_{m,n}$, one has $u_2(x, y, t)$, $v_2(x, y, t)$. Then the Taylor series for displacements of neighboring masses may be written, e.g.,

$$x_{m\pm1,n} = u_1 \pm h\, u_{1,x} + \frac{h^2}{2}u_{1,xx},\ x_{m,n\pm1} = u_1 \pm h\, u_{1,y} + \frac{h^2}{2}u_{1,yy},$$

$$x_{m\pm1,n\pm1} = u_1 \pm h\,(u_{1,x} + u_{1,y}) + \frac{h^2}{2}\left(u_{1,xx} + 2u_{1,xy} + u_{1,yy}\right) + \ldots$$

$$x_{m\pm1,n\mp1} = u_1 \pm h\,(u_{1,x} - u_{1,y}) + \frac{h^2}{2}\left(u_{1,xx} - 2u_{1,xy} + u_{1,yy}\right) + ...$$

and similarly for y-components of displacements. Then the continuum limit of Eqs. (3)–(6) up to terms of order h^2 results in the coupled equations,

$$m_1\,u_{1,tt} - 2C_1(u_2 - u_1) - C_1\,h^2\,u_{2,xx} - C_2\,h^2\,(u_{1,xx} + 2v_{1,xy} + u_{1,yy}) = 0, \quad (7)$$

$$m_1\,v_{1,tt} - 2C_1(v_2 - v_1) - C_1\,h^2\,v_{2,yy} - C_2\,h^2(v_{1,xx} + 2u_{1,xy} + v_{1,yy}) = 0, \quad (8)$$

$$m_2\,u_{2,tt} - 2C_1(u_1 - u_2) - C_1\,h^2\,u_{1,xx} - C_2\,h^2\,(u_{2,xx} + 2v_{2,xy} + u_{2,yy}) = 0, \quad (9)$$

$$m_2\,v_{2,tt} - 2C_1(v_1 - v_2) - C_1\,h^2\,v_{1,yy} - C_2\,h^2\,(v_{2,xx} + 2u_{2,xy} + v_{2,yy}) = 0. \quad (10)$$

3.2 Continuum Equations in New Variables

Let us introduce new variables,

$$U = \frac{m_1\,u_1 + m_2\,u_2}{m_1 + m_2},\ V = \frac{m_1\,v_1 + m_2\,v_2}{m_1 + m_2}, \quad (11)$$

$$u = \frac{u_1 - u_2}{h},\ v = \frac{v_1 - v_2}{h}. \quad (12)$$

The variables (11) account for the movement of center of masses, while the variables (12) describe relative displacements of the neighboring masses, they are responsible for a microstructure. Then the original variables may be expressed as

$$u_1 = U + \frac{m_2\,h}{m_1 + m_2}\,u,\ u_2 = U - \frac{m_1\,h}{m_1 + m_2}\,u,$$

$$v_1 = V - \frac{m_1\,h}{m_1 + m_2}\,v,\ v_2 = V + \frac{m_2\,h}{m_1 + m_2}\,v.$$

It allows us to transform Eqs. (7)–(10) to equations

$$(m_1 + m_2)U_{tt} = (C_1 + C_2)h^2\left(2U_{xx} + \frac{m_2 - m_1}{m_1 + m_2}\,h\,u_{xx}\right) +$$

$$C_2h^2\left(2U_{yy} + 4V_{xy} + \frac{m_2 - m_1}{m_1 + m_2}\,h(u_{yy} + 2v_{xy})\right), \quad (13)$$

$$(m_1+m_2)V_{tt} \;=\; (C_1+C_2)\left(\,2V_{yy}+\frac{m_2-m_1}{m_1+m_2}\,h\,v_{yy}\,\right)$$

$$C_2h^2\left(\,V_{yy}+4U_{xy}+\frac{m_2-m_1}{m_1+m_2}\,h(v_{xx}+2u_{xy})\,\right), \tag{14}$$

$$u_{tt} \;=\; -\,\frac{2C_1(m_1+m_2)}{m_1m_2}\,u+\frac{(C_1+C_2)(m_2-m_1)}{m_1m_2}\,hU_{xx}+$$

$$\frac{h^2}{m_1m_2(m_1+m_2)}\left(\,C_2(m_1^2+m_2^2)-2C_1m_1m_2\,\right)u_{xx}+\frac{(m_2-m_1)hC_2}{m_1m_2}\left(\,U_{yy}+2V_{xy}\,\right)+$$

$$\frac{h^2(m_1^2+m_2^2)C_2}{m_1m_2(m_1+m_2)}\left(\,u_{yy}+2v_{xy}\,\right), \tag{15}$$

$$v_{tt} \;=\; -\,\frac{2C_1(m_1+m_2)}{m_1m_2}\,v+\frac{(C_1+C_2)(m_2-m_1)}{m_1m_2}\,hV_{yy}+$$

$$\frac{h^2}{m_1m_2(m_1+m_2)}\left(\,C_2(m_1^2+m_2^2)-2C_1m_1m_2\,\right)v_{yy}+\frac{(m_2-m_1)hC_2}{m_1m_2}\left(\,V_{xx}+2U_{xy}\,\right)+$$

$$\frac{h^2(m_1^2+m_2^2)C_2}{m_1m_2(m_1+m_2)}\left(\,v_{xx}+2u_{xy}\,\right). \tag{16}$$

3.3 Reconstruction of Continuum Potential Energy

Equations of motion (13)–(16) allow us to reconstruct the kinetic and potential energies in variables U, V, u and v. Indeed these equations may be obtained using the Hamilton-Ostrogradsky variational principle of the form,

$$\delta S \;=\; \delta\int_{t_0}^{t_1}dt\int_{-\infty}^{\infty}dx\int_{-\infty}^{\infty}\mathscr{L}\,dy=0,$$

where $\mathscr{L}$ is the Lagrangian density,

$$\mathscr{L} \;=\; K-\Pi$$

where K is the kinetic energy density, Π is the density of the potential energy. For kinetic energy one can assume

$$2K=\rho_1U_t^2+\rho_2V_t^2+\rho_3u_t^2+\rho_4v_t^2.$$

The left-hand sides of Eqs. (13)–(16) should appear due to utilization of the variational principle to the kinetic energy. However, the coefficients ρ_1 and ρ_2 should have the dimension of density. Then it is necessary to divide both sides of Eqs. (13), (14) by h^3. Then one obtains

$$\rho_1 = \rho_2 = \frac{m_1 + m_2}{h^3}$$

The variables u, v are dimensionless, therefore, the dimension of ρ_3, ρ_4 should be kg/m. Both sides Eqs. (15), (16) are conveniently divided by $(m_1 + m_2)h/(m_1 m_2)$. Then one obtains for ρ_3, ρ_4

$$\rho_3 = \rho_4 = \frac{m_1 m_2}{(m_1 + m_2)h}.$$

Now the r.h.s. in Eqs. (13), (14) divided by h^3 contain coefficients having dimensions of elastic constants, N/m^2 since the dimension of rigidities C_i is N/m. The suitable functional form of the density of potential energy is

$$\begin{aligned}\Pi \;=\; & \frac{C_1}{h}\left(u^2+v^2\right)+\frac{C_1+C_2}{h}\left(U_x^2+V_y^2\right)+\frac{C_2}{h}\left(U_y^2+V_x^2+2U_xV_y+U_yV_x\right)+\\ & \frac{h(C_2(m_1^2+m_2^2)-2C_1m_1m_2)}{2(m_1^2+m_2^2)}\left(u_x^2+v_y^2\right)+\frac{(m_2-m_1)(C_1+C_2)}{m_1+m_2}\left(u_xU_x+v_yV_y\right)+\\ & \frac{C_2\,h(m_1^2+m_2^2)}{2(m_1+m_2)^2}\left(u_y^2+v_x^2+2u_yv_x+2u_xv_y\right)+\frac{C_2(m_2-m_1)}{m_1+m_2}\left(u_yU_y+v_xV_x+u_yV_x+\right.\\ & \left.u_xV_y+v_yU_x+v_xU_y\right)\end{aligned} \tag{17}$$

3.4 Introduction of Nonlinearity

Weakly nonlinear modeling consists in an addition of power series terms in the discrete equations of motion. In the 1D case, it was done in [6]. Similarly, highly nonlinear terms via the sine function may be used, see [5] for 1D case. Then the above mentioned procedure of the continuum limit and transformation to the variables (11), (12) may be applied.

Alternatively, a phenomenological approach may be used. In the 1D case, it was discussed in [3]. In this case nonlinearity is added already in the continuum equations of motion or in the continuum expression for the energy [1, 2]. In the 2D problem, it was suggested in [4] to look for the nonlinear part of the energy in the form

$$\Pi_{nl} = \Big(p - s_{xx}\, U_x - s_{xy}(U_y + V_x) - s_{yy}\, V_y \Big) \Big(1 - \cos(u + v) \Big) \tag{18}$$

where F is a constant. The parameter p is associated in [4] with one half of the energy of activation of rigid shift of the lattice. The coefficients s_{ij} account for a nonlinear coupling between macro- and micro components of the model. Another choice for the argument of the cosine function has been suggested in [2] where $\cos(\sqrt{u^2 + v^2})$ was suggested.

The complete potential energy is

$$\Pi_c = \Pi + \Pi_{nl}, \tag{19}$$

where Π is defined by Eq. (17).

4 Conclusion

An approach alternative to that used in [4] is developed to model two-dimensional dynamics of diatomic lattices. The key point of the approach is to obtain continuum expression for the kinetic and potential energies used the equations of motion obtained as continuum limit of the discrete equations of motion. Such procedure looks stronger than that used in [4] where pure continuum modeling is used. Now we don't need in any assumptions to construct the expression of the energy and about parameters of the model. The constants of our model of the energy are connected with the constants of the original discrete lattice model.

The obtaining of the expressions for the energies is very important for the statement of the boundary value problems. A modification of the variational principle Sect. 3.3 by addition of the elementary work of external forces allows us to study finite size bodies subjected to external loading. Moreover, the reasonable or natural boundary conditions appear due to utilization of the variational principle.

An introduction of nonlinearity in the model requires stronger approach then the above mentioned phenomenological one. In the one-dimensional case, it was done in [5] where nonlinear terms were obtained for diatomic chain using the continuum limit the discrete model. The extension of this procedure to the two-dimensional case will be the subject of future work.

Acknowledgements The work has been supported by the Russian Foundation for Basic Researches, grant No 17-01-00230-a. It was also partially supported by the grant 16-01-00068-a of the Russian Foundation for Basic Researches.

References

1. Aero, E.L.: Micromechanics of a double continuum in a model of a medium with variable periodic structure. J. Eng. Math. **55**, 81–95 (2002)
2. Aero, E.L., Bulygin, A.N.: Strongly nonlinear theory of nanostructure formation owing to elastic and nonelastic strains in crystalline solids. Mech. Solids **42**, 807–822 (2007)
3. Porubov, A.V., Aero, E.L., Maugin, G.A.: Two approaches to study essentially nonlinear and dispersive properties of the internal structure of materials. Phys. Rev. E **79**, 046608 (2009)
4. Aero, E.L., Bulygin, A.N., Pavlov, Y.V.: The solutions of nonlinear equations of flat deformation of the crystal media allowing martensitic transformations. In: Indeitsev, D.I., Krivtsov, A.M. (eds.) In: Proceedings of the XLV Summer School—Conference Advanced Problems in Mechanics, pp. 21–30, St. Petersburg (2017)
5. Porubov, A.V.: Modeling of strongly nonlinear effects in diatomic lattices. Arch. Appl. Mech. **84**, 1533–1538 (2014)
6. Porubov, A.V., Andrianov, I.V.: Nonlinear waves in diatomic crystals. Wave Motion **50**, 1153–1160 (2013)
7. Born, M., Huang, K.: Dynamical Theory of Crystal Lattices. Clarendon Press, Oxford (1954)
8. Askar, A.: Lattice Dynamical Foundations of Continuum Theories. World Scientific, Series in Theoretical and Applied Mechanics, vol. 2 (1985)
9. Kevrekidis, P.G.: Non-linear waves in lattices: past, present, future. IMA J. Appl. Math. 1–35 (2010)
10. Ostoja-Starzewski, M.: Lattice models in micromechanics. Appl. Mech. Rev. **55**, 35–60 (2002)
11. Andrianov, I.V., Awrejcewicz, J., Weichert, D.: Improved continuous models for discrete media. Math. Probl. Eng. (Open Access), Article ID 986242, 35 pages (2010). https://doi.org/10.1155/2010/986242
12. Maugin, G.A.: Nonlinear Waves in Elastic Crystals. Oxford University Press, UK (1999)
13. Brillouin, L., Parodi, M.: Wave Propagation in Periodic Structures. Dover, New York (1953)
14. Yajima, N., Satsuma, J.: Soliton solutions in a diatomic lattice system. Prog. Theory Phys. **62**, 370–378 (1979)
15. Pnevmatikos, St., Remoissenet, M., Flytzanis, N.: Propagation of acoustic and optical solitons in nonlinear diatomic chains. J. Phys. C: Solid State Phys. **16**, L305–L310 (1983)
16. Collins, M.A.: Solitons in the diatomic chain. Phys. Rev. **31**, 1754–1762 (1985)
17. Pnevmatikos, St., Flytzanis, N., Remoissenet, M.: Soliton dynamics of nonlinear diatomic lattices: Phys. Rev. B **33**, 2308–2311 (1986)
18. Kosevich, A.M., Kovalev, A.S.: Self-localization of vibrations in a one-dimensional anharmonic chain. Sov. Phys. JETP **40**, 891–896 (1975)
19. Manevich L.I., et al.: Solitons in non-degenerated bistable systems. Phys. Usp. **37**, 859–879 (1994)
20. Maugin, G.A., Pouget, J., Drouot, R., Collet, B.: Nonlinear electromechanical couplings. Wiley, UK (1992)
21. Sayadi, M.K., Pouget, J.: Soliton dynamics in a microstructured lattice model. J. Phys. A: Math. Gen. **24**, 2151–2172 (1991)
22. Erofeev, V.I., Pavlov, I.S.: Parametric identification of crystals having a cubic lattice with negative Poisson's ratios. J. Appl. Mech. Tech. Phys. **56**, 1015–1022 (2015)
23. Erofeev, V.I.: Wave Processes in Solids with Microstructure. World Scientific, Singapore (2002)
24. Eremeyev, V.A., Lebedev, L.P., Altenbach, H.: Foundations of Micropolar Mechanics. Springer, Heidelberg (2013)

Mechanics of Metamaterials: An Overview of Recent Developments

H. Reda, N. Karathanasopoulos, K. Elnady, J. F. Ganghoffer and H. Lakiss

Abstract The emergence of additive manufacturing in combination with the advancement of engineering analysis tools has led to a new paradigm in the design of materials, in which the organization of matter and topology plays a central role. A new class of artificial materials has emerged that exhibit static and dynamic properties typically not encountered in natural materials and have been named as metamaterials. In the current work, we present recent advances made in the field, relating to both the static attributes and to the wave propagation characteristics of metamaterials under small and large strains. In particular, we present a class of anti-auxetic inner material architectures with positive and high Poissons ratio values which lead to metamaterials of controlled anisotropy. Thereupon, we study the influence of the degree of anisotropy on the wave propagation characteristics under small strains. Moreover, we analyze the effect of geometrical nonlinearities on the propagation of longitudinal and shear waves in two-dimensional hexagonal-shaped architectured lattices viewed as effective 1D and 2D media, while we showcase the potential of non-auxetic architectures to reach auxetic ones through a kinematic control in the large strains regime. What is more, we analyze the role of the considered nonlinearity in the nature of propagating waves, identifying strain thresholds beyond which both supersonic and subsonic modes emerge.

H. Reda · H. Lakiss
Faculty of Engineering, Beirut, Lebanon
e-mail: hilalreda@hotmail.com

H. Lakiss
e-mail: hassanlakissr@yahoo.com

N. Karathanasopoulos
Institute for Computational Science, ETH Zurich, Zurich, Switzerland
e-mail: nkaratha@ethz.ch

K. Elnady
Lemta University of Lorraine, Lorraine, France
e-mail: khaled.el-nady@univ-lorraine.fr

J. F. Ganghoffer (✉)
LEM3, CNRS, University of Lorraine, Lorraine, France
e-mail: jean-francois.ganghoffer@univ-lorraine.fr

F. dell'Isola et al. (eds.), *Advances in Mechanics of Microstructured Media and Structures*, Advanced Structured Materials 87,
https://doi.org/10.1007/978-3-319-73694-5_16

1 Introduction

In the conventional approach, the development of new materials is done at the scale of 'atoms', which is considered as the primal material unit (bottom-up approach). In the last decades, the focus has been set at a higher scale, substituting the notion of atoms with that of material building blocks. Material building blocks are periodic or non-periodic artificial microstructural topologies, specifically architectured to provide an enhanced macroscopic response for certain properties of interest. The artificial design of the resulting material, along with the extraordinary properties typically not encountered in natural materials, required a specific wording for this new class of artificial materials. The wording 'metamaterials' has been selected as the most representative wording, noting that the prefix 'meta' means in Greek to exceed, to go beyond natural materials [1]. Metamaterials derive their properties not from the ones of their base material, but from the design of their microstructure. The microstructures density, shape, size and structural arrangement are responsible for the enhanced or exotic behavior observed at the macroscale. By appropriately tuning the microstructures design, electromagnetic waves can be enhanced, absorbed, blocked or bent and structural properties can be considerably upgraded [2]. This observation has fostered extensive studies in different research directions. By that means, new frontiers have been opened in a series of different fields, such as in optics (superlens), signal transmission and energy harvesting [3]. More recently, the metamaterial concept has been carried over to mechanical/acoustic properties as well. In the field of mechanics, the design, modeling and testing of rationally designed metamaterial microstructures in two and three dimensions are much less advanced than their electromagnetic counterparts and is an emerging field. For the effective mechanical and electromagnetic properties of metamaterials to be determined, a link between the microstructural and mesostructural scale (equivalent continuum scale) needs to be set.

The Poissons ratio has been for centuries regarded as a metric for the mechanical performance of materials and structures [4]. It characterizes their volumetric response and is defined as positive, when the material contracts in the plane lying perpendicular to its loading direction. Most common engineering materials have positive Poissons ratios. In particular, ceramics, metals and glass structures have typical Poissons ratio values between 0.25 and 0.4, while rubbers have values slightly below 0.5. For isotropic three dimensional materials, Poissons ratio values are bounded between -1 and 0.5. In the isotropic case, Poissons ratio is uniquely coupled to the materials shear and bulk modulus G and K respectively, upon rather simple relations. In particular, both K and G are reversely related to the Poissons ratio, with K defined as $K = E/(3(1 - 2 * \nu))$ and G as $G = E/(2(1 + \nu))$. The Poissons ratio completely defines the shear to the bulk modulus ratio value, while its bounded nature $-1 \leq \nu < 0.5$ constrains the ratio K/G (a sole function of the Poissons ratio within isotropy) to lie within a certain range, as schematically depicted in Fig. 1.

Up to now a considerable amount of works has been dedicated to the conception and analysis of auxetic metamaterials, namely materials with negative Poisson's

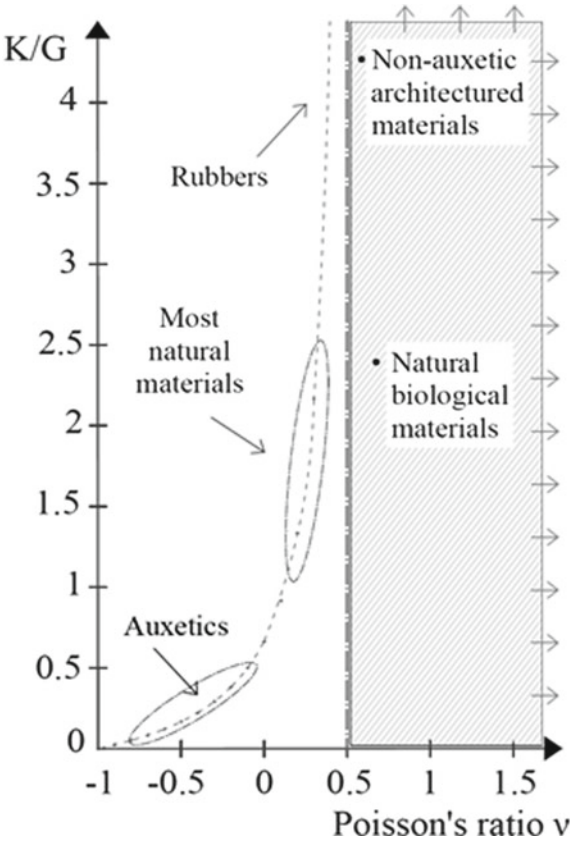

Fig. 1 Bulk to shear modulus ratio versus Poisson's ratio for different material classes

ratios [5]. In particular, the mechanical properties of chiral lattices, hexa- and tetrachiral cellular solids have been studied [6, 7]. Auxetics have found a wide range of applications in different fields, as for example in the aerospace and automotive industry, primarily due to their superior shear strength and reduced overall structural weight [8].

The Poisson's ratio offers a fundamental metric to compare the material performance [9]. While for isotropic materials the Poisson's ratio value is limited in between −1 and 0.5, anisotropic materials can well exceed these limits. The necessity to induce a certain degree of anisotropy in order to achieve non-conventional mechanical behaviours has been recognized in a series of engineering fields, amongst others in morphing wing engineering applications [10]. Thereupon, successful morphing in aerospace or wind energy engineering has been directly associated with the development and usage of materials that exhibit a combination of low stiffness and high Poisson's ratio in the one material direction to 'minimize actuation energy', combined with a high stiffness in its perpendicular material direction to adequately support aerodynamic loads [11]. Certain honeycomb and hybrid accordion

cellular solids have been shown to satisfy the previously described stiffness characteristics [12, 13]. Lately, polygonal-shaped unit cell architectures have been shown to yield metamaterials of controlled static mechanical properties upon low effective density values [14]. Lightweight material designs of controlled anisotropy that combine stiff and soft material directions are favorable amongst others for space-frame structures, metallic filters and ceramics [15]. What is more, the development of architectured lightweight materials with a soft material direction has been directly related to the advancement of soft-robotics and damping structures [16, 17]. Moreover, in the realm of bio-engineering, the restoration of ligaments and tendons with biosubstitute materials that can inherently emulate the native tissue mechanics (large Poissons ratio values), constitutes an ongoing engineering challenge in the search of the optimal artificial material [18, 19].

The metamaterial's static properties are directly related to their wave propagation characteristics. Acoustic metamaterials raise a continuously increasing interest in both physicists and mechanician communities, sometimes with different but complementary viewpoints, see [20]. One promising research direction is the design of metamaterials having microstructures which present a strong contrast in the microscopic properties of their constituents, thus generating generalized continuum models when homogenized [21–23]. The presence of a microstructure entails that some effective properties of the substitution continuum replacing the initial microstructure (which may be discrete, like in network materials) may diverge or vanish when considering the macro-properties obtained by homogenization. Cauchy continuum theory may not be accurate enough to capture the specific unusual wave propagation features brought by materials with a microstructures or for some natural materials with highly heterogeneous hierarchical microstructures [24], when modeling them at a continuum level. The introduction of more sophisticated models than Cauchy continuum like continua with microstructure or generalized continua is mandatory in order to account in a satisfactorily manner the unexpected effects brought by the microstructure on wave propagation [26, 28]; recent works have been devoted to network materials modeled as effective micropolar or second gradient continua, [25, 27, 28], giving rise to partial or full band gaps.

Control of the propagation of sound waves is mostly accomplished through negative values of constitutive parameters, like bulk modulus, mass density, Poisson ratio and also via chirality. The density and bulk modulus are the analogs of electromagnetic parameters, respectively permittivity and permeability in negative index materials. Composite media presenting a negative effective bulk modulus of a negative effective mass density have been produced in [30–32], where auxetic materials were studied. A vanishing shear modulus but finite bulk modulus has been obtained for the pentamode structures by producing anisotropic variants of them in [33]. The physical mechanisms behind such unusual effects are the trapping of energy of macroscopic waves in microscopic degrees of freedom (abbreviated in the sequel as dof), which may be described by adopting the framework of generalized continua. Different literature works highlight—see [34] and references therein that the coupling between macroscopic and microscopic dof and non-linearities are two essential mechanisms responsible for the generation of frequency band gaps in wave propagation problems.

However, while the elastic wave propagation has been extensively analyzed in the literature [35–38], only few works have so far been dedicated to wave propagation in nonlinear periodic structures [39, 40]. The propagation of waves in pre-deformed periodic structures is accompanied by a number of new phenomena that are different and can not be observed for linear media, such as amplitude-dependent dispersion relations [41]. By varying the applied deformation, it is possible to synthesize anisotropic materials in which the elastic rigidity matrix increases incrementally. Few works have described the variation of the material upon finite deformations [44, 45]. The range of deformation is limited by stability considerations, which have been captured by dedicated constitutive models [42, 43].

In the current contribution we adress the following key issues:

1. The design of so-called anti-auxetic structures exhibiting high positive Poissons coefficients and the influence of such anti-auxetic features on the metamaterials wave propagation properties.
2. The influence of geometrical nonlinearities on the static and wave propagation characteristics of architectured materials.
3. The role of the degree of non-linearity on the nature of the propagating waves.

The present work is organized as follows: the design of network anti-auxetic inner material architectures of controlled anisotropy is discussed in Sect. 2, whereby the effect of anisotropy on the wave propagation characteristics is analyzed. In Sect. 3, large strain aspects are presented: in particular, the potential of auxetic materials to reach non-auxetic behaviours through appropriate strain applications, along with the effect of large strains on the wave propagation characteristics of architectured media are analyzed. In Sect. 4, we discuss the role of the considered degree of nonlinearity on the nature of the propagating waves in an 1D context, correlating this factor to the appearance of supersonic and subsonic modes. We conclude in Sect. 5 by a summary of the main results of this work.

2 Anti-auxetic 2D Architectured Materials Under Small Strains

2.1 Orthotropic Lattice Architectures of Controlled Static Properties

We analyze a class of two-dimensional, non-auxetic metamaterials of controlled anisotropy which make use of polygonal-shaped unit-cell architectures (Fig. 1). In particular, we employ diamond and octagon-shaped lattice architectures, which allow us to create metamaterials with effective moduli ratio values E_2^*/E_1^* that can be controlled through the appropriate choice of the unit-cell's inner design parameters, namely: member orientation θ, number and geometry of strengthening elements and slenderness ratio values η (Fig. 2). In the unit cell shown as an insert in Fig. 1 is

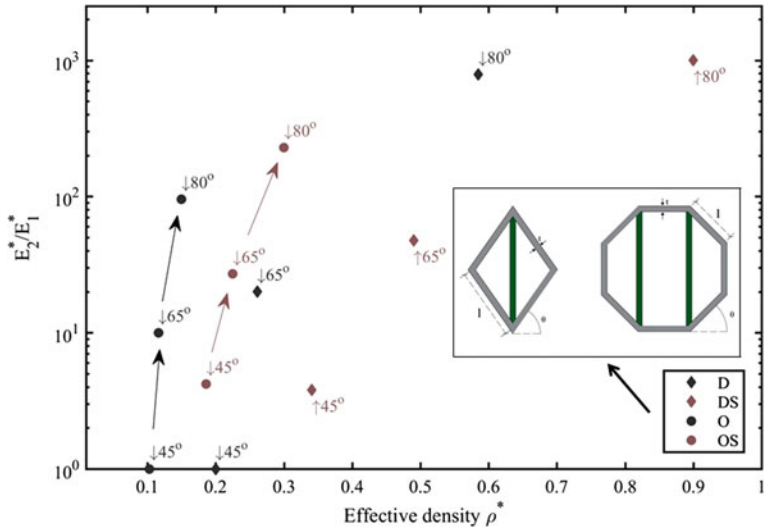

Fig. 2 Effective material moduli ratio values E_2^*/E_1^* as a function of the effective unit-cell density ρ^* for diamond and octagon-shaped lattice structures with and without inner strengthenings

then repeated by translation in both directions of the plane so that a periodic network is built; the structural network elements are modeled as beams and are connected at junction nodes endowed with a certain in-plane flexural rigidity. As will be explained later on, the existing local rotation at these connecting nodes shall be condensed at the level of the constructed effective continuum [14], we have computed the effective material properties of the previously reported lattice architectures in a parametric manner, using the discrete homogenization method provided in [46]. In the Appendix, we furnish closed-form expressions of the normal effective material moduli ${E_1}^*$ and ${E_2}^*$ and effective density values ρ^* as a function of the unit-cell geometry parameters. In Fig. 2, we provide an Eshelby-type diagram of the moduli ratios as a function of the density. To that scope, we present a subset of diamond and octagon-shaped unit-cell architectures without strengthening (D, O) and with a single and two inner vertical strengthening elements respectively (DS, OS) of equal outer sides length and a slenderness ratio $\eta = L/t = 10$.

Figure 2 suggests that octagon-shaped unit-cell lattice architectures yield artificial materials of highly tunable moduli ratio values E_2^*/E_1^* (E_2^*/E_1^* being the effective material moduli in the horizontal and vertical material direction accordingly), thus of tunable anisotropy. In particular, the material moduli ratio can range between unity and approximately 100 for non-strengthened configurations (O) upon appropriate modulations of the lattices outer elements design angle θ. The insertion of inner strengthening elements extends the feasible range of ratio values to a maximum of approximately 250 for the strengthened octagon-shaped unit-cell lattice architectures (OS). The corresponding maximum anisotropy values for diamond-shaped lattice architectures (DS) are approximately four times the ones created by octagon-shaped

lattices; however for considerably higher effective density values ρ^*. We note that the slenderness ratio η of each unit cell architecture can be used as an additional degree of freedom in the attainment of a desirable combination of ρ^*, E_2^*/E_1^* values, with higher η values to correspond to lower effective density values ρ^*.

2.2 Wave Propagation Attributes of 2D Anti-auxetic Material Architectures of High Anisotropy

The artificial materials degree of anisotropy—characterized by the ${E_2}^*/{E_1}^*$ value—directly affects its wave propagation characteristics. The latter can be obtained for an effective two-dimensional Cauchy medium through the solution of the dynamic equilibrium equation:

$$\frac{\partial \sigma_{xx}}{\partial x} + \frac{\partial \sigma_{xy}}{\partial y} = \rho^* \ddot{u}, \qquad \frac{\partial \sigma_{yx}}{\partial x} + \frac{\partial \sigma_{yy}}{\partial y} = \rho^* \ddot{v} \tag{1}$$

where σ_{xx}, σ_{yy} and σ_{xy}, σ_{yx} stand for the normal and shear stresses accordingly, characterized by two independent planar kinematic degrees of freedom u and v to which they are related to, through the effective material density ρ^* the overhead dot over the displacement in (Eq. 1) denotes the time derivative. Employing a harmonic planar wave Ansatz $u(x, y, t) = U \exp(i\omega t - i(\kappa_1 x + \kappa_2 y))$ and $v(x, y, t) = V \exp(i\omega t - i(\kappa_1 x + \kappa_2 y))$ for the horizontal and vertical displacement components, $\kappa_1 = |k| \cos\beta$ and $\kappa_2 = |k| \sin\beta$ being the components of the wave vector κ and ω the wave frequency, the phase velocity $c_p = \omega/|k|$ can be computed as a function of the wave propagation direction β. In [14], we have shown that the level of anisotropy—expressed through the E_2^*/E_1^* ratio—directly affects the phase velocity characteristics for both longitudinal and shear waves. Figure 3 provides a schematic representation of the correlation between the phase velocity c_p and the propagation direction β for longitudinal (L) and shear waves (S) for two metamaterial designs: an isotropic one with $E_2^*/E_1^* = 1$ and a highly anisotropic one with $E_2^*/E_1^* = 784$. The results are normalized with respect to the corresponding beam phase velocity $\sqrt{E_s/\rho_s}$, E_s being the constituents materials modulus and ρ_s its density ($E_s = 200\,GPa$, $\rho_s = 7700\,kg/m^3$, $\eta = 1/15$).

Figure 3 demonstrates a considerable difference between isotropic and highly anisotropic artificial material designs. While for isotropic metamaterials non-zero phase velocities are obtained for both modes of propagation (L, S) irrespective of the direction of propagation β, for anisotropic designs the metamaterial acts as a complete shear wave isolator in the $\beta \to 0,\ \pi,\ -\pi$ material direction (Fig. 3, right). The latter corresponds to the soft material direction, thus to the E_1^* material directions of Fig. 2. Contrariwise, in the high modulus, stiff material direction (E_2^* in Fig. 2), an effective transmitter behaviour is observed for the longitudinal waves. It needs to be noted that the previously reported characteristics pertain not only to metamaterials

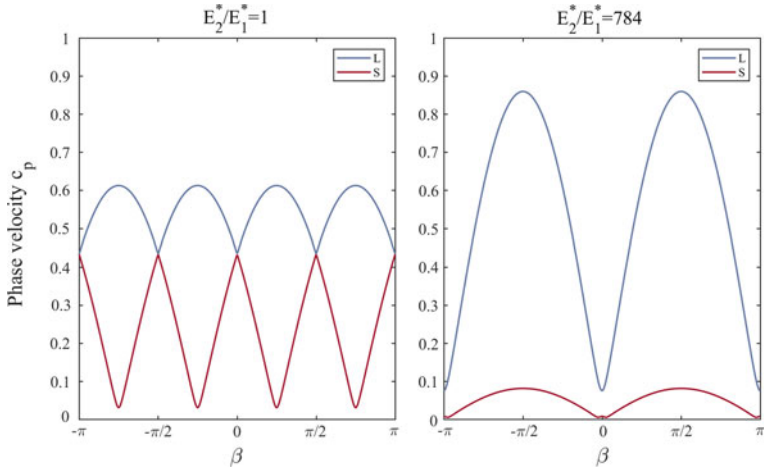

Fig. 3 Phase velocity c_p dependence on the wave propagation direction β for longitudinal (L) and shear waves (S) for an isotropic ($E_2{}^*/E_1{}^* = 1$, left) and a highly anisotropic material ($E_2{}^*/E_1{}^* = 784$, right) obtained for diamond-shaped lattice architectures of 45 and 80° accordingly

architectured with diamond-shaped lattices, but also for any unit cell configuration of high anisotropy ratio E_2^*/E_1^* of the type, as indicated by the study of the D, O, DS, OS unit-cell lattice architectures. The reader is referred to [14] for an elaborate analysis of the static and acoustic wave propagation attributes of the previously reported lattice designs. We have accordingly shown that the modification of the inner design of architectured material has a significant impact on their acoustic properties. The change of topology at the level of a representative unit cell can be achieved by the application of large deformations, as exposed in the next sections.

3 Static and Wave Propagation Characteristics of Architectured Materials Under Large Strains

We next develop homogenization schemes for the computation of the large strains response of periodic networks in order to derive their effective elastic response accounting for large changes of their geometry.

3.1 Microscopic and Mesoscopic Nonlinear Homogenization Problems

The adopted computational method of the effective nonlinear response of network materials relies on a two steps methodology: the ground state effective moduli are first evaluated in the initial small strains regime, followed by the evaluation of the nonlinear subsequent response, based on the update of the lattice configuration (geometry) when subjected to an increased kinematic loading imposed over the identified unit cell. We rely for the purpose of computing the effective nonlinear response on the discrete homogenization method (abbreviated DH method in the sequel) to replace the initially discrete structure by a nonlinear elastic effective continuum.

The homogenization of the periodic network towards a Cauchy continuum at the mesoscopic level relies on the condensation of the existing nodal rotations (which exist at the crossing nodes between the structural elements of the network), which are expressed versus the deformation applied over the unit cell, using the equilibrium equations. We refer the reader for more details related to the asymptotic homogenisation technique to the recent works on the topic [46, 47]. The homogenization methods accounts for the large changes of network configurations occurring due to the large imposed kinematic loadings. We note that since the flexural rigidity of the beam elements is commonly much lower than their tensile rigidity, it is likely that geometrical nonlinearities will be the dominant mechanism at the microscale. The lattice geometry is updated at each new increment of the external load applied to the unit cell boundary, based on which new effective properties are evaluated. The main steps of the DH method leading to the nonlinear response of the homogenized continuum are written in algorithmic format below. Note that although the main source of nonlinearities at microscopic level is the modification of the network geometry, the obtained constitutive law at the mesoscopic level is a nonlinear relation between stress and strain. The computation of the large deformation response of network materials goes through the following main steps:

For each kinematic increment $\Delta\mathbf{E}_{Gn}^{(k)}$ and iteration k inside the increment loop:

1. Compute the effective mechanical properties in the linear regime based on the linear discrete homogenization framework;
2. Define the incremental strain applied over the RUC.
3. Compute the incremental Second Piola-Kirchhoff stress tensor.
4. $\Delta\mathbf{S}_n^{(k)} = K_{T,n}^S : \Delta\mathbf{E}_{Gn}^{(k)}$
5. Check convergence at iteration k. if it is attained, go to next step.
6. Compute the incremental deformation gradient and its Jacobean.
7. Update Cauchy stress and couple stress at increment $(n+1)$ by a push forward of their Lagrangian counterpart from configuration Ω_n to Ω_{n+1}:

$$\sigma_{n+1}^{(k)} = J_n^{-1}\mathbf{F}_n.\left\{\mathbf{S}_n^{(k)} + \Delta\mathbf{S}_n^{(k)}\right\}.\mathbf{F}_n^T = \underbrace{\left(J_n^{-1}\mathbf{F}_n.\mathbf{S}_n^{(k)}.\mathbf{F}_n^T\right)}_{\sigma_n^{(k)}} + \underbrace{\left(J_n^{-1}\mathbf{F}_n.\left(\Delta\mathbf{S}_n^{(k)}\right).\mathbf{F}_n^T\right)}_{\Delta\sigma_n^{(k)}}$$

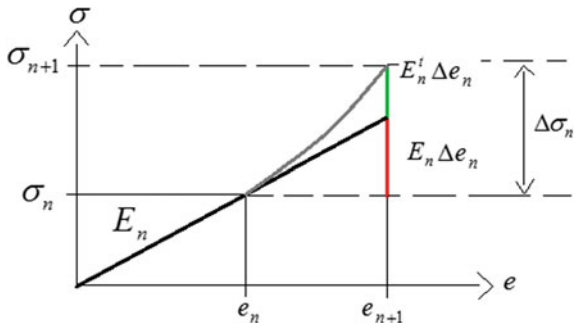

Fig. 4 Incremental Cauchy stress versus the linearized strain between steps n and $n+1$

8. Update the network configuration from Ω_n to Ω_{n+1}
9. Repeat steps 1–7 up to the maximum applied strain over the unit cell.

Since the DH method is predictive, it can be conceived as a virtual testing method (instead of doing real measurements, which can be costly) to provide a database of uniaxial, biaxial and simple shear responses to identify a strain energy density for an assumed hyperelastic effective homogeneous material. In view of the analysis of nonlinear wave propagation, we express the increment of Kirchhoff stress $\Delta\tau_n$ (denoting the linearized tensor-valued function $\tau_n = J_n\sigma_n$) versus the corresponding increment of the Euler-Almansi tensor $\Delta\mathbf{e}_n = \frac{1}{2}\left(grad\,\Delta\mathbf{u}_n + grad^T\,\Delta\mathbf{u}_n\right)$ as follows:

$$\Delta\tau_n = J_n\mathbf{c}_n : grad\Delta\mathbf{u}_n = J_n\mathbf{c}_n : \Delta\mathbf{e}_n \tag{2}$$

We have introduced in Eq. 2 the fourth order tensor $\mathbf{c}_n$ of the tangent moduli in the actual configuration (the symbol $\Delta(.)$ denotes here and in the sequel the infinitesimal variation of any quantity), obtained from the material tangent stiffness tensor $K^S_{T,n}$ identified by the discrete homogenization method by a push-forward, expressed in component form by the relation:

$$c_{abcd} = J^{-1}F_{aA}F_{bB}F_{cC}F_{dD}K^S_{T,n_{ABCD}} \tag{3}$$

Introducing grad(.) the gradient operator with respect to the actual coordinates, with the relation $grad\Delta\mathbf{u}_n = Grad\Delta\mathbf{u}_n.\mathbf{F}^{-1}$, a straightforward computation leads based on Eq. 3 to the expression of the increment of Cauchy stress versus the increment of the Eulerian strain tensor:

$$\Delta\sigma_n = \mathbf{c}_n : \Delta\mathbf{e}_n - Tr(grad\Delta\mathbf{u}_n)\sigma_n = \mathbf{c}_n : \Delta\mathbf{e}_n - Tr\left(\Delta\mathbf{e}_n\right)\sigma_n \tag{4}$$

This last relation entails that one can write the increment of Cauchy stress as a first order approximation based on the tangent Eulerian stiffness tensor $\mathbf{c}_n$, augmented by a nonlinear corrective term function of the incremental linearized strain $\Delta\mathbf{e}_n$ (the last term in Eq. 4), as illustrated in Fig. 4.

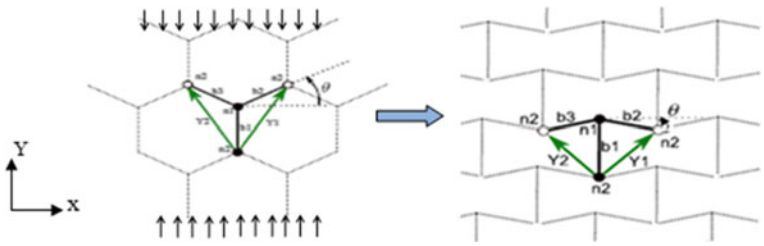

Fig. 5 Classical hexagonal lattice under a compressive loading

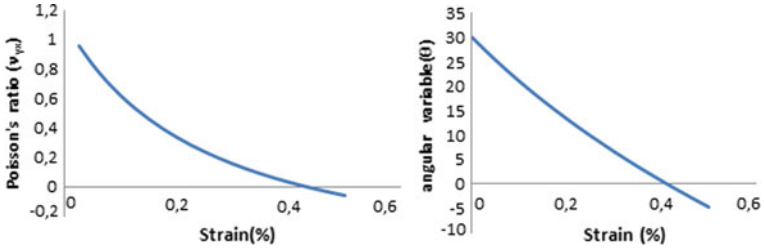

Fig. 6 Change of Poissons ratio (left) and angular variable θ (right) versus the applied compressive strain for the hexagonal lattice

A dedicated code has been constructed from the proposed algorithm, in order to solve for the nodal kinematical unknowns (the displacements of each beam) within the repetitive unit cell. The code uses an input file the reference unit cell topology and micromechanical properties, and delivers as an output the homogenized mechanical properties (classical moduli and Poissons ratio) and the nonlinear stress-strain response for a given deformation path imposed over the RUC.

3.2 Control of the Transition from Non-auxetic to Auxetic Behaviors by Large Strains

As an application of the proposed methodology, the transformation from the non-auxetic hexagonal to the auxetic configuration (re-entrant) of the same lattice is computed, based on a control by the imposed compressive strain (along the y-direction). This transition is evidenced by the evolution of Poissons ratio versus the compressive strain applied along the y direction. The classical hexagonal lattice becomes re-entrant under compression, thus it exhibits a transition from a non auxetic to an auxetic behaviour, as illustrated in Fig. 5.

This transition is evidenced by the evolution of Poissons ratio and the angular variable versus the compressive strain along the y direction of compression, indicated in Fig. 6.

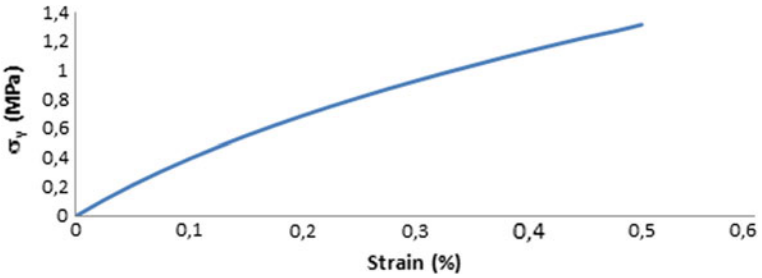

Fig. 7 Compressive Cauchy stress versus strain for the classical hexagonal lattice

The y-component of Cauchy stress (its absolute value is plotted) increases in a monotonous way versus the compressive strain (its absolute value), evaluated as $\epsilon = \lambda_y - 1$, as shown in Fig. 7.

The Poissons ratio becomes negative for strains as large as 50% (compressive strains are counted positively on Fig. 7), indicating a transition towards an auxetic structure, while the compressive stress reaches some plateau before increasing again in the auxetic regime. Based on the effective large strains response, we next evaluate the impact of large applied pre-deformations on the acoustic properties of network materials.

3.3 Effective Incremental Frequency and Phase Velocity of a 1D Microstructured Beam

The dynamical analysis under large strains is first performed in a 1D context, a situation that can be illustrated by a macroscopic beam including a repetitive microstructure. In order to present the 1D method in such a 1D context, we rewrite the incremental nonlinear constitutive law of Sect. 3.1 in the 1D context as follows:

$$\Delta\sigma_n = \left(E_n + E_n^t\right) \Delta e_n \tag{5}$$

where $\Delta\sigma_n$ is the incremental Cauchy stress at increment n, E_n the homogenized beam Youngs modulus (at increment n), $e_n = \frac{\partial u}{\partial x}_{|n}$ the 1D linearized strain with increment Δe_n, and E_n^t the corrected incremental Young modulus accounting for the nonlinear correction to the linear term $E_n \Delta e_n$ in Sect. 3.1, itself depending on the linearized strain increment. Previous incremental constitutive law describes the beam response to an imposed increment of deformation gradient, itself equal to the small strains increment, term $\Delta F_n(x) = \Delta\left(gradu_n(x)\right) \equiv \Delta e_n(x)$.

The incremental nonlinear elastic constitutive law written in Sect. 3.1 is next applied to the analysis of wave propagation through a pre-strained nonlinear microstructured beam, incorporating many unit cells repeated by periodicity along

the longitudinal direction submitted to an incremental strain. All fields in Sect. 3.1 depend upon the variable x, which is the beam axial coordinate; periodicity of the microstructure along x implies that the beam is considered as macro-homogeneous, so that the fields experience a smooth variation with x. Omitting index n, the dynamical incremental equilibrium equation for the continuous displacement of the homogenized continuum writes based on the effective constitutive model given in Eq. 5 as:

$$div\Delta\sigma_n = \rho_{n+1}\frac{\partial^2\Delta u_n}{\partial t^2} \Rightarrow \left(E_n + E_n^t\right)\frac{\partial\Delta e_n}{\partial x} = \rho_{n+1}\frac{\partial^2\Delta u_n}{\partial t^2} \tag{6}$$

in which ρ_{n+1} is the effective medium density of the deformed structure at increment $n+1$. A small parameter υ is introduced in Eq. 6 to enforce the weak nonlinearity through the relation $\upsilon\bar{E}_n^t = E_n^t$, which defines a perturbed modulus (the introduced modulus $\bar{E}_n^t$ has the same physical dimension as modulus E_n^t); the parameter υ facilitates the asymptotic developments in the Linstedt-Poincar method [27]. The first step in the analysis of the nonlinear dispersion relation in the continuum medium is the introduction of the dimensionless time $\tau = \omega t$ in the dynamical equilibrium equation, thus leading to the asymptotic expansion of the frequency, effective density and axial displacement, successively. Substituting the asymptotic expansion expressions into the weakly nonlinear wave Eq. 6 and ordering versus the successive powers of the small parameter produces a set of equations as follows:

$$\begin{aligned}
&O\left(\upsilon^0\right): \quad E_n\frac{\partial^2\Delta u_n^0}{\partial x^2} - \rho_{n+1}^0\left(\omega_{n+1}^0\right)^2\frac{\partial^2\Delta u_n^0}{\partial\tau^2} = 0\\
&O\left(\upsilon^1\right): \quad E_n\frac{\partial^2\Delta u_n^1}{\partial x^2} - \rho_{n+1}^0\left(\omega_{n+1}^0\right)^2\frac{\partial^2\Delta u_n^1}{\partial\tau^2} =\\
&2\rho_{n+1}^0\,\omega_{n+1}^0\omega_{n+1}^1\frac{\partial^2\Delta u_n^0}{\partial\tau^2} + \rho_{n+1}^1\left(\omega_{n+1}^0\right)^2\frac{\partial^2\Delta u_n^0}{\partial\tau^2} - \bar{E}_n^t\frac{\partial^2\Delta u_n^0}{\partial x^2}
\end{aligned} \tag{7}$$

The solution of the $O\left(\upsilon^0\right)$ term equation is well-known and is given by planar harmonic waves of frequency ω_{n+1}^0 (ω_{n+1}^0, ρ_{n+1}^0 are the frequency and density at increment n respectively and which will later on be denoted ω_n, ρ_n). The linear kernel of order $O\left(\upsilon^1\right)$ is similar to the linear kernel of order $O\left(\upsilon^0\right)$. Cancelling the secular terms (the terms multiplied by $\cos(\tau - kx)$) results in an equation containing the incremental angular frequency ω_{n+1}^1 and the effective incremental Youngs modulus $\bar{E}_n$. Thus, the frequency for the new structure configuration is updated versus the actual tangent modulus and density by the relation:

$$\omega_{n+1} = \left(3 - \frac{\rho_{n+1}}{\rho_n}\right)\frac{\omega_n}{2} + \frac{E_n^t k^2}{2\rho_n\,\omega_n} \tag{8}$$

The quantities ρ_n, ω_n therein are the effective density and angular frequency of the medium at increment n, according to the $O\left(\upsilon^0\right)$ equation, ρ_{n+1} is the density for the new configuration and k the wavenumber. The effective incremental phase velocity is given by the following relation versus the updated density and tangent modulus:

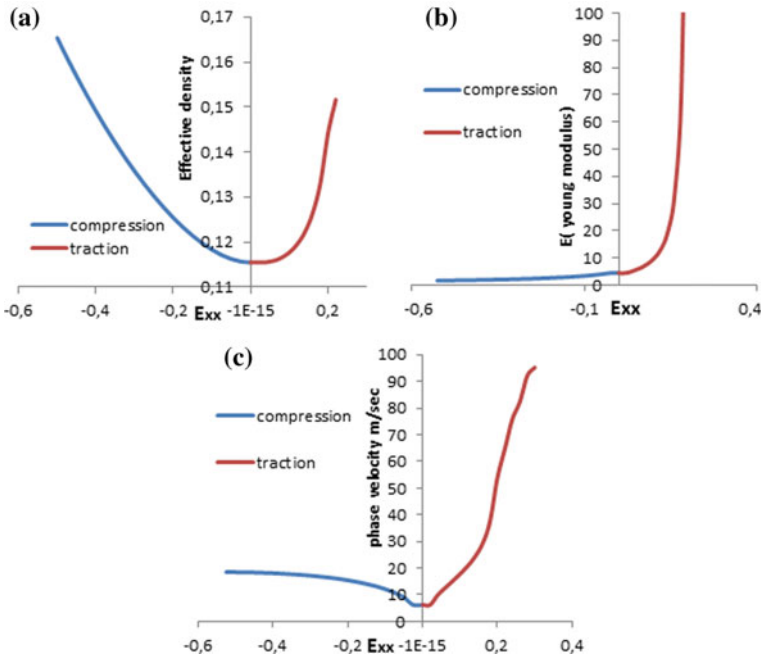

Fig. 8 Density (**a**), Young modulus (**b**) and phase velocity (**c**) variations versus the imposed tensile and compressive strain for a beam incorporating a hexagonal repetitive microstructure

$$c_{n+1} = \left(3 - \frac{\rho_{n+1}}{\rho_n}\right)\frac{c_n}{2} + \frac{E_n^t}{2\rho_n c_n} \tag{9}$$

We subsequently analyze the wave propagation characteristics of the hexagonal lattice introduced in Sect. 3.2. Figure 8 indicates that the imposed compression has a significant effect on the incremental phase velocity, which is much more pronounced in traction than in compression, due to the fact that Young modulus varies very little under (Fig. 8b) compression while the density increases (Fig. 8a). The strong variation of Young modulus under traction (Fig. 8b) counterbalances the increase of density (Fig. 8a) so that the phase velocity in turn increases under a tensile loading (Fig. 8c). These results entail overall that the dynamical behavior of the material will be modified by decreasing the wave velocity, especially by imposing a compressive strain before sending waves into the structure. This feature is especially interesting in situations in which dissipation occurs, since compression tends (as dissipation) to increase wave absorption phenomena.

3.4 Incremental Dispersion Relation and Phase Velocity in 2D Homogenized Media

In a 2D context, the constitutive law governing the evolution of the homogenized network material subjected to large deformation gradients writes relying on the developments at the end of Sect. 2 and as an extension of Sect. 3.3:

$$\Delta\left[\sigma_{xx},\ \sigma_{yy},\ \sigma_{xy}\right]_n^T = \left(c_n + c_n^t\right)\Delta\left[e_{xx},\ e_{yy},\ e_{xy}\right]_n^T \tag{10}$$

where c_n is the tangent stiffness matrix of the effective continuum at increment, c_n^t the corrected tangent stiffness matrix, and $\left[\sigma_{xx},\ \sigma_{yy},\ \sigma_{xy},\ \right]_n^T$, $\left[e_{xx},\ e_{yy},\ e_{xy}\right]_n^T$ are successively the vectors condensing the three independent components of the Cauchy stress tensor σ and small strain tensor $\mathbf{e} := \frac{1}{2}\left(grad\mathbf{u} + grad^T\mathbf{u}\right)$, itself built as the symmetrical part of the gradient of the displacement field, vector $\mathbf{u}$. Using the same methodology as in the previous 1D context, and restricting to centro-symmetrical structures for which the coupling coefficients vanish (the following components of the rigidity matrix vanish, $a_{13} = a_{23} = a_{31} = a_{32} = 0,\ a_{12} = a_{21}$), we express the nonlinear frequency for the new configuration (resulting from the applied gradient of deformation) in an incremental scheme versus the effective density of the medium as:

$$\begin{aligned}
\omega_{n+1}^l &= \left(3 - \frac{\rho_{n+1}}{\rho_{n+1}^0}\right)\frac{\omega_n^l}{2} + \frac{1}{\rho_{n+1}^0\,\omega_n^l}\left(\tfrac{1}{4}a_{11}k_1^2 + \tfrac{1}{4}a_{22}k_2^2 + \tfrac{1}{4}a_{33}k_1^2 + \tfrac{1}{4}a_{33}k_2^2\right.\\
&\quad \left. + \tfrac{1}{4}\sqrt{a_{11}^2k_1^4 - 2a_{11}a_{22}k_1^2k_2^2 - 2a_{11}a_{33}k_1^4 + 2a_{11}a_{33}k_1^2k_2^2 + 4a_{11}^2k_1^2k_2^2 + f_1}\right.\\
f_1 &= 8a_{12}a_{33}k_1^2k_2^2a_{22}^2k_2^4 + 2a_{22}a_{33}k_1^2k_2^2 - 2a_{22}a_{33}k_2^4 + a_{33}^2k_1^4 + 2a_{33}^2k_1^2k_2^2 + a_{33}^2k_2^4)\\
\omega_{n+1}^t &= \left(3 - \frac{\rho_{n+1}}{\rho_{n+1}^0}\right)\frac{\omega_n^l}{2} + \frac{1}{\rho_{n+1}^0\,\omega_n^t}\left(\tfrac{1}{4}a_{11}k_1^2 + \tfrac{1}{4}a_{22}k_2^2 + \tfrac{1}{4}a_{33}k_1^2 + \tfrac{1}{4}a_{33}k_2^2\right.\\
&\quad \left. - \tfrac{1}{4}\sqrt{a_{11}^2k_1^4 - 2a_{11}a_{22}k_1^2k_2^2 - 2a_{11}a_{33}k_1^4 + 2a_{11}a_{33}k_1^2k_2^2 + 4a_{11}^2k_1^2k_2^2 + f_1}\right.
\end{aligned} \tag{11}$$

and shear modes respectively, $\omega_n^{l,t}$ is the frequency of the increment and the coefficients a_{ij} are the components of the incremental stiffness matrix. In order to highlight the non-isotropic dynamical behaviour of the re-entrant hexagonal configurations and the impact of applied deformation on the dispersive characteristics, we plot the phase velocity for the hexagonal lattice submitted to a gradient of deformation corresponding to compression (Fig. 9) and shear (Fig. 10) successively.

The regular hexagonal lattice has an initial isotropic behavior for both the longitudinal and shear modes (in the low frequency range), as indicated in Figs. 9 and 10 by the corresponding circular phase velocity shape of snapshots (a) in the absence of deformation. What is more, the low frequency behavior both for longitudinal and shear modes is non-dispersive. An anisotropic behavior appears when we employ rather than a regular a re-entrant configuration, which occurs for $E_{yy} = 0.5$. The degree of anisotropy becomes higher as the level of compression increases, due to the modification of the lattice geometry; the anisotropic behavior of the re-entrant

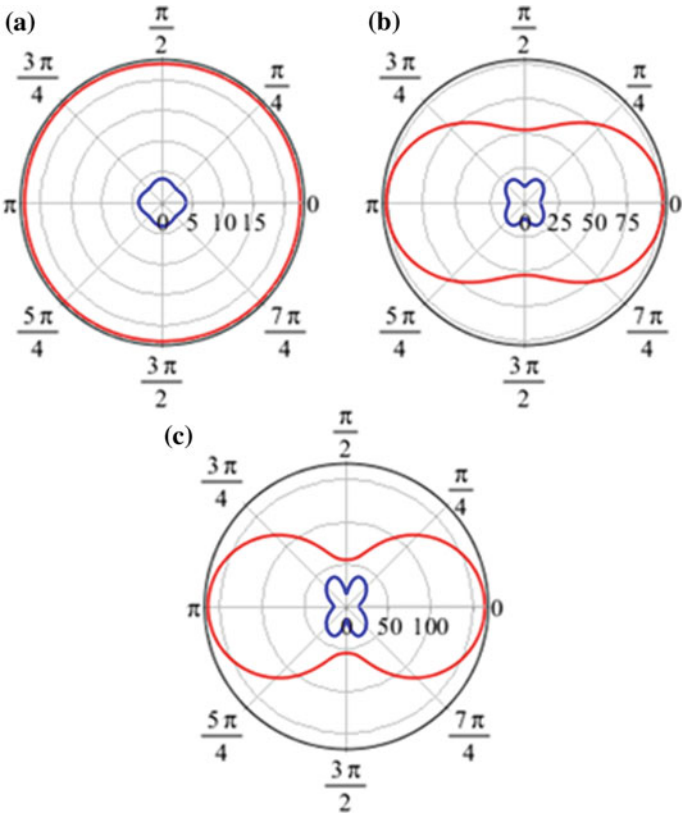

Fig. 9 Phase velocity in the longitudinal (red) and shear (blue) modes for the hexagonal lattice for different compression strain loadings (here measured positively) **a** $E_{yy} = 0$, **b** $E_{yy} = 0.25$ **c** $E_{yy} = 0.5$

lattice is markedly visible from the irregular shape of the phase velocity plot for the longitudinal and shear modes [37].

4 Modification of the Nature of Propagating Waves According to the Degree of Nonlinearity in 1D Elastic Microstructured Beams

In order to analyze the effect of the considered degree of nonlinearity on the nature of the propagating waves, we consider the complete kinematics of its inner elements. For extensible beams, it can be shown that the energy density of a nonlinear second gradient medium takes the more general form [48]:

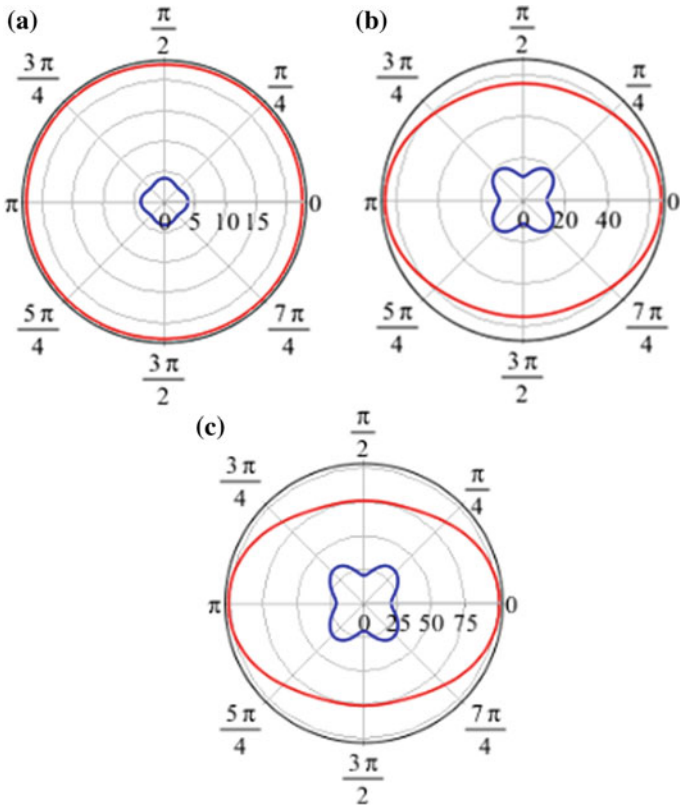

Fig. 10 Phase velocity in the longitudinal (red) and shear (blue) modes for the hexagonal lattice for different shear loads **a** $E_{xy} = 0$, **b** $E_{xy} = 0.15$ **c** $E_{xy} = 0.275$

$$Ws = Ws_1 + Ws_2 + Ws_3 \tag{12}$$

where Ws_1 and Ws_2 are the first and second order contributions of the strain energy density in small strain and Ws_3 is the contribution of the strain energy density accounting for the presence of large strains. We consider a nonlinear beam kinematics at the discrete level of the unit cell, which after homogenization lead to a nonlinear second gradient effective continuum. Its kinematics are characterized by the first and second gradient of the scalar displacement field. The strain energy density expression defined in Eq. 12 incorporates the contributions of both the first order Piola-Kirchhoff stress tensor and of the second order hyperstress tensor. The latter are given in component form as follows:

$$\sigma_{ij} = \frac{\partial \left(Ws_1 + Ws_3\right)}{\partial \left(\partial u_i / \partial x_j\right)}, \quad S_{ijk} = \frac{\partial \left(Ws_2\right)}{\partial \left(\partial^2 u_{ij} / \partial {x_k}^2\right)} \tag{13}$$

The equations of motion for a second gradient medium along the directions then write in index form as follows:

$$\left(\frac{\partial \sigma_{ij}}{\partial x_j}\right) - \frac{\partial^2 S_{ijk}}{\partial x_j \partial x_k} = \rho^* \ddot{u}_j,\ j = 1, 2 \tag{14}$$

The effective density therein is given in general by $\rho^* = M_1/A_{cell}$, with M_1 the mass of the set of lattice beams within the unit cell and A_{cell} the area of the periodic unit cell in 2D. From Eq. 14, we obtain two differential equations that describe the propagation of longitudinal waves polarized in the direction of incident waves, and of shear waves polarized in a direction perpendicular to the direction of the incident wave. The longitudinal and shear modes are coupled via the linear (Cauchy and Second gradient) and nonlinear kinematic parameters.

We subsequently analyze the propagation of longitudinal waves in a 1D continuum beam at the macro level, considering a microstructured beam which incorporates periodic hexagonal unit cells along the length direction, and only one unit cell in its thickness direction and subject to uniaxial loading ($\sigma_{xx} \neq 0$ and $\epsilon_{xx} \neq 0$). Expanding the total work of the architectured lattice [48], the extensible energy density of the homogenized hexagonal lattice can be written in closed form versus the slenderness ratio β and the angle θ in the x-direction:

$$\begin{aligned} W = \frac{E\beta}{\cos(\theta)} (& \underbrace{\varepsilon_{xx}^2 \left(4\sin(\theta)\cos(\theta) + 4\cos(\theta) + 3\sin(\theta) + 3 - 4\cos^3(\theta)\right)}_{Linear\ part} \\ & \underbrace{-2\varepsilon_{xx}^3 (2\cos^3(\theta) + 2\cos^2(\theta)\sin(\theta) + 5\cos^2(\theta) - 4\cos(\theta)\sin(\theta)}_{Non\ Linear\ part} \\ & \underbrace{- 4\cos(\theta) - 6\sin(\theta) - 6)}_{Non\ Linear\ part} \\ & \underbrace{+ \frac{1}{4} L^2 (\beta + 1) \varepsilon_{xx,x}^2 (2\sin(\theta)\cos^4(\theta) + 6\cos^4(\theta) - 11\sin(\theta)\cos^2(\theta)}_{Second\ gradient\ part} \\ & \underbrace{- 17\cos^2(\theta) + 12\sin(\theta) + 12}_{Second\ gradient\ part} \end{aligned} \tag{15}$$

Using Eq. 15, we easily obtain the specific expressions of the first order Piola-Kirchhoff stress and hyperstress tensors based on the general definitions introduced in Eqs. 12 and 13. Inserting these expressions into the equation of motion (Eq. 14), we obtain the homogenized nonlinear wave equation:

$$E_1 \frac{\partial^2 u}{\partial x^2} + E_2 \frac{\partial^2 u}{\partial x^2} \frac{\partial u}{\partial x} + E_3 \frac{\partial^4 u}{\partial x^4} = \rho^* \frac{\partial^2 u}{\partial t^2} \tag{16}$$

where u is the longitudinal displacement, E_1 the linear effective modulus derived from the linear part of the energy equation, E_2 the nonlinear effective modulus characteristic of the large deformation behavior (nonlinear part) and E_3 the second order effective modulus, characterizing the second order gradient behavior. The equation of motion (Eq. 16) describes the quasi-static (dispersive) behavior of waves propagating within the periodic lattice. Let us note that the second order modulus E_3 on Eq. 16 is always negative. This means that the presence of a microstructure results in positive dispersion, so that increasing the wavenumber leads to increase the phase velocity. The problem under consideration in Eq. 16 represents a Boussinesq-type equation. A set of elliptic functions depending on the degree of nonlinearity are presented explicitly as a solution in [49]; they are described by a universal coefficient s which does not depend on the mechanical properties of the material, but takes into account the shape, the period and the velocity of propagating waves within the material. It may be considered as a quantitative measure of how much the nonlinearity mode differs from the linear one. The solution of Eq. 16 can then be expressed as [49]:

$$u(z) = \int -\frac{A}{2} + \frac{A\,s^2}{2\left(1 - {}^{E(s)}/_{K(s)}\right)} sn^2\left(\frac{k_0}{2}z, s\right)dz \tag{17}$$

where the reduced variable $z = x - \frac{w}{k}t$ has been introduced. We shall consider the following non-dimensional system parameters: the product $k \cdot L$ is the dimensionless wavenumber, $\frac{\omega_0 L}{\sqrt{\frac{E}{\rho}}}$ is the dimensionless frequency, $\frac{v_p}{\sqrt{\frac{E}{\rho}}}$ and $\frac{v_g}{\sqrt{\frac{E}{\rho}}}$ are the dimensionless phase and group velocities respectively, with parameters E, ρ and L therein the Young modulus, the density and length of the beam respectively. We represent in Fig. 11 the dispersion relation for different values of the nonlinear parameter s for the re-entrant hexagon lattice (case $\theta \leq 0$). In the analysis to follow, v_p and v_{p0} are the phase velocities for the nonlinear and linear medium respectively.

For a weak nonlinearity, a supersonic mode occurs and the dispersion curves lie above the linear dispersion curve ($v = v_0$). For higher nonlinearity, the waves changes from a supersonic to an evanescent subsonic mode at approximately s = 0.7 and the dispersion curves drops below the linear case and vanish for certain values of k. In a nonlinear situation, the second order gradient anisotropic continuum has two propagation modes (subsonic and supersonic), whereas Cauchy or micropolar continua only have supersonic modes, for which an increase of the frequency with the wavenumber occurs. Figure 12 suggests that the group velocity tends to zero when the wave frequency of all evanescent subsonic modes approaches their higher value. The vanishing of mode occurs when $v_g \to -\infty$, which means that the total energy of the medium is completely dissipated. In the case of supersonic modes, as the wavenumber k increases, the accumulated energy in the medium (increasing in the group velocity) provides an increase in the dispersion relation (Fig. 13).

A relation between the phase and group velocities is obtained after a lengthy calculation starting from the dynamical equilibrium equation and the definition of the group velocity. It can be seen that for a weak nonlinearity, the phase velocity exceeds

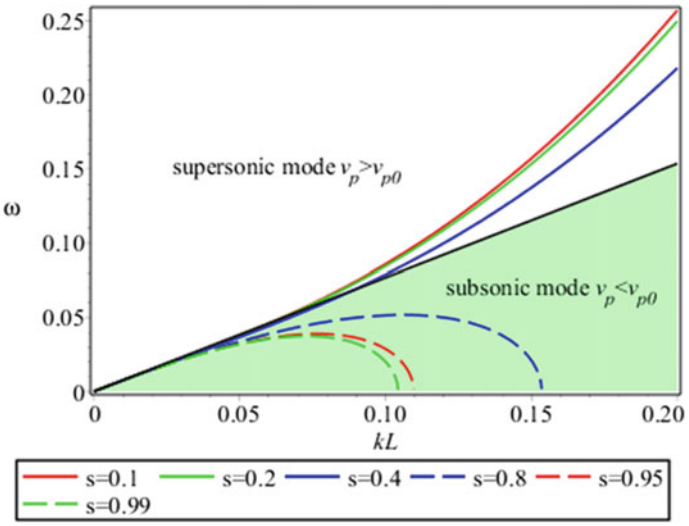

Fig. 11 Dispersion relation for different values of s for the hexagonal re-entrant lattice, $\theta = -\frac{\pi}{6}$

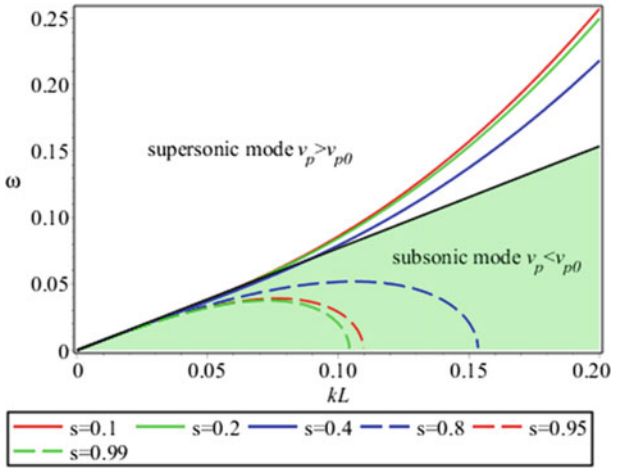

Fig. 12 Dispersion relation for different values of s for the hexagonal re-entrant lattice, $\theta = -\frac{\pi}{6}$

the phase velocity and describes a supersonic mode, while for a higher nonlinearity, the wave changes from a supersonic to subsonic mode (approximately for $s = 0.7$).

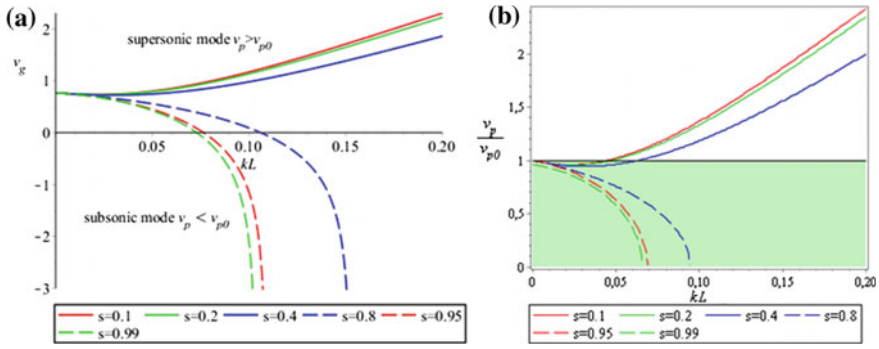

Fig. 13 Group velocities (**a**) and phase velocities (**b**) for different values of s for the regular hexagon with $\theta = \frac{\pi}{6}$

5 Conclusions

In the current work, we have presented recent advances in the design and analysis of metamaterials, with respect to their static and wave propagation characteristics. More specifically, we presented a class of two-dimensional anti-auxetic inner material architectures that allowed for the creation of metamaterials of controlled anisotropy. We subsequently correlated the level of anisotropy with the wave propagation attributes of the architectured material, noting the creation of isolating propagating material directions in a systematic manner. What is more, we studied the large strain behavior of architectured media. To that scope, we showcased the potential of creating auxetic metamaterials from non-auxetic ones in the large strain regime, while we quantified the effect of large compressive and shear loads in the wave propagation characteristics of hexagonal lattices. We noted significant effects of the applied large deformation on the frequency and phase velocity of the propagating waves, as well as on the dispersion relation. What is more, we analyzed the role of the considered nonlinearity on the nature of the propagating waves, deriving a relation between the phase and group velocities and the level of nonlinearity.

We hope that the provided insights and elaborated methodologies function as a basis and inspiration for further developments in the design and analysis of novel metamaterials for static and acoustic applications.

Appendix

The effective densities of the diamond and octagon-shaped lattice architectures (D, DS, O, OS) are given in parametric form with respect to their slenderness $\eta = t/L$, $c = \cos\theta$, $s = \sin\theta$ (Fig. 2) and the constituents material density ρ_s, as follows:

$$\begin{aligned} \rho_D^* &= \frac{\rho_s\,\eta}{cs}, \quad \rho_{DS}^* = \frac{\rho_s(1+s)\,\eta}{cs} \\ \rho_O^* &= \frac{6\rho_s\,\eta}{(2c+1)\,(2s+1)}, \quad \rho_{OS}^* = \frac{\rho_s\,\eta\,(6+2\,(1+2s))}{(2c+1)\,(2s+1)} \end{aligned} \tag{18}$$

The effective mechanical moduli E_1^* and E_2^* for the diamond-shaped lattice metamaterials without (D) and with (DS) inner strengthenings are given in Eq. 19. The moduli are normalized with respect to the modulus E_s of the constitutive material and are provided in closed-form as functions of the aspect ratio η and angle θ of the lattice's unit cell. We note that in [14], the corresponding expressions of the effective moduli have been additively normalized with respect to the unit-cell density values.

$$\begin{aligned} E_1^{*D} &= -\frac{\eta^3 c}{s\left(c^2-\eta^2c^2-1\right)}, \quad E_2^{*D} = \frac{\eta^3 s}{c\left(c^2-\eta^2c^2+\eta^2\right)} \\ E_1^{*DS} &= \frac{\eta\left(s-s\eta^2-1\right)c}{c^2s\left(1-\eta^2\right)+(s-1)\left(c^2+\eta^2\right)-2s+1} \\ E_2^{*DS} &= \frac{\eta\left(c^2+\left(c^2-1\right)\left(\eta^4-2\eta^2\right)c\right)}{c^4\left(1-2\eta^2\right)+\eta^4\left(c^4+c^2s-2c^2-s+1\right)+c^2\eta^2(2-s)} \end{aligned} \tag{19}$$

The effective moduli for the octagon-shaped lattice metamaterials without (O) and with (OS) inner strengthenings are given accordingly in Eq. 20, as follows:

$$\begin{aligned} E_1^{*O} &= -\frac{1}{2}\frac{\eta^3(2c+1)}{\left(\left(1-\eta^2\right)c^2-1-\eta^2\right)(s+0.5)}, \quad E_2^{*O} = \frac{\eta^3(2s+1)}{\left(c^2-\eta^2c^2+2\eta^2\right)(2c+1)} \\ E_1^{*OS} &= \frac{1}{4}\frac{\eta\left(2c^2-2\eta^2c^2+2\eta^2s+s\eta^2\right)(2c+1)}{\left(1-\eta^2\right)\left(c^4-sc^2\right)+\left(-\frac{9}{4}+\frac{1}{4}\eta^2\right)c^2+3\left(1+\eta^2\right)\left(s+\frac{3}{4}\right)} \\ E_2^{*OS} &= \frac{\eta\left(2c^2-2\eta^2c^2+2\eta^2s+s\eta^2\right)}{\left(c^2-\eta^2c^2+2\eta^2\right)(2c+1)} \end{aligned} \tag{20}$$

References

1. Cui, T.J., Smith, D.R., Liu, R.P.: Metamaterials: Theory Design and Applications. Springer (2010)
2. Smith, D.R., Pendry, J.B.: Homogenization of metamaterials by field averaging. J. Optic. Soc. Am. B **23**(3), 391 (2006)
3. Engheta, N., Ziolkowski, R.W.: Metamaterials: Physics and Engineering Explorations (2006)
4. Greaves, G.N.: Poisson's ratio over two centuries: challenging hypotheses. Notes Rec. R. Soc. London **67**(2012), 37–58 (2013)
5. Liu, Y., Hu, H.: A review on auxetic structures and polymeric materials. Sci. Res. Essays **5**(10), 1052–1063 (2010)
6. Spadoni, A., Ruzzene, M.: Elasto-static micropolar behavior of a chiral auxetic lattice. J. Mech. Phys. Solids **60**(1), 156–171 (2012)
7. Bacigalupo, A., Gambarotta, L.: Homogenization of periodic hexa- and tetrachiral cellular solids. Compos. Struct. **116**(1), 461–476 (2014)
8. Prawoto, Y.: Seeing auxetic materials from the mechanics point of view: a structural review on the negative Poisson's ratio. Comput. Mater. Sci. **58**, 140–153 (2012)
9. Greaves, G.N., Greer, A.L., Lakes, R.S., Rouxel, T.: Poisson's ratio and modern materials. Nat. Mater. **10**, 823–838 (Oct. 2011)
10. Lachenal, X., Daynes, S., Weaver, P.M.: Review of morphing concepts and materials for wind turbine blade applications. Wind Energy **16**(2012), 283–307 (2013)

11. Kingnid, R.O., Farhan, G.: Zero poissons ratio cellular honeycombs for ex skins undergoing onedimensional morphing. J. Intelligen. Mater. Syst. Struct. **21**(17), 1737–1753 (2010)
12. Attard, D., Grima, J.N.: Modelling of hexagonal honeycombs exhibiting zero Poisson's ratio. physica status solidi (b) **248**(1), 52–59 (2011)
13. Gong, X., Huang, J., Scarpa, F., Liu, Y., Leng, J.: Zero Poisson 's ratio cellular structure for two-dimensional morphing applications. Compos. Struct. **134**, 384–392 (2015)
14. Karathanasopoulos, N., Reda, H., Ganghoffer, J.-F.: Designing two-dimensional metamaterials of controlled static and dynamic properties. Comput. Mater. Sci. **138**, 323–332 (2017)
15. Zheng, X., Lee, H., Weisgraber, T.H., Shuste, M., DeOtte, J., Duoss, E.B., Kuntz, J.D., Biener, M.M., Ge, Q., Jackson, J.A., Kucheyev, S.O., Fang, N.X., Spadaccini, C.M.: Ultralight, ultrastiff mechanical metamaterials. Science **344**(6190), 1373–1377 (2014)
16. Babaee, S., Shim, J., Weaver, J.C., Chen, E.R., Patel, N., Bertoldi, K.: 3D soft metamaterials with negative Poisson's ratio. Adv. Mat. **25**(36), 5044–5049 (2013)
17. Jiang, Y., Wang, Q.: Highly-stretchable 3D-architected mechanical metamaterials, Nature (2016)
18. Karathanasopoulos, N., Angelikopoulos, P., Papadimitriou, C., Koumoutsakos, P.: Bayesian identication of the tendon fascicles structural composition using finite element models for helical geometries. Comput. Methods Appl. Mech. Eng. **313**, 744–758 (2017)
19. Abdolhamid, M.-P., Ahmad, O., Ali, M.: Tendon Tissue Engineering and its role on healing of the experimentally induced large tendon defect model in rabbits: a comprehensive in vivo study. PLoS One, **8**(9) (2013)
20. Engheta, N., Ziolkowski, R.W.: Metamaterials: Physics and Engineering Explorations, Wiley (2006)
21. Alibert, J.J., Seppecher, P., dell'Isola, F.: Truss modular beams with deformation energy depending on higher displacement gradients. Math. Mech. Solids **8**, 51–73 (2003)
22. Forest, S., Sievert, R.: Nonlinear microstrain theories. Int. J. Solids Struct. **43**, 7224–7245 (2006)
23. Forest, S.: Micromorphic Approach for gradient elasticity, viscoplasticity, and damage. J. Eng. Mech. **135**(3), 117–131 (2009)
24. Buechner, P.M., Lakes, R.S.: Size effects in the elasticity and viscoelasticity of bone. Biomechan. Model. Mechanobiol. **1**, 295–301 (2003)
25. Manktelow, K., Leamy, M.J., Ruzzene, M.: Topology design and optimization of nonlinear periodic materials. J. Mech. Phys. Solids **61**(12), 2433–2453 (2013a)
26. Manktelow, K., Leamy, M.J., Ruzzene, M.: Comparison of asymptotic and transfer matrix approaches for evaluating intensity-dependent dispersion in nonlinear photonic and phononic crystals. Wave Motion **50**, 494–508 (2013b)
27. Narisetti, R.K., Ruzzene, M., Leamy, M.J.: Study of Wave Propagation in Strongly Nonlinear Periodic Lattices Using a Harmonic Balance Approach. Wave Motion **49**, 394–410 (2012)
28. Placidi, L., Rosi, G., Giorgio, I., Madeo, A.: Reflection and transmission of plane waves at surfaces carrying material properties and embedded in second-gradient materials. Math. Mech. Solids (2013). https://doi.org/10.1177/1081286512474016
29. Eremeyev, V.A., Pietraszkiewicz, W.: The nonlinear theory of elastic shells with phase transitions. J. Elast. **74**(1), 67–86 (2004)
30. Lee, S.H., Park, C.M., Seo, Y.M., Wang, Z.G., Kim, C.K.: Composite acoustic medium with simultaneously negative density and modulus. Phys. Rev. Lett. **104**(5), (2010)
31. Kolpakovs, A.G.: Determination of the average characteristics of elastic frameworks. J. Appl. Math. Mech. **49**(6), 739–745 (1985)
32. Xu, B., Arias, F., Brittain, S.T., Zhao, X.-M., Grzybowski, B., Torquato, S., Whitesides, G.M.: Making negative Poissons ratio microstructures by soft lithography. Advanc. Mater. **11**(14), 1186–1189 (1999)
33. Christensen, J., de Abajo, F.: Anisotropic metamaterials for full control of acoustic waves. Phys. Rev. Lett. **108**(12), (2012)
34. Del Vescovo, D., Fregolent, A.: Theoretical and experimental dynamic analysis aimed at the improvement of an acoustic method for fresco detachment diagnosis. Mech. Syst. Signal Process. **23**(7), 2312–2319 (2009)

35. Phani, A.S., Woodhouse, J., Fleck, N.A.: Wave propagation in two-dimensional periodic lattices. J. Acoust. Soc. Am. **119**(4), 1995–2005 (2006)
36. Reda, H., Rahali, Y., Ganghoffer, J.F., Lakiss, H.: Wave propagation in 3D viscoelastic auxetic and textile materials by homogenized continuum micropolar models. Comp. Struct. **141**, 328–345 (2016)
37. Gonella, S., Ruzzene, M.: Homogenization and equivalent in-plane properties of two-dimensional periodic lattices. Int. J. Solids Struct. **45**(10), 2897–2915 (2008)
38. Bacigalupo, A., Gambarotta, L.: Homogenization of periodic hexa- and tetrachiral cellular solids. Comp. Struct. **116**, 461–476 (2014)
39. Reda, H., Rahali, Y., Ganghoffer, J.F., Lakiss, H.: Wave propagation analysis in 2D nonlinear hexagonal periodic networks based on second order gradient nonlinear constitutive models. Int. J. Nonlin. Mech. **87**, 85–96 (2016)
40. Reda, H., Rahali, Y., Ganghoffer, J.F., Lakiss, H.: Nonlinear dynamical analysis of 3D textiles based on second order gradient homogenized media. Comp. Struct. **154**, 538–555 (2016)
41. Manktelow, K., Narisetti, R.K., Leamy, M.J., Ruzzene, M.: Finite-element based perturbation analysis of wave propagation in nonlinear periodic structures. J. Mech. Syst. Signal Proc. **39**, 32–46 (2013)
42. Danescu, A.: Bifurcation in the traction problem for a transversely isotropic material. Math. Proc. Cambridge Philos. Soc. **110**, 385–394 (1991)
43. Dorfmann, A., Ogden, R.W.: A constitutive model for the Mullins effect with permanent set in particle-reinforced rubber. Int. J. Solids Struct. **41**, 1855–1878 (2004)
44. Kurashige, K.: Instability of a transversely isotropic elastic slab subjected to axial. Appl. Mech. **48**, 351–356 (1981)
45. El Nady, K., Ganghoffer, J.F.: Computation of the effective mechanical response of biological networks accounting for large configuration changes. J. Mech. Behav. Biomed. Mat. **58**, 28–44 (2015)
46. Dos Reis, F., Ganghoffer, J.F.: Construction of micropolar models from lattice homogenization. Comput. Struct. **112–113** (2012) 354–363
47. El Nady, K., Goda, I., Ganghoffer, J.F.: Computation of the effective nonlinear mechanical response of lattice materials considering geometrical nonlinearities. Comp. Mech. **58** (2016) 1–23
48. Rahali, Y., Giorgio, I., Ganghoffer, J.F., dell'Isola, F.: Homogenization la Piola produces second gradient continuum models for linear pantographic lattices. Int. J. Eng. Sci. **97**, 148–172 (2015)
49. Andrianov, I.V., Danishevs'kyy, V.V., Ryzhkov, O.I., Weichert, D.: Numerical study of formation of solitary strain waves in a nonlinear elastic layered composite material. Wave Motion **51**, 405–417 (2014)

Acoustic Approximation of the Governing Equations of Liquid Crystals Under Weak Thermomechanical and Electrostatic Perturbations

Vladimir Sadovskii and Oxana Sadovskaya

Abstract A simplified mathematical model of thermomechanical behavior of a liquid crystal in nematic phase under weak mechanical and thermal perturbations as a micropolar viscoelastic medium with rotating particles is constructed. This model is based on the assumption that potential energy of elastic deformation depends on four parameters—the change in volume, angle of relative rotation of particles, first invariant of curvature measure and entropy. The heat conduction process is described taking into account the anisotropy of a material due to the difference in coefficients of thermal conductivity along the axis of orientation of particles and in the transverse direction. Influence of electric field on the layer of a liquid crystal is modeled by means of the equations of electrostatics for an inhomogeneous anisotropic medium. In the plane formulation, the parallel computational algorithm is worked out on the basis of splitting method with respect to spatial variables, Godunov's gap decay method, Ivanov's method of constructing finite-difference schemes with controlled dissipation properties and method of straight lines for finding electric field. The algorithm is implemented using the CUDA technology for computer systems with graphics accelerators. Results of computations of wave motions demonstrating the efficiency of proposed method and algorithm are represented. It is shown that the effect of orientational thermoelasticity of a liquid crystal in the form of re-orientation of particles in an inhomogeneous temperature field can only be evident in the presence of tangential stresses at the boundary. The modes of resonance excitation in a liquid crystal at the eigenfrequency of rotational motion of particles are analyzed numerically.

V. Sadovskii (✉) · O. Sadovskaya
Siberian Branch of the Russian Academy of Sciences, Institute of Computational Modeling, Akademgorodok 50/44, Krasnoyarsk 660036, Russia
e-mail: sadov@icm.krasn.ru

O. Sadovskaya
e-mail: o_sadov@icm.krasn.ru

F. dell'Isola et al. (eds.), *Advances in Mechanics of Microstructured Media and Structures*, Advanced Structured Materials 87,
https://doi.org/10.1007/978-3-319-73694-5_17

1 Introduction

Liquid crystals (mesomorphic materials) have wide applications due to unusual combination of properties of fluidity and elastic anisotropy, which appear in a certain range of temperature under weak external effects of different physical nature—mechanical, thermal, electromagnetic, magnetic, or optical. Such materials are used in optical instrumentation: data logging, display, processing and storage devices; in medical and technical diagnostics, in particular, in thermography.

Physical properties of liquid crystals and their response to different external actions are described in the monographs [7, 16, 53]. The simplest mathematical model of the static state of a liquid crystal as an elastic continuous medium is developed by Oseen and Frank [14, 33] (see [48]). In this model, the elastic energy is represented as a quadratic form relative to derivatives of the vector–director with respect to the spatial coordinates. In isotropic case the quadratic form is determined by three independent phenomenological parameters—the Frank coefficients, characterizing the elastic resistance of a liquid crystal to a change in curvature. Equilibrium equations follow from the variational principle of minimum of free elastic energy for fixed boundary conditions, and have the form of second-order partial differential equations relative to the vector–director. An obvious drawback of this approach is that it does not take into account the effect of translational motion of the liquid crystal molecules due to the mechanical action at the boundary of normal pressure and tangential stresses, as well as the thermal action that leads to inhomogeneous volumetric expansion of a medium. The Oseen model can not be generalized for the analysis of dynamic, in particular, wave effects, in which the D'Alembert inertial forces of translational and rotational motion play an important role.

A more meaningful approach to mathematical modeling of deformation of a liquid crystal is based on the notion that a liquid crystal is a fine-dispersed continuum, at each point of which the elongated particles—molecules of the liquid crystal or domains of co-oriented molecules—can move in accordance with laws of the dynamics of viscous or inviscid fluid and can rotate relative to the fluid, with elastic or viscoelastic resistance to rotation. The basis for this approach is the fundamental work by the Cosserat brothers [8], where the equations of an elastic couple-stress continuum were deduced. For the first time, the model of a liquid crystal was proposed by Ericksen [10]. Using thermodynamic principles this model was developed by Aero and his followers [1–3], Eringen and Lee [11, 12, 26], Leslie [27], as well as, later, by Kondaurov [23], Kalugin [21] and other researchers [5, 28, 29]. The theory of structurally inhomogeneous continuum with rotational degrees of freedom was applied to the simulation of elastic crystals under dynamic loading in [19, 30].

In [38, 39, 41] the system of nonlinear equations of the Cosserat theory of elasticity and the system of reduced momentless model, taking into account rotational degrees of freedom of particles, are represented in a thermodynamically consistent form of the conservation laws. This ensures hyperbolicity and mathematical correctness of the formulation of boundary-value problems for the mentioned systems. Accounting viscosity in accordance with the Maxwell theory, as is done in the

models of liquid crystals, brings additional summands, free from derivatives with respect to spatial variables, in equations of the Cosserat elastic medium but does not change the type of the system. Thus, actually, there exists a consistent mathematical model which adequately describes experimentally discovered qualitative behavioral characteristics of a material in a mesomorphic aggregate state. However, this model is so complicated that the analytical apparatus available for its study is almost fully limited to direct computational methods. A considerable obstruction is put by the demand of presetting the model parameters and functions of state, which need special physical experiments to be determined. For a detailed study of processes running in liquid crystals, it is more appropriate to derive simpler model variants describing specific cases of motion.

This chapter deals with developing and analyzing an acoustic approximation of the model of a nematic liquid crystal as a micropolar medium using high-performance computations. The model of elastic acoustic approximation without taking into account couple stresses was obtained in [40, 43]. The modernization of the model, as described below in this chapter, consists in accounting the moment interactions, caused by a change in the internal curvature, and the dissipative viscoelastic processes at arbitrary rotations of the particles.

2 Governing Equations

2.1 Integral Conservation Laws

Transition from the microscopic description of a liquid crystal medium as a discrete mechanical system, composed of a large number of particles—elongated molecules of the liquid crystal, to the continuous macroscopic description is based on the averaging procedure. Common in the continuum mechanics, Lagrangian characteristics of motion—the initial density ρ and the velocity vector $\boldsymbol{v}$—are estimated in terms of the masses m_k and the velocity vectors $\boldsymbol{v}_k$ of particles in a specified volume V in the initial state, using the known formulas:

$$\rho = \lim_{V\to 0} \frac{1}{|V|} \sum_{k=1}^{N} m_k, \quad \rho \boldsymbol{v} = \lim_{V\to 0} \frac{1}{|V|} \sum_{k=1}^{N} m_k \boldsymbol{v}_k. \tag{1}$$

Here the vanishing V is understood as the volume contraction to a fixed point. Similarly, the Lagrangian characteristics of rotational motion are introduced—the bulk density of moment of inertia $\boldsymbol{J}$, which is a second-order symmetric and positive definite tensor, and the angular velocity vector $\boldsymbol{\omega}$:

$$\boldsymbol{J} = \lim_{V\to 0} \frac{1}{|V|} \sum_{k=1}^{N} \boldsymbol{j}_k, \quad \boldsymbol{J} \cdot \boldsymbol{\omega} = \lim_{V\to 0} \frac{1}{|V|} \sum_{k=1}^{N} \boldsymbol{j}_k \cdot \boldsymbol{\omega}_k, \tag{2}$$

where $\boldsymbol{j}_k$ and $\boldsymbol{\omega}_k$ are, respectively, the tensors of inertia and the angular velocity vectors of particles in the volume V.

The analysis of dimensions shows that the resultant averaging model takes into account the material microstructure, the characteristic linear dimension of which has the following upper and lower limits:

$$d_+ = \max_{|\boldsymbol{\nu}|=1} \sqrt{\frac{\boldsymbol{\nu}\cdot\boldsymbol{J}\cdot\boldsymbol{\nu}}{\rho}}, \quad d_- = \min_{|\boldsymbol{\nu}|=1} \sqrt{\frac{\boldsymbol{\nu}\cdot\boldsymbol{J}\cdot\boldsymbol{\nu}}{\rho}}.$$

Subject to a situation, the parameters d_+ and d_- can be associated with the longitudinal and transverse dimensions of a liquid crystal molecule, or, more strictly, with the size of a domain of co-oriented molecules that carry out "on an average" joint translational and rotational motion. Physical observations show that the domain structure of a liquid crystal is formed by combining 10^4–10^5 molecules with the same or similar orientation [45]. For simplicity, we will assume hereinafter that the domains have a form of elongated rods of the given length a.

The formulas (1), (2) are the methodological basis to formulate the integral laws of conservation of momentum, angular momentum and energy, resulting from averaging in a system of discrete conservation laws, and the Clausius–Duhem integral inequality for irreversible processes:

$$\begin{aligned}
&\frac{\partial}{\partial t}\int_V \rho\boldsymbol{\nu}\,dV = \int_\Gamma \boldsymbol{\sigma}\cdot\boldsymbol{\nu}\,d\Gamma + \int_V \boldsymbol{f}\,dV,\\
&\frac{\partial}{\partial t}\int_V \left(\boldsymbol{J}\cdot\boldsymbol{\omega} + \rho\boldsymbol{x}\times\boldsymbol{\nu}\right)dV = \int_\Gamma (\boldsymbol{x}\times\boldsymbol{\sigma} + \boldsymbol{\mu})\cdot\boldsymbol{\nu}\,d\Gamma + \int_V \left(\boldsymbol{x}\times\boldsymbol{f} + \boldsymbol{g}\right)dV,\\
&\frac{\partial}{\partial t}\int_V \left(\rho\frac{\boldsymbol{\nu}^2}{2} + \frac{1}{2}\boldsymbol{\omega}\cdot\boldsymbol{J}\cdot\boldsymbol{\omega} + W\right)dV = \int_\Gamma (\boldsymbol{\nu}\cdot\boldsymbol{\sigma} + \boldsymbol{\omega}\cdot\boldsymbol{\mu} - \boldsymbol{h})\cdot\boldsymbol{\nu}\,d\Gamma +\\
&\qquad\qquad + \int_V (\boldsymbol{\nu}\cdot\boldsymbol{f} + \boldsymbol{\omega}\cdot\boldsymbol{g} + H)\,dV,\\
&\frac{\partial}{\partial t}\int_V s\,dV \geqslant -\int_\Gamma \frac{\boldsymbol{h}\cdot\boldsymbol{\nu}}{T}\,d\Gamma + \int_V \frac{H}{T}\,dV.
\end{aligned} \tag{3}$$

Here V is an arbitrary domain with a piecewise-smooth boundary Γ, selected in initial (undeformed) state of a medium; $\boldsymbol{\nu}$ is the vector of outward normal to the boundary; $\boldsymbol{\sigma}$ is the Piola–Kirchhoff asymmetric stress tensor; $\boldsymbol{\mu}$ is the asymmetric tensor of couple stresses; W is the internal energy in a unit volume; $\boldsymbol{h}$ is the heat flux vector; $\boldsymbol{f}$ and $\boldsymbol{g}$ are the bulk densities of the body forces and couple stresses, which are nonzero, for example, when taking into account the influence of external electric fields on a crystal; H is the intensity of internal heat sources; s and T are, respectively, the bulk density of entropy and absolute temperature. The couple stresses caused by curvature of the internal structure of a medium due to the spatially inhomogeneous rotation of the medium particles are assumed negligible.

2.2 Kinematics of a Micropolar Medium

Translational motion in a liquid crystal is described by the equation $\boldsymbol{x} = \boldsymbol{\xi} + \boldsymbol{u}(\boldsymbol{\xi}, t)$, connecting the Lagrangian and Eulerian vectors of a particle's center of masses by the displacement vector $\boldsymbol{u}$. In the general theory of a micropolar medium, the strain tensor $\boldsymbol{\Lambda} = \boldsymbol{R}^* \cdot \boldsymbol{x}_{\boldsymbol{\xi}}$ is used as a measure of deformation, where $\boldsymbol{R}$ is the orthogonal tensor of rotational motion of a particle, $\boldsymbol{x}_{\boldsymbol{\xi}}$ is the distortion tensor, the asterisk denotes the conjugation operation. The antisymmetric tensor of angular velocity of a particle is calculated by the formula: $\boldsymbol{\Omega} = \dot{\boldsymbol{R}} \cdot \boldsymbol{R}^*$. Here and further dot over a symbol means partial derivative with respect to time.

The distortion tensor can be expanded into a product of orthogonal and symmetric tensors: $\boldsymbol{x}_{\boldsymbol{\xi}} = \boldsymbol{R}_e \cdot \boldsymbol{C}$. Here $\boldsymbol{R}_e$ is the tensor of transfer rotation of a particle, $\boldsymbol{C}$ is the Cauchy–Green strain measure. Relative rotation of a particle is described by the orthogonal tensor $\boldsymbol{R}_r$, that satisfies the equations: $\boldsymbol{R} = \boldsymbol{R}_e \cdot \boldsymbol{R}_r$, $\boldsymbol{\Lambda} = \boldsymbol{R}_r^* \cdot \boldsymbol{C}$. In accordance with the former equation, rotational motion is a superposition of relative rotation and transfer rotation.

Note, that by a given tensor $\boldsymbol{\Lambda}$ one can define both the Cauchy–Green strain measure $\boldsymbol{C}^2 = \boldsymbol{\Lambda}^* \cdot \boldsymbol{\Lambda}$ and the relative rotation tensor $\boldsymbol{R}_r = \boldsymbol{C} \cdot \boldsymbol{\Lambda}^{-1}$. Hence, as for the latter equation, the chosen strain measure $\boldsymbol{\Lambda}$ describes simultaneously two factors, that lead to the change of internal energy—the deformation of a medium and the relative rotation of particles [38].

The complete description of the strain state in a liquid crystal, aside from the tensor $\boldsymbol{\Lambda}$, uses a special curvature tensor $\boldsymbol{M}$, calculated in terms of the rotation tensor $\boldsymbol{R}$ and its derivatives in the Lagrangian coordinates $\boldsymbol{R}_{,k} = \partial \boldsymbol{R} / \partial \xi_k$ $(k = 1, 2, 3)$. The construction of this tensor is suggested in [42]. Let $\boldsymbol{M}^{(k)} = \boldsymbol{R}_{,k} \cdot \boldsymbol{R}^*$ be the antisymmetric curvature tensors along the coordinate lines. The Darboux vectors fitting with these tensors are assigned by the columns of $\boldsymbol{M}$:

$$\boldsymbol{M} = \begin{pmatrix} M_{11} & M_{12} & M_{13} \\ M_{21} & M_{22} & M_{23} \\ M_{31} & M_{32} & M_{33} \end{pmatrix}, \quad \boldsymbol{M}^{(k)} = \begin{pmatrix} 0 & -M_{3k} & M_{2k} \\ M_{3k} & 0 & -M_{1k} \\ -M_{2k} & M_{1k} & 0 \end{pmatrix}.$$

Differentiating $\boldsymbol{M}^{(k)}$ with respect to time and $\boldsymbol{\Omega}$ with respect to the variables ξ_k yields kinematic equations $\dot{\boldsymbol{M}}^{(k)} = \boldsymbol{\Omega}_{,k} + \boldsymbol{\Omega} \cdot \boldsymbol{M}^{(k)} - \boldsymbol{M}^{(k)} \cdot \boldsymbol{\Omega}$ that admit, collectionwise, the tensor representation:

$$\dot{\boldsymbol{M}} = \boldsymbol{\omega}_{\boldsymbol{\xi}} + \boldsymbol{\Omega} \cdot \boldsymbol{M}. \tag{4}$$

The validity of this representation is readily tested with the componentwise writing of the tensors in the Cartesian coordinate system. It follows from (4) that $\boldsymbol{M}$ is neither an invariant nor an indifferent tensor, i.e. it changes both under rotation of the current configuration and under rotation of the original configuration.

It can be shown that under rotation of the current configuration $d\boldsymbol{x}' = \boldsymbol{O} \cdot d\boldsymbol{x}$ this tensor transforms in accordance with the law $\boldsymbol{M}' = \boldsymbol{O} \cdot \boldsymbol{M}$. In fact, since the rotation tensor $\boldsymbol{O}$ is independent on time, then

$$\boldsymbol{R}' = \boldsymbol{O}\cdot\boldsymbol{R}, \quad \boldsymbol{\Omega}' = \dot{\boldsymbol{R}}'\cdot\boldsymbol{R}'^{*} = \boldsymbol{O}\cdot\dot{\boldsymbol{R}}\cdot\boldsymbol{R}^{*}\cdot\boldsymbol{O}^{*} = \boldsymbol{O}\cdot\boldsymbol{\Omega}\cdot\boldsymbol{O}^{*}, \quad \boldsymbol{\omega}' = \boldsymbol{O}\cdot\boldsymbol{\omega}.$$

Consequently, Eq. (4) reduces to equation $\dot{\boldsymbol{M}}' = \boldsymbol{O}\cdot\boldsymbol{\omega}_{\boldsymbol{\xi}} + \boldsymbol{O}\cdot\boldsymbol{\Omega}\cdot\boldsymbol{O}^{*}\cdot\boldsymbol{M}'$, having the solution: $\boldsymbol{M}' = \boldsymbol{O}\cdot\boldsymbol{M}$.

By the same law goes the distortion tensor $\boldsymbol{x}_{\boldsymbol{\xi}}$, for instance, which is used to determine the invariant strain measure $\boldsymbol{x}^{*}_{\boldsymbol{\xi}}\cdot\boldsymbol{x}_{\boldsymbol{\xi}}$, involved in the Lagrangian representation of motion in a classic elastic medium, and an indifferent measure $\boldsymbol{x}_{\boldsymbol{\xi}}\cdot\boldsymbol{x}^{*}_{\boldsymbol{\xi}}$, included in the Eulerian representation [24]. The both measures are independent on rotation of a medium element as a rigid whole, which does not influence the potential energy of deformation. Similarly, the invariance is the property of the product $\boldsymbol{M}^{*}\cdot\boldsymbol{M}$, that will be used as an independent parameter of state to construct constitutive equations accounting for the couple properties of a medium, and that leads to a thermodynamically consistent system of conservation laws, as it will be illustrated below.

It is noteworthy, that the selected curvature measure differs from the conventionally used measures [34], defined by nonsymmetric invariant tensors. As judged by the analogy with the strain measure, the symmetrized measure $\boldsymbol{M}^{*}\cdot\boldsymbol{M}$ eliminates "excessive" degrees of freedom, having no influence on potential energy of strain state.

In the case of weak perturbations, when gradients of displacements are small, the approximation holds true:

$$\boldsymbol{R}_{e} \approx \boldsymbol{I} + \frac{1}{2}(\boldsymbol{u}_{\boldsymbol{x}} - \boldsymbol{u}^{*}_{\boldsymbol{x}}), \quad \boldsymbol{C} \approx \boldsymbol{I} + \frac{1}{2}(\boldsymbol{u}_{\boldsymbol{x}} + \boldsymbol{u}^{*}_{\boldsymbol{x}}), \quad \boldsymbol{R}\cdot\dot{\boldsymbol{\Lambda}} = \boldsymbol{v}_{\boldsymbol{x}} - \boldsymbol{\Omega}, \tag{5}$$

where $\boldsymbol{I}$ is a unit tensor, $\boldsymbol{v} = \dot{\boldsymbol{u}}$ is a particle velocity vector. In a Cartesian coordinate system, the tensors $\boldsymbol{\Omega}$ and $\boldsymbol{u}_{\boldsymbol{x}}$ are defined by the matrices:

$$\boldsymbol{\Omega} = \begin{bmatrix} 0 & -\omega_3 & \omega_2 \\ \omega_3 & 0 & -\omega_1 \\ -\omega_2 & \omega_1 & 0 \end{bmatrix}, \quad \boldsymbol{u}_{\boldsymbol{x}} = \begin{bmatrix} u_{1,1} & u_{1,2} & u_{1,3} \\ u_{2,1} & u_{2,2} & u_{2,3} \\ u_{3,1} & u_{3,2} & u_{3,3} \end{bmatrix}.$$

The angular velocity tensor is identified with the angular velocity vector $\boldsymbol{\omega}$, whose coordinates are $(\omega_1, \omega_2, \omega_3)$. The tensor $\boldsymbol{R}_r$ can be calculated using the general formula for orthogonal tensors [17]:

$$\boldsymbol{R}_r = \boldsymbol{I} + \sin\phi_r\,\boldsymbol{Q} + (1 - \cos\phi_r)\,\boldsymbol{Q}^2.$$

Here $\boldsymbol{Q}$ is the antisymmetric tensor:

$$\boldsymbol{Q} = \begin{bmatrix} 0 & -q_3 & q_2 \\ q_3 & 0 & -q_1 \\ -q_2 & q_1 & 0 \end{bmatrix}, \quad q_1^2 + q_2^2 + q_3^2 = 1,$$

ϕ_r is the angle of relative rotation of particles, defined in terms of trace of the tensor $\boldsymbol{R}_r$: $\cos\phi_r = (\mathrm{tr}\,\boldsymbol{R}_r - 1)/2$. The vector $\boldsymbol{q}$ with the coordinates (q_1, q_2, q_3) satisfies the equality: $\boldsymbol{R}_r \cdot \boldsymbol{q} = \boldsymbol{q}$, which means that it determines the direction for instantaneous axis of relative rotation.

In the framework of the approximation (5), $\boldsymbol{\Omega} = \dot{\boldsymbol{R}}_e + \dot{\boldsymbol{R}}_r \cdot \boldsymbol{R}_r^*$. Omitting the calculations of the product $\dot{\boldsymbol{R}}_r \cdot \boldsymbol{R}_r^*$, where the easy-to-test equalities $\boldsymbol{Q}^3 = -\boldsymbol{Q}, \boldsymbol{Q}^4 = -\boldsymbol{Q}^2$ and $\boldsymbol{Q} \cdot \dot{\boldsymbol{Q}} \cdot \boldsymbol{Q} = 0$ are essentially used, one can find the tensor of angular velocity:

$$\boldsymbol{\Omega} = \frac{1}{2}(\boldsymbol{v}_{\boldsymbol{x}} - \boldsymbol{v}_{\boldsymbol{x}}^*) + \dot{\phi}_r\,\boldsymbol{Q} + \sin\phi_r\,\dot{\boldsymbol{Q}} + (1 - \cos\phi_r)\,(\boldsymbol{Q} \cdot \dot{\boldsymbol{Q}} - \dot{\boldsymbol{Q}} \cdot \boldsymbol{Q}).$$

In the coordinate form this tensor equation leads to three scalar equations:

$$\begin{aligned} q_1\,\dot{\phi}_r &= \omega_{r\,1} - \dot{q}_1 \sin\phi_r - (1 - \cos\phi_r)(q_2\,\dot{q}_3 - \dot{q}_2\,q_3), \\ q_2\,\dot{\phi}_r &= \omega_{r\,2} - \dot{q}_2 \sin\phi_r - (1 - \cos\phi_r)(q_3\,\dot{q}_1 - \dot{q}_3\,q_1), \\ q_3\,\dot{\phi}_r &= \omega_{r\,3} - \dot{q}_3 \sin\phi_r - (1 - \cos\phi_r)(q_1\,\dot{q}_2 - \dot{q}_1\,q_2), \end{aligned} \tag{6}$$

where

$$\omega_{r\,1} = \omega_1 - \frac{v_{3,2} - v_{2,3}}{2}, \quad \omega_{r\,2} = \omega_2 - \frac{v_{1,3} - v_{3,1}}{2}, \quad \omega_{r\,3} = \omega_3 - \frac{v_{2,1} - v_{1,2}}{2}$$

are projections of the vector of relative angular velocity $\boldsymbol{\omega}_r$. After simple transformations of the above equations, taking into account that $q_1\,\dot{q}_1 + q_2\,\dot{q}_2 + q_3\,\dot{q}_3 = 0$, we obtain an equation for the angle of relative rotation of a particle:

$$\dot{\phi}_r = \omega_{r\,1} q_1 + \omega_{r\,2} q_2 + \omega_{r\,3} q_3.$$

On the other hand, from (6) also follows a system of equations for determining the unit vector $\boldsymbol{q}$:

$$\begin{pmatrix} \dot{q}_1 \\ \dot{q}_2 \\ \dot{q}_3 \end{pmatrix} = \frac{1}{\Delta} \begin{pmatrix} a^2 + b^2 q_1^2 & a\,b\,q_3 + b^2 q_1\,q_2 & -a\,b\,q_2 + b^2 q_1\,q_3 \\ -a\,b\,q_3 + b^2 q_1\,q_2 & a^2 + b^2 q_2^2 & a\,b\,q_1 + b^2 q_2\,q_3 \\ a\,b\,q_2 + b^2 q_1\,q_3 & -a\,b\,q_1 + b^2 q_2\,q_3 & a^2 + b^2 q_3^2 \end{pmatrix} \times \\ \times \begin{pmatrix} \omega_{r\,1} - q_1\,\dot{\phi}_r \\ \omega_{r\,2} - q_2\,\dot{\phi}_r \\ \omega_{r\,3} - q_3\,\dot{\phi}_r \end{pmatrix}, \quad a = \sin\phi_r, \quad b = 1 - \cos\phi_r, \quad \Delta = 2\,a\,b. \tag{7}$$

Note that if the relative rotation angle ϕ_r is a multiple of π, then it follows from the system (7) that the vector $\boldsymbol{q}$ is parallel to the relative angular velocity vector $\boldsymbol{\omega}_r$. And if $\boldsymbol{\omega}_r = 0$, then this vector can be chosen arbitrarily.

Since in the case of small strains the Lagrangian and Euler variables are identified, equations for the curvature tensor are taken in the form (4) accurate to a replacement the index $\boldsymbol{\xi}$ by the index $\boldsymbol{x}$. The inertia tensor $\boldsymbol{J}$ changes with time according to the equation $\boldsymbol{J} = \boldsymbol{R} \cdot \boldsymbol{J}_0 \cdot \boldsymbol{R}^*$, that is substantiated by the transition to the co-moving

coordinate system connected with the rotating particle. Here $\boldsymbol{J}_0$ is the inertia tensor in the initial state of a medium. If in the technological process of obtaining a liquid crystal the domains of molecules are differently oriented, then the initial distribution of $\boldsymbol{J}_0$ in volume is nonuniform, it must be specified by a suitable equation describing the process. The time differentiation results in the following equality, used in some studies, for instance, in [23] as the equation for determining the inertia tensor:

$$\dot{\boldsymbol{J}} = \dot{\boldsymbol{R}} \cdot \boldsymbol{J}_0 \cdot \boldsymbol{R}^* + \boldsymbol{R} \cdot \boldsymbol{J}_0 \cdot \dot{\boldsymbol{R}}^* = \boldsymbol{\Omega} \cdot \boldsymbol{J} - \boldsymbol{J} \cdot \boldsymbol{\Omega}. \tag{8}$$

Initial distribution of the inertia tensor serves as the Cauchy condition for this equation.

2.3 Constitutive Equations

For continuous motions with small displacement gradients, the Eulerian and Lagrangian variables are identified. In this case, the integral conservation laws (3), using the Green formula and the equality $\boldsymbol{\omega} \cdot \dot{\boldsymbol{J}} \cdot \boldsymbol{\omega} = 0$ valid in view of (8), are transformed into the differential equations and inequality:

$$\begin{gathered} \rho \dot{\boldsymbol{v}} = \operatorname{div} \boldsymbol{\sigma} + \boldsymbol{f}, \quad \frac{\partial}{\partial t}\left(\boldsymbol{J} \cdot \boldsymbol{\omega}\right) = \operatorname{div} \boldsymbol{\mu} + 2\boldsymbol{\sigma}^a + \boldsymbol{g}, \\ W = \boldsymbol{\sigma}^* : (\boldsymbol{v}_{\boldsymbol{x}} - \boldsymbol{\Omega}) + \boldsymbol{\mu}^* : \boldsymbol{\omega}_{\boldsymbol{x}} - \operatorname{div} \boldsymbol{h} + H, \quad T\dot{s} \geqslant -\operatorname{div} \boldsymbol{h} + \frac{\boldsymbol{h} \cdot T_{\boldsymbol{x}}}{T} + H, \end{gathered} \tag{9}$$

where $\boldsymbol{\sigma}^a$ is a vector associated with the antisymmetric part $(\boldsymbol{\sigma} - \boldsymbol{\sigma}^*)/2$ of the stress tensor; a colon denotes double convolution of the tensors.

According to the method of internal thermodynamic parameters [31], let's assume that the state of a liquid crystal is determined by four independent parameters—the bulk strain $\theta = \operatorname{div} \boldsymbol{u} = \operatorname{tr} \boldsymbol{u}_{\boldsymbol{x}}$, the elastic (reversible) component ϕ_r' of the relative rotation angle, the linear invariant $\psi = \boldsymbol{M}^* : \boldsymbol{M}$ of the curvature measure $\boldsymbol{M}^* \cdot \boldsymbol{M}$, and the entropy s. The viscous component $\phi_r'' = \phi_r - \phi_r'$ of the rotation angle is defined by the Maxwell model of viscoelasticity. With such assumptions, the equation of the system (9), characterizing the change in internal energy, acquires the form:

$$\begin{gathered} \frac{\partial W}{\partial \theta} \operatorname{tr} \boldsymbol{v}_{\boldsymbol{x}} + \frac{\partial W}{\partial \phi_r'} \dot{\phi}_r' + \frac{\partial W}{\partial \psi} \dot{\psi} + \frac{\partial W}{\partial s} \dot{s} = \boldsymbol{\sigma}^* : \left(\frac{\boldsymbol{v}_{\boldsymbol{x}} + \boldsymbol{v}_{\boldsymbol{x}}^*}{2} - \dot{\phi}_r \boldsymbol{Q} \right) - \\ - \sin \phi_r \, \boldsymbol{\sigma}^* : \dot{\boldsymbol{Q}} - (1 - \cos \phi_r) \boldsymbol{\sigma}^* : (\boldsymbol{Q} \cdot \dot{\boldsymbol{Q}} - \dot{\boldsymbol{Q}} \cdot \boldsymbol{Q}) + \boldsymbol{\mu}^* : \boldsymbol{\omega}_{\boldsymbol{x}} - \operatorname{div} \boldsymbol{h} + H. \end{gathered} \tag{10}$$

Considering functional independence of thermodynamic parameters of the state, the above equation yields the constitutive relationships of reversible deformation:

$$\begin{aligned}
&\operatorname{diag}\boldsymbol{\sigma} = \frac{\partial W}{\partial \theta}\boldsymbol{I}, \quad \boldsymbol{\sigma} - \operatorname{diag}\boldsymbol{\sigma} = -(\boldsymbol{\sigma} - \operatorname{diag}\boldsymbol{\sigma})^*, \quad \boldsymbol{\sigma}^* : \boldsymbol{Q} = -\frac{\partial W}{\partial \phi_r'},\\
&\boldsymbol{\mu} = 2\,\frac{\partial W}{\partial \psi}\boldsymbol{M}, \quad \sin\phi_r\,\boldsymbol{\sigma}^* : \dot{\boldsymbol{Q}} - (1-\cos\phi_r)\,\boldsymbol{\sigma}^* : (\boldsymbol{Q}\cdot\dot{\boldsymbol{Q}} - \dot{\boldsymbol{Q}}\cdot\boldsymbol{Q}) = 0.
\end{aligned} \tag{11}$$

The equation for couple stresses is obtained with the help of the chain of equalities

$$\boldsymbol{M}^* : \dot{\boldsymbol{M}} = \boldsymbol{M}^* : \boldsymbol{\omega}_{\boldsymbol{x}} + \boldsymbol{M}^* : \boldsymbol{\Omega} : \boldsymbol{M} = \boldsymbol{M}^* : \boldsymbol{\omega}_{\boldsymbol{x}},$$

which is true because of the symmetry of tensor $\boldsymbol{M}^* \cdot \boldsymbol{M}$. The latter relation in (11) ensues from independence of internal energy on the direction of axis of relative rotation of a particle. In the Cartesian coordinates, this relation is reduced to a linear equation

$$A_1\,\dot{q}_1 + A_2\,\dot{q}_2 + A_3\,\dot{q}_3 = 0 \tag{12}$$

with coefficients

$$\begin{aligned}
A_1 &= \sin\phi_r\,(\sigma_{32} - \sigma_{23}) - (1-\cos\phi_r)\big((\sigma_{21} - \sigma_{12})\,q_2 - (\sigma_{13} - \sigma_{31})\,q_3\big),\\
A_2 &= \sin\phi_r\,(\sigma_{13} - \sigma_{31}) + (1-\cos\phi_r)\big((\sigma_{21} - \sigma_{12})\,q_1 - (\sigma_{32} - \sigma_{23})\,q_3\big),\\
A_3 &= \sin\phi_r\,(\sigma_{21} - \sigma_{12}) - (1-\cos\phi_r)\big((\sigma_{13} - \sigma_{31})\,q_1 - (\sigma_{32} - \sigma_{23})\,q_2\big).
\end{aligned} \tag{13}$$

The variable quantities $\dot{q}_1$, $\dot{q}_2$, $\dot{q}_3$, included in (12), are correlated by the condition $q_1\,\dot{q}_1 + q_2\,\dot{q}_2 + q_3\,\dot{q}_3 = 0$ of the normalization of vector $\boldsymbol{q}$. According to the Lagrange rule, from this it follows that $A_k = \lambda\,q_k$ $(k = 1, 2, 3)$, where λ is an undetermined multiplier. The system of equations (13) limits a general form of the stress tensor. The direct calculation of the system determinant

$$\begin{vmatrix}
\sin\phi_r & (1-\cos\phi_r)\,q_3 & -(1-\cos\phi_r)\,q_2\\
-(1-\cos\phi_r)\,q_3 & \sin\phi_r & (1-\cos\phi_r)\,q_1\\
(1-\cos\phi_r)\,q_2 & -(1-\cos\phi_r)\,q_1 & \sin\phi_r
\end{vmatrix} = \sin\phi_r\,(1-\cos\phi_r)^2$$

shows that it is different from zero, if $\phi_r \neq 0$. In this case, the tangential stresses are uniquely defined for a given λ. Taking into account the remaining relationships, we have:

$$\boldsymbol{\sigma} = -p\,\boldsymbol{I} + \tau\,\boldsymbol{Q} = \begin{bmatrix}
-p & -\tau\,q_3 & \tau\,q_2\\
\tau\,q_3 & -p & -\tau\,q_1\\
-\tau\,q_2 & \tau\,q_1 & -p
\end{bmatrix}, \quad p = -\frac{\partial W}{\partial \theta}, \quad \tau = -\frac{1}{2}\,\frac{\partial W}{\partial \phi_r'}. \tag{14}$$

It is worthy of noting that, when $\phi_r = 0$, the vector $\boldsymbol{q}$, assigning the direction of relative rotation axis, is arbitrary and, thus, the formulas (14) are valid as well.

So, the constitutive equations (11), along with the moment interaction of the domains of a liquid crystal caused by a change in the internal curvature, or, simply speaking, the inhomogeneity of the rotation field (see Fig. 1), also take into account

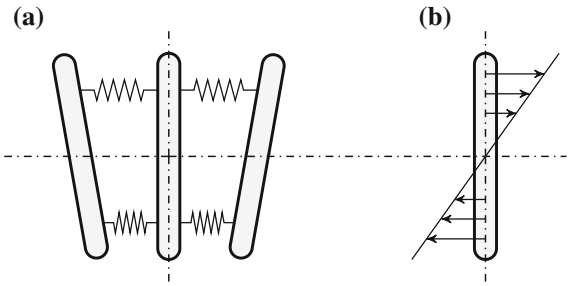

Fig. 1 Scheme of moment interaction of domains (**a**) and a distribution of normal stresses caused by a change in the internal curvature (**b**)

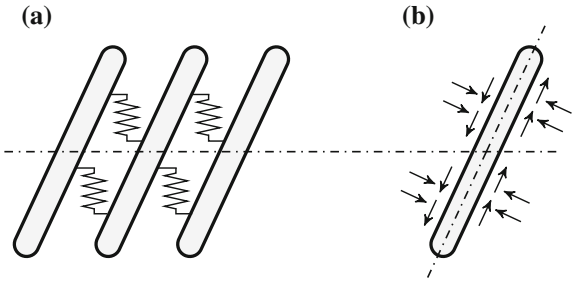

Fig. 2 Scheme of shear deformation of a liquid crystal (**a**) and diagram of distribution of tangential stress and pressure (**b**)

the appearance of pressure and tangential stresses due to elastic or viscoelastic resistance to rotational and translational degrees of freedom (Fig. 2).

Besides the derived equations, (10) yields an equation of heat inflow:

$$T\dot{s} = -\dot{\phi}_r'' \boldsymbol{\sigma}^* : \boldsymbol{Q} - \operatorname{div} \boldsymbol{h} + H, \tag{15}$$

where the first term on the right-hand side, which is equal to $-2\,\tau\,\dot{\phi}_r''$, represents a dissipative power of viscous processes. According to the Maxwell model of viscoelasticity, such processes in a liquid crystal are described by the Stokes law: $\tau = -\eta\,\dot{\phi}_r''$, where η is an empirical coefficient of viscosity. The Clausius–Duhem differential inequality, included in (9), produces an equation for temperature, $T = \partial W/\partial s$, and an inequality for thermal conductivity, $\boldsymbol{h} \cdot T_{\boldsymbol{x}} \leqslant 0$.

2.4 Equations of a Spatial Model

Specifying the equations of state (14), we accept the following expressions for internal energy and entropy:

$$W = \frac{\kappa}{2}\,\theta^2 + \beta\,T_0\,\theta + 2\,\alpha(\phi_r')^2 + \frac{\gamma}{2}\psi^2 + c\,T, \quad s = \beta\,\theta + c\,\ln\frac{T}{T_0}.$$

Here κ is the isothermal bulk compression modulus, α is the modulus of elastic resistance of a medium to the rotation of particles, β is the coefficient of thermal expansion, γ is the modulus of elastic resistance to the action of couple stresses with the change in curvature, T_0 is the initial temperature, c is the specific heat capacity per unit volume. With such specification, the left-hand side of the heat inflow equation (15) is equal to: $c\,\dot{T} + \beta\,T\dot{\theta}$, the hydrostatic pressure satisfies the Duhamel–Neumann law: $p = -\kappa\,\theta + \beta(T - T_0)$, the tangential stress and couple stresses obey the Cosserat law: $\tau = -2\,\alpha\,\phi_r'$, $\boldsymbol{\mu} = 2\,\gamma\,\boldsymbol{M}$. By virtue of the Stokes law, the equation for tangential stress takes the form: $\dot{\tau} = -2\,\alpha\,(\dot{\phi}_r + \tau/\eta)$.

If we neglect the dependence of the elastic potential energy on the volume deformation and on the temperature factors, leaving only the square of the linear invariant ψ of the curvature measure, then we obtain a variant of the model, whose constitutive equations are the equations of Oseen type with the coincident Frank orientational elasticity coefficients. This coincidence is a consequence of the assumption that the elastic potential is independent on quadratic and cubic invariants of the tensor $\boldsymbol{M}^* : \boldsymbol{M}$. If we take this dependence into account, then within the framework of this approach we obtain nonlinear constitutive equations that are different from the Oseen–Frank ones.

For the correct description of finite rotations of the liquid crystal particles, the quadratic term in the potential, connected with the rotational degrees of freedom, can be replaced by a more general nonlinear expression. However, such replacement will hardly result in significant refinement of the model since, in fact, the elastic component of the rotation angle remains always small and the finite rotations accumulate in the course of time owing to the viscous component.

In a spatial case, there is a simple method for accounting the anisotropy of a liquid crystal via the vector–director $\boldsymbol{n}$ oriented along molecules of a crystal. Rotation of the vector–director is described by the tensor $\boldsymbol{R}$, consequently, $\boldsymbol{n} = \boldsymbol{R} \cdot \boldsymbol{n}^0$, $\dot{\boldsymbol{n}} = \dot{\boldsymbol{R}} \cdot \boldsymbol{n}^0$ and $\dot{\boldsymbol{n}} = \boldsymbol{\Omega} \cdot \boldsymbol{n}$, where $\boldsymbol{n}^0$ is the initial position of $\boldsymbol{n}$.

Calculating the Cartesian components of the inertia tensor for a liquid crystal particle of the linear shape assumed, from the known formulas of the mechanics of rigid bodies:

$$J_{kl} = \int\limits_m (\delta_{kl}\,|\boldsymbol{x}|^2 - x_k x_l)\,dm, \quad dm = \frac{m}{a}\,dz, \quad x_k = z\,n_k, \quad -\frac{a}{2} \leqslant z \leqslant \frac{a}{2},$$

where δ_{kl} is the Kronecker delta, a and m are the length and mass of a molecule (domain), we derive the following expression for the inertia tensor:

$$\boldsymbol{J} = \frac{\rho\,a^2}{12} \begin{bmatrix} 1 - n_1^2 & -n_1 n_2 & -n_1 n_3 \\ -n_1 n_2 & 1 - n_2^2 & -n_2 n_3 \\ -n_1 n_3 & -n_2 n_3 & 1 - n_3^2 \end{bmatrix}. \tag{16}$$

This tensor automatically satisfies the Eq. (8). In the initial state the distribution of inertia tensor occurs to be dependent on the initial distribution of the vector–

director $\boldsymbol{n}_0$. Setting the orientation of vector–director in a volume, one can simulate, for example, the chiral phase of a liquid crystal. To model the smectic phase, it is necessary to specify a more complex layered structure with certain gap conditions at interfaces between the layers.

Let $æ^{\parallel}$ and $æ^{\perp}$ be the coefficients of thermal conductivity of a liquid crystal in the direction of orientation of its molecules and in the transverse direction, respectively. In this case, the thermal conductivity tensor can be represented in a dyadic form as

$$\boldsymbol{æ} = æ^{\parallel}\,\boldsymbol{n}\,\boldsymbol{n} + æ^{\perp}\boldsymbol{n}'\boldsymbol{n}' + æ^{\perp}\boldsymbol{n}''\boldsymbol{n}'',$$

where $\boldsymbol{n}'$ and $\boldsymbol{n}''$ are the unit vectors forming a Cartesian system together with $\boldsymbol{n}$. With the arbitrarily taken vectors $\boldsymbol{n}'$ and $\boldsymbol{n}''$, we have:

$$\boldsymbol{æ} = æ^{\perp}\begin{bmatrix}1&0&0\\0&1&0\\0&0&1\end{bmatrix} + (æ^{\parallel} - æ^{\perp})\begin{bmatrix}n_1^2 & n_1 n_2 & n_1 n_3\\ n_1 n_2 & n_2^2 & n_2 n_3\\ n_1 n_3 & n_2 n_3 & n_3^2\end{bmatrix}. \tag{17}$$

At the initial time instant the distribution of the thermal conductivity tensor over the volume is consistent with a given distribution of the vector–director $\boldsymbol{n}_0$.

By the Fourier law, the heat flux vector is linearly dependent on the temperature gradient: $\boldsymbol{h} = -\boldsymbol{æ}\cdot T_{\boldsymbol{x}}$.

The complete system of equations in an expanded form comprises the equations of translational and rotational motion:

$$\begin{aligned}
&\rho\,\dot v_1 = -p_{,1} - (\tau\,q_3)_{,2} + (\tau\,q_2)_{,3} + f_1,\\
&\rho\,\dot v_2 = -p_{,2} + (\tau\,q_3)_{,1} - (\tau\,q_1)_{,3} + f_2,\\
&\rho\,\dot v_3 = -p_{,3} - (\tau\,q_2)_{,1} + (\tau\,q_1)_{,2} + f_3,\\
&\frac{\partial}{\partial t}\big(J_{jk}\,\omega_k\big) = \mu_{jk,k} + 2\,\tau\,q_j + g_j,
\end{aligned} \tag{18}$$

the constitutive equations:

$$\begin{aligned}
&\dot p = -\,\kappa\,(v_{1,1} + v_{2,2} + v_{3,3}) + \beta\,\dot T,\\
&\dot\tau = \alpha\,(v_{3,2} - v_{2,3} - 2\,\omega_1)\,q_1 + \alpha\,(v_{1,3} - v_{3,1} - 2\,\omega_2)\,q_2 +\\
&\quad + \alpha\,(v_{2,1} - v_{1,2} - 2\,\omega_3)\,q_3 - 2\,\alpha\,\tau/\eta,\\
&\mu_{jk} = 2\,\gamma\,M_{jk},
\end{aligned} \tag{19}$$

the kinematic equations for curvatures:

$$\begin{aligned}
&\dot M_{ii} = \omega_{i,i} - \omega_j M_{ki} + \omega_k M_{ji}, \quad \dot M_{ij} = \omega_{i,j} - \omega_j M_{kj} + \omega_k M_{jj},\\
&\dot M_{ik} = \omega_{i,k} - \omega_j M_{kk} + \omega_k M_{jk} \quad (j = i+1 \text{ and } k = j+1 \bmod 3),
\end{aligned} \tag{20}$$

the heat conduction equation:

$$c\,\dot T = -\,h_{1,1} - h_{2,2} - h_{3,3} - \beta\,T(v_{1,1} + v_{2,2} + v_{3,3}) + 2\,\tau^2/\eta + H \tag{21}$$

($h_k = -æ_{k1}\,T_{,1} - æ_{k2}\,T_{,2} - æ_{k3}\,T_{,3}$), the Eq. (7) for projections of the vector $\boldsymbol{q}$, and the equations for projections of the vector–director:

$$\dot{n}_1 = -\omega_3\,n_2 + \omega_2\,n_3, \quad \dot{n}_2 = \omega_3\,n_1 - \omega_1\,n_3, \quad \dot{n}_3 = -\omega_2\,n_1 + \omega_1\,n_2. \tag{22}$$

The components of the tensors of inertia and thermal conductivity are given by the formulas (16) and (17). Here and further the Einstein rule of summation over repeated indices is applied; index k after a comma denotes partial derivative with respect to x_k; $i, j, k = 1, 2, 3$.

2.5 *Equations of Plane Motion*

For plane motion, the Eqs. (16)–(22) are essentially simplified, since the vector–director can be calculated in terms of the angle ϕ, which is equal to the sum of the initial angle ϕ_0 of orientation with respect to the abscissa axis x_1 and the angles of transference ϕ_e and relative ϕ_r rotation of the liquid crystal molecules; the vector $\boldsymbol{q}$, used to assign the axis of relative rotation, coincides with the unit vector of the coordinate axis that is perpendicular to the plane of motion. The complete system takes the form:

$$\begin{aligned}
&\rho\,\dot{v}_1 = -p_{,1} - \tau_{,2} + f_1, \qquad \rho\,\dot{v}_2 = \tau_{,1} - p_{,2} + f_2,\\
&\dot{p} = -\kappa\,(v_{1,1} + v_{2,2}) + \beta\,\dot{T}, \quad \dot{\tau} = \alpha\,(v_{2,1} - v_{1,2}) - 2\,\alpha\,(\omega + \tau/\eta),\\
&J\,\dot{\omega} = \mu_{1,1} + \mu_{2,2} + 2\,\tau + g, \quad \dot{\mu}_1 = 2\,\gamma\,\omega_{,1}, \quad \dot{\mu}_2 = 2\,\gamma\,\omega_{,2},\\
&c\,\dot{T} = \left(æ_{11}\,T_{,1} + æ_{12}\,T_{,2}\right)_{,1} + \left(æ_{12}\,T_{,1} + æ_{22}\,T_{,2}\right)_{,2} -\\
&\qquad -\beta\,T\,(v_{1,1} + v_{2,2}) + 2\,\tau^2/\eta + H,\\
&æ_{11} = æ^{\parallel}\cos^2\phi + æ^{\perp}\sin^2\phi, \quad æ_{12} = (æ^{\parallel} - æ^{\perp})\sin\phi\cos\phi,\\
&æ_{22} = æ^{\parallel}\sin^2\phi + æ^{\perp}\cos^2\phi, \quad \dot{\phi} = \omega.
\end{aligned} \tag{23}$$

Inhomogeneous distribution of orientation of molecules in volume is given by nonuniform initial data $\phi = \phi_0(x_1, x_2)$ at $t = 0$.

For convenience, it is possible to represent the system (23) as the subsystem of equations of acoustics for a liquid crystal and the coupled equation of heat conduction. The acoustics subsystem is written in a matrix form:

$$\mathsf{A}\,\dot{\mathbf{U}} = \mathsf{B}^1\,\mathbf{U}_{,1} + \mathsf{B}^2\,\mathbf{U}_{,2} + \mathsf{S}\,\mathbf{U} + \mathbf{F}, \tag{24}$$

where

$$\mathbf{U}=\begin{bmatrix} v_1\\ v_2\\ p\\ \tau\\ \omega\\ \mu_1\\ \mu_2 \end{bmatrix},\quad \mathsf{A}=\begin{bmatrix} \rho & 0 & 0 & 0 & 0 & 0 & 0\\ 0 & \rho & 0 & 0 & 0 & 0 & 0\\ 0 & 0 & 1/\kappa & 0 & 0 & 0 & 0\\ 0 & 0 & 0 & 1/\alpha & 0 & 0 & 0\\ 0 & 0 & 0 & 0 & J & 0 & 0\\ 0 & 0 & 0 & 0 & 0 & 1/(2\gamma) & 0\\ 0 & 0 & 0 & 0 & 0 & 0 & 1/(2\gamma) \end{bmatrix},$$

$$\mathsf{B}^k=\begin{bmatrix} 0 & 0 & k-2 & 1-k & 0 & 0 & 0\\ 0 & 0 & 1-k & 2-k & 0 & 0 & 0\\ k-2 & 1-k & 0 & 0 & 0 & 0 & 0\\ 1-k & 2-k & 0 & 0 & 0 & 0 & 0\\ 0 & 0 & 0 & 0 & 0 & 2-k & k-1\\ 0 & 0 & 0 & 0 & 2-k & 0 & 0\\ 0 & 0 & 0 & 0 & k-1 & 0 & 0 \end{bmatrix},$$

$$\mathsf{S}=\begin{bmatrix} 0 & 0 & 0 & 0 & 0 & 0 & 0\\ 0 & 0 & 0 & 0 & 0 & 0 & 0\\ 0 & 0 & 0 & 0 & 0 & 0 & 0\\ 0 & 0 & 0 & -2/\eta & -2 & 0 & 0\\ 0 & 0 & 0 & 2 & 0 & 0 & 0\\ 0 & 0 & 0 & 0 & 0 & 0 & 0\\ 0 & 0 & 0 & 0 & 0 & 0 & 0 \end{bmatrix},\quad \mathbf{F}=\begin{bmatrix} f_1\\ f_2\\ \beta\dot{T}/\kappa\\ 0\\ g\\ 0\\ 0 \end{bmatrix}.$$

The matrices A and B^k $(k=1,2)$ are symmetric, besides the matrix A is positive definite, consequently, the differential operator of (24) is hyperbolic by Friedrichs [15]. With the thermal expansion neglected, i.e. if $\beta=0$, the subsystem (24) is separated as independent one. For this subsystem, the Cauchy problem with the initial data $\mathbf{U}\big|_{t=0}=\mathbf{U}^0(x_1,x_2)$ and the boundary-value problems with dissipative boundary conditions of general form are well-posed. Boundary conditions are formulated in terms of v_1, v_2, p, τ, ω, μ_1, μ_2 and ensure fulfillment of the following inequality at points of the boundary:

$$\begin{gathered} \Delta\mathbf{U}(\nu_1\,\mathsf{B}^1+\nu_2\,\mathsf{B}^2)\,\Delta\mathbf{U}\leqslant 0:\\ -\Delta v_1(\nu_1\,\Delta p+\nu_2\,\Delta\tau)+\Delta v_2(\nu_1\,\Delta\tau-\nu_2\,\Delta p)+\Delta\omega\,(\nu_1\,\Delta\mu_1+\nu_2\,\Delta\mu_2)\leqslant 0. \end{gathered}\tag{25}$$

Here ν_1 and ν_2 are the projections of unit vector of external normal to the boundary, $\Delta\mathbf{U}=\mathbf{U}'-\mathbf{U}$, $\mathbf{U}'$ and $\mathbf{U}$ are the arbitrary vector–functions satisfying the boundary conditions.

Judging by expanded form of the inequality (25), among the dissipative conditions are, for instance, boundary conditions set in terms of the translational and angular velocities as well as in terms of the stress and couple stress vectors on the boundary, which are customary for the elasticity theory. The dissipative conditions are also the mixed-type boundary conditions specifying the translational velocity, normal to

the boundary, and the tangential stress or, vice versa, the tangential velocity and the normal stress, as in the contact problems of elasticity.

The characteristic equation of the subsystem (24):

$$\det\left(\lambda\,\mathsf{A} - \nu_1\,\mathsf{B}^1 - \nu_2\,\mathsf{B}^2\right) = 0$$

has one zero root: $\lambda = 0$, corresponding to the contact discontinuities, and six non-zero roots: $\lambda = \pm c_1, \pm c_2, \pm c_3$, defining the velocities of weak shock waves in a liquid crystal: $c_1 = \sqrt{\kappa/\rho}$ (for longitudinal waves), $c_2 = \sqrt{\alpha/\rho}$ (for transverse waves) and $c_3 = \sqrt{2\,\gamma/J}$ (for rotational waves).

It may be noted, that in the acoustic approximation, as distinct from the classical acoustics, the elastic resistance of a liquid crystalline medium to rotational motion of the particles initiates the transverse waves.

3 Computational Algorithm

3.1 Two-Cyclic Splitting Method

Numerical solution of boundary-value problems for the system (23) is carried out by means of the procedure of splitting with respect to spatial variables [32]. The two-cyclic splitting is used, where at each time step $(t,\ t + \Delta t)$ the next series of one-dimensional problems is solved:

$$\begin{aligned}
&\mathsf{A}\,\dot{\mathbf{U}}^{(1)} = \mathsf{B}^1\,\mathbf{U}^{(1)}_{,1} + F^{(1)}, \quad c\,\dot{T}^{(1)} = \left(æ_{11}\,T^{(1)}_{,1} + æ_{12}\,T^{(0)}_{,2}\right)_{,1} - \beta\,T^{(0)}\,v^{(1)}_{1,1},\\
&\mathsf{A}\,\dot{\mathbf{U}}^{(2)} = \mathsf{B}^2\,\mathbf{U}^{(2)}_{,2} + F^{(2)}, \quad c\,\dot{T}^{(2)} = \left(æ_{12}\,T^{(1)}_{,1} + æ_{22}\,T^{(2)}_{,2}\right)_{,2} - \beta\,T^{(1)}\,v^{(2)}_{2,2},\\
&\mathsf{A}\,\dot{\mathbf{U}}^{(3)} = \mathsf{S}\,\mathbf{U}^{(3)}, \qquad\qquad c\,\dot{T}^{(3)} = 2(\tau^{(3)})^2/\eta + H,\\
&\mathsf{A}\,\dot{\mathbf{U}}^{(4)} = \mathsf{B}^2\,\mathbf{U}^{(4)}_{,2} + F^{(4)}, \quad c\,\dot{T}^{(4)} = \left(æ_{12}\,T^{(3)}_{,1} + æ_{22}\,T^{(4)}_{,2}\right)_{,2} - \beta\,T^{(3)}\,v^{(4)}_{2,2},\\
&\mathsf{A}\,\dot{\mathbf{U}}^{(5)} = \mathsf{B}^1\,\mathbf{U}^{(5)}_{,1} + \mathbf{F}^{(5)}, \quad c\,\dot{T}^{(5)} = \left(æ_{11}\,T^{(5)}_{,1} + æ_{12}\,T^{(4)}_{,2}\right)_{,1} - \beta\,T^{(4)}\,v^{(5)}_{1,1}.
\end{aligned} \tag{26}$$

The vector–function $\mathbf{U}^{(0)}$ and the temperature distribution $T^{(0)}$ are taken from the previous time step computations, or from initial data of the problem if $t = 0$. The vectors

$$\mathbf{F}^{(1)} = \begin{bmatrix} f_1 \\ 0 \\ \beta\,\dot{T}^{(1)}/\kappa \\ 0 \\ g/2 \\ 0 \\ 0 \end{bmatrix}, \quad \mathbf{F}^{(2)} = \begin{bmatrix} 0 \\ f_2 \\ \beta\,\dot{T}^{(2)}/\kappa \\ 0 \\ g/2 \\ 0 \\ 0 \end{bmatrix},$$

$$\mathbf{F}^{(4)} = \begin{bmatrix} 0 \\ f_2 \\ \beta\,\dot{T}^{(4)}/\kappa \\ 0 \\ g/2 \\ 0 \\ 0 \end{bmatrix}, \quad \mathbf{F}^{(5)} = \begin{bmatrix} f_1 \\ 0 \\ \beta\,\dot{T}^{(5)}/\kappa \\ 0 \\ g/2 \\ 0 \\ 0 \end{bmatrix}$$

are chosen in that form on account of total approximation of equations of two-dimensional model. The initial data for one-dimensional systems of equations at the splitting stages and the solution attached to a new time level are given by the formulas:

$$\begin{aligned}
&\mathbf{U}^{(1)}(t) = \mathbf{U}(t), && T^{(1)}(t) = T(t),\\
&\mathbf{U}^{(2)}(t) = \mathbf{U}^{(1)}(t + \Delta t/2), && T^{(2)}(t) = T^{(1)}(t + \Delta t/2),\\
&\mathbf{U}^{(3)}(t) = \mathbf{U}^{(2)}(t + \Delta t/2), && T^{(3)}(t) = T^{(2)}(t + \Delta t/2),\\
&\mathbf{U}^{(4)}(t + \Delta t/2) = \mathbf{U}^{(3)}(t + \Delta t), && T^{(4)}(t + \Delta t/2) = T^{(3)}(t + \Delta t),\\
&\mathbf{U}^{(5)}(t + \Delta t/2) = \mathbf{U}^{(4)}(t + \Delta t), && T^{(5)}(t + \Delta t/2) = T^{(4)}(t + \Delta t),\\
&\mathbf{U}(t + \Delta t) = \mathbf{U}^{(5)}(t + \Delta t), && T(t + \Delta t) = T^{(5)}(t + \Delta t).
\end{aligned} \tag{27}$$

The advantage of two-cyclic splitting method, as compared with the conventional method, having only one cycle, is that it preserves the second-order approximation if the second-order schemes are used for the solution of one-dimensional systems.

The boundary-value problems for the systems (26) with the initial data (27) and the given boundary conditions are solved by means of the predictor–corrector finite-difference scheme, based on Godunov's gap decay method [18] (for the subsystem of acoustic equations) and Ivanov's scheme with controlled dissipation of energy [20] (for the heat conduction equation).

For the subsystem of acoustics, at the predictor step in the x_1 direction the homogeneous equations on characteristics are used:

$$\begin{aligned}
&dx_1 = \pm c_1'\,dt: \quad dI_1^{\pm} = 0, \quad I_1^{\pm} = \rho\,c_1'\,v_1 \pm p,\\
&dx_1 = \pm c_2\,dt: \quad dI_2^{\pm} = 0, \quad I_2^{\pm} = \rho\,c_2\,v_2 \mp \tau,\\
&dx_1 = \pm c_3\,dt: \quad dI_3^{\pm} = 0, \quad I_3^{\pm} = J\,c_3\,\omega \mp \mu_1,
\end{aligned} \tag{28}$$

where $c_1' = \sqrt{\kappa'/\rho}$ is the velocity of longitudinal waves, calculated by the adiabatic bulk compression modulus $\kappa' = \kappa + \beta^2 T_0/c$. Owing to replacement of the characteristic velocity c_1 of the acoustics subsystem by the velocity c_1', the resultant equations take into account the influence of additional terms in (26), connected with thermal expansion of a medium.

The Eq. (28) allow to define the values with fractional indices $j - 1/2$ referred to the lateral faces of meshes of a grid in the plane x_1, t:

$$\begin{aligned} v_{1\,j-1/2} &= \frac{I^+_{1\,j-1} + I^-_{1j}}{2\,\rho\,c_1'}, \quad & p_{j-1/2} &= \frac{I^+_{1\,j-1} - I^-_{1j}}{2}, \\ v_{2\,j-1/2} &= \frac{I^+_{2j} + I^-_{2\,j-1}}{2\,\rho\,c_2}, \quad & \tau_{j-1/2} &= \frac{I^+_{2j} - I^-_{2\,j-1}}{2}, \\ \omega_{j-1/2} &= \frac{I^+_{3j} + I^-_{3\,j-1}}{2\,J\,c_3}, \quad & \mu_{1\,j-1/2} &= \frac{I^+_{3j} - I^-_{3\,j-1}}{2} \end{aligned} \tag{29}$$

(the internal nodes of meshes are indicated by integer indices j; $j = 2, \ldots, N_1$). At the boundary nodes, these values are found from the boundary conditions and equations on incoming characteristics. To improve the accuracy of the solution of acoustic equations, at the predictor step the procedure of ENO-reconstruction for the Riemann invariants $I_1^{\pm}$, $I_2^{\pm}$ and $I_3^{\pm}$ is used, well-reputed in solving a wide range of problems [25, 38, 46]. At the corrector step, the solution at the centers of the upper faces of the meshes is obtained from the system of differential equations:

$$\mathsf{A}\,\frac{\mathbf{U}^j - \mathbf{U}_j}{\Delta t/2} = \mathsf{B}^1\,\frac{\mathbf{U}_{j+1/2} - \mathbf{U}_{j-1/2}}{\Delta x_1} + \mathbf{F}_j. \tag{30}$$

Similar computations are performed in the x_2 direction. The resultant splitting scheme is stable relative to round-off errors, if the one-dimensional Courant–Friedrichs–Lewy stability condition $c_1'\,\Delta t/2 \leqslant \Delta x_k$ is fulfilled (we supposed here, that longitudinal waves have maximal velocity).

The systems of ordinary differential equations of the form $\mathsf{A}\,\dot{\mathbf{U}} = \mathsf{S}\,\mathbf{U}$ is solved by means of the Crank–Nicolson implicit difference scheme:

$$\mathsf{A}\,\frac{\mathbf{U}^j - \mathbf{U}_j}{\Delta t} = \mathsf{S}\,\frac{\mathbf{U}^j + \mathbf{U}_j}{2}, \tag{31}$$

which possesses the second-order accuracy, is unconditionally stable and preserves mechanical energy of the system. These properties are of key importance, as the equations of the system contain a small parameter—the moment of inertia J, proportional to a squared characteristic size of a liquid crystal domain, that leads to certain computational difficulties.

3.2 Scheme for Heat Conduction Equation

At the stages of splitting method, the one-dimensional problems are solved in the following sequence: implementation of the predictor step for the subsystem of acoustic equations, first; solution of the coupled heat conduction equation, second; and, finally, accomplishment of the corrector step for the matrix system, the right-hand side of which depends on temperature. For the numerical solution of one-dimensional heat conduction equations, we construct a special finite-difference scheme of the predictor–corrector type, consistent with the scheme for one-dimensional acoustics systems by the stability criterion. The method of construction of schemes with controlled dissipation of energy, worked out by Ivanov [20] for solving problems of the dynamics of elastic bodies, plates and shells, is applied. According to the said method, the heat conduction equation in the form of the system:

$$c\,\dot{T} = -\,h_{,k}, \quad h = -\,æ\,T_{,k} + f$$

in the x_k direction is replaced by the extended system:

$$c\,\dot{T} = -\,h'_{,k}, \quad h = -\,æ\,T'_{,k} + f,$$

where the unknown functions T' and h' differ, generally speaking, from T and h. For the extended system, the next equation holds:

$$\frac{c}{2}\,\frac{\partial T^2}{\partial t} + æ\,(T'_{,k})^2 = -\,(T'h')_{,k} + f\,T'_{,k} + (T' - T)\,h'_{,k} + (h' - h)\,T'_{,k}. \tag{32}$$

The closing equations to the extended system are taken in the form:

$$\begin{bmatrix} T' - T \\ h' - h \end{bmatrix} = -\,\mathsf{D} \begin{bmatrix} h'_{,k} \\ T'_{,k} \end{bmatrix}, \quad \mathsf{D} = \begin{bmatrix} D_{11} & D_{12} \\ D_{21} & D_{22} \end{bmatrix}, \tag{33}$$

where D is given positively semidefinite matrix. In this case, the expression

$$(T' - T)\,h'_{,k} + (h' - h)\,T'_{,k}$$

on the right-hand side of (32) is a nonpositive quadratic form relative to derivatives of T' and h' with respect to x_k, and its coefficients are elements of the matrix D. The Eq. (32) is transformed into the inequality:

$$\frac{c}{2}\,\frac{\partial T^2}{\partial t} + æ(T'_{,k})^2 \leqslant -\,(T'h')_{,k} + f\,T'_{,k}.$$

Using this inequality one can obtain a priory estimates, which allow to prove the uniqueness and continuous dependence on initial data of the solutions of boundary-value problems with dissipative boundary conditions for the extended system.

In fact, in constructing a finite-difference scheme, these reasoning are repeated at the discrete level. The discrete analog of the extended system takes the form:

$$c\,\frac{T^j - T_j}{\Delta t/2} = -\,\frac{h_{j+1/2} - h_{j-1/2}}{\Delta x_k}, \quad h^j = -\,æ_j\,\frac{T_{j+1/2} - T_{j-1/2}}{\Delta x_k} + f_j. \tag{34}$$

Here, as earlier, the values with integer superscripts and subscripts approximating basic functions are referred to the upper and lower faces of the space-time mesh of the grid, and the values with the half-integer subscripts approximating auxiliary functions are referred to the lateral faces of the mesh. The solution is constructed with the time step $\Delta t/2$, as required for the splitting stages.

The discrete analog of the Eq. (32) results from multiplication of the first and second equations in (34) by the half-sums $(T^j + T_j)/2$ and $(T_{j+1/2} + T_{j-1/2})/2$, respectively. Finally, we have

$$c\,\frac{(T^j)^2 - T_j^2}{\Delta t} + æ_j\,\frac{(T_{j+1/2} - T_{j-1/2})^2}{\Delta x_k^2} = -\,\frac{(Th)_{j+1/2} - (Th)_{j-1/2}}{\Delta x_k} + \\ + f_j\,\frac{T_{j+1/2} + T_{j-1/2}}{\Delta x_k} + \left(\frac{T_{j+1/2} + T_{j-1/2}}{2} - \frac{T^j + T_j}{2}\right)\frac{h_{j+1/2} - h_{j-1/2}}{\Delta x_k} + \\ + \left(\frac{h_{j+1/2} + h_{j-1/2}}{2} - h^j\right)\frac{T_{j+1/2} - T_{j-1/2}}{\Delta x_k}.$$

The closing equations to approximate (33) are taken as:

$$\begin{bmatrix} T_{j+1/2} + T_{j-1/2} - T^j - T_j \\ h_{j+1/2} + h_{j-1/2} - 2\,h^j \end{bmatrix} = -\,\frac{2}{\Delta x_k}\,\mathsf{D}\begin{bmatrix} h_{j+1/2} - h_{j-1/2} \\ T_{j+1/2} - T_{j-1/2} \end{bmatrix}. \tag{35}$$

Using the method of a priori estimates allows proving the step-by-step stability of the resultant finite-difference scheme in the root-mean-square norm, if the dissipative boundary conditions are assigned at the boundary of the solution domain. The dissipativeness supposes fulfillment of the next inequalities: $(\Delta T\,\Delta h)_{1/2} \leqslant 0$, $(\Delta T\,\Delta h)_{N_k+1/2} \geqslant 0$ for differences of functions satisfying these conditions.

The scheme (34), (35) approximates the heat conduction equation only if elements of the matrix D are small, i.e. if $\mathsf{D} = O(\Delta x_k)$. For simplicity, in the capacity of D, we choose a special-form matrix with a single non-zero element, $2\,D_{11} = \Delta x_k\,d - \Delta t/(2\,c) \geqslant 0$ with free parameter d. According to the Courant–Friedrichs–Lewy condition, $\Delta t = 2\,K\,\Delta x_k/c_1'$, where $K \leqslant 1$. Consequently, given that choice, it is required to assign $d \geqslant K/(c_1' c)$ for the stability of calculations.

The system of equations (35) transforms into:

$$2\,T_j - T_{j+1/2} - T_{j-1/2} = (h_{j+1/2} - h_{j-1/2})\,d, \quad 2\,h^j = h_{j+1/2} + h_{j-1/2}. \tag{36}$$

Expressing the heat fluxes from (36) using the second equation from (34):

$$h_{j\pm1/2} = \mp\frac{T_{j+1/2} - 2T_j + T_{j-1/2}}{2\,d} - æ_j\frac{T_{j+1/2} - T_{j-1/2}}{\Delta x_k} + f_j, \tag{37}$$

after shift with respect to j, we obtain a system of equations to find nodal values of temperature with half-integer subscripts:

$$\begin{aligned} &A_{j+1/2}\,T_{j+3/2} + C_{j+1/2}\,T_{j+1/2} + B_{j+1/2}\,T_{j-1/2} = G_{j+1/2},\\ &A_{j+1/2} = \frac{1}{2} - \frac{d}{\Delta x_k}\,æ_{j+1}, \quad B_{j+1/2} = \frac{1}{2} - \frac{d}{\Delta x_k}\,æ_j,\\ &C_{j+1/2} = 1 + \frac{d}{\Delta x_k}\,(æ_{j+1} + æ_j), \quad G_{j+1/2} = T_{j+1} + T_j - (f_{j+1} - f_j)\,d. \end{aligned} \tag{38}$$

The system (38) with given boundary conditions in terms of temperature or in terms of heat fluxes at the boundary, connected with the temperature by formulas (37), is realized by means of the tridiagonal matrix algorithm. It can be shown that the matrix of this system satisfies the condition of diagonal dominance in each case: $|C_{j+1/2}| > |A_{j+1/2}| + |B_{j+1/2}|$, which ensures the stability of the tridiagonal matrix algorithm. This is how the predictor of the scheme for solution of the heat conduction equation is implemented. The corrector of the scheme is performed according to Eq. (34).

3.3 Comparison with Exact Solution

To test the algorithm for solution of the heat conduction equation, the computations of unsteady temperature field in an anisotropic liquid crystal were performed. Internal heat sources were neglected. The initial temperature field on computational domain in the form of unit square and the boundary values of temperature were given in accordance with the exact solution in terms of dimensionless variables:

$$T = T_0\,\mathrm{e}^{-\lambda t}\sin(\pi\,k\,\xi_1)\cos(\pi\,m\,\xi_2), \qquad \begin{bmatrix}\xi_1\\ \xi_2\end{bmatrix} = \begin{bmatrix}\cos\phi & \sin\phi\\ -\sin\phi & \cos\phi\end{bmatrix}\begin{bmatrix}x_1\\ x_2\end{bmatrix},$$

$$c\,\lambda = \pi^2 k^2\,æ^{\parallel} + \pi^2 m^2 æ^{\perp}.$$

The coefficients of thermal conductivity in the direction of orientation of particles and in the transverse direction differed two times: $æ^{\parallel} = 2\,æ^{\perp}$. Figure 3a corresponds to the dimensionless coefficients $k = 0.5$, $m = 3$, and Fig. 3b corresponds to $k = 2$, $m = 3$. In computations, the particles of a liquid crystal were oriented at the angles $\phi = 30°$, $45°$, $60°$ and $90°$ (from left to right in Fig. 3). The computations were carried out for $\Delta t = 1.75\,c\,\Delta x_k\,d$. If $\Delta t = 2\,c\,\Delta x_k\,d$, then the artificial dissipation of energy is absent in the scheme of solution of one-dimensional problems. It follows

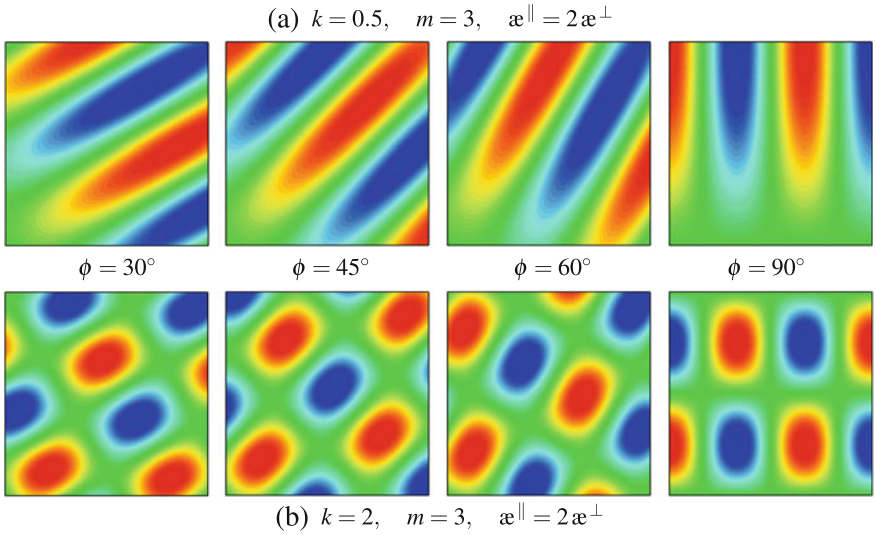

Fig. 3 Numerical solution of the anisotropic heat conduction equation: The temperature fields at different values of k and ϕ

from the Lax convergence theorem that the scheme in this case possesses the second-order accuracy relative to Δt and Δx_k. Decreasing of the time step, which is accompanied by dissipation, is necessary to ensure the stability of the splitting scheme.

3.4 Parallel Implementation of Algorithm

Computational algorithm for simulation of thermomechanical behavior of a liquid crystal in two-dimensional case is implemented as a parallel program for computers with graphic accelerators. The program is coded using the C programming language and the CUDA (Compute Unified Device Architecture) technology. Parallelization is carried out at the stages of splitting.

GPU (Graphics Processing Unit) is focused on the implementation of programs with a large amount of computation. Due to the large number of parallel working cores, it turns an ordinary computer into a supercomputer with the computing speed of hundreds of times higher than the PC, using only the computing power of the CPU (Central Processing Unit). All computations are performed on the GPU, which is a coprocessor to the CPU. The computational domain is divided into square blocks containing the same number of threads. Each block is an independent set of interacting threads, threads of different blocks can not communicate with each other. Due to the identifiers available in the CUDA, each thread is associated with the mesh of finite-difference grid. In parallel mode, the threads of a graphic device perform

operations of the same type in the meshes of grid on the calculation of solution at each time step.

At the beginning of program, on CPU the dimensions of finite-difference grid and all necessary constants are preset, as well as the one-dimensional arrays are described and the initial data are specified for nine main values represented by two components v_1 and v_2 of the velocity vector, angular velocity ω, rotation angle ϕ, pressure p, tangential stress τ, couple stresses μ_1 and μ_2, and temperature T. Simultaneously, on GPU the memory is allocated for arrays of these values and other auxiliary values required. Then, the constants and arrays are copied from CPU to GPU. The right-hand sides f_1, f_2 and g of Eq. (23) are calculated by the equations of electrostatic perturbation, presented in Sect. 5. At each time step, five stages of the splitting method (26), (27) are fulfilled sequentially. At four splitting stages, GPU performs the following kernels (procedures): predictor for the system of acoustic equations (29) and corresponding boundary conditions; calculation of the coefficients of the tridiagonal matrix algorithm and implementation of this algorithm to find the temperature (38); boundary conditions and predictor for the heat flux (37); corrector of the scheme (30), (34), general for all values. At the first and fifth stages of splitting, all these kernels are executed in the x_1 direction, at the second and fourth stages these kernels are executed in the x_2 direction. At the third splitting stage, GPU performs a single kernel of recomputation of the values by the Crank–Nicolson scheme (31). For the purpose of analyzing the computational results at the control points in time, the solution is copied from GPU to CPU and, based on the obtained data files, level curves of the unknown values are drawn by means of graphical tools of the personal computer.

The necessity of high-performance computing is connected with the fact that steps of computational grid with respect to spatial variables must be consistent with small parameters—the characteristic linear sizes of the material microstructure—$d_{\pm}$. The satisfactory accuracy of computations is reached with very fine grids. This leads to high-dimensional problems, requiring considerable computer resources. Main features of the technology of parallel computing using GPUs in the problems of mechanics and physics are described, for example, in [13, 22].

Similar algorithm and parallel program for its implementation were proposed earlier in [36] for the model, neglecting the moment interactions and the influence of electric field on a liquid crystal. A series of numerical calculations has been performed on the high-performance computational server Flagman with 8 graphic solvers Tesla C2050 (448 CUDA cores on each GPU) of the Institute of Computational Modeling SB RAS (Krasnoyarsk), demonstrating the efficiency of proposed algorithm and program.

Figure 4 shows a graph of the dependence of acceleration of the parallel program on the dimension $N \times N$ of a finite-difference grid (N takes the values: 10, 100, 200, 400, 600, …, 3000, 3200). As compared with the corresponding sequential program, the parallel program speedup is about 25 times on the grids of 1000×1000 meshes and above.

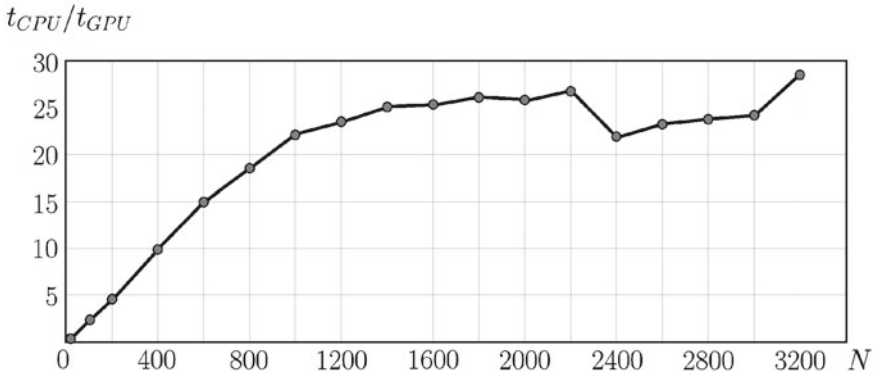

Fig. 4 Acceleration of the program on GPU as compared with CPU

4 Resonant Excitation

4.1 Klein–Gordon Equation

As a result of simple transformations, the separate equation for tangential stress can be obtained from the system (23), if curvature and influence of couple stresses are small. This is the Klein–Gordon equation:

$$\frac{\ddot{\tau}}{\alpha}+\frac{2\,\dot{\tau}}{\eta}=\frac{1}{\rho}\left(\tau_{,11}+\tau_{,22}\right)-\frac{4\,\tau}{J}+r,\quad r=\frac{1}{\rho}\left(f_{2,1}-f_{1,2}\right)-\frac{2\,g}{J}, \tag{39}$$

which can be used for the verification of suggested algorithm. First of all, it shows that if at initial time the liquid crystal is in a natural state with $v_1 = v_2 = \omega = \tau = 0$ and if the body forces and moments are negligibly small, while the tangential stress is equal to zero along the whole boundary, then the tangential stress remains zero everywhere in the crystal domain at each subsequent instant of time. This property holds true independently on the character of distribution of pressure and temperature. It appears from this property that, for instance, it is impossible to change orientation of the liquid crystal particles under thermal effect if the boundary is stress-free. Thus, judging by the Eq. (39), the effect of orientational thermoelasticity of a liquid crystal, being the subject of discussion in [9, 35, 52, 54], is associated with the appearance of tangential stresses at the boundary.

The homogeneous equation (39) for tangential stress has exponential solutions of the type $\tau = \tau_0 \exp \lambda\, t$, which are independent on the spatial coordinates. In these solutions, the constant λ is determined from a quadratic equation with the roots:

$$\lambda_{1;2}=-\frac{\alpha}{\eta}\pm 2\,\pi\, i\,\nu_*,\quad \nu_*=\frac{\alpha}{2\,\pi\,\eta}\sqrt{\frac{4\,\eta^2}{\alpha\,J}-1}\quad (i^2=-1), \tag{40}$$

that may be both real and complex depending on parameters of a medium. The real roots at low viscosity $\eta \leqslant \alpha\, J/4$ describe the smoothly damped rotations of parti-

cles. At high viscosity $\eta > \alpha J/4$ the damped oscillation modes appear with cyclic frequency ν_* and relaxation time $t_* = \eta/\alpha$.

The frequency ν_* is, in fact, a phenomenological parameter of the material, independent on size of a liquid crystal and its boundary conditions. In [37, 38, 44], based on the exact solutions and computational procedures, it was shown that this frequency is a resonance frequency for an elastic Cosserat medium: a periodic external loading with such frequency can excite the resonance of rotational motion of the particles.

In computations for the Klein–Gordon equation the following finite-difference scheme "cross" is used:

$$\frac{\tau_{j_1j_2}^{n+1} - 2\,\tau_{j_1j_2}^{n} + \tau_{j_1j_2}^{n-1}}{\alpha\,\Delta t^2} + \frac{\tau_{j_1j_2}^{n+1} - \tau_{j_1j_2}^{n-1}}{\eta\,\Delta t} = \frac{\tau_{j_1+1j_2}^{n} - 2\,\tau_{j_1j_2}^{n} + \tau_{j_1-1j_2}^{n}}{\rho\,\Delta x_1^2} + \\ + \frac{\tau_{j_1j_2+1}^{n} - 2\,\tau_{j_1j_2}^{n} + \tau_{j_1j_2-1}^{n}}{\rho\,\Delta x_2^2} - \frac{4\,\tau_{j_1j_2}^{n}}{J} + r_{j_1j_2}^{n}. \tag{41}$$

The stability condition for the scheme (41) can be obtained by the Fourier spectral analysis in the form:

$$\frac{\alpha}{\rho}\,\Delta t^2 \leqslant \left(\frac{1}{\Delta x_1^2} + \frac{1}{\Delta x_2^2} + \frac{\rho}{J}\right)^{-1}.$$

However, taking into account that the moment of inertia J is a small quantity, in practice it should be used the value of the time step, which is considerably less than the limit by the formula (41), choosing it for reasons of approximation.

To perform the numerical computations within the framework of proposed model, the parameters of the liquid crystal 5CB were found by summarizing the literature data [4, 7, 47]. The initial temperature is $T_0 = 297°\,\mathrm{K}$, the density is $\rho = 1022\,\mathrm{kg/m^3}$, the time of relaxation is $t_* = 10^{-7}\,\mathrm{s}$, the bulk compression modulus and the rotational modulus are $\kappa = 11.1$ and $\alpha = 0.161\,\mathrm{GPa}$, the coefficient of thermal expansion is $\beta = 3.33\,\mathrm{MPa/K}$, the heat capacity coefficient is $c = 1.02\,\mathrm{MJ/(m^3\,K)}$, and the thermal conductivity coefficients are $æ^{\parallel} = 0.226$, $æ^{\perp} = 0.135\,\mathrm{W/(m\,K)}$. The inertia moment $J = 1.33 \times 10^{-10}\,\mathrm{kg/m}$ was calculated from the formula (16) via the size of the domain $a = 1.25\,\mu\mathrm{m}$. The parameter α was defined in accordance with (40) by the given resonance frequency $\nu_* = 350\,\mathrm{MHz}$. The presence of the resonance in liquid crystal 5CB at that frequency was established experimentally in [6]. The cause of the resonance is beyond this discussion. In calculation of α, we supposed the resonance was caused by the rotational motion of particles.

With the given elasticity moduli, the velocities of elastic waves in the liquid crystal are $c_1 = 3300$ and $c_2 = 397\,\mathrm{m/s}$. The main variable parameter in the model is the characteristic size of the domain a, the minimum value of which is equal to the size of 5CB molecules, $a_0 = 1.87\,\mathrm{nm}$. Apparently, for a more exact definition of the parameter, it is necessary to apply the methods of the molecular dynamics. The computations, based on the Eq. (39) and the system (23), shown that the reduction in size

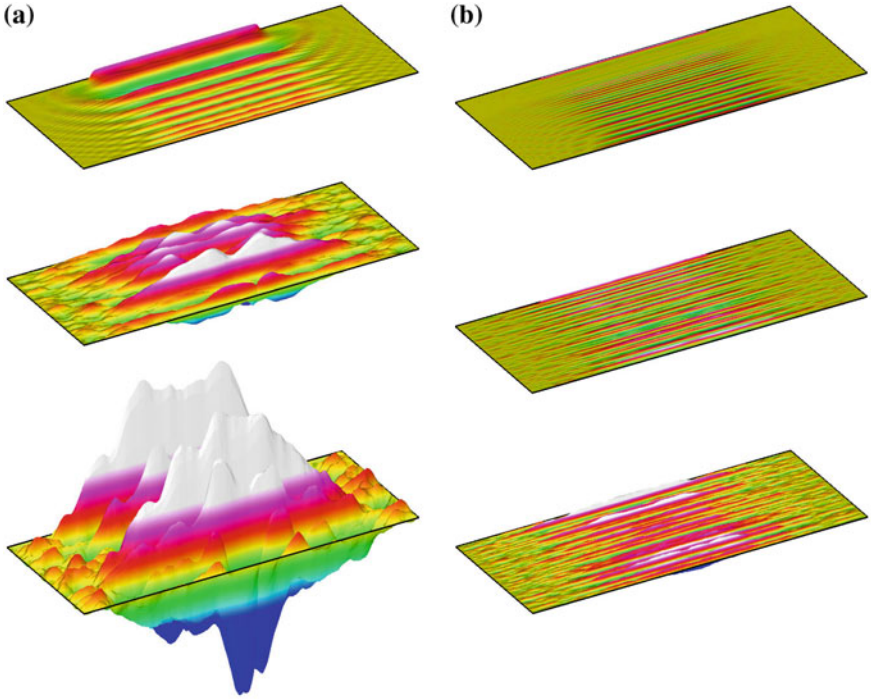

Fig. 5 Numerical solution of the Klein–Gordon equation: The fields of tangential stress τ at different time moments. **a** Resonance frequency, **b** Nonresonance frequency

of the domain by an order as compared with the accepted value leads to nearly three times decrease in the velocity of transverse waves. The computation time essentially grows in this case, while the qualitative pattern, considering the change in the time scale, is scarcely altered.

Figure 5 illustrates the computations for a liquid crystal under periodic loading. At $t = 0$ the crystal is in a natural stress-free state with the initial temperature T_0. At $t > 0$ at a part of the upper boundary $l_1 - l_0 \leqslant 2x_1 < l_1 + l_0$ of the computational domain $0 \leqslant x_1 \leqslant l_1$, $0 \leqslant x_2 \leqslant l_2$, a uniformly distributed tangential stress is assigned that varies sinusoidally with a frequency ν: $\tau = \tau_0 \sin(2\pi\nu t)$. At the rest part of the upper boundary, the conditions of free heat-insulated surface are set: $p = 0$, $\tau = 0$ and $h_2 = 0$. The tangential stress zone is also heat-insulated. At the vertical boundaries of the computational domain, the symmetry conditions hold true: $v_1 = 0$, $\tau = 0$ and $h_1 = 0$; at the lower boundary, the conditions of slipping are fulfilled: $v_2 = 0$, $\tau = 0$ and $T = T_0$.

Geometrical parameters of the problem: $l_1 = 100$, $l_2 = 40$ and $l_0 = 50\,\mu\text{m}$ are chosen in accordance with the scheme of the experiment, described in [54]. The computations were performed for the resonance frequency $\nu = \nu_*$ (Fig. 5a) and nonresonance frequency $\nu = \nu_*/1.5$ (Fig. 5b). As follows from the comparison of the results

in Fig. 5 showing the distribution of tangential stress at successive time moments ($t = 0.266$, 0.798 and 1.33 μs), at the frequency ν_* the amplitudes increase with time, which is indicative of a resonance. As the computations revealed, this resonance appears regardless of the layer thickness l_2. The computations were performed by the program for solving the Eq. (39). Numerical solution of the system (23) using the reconstruction procedure yields close results. Without the reconstruction the used finite-difference scheme features large artificial viscosity, smoothes off the solution and suppresses the resonance.

4.2 Computations Based on Full Model

Figure 6 presents the results of computations of the liquid crystal loading by the uniformly distributed hydrostatic pressure $p = p_0 \sin(2\pi\nu t)$ at the part of upper boundary for the same frequencies ($t = 0.024$, 1.584 and 3.96 μs from top to down). At $\nu = \nu_*$ the pressure amplitude grows inside the computational domain with time, but the resonance in this case is not associated with the rotational motion of particles, since tangential stress is zero everywhere according to the homogeneous equation (39) without the right hand part. This is the resonance of longitudinal motion, which disappears with the change of the layer thickness l_2. Computations by the known formula for the resonance frequencies in an elastic layer with one fixed boundary:

$$\nu^k = \frac{2k+1}{4}\frac{c_1'}{l_2} \quad (k = 0, 1, 2, \ldots)$$

show that Fig. 6a corresponds to the seventh resonance mode ($k = 7$). The frequency $\nu = \nu_*/1.5$ lies between ν^4 and ν^5, therefore, there in no resonance in Fig. 6b.

The results of numerical simulation of the thermal effects in a liquid crystal are represented in Fig. 7 ($t = 0.0079$, 0.0158 and 0.079 μs from top to down). Generally, the previous loading scheme is repeated but at a part of the upper boundary $l_1 - l_0 \leqslant 2x_1 < l_1 + l_0$ zero velocities and the constant temperature $T = T_0 + \Delta T$ (with the increment $\Delta T = 2.5\,^\circ\mathrm{K}$) are specified. This scheme corresponds to the action on a crystal of a heated indenter with the condition of adhesion fulfilled at the surface. Due to thermal expansion of a liquid crystal, the pressure waves appear near the boundary (Fig. 7a) with an amplitude approximately of 50 kPa. These waves propagate inward the crystal with the velocity of longitudinal waves and are reflected from the lower boundary as from a rigid wall. Because of the low thermal conductivity, the temperature propagates inside the crystal very slowly, so the effect of thermal anisotropy at the considered times almost does not show itself. At the points $x_1 = (l_1 \pm l_0)/2$ of changeover of the type of the boundary conditions, the peaks of tangential stress arise (Fig. 7b) with the amplitude of about 0.5 kPa, which initiate the transverse waves, and this eventually leads to a change in the initial orientation of particles.

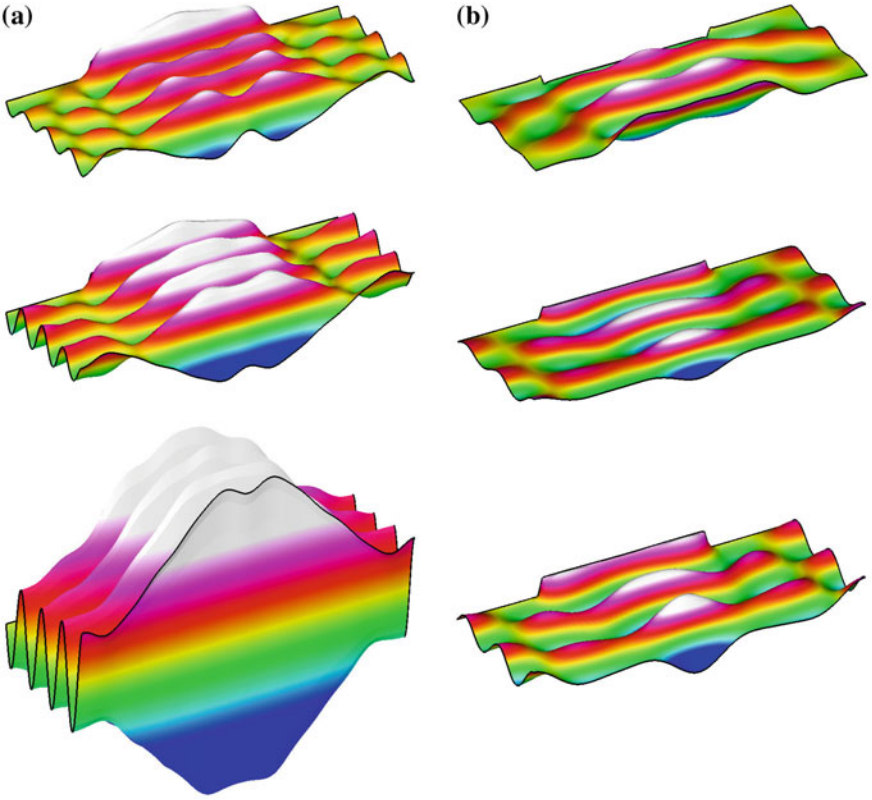

Fig. 6 Resonance excitation of a liquid crystal by hydrostatic pressure: The fields of pressure p at different time moments. **a** Resonance frequency, **b** Nonresonance frequency

4.3 Two Equation of the Second Order

The system of equations (23) of the plane strain state can be reduced to pair of equations of the second order. Let's consider how to obtain the subsystem for tangential stress and angular velocity. Differentiating the first equation of (23) by x_1, the second equation by x_2 and subtracting the second from the first, we find:

$$\rho\left(\dot{v}_{1,2} - \dot{v}_{2,1}\right) = -\triangle\tau + f_{1,2} - f_{2,1},$$

where $\triangle$ is the Laplace operator. In view of this expression and also expressions for $\dot{\mu}_1$ and $\dot{\mu}_2$, after differentiation of corresponding equations of the system by t, we obtain a separate subsystem for τ and ω:

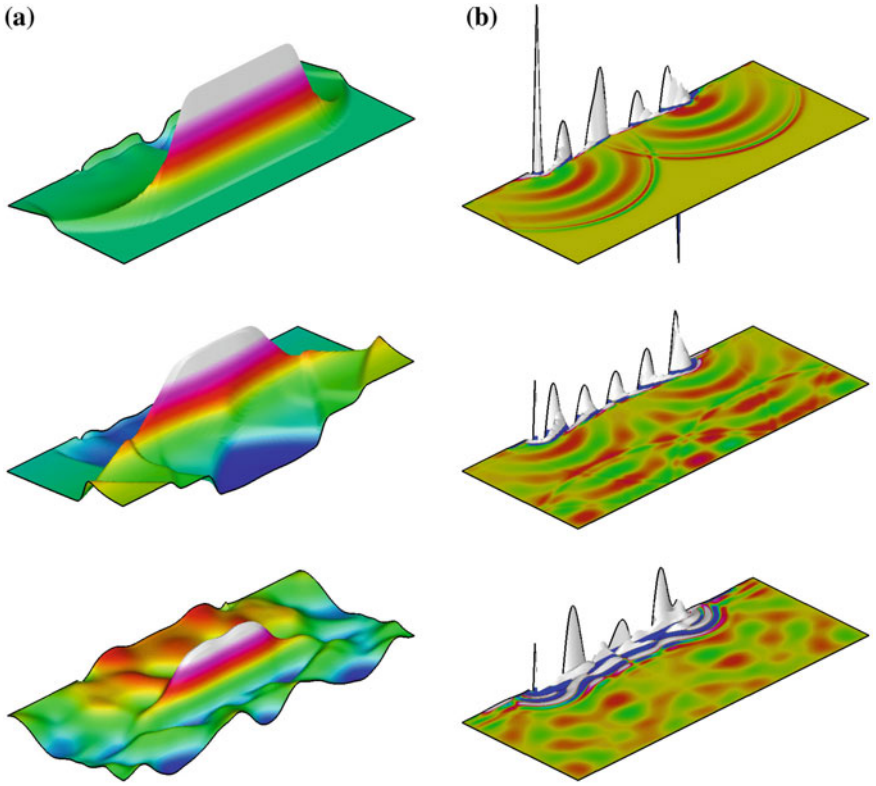

Fig. 7 Thermal perturbation of a liquid crystal: The fields of pressure p (**a**) and tangential stress τ (**b**) at different time moments

$$\begin{aligned} &\ddot{\tau} + \frac{2\,\alpha}{\eta}\,\dot{\tau} + 2\,\alpha\,\dot{\omega} = \frac{\alpha}{\rho}\,(\triangle\tau - f_{1,2} + f_{2,1}),\\ &J\ddot{\omega} - 2\,\dot{\tau} = 2\,\gamma\,\triangle\,\omega + \dot{g}. \end{aligned} \tag{42}$$

Initial data for the system (42) have the following form:

$$\begin{aligned} &\tau\big|_{t=0} = \tau^0, \quad \dot{\tau}\big|_{t=0} = \alpha\big(\nu^0_{2,1} - \nu^0_{1,2}\big) - 2\,\alpha\Big(\omega^0 + \frac{\tau^0}{\eta}\Big),\\ &\omega\big|_{t=0} = \omega^0, \quad \dot{\omega}\big|_{t=0} = \frac{1}{J}\Big(2\,\tau^0 + \mu^0_{1,1} + \mu^0_{2,2} + g\big|_{t=0}\Big), \end{aligned} \tag{43}$$

where ν^0_1, ν^0_2, ω^0, τ^0, μ^0_1, μ^0_2 are given constants at the initial time moment. Boundary conditions may be defined in terms of τ, ω and also in terms of some combinations of $\tau_{,1}$, $\tau_{,2}$ and $\omega_{,1}$, $\omega_{,2}$.

Computational algorithm is developed for numerical solution of the system of equations (42) with the initial data (43). The unknown variables are the tangential

stress τ and the angular velocity ω within computational domain. The explicit finite-difference scheme "cross" of the second order approximation by x_1, x_2 and t is used.

If volume forces and couple forces are equal to zero, then equations of the system (42) at each time step are approximated by replacing the derivatives with respect to time and spatial variables by the finite differences:

$$\frac{\tau_{j_1 j_2}^{n+1} - 2\,\tau_{j_1 j_2}^{n} + \tau_{j_1 j_2}^{n-1}}{\Delta t^2} + \frac{\alpha}{\eta}\,\frac{\tau_{j_1 j_2}^{n+1} - \tau_{j_1 j_2}^{n-1}}{\Delta t} + \alpha\,\frac{\omega_{j_1 j_2}^{n+1} - \omega_{j_1 j_2}^{n-1}}{\Delta t} =$$
$$= \frac{\alpha}{\rho}\left(\frac{\tau_{j_1+1 j_2}^{n} - 2\,\tau_{j_1 j_2}^{n} + \tau_{j_1-1 j_2}^{n}}{\Delta x_1^2} + \frac{\tau_{j_1 j_2+1}^{n} - 2\,\tau_{j_1 j_2}^{n} + \tau_{j_1 j_2-1}^{n}}{\Delta x_2^2}\right),$$
$$\frac{\omega_{j_1 j_2}^{n+1} - 2\,\omega_{j_1 j_2}^{n} + \omega_{j_1 j_2}^{n-1}}{\Delta t^2} - \frac{1}{J}\,\frac{\tau_{j_1 j_2}^{n+1} - \tau_{j_1 j_2}^{n-1}}{\Delta t} =$$
$$= \frac{2\,\gamma}{J}\left(\frac{\omega_{j_1+1 j_2}^{n} - 2\,\omega_{j_1 j_2}^{n} + \omega_{j_1-1 j_2}^{n}}{\Delta x_1^2} + \frac{\omega_{j_1 j_2+1}^{n} - 2\,\omega_{j_1 j_2}^{n} + \omega_{j_1 j_2-1}^{n}}{\Delta x_2^2}\right),$$

where $j_1 = 2, \ldots, N_1 - 1$ and $j_2 = 2, \ldots, N_2 - 1$. Next, $\omega_{j_1 j_2}^{n+1}$ can be expressed from the second equation:

$$\omega_{j_1 j_2}^{n+1} = 2\,\omega_{j_1 j_2}^{n} - \omega_{j_1 j_2}^{n-1} + \frac{\Delta t}{J}\left(\tau_{j_1 j_2}^{n+1} - \tau_{j_1 j_2}^{n-1}\right) + \frac{2\,\gamma\,\Delta t^2}{J}\times$$
$$\times\left(\frac{\omega_{j_1+1 j_2}^{n} - 2\,\omega_{j_1 j_2}^{n} + \omega_{j_1-1 j_2}^{n}}{\Delta x_1^2} + \frac{\omega_{j_1 j_2+1}^{n} - 2\,\omega_{j_1 j_2}^{n} + \omega_{j_1 j_2-1}^{n}}{\Delta x_2^2}\right). \tag{44}$$

Substituting (44) into the first equation, we obtain the formula for $\tau_{j_1 j_2}^{n+1}$:

$$\left(\frac{\alpha}{J} + \frac{\alpha}{\eta\,\Delta t} + \frac{1}{\Delta t^2}\right)\tau_{j_1 j_2}^{n+1} = \frac{2}{\Delta t^2}\,\tau_{j_1 j_2}^{n} +$$
$$+ \left(\frac{\alpha}{J} + \frac{\alpha}{\eta\,\Delta t} - \frac{1}{\Delta t^2}\right)\tau_{j_1 j_2}^{n-1} + \frac{2\,\alpha}{\Delta t}\left(\omega_{j_1 j_2}^{n-1} - \omega_{j_1 j_2}^{n}\right) +$$
$$+ \frac{\alpha}{\rho}\left(\frac{\tau_{j_1+1 j_2}^{n} - 2\,\tau_{j_1 j_2}^{n} + \tau_{j_1-1 j_2}^{n}}{\Delta x_1^2} + \frac{\tau_{j_1 j_2+1}^{n} - 2\,\tau_{j_1 j_2}^{n} + \tau_{j_1 j_2-1}^{n}}{\Delta x_2^2}\right) - \tag{45}$$
$$- \frac{2\,\alpha\,\gamma\,\Delta t}{J}\left(\frac{\omega_{j_1+1 j_2}^{n} - 2\,\omega_{j_1 j_2}^{n} + \omega_{j_1-1 j_2}^{n}}{\Delta x_1^2} + \right.$$
$$\left. + \frac{\omega_{j_1 j_2+1}^{n} - 2\,\omega_{j_1 j_2}^{n} + \omega_{j_1 j_2-1}^{n}}{\Delta x_2^2}\right).$$

Calculating tangential stress by the formula (45) and then angular velocity by the formula (44) at each time step, one can find numerical solution of the problem.

The considered finite-difference scheme has the second-order approximation by time and spatial variables. According to the Lax theorem, the sequence of approximate solutions converges to the exact solution with the second order, too. It is easy to write similar scheme in the case, when the volume forces or couple forces are not equal to zero.

4.4 Stability of the Scheme

Under analysis of the stability of the finite-difference scheme for simplicity let's neglect the viscous term tending $\eta \to \infty$. This simplification is based on the assumption that viscosity increases the reserve of stability of the scheme. According to the Fourier method, let

$$\tau^n_{j_1 j_2} = \lambda^n \, \hat{\tau} \, e^{i(j_1\alpha_1 + j_2\alpha_2)}, \quad \omega^n_{j_1 j_2} = \lambda^n \, \hat{\omega} \, e^{i(j_1\alpha_1 + j_2\alpha_2)}. \tag{46}$$

Substituting these values into the first equation of the system (42) and dividing both sides of the equation by $\lambda^n e^{i(j_1\alpha_1 + j_2\alpha_2)}$, we get:

$$\frac{\lambda - 2 + 1/\lambda}{\Delta t^2}\,\hat{\tau} + \alpha\,\frac{\lambda - 1/\lambda}{\Delta t}\,\hat{\omega} = \frac{\alpha}{\rho}\left(\frac{e^{i\alpha_1} - 2 + e^{-i\alpha_1}}{\Delta x_1^2} + \frac{e^{i\alpha_2} - 2 + e^{-i\alpha_2}}{\Delta x_2^2}\right)\hat{\tau}.$$

Consequently,

$$\left(\frac{\lambda^2 - 2\,\lambda + 1}{\Delta t^2} + \frac{4\,\alpha}{\rho}\,\lambda\left(\frac{\sin^2(\alpha_1/2)}{\Delta x_1^2} + \frac{\sin^2(\alpha_2/2)}{\Delta x_2^2}\right)\right)\hat{\tau} + \alpha\,\frac{\lambda^2 - 1}{\Delta t}\,\hat{\omega} = 0.$$

After similar calculations for the second equation of (42) we find:

$$\left(\frac{\lambda^2 - 2\,\lambda + 1}{\Delta t^2} + \frac{8\,\gamma}{J}\,\lambda\left(\frac{\sin^2(\alpha_1/2)}{\Delta x_1^2} + \frac{\sin^2(\alpha_2/2)}{\Delta x_2^2}\right)\right)\hat{\omega} - \frac{1}{J}\,\frac{\lambda^2 - 1}{\Delta t}\,\hat{\tau} = 0.$$

To obtain the characteristic equation, we form the matrix of coefficients under $\hat{\tau}$ and $\hat{\omega}$:

$$\begin{vmatrix} \dfrac{(\lambda-1)^2}{\Delta t^2} + \dfrac{4\,\alpha}{\rho}\,\lambda A & \alpha\,\dfrac{\lambda^2 - 1}{\Delta t} \\ -\dfrac{1}{J}\,\dfrac{\lambda^2 - 1}{\Delta t} & \dfrac{(\lambda^2-1)^2}{\Delta t^2} + \dfrac{8\,\gamma}{J}\,\lambda A \end{vmatrix} = 0,$$

where $A = \dfrac{\sin^2(\alpha_1/2)}{\Delta x_1^2} + \dfrac{\sin^2(\alpha_2/2)}{\Delta x_2^2}$. Introducing the notations

$$a_1 = \frac{\alpha}{\rho}\,A\,\Delta t^2, \quad a_2 = \frac{2\,\gamma}{J}\,A\,\Delta t^2, \quad a_3 = \frac{\alpha}{J}\,\Delta t^2,$$

one can calculate the determinant:

$$(1 + a_3)(\lambda^2 - 1)^2 + 4\,\lambda\,(\lambda - 1)^2\,(a_1 + a_2 - 1) + 16\,\lambda^2 a_1\,a_2 = 0.$$

So, let us consider three cases with different values of a_1, a_2 and a_3:

(1) If $a_2 = 0$ (i.e. if $\gamma = 0$), then the characteristic equation can be solved in explicit form. Its two roots coincide and are equal to 1, two more roots are solutions of the quadratic equation $(1 + a_3)(\lambda + 1)^2 + 4\,\lambda\,(a_1 - 1) = 0$. By Viet's theorem, the product of these roots is equal to 1. Therefore, in the case of real roots, when the discriminant is positive, one of them is strictly greater than one. This is the case of instability of the scheme. The scheme is stable, if the discriminant is less than or equal to zero. In this case, the roots are complex conjugate, consequently, $|\lambda_1| = |\lambda_2| = 1$. Thus, from the nonpositivity of discriminant

$$\left(1 - 2\,\frac{1 - a_1}{1 + a_3}\right)^2 - 1 \leqslant 0 \quad \Leftrightarrow \quad a_1 \leqslant 1$$

the spectral condition of stability of the scheme is follows:

$$\frac{\alpha}{\rho}\,\Delta t^2 \leqslant \left(\frac{1}{\Delta x_1^2} + \frac{1}{\Delta x_2^2}\right)^{-1}.$$

(2) If $a_1 = 0$ (i.e. if $\alpha = 0$), then the corresponding quadratic equation can be written as: $(1 + a_3)(\lambda + 1)^2 + 4\,\lambda\,(a_2 - 1) = 0$. Repeating the previous arguments, we obtain the condition of nonpositivity of the discriminant: $a_2 \leqslant 1$, from which follows the stability condition of the scheme:

$$\frac{\gamma}{j}\,\Delta t^2 \leqslant \left(\frac{1}{\Delta x_1^2} + \frac{1}{\Delta x_2^2}\right)^{-1}.$$

(3) If $a_1 + a_2 = 1$, then the characteristic equation is reduced to the biquadratic equation $(1 + a_3)(\lambda^2 - 1)^2 + 16\,\lambda^2\,a_1\,a_2 = 0$. Making the change $z = \lambda^2$, we obtain a quadratic equation, whose roots are complex conjugate and lie on the unit circle under the condition that discriminant is nonpositive:

$$\left(1 - 8\,\frac{a_1\,a_2}{1 + a_3}\right)^2 - 1 \leqslant 0 \quad \Leftrightarrow \quad 4\,a_1\,a_2 \leqslant 1 + a_3.$$

Since $a_1 + a_2 = 1$, the last inequality is reduced to the form: $4\,a_1\,a_2 \leqslant (a_1 + a_2)^2 + a_3$, i.e. $0 \leqslant (a_1\,a_2)^2 + a_3$, and is automatically satisfied. The condition $a_1 + a_2 = 1$ means that

$$\left(\frac{\alpha}{\rho} + \frac{\gamma}{j}\right)\Delta t^2 = \left(\frac{\sin^2(\alpha_1/2)}{\Delta x_1^2} + \frac{\sin^2(\alpha_2/2)}{\Delta x_2^2}\right)^{-1}.$$

For fixed values of α_1 and α_2, this choice of time step gives $|\lambda| = 1$. The corresponding solution (46) is bounded. Without calculating the roots of characteristic equation, one can prove that it remains bounded also for smaller time steps.

Let us prove a more general statement. Let $||u^n||$ be an arbitrary norm on the space of solutions of a two-layer homogeneous difference scheme with constant step operator L, the special case of which is the scheme (44), (45). Then if the norm of the solution does not increase under transition to a new time level in computations with the step $\overline{\Delta t}$, it does not increase in computations with a smaller step $\Delta t < \overline{\Delta t}$.

The proof essentially relies on the property of convexity of the norm—a consequence of its positive homogeneity and the triangle inequality:

$$||\chi\,\bar{u} + (1-\chi)\,u|| \leqslant \chi\,||\bar{u}|| + (1-\chi)||u|| \quad (0 \leqslant \chi \leqslant 1).$$

The transition to a new time level in the scheme is carried out by the formulas

$$u^{n+1} = u^n + \Delta t\,L\,u^n, \quad \bar{u}^{n+1} = u^n + \overline{\Delta t}\,L\,u^n,$$

with the help of which it can be shown that

$$u^{n+1} = u^n + \chi\,\overline{\Delta t}\,L\,u^n = \chi\,\bar{u}^{n+1} + (1-\chi)\,u^n, \quad \chi = \Delta t/\overline{\Delta t} \in (0,1).$$

By assumption, $||\bar{u}^{n+1}|| \leqslant ||u^n||$. Consequently,

$$||u^{n+1}|| \leqslant \chi\,||\bar{u}^{n+1}|| + (1-\chi)||u^n|| \leqslant ||u^n||,$$

which was to be proved.

Because of boundedness of the solutions $u^n = (\tau^n, \omega^n)$ in the form (46) for all possible values of the parameters α_1 and α_2, we obtain the following condition:

$$\left(\frac{\alpha}{\rho} + \frac{\gamma}{j}\right)\Delta t^2 \leqslant \left(\frac{1}{\Delta x_1^2} + \frac{1}{\Delta x_2^2}\right)^{-1}. \tag{47}$$

Strictly speaking, this condition is a necessary spectral condition for the stability of the scheme only in two particular cases (1) and (2). In the general case, it guarantees the boundedness of solutions in the form (46), which is very important from a practical point of view, but it is not known whether such solutions are growing if this condition is violated. In addition, neither the condition (47) nor the necessary spectral Fourier stability condition, generally speaking, are not sufficient conditions and thus do not guarantee stability, which may depend, for example, on the method of approximation of boundary conditions. However, in practice, computations based on the described scheme with choosing a time step in accordance with the condition (47) showed stable computational results.

4.5 Numerical Results

For one-dimensional problem on the action of tangential stress $\tau = \hat{\tau}\, e^{i(f\,t - k\,x_2)}$ at one of the boundaries of computational domain, the comparison of the numerical solution by described parallel program and the exact solution was carried out.

Substituting $\tau = \hat{\tau}\, e^{i(f\,t-k\,x_2)}$, $\omega = \hat{\omega}\, e^{i(f\,t-k\,x_2)}$ in the equations of system (42) after simplification we obtain:

$$\Big(-f^2 + \frac{2\,i\,\alpha f}{\eta} + \frac{\alpha\,k^2}{\rho}\Big)\hat{\tau} + 2\,i\,\alpha f\,\hat{\omega} = 0, \quad -\frac{2\,if}{J}\,\hat{\tau} + \Big(\frac{2\,\gamma\,k^2}{J} - f^2\Big)\hat{\omega} = 0.$$

Calculating the determinant of this system, one can find the expression for $k^{\pm}$:

$$k^{\pm} = \sqrt{\frac{\rho J f}{4\,\alpha\,\gamma}\Big(d \pm \sqrt{d^2 - 8\,\frac{\alpha\,\gamma}{\rho J}\Big(f^2 - \frac{2\,i\,\alpha f}{\eta} - \frac{4\,\alpha}{J}\Big)}\Big)},$$

$k^{\pm} = k_1^{\pm} + i\,k_2^{\pm}$ are the wave numbers, $d = \Big(\frac{\alpha}{\rho} + \frac{2\,\gamma}{J}\Big)f - 4\,i\,\frac{\alpha\,\gamma}{\eta\,J}$.

The characteristic dispersion curves are represented in Figs. 8 and 9: dependence of the phase velocity $c^{\pm} = f/\mathrm{Re}\,k^{\pm}$ on the frequency $\nu = f/(2\,\pi)$ and dependence of the damping decrement $\lambda^{\pm} = -1/\mathrm{Im}\,k^{\pm}$ on the frequency ν for $k^{\pm}$. The dashed line corresponds to the eigenfrequency of rotational motion of the particles of a crystal:

$$\nu_* = \frac{1}{\pi}\sqrt{\frac{\alpha}{J}}. \tag{48}$$

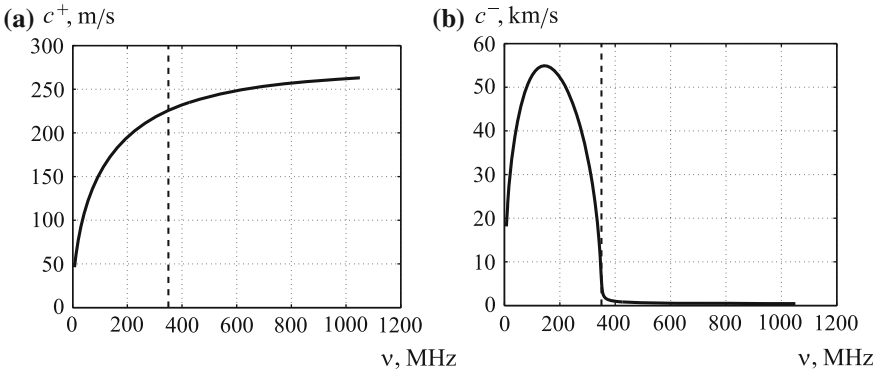

Fig. 8 Dependence of phase velocity on frequency: **a** for k^{+}, **b** for k^{-}

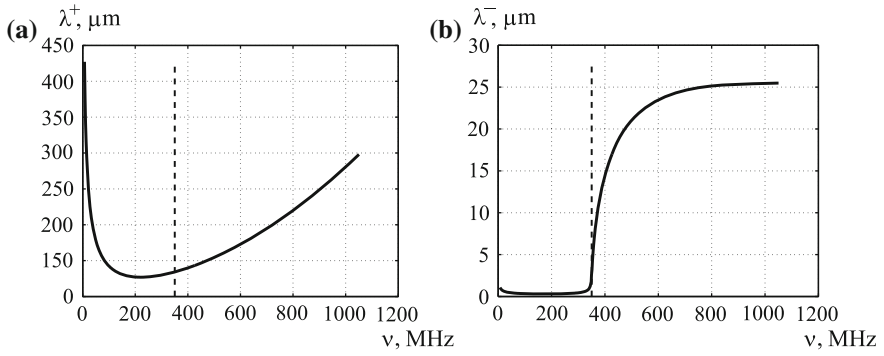

Fig. 9 Dependence of damping decrement on frequency: **a** for k^+, **b** for k^-

Computations were performed for the liquid crystal 5CB with the next parameters [6]: $\rho = 1022\,\mathrm{kg/m^3}, j = 1.33 \times 10^{-10}\,\mathrm{kg/m}, \alpha = 0.161\,\mathrm{GPa}, \gamma = 10\,\mu\mathrm{N}$, $\eta = 10\,\mathrm{Pa\,s}$. For this crystal $\nu_* = 350\,\mathrm{MHz}$. The size of a domain is $4\,\mu\mathrm{m}$.

Initial data and boundary conditions for one-dimensional problem are determined from the next equations:

$$\mathrm{Re}\,\hat{q} = e^{k_2 x_2}\big(\hat{q}_1 \cos(f\,t - k_1\,x_2) - \hat{q}_2 \sin(f\,t - k_1\,x_2)\big),$$
$$\mathrm{Re}\,\hat{\omega} = e^{k_2 x_2}\big(\hat{\omega}_1 \cos(f\,t - k_1\,x_2) - \hat{\omega}_2 \sin(f\,t - k_1\,x_2)\big).$$

Figure 10 shows the results of numerical solution for described above parameters: dependence of $\mathrm{Re}\,\omega$ on x_2 for k^+ and k^- at one of the time moments. The dimension of a finite-difference grid is 1000 meshes. The relative error is 3×10^{-3} in calculations for k^+ and 5×10^{-4} in calculations for k^-.

To verify the proposed parallel program for two-dimensional problems, a series of numerical calculations was carried out on the computational server Flagman of

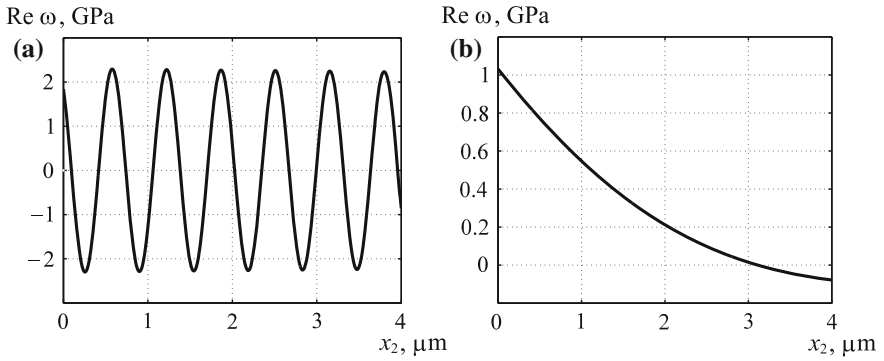

Fig. 10 Dependence of angular velocity on coordinate: **a** for k^+, **b** for k^-

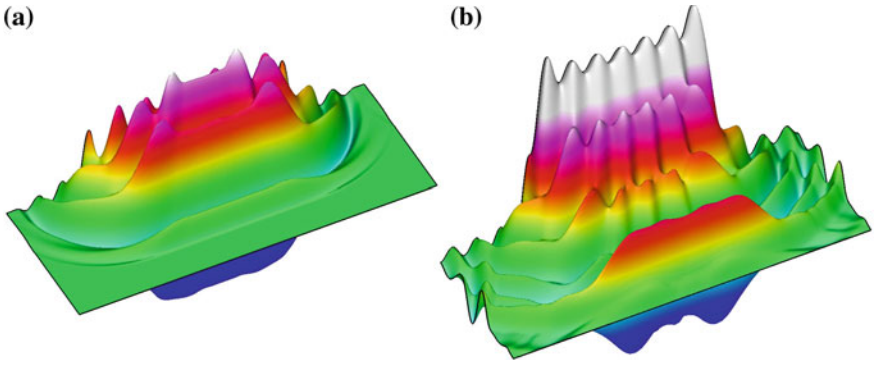

Fig. 11 Periodic action of tangential stress at the upper boundary: The fields of angular velocity ω at different time moments

ICM SB RAS. In Fig. 11 one can see the results of computations for the problem on periodic action of a tangential stress on the part of upper boundary of computational domain. Initial data are zero. The boundary conditions at the upper boundary: $\tau = \bar{\tau}\ \sin(2\,\pi\,\nu\,t)$, if $|x_1 - x_1^c| \leqslant l$, and $\tau = 0$, if $|x_1 - x_1^c| > l$; $\omega_{,2} = 0$. Here x_1^c is the center of zone, where the load acts, l is the radius of this zone. In computations $x_1^c = 5\,\mu\text{m}$, $l = 2.5\,\mu\text{m}$. The lower boundary is fixed, at the left and right boundaries the periodicity conditions are given. The frequency ν is equal to the resonance frequency $\nu_* = 350\,\text{MHz}$. The size of rectangular computational domain is $100\,\mu\text{m} \times 40\,\mu\text{m}$, the dimension of a finite-difference grid is 2560×1024 meshes. Computations were performed for the liquid crystal 5CB with the parameters: $\rho = 1022\,\text{kg/m}^3$, $j = 1.33 \times 10^{-7}\,\text{kg/m}$, $\alpha = 0.161\,\text{GPa}$, $\gamma = 1\,\text{mN}$, $\eta = 100\,\text{Pa s}$. The fields of angular velocity are shown in Fig. 11.

Computational algorithm for solution of the subsystem (42) for tangential stress and angular velocity, parallel program of its realization and some numerical results are represented in [50, 51].

5 Perturbation by Electric Field

5.1 Statement of the Problem

Let's consider a layer of a liquid-crystal medium, extended in the horizontal direction, under the action of a periodic electric field, created by the appearance of charges on the plates of a capacitor. The periodicity of electric field is because of the periodicity of arrangement of the plates at the same distance l from each other both on the upper side and on the lower side of a liquid crystal (Fig. 12). It is assumed that the horizontal sizes $l^{\pm}$ of the capasitor plates are less than l. Changing the charges

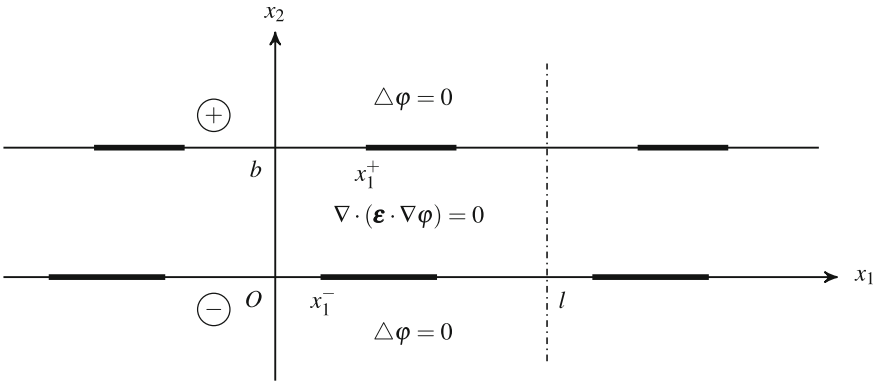

Fig. 12 Scheme of perturbation of a liquid-crystal layer by electric field

in time leads to a rapid change of electric field, which is described by the quasistatic dependence of the electric field $\boldsymbol{E}$ on time as on a parameter.

In the exterior part of a layer, the potential φ of the electric field $\boldsymbol{E} = -\nabla\varphi$ satisfies the Laplace equation: $\triangle\varphi = 0$ for $x_2 < 0$ and $x_2 > b$ (b is the thickness of a layer, ∇ is the Hamiltonian operator). Inside the layer the equation, taking into account the anisotropy of a medium, is fulfilled: $\nabla \cdot (\boldsymbol{\varepsilon} \cdot \nabla\varphi) = 0$, where $\boldsymbol{\varepsilon}$ is the tensor of dielectric permittivity of a liquid crystal, depending on the orientation of domains:

$$\begin{aligned} &\boldsymbol{\varepsilon} = \begin{pmatrix} \varepsilon_{11} & \varepsilon_{12} \\ \varepsilon_{12} & \varepsilon_{22} \end{pmatrix}, \quad \varepsilon_{11} = \varepsilon^{\parallel} \cos^2\theta + \varepsilon^{\perp} \sin^2\theta, \\ &\varepsilon_{12} = (\varepsilon^{\parallel} - \varepsilon^{\perp}) \cos\theta \sin\theta, \quad \varepsilon_{22} = \varepsilon^{\parallel} \sin^2\theta + \varepsilon^{\perp} \cos^2\theta, \end{aligned} \tag{49}$$

$\varepsilon^{\parallel}$ and $\varepsilon^{\perp}$ are the dielectric permeabilities in the direction of molecules and in the transverse direction, θ is the inclination angle of a liquid crystal domain to the abscissa axis.

Taking into account the periodicity of the problem, we can consider only a part of the layer of length l. The electric potential on the plates is distributed uniformly:

$$\begin{aligned} &\varphi^+ = \varphi = \varphi^0 && \text{for } x_2 = b, \ x_1^+ \leqslant x_1 < x_1^+ + l^+, \\ &\varphi = \varphi^-, \quad \varphi_{,1} = 0 && \text{for } x_2 = 0, \ x_1^- \leqslant x_1 < x_1^- + l^-. \end{aligned}$$

Hereinafter $\varphi^{\pm}$ are the limit values of the potential at the boundaries of a liquid crystal from the outside (above and below relative to the layer); φ without indices denotes the values on the same boundaries from the inside of the layer; φ^0 is a given constant, which is selected depending on the intensity of electric field; $x_1^{\pm}$ are the coordinates of the left ends of the upper and lower plates of a capacitor, located, generally speaking, non-symmetrically within the selected part of the layer.

At the rest parts of the boundary, where a liquid crystal is bordered by air (vacuum), the following conditions are satisfied:

$$\varphi^+ = \varphi,\ \varphi^+_{,2} = \varepsilon_{12}\,\varphi_{,1} + \varepsilon_{22}\,\varphi_{,2} \qquad \text{for } x_2 = b,$$
$$\varphi = \varphi^-,\ \varepsilon_{12}\,\varphi_{,1} + \varepsilon_{22}\,\varphi_{,2} = \varphi^-_{,2} \qquad \text{for } x_2 = 0.$$

These conditions result from the continuity of electric potential at the interfaces between media, and the continuity of the normal component of the electric induction vector $\boldsymbol{D} = \varepsilon_0\,\boldsymbol{\varepsilon}\cdot\boldsymbol{E}$ ($\varepsilon_0 = 8.8541878172206\times 10^{-12}$ F/m).

In the presence of electric field, the domains of a liquid crystal undergo the action of bulk forces $\boldsymbol{f} = (\boldsymbol{P}\cdot\nabla)\boldsymbol{E}$ and couple forces $\boldsymbol{g} = \boldsymbol{P}\times\boldsymbol{E}$, where $\boldsymbol{P} = \varepsilon_0\,\boldsymbol{\chi}\,\boldsymbol{E}$ is the vector of electric polarization, $\boldsymbol{\chi} = \boldsymbol{\varepsilon} - \boldsymbol{I}$ is the dielectric susceptibility tensor.

Taking into account plane symmetry of the problem, these formulas can be represented in the form:

$$(f_1, f_2) = \varepsilon_0\big(\chi_{11}\,\varphi_{,1} + \chi_{12}\,\varphi_{,2}\big)\big(\varphi_{,11},\ \varphi_{,12}\big) + \varepsilon_0\big(\chi_{12}\,\varphi_{,1} + \chi_{22}\,\varphi_{,2}\big)\big(\varphi_{,12},\ \varphi_{,22}\big),$$
$$g = \varepsilon_0\big(\chi_{11} - \chi_{22}\big)\varphi_{,1}\,\varphi_{,2} - \varepsilon_0\,\chi_{12}\big((\varphi_{,1})^2 - (\varphi_{,2})^2\big).$$

It is necessary to take into account the forces and couple forces as the right-hand sides of equations of the acoustic approximation of a liquid crystal. In turn, a change in the spatial orientation of the domains due to the action of forces and couple forces leads to a change in the dielectric permittivity tensor, and, thus, the electric field changes. In addition, it is necessary to take into account the heating of a liquid crystal due to the dissipation of energy of the electric field.

5.2 Numerical Method

Solution of the Laplace equation in the exterior of a layer is constructed by means of the method of straight lines. To do this, we introduce a uniform partition of the segment $[0, l]$ of the x_1 axis with step $\Delta x_1 = l/N_1$. The derivatives with respect to x_1 are replaced by finite differences of the second order of approximation:

$$\frac{\varphi_{j_1+1} - 2\,\varphi_{j_1} + \varphi_{j_1-1}}{\Delta x_1^2} + \frac{d^2\varphi_{j_1}}{dx_2^2} = 0 \quad (j_1 = 1, 2, \ldots, N_1 - 1). \tag{50}$$

Here φ_{j_1} are unknown functions depending on x_2 and satisfying the periodicity condition: $\varphi_{N_1} = \varphi^0$.

Let $w = \exp(2\,\pi\,i/N_1)$. As is known, the system of vectors

$$\mathbf{W}^k = \left(1, w^{-k}, w^{-2k}, \ldots, w^{-(N_1-1)k}\right) \quad (k = 0, 1, \ldots, N_1 - 1)$$

forms an orthogonal basis in the N_1-dimensional complex space. Vector–function $(\varphi_0, \varphi_1, \ldots, \varphi_{N_1-1})$ can be represented as an expansion in this basis:

$$\varphi_{j_1}(x_2) = \frac{1}{N_1}\sum_{k=0}^{N_1-1} y_k\, w^{-j_1 k} \quad \text{with coefficients} \quad y_k(x_2) = \sum_{j_1=0}^{N_1-1} \varphi_{j_1}\, w^{j_1 k}.$$

In fact, these are the formulas for the discrete fast Fourier transform and the inverse fast Fourier transform. Substitution in the system of equations (50) leads to independent equations for the expansion coefficients

$$\frac{d^2 y_k}{dx_2^2} = \lambda_k\, y_k, \quad \lambda_k = \frac{4}{\Delta x_1^2}\sin^2\frac{\pi\, k}{N_1}.$$

Hence, $y_k = C_k^+ \exp\bigl(-\sqrt{\lambda_k}\,(x_2 - b)\bigr) + C_k^- \exp\bigl(\sqrt{\lambda_k}\,x_2\bigr)$, where $C_k^\pm$ are arbitrary constants of integration. Since the electric potential is limited in the exterior of a liquid-crystal layer, we should assume $C_k^- = 0$ for the upper half-plane ($x_2 > b$) and $C_k^+ = 0$ for the lower half-plane ($x_2 < 0$). Considering that the electric potential, which is determined up to an additive constant, tends to zero at infinity, it is also necessary to assume $C_0^\pm = 0$.

Equation for the potential in a rectangular region occupied by a liquid crystal is solved by an iterative method with the help of recurrent recalculation using the formula:

$$\bar{\varepsilon}\ \triangle\,\hat{\varphi} = \bar{\varepsilon}\ \triangle\,\varphi - \nabla\cdot(\boldsymbol{\varepsilon}\cdot\nabla\varphi). \tag{51}$$

According to this formula, at each step an anisotropic medium is replaced by a homogeneous and isotropic medium with dielectric permittivity $\bar{\varepsilon}$, with charges distributed inside it. The right-hand side of Eq. (51) is calculated on the previous approximation of electric potential, the value $\bar{\varepsilon}$ is chosen from reasons of the fastest convergence of iterations. Condition of termination of the iterative process is applied in the usual form: $||\hat{\varphi} - \varphi|| \leqslant \delta\,||\varphi||$, with a predetermined admissible error δ and an uniform norm.

To solve the obtained Poisson equation with respect to a new approximation of the potential $\hat{\varphi}$ on a uniform grid, consistent with grid of the method of straight lines, a difference scheme of the second order of approximation is considered:

$$\begin{aligned}
&\frac{\hat{\varphi}_{j_1+1\,j_2} - 2\,\hat{\varphi}_{j_1 j_2} + \hat{\varphi}_{j_1-1\,j_2}}{\Delta x_1^2} + \frac{\hat{\varphi}_{j_1 j_2+1} - 2\,\hat{\varphi}_{j_1 j_2} + \hat{\varphi}_{j_1 j_2-1}}{\Delta x_2^2} = q_{j_1 j_2},\\
&q_{j_1 j_2} = \frac{\varphi_{j_1+1\,j_2} - 2\,\varphi_{j_1 j_2} + \varphi_{j_1-1\,j_2}}{\Delta x_1^2} + \frac{\varphi_{j_1 j_2+1} - 2\,\varphi_{j_1 j_2} + \varphi_{j_1 j_2-1}}{\Delta x_2^2} -\\
&\quad - \frac{d_{1\,j_1+1/2\,j_2} - d_{1\,j_1-1/2\,j_2}}{\bar{\varepsilon}\,\Delta x_1} - \frac{d_{2\,j_1 j_2+1/2} - d_{2\,j_1 j_2-1/2}}{\bar{\varepsilon}\,\Delta x_2},
\end{aligned} \tag{52}$$

where $j_2 = 1, 2, \ldots, N_2 - 1$. For brevity, the following notations are used:

$$d_{1j_1+1/2j_2} = \varepsilon_{11j_1+1/2j_2}\frac{\varphi_{j_1+1j_2}-\varphi_{j_1j_2}}{\Delta x_1} + \\ + \varepsilon_{12j_1+1/2j_2}\frac{\varphi_{j_1+1j_2+1}-\varphi_{j_1+1j_2-1}+\varphi_{j_1j_2+1}-\varphi_{j_1j_2-1}}{4\,\Delta x_2},$$

$$d_{2j_1j_2+1/2} = \varepsilon_{12j_1j_2+1/2}\frac{\varphi_{j_1+1j_2+1}-\varphi_{j_1-1j_2+1}+\varphi_{j_1+1j_2}-\varphi_{j_1-1j_2}}{4\,\Delta x_1} + \\ + \varepsilon_{22j_1j_2+1/2}\frac{\varphi_{j_1j_2+1}-\varphi_{j_1j_2}}{\Delta x_2}.$$

Solution of the discrete equation (52) is constructed by expansion in the basis vectors $\mathbf{W}^k$, according to which

$$\hat{\varphi}_{j_1j_2} = \frac{1}{N_1}\sum_{k=0}^{N_1-1}\hat{y}_{kj_2}\,w^{-j_1k}.$$

For the expansion coefficients the system of equations is fulfilled:

$$-\lambda_k\,\hat{y}_{kj_2} + \frac{\hat{y}_{kj_2+1}-2\,\hat{y}_{kj_2}+\hat{y}_{kj_2-1}}{\Delta x_2^2} = r_{kj_2}, \quad r_{kj_2} = \sum_{j_1=0}^{N_1-1} q_{j_1j_2}\,w^{j_1k}.$$

The tridiagonal matrix algorithm is applied to the solution of obtained system. First the particular solution $\hat{y}^0_{kj_2}$ of an inhomogeneous system with homogeneous boundary conditions $\hat{y}^0_{k0} = \hat{y}^0_{kN_2} = 0$ is calculated. Then two solutions $\hat{y}^+_{kj_2}$ and $\hat{y}^-_{kj_2}$ of a homogeneous system with boundary conditions $\hat{y}^+_{k0} = 0$, $\hat{y}^+_{kN_2} = 1$ and $\hat{y}^-_{k0} = 1$, $\hat{y}^-_{kN_2} = 0$ are calculated similarly. Because of linearity, the general solution of original system has the form:

$$\hat{y}_{kj_2} = \hat{y}^0_{kj_2} + A^+_k\,\hat{y}^+_{kj_2} + A^-_k\,\hat{y}^-_{kj_2}.$$

Constants $A^\pm_k$ together with constants $C^\pm_k$, through which the electric potential is determined in the exterior of a layer, are found from boundary conditions on the capacitor plates and conditions for gluing (sewing) together solutions at the free boundary of a liquid crystal. Conditions of continuity of the potential under passing through the boundaries of a layer allow to exclude $C^\pm_k$: $C^+_k = A^+_k$, $C^-_k = A^-_k$.

Conditions on the plates of a capacitor are reduced to the equations:

$$\sum_{k=0}^{N_1-1} C^+_k w^{-j_1k} = N_1\,\varphi^0, \qquad \text{if } x^+_1 < j_1\,\Delta x_1 < x^+_1 + l^+,$$

$$\sum_{k=0}^{N_1-1} C^-_k(1-w^k)\,w^{-j_1k} = 0, \text{ if } x^-_1 < j_1\,\Delta x_1 < x^-_1 + l^-.$$

Taking into account the formulas

$$\frac{d\varphi^{\pm}_{j_2}}{dx_2} = \mp \frac{1}{N_1} \sum_{k=0}^{N_1-1} \sqrt{\lambda_k}\, C^{\pm}_k\, w^{-j_1 k}, \quad \frac{d\varphi^{\pm}_{j_2}}{dx_1} \approx \frac{1}{N_1} \sum_{k=0}^{N_1-1} C^{\pm}_k\, (1 - w^k)\, w^{-j_1 k},$$

the remaining bonding conditions are transformed into the following equations:

$$\sum_{k=0}^{N_1-1} \left(C^{+}_k \left(\sqrt{\lambda_k} + \varepsilon_{12 j_1 N_2} \frac{1 - w^k}{\Delta x_1} + \varepsilon_{22 j_1 N_2} \frac{1 - \hat{y}^{+}_{k N_2 - 1}}{\Delta x_2} \right) - \right.$$
$$\left. - \varepsilon_{22 j_1 N_2} \frac{\hat{y}^{0}_{k N_2 - 1} + C^{-}_k \hat{y}^{+}_{k N_2 - 1}}{\Delta x_2} \right) w^{-j_1 k} = 0$$

for subscript j_1 lying outside the indicated limits on the upper boundary of the layer, and the equations:

$$\sum_{k=0}^{N_1-1} \left(C^{-}_k \left(-\sqrt{\lambda_k} + \varepsilon_{12 j_1 0} \frac{1 - w^k}{\Delta x_1} - \varepsilon_{22 j_1 0} \frac{1 - \hat{y}^{-}_{k 1}}{\Delta x_2} \right) + \right.$$
$$\left. + \varepsilon_{22 j_1 0} \frac{\hat{y}^{0}_{k 1} + C^{+}_k \hat{y}^{+}_{k 1}}{\Delta x_2} \right) w^{-j_1 k} = 0$$

for subscript j_1 lying outside the indicated limits on the lower boundary. As a result, we obtain a closed system of equations for determining the constants $C^{\pm}_k$, which is solved by means of the LU-decomposition method.

Under numerical realization of the algorithm the value of φ^0, which depends on the intensity of the action, is taken as $\varphi^0 = 1$. Then, taking into account the linearity of the problem with respect to the electric potential, the obtained solution is multiplied by a size coefficient corresponding to a given difference of potentials on the capacitor plates.

5.3 Computational Results

The parallel program implementing this computational algorithm is in the process of debugging and verification. The CUDA technology for computer systems with GPUs is used. Stages of the algorithm are executed sequentially, the parallelization of computations is performed inside each of the stages. The program contains modules that implement the method of straight lines with the use of the tridiagonal matrix algorithm, the Fourier transform and the SLAE solution method by means of the LU-decomposition, and also modules realizing an iterative method for solving the equation for potential with the help of a recurrence relation. In the future, it is planned to embed this program into the previously developed software package for mathematical model describing the thermomechanical properties of liquid crystals [36, 49].

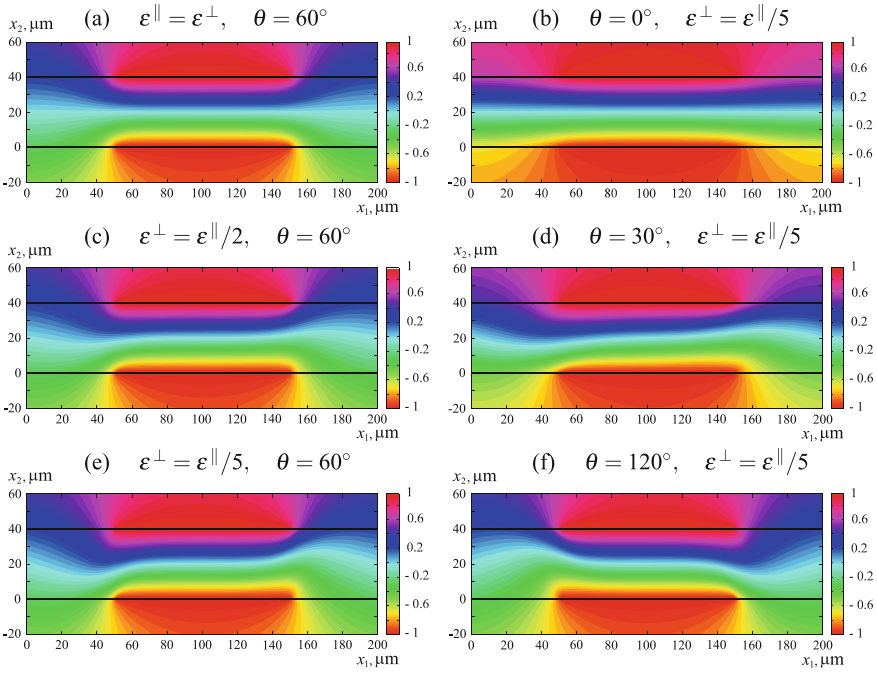

Fig. 13 Perturbation of a liquid-crystal layer by electric field (case of symmetric plates of a capacitor): Level curves of $Re(\varphi)$ at different values of $\varepsilon^{\parallel}$, $\varepsilon^{\perp}$ and θ

Figures 13 and 14 demonstrate the results of computations performed for a liquid crystal 5CB of size $200\,\mu m \times 40\,\mu m$. In the first case, the capacitor plates are located symmetrically, they have the same length $l^{\pm} = 100\,\mu m$ and coordinates of the left ends $x_1^{\pm} = 50\,\mu m$ (Fig. 13). In the second case, the plates are non-symmetric, $l^{+} = 50\,\mu m$ and $x_1^{+} = 50\,\mu m$ for the upper plate, $l^{-} = 20\,\mu m$ and $x_1^{-} = 150\,\mu m$ for the lower plate (Fig. 14). The angle of inclination of molecules of a liquid crystal to the abscissa axis is $\phi = 60^{\circ}$, and the dielectric permeabilities in the direction of molecules and in the transverse direction are varied: $\varepsilon^{\parallel} = \varepsilon^{\perp}$ in Figs. 13a and 14a; $\varepsilon^{\perp} = \varepsilon^{\parallel}/2$ in Figs. 13c and 14c; $\varepsilon^{\perp} = \varepsilon^{\parallel}/5$ in Figs. 13e and 14e. Similarly, the dielectric permeabilities are the same: $\varepsilon^{\perp} = \varepsilon^{\parallel}/5$, and the inclination angle are varied: $\theta = 0^{\circ}$ in Figs. 13b and 14b; $\theta = 30^{\circ}$ in Figs. 13d and 14d; $\theta = 120^{\circ}$ in Figs. 13f and 14f. Level curves of $Re(\varphi)$ are represented. Horizontal lines show the boundaries of a liquid-crystal layer. Outside the layer, above and below, computational domains of the size $200\,\mu m \times 20\,\mu m$ are considered.

Proposed parallel computational algorithm will be used for simulation the behavior of liquid crystals under the influence of an electric field.

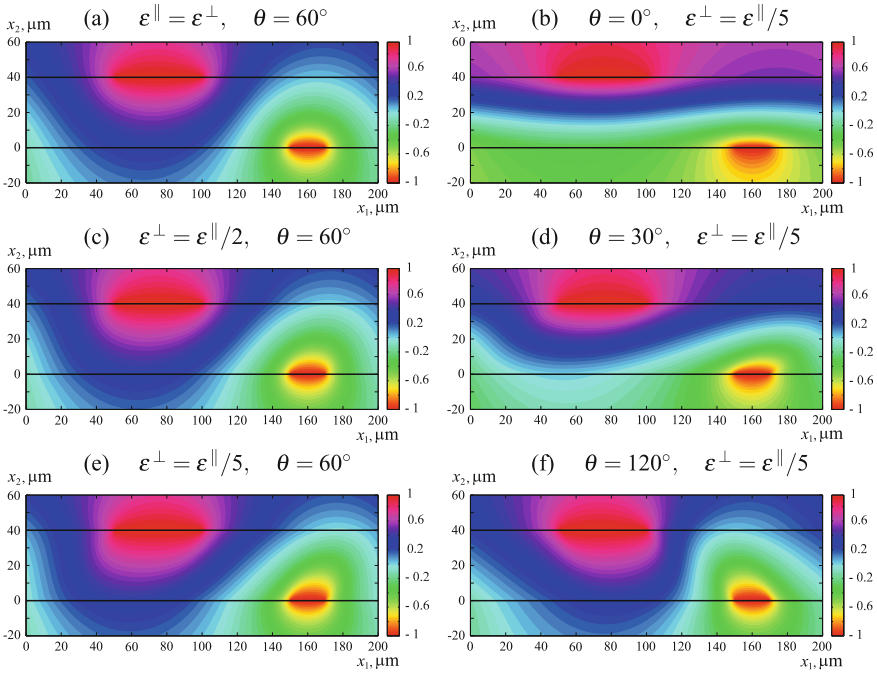

Fig. 14 Perturbation of a liquid-crystal layer by electric field (case of non-symmetric plates of a capacitor): Level curves of $Re(\varphi)$ at different values of $\varepsilon^{\parallel}$, $\varepsilon^{\perp}$ and θ

6 Conclusions

For the description of thermomechanical processes running in liquid crystals exposed to weak external effects, the simplified mathematical model is developed accounting for mutual influence of three different physical factors—transfer of acoustic energy due to translational motion of particles, viscoelastic rotation of particles under appearing tangential stresses and anisotropic thermal diffusion. The efficient shock-capturing algorithms are worked out for numerical solution of boundary-value problems on the basis of the model equations. The algorithms are implemented by the CUDA technology for computer systems with GPUs. It was demonstrated that, in the framework of the simplified model, re-orientation of particles under localized thermal impact can only happen if tangential stresses appear at the boundary of a liquid crystal due to external conditions of loading and fixing. The performed series of computations of resonant excitation of a medium at the frequency of characteristic oscillations of rotational motion of particles has yielded that the resonance is observed irrespectively of the size of a liquid crystal as distinguished from elastic resonances of longitudinal and transverse motion. Numerical algorithm for modeling the excitation of liquid crystals by electric field is suggested, which can be used for simulation of known physical observations, such as Frederix effect, etc.

Acknowledgements This work was supported by the Complex Fundamental Research Program no. II.2P "Integration and Development" of Siberian Branch of the Russian Academy of Sciences (project no. 0356-2016-0728).

References

1. Aero, E.L., Bulygin, A.N.: Equations of motion of nematic liquid-crystal media. J. Appl. Math. Mech. **35**(5), 831–843 (1971). https://doi.org/10.1016/0021-8928(71)90081-5
2. Aero, E.L., Bulygin, A.N.: Kinematics of nematic liquid crystals. Int. Appl. Mech. **8**(3), 306–313 (1972). https://doi.org/10.1007/BF00887448
3. Aero, E.L., Bulygin, A.N., Kuvshinskii, E.V.: Asymmetric hydromechanics. J. Appl. Math. Mech. **29**(2), 333–346 (1965). https://doi.org/10.1016/0021-8928(65)90035-3
4. Ahlers, G., Cannell, D.S., Berge, L.I., Sakurai, S.: Thermal conductivity of the nematic liquid crystal 4-n-pentil-4′-cyanobiphenil. Phys. Rev. E **49**(1), 545–553 (1994). https://doi.org/10.1103/PhysRevE.49.545
5. de Andrade Lima, L.R.P., Rey, A.D.: Superposition and universality in the linear viscoelasticity of Leslie–Ericksen liquid crystals. J. Rheol. **48**(5), 1067–1084 (2004). https://doi.org/10.1122/1.1773784
6. Belyaev, B.A., Drokin, N.A., Shabanov, V.F., Shepov, V.N.: Dielectric anisotropy of 5CB liquid crystal in a decimeter wavelength range. Phys. Solid State **42**(3), 577–579 (2000). https://doi.org/10.1134/1.1131251
7. Blinov, L.M.: Structure and Properties of Liquid Crystals. Springer, Heidelberg, New York, Dordrecht, London (2011). https://doi.org/10.1007/978-90-481-8829-1
8. Cosserat, E., Cosserat, F.: Théorie des corps déformables. In: Chwolson, O.D. (ed.) Traité Physique, pp. 953–1173. Librairie Scientifique A. Hermann et Fils, Paris (1909)
9. Demenev, E.I., Pozdnyakov, G.A., Trashkeev, S.I.: Nonlinear orientation interaction of nematic liquid crystal with thermal flow. Pisma v ZhTF **35**(14), 76–83 (2009) (in Russian)
10. Ericksen, J.L.: Conservation laws for liquid crystals. Trans. Soc. Rheol. **5**(1), 23–34 (1961). https://doi.org/10.1122/1.548883
11. Eringen, A.C.: Theory of micropolar fluids. Indiana Univ. Math. J. **16**(1), 1–18 (1967). https://doi.org/10.1512/iumj.1967.16.16001
12. Eringen, A.C.: Micropolar theory of liquid crystals. In: Jonson, J.F., Porter, R.S. (eds.) Liquid Crystals and Ordered Fluids, vol. 3, pp. 443–474. Plenum Press, New York (1978)
13. Farber, R.: CUDA Application Design and Development, 1st edn. Morgan Kaufmann/Elsevier, Amsterdam, Boston, Heidelberg, London, New York, Oxford, Paris, San Diego, San Francisco, Singapore, Sydney, Tokyo (2011)
14. Frank, F.C.: On the theory of liquid crystals. Disc. Faraday Soc. **25**, 19–28 (1958)
15. Friedrichs, K.O.: Symmetric hyperbolic linear differential equations. Commun. Pure Appl. Math. **7**(2), 345–392 (1954). https://doi.org/10.1002/cpa.3160070206
16. de Gennes, P.G., Prost, J.: The Physics of Liquid Crystals, 2nd edn. International Series of Monographs on Physics, vol. 83. Clarendon Press, Oxford (1995)
17. Godunov, S.K., Mikhailova, T.Yu.: Representation of Rotation Group and Spherical Functions. Nauchnaya Kniga, Novosibirsk (1998) (in Russian)
18. Godunov, S.K., Zabrodin, A.V., Ivanov, M.Ya., Kraiko, A.N., Prokopov, G.P.: Numerical Solving Many-Dimensional Problems of Gas Dynamics. Nauka, Moscow (1976) (in Russian)
19. Grekova, E.F., Maugin, G.A.: Modelling of complex elastic crystals by means of multi-spin micromorphic media. Int. J. Eng. Sci. **43**(5–6), 494–519 (2005). https://doi.org/10.1016/j.ijengsci.2004.08.016
20. Ivanov, G.V., Volchkov, Yu.M, Bogulskii, I.O., Anisimov, S.A., Kurguzov, V.D.: Numerical Solution of Dynamic Elastic-Plastic Problems of Deformable Solids. Sib. Univ. Izd., Novosibirsk (2002) (in Russian)

21. Kalugin, A.G.: Mechanics of Anisotropic Liquids. Izd., CPI MMF MGU, Moscow (2005) (in Russian)
22. Kirk, D.B., Hwu, W.W.: Programming Massively Parallel Processors: A Hands-on Approach, 2nd edn. Morgan Kaufmann/Elsevier, Amsterdam, Boston, Heidelberg, London, New York, Oxford, Paris, San Diego, Singapore, Sydney, Tokyo (2013)
23. Kondaurov, V.I.: Non-linear equations of the dynamics of an elastic micropolar medium. J. Appl. Math. Mech. **48**(3), 291–299 (1984). https://doi.org/10.1016/0021-8928(84)90135-7
24. Kondaurov, V.I., Fortov, V.E.: Fundamentals of the Thermomechanics of a Condensed Medium. Izd., MFTI, Moscow (2002) (in Russian)
25. Kulikovskii, A.G., Pogorelov, N.V., Semenov, A.Yu.: Mathematical Aspects of Numerical Solution of Hyperbolic Systems. Series of Monographs and Surveys in Pure and Applied Mathematics, vol. 118. Chapman & Hall/CRC, Boca Raton, London, New York, Washington (2001)
26. Lee, J.D., Eringen, A.C.: Wave propagation in nematic liquid crystals. J. Chem. Phys. **54**(12), 5027–5034 (1971). https://doi.org/10.1063/1.1674793
27. Leslie, F.M.: Some constitutive equations for liquid crystals. Arch. Ration. Mech. Anal. **28**(4), 265–283 (1968). https://doi.org/10.1007/BF00251810
28. Lhuillier, D.: Micropolar fluids: from nematic liquid crystals to liquid-like granular media. In: Maugin, G.A., Metrikine, A.V. (eds.) Mechanics of Generalized Continua, Series of Advanced in Mechanics and Mathematics, vol. 21, pp. 47–54. Springer, Heidelberg, New York, Dordrecht, London (2010). https://doi.org/10.1007/978-1-4419-5695-8
29. Lhuillier, D., Rey, A.D.: Nematic liquid crystals and ordered micropolar fluids. J. Non-Newtonian Fluid Mech. **120**(1–3), 169–174 (2004). https://doi.org/10.1016/j.jnnfm.2004.01.018
30. Maugin, G.A.: Nonlinear Waves in Elastic Crystals. Oxford Mathematical Monographs. Oxford University Press, Oxford (1999)
31. Maugin, G.A., Drouot, R.: Internal variables and the thermodynamics of macromolecule solutions. Int. J. Eng. Sci. **21**(7), 705–724 (1983). https://doi.org/10.1016/0020-7225(83)90056-3
32. Marchuk, G.I.: Splitting Methods. Nauka, Moscow (1988) (in Russian)
33. Oseen, C.W.: The theory of liquid crystals. Trans. Faraday Soc. **29**, 883–900 (1933)
34. Pietraszkiewicz, W., Eremeev, V.A.: On natural strain measures of the non-linear micropolar continuum. Int. J. Solids Struct. **46**(3–4), 774–787 (2009). https://doi.org/10.1016/j.ijsolstr.2008.09.027
35. Prishchepa, O.O., Shabanov, A.V., Zyryanov, V.Ya.: Transformation of director configuration upon changing boundary conditions in droplets of nematic liquid crystal. JETP Lett. **79**(6), 257–261 (2004). https://doi.org/10.1134/1.1759405
36. Sadovskaya, O.V.: Numerical simulation of the dynamics of a liquid crystal in the case of plane strain using GPUs. AIP Conf. Proc. **1629**, 303–310 (2014). https://doi.org/10.1063/1.4902286
37. Sadovskaya, O.V., Sadovskii, V.M.: Analysis of rotational motion of material microstructure particles by equations of the Cosserat elasticity theory. Acoust. Phys. **56**(6), 942–950 (2010). https://doi.org/10.1134/S1063771010060199
38. Sadovskaya, O., Sadovskii, V.: Mathematical Modeling in Mechanics of Granular Materials. In: Altenbach, H. (ed.), Series of Advanced Structured Materials, vol. 21. Springer, Heidelberg, New York, Dordrecht, London (2012). https://doi.org/10.1007/978-3-642-29053-4
39. Sadovskii, V.M.: Thermodynamically consistent system of conservation laws of nonsymmetric elasticity theory. Far Eastern Math. J. **11**(2), 201–212 (2011) (in Russian)
40. Sadovskii, V.M.: Equations of the dynamics of a liquid crystal under the influence of weak mechanical and thermal perturbations. AIP Conf. Proc. **1629**, 311–318 (2014). https://doi.org/10.1063/1.4902287
41. Sadovskii, V.M.: Thermodynamically consistent equations of the couple stress elasticity. Far Eastern Math. J. **16**(2), 209–222 (2016) (in Russian)

42. Sadovskii, V.: On thermodynamically consistent form of nonlinear equations of the Cosserat theory. Eng. Trans. **65**(1), 201–208 (2017)
43. Sadovskii, V.M., Sadovskaya, O.V.: On the acoustic approximation of thermomechanical description of a liquid crystal. Phys. Mesomech. **16**(4), 312–318 (2013). https://doi.org/10.1134/S102995991304005X
44. Sadovskii, V.M., Sadovskaya, O.V., Varygina, M.P.: Numerical solution of dynamic problems in couple-stressed continuum on multiprocessor computer systems. Int. J. Numer. Anal. Model. B **2**(2–3), 215–230 (2011)
45. Shibaev, V.P., Freidzon, Ya.S., Kostromin, S.G.: Molecular architecture and structure of thermotropic liquid crystal polymers with mesogenic side groups. In: Shibaev, V.P., Lam, L. (eds.) Liquid Crystalline and Mesomorphic Polymers, pp. 77–120. Springer, New York (1994). https://doi.org/10.1007/978-1-4613-8333-8
46. Shu, C.-W.: Essentially non-oscillatory and weighted essentially non-oscillatory schemes for hyperbolic conservation laws. In: Quarteroni, A. (ed.) Advanced Numerical Approximation of Nonlinear Hyperbolic Equations. Series of Lecture Notes in Mathematics, vol. 1697, pp. 325–432. Springer, Berlin, Heidelberg, New York (1998). https://doi.org/10.1007/BFb0096355
47. Skarp, K., Lagerwall, S.T., Stebler, B.: Measurement of hydrodynamic parameters for nematic 5CB. Mol. Cryst. Liq. Cryst. **60**(3), 215–236 (1980). https://doi.org/10.1080/00268948008072401
48. Sluckin, T.J., Dunmur, D.A., Stegemeyer, H. (eds.) Crystals that Flow: Classic Papers in the History of Liquid Crystals. CRC Press, London (2004). https://doi.org/10.1201/9780203022658
49. Smolekho, I.V.: Parallel implementation of the algorithm for description of thermoelastic waves in liquid crystals. Young Sci. **11**(91), 107–112 (2015) (in Russian)
50. Smolekho, I., Sadovskaya, O., Sadovskii, V.: Numerical analysis of acoustic waves in a liquid crystal taking into account couple-stress interaction. In: CEUR Workshop Proceedings: Mathematical and Information Technologies (MIT–2016), vol. 1839, pp. 473–486 (2017)
51. Smolekho, I.V., Sadovskaya, O.V., Sadovskii, V.M.: Numerical modeling of acoustic waves in a liquid crystal using CUDA technology. Comput. Technol. **22**(Spec. Iss.), 87–98 (2017) (in Russian)
52. Sutormin, V.S., Krakhalev, M.N., Prishchepa, O.O.: Thermo-induced transformations of director configuration within nematic droplets dispersed in polyvinylpyrrolidone. J. SFU: Mathem. Phys. **2**(3), 352–359 (2009) (in Russian)
53. Tomilin, M.G., Pestov, S.M.: Properties of Liquid Cristalline Materials. Politekhnika, St. Petersburg (2005). (in Russian)
54. Trashkeev, S.I., Britvin, A.V.: Thermal-oriented effect in a nematic liquid crystal. ZhTF **81**(6), 1–7 (2011) (in Russian)

Effect of Surface Stresses on Stability of Elastic Circular Cylinder

Denis N. Sheydakov

Abstract The present research is dedicated to the buckling analysis of nonlinearly elastic cylinders with surface stresses. In the framework of Gurtin–Murdoch model, we have studied the stability of a solid circular cylinder subjected to the axial compression-extension and the external pressure. For an arbitrary isotropic material, the system of linearized equilibrium equations is derived, which describes the behavior of a cylinder in a perturbed state. By means of a special substitution, the study of stability is reduced to solving a linear homogeneous boundary-value problem for a system of three ordinary differential equations. For two specific models of bulk material (Harmonic model and Blatz–Ko model), the buckling analysis has been carried out for a circular cylinder made of aluminum in the case of a simple axial compression. It was found, in particular, that the stability of the cylinder increases with a decrease of its overall size. This effect is due to the influence of surface stresses. It is negligible at macroscale, but becomes quite significant at micro- and nanoscale.

1 Introduction

The problem of equilibrium stability for deformable bodies is of major importance both from theoretical and practical points of view, because the exhaustion of bearing capacity and the collapse of engineering structures quite often occurs due to the buckling under external loads. Due to the development of modern technologies and the appearance of new materials, the problem of stability analysis while taking into account the various surface phenomena becomes relevant [11]. Recently, for modeling such phenomena, especially in nanomechanics [1, 4, 16], the theory of elasticity with surface stresses has received development. In this theory, in addition to the ordinary stresses distributed in the volume, the independent surface stresses are also

D. N. Sheydakov (✉)
South Scientific Center of Russian Academy of Sciences, Chekhova Ave. 41, 344006 Rostov-on-Don, Russia
e-mail: sheidakov@mail.ru

F. dell'Isola et al. (eds.), *Advances in Mechanics of Microstructured Media and Structures*, Advanced Structured Materials 87,
https://doi.org/10.1007/978-3-319-73694-5_18

taken into account at the boundary of the body or its part. These stresses generalize the well-known in hydromechanics scalar surface tension to the case of solids. The introduction of surface stresses allows, in particular, describing the size effect typical for nanomaterials [3, 9, 15].

The present research is dedicated to the buckling analysis of nonlinearly elastic cylinders with surface stresses. To take into account the influence of the latter, the Gurtin–Murdoch model [6] is used, which from the mechanical point of view is equivalent to a deformable body with glued elastic membrane. In this case, the stress resultant tensor acting in the membrane can be interpreted as surface stresses.

2 Equilibrium of Body with Surface Stresses

In the framework of Gurtin–Murdoch model [6], the set of static equations for a nonlinearly elastic body with surface stresses in the absence of body forces consists of the equilibrium equations

$$\overset{\circ}{\nabla} \cdot \mathbf{D} = \mathbf{0} \tag{1}$$

the equilibrium conditions on the part of the body surface Ω_s, where the surface stresses are acting

$$\left(\mathbf{n} \cdot \mathbf{D} - \overset{\circ}{\nabla}_s \cdot \mathbf{D}_s \right) \Big|_{\Omega_s} = \mathbf{t} \tag{2}$$

the constitutive equations

$$\mathbf{D} = \mathbf{P} \cdot \mathbf{C}, \qquad \mathbf{P} = 2\frac{\partial W(\mathbf{G})}{\partial \mathbf{G}}, \qquad \mathbf{D}_s = \mathbf{P}_s \cdot \mathbf{C}_s, \qquad \mathbf{P}_s = 2\frac{\partial W_s(\mathbf{G}_s)}{\partial \mathbf{G}_s} \tag{3}$$

and the geometric relations

$$\mathbf{G} = \mathbf{C} \cdot \mathbf{C}^{\mathrm{T}}, \qquad \mathbf{C} = \overset{\circ}{\nabla} \mathbf{R}, \qquad \mathbf{G}_s = \mathbf{C}_s \cdot \mathbf{C}_s^{\mathrm{T}}, \qquad \mathbf{C}_s = \overset{\circ}{\nabla}_s \mathbf{R} \Big|_{\Omega_s} \tag{4}$$

Here $\mathbf{D}$ and $\mathbf{P}$ are the Piola and Kirchhoff stress tensors, respectively; $\overset{\circ}{\nabla}$ is the three-dimensional nabla-operator in Lagrangian coordinates; $\overset{\circ}{\nabla}_s$ is the surface nabla-operator; $\mathbf{D}_s$ and $\mathbf{P}_s$ are the surface stress tensors of the Piola and Kirchhoff type; $\mathbf{n}$ is the unit vector normal to the surface of the undeformed body; $\mathbf{t}$ is the surface loads vector; W and W_s are the bulk and surface strain energy densities, respectively; $\mathbf{G}$ and $\mathbf{G}_s$ are the Cauchy–Green strain tensors in the volume and on the surface of the body; $\mathbf{C}$ and $\mathbf{C}_s$ are the deformation gradients; and $\mathbf{R}$ is the position vector in the actual configuration.

Taking (3) into account, the following relations are valid for the Kirchhoff stress tensor $\mathbf{P}$ in the case of an isotropic body [8, 10]:

$$\mathbf{P} = \sum_{k=1}^{3} \chi_k \mathbf{d}_k \otimes \mathbf{d}_k, \qquad \chi_k = 2\frac{\partial W(G_1, G_2, G_3)}{\partial G_k}, \qquad \mathbf{G} = \sum_{k=1}^{3} G_k \mathbf{d}_k \otimes \mathbf{d}_k \tag{5}$$

where $G_k, \mathbf{d}_k (k = 1, 2, 3)$ are the eigenvalues and eigenvectors of the Cauchy–Green strain tensor $\mathbf{G}$. At the same time, the expression for the surface stress tensor of Kirchhoff type $\mathbf{P}_s$ takes the form [1]:

$$\mathbf{P}_s = \kappa_1 \mathbf{I}_s + 2\kappa_2 \mathbf{G}_s, \qquad \kappa_\alpha = 2\frac{\partial W_s(j_1, j_2)}{\partial j_\alpha}, \qquad j_\alpha = \mathrm{tr}\mathbf{G}_s^\alpha, \qquad \alpha = 1, 2 \tag{6}$$

Here j_1, j_2 are the invariants of the surface Cauchy–Green strain tensor $\mathbf{G}_s$; $\mathbf{I}$ and $\mathbf{I}_s = \mathbf{I} - \mathbf{n} \otimes \mathbf{n}$ are the three-dimensional and surface unit tensors, respectively.

3 Circular Cylinder with Surface Stresses

Consider a homogeneous circular cylinder of radius r_0 and length l. We assume that the surface stresses are acting on its lateral surface Ω_0 $(r = r_0)$, i.e. $\Omega_s = \Omega_0$. In the case of axial compression-extension of the cylinder under external hydrostatic pressure, the position vector $\mathbf{R}$ is given by the following relations [13, 17]:

$$\begin{aligned} &\mathbf{R} = \gamma r \mathbf{e}_R + \alpha z \mathbf{e}_Z \\ &R = \gamma r, \qquad \Phi = \varphi, \qquad Z = \alpha z \\ &0 \le r \le r_0, \qquad 0 \le \varphi \le 2\pi, \qquad 0 \le z \le l \end{aligned} \tag{7}$$

where r, φ, z are the cylindrical coordinates in the reference state (Lagrangian coordinates); R, Φ, Z are the Eulerian cylindrical coordinates; $\{\mathbf{e}_r, \mathbf{e}_\varphi, \mathbf{e}_z\}$ and $\{\mathbf{e}_R, \mathbf{e}_\Phi, \mathbf{e}_Z\}$ are the orthonormal vector bases of Lagrangian and Eulerian coordinates, respectively; α is the given ratio of compression-extension along the axis of the cylinder; and γ is the unknown constant that characterizes the radial deformation of the cylinder.

According to the expressions (4), (7), the deformation gradients in the volume and on the surface are:

$$\mathbf{C} = \gamma \mathbf{e}_r \otimes \mathbf{e}_R + \gamma \mathbf{e}_\varphi \otimes \mathbf{e}_\Phi + \alpha \mathbf{e}_z \otimes \mathbf{e}_Z, \qquad \mathbf{C}_s = \gamma \mathbf{e}_\varphi \otimes \mathbf{e}_\Phi + \alpha \mathbf{e}_z \otimes \mathbf{e}_Z \tag{8}$$

From the relations (4), (8) we obtain the expressions for the corresponding Cauchy–Green strain tensors

$$\mathbf{G} = \gamma^2 \mathbf{e}_r \otimes \mathbf{e}_r + \gamma^2 \mathbf{e}_\varphi \otimes \mathbf{e}_\varphi + \alpha^2 \mathbf{e}_z \otimes \mathbf{e}_z, \qquad \mathbf{G}_s = \gamma^2 \mathbf{e}_\varphi \otimes \mathbf{e}_\varphi + \alpha^2 \mathbf{e}_z \otimes \mathbf{e}_z \tag{9}$$

It is obvious that for the considered initial strain state the eigenvectors $\mathbf{d}_k$ $(k = 1, 2, 3)$ of the Cauchy–Green strain tensor coincide with the vector basis of Lagrangian cylindrical coordinates, i.e. $\mathbf{d}_1 = \mathbf{e}_r$, $\mathbf{d}_2 = \mathbf{e}_\varphi$, $\mathbf{d}_3 = \mathbf{e}_z$, and the eigenvalues G_k are: $G_1 = G_2 = \gamma^2$, $G_3 = \alpha^2$.

Thus, taking (5), (6) into account, the following relations are valid for the Kirchhoff stress tensors:

$$\begin{aligned} \mathbf{P} &= \chi_1 \mathbf{e}_r \otimes \mathbf{e}_r + \chi_2 \mathbf{e}_\varphi \otimes \mathbf{e}_\varphi + \chi_3 \mathbf{e}_z \otimes \mathbf{e}_z \\ \mathbf{P}_s &= \left(\kappa_1 + 2\gamma^2 \kappa_2\right) \mathbf{e}_\varphi \otimes \mathbf{e}_\varphi + \left(\kappa_1 + 2\alpha^2 \kappa_2\right) \mathbf{e}_z \otimes \mathbf{e}_z \end{aligned} \tag{10}$$

Substituting the above expressions in (3), we find a representation of the Piola stress tensor $\mathbf{D}$ and the surface stress tensor of the Piola type $\mathbf{D}_s$ in the case of axial compression-extension of the cylinder under external pressure

$$\begin{aligned} \mathbf{D} &= \gamma \chi_1 \mathbf{e}_r \otimes \mathbf{e}_R + \gamma \chi_2 \mathbf{e}_\varphi \otimes \mathbf{e}_\Phi + \alpha \chi_3 \mathbf{e}_z \otimes \mathbf{e}_Z \\ \mathbf{D}_s &= \gamma \left(\kappa_1 + 2\gamma^2 \kappa_2\right) \mathbf{e}_\varphi \otimes \mathbf{e}_\Phi + \alpha \left(\kappa_1 + 2\alpha^2 \kappa_2\right) \mathbf{e}_z \otimes \mathbf{e}_Z \end{aligned} \tag{11}$$

It follows from (11) that the equilibrium equations (1) are automatically satisfied if $\chi_1 = \chi_2$. The equilibrium conditions (2) on the lateral surface of the cylinder $(r = r_0)$ under hydrostatic pressure p (referred to the unit area of the deformed configuration) are written as follows:

$$\chi_1 + \frac{\kappa_1 + 2\gamma^2 \kappa_2}{r_0} = -\alpha p \tag{12}$$

By solving the Eq. (12) at given densities W, W_s of the bulk and surface strain energy, we find the unknown constant γ.

4 Linearized Equilibrium Equations

Consider a small perturbation of the initial strain state described above. We assume that the perturbed equilibrium state of a circular cylinder exists under the same external loads and is determined by the position vector $\tilde{\mathbf{R}} = \mathbf{R} + \eta \mathbf{v}$. Here η is the small parameter and $\mathbf{v}$ is the vector of additional displacements.

The linearized equilibrium equations for a nonlinearly elastic medium have the form [5, 10]:

$$\overset{\circ}{\nabla} \cdot \mathbf{D}^\bullet = \mathbf{0}, \qquad \mathbf{D}^\bullet = \left[\frac{d}{d\eta} \mathbf{D}\left(\mathbf{R} + \eta \mathbf{v}\right)\right]_{\eta=0} \tag{13}$$

$$\mathbf{D}^\bullet = \mathbf{P}^\bullet \cdot \mathbf{C} + \mathbf{P} \cdot \overset{\circ}{\nabla} \mathbf{v} \tag{14}$$

Here $\mathbf{D}^\bullet$ and $\mathbf{P}^\bullet$ are the linearized Piola and Kirchhoff stress tensors, respectively. In order to find the expression for the latter, a linearization of the constitutive relations

(5) is carried out [12]

$$\begin{aligned}\mathbf{P}^{\bullet} &= \sum_{k=1}^{3}\left(\chi_k^{\bullet}\mathbf{d}_k\otimes\mathbf{d}_k+\chi_k\mathbf{d}_k^{\bullet}\otimes\mathbf{d}_k+\chi_k\mathbf{d}_k\otimes\mathbf{d}_k^{\bullet}\right)\\ \mathbf{G}^{\bullet} &= \sum_{k=1}^{3}\left(G_k^{\bullet}\mathbf{d}_k\otimes\mathbf{d}_k+G_k\mathbf{d}_k^{\bullet}\otimes\mathbf{d}_k+G_k\mathbf{d}_k\otimes\mathbf{d}_k^{\bullet}\right)\end{aligned} \tag{15}$$

By taking into account the fact that vectors $\mathbf{d}_k$ and $\mathbf{d}_k^{\bullet}$ $(k=1,2,3)$ are mutually orthogonal, i.e. $\mathbf{d}_k\cdot\mathbf{d}_k^{\bullet}=0$, following (15) we obtain $(m,n=1,2,3;\ k\neq m\neq n)$

$$\mathbf{d}_k\cdot\mathbf{P}^{\bullet}\cdot\mathbf{d}_k=\chi_k^{\bullet},\qquad \mathbf{d}_k\cdot\mathbf{P}^{\bullet}\cdot\mathbf{d}_m=B_n\mathbf{d}_k\cdot\mathbf{G}^{\bullet}\cdot\mathbf{d}_m,\qquad B_n=\frac{\chi_k-\chi_m}{G_k-G_m} \tag{16}$$

where the relations for $\chi_k^{\bullet}$ have the form:

$$\chi_k^{\bullet}=\sum_{n=1}^{3}\chi_{kn}G_n^{\bullet},\qquad \chi_{kn}=\frac{\partial\chi_k(G_1,G_2,G_3)}{\partial G_n},\qquad G_n^{\bullet}=\mathbf{d}_n\cdot\mathbf{G}^{\bullet}\cdot\mathbf{d}_n$$

Equations (16) represent all components of the linearized Kirchhoff stress tensor $\mathbf{P}^{\bullet}$ in the basis $\{\mathbf{d}_1,\mathbf{d}_2,\mathbf{d}_3\}$ through the components of the linearized Cauchy–Green strain tensor $\mathbf{G}^{\bullet}$, while the tensor $\mathbf{G}^{\bullet}$ itself is

$$\mathbf{G}^{\bullet}=\overset{\circ}{\nabla}\mathbf{v}\cdot\mathbf{C}^{\mathrm{T}}+\mathbf{C}\cdot\overset{\circ}{\nabla}\mathbf{v}^{\mathrm{T}} \tag{17}$$

According to (2), the linearized equilibrium conditions on the lateral surface of the cylinder $(r=r_0)$ take the form [1, 8]:

$$\left(\mathbf{e}_r\cdot\mathbf{D}^{\bullet}-\overset{\circ}{\nabla}_s\cdot\mathbf{D}_s^{\bullet}\right)\Big|_{r=r_0}=-pJ\mathbf{e}_r\cdot\mathbf{C}^{-\mathrm{T}}\cdot\left[(\nabla\cdot\mathbf{v})\mathbf{I}-\nabla\mathbf{v}^{\mathrm{T}}\right],\qquad J=\det\mathbf{C} \tag{18}$$

Here ∇ is the three-dimensional nabla-operator in Eulerian coordinates; $\mathbf{D}_s^{\bullet}$ is the linearized surface stress tensor of the Piola type, for which, taking into account the expressions (3), (6), the following relations are valid

$$\mathbf{D}_s^{\bullet}=\mathbf{P}_s^{\bullet}\cdot\mathbf{C}_s+\mathbf{P}_s\cdot\overset{\circ}{\nabla}_s\mathbf{v}_s,\qquad \mathbf{P}_s^{\bullet}=\kappa_1^{\bullet}\mathbf{I}_s+2\kappa_2^{\bullet}\mathbf{G}_s+2\kappa_2\mathbf{G}_s^{\bullet} \tag{19}$$

where $(\alpha=1,2)$

$$\begin{aligned}&\kappa_{\alpha}^{\bullet}=\sum_{\beta=1}^{2}\kappa_{\alpha\beta}j_{\beta}^{\bullet},\quad \kappa_{\alpha\beta}=\frac{\partial\kappa_{\alpha}(j_1,j_2)}{\partial j_{\beta}},\quad j_1^{\bullet}=\mathrm{tr}\mathbf{G}_s^{\bullet},\quad j_2^{\bullet}=2\mathrm{tr}\left(\mathbf{G}_s\cdot\mathbf{G}_s^{\bullet}\right)\\ &\mathbf{G}_s^{\bullet}=\overset{\circ}{\nabla}_s\mathbf{v}_s\cdot\mathbf{C}_s^{\mathrm{T}}+\mathbf{C}_s\cdot\overset{\circ}{\nabla}_s\mathbf{v}_s^{\mathrm{T}},\qquad \mathbf{v}_s=\mathbf{v}\big|_{r=r_0}\end{aligned} \tag{20}$$

Here $\mathbf{P}_s^\bullet$ is the linearized surface stress tensors of the Kirchhoff type; $\mathbf{G}_s^\bullet$ is the linearized surface strain tensor of the Cauchy–Green type; and $\mathbf{v}_s$ is the vector of additional displacements of the lateral surface.

We assume that there is no friction at the ends of the cylinder ($z = 0, l$) and constant normal displacement is given. This leads to the following linearized boundary conditions [13, 14]:

$$\mathbf{e}_z \cdot \mathbf{D}^\bullet \cdot \mathbf{e}_R\big|_{z=0,l} = \mathbf{e}_z \cdot \mathbf{D}^\bullet \cdot \mathbf{e}_\Phi\big|_{z=0,l} = \mathbf{e}_z \cdot \mathbf{v}|_{z=0,l} = 0 \tag{21}$$

The vector of additional displacements $\mathbf{v}$ in the basis of Eulerian cylindrical coordinates is written as:

$$\mathbf{v} = v_R\mathbf{e}_R + v_\Phi\mathbf{e}_\Phi + v_Z\mathbf{e}_Z \tag{22}$$

Taking into account the expressions (8), (10), (14), (16), (17), (22) and the fact that in the considered unperturbed state $\mathbf{d}_1 = \mathbf{e}_r$, $\mathbf{d}_2 = \mathbf{e}_\varphi$, $\mathbf{d}_3 = \mathbf{e}_z$, the components of the linearized Piola stress tensor $\mathbf{D}^\bullet$ in the basis of cylindrical coordinates take the form:

$$\begin{aligned}
\mathbf{e}_r \cdot \mathbf{D}^\bullet \cdot \mathbf{e}_R &= \frac{2\gamma^2\chi_{12}}{r}\left(\frac{\partial v_\Phi}{\partial\varphi} + v_R\right) + \left(\chi_1 + 2\gamma^2\chi_{11}\right)\frac{\partial v_R}{\partial r} + 2\alpha\gamma\chi_{13}\frac{\partial v_Z}{\partial z}\\
\mathbf{e}_r \cdot \mathbf{D}^\bullet \cdot \mathbf{e}_\Phi &= \left(\chi_1 + \gamma^2 B_3\right)\frac{\partial v_\Phi}{\partial r} + \frac{\gamma^2 B_3}{r}\left(\frac{\partial v_R}{\partial\varphi} - v_\Phi\right)\\
\mathbf{e}_r \cdot \mathbf{D}^\bullet \cdot \mathbf{e}_Z &= \left(\chi_1 + \alpha^2 B_2\right)\frac{\partial v_Z}{\partial r} + \alpha\gamma B_2\frac{\partial v_R}{\partial z}\\
\mathbf{e}_\varphi \cdot \mathbf{D}^\bullet \cdot \mathbf{e}_R &= \gamma^2 B_3\frac{\partial v_\Phi}{\partial r} + \frac{\chi_2 + \gamma^2 B_3}{r}\left(\frac{\partial v_R}{\partial\varphi} - v_\Phi\right)\\
\mathbf{e}_\varphi \cdot \mathbf{D}^\bullet \cdot \mathbf{e}_\Phi &= \frac{\chi_2 + 2\gamma^2\chi_{22}}{r}\left(\frac{\partial v_\Phi}{\partial\varphi} + v_R\right) + 2\gamma^2\chi_{12}\frac{\partial v_R}{\partial r} + 2\alpha\gamma\chi_{23}\frac{\partial v_Z}{\partial z}\\
\mathbf{e}_\varphi \cdot \mathbf{D}^\bullet \cdot \mathbf{e}_Z &= \frac{\chi_2 + \alpha^2 B_1}{r}\frac{\partial v_Z}{\partial\varphi} + \alpha\gamma B_1\frac{\partial v_\Phi}{\partial z}\\
\mathbf{e}_z \cdot \mathbf{D}^\bullet \cdot \mathbf{e}_R &= \left(\chi_3 + \gamma^2 B_2\right)\frac{\partial v_R}{\partial z} + \alpha\gamma B_2\frac{\partial v_Z}{\partial r}\\
\mathbf{e}_z \cdot \mathbf{D}^\bullet \cdot \mathbf{e}_\Phi &= \left(\chi_3 + \gamma^2 B_1\right)\frac{\partial v_\Phi}{\partial z} + \frac{\alpha\gamma B_1}{r}\frac{\partial v_Z}{\partial\varphi}\\
\mathbf{e}_z \cdot \mathbf{D}^\bullet \cdot \mathbf{e}_Z &= \frac{2\alpha\gamma\chi_{23}}{r}\left(\frac{\partial v_\Phi}{\partial\varphi} + v_R\right) + 2\alpha\gamma\chi_{13}\frac{\partial v_R}{\partial r} + \left(\chi_3 + 2\alpha^2\chi_{33}\right)\frac{\partial v_Z}{\partial z}
\end{aligned} \tag{23}$$

Similarly, according to the relations (8)–(10), (19), (20), (22), the components of the linearized surface stress tensor of the Piola type $\mathbf{D}_s^\bullet$ are written as follows:

$$
\begin{aligned}
\mathbf{e}_{\varphi}\cdot\mathbf{D}_s^{\bullet}\cdot\mathbf{e}_R &= \frac{\kappa_1+2\gamma^2\kappa_2}{r_0}\left(\frac{\partial v_R^s}{\partial\varphi}-v_{\Phi}^s\right)\\
\mathbf{e}_{\varphi}\cdot\mathbf{D}_s^{\bullet}\cdot\mathbf{e}_{\Phi} &= 2\alpha\gamma\xi_{12}\frac{\partial v_Z^s}{\partial z}+\frac{\kappa_1+2\gamma^2\left(3\kappa_2+\xi_1\right)}{r_0}\left(\frac{\partial v_{\Phi}^s}{\partial\varphi}+v_R^s\right)\\
\mathbf{e}_{\varphi}\cdot\mathbf{D}_s^{\bullet}\cdot\mathbf{e}_Z &= 2\alpha\gamma\kappa_2\frac{\partial v_{\Phi}^s}{\partial z}+\frac{\kappa_1+2\left(\alpha^2+\gamma^2\right)\kappa_2}{r_0}\frac{\partial v_Z^s}{\partial\varphi}\\
\mathbf{e}_{z}\cdot\mathbf{D}_s^{\bullet}\cdot\mathbf{e}_R &= \left(\kappa_1+2\alpha^2\kappa_2\right)\frac{\partial v_R^s}{\partial z}\\
\mathbf{e}_{z}\cdot\mathbf{D}_s^{\bullet}\cdot\mathbf{e}_{\Phi} &= \frac{2\alpha\gamma\kappa_2}{r_0}\frac{\partial v_Z^s}{\partial\varphi}+\left(\kappa_1+2\left(\alpha^2+\gamma^2\right)\kappa_2\right)\frac{\partial v_{\Phi}^s}{\partial z}\\
\mathbf{e}_{z}\cdot\mathbf{D}_s^{\bullet}\cdot\mathbf{e}_Z &= \frac{2\alpha\gamma\xi_{12}}{r_0}\left(\frac{\partial v_{\Phi}^s}{\partial\varphi}+v_R^s\right)+\left(\kappa_1+2\alpha^2\left(3\kappa_2+\xi_2\right)\right)\frac{\partial v_Z^s}{\partial z}\\
\mathbf{e}_{r}\cdot\mathbf{D}_s^{\bullet} &= \mathbf{0}
\end{aligned}
\tag{24}
$$

$$
\xi_1=\kappa_{11}+4\gamma^2\kappa_{12}+4\gamma^4\kappa_{22},\qquad \xi_2=\kappa_{11}+4\alpha^2\kappa_{12}+4\alpha^4\kappa_{22}
$$

$$
\xi_{12}=\kappa_{11}+2\left(\alpha^2+\gamma^2\right)\kappa_{12}+4\alpha^2\gamma^2\kappa_{22}
$$

$$
v_R^s=v_R\big|_{r=r_0},\qquad v_{\Phi}^s=v_{\Phi}\big|_{r=r_0},\qquad v_Z^s=v_Z\big|_{r=r_0}
$$

Expressions (13), describing the perturbed state of equilibrium for a solid circular cylinder, constitute a system of three partial differential equations with respect to three unknown functions v_R, v_{Φ}, v_Z. Substitution [13, 14]

$$
\begin{aligned}
v_R &= V_R(r)\cos n\varphi\cos\beta z\\
v_{\Phi} &= V_{\Phi}(r)\sin n\varphi\cos\beta z\\
v_Z &= V_Z(r)\cos n\varphi\sin\beta z
\end{aligned}
\tag{25}
$$

$$
\beta=\pi m/l,\qquad m=0,1,\ldots\qquad n=0,1,\ldots
$$

leads to the separation of variables φ and z in these equations and allows to satisfy the linearized boundary conditions (21).

Taking into account the relations (23), (25), we write the equations of neutral equilibrium (13) in scalar form:

$$
\begin{aligned}
&\left(\chi_1+2\gamma^2\chi_{11}\right)\left(V_R''+\frac{V_R'}{r}\right)-\frac{n}{r^2}\left(2\chi_2+2\gamma^2\chi_{22}+\gamma^2B_3\right)V_{\Phi}\\
&-\frac{1}{r^2}\left(\chi_2+2\gamma^2\chi_{22}+r^2\beta^2\left[\chi_3+\gamma^2B_2\right]+n^2\left[\chi_2+\gamma^2B_3\right]\right)V_R\\
&\qquad+\frac{n\gamma^2}{r}\left(B_3+2\chi_{12}\right)V_{\Phi}'+\alpha\beta\gamma\left(B_2+2\chi_{13}\right)V_Z'=0
\end{aligned}
$$

$$
\begin{gathered}
\left(\chi_1+\gamma^2 B_3\right)\left(V_{\Phi}''+\frac{V_{\Phi}'}{r}\right)-\frac{n}{r^2}\left(2\chi_2+2\gamma^2\chi_{22}+\gamma^2 B_3\right)V_R \\
-\frac{1}{r^2}\left(\chi_2+\gamma^2 B_3+r^2\beta^2\left[\chi_3+\gamma^2 B_1\right]+n^2\left[\chi_2+2\gamma^2\chi_{22}\right]\right)V_{\Phi} \\
-\frac{n\gamma^2}{r}\left(B_3+2\chi_{12}\right)V_R'-\left(B_1+2\chi_{23}\right)\frac{\alpha\beta\gamma n}{r}V_Z=0 \\
\left(\chi_1+\alpha^2 B_2\right)\left(V_Z''+\frac{V_Z'}{r}\right)-\alpha\beta\gamma\left(B_2+2\chi_{13}\right)\left(V_R'+\frac{nV_{\Phi}+V_R}{r}\right) \\
-\frac{1}{r^2}\left(r^2\beta^2\left[\chi_3+2\alpha^2\chi_{33}\right]+n^2\left[\chi_2+\alpha^2 B_1\right]\right)V_Z=0
\end{gathered}
\tag{26}
$$

According to the expressions (23)–(25), the linearized equilibrium conditions (18) on the lateral surface of the cylinder are written as follows:

$$
\begin{gathered}
\frac{1}{r_0^2}\left(\alpha r_0 p+\tau\kappa_1+2\left(\alpha^2\beta^2 r_0^2+\gamma^2\left[n^2+3\right]\right)\kappa_2+2\gamma^2\left[r_0\chi_{12}+\xi_1\right]\right)V_R\left(r_0\right) \\
+\left(\chi_1+2\gamma^2\chi_{11}\right)V_R'\left(r_0\right)+\beta\gamma\left(p+2\alpha\left[\chi_{13}+\frac{\xi_{12}}{r_0}\right]\right)V_Z\left(r_0\right) \\
+\frac{n}{r_0^2}\left(\alpha r_0 p+2\gamma^2 r_0\chi_{12}+2\kappa_1+2\gamma^2\left[4\kappa_2+\xi_1\right]\right)V_{\Phi}\left(r_0\right)=0 \\
\frac{1}{r_0}\left(\alpha r_0 p+\tau\kappa_1-\gamma^2 r_0 B_3+2\left(\alpha^2\beta^2 r_0^2+\gamma^2\left[2n^2+\tau\right]\right)\kappa_2+2n^2\gamma^2\xi_1\right)V_{\Phi}\left(r_0\right) \\
+\left(\chi_1+\gamma^2 B_3\right)V_{\Phi}'\left(r_0\right)+\frac{2\alpha\beta\gamma n}{r_0}\left(\kappa_2+\xi_{12}\right)V_Z\left(r_0\right) \\
+\frac{n}{r_0^2}\left(\alpha r_0 p+2\kappa_1+\gamma^2\left[8\kappa_2+2\xi_1-r_0 B_3\right]\right)V_R\left(r_0\right)=0 \\
\frac{1}{r_0^2}\left(\left(\tau-1\right)\kappa_1+2\left(n^2\gamma^2+\alpha^2\left[n^2+3\beta^2 r_0^2\right]\right)\kappa_2+2\alpha^2\beta^2 r_0^2\xi_2\right)V_Z\left(r_0\right) \\
+\left(\chi_1+\alpha^2 B_2\right)V_Z'\left(r_0\right)+\beta\gamma\left(p+\alpha\left[\frac{2\xi_{12}}{r_0}-B_2\right]\right)V_R\left(r_0\right) \\
+\frac{2\alpha\beta\gamma n}{r_0}\left(\kappa_2+\xi_{12}\right)V_{\Phi}\left(r_0\right)=0
\end{gathered}
\tag{27}
$$

$$
\tau=n^2+\beta^2 r_0^2+1
$$

Thus, the stability analysis of a solid circular cylinder with surface stresses is reduced to solving a linear homogeneous boundary-value problem (26), (27) for a system of three ordinary differential equations. For its solvability, it is necessary to formulate three additional conditions at $r=0$, which can be obtained by requiring the boundedness of unknown functions V_R, V_{Φ}, V_Z and their derivatives [13, 14]:

$$\begin{aligned} n = 0: &\quad V_R(0) = V_\Phi(0) = V_Z'(0) = 0 \\ n = 1: &\quad V_R'(0) = V_\Phi'(0) = V_Z(0) = 0 \end{aligned} \tag{28}$$

5 Numerical Results

As an example, in this paper we have studied the stability of a solid circular cylinder made of aluminum in the case of a simple axial compression ($p = 0, \alpha \le 1$). Two different models of bulk material were considered:

1) Harmonic model [7] ($\lambda_1, \lambda_2, \lambda_3$ are the principal stretches)

$$W = \frac{1}{2}\lambda\left(\lambda_1 + \lambda_2 + \lambda_3 - 3\right)^2 + 2\mu\left[\left(\lambda_1 - 1\right)^2 + \left(\lambda_2 - 1\right)^2 + \left(\lambda_3 - 1\right)^2\right]$$

$$\lambda_k = \sqrt{G_k}, \qquad k = 1, 2, 3$$

2) Blatz–Ko model [2] (I_1, I_2, I_3 are the principal invariants of the Cauchy–Green strain tensor)

$$W = \frac{1}{2}\mu b\left(I_1 + \frac{I_3^{-a} - 1}{a} - 3\right) + \frac{1}{2}\mu(1 - b)\left(\frac{I_2}{I_3} + \frac{I_3^a - 1}{a} - 3\right), \qquad a = \frac{\lambda}{2\mu}$$

$$I_1 = G_1 + G_2 + G_3, \qquad I_2 = G_1G_2 + G_1G_3 + G_2G_3, \qquad I_3 = G_1G_2G_3$$

The surface strain energy density was assumed to be a quadratic function of the invariants j_1, j_2 [1]:

$$W_s = \frac{1}{8}\lambda_s\left(j_1 - 2\right)^2 + \frac{1}{4}\mu_s\left(j_2 - 2j_1 + 2\right)$$

The following values of bulk λ, μ and surface λ_s, μ_s elastic moduli were used for the aluminum [4]:

$$\lambda = 52.05 \text{ GPa}, \quad \mu = 34.7 \text{ GPa}, \quad \lambda_s = -3.49 \text{ Pa} \cdot \text{m}, \quad \mu_s = 6.22 \text{ Pa} \cdot \text{m}$$

For convenience, the following dimensionless parameters were introduced: relative axial compression $\delta = 1 - \alpha$, length-to-radius ratio $l^* = l/r_0$, and relative radius $r_0^* = r_0\mu/\mu_s$.

By numerical solution of the linearized boundary-value problem (26)–(28) we found the spectra of critical values of the relative axial compression δ, corresponding to the different buckling modes of the solid circular cylinder with surface stresses. By analyzing these spectra the critical axial compression δ_c was obtained for cylinders of various sizes. In the present paper we studied the stability of relatively long cylinders ($l^* \ge 10$). According to the results, in this case the bending buckling ($n = 1$) occurs

at the lowest loads, and the critical axial compression δ_c corresponds to the first bending mode ($m = 1, n = 1$).

Figures 1, 2 and 3 illustrate the influence of the overall size (scale) of the cylinder on its stability. The graphs show the dependencies (solid lines) of the critical axial compression δ_c on the relative radius r_0^* (size parameter) for cylinders with different length-to-radius ratio l^*. According to the results obtained, for both models of bulk material the stability of the cylinder increases with a decrease in size. This effect is due to the influence of surface stresses. It is negligible at macroscale, but becomes quite significant at micro- and nanoscale ($r_0^* \leq 50$). For reference, the graphs also show the results of the stability analysis for cylinders without surface stresses (dashed lines). As expected, these results do not depend on the overall size (scale) of the cylinder.

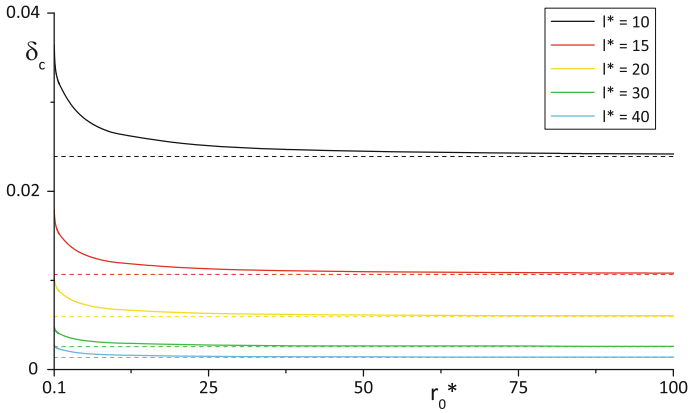

Fig. 1 Size effect on stability of aluminum cylinder with surface stresses. Harmonic model

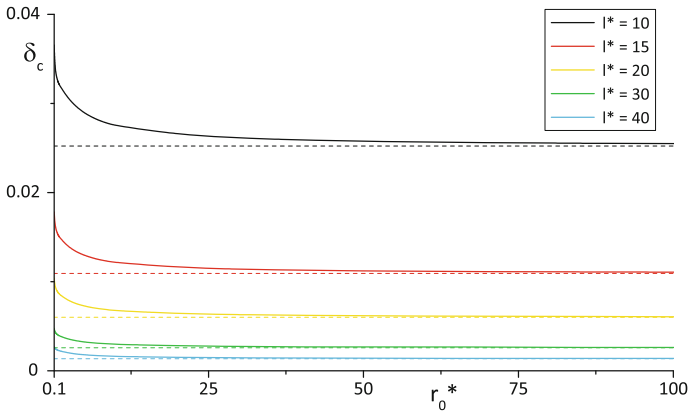

Fig. 2 Size effect on stability of aluminum cylinder with surface stresses. Blatz–Ko model ($b = 0$)

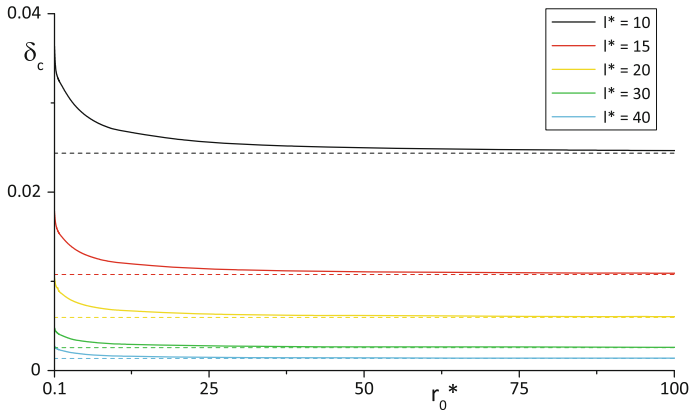

Fig. 3 Size effect on stability of aluminum cylinder with surface stresses. Blatz–Ko model ($b = 1$)

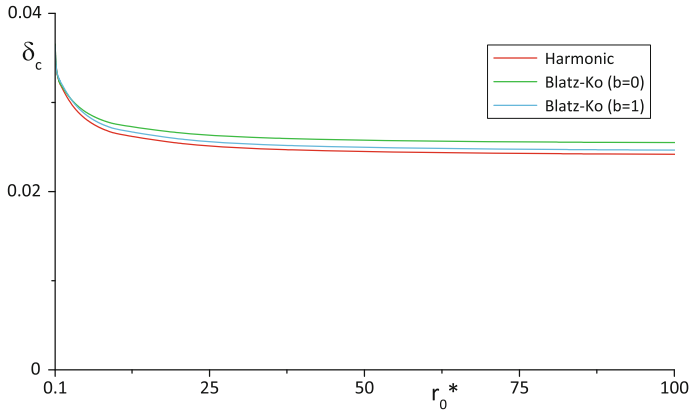

Fig. 4 Comparison of the results for the different models of bulk material ($l^* = 10$)

A comparison of the results for the considered models of bulk material is shown in Fig. 4. It can be seen from the graphs that in the case of Blatz–Ko model the cylinder is generally more stable. This statement is valid for any relatively long ($l^* \geq 10$) solid circular cylinders.

6 Conclusion

In the framework of bifurcation approach, we studied the stability of a nonlinearly elastic solid circular cylinder with surface stresses. For an arbitrary isotropic material, the system of linearized equilibrium equations was derived, which describes

the behavior of a cylinder in a perturbed state. By means of a special substitution, the study of stability was reduced to solving a linear homogeneous boundary-value problem (26)–(28) for a system of three ordinary differential equations. For two specific models of bulk material (Harmonic model and Blatz–Ko model), the buckling analysis has been carried out for a circular cylinder made of aluminum in the case of a simple axial compression ($p = 0, \alpha \leq 1$). As a result, it was found that the stability of the cylinder increases with a decrease of its overall size. This effect is due to the influence of surface stresses. It is negligible at macroscale, but becomes quite significant at micro- and nanoscale ($r_0^* \leq 50$).

Acknowledgements This work was supported by the Russian Foundation for Basic Research (grants 16-08-00802-a, 16-01-00647-a, 16-48-230068-r_a).

References

1. Altenbach, H., Morozov, N.F. (eds.): Surface Effects in Solid Mechanics—Models, Simulations, and Applications. Springer, Berlin (2013)
2. Blatz, P.J., Ko, W.L.: Application of finite elastic theory to the deformation of rubbery materials. Trans. Soc. Rheol. **6**, 223–251 (1962)
3. Cuenot, S., Fretigny, C., Demoustier-Champagne, S., Nysten, B.: Surface tension effect on the mechanical properties of nanomaterials measured by atomic force microscopy. Phys. Rev. B **69**(16), 165410 (2004)
4. Duan, H.L., Wang, J., Karihaloo, B.L.: Theory of elasticity at the nanoscale. In: Advances in Applied Mechanics, vol. 42, pp. 1–68. Elsevier, San Diego (2008)
5. Green, A.E., Adkins, J.E.: Large Elastic Deformations and Non-Linear Continuum Mechanics. Clarendon Press, Oxford (1960)
6. Gurtin, M.E., Murdoch, A.I.: A continuum theory of elastic material surfaces. Arch. Ration. Mech. Anal. **57**(4), 291–323 (1975)
7. John, F.: Plane strain problems for a perfectly elastic material of harmonic type. Commun. Pure Appl. Math. **13**, 239–296 (1960)
8. Lurie, A.I.: Non-linear Theory of Elasticity. North-Holland, Amsterdam (1990)
9. Miller, R.E., Shenoy, V.B.: Size-dependent elastic properties of nanosized structural elements. Nanotechnology **11**(3), 139–147 (2000)
10. Ogden, R.W.: Non-linear Elastic Deformations. Dover, Mineola (1997)
11. Ogden, R.W., Steigmann, D.J., Haughton, D.M.: The effect of elastic surface coating on the finite deformation and bifurcation of a pressurized circular annulus. J. Elast. **47**(2), 121–145 (1997)
12. Sheydakov, D.N.: Stability of a rectangular plate under biaxial tension. J. Appl. Mech. Tech. Phys. **48**(4), 547–555 (2007)
13. Sheydakov, D.N.: Buckling of elastic composite rod of micropolar material subject to combined loads. In: Altenbach, H., Erofeev, V., Maugin, G. (eds.) Mechanics of Generalized Continua—From Micromechanical Basics to Engineering Applications. Advanced Structured Materials, vol. 7, pp. 255–271. Springer, Berlin (2011)
14. Sheydakov, D.N.: On Stability of Inhomogeneous Elastic Cylinder of Micropolar Material. In: Altenbach, H., Mikhasev, G.I. (eds.) Shell and Membrane Theories in Mechanics and Biology. Advanced Structured Materials, vol. 45, pp. 289–300. Springer, Berlin (2015)
15. Wang, J., Duan, H.L., Huang, Z.P., Karihaloo, B.L.: A scaling law for properties of nanostructured materials. P. Roy. Soc. Lond. A **462**(2069), 1355–1363 (2006)

16. Wang, J., Huang, Z., Duan, H., Yu, S., Feng, X., Wang, G., Zhang, W., Wang, T.: Surface stress effect in mechanics of nanostructured materials. Acta Mech. Solida Sinca **24**, 52–82 (2011)
17. Zubov, L.M.: Nonlinear Theory of Dislocations and Disclinations in Elastic Bodies. Springer, Berlin (1997)

Spherically Symmetric Deformations of Micropolar Elastic Medium with Distributed Dislocations and Disclinations

Anastasia A. Zelenina and Leonid M. Zubov

Abstract We discuss the problem of eigenstresses caused by distributed dislocations and disclinations in a hollow solid sphere of linearly elastic isotropic micropolar material. For any spherically symmetric distribution of dislocations and disclinations the exact solution of the boundary value problem is obtained. The derived solution is expressed in primary functions. The spherically symmetric eigenstresses problem is also resolved in the framework of the classical theory of elasticity that is without couple stresses.

Keywords The dislocations and disclinations densities · Couple stress Spherically symmetric tensor fields · Eigenstresses · Exact solution

1 Introduction

A common feature of the structure of solids is a micro nonhomogeneity. To account the materials micro nonhomogeneity in the framework of continuum mechanics the model of the micropolar body can be applied, i.e. the model of a medium with couple stresses and the rotational interaction of material particles. The model of the micropolar medium, also called the Cosserat continuum, is often used for the description of grain polycrystalline bodies, polymers, composites, suspensions, liquid crystals, geophysical structures, biological tissues, nanostructured materials, see e.g. [1–9] and the extended bibliography therein.

Another important element of the microstructure of solids are defects of the crystal lattice such as dislocations and disclinations. In many cases, the number

A. A. Zelenina
Rostov State Transport University, Rostovskogo Strelkovogo Polka Narodnogo Opolcheniya Sq. 2, 344038 Rostov-on-Don, Russia
e-mail: a.zelenina@gmail.com

L. M. Zubov (✉)
Southern Federal University, Milchakova Ave. 8a, 344092 Rostov-on-Don, Russia
e-mail: zubovl@yandex.ru

F. dell'Isola et al. (eds.), *Advances in Mechanics of Microstructured Media and Structures*, Advanced Structured Materials 87,
https://doi.org/10.1007/978-3-319-73694-5_19

of dislocations and disclinations in a bounded volume of the body is very large. So instead of considering a discrete set of defects it more efficient to analyze the continuous distribution of defects and use the theory of distributed dislocations and disclinations. The continuum dislocations theory in non-polar elastic bodies, i.e. in the simple materials was described, for example, in [10–19]. The theory of continuously distributed dislocations and disclinations in micropolar media is described in [16, 20, 21]. Up to our knowledge, nowadays in the literature there are practically no solutions presented for static boundary value problems of the micropolar elastic bodies with distributed dislocations and disclinations. This is because of the complexity of the system of governing differential equations, which in general case consists of six equilibrium equations for stresses and couple stresses and eighteen incompatibility equations regarding the metric and bending deformations. In the paper within the framework of the linear isotropic micropolar elasticity theory we find the exact solution of the eigenstresses problem in hollow solid sphere with spherically symmetric distribution of dislocations and disclinations. The solution is given in elementary functions. The solution is also compared with solution of the same problem obtained within the framework of the classic linear theory of elasticity of non-polar materials.

2 Input Relations

The system of static equations of a linear elastic isotropic micropolar body consists of the equilibrium equations for the stresses [4–6]

$$\mathrm{div}\mathbf{T} + \mathbf{f} = 0, \quad \mathrm{div}\mathbf{M} + \mathbf{T}_{\times} + \mathbf{h} = 0 \tag{1}$$

constitutive relations

$$\begin{aligned} \mathbf{T} &= \lambda \mathbf{E}\mathrm{tr}\,\boldsymbol{\varepsilon} + (\mu + \tau)\boldsymbol{\varepsilon} + (\mu - \tau)\boldsymbol{\varepsilon}^T \\ \mathbf{M} &= \nu \mathbf{E}\mathrm{tr}\boldsymbol{\kappa} + (\gamma + \eta)\boldsymbol{\kappa} + (\gamma - \eta)\boldsymbol{\kappa}^T \end{aligned} \tag{2}$$

and the geometric relations

$$\boldsymbol{\varepsilon} = \mathrm{grad}\mathbf{u} + \mathbf{E} \times \boldsymbol{\theta}, \quad \boldsymbol{\kappa} = \mathrm{grad}\boldsymbol{\theta} \tag{3}$$

Here $\mathbf{T}$ is the stress tensor, $\mathbf{M}$ is the couple stress tensor, $\boldsymbol{\varepsilon}$ is the non-symmetric metric strain tensor, $\boldsymbol{\kappa}$ is the bending strain tensor called also the wryness tensor, see [22, 23], $\boldsymbol{\theta}$ is the microrotation vector field, $\mathbf{u}$ is the displacement field of the elastic medium, $\mathbf{E}$ is the unit tensor. λ, μ, τ, ν, γ, η are the elastic modules, $\mathbf{f}$ is the volume density of mass forces, $\mathbf{h}$ is the volume density of mass moments. The div and grad operators are defined as in [24, 25]. The symbol $\mathbf{T}_{\times}$ denotes the vector invariant of a second-order tensor:

$$\mathbf{T}_{\times} = (T_{sk}\mathbf{r}^{s} \otimes \mathbf{r}^{k})_{\times} = T_{sk}\mathbf{r}^{s} \times \mathbf{r}^{k}$$

where $\mathbf{r}^{s}$, $s = 1, 2, 3$, is a vector basis, see e.g. [25].

To introduce the dislocations density in the micropolar medium let us consider the problem of determination of the displacement field $\mathbf{u}(\mathbf{r})$ for a given strain tensor field $\boldsymbol{\varepsilon}(\mathbf{r})$ and microrotation vector field $\boldsymbol{\theta}(\mathbf{r})$ defined in multiply-connected domain v. Here $\mathbf{r}$ is the radius-vector of point in the 3D space. The fields $\boldsymbol{\varepsilon}$ and $\boldsymbol{\theta}$ are assumed to be differentiable and single-valued. According to (3)

$$\mathrm{grad}\mathbf{u} = \boldsymbol{\varepsilon} - \mathbf{E} \times \boldsymbol{\theta}, \tag{4}$$

in the case of the multiply-connected domain vector field $\mathbf{u}(\mathbf{r})$ can not be uniquely determined, in general. This results in the appearance of translational dislocations [10–12] in the body, each of which is characterized by the Burgers vector

$$\mathbf{b}_{N} = \oint\limits_{\gamma_N} d\mathbf{r} \cdot (\boldsymbol{\varepsilon} - \mathbf{E} \times \boldsymbol{\theta}), \quad N = 1, 2, \ldots N_0 \tag{5}$$

Here γ_N is an arbitrary simple closed contour enclosing the axis of the Nth dislocation. The total Burgers vector of the discrete set of N_0 dislocations is defined according to (5) by the relation

$$\mathbf{B} = \sum_{N=1}^{N_0} \mathbf{b}_{N} = \sum_{N=1}^{N_0} \oint\limits_{\gamma_N} d\mathbf{r} \cdot (\boldsymbol{\varepsilon} - \mathbf{E} \times \boldsymbol{\theta}) \tag{6}$$

Using the known properties of contour integrals the sum of integrals in (6) can be replaced by a single integral over the closed contour γ_0 surrounding the lines of all N_0 dislocations as follows

$$\mathbf{B} = \oint\limits_{\gamma_0} d\mathbf{r} \cdot (\boldsymbol{\varepsilon} - \mathbf{E} \times \boldsymbol{\theta}) \tag{7}$$

Following [13, 14] we passed from a discrete set of dislocations to their continuous distribution, transforming the integral (7) by Stokes' formula

$$\mathbf{B} = \int\limits_{\sigma_0} \mathbf{n} \cdot \mathrm{rot}(\boldsymbol{\varepsilon} - \mathbf{E} \times \boldsymbol{\theta}) d\sigma \tag{8}$$

Here σ_0 is the surface drawn over γ_0, $\mathbf{n}$ is the unit normal to σ_0. The relationship (8) allows to introduce the density of continuously distributed dislocations $\boldsymbol{\alpha}$ as a second-order tensor, whose flux across any surface yields the total Burgers vector of the dislocations crossing this surface

$$\mathrm{rot}(\boldsymbol{\varepsilon} - \mathbf{E} \times \boldsymbol{\theta}) = \boldsymbol{\alpha} \tag{9}$$

Let us assume that elastic body with continuously distributed dislocations occupies the multiply-connected domain and state the problem on rotation field $\boldsymbol{\theta}(\mathbf{r})$ determination in multiply-connected domain with single-valued and differentiable fields $\boldsymbol{\varepsilon}$ and $\boldsymbol{\kappa}$. Now we do not use the requirement that the rotations are single-valued. By analogy with (4) the system of equations with respect to vector $\boldsymbol{\theta}$ takes the form

$$\mathrm{grad}\boldsymbol{\theta} = \boldsymbol{\kappa} \tag{10}$$

In the case of multiply-connected domain it has not uniquely defined solution, in general, that means existence in the body of rotational linear defects, i.e. disclinations [16–19]. The certain disclination is characterized by Frank's vector $\mathbf{q}_N$

$$\mathbf{q}_N = \oint\limits_{\gamma_N} d\mathbf{r} \cdot \boldsymbol{\kappa}, \quad N = 1, 2, \ldots N_0 \tag{11}$$

The total Frank's vector of a discrete disclinations set can, in accordance with (11), be represented as

$$\mathbf{Q} = \sum_{N=1}^{N_0} \mathbf{q}_N = \sum_{N=1}^{N_0} \oint\limits_{\gamma_N} d\mathbf{r} \cdot \boldsymbol{\kappa} \tag{12}$$

In a similar way we passed from a discrete set of disclinations to their continuous distribution and define the density of distributed disclinations $\boldsymbol{\beta}$ as a second-order tensor, whose flux across any surface yields the total Frank vector of all disclinations crossing this surface. This definition leads to the relation $\mathrm{rot}\boldsymbol{\kappa} = \boldsymbol{\beta}$.

Thus, in the presence of distributed dislocations and disclinations, the geometric relations (3) are transformed to the incompatibility equations with regard to the metric and bending deformations

$$\mathrm{rot}\boldsymbol{\varepsilon} - \boldsymbol{\kappa}^T + \mathbf{E}\mathrm{tr}\boldsymbol{\kappa} = \boldsymbol{\alpha} \tag{13}$$

$$\mathrm{rot}\boldsymbol{\kappa} = \boldsymbol{\beta} \tag{14}$$

The Eq. (13) is derived from the relationship (9) and expression of the tensor $\boldsymbol{\kappa}$ in (3). The incompatibility equation (13) and (14) are deduced earlier in [16] with another method. If $\boldsymbol{\alpha} \neq 0$ and $\boldsymbol{\beta} \neq 0$, the fields of displacements $\mathbf{u}$ and rotations $\boldsymbol{\theta}$ do not exist. If $\boldsymbol{\alpha} \neq 0$ but $\boldsymbol{\beta} = 0$, the displacements field does not exist and there exists a rotation field. In what follows we assume that the dislocations and disclinations densities are given tensor functions of coordinates, as mass loads $\mathbf{f}$ and $\mathbf{h}$. These functions cannot be taken arbitrarily, since they obey the equations of continuity [16].

$$\mathrm{div}\boldsymbol{\alpha} + \boldsymbol{\beta}_{\times} = 0, \quad \mathrm{div}\boldsymbol{\beta} = 0 \tag{15}$$

The Eq. (15) are easy to obtain as a necessary condition of solvability of incompatibility equations (13) and (14) by exclusion of the unknown functions $\boldsymbol{\varepsilon}$ and $\boldsymbol{\kappa}$.

3 Spherically Symmetric State

Considering the problem for a hollow sphere we introduce spherical coordinates r, φ, θ by formula

$$x_1 = r\cos\varphi\cos\theta, \quad x_2 = r\sin\varphi\cos\theta, \quad x_3 = r\sin\theta,$$

here x_1, x_2, x_3 is the Cartesian coordinates, r ($r_1 \le r \le r_0$) is the radial coordinate, φ ($0 \le \varphi \le 2\pi$) is the longitude, θ ($-\frac{\pi}{2} \le \theta \le \frac{\pi}{2}$) is the latitude. Unit vectors tangent to the lines of spherical coordinates are denoted by $\mathbf{e}_r$, $\mathbf{e}_\varphi$, $\mathbf{e}_\theta$. The dislocations and disclinations density tensors take the form

$$\boldsymbol{\alpha} = \alpha_1(r)\mathbf{g} + \alpha_2(r)\mathbf{d} + \alpha_3(r)\mathbf{e}_r \otimes \mathbf{e}_r \tag{16}$$

$$\boldsymbol{\beta} = \beta_1(r)\mathbf{g} + \beta_2(r)\mathbf{d} + \beta_3(r)\mathbf{e}_r \otimes \mathbf{e}_r \tag{17}$$

$$\mathbf{g} = \mathbf{e}_\varphi \otimes \mathbf{e}_\varphi + \mathbf{e}_\theta \otimes \mathbf{e}_\theta, \quad \mathbf{d} = \mathbf{e}_\varphi \otimes \mathbf{e}_\theta - \mathbf{e}_\theta \otimes \mathbf{e}_\varphi \tag{18}$$

The tensor fields (16) and (17) have a spherical symmetry in the sense that their components in the basis $\mathbf{e}_r$, $\mathbf{e}_\varphi$, $\mathbf{e}_\theta$ on each spherical surface $r = \mathrm{cons}t$ are the same at all points of the spherical surface and the tensors $\boldsymbol{\alpha}$, $\boldsymbol{\beta}$ invariant under rotations about the radial axis, i.e. about $\mathbf{e}_r$ vector. The last property means that for any function $\chi(r)$ there is the identity

$$\boldsymbol{\Omega} \cdot \boldsymbol{\alpha} \cdot \boldsymbol{\Omega}^T = \boldsymbol{\alpha}$$

$$\boldsymbol{\Omega} = \mathbf{g}\cos\chi(r) + \mathbf{d}\sin\chi(r) + \mathbf{e}_r \otimes \mathbf{e}_r$$

The first summand in (16) describes the distribution of screw dislocations the axes of which coincide with the parallels and meridians, the last summand describes the distribution of screw dislocations with radial axis. The meaning of the (16) corresponds to a distribution of edge dislocations.

The first summand in (17) describes the distribution of wedge disclinations the axes of which coincide with the parallels and meridians, whereas the last summand describes the distribution of wedge disclinations with radial axis. The meaning of the (17) corresponds to a distribution of twist disclinations.

In order to specify loadings, we assume spherically symmetric vector fields

$$\mathbf{f} = f(r)\mathbf{e}_r, \quad \mathbf{h} = h(r)\mathbf{e}_r \tag{19}$$

Using the constitutive relations (2) the equilibrium equations (1) can be easily converted into a system of two vector equations for tensor functions $\boldsymbol{\varepsilon}$ and κ. They should connect the two tensor incompatibility equations (13) and (14). Thus, we obtain the system of 24 scalar equations for 18 unknown scalar functions, i.e. for components of the tensors $\boldsymbol{\varepsilon}$ and κ. The spherically symmetric solution of this system will be obtained similar to (16)

$$\begin{aligned} \boldsymbol{\varepsilon} &= \varepsilon_1(r)\mathbf{g} + \varepsilon_2(r)\mathbf{d} + \varepsilon_3(r)\mathbf{e}_r \otimes \mathbf{e}_r \\ \boldsymbol{\kappa} &= \kappa_1(r)\mathbf{g} + \kappa_2(r)\mathbf{d} + \kappa_3(r)\mathbf{e}_r \otimes \mathbf{e}_r \end{aligned} \tag{20}$$

With (2) and (19) for isotropic material we get

$$\begin{aligned} \mathbf{T} &= t_1(r)\mathbf{g} + t_2(r)\mathbf{d} + t_3(r)\mathbf{e}_r \otimes \mathbf{e}_r \\ \mathbf{M} &= m_1(r)\mathbf{g} + m_2(r)\mathbf{d} + m_3(r)\mathbf{e}_r \otimes \mathbf{e}_r \end{aligned} \tag{21}$$

On the basis of (16) and (17), the tensor incompatibility equations (13) is transformed to the three scalar ordinary differential equations

$$\frac{1}{r}(r\varepsilon_2)' = \alpha_1 - \kappa_1 - \kappa_3, \quad \frac{\varepsilon_3 - \varepsilon_1}{r} - \varepsilon_1' = \alpha_2 - \kappa_2, \quad \frac{2\varepsilon_2}{r} = \alpha_3 - 2\kappa_1 \tag{22}$$

whereas the tensor incompatibility equations (14) is also results into the three equations

$$\frac{1}{r}(r\kappa_2)' = \beta_1, \quad \frac{\kappa_3 - \kappa_1}{r} - \kappa_1' = \beta_2, \quad \frac{2\kappa_2}{r} = \beta_3 \tag{23}$$

Two vector continuity equations (15) are reduced to two scalar differential equations

$$\alpha_3' + \frac{2}{r}(\alpha_3 - \alpha_1) + 2\beta_2 = 0, \quad \beta_3' + \frac{2}{r}(\beta_3 - \beta_1) = 0 \tag{24}$$

The continuity equations (24) does not include the density of edge dislocations function $\alpha_2(r)$. So this function can be arbitrary, including the Dirac delta-function.

With (21) the equilibrium equations (1) are equivalent to the following

$$t_3' + \frac{2}{r}(t_3 - t_1) + f(r) = 0, \quad m_3' + \frac{2}{r}(m_3 - m_1) + 2t_2 + h(r) = 0 \tag{25}$$

It's easy to check that the first equation of (22) is not independent since it follows from the third Eq. (22), the second Eq. (23) and the first Eq. (24). Similarly, the first equation of (23) is a consequence of the third relation (23) and the second relation (24). Thus, there are four independent incompatibility equations.

If we express in the equilibrium equation (25) the components of the stress tensor t_s and the couple stress tensor m_k with the help of constitutive relations (2) through the values ε_k and κ_s, we get two differential equations for functions $\varepsilon_k(r)$, $\kappa_s(r)$.

Adding to these another four incompatibility equations, we will have 6 ordinary differential equations with 6 unknown functions: $\varepsilon_1, \varepsilon_2, \varepsilon_3, \kappa_1, \kappa_2, \kappa_3$.

Thus, even in the total system of resolving Eqs. (1), (2), (13) and (14) the number of equations exceeds the number of unknown functions, in the case of a spherically symmetric deformation, the number of ordinary differential equations coincides with the number of unknown functions.

For the spherically symmetric state we rewrite the constitutive relations in the following form

$$t_1 = 2(\lambda+\mu)\varepsilon_1 + \lambda\varepsilon_3, \quad t_2 = 2\tau\varepsilon_2, \quad t_3 = 2\lambda\varepsilon_1 + (\lambda+2\mu)\varepsilon_3 \tag{26}$$

$$m_1 = 2(\nu+\gamma)\kappa_1 + \nu\kappa_3, \quad m_2 = 2\eta\kappa_2, \quad m_3 = 2\nu\kappa_1 + (\nu+2\gamma)\kappa_3 \tag{27}$$

Proceeding from (22) and (26) we obtain

$$\varepsilon_2 = \frac{r\alpha_3}{2} - r\kappa_1, \quad t_2 = \tau r\alpha_3 - 2\tau r\kappa_1$$

Therefore, the second equilibrium equations (25) will be sought in the following form

$$m_3^{/} + \frac{2}{r}(m_3 - m_1) - 4\tau r\kappa_1 + 2\tau r\alpha_3 + h(r) = 0 \tag{28}$$

It follows from (23), (27) that

$$\kappa_3 = r\kappa_1^{/} + \kappa_1 + r\beta_2,$$

$$m_1 = (3\nu+2\gamma)\kappa_1 + \nu r\kappa_1^{/} + \nu r\beta_2 \tag{29}$$

$$m_3 = (3\nu+2\gamma)\kappa_1 + (\nu+2\gamma)r\kappa_1^{/} + (\nu+2\gamma)r\beta_2 \tag{30}$$

$$m_3 - m_1 = 2\gamma r\kappa_1^{/} + 2\gamma r\beta_2$$

$$m_3^{/} = (\nu+2\gamma)r\kappa_1^{//} + 4(\nu+\gamma)\kappa_1^{/} + (\nu+2\gamma)(r\beta_2)^{/} \tag{31}$$

With (29)–(31) relation (28) becomes the equation for the function $\kappa_1(r)$

$$\begin{aligned} &r^2\kappa_1^{//} + 4r\kappa_1^{/} - \frac{4\tau}{\nu+2\gamma}r^2\kappa_1 = \\ &= -\frac{r}{\nu+2\gamma}\left[(\nu+2\gamma)(r\beta_2)^{/} + 4\gamma\beta_2 + 2\tau r\alpha_3 + h\right] \end{aligned} \tag{32}$$

The right side of the Eq. (32) contains given functions $\beta_2(r)$, $\alpha_3(r)$, $h(r)$. After determining the unknown function $\kappa_1(r)$, the function $\kappa_3(r)$ can be determined from the second relation (23), and the function $\kappa_2(r)$ we can find directly.

Now let us deduce an equation for the function $\varepsilon_1(r)$. Using (22) we get

$$\varepsilon_3 = (r\varepsilon_1)' + r\alpha_2 - \frac{1}{2}r^2\beta_3 \tag{33}$$

and on the basis of (26) we have

$$t_3 - t_1 = 2\mu(\varepsilon_3 - \varepsilon_1) \tag{34}$$

Substitute (33) into (34) we have

$$t_3 - t_1 = 2\mu\left[(r\varepsilon_1)' + r\alpha_2 - \frac{1}{2}r^2\beta_3 - \varepsilon_1\right] \tag{35}$$

Further, differentiating the third relation in (26) and using (33), we obtain

$$\begin{aligned} t_3' &= 2\lambda\varepsilon_1' + (\lambda + 2\mu)\varepsilon_3' = \\ &= 2\lambda\varepsilon_1' + (\lambda + 2\mu)\left[(r\varepsilon_1)'' + (r\alpha_2)' - \frac{1}{2}(r^2\beta_3)'\right] \end{aligned} \tag{36}$$

We transform (35) into

$$\frac{t_3 - t_1}{r} = 2\mu\left(\varepsilon_1' + \alpha_2 - \frac{1}{2}r\beta_3\right) \tag{37}$$

Substituting (36) and (37) to the first equilibrium equation (25), we obtain the equation for $\varepsilon_1(r)$

$$\begin{aligned} &(\lambda + 2\mu)r\varepsilon'' + 4(\lambda + 2\mu)\varepsilon_1' = \\ &= (\lambda + 2\mu)\left[\frac{1}{2}(r^2\beta_3)' - (r\alpha_2)'\right] + 4\mu\left(\frac{1}{2}r\beta_3 - \alpha_2\right) - f \end{aligned} \tag{38}$$

The homogeneous equation (38) is an equation of Euler's type and can be solved elementary. The inhomogeneous equations (38) can be solved by the above technique.

Once the functions ε_1 and κ_1 are found, the other unknowns can be determined directly with (22) and (23). And then with the use of (26) and (27) it is possible to find all stresses.

4 Solution of the Eigenstresses Problem in a Hollow Solid Sphere from Micropolar Material

Let us consider the differential equations (32) and (38)

$$r^2\kappa_1^{//} + 4r\kappa_1^{/} - br^2\kappa_1 = G(r), \quad b = \frac{4\tau}{\nu + 2\gamma} \tag{39}$$

$$G(r) = -\frac{r}{\nu + 2\gamma}\left[(\nu + 2\gamma)(r\beta_2)^{/} + 4\gamma\beta_2 + 2\tau r\alpha_3 + h\right]$$

$$(\lambda + 2\mu)r\varepsilon_1^{//} + 4(\lambda + 2\mu)\varepsilon_1^{/} = F(r) \tag{40}$$

$$F(r) = (\lambda + 2\mu)\left[\frac{1}{2}(r^2\beta_3)^{/} - (r\alpha_2)^{/}\right] + 4\mu\left(\frac{1}{2}r\beta_3 - \alpha_2\right) - f$$

where the right sides are expressed through the given functions describing the distribution of dislocations, disclinations and mass loads. As for the eigenstresses problem there are no external mass and surface loads we assume that $\mathbf{f} = \mathbf{h} = 0$, and the boundary conditions on the inner and outer spherical boundaries of the ball have the form

$$\begin{aligned} m_3(r)|_{r=r_1} &= 0, \quad m_3(r)|_{r=r_0} = 0 \\ t_3(r)|_{r=r_1} &= 0, \quad t_3(r)|_{r=r_0} = 0 \end{aligned} \tag{41}$$

In the case of $b > 0$ the general solution of the differential equations (39) has the form

$$\begin{aligned} \kappa_1(r) = \frac{1}{r^3}&\left(A_1 e^{-\sqrt{b}r}(br + \sqrt{b}) + A_2 e^{\sqrt{b}r}(br - \sqrt{b})\right) + \\ &+ \frac{1}{2b^2r^3}\left[\mathrm{e}^{-\sqrt{b}r}(br + \sqrt{b})\int\left(\frac{1}{r} - \sqrt{b}\right)G(r)\mathrm{e}^{\sqrt{b}r}\mathrm{d}r - \right. \\ &\left. -\mathrm{e}^{\sqrt{b}r}(br - \sqrt{b})\int\left(\frac{1}{r} + \sqrt{b}\right)G(r)\mathrm{e}^{-\sqrt{b}r}\mathrm{d}r\right] \end{aligned} \tag{42}$$

For the differential equations (39) in the case of $b < 0$ we obtain the general solution

$$\kappa_1(r) = \kappa_1(r) = \frac{1}{r^3}\left(A_1 e^{r\sqrt{-b}}(br + I\sqrt{b}) + A_2 e^{-r\sqrt{-b}}(br - I\sqrt{b})\right) + \\ + \frac{1}{2r^3 b}\left[e^{r\sqrt{-b}}(I\sqrt{b} + rb)\int \frac{G(r)r\left(I\sqrt{b} - rb\right)\mathrm{e}^{-r\sqrt{-b}}}{r^2\sqrt{(-b)^3} + I\sqrt{b} - \sqrt{-b}}\mathrm{d}r - \right. \\ \left. - e^{-r\sqrt{-b}}(I\sqrt{b} - rb)\int \frac{G(r)r\left(I\sqrt{b} + rb\right)\mathrm{e}^{r\sqrt{-b}}}{r^2\sqrt{(-b)^3} + I\sqrt{b} - \sqrt{-b}}\mathrm{d}r\right] \tag{43}$$

For the inhomogeneous differential equations (40) we obtain the general solution

$$\varepsilon_1(r) = B_1 + \frac{B_2}{r^3} + \frac{1}{\lambda + 2\,\mu}\int \frac{1}{r^4}\left(\int F(r)r^3\mathrm{d}r\right)\mathrm{d}r \tag{44}$$

Constants A_1, A_2, B_1, B_2 have to be determined from boundary conditions (41). Thus, for (42), (43), and (44) with the boundary conditions (41) it is possible to find exact solutions of the eigenstresses problem.

5 Spherically Symmetric State with a Non-polar Elastic Medium with Distributed Dislocations and Disclinations

Let us also consider the problem of a hollow sphere equilibrium within the framework of the classic linear theory of elasticity, i.e. for a simple (non-polar) material. In this case, the Cauchy stress tensor $\mathbf{T}$ is symmetric and the system of equations of statics of an isotropic body in the absence of distributed defects has the form [24]

$$\mathrm{div}\mathbf{T} + \mathbf{f} = 0 \tag{45}$$

$$\mathbf{T} = \lambda\mathbf{E}\mathrm{tr}\mathbf{e} + 2\mu\mathbf{e} \tag{46}$$

$$\mathbf{e} = \frac{1}{2}\left[\mathrm{grad}\mathbf{u} + (\mathrm{grad}\mathbf{u})^T\right] \tag{47}$$

Derivation of incompatibility equations for a simple elastic material with dislocations and disclinations is similar to that outlined in Sect. 1. With (47) it is given by

$$\mathrm{grad}\mathbf{u} = \mathbf{e} - \mathbf{E}\times\boldsymbol{\varphi} \tag{48}$$

here $\boldsymbol{\varphi}$ is the linear rotation vector [24]. Considering the problem of determining the displacement field $\mathbf{u}$ for a given in multiply-connected domain unique fields of the symmetric strain tensor $\mathbf{e}$ and rotation vector $\boldsymbol{\varphi}$, and arguing as in Sect. 1, we come

to the expression of a tensor density of dislocations

$$\mathrm{rot}\mathbf{e} - \mathrm{rot}(\mathbf{E} \times \boldsymbol{\varphi}) = \boldsymbol{\alpha} \tag{49}$$

Equation (49) can be transformed as follows

$$\mathrm{grad}\boldsymbol{\varphi} = (\mathrm{rot}\mathbf{e})^T + \frac{1}{2}\mathbf{E}\mathrm{tr}\boldsymbol{\alpha} - \boldsymbol{\alpha}^T \tag{50}$$

We consider (50) as a system of equations for determination of the rotation vector field in a multiply-connected domain with given fields $\mathbf{e}$ and $\boldsymbol{\alpha}$. Repeating the arguments of Sect. 1, we obtain an expression for the tensor of disclination density $\boldsymbol{\beta}$

$$\boldsymbol{\beta} = \mathrm{rot}(\mathrm{rot}\mathbf{e})^T - \mathrm{rot}\left(\boldsymbol{\alpha}^T - \frac{1}{2}\mathbf{E}\mathrm{tr}\boldsymbol{\alpha}\right) \tag{51}$$

Considering the $\boldsymbol{\alpha}$ and $\boldsymbol{\beta}$ tensor fields as given quantities whereas the symmetric strain tensor $\mathbf{e}$ as the unknown function, from (51) we get the incompatibility equation of the classic theory of elasticity

$$\mathrm{rot}(\mathrm{rot}\mathbf{e})^T = \mathrm{rot}\left(\boldsymbol{\alpha}^T - \frac{1}{2}\mathbf{E}\mathrm{tr}\boldsymbol{\alpha}\right) + \boldsymbol{\beta} \tag{52}$$

As it is known [24], the tensor $\mathrm{rot}(\mathrm{rot}\mathbf{P})^T$ is symmetric, if $\mathbf{P} = \mathbf{P}^T$. Therefore, a necessary condition for the solvability of equations (52) is the symmetry requirement of the right side. This leads to the relation $\mathrm{div}\boldsymbol{\alpha} + \boldsymbol{\beta}_{\times} = 0$. The second solvability condition can be obtained by applying divergence operator to Eq. (52) and has the form $\mathrm{div}\boldsymbol{\beta} = 0$. Thus, the conditions of solvability of the incompatibility equations (52) coincide with the continuity equations (15) of the micropolar theory of elasticity.

Because of the symmetry of tensors $\mathbf{e}$ and $\mathbf{T}$ the spherically symmetric solution of equilibrium equations (45) and the incompatibility equations (52) for simple linearly elastic isotropic material should be sought in the form

$$\mathbf{e} = e_1(r)\mathbf{g} + e_3(r)\mathbf{e}_r \otimes \mathbf{e}_r, \quad \mathbf{T} = t_1(r)\mathbf{g} + t_3(r)\mathbf{e}_r \otimes \mathbf{e}_r \tag{53}$$

Considering (16), (17) and continuity equations (24) the right part of the incompatibility equations (52) takes the form

$$\mathrm{rot}\left(\boldsymbol{\alpha}^T - \frac{1}{2}\mathbf{E}\mathrm{tr}\boldsymbol{\alpha}\right) + \boldsymbol{\beta} = \left[\beta_1 - \frac{1}{r}(r\alpha_2)'\right]\mathbf{g} + \left(\beta_3 - \frac{2\alpha_2}{r}\right)\mathbf{e}_r \otimes \mathbf{e}_r \tag{54}$$

Components of the dislocation densities α_1, α_3 and the component β_2 of disclination density are not included in the expression (54). This means that the components of distributed defects do not affect the stress state of solid sphere made of linear elastic nonpolar material, whereas in the micropolar material, these defects manifest themselves, i.e. creating their own stresses. Note that the dislocation densities α_1

and α_3 manifest themselves also in the framework of nonlinear elasticity theory of simple materials [26]. In other words, these dislocations in non-polar material cause nonlinear effects. Using (53) and taking into account the continuity equations (15) the tensor incompatibility equations (54) is reduced to one scalar equation

$$\frac{de_1}{dr} + \frac{e_1 - e_3}{r} = \frac{r}{2}\beta_3 - \alpha_2 \tag{55}$$

Vector equilibrium equations (46) with $\mathbf{f} = 0$ on the basis of (53) results in one scalar equation. By using constitutive relations (46) this equation is converted to a differential equation for functions $e_1(r)$ and $e_3(r)$. The latter by means of (55) is the equation of the second order with respect to function $e_1(r)$. This equation not differs from Eq. (36) corresponding to the micropolar material.

6 Conclusion

Using the concept of spherical symmetric tensor field, we reduced a complex system of differential equilibrium equations of the micropolar elastic medium with distributed dislocations and disclinations to two ordinary differential equations. We demonstrate that it is possible to find exact solution of the problem of eigenstresses in a hollow solid sphere made of micropolar material for any spherically symmetric distribution of dislocations and disclinations. This problem is also solved within the framework of the classical theory of elasticity which does not take into account the couple stresses. We established that in this case some components of the dislocations and disclinations density tensors do not affect the stress state of the solid sphere, i.e. the effect of these defects may not be identified in the framework of the classical theory of elasticity.

Acknowledgements This work was supported by the Russian Foundation for Basic Research (grant 18-01-00203).

References

1. Aero, E.L., Kuvshinskii, E.V.: Fundamental equations of the theory of elastic media with rotationally interacted particles. Sov. Phys. Solid State **2**(7), 1272–1281 (1961)
2. Aero, E.L., Kuvshinskii, E.V.: Continuum theory of asymmetric elasticity. Equilibrium of an isotropic body (in Russian). Fisika Tverdogo Tela **2**, 2689–2699 (1964)
3. Koiter, V.T.: Couple-stresses in the theory of elasticity. Pt. I-II. Proc. Koninkl. Neterl. Akad. Weten. **67**, 17–44 (1964)
4. Pal'mov, V.A.: Fundamental equations of the theory of asymmetric elasticity. J. Appl. Math. Mech. **28**(6), 1341–1345 (1964)
5. Morozov, N.F.: Mathematical Problems of Theory of Cracks. Nauka, Moscow (1984) (in Russian)

6. Nowacki, W.: Theory of Asymmetric Elasticity. Pergamon Press, Oxford (1986)
7. Eringen, A.C.: Microcontinuum Fields Theories. I. Foundations and Solids, Springer, New York (1999)
8. Zelenina, A.A., Zubov, L.M.: Quasi-solid states of micripolar elastic bodies. Dokl. Phys. **62**(1), 30–33 (2017)
9. Zubov, L.M.: Static-geometric analogy in the micropolar theory of elasticity. Dokl. Phys. **62**(9), 434–437 (2017)
10. Eshelby, J.D.: The continuum theory of lattice defects. In: Seitz, F., Turnbull, D. (eds.) Solid State Physics, vol. 3, pp. 79–144. Academic Press, New York (1956)
11. Landau, L.D., Lifshitz, E.M.: Theory of Elasticity. Theoretical Physics, vol. 7. Pergamon, Oxford (1975)
12. Kröner, E.: Allgemeine Kontinuums theorie der Versetzungen und Eigenspannungen. Arch. Ration. Mech. Anal. **4**, 273–334 (1960)
13. Nye, J.F.: Some geometrical relations in dislocated crystals. Acta Metall. **1**(2), 153–162 (1953)
14. Vakulenko, A.A: The relationship of micro- and macroproperties in elastic-plastic media (in Russian). Itogi Nauki Tekh., Ser.: Mekh. Deform. Tverd. Tela. **22**, 3 (1991)
15. Gutkin, M.Y., Ovid'ko, I.A.: Plastic Deformation in Nanocrystalline Materials. Springer, Berlin (2004)
16. De Wit, R.: Continual Theory of Disclinations. Mir, Moscow (1977) (in Russian)
17. Zubov, L.M.: Nonlinear Theory of Dislocations and Disclinations in Elastic Bodies. Springer, Berlin (1997)
18. Romanov, A.E.: Mechanics and physics of disclinations in solids. Eur. J. Mech. A Solids **22**, 727–741 (2003)
19. Derezin, S.V., Zubov, L.M.: Disclinations in nonlinear elasticity. Ztschr. Angew. Math. und Mech. **91**, 433–442 (2011)
20. Zubov, L.M.: Continuously distributed dislocations and disclinations in nonlinearly elastic micropolar media. Dokl. Phys. **49**(5), 308–310 (2004)
21. Zubov, L.M.: The continuum theory of dislocations and disclinations in nonlinearly elastic micropolar media. Izv. RAN. MTT. No **1**, 18–27 (2011)
22. Pietraszkiewicz, W., Eremeyev, V.A.: On natural strain measures of the non-linear micropolar continuum. Int. J. Solids Struct. **46**(3), 774–787 (2009)
23. Pietraszkiewicz, W., Eremeyev, V.A.: On vectorially parameterized natural strain measures of the non-linear Cosserat continuum. Int. J. Solids Struct. **46**(11), 2477–2480 (2009)
24. Lurie, A.: Theory of Elasticity. Springer, Berlin (2005)
25. Lebedev, L.P., Cloud, M.J., Eremeyev, V.A.: Tensor Analysis with Applications in Mechanics. World Scientific, New Jersey (2010)
26. Zubov, L.M.: Spherically symmetric solutions in the nonlinear theory of dislocations. Dokl. Phys. **59**(9), 419–422 (2014)